DREIDIMENSIONALE GERÜSTE AUS REKOMBINANTEN SPINNENSEIDENPROTEINEN FÜR BIOMEDIZINISCHE ANWENDUNGEN

DISSERTATION

zur Erlangung des akademischen Grades

- DOKTOR DER NATURWISSENSCHAFTEN -

Im Promotionsprogramm „Molekulare Biowissenschaften“ der Bayreuther Graduiertenschule für Mathematik und Naturwissenschaften der Universität Bayreuth

(BayNAT)

vorgelegt von

Kristin Schacht

(Master of Science)

Bayreuth 2016

Die vorliegende Arbeit wurde in der Zeit von Februar 2012 bis Februar 2016 in Bayreuth am Lehrstuhl Biomaterialien unter der Betreuung von Herrn Prof. Dr. Thomas Scheibel angefertigt.

Vollständiger Abdruck der von der Bayreuther Graduiertenschule für Mathematik und Naturwissenschaften (BayNAT) der Universität Bayreuth genehmigten Dissertation zur Erlangung des akademischen Grades eines Doktors der Naturwissenschaften (Dr. rer. nat).

Dissertation eingereicht am: 18.02.2016

Zulassung durch das Leitungsgremium: 22.02.2016

Wissenschaftliches Kolloquium: 16.09.2016

Amtierender Direktor: Prof. Dr. Stephan Kümmel

Prüfungsausschuss:

Prof. Dr. Thomas Scheibel (Erstgutachter)

PD Dr. Stefan Geimer (Zweitgutachter)

Prof. Dr. Stephan Schwarzinger (Vorsitz)

Prof. Dr. Stefan Schuster

(Prof. Dr. Carsten Werner (Drittgutachter))

INHALTSVERZEICHNIS

Zusammenfassung I
Summary IV
1 Einleitung 1
1.1 Gewebezüchtung (*Tissue Engineering*) 1
1.2 Zell-Matrix-Interaktionen 5
1.2.1 Unspezifische Interaktionen 6
1.2.2 Spezifische Interaktionen 6
1.3 Dreidimensionale Gerüste 9
1.3.1 Anforderungen 9
1.3.2 Schäume 11
1.3.3 Hydrogele 13
1.4 Biofabrikation in der Gewebezüchtung 16
1.4.1 Fabrikationssysteme 17
1.4.2 Biotinten 22
1.5 Spinnenseide 33
1.5.1 Natürliche Spinnenseide 33
1.5.2 Herstellung rekombinanter Spinnenseide 36
1.5.3 Spinnenseidenproteine für biomedizinische Anwendungen 38
2 Zielsetzung 41
3 Synopsis 43
3.1 Mittels *Salt leaching* hergestellte Schäume als 3D-*Scaffolds* 45
3.2 Spinnenseidenhydrogele als neue Biotinte für den 3D-Druck 49
3.3 Optimierung der Überlebensrate von eingekapselten Zellen in der Biotinte 52
4 Literaturverzeichnis 56
5 Darstellung des Eigenanteils 71
6 Publikationsliste 74
7 Teilarbeiten 75
Teilarbeit I 75
Teilarbeit II 93
Teilarbeit III 111
Teilarbeit IV 117
Teilarbeit V 127
Teilarbeit VI 141
Teilarbeit VII 187
Danksagung 193
Erklärung 195

ZUSAMMENFASSUNG

Das Ziel der Gewebezüchtung (*Tissue Engineering*) ist die Wiederherstellung, Erhaltung oder Optimierung von biologischen Gewebefunktionen und sogar ganzen Organen. Bei komplexen und schwerwiegenderen Verletzungen wird eine Trägermatrix bzw. ein 3D-Gerüst (*Scaffold*) benötigt. Die Gerüste aus Polymeren, Keramiken oder Metallen werden durch traditionelle oder additive Fertigungsverfahren hergestellt, bevor die Besiedelung der Zellen und Kultivierung erfolgt. Um Zelladhäsion, -migration, -proliferation und -differenzierung zu ermöglichen, müssen die 3D-*Scaffolds* viele Anforderungen erfüllen. Zum einen spielen die Oberflächenladung und Benetzbarkeit sowie die Topographie der Gerüste eine entscheidende Rolle. Zum anderen müssen die Porengröße, Porosität sowie mechanischen Eigenschaften der Gerüste die Zelladhäsion erlauben und fördern. Aufgrund ihrer Biokompatibilität werden für die Herstellung dieser Gerüste vor allem Biopolymere verwendet. Je nach Anwendungsgebiet und Zelllinie müssen die Materialien und Gerüsteigenschaften angepasst werden, so dass die natürliche extrazelluläre Matrix möglichst genau nachgeahmt wird.

Zu den traditionellen Fertigungsverfahren zählen u. a. die Gefriertrocknung und das Auslaugen von Salzen (*Salt leaching*). Durch das Variieren der Salzpartikelgröße und der Parameter während des Einfrierens können Gerüste mit definierten Poren hergestellt werden. Ein entscheidender Nachteil dieser Methoden ist die fehlende Genauigkeit bei der Herstellung der Gerüste und die komplizierte Steuerung und Regulierung der inneren Struktur. Deshalb werden additive Fertigungsverfahren, wie z. B. die Stereolithographie und der 3D-Druck, eingesetzt. Durch einen automatisierten Prozess können komplexe dreidimensionale Strukturen computergesteuert aufgebaut werden. Bei den meisten additiven Fertigungsverfahren erfolgt die Verarbeitung unter extremen Bedingungen (hohe Temperaturen, Drücke), weil klassische Werkstoffe verwendet werden. Deshalb erfolgt die Besiedelung der *Scaffolds* mit Zellen auch hier erst nach der Herstellung. Allerdings kann dadurch die Zellbesiedelung des Gerüstes teilweise inhomogen erfolgen sowie das Gewebewachstum ungleichmäßig sein.

Eine vielversprechende Alternative zur klassischen Gewebezüchtung ist die Biofabrikation, bei der durch eine automatisierte Herstellung biologisch funktionale Produkte mit struktureller Organisation aus lebenden Zellen, bioaktiven Molekülen oder Biomaterialien durch Biodrucken oder Bioassemblierung und nachfolgender Reifung entstehen. Durch Prozesse, wie z. B. Tintenstrahldruck, Dispensdruck und laserinduzierter Vorwärtstransfer, können hierarchische, dem natürlichen Gewebe nachempfundene Strukturen erzeugt werden, die

eine schnelle Vaskularisierung und Ausbildung funktionaler Komponenten ermöglichen. Die eingesetzten Materialien, vor allem Hydrogele, müssen bei diesen Methoden sowohl druckbar als auch biokompatibel sein. Hydrogele aus natürlichen Polymeren, wie z. B. Alginat und Gelatine, sind bereits in der Biofabrikation als druckbare Materialien (Biotinten) etabliert. Dennoch wird intensiv an alternativen Biomaterialien geforscht, um beispielsweise die Formstabilität der gedruckten 3D-Konstrukte und deren Biokompatibilität zu erhöhen. Die Verwendung von natürlichen Polysacchariden und Proteinen ist vor allem durch deren variierende Qualität und das mögliche Auslösen von immunogenen Reaktionen und Krankheitsübertragungen begrenzt. Deshalb ist es von großem Interesse, dass neue Biopolymere entwickelt werden, die in dieser Komplexität und Funktionalität in der Natur nicht vorkommen.

Spinnenseide ist aufgrund ihrer Biokompatibilität und Bioabbaubarkeit eine vielversprechende Alternative für die Gewebezüchtung. Designte Spinnenseidenproteine eADF4(C16) und deren Varianten, die auf der repetitiven Kernsequenz des *Dragline*-Seidenproteins *Araneus diadematus* Fibroin 4 (ADF4) der europäischen Gartenkreuzspinne (*Araneus diadematus*) basieren, können heutzutage biotechnologisch effizient hergestellt werden. Ein Vorteil der rekombinanten Herstellung ist, dass die Proteine genetisch modifiziert werden können. Nach der biotechnologischen Herstellung können die rekombinanten Spinnenseidenproteine in verschiedene Morphologien, wie z. B. Schäume und Hydrogele überführt werden.

Im Rahmen dieser Dissertation wurden durch unterschiedliche Herstellungsverfahren 3D-*Scaffolds* aus dem rekombinanten Spinnenseidenprotein eADF4(C16) und der mit einer Zelladhäsionsdomäne modifizierten Variante eADF4(C16)-RGD hergestellt. Zunächst wurden, durch das Auslaugen von Salz, Schäume mit einer definierten und steuerbaren Porengröße (30 – 440 µm), Porosität (> 91 %) und mechanischen Eigenschaften im Bereich von Weichgeweben produziert. Zudem waren die Schäume proteolytisch abbaubar, so dass sie nach und nach von der natürlichen extrazellulären Matrix ersetzt werden konnten. Die Analyse der Biokompatibilität dieser porösen Strukturen zeigte, dass Mausfibroblasten auf den Schäumen aus eADF4(C16) nicht adhärieren und proliferieren können, dies aber durch die Einführung des Zelladhäsionsmotivs RGD ermöglicht wird. Die Zellen waren durch die Offenporigkeit und Interkonnektivität des Schaumes im gesamten Gerüst gleichmäßig verteilt. Die Ergebnisse zeigten, dass die Schäume aus den rekombinanten Spinnenseidenproteinen attraktiv für den Einsatz als Trägermatrix in der Gewebezüchtung sind.

Da durch einen computergesteuerten automatisierten Herstellungsprozess die äußere und innere Struktur von Gerüststrukturen besser reguliert werden können, wurde im zweiten Teil

der Arbeit das Potential von Hydrogelen aus rekombinanten Spinnenseidenproteinen als Biotinte evaluiert. Die selbstassemblierten Hydrogele konnten aufgrund der schnellen, reversiblen supramolekularen Wechselwirkungen der Proteine und des scherverdünnenden Verhaltens des Proteinnetzwerkes direkt mittels Dispensdruck verarbeitet werden. Es entstanden mehrlagige, formstabile 3D-Konstrukte, die nicht durch zusätzliche Quervernetzer mechanisch stabilisiert werden mussten. Vor dem Drucken wurden zu der eADF4(C16)-Spinnenseidenlösung humane Fibroblasten gemischt, deren Zugabe weder einen Einfluss auf die physikalische Gelbildung noch auf den Druckprozess hatte. Die Zellen überlebten den Druckprozess und waren über sieben Tage vital. Allerdings sank während des Gelbildungsprozesses die durchschnittliche Viabilität der Zellen um ca. 30 %. Außerdem zeigten die eingekapselten Zellen nach einer Woche noch keine gespreitete Zellmorphologie. Deshalb wurde untersucht, wie die Überlebens- und Proliferationsrate der Zellen verbessert werden kann. Sowohl durch die Seidenproteinkonzentration als auch die Integration der funktionalen Gruppe RGD konnte die Proliferation der Zellen initiiert werden. Über einen Zeitraum von 15 Tagen proliferierten sowohl Fibroblasten als auch Myoblasten in den Hydrogelen aus eADF4(C16)-RGD.

Die durch die *Salt leaching*-Methode und die Biofabrikation hergestellten 3D-*Scaffolds* sind vielversprechend für die Gewebezüchtung, da nicht nur die Gerüsteigenschaften (z. B. durch Variation der Proteinkonzentration), sondern auch deren Biokompatibilität gesteuert werden können.

SUMMARY

The aim of tissue engineering is to restore, maintain or optimize biological tissue functions and to potentially replace whole organs. To reach this aim, a 3D scaffold for the guidance of cells is required. The scaffolds comprise polymers, ceramics or metals and can be produced by various processes (i. e. additive manufacturing). Independent of the processing method, there are many requirements these scaffolds have to fulfill: they have to support cell adhesion, migration, proliferation and differentiation. On one side the hydrophobicity, surface charge and topography of the scaffolds are important. On the other side pore size, porosity, and mechanical properties of the scaffolds have to be adjusted to allow and promote cell adhesion. Due to their biocompatibility, especially biopolymers can be used as scaffold materials. Depending on the field of application, material and scaffold properties need to mimic the natural extracellular matrix as closely as possible.

Traditional manufacturing methods include for example freeze-drying and salt leaching. By variation of the parameters during freezing or the salt particle size, scaffolds with defined pores can be produced. An important disadvantage of these methods is the lack of accuracy in the production of the scaffolds and the lack of control over the internal structure. Therefore, additive manufacturing, such as stereolithography and 3D printing have been used. Most of these techniques are carried out under extreme conditions (e. g. high temperatures, pressures), since conventional materials are employed. However, the cell cultivation of the scaffold occurred after manufacturing and the placement of cells in the scaffold is not controlled.

A promising alternative to traditional tissue engineering is biofabrication, also called bioprinting, the simultaneously processing of cells, signaling molecules and materials into 3D constructs. The hierarchical structures of the natural tissue can be achieved by automated processes, such as inkjet printing, robotic dispensing and laser induced forward transfer. Imitating natural structures enables rapid vascularization and formation of functional components. One of the greatest challenges within the field of biofabrication is the development of process-compatible materials.

The materials used in biofabrication, especially hydrogels, must be both printable and biocompatible. Hydrogels made of natural polymers, such as alginate and gelatin are already established as bio-printable materials (bioinks). Nevertheless, further research for alternative biomaterials for example to increase form stability of the printed 3D constructs and their biocompatibility must be done. The use of natural polysaccharides and proteins is limited

primarily by the varying quality and the possible induction of immunogenic reactions and diseases.

Spider silk is a promising candidate in tissue engineering due to its biocompatibility and biodegradability. The recombinant spider silk proteins eADF4(C16) and its modified variant eADF4(C16)-RGD are based on the repetitive core sequence of the dragline silk protein ADF4 (*Araneus diadematus* fibroin 4) of the European garden spider (*Araneus diadematus*). The biotechnological production of these proteins enables a high amount with consistent quality. The proteins can be genetically modified and processed into different three-dimensional morphologies, such as foams and hydrogels.

In this thesis different manufacturing processes were used to prepare 3D scaffolds made of eADF4(C16) and eADF4(C16)-RGD. First, foams with defined pore sizes (30 - 440 µm), controlled porosity (> 91 %) and mechanical properties in the range of soft tissues were produced by salt leaching. The foams were proteolytically degradable, and can be gradually replaced by the natural extracellular matrix. The analysis of the biocompatibility of these porous structures showed that mouse fibroblasts cannot adhere or proliferate on foams made of eADF4(C16). The adhesion and proliferation could be significantly improved by the introduction of the cell adhesion motif RGD. The cells were homogeneously distributed over such a scaffold due to its open porosity and interconnectivity.

Since the outer and inner structure of a 3D-printed scaffold can be better adjusted by a computer controlled automated manufacturing process, the potential of hydrogels made of recombinant spider silk proteins as bioink was evaluated. The self-assembled hydrogels could be printed by robotic dispensing due to the rapid reversible supramolecular interactions of the proteins and the shear-thinning behavior of the protein networks. Multi-layer, form stable 3D constructs could be printed without the need of crosslinker or additives to stabilize the constructs. Before printing, human fibroblasts were added to the eADF4(C16) spider silk solution. The addition of the cells had no impact on the physical gelation and the printing process. In addition, the cells survived the printing process and were viable for more than seven days. Incubation of the hydrogel without the addition of fresh media resulted in a decrease in the viability of the cells by approximately 30 %. In addition, the encapsulated cells showed round cell morphology after one week. In order to improve the cell proliferation rate and morphology, the fabrication of the bioink was optimized. The survival and proliferation of the cells could be controlled by the spider silk protein concentration and the introduction of the functional group RGD. Over a period of 15 days encapsulated fibroblasts and myoblasts proliferated well in the hydrogels made of eADF4(C16)-RGD.

Summary

The spider silk 3D scaffolds produced by salt leaching and biofabrication are promising candidates for tissue engineering, because both the scaffold's properties and its biocompatibility can be controlled i. e. by the protein concentration and the introduction of functional groups.

1 EINLEITUNG

1.1 GEWEBEZÜCHTUNG (*TISSUE ENGINEERING*)

Die Gewebezüchtung bzw. das *Tissue Engineering* wurde 1993 definiert als „ein interdisziplinärer Bereich, der die Prinzipien der Ingenieurs- und Biowissenschaften vereint, um biologische Substitute zu entwickeln, die biologische Gewebefunktionen und ganze Organe wiederherstellen, erhalten oder verbessern sollen“.[1] In den vergangenen zwei Jahrzehnten kam es in der Gewebezüchtung zu beträchtlichen Fortschritten in den verschiedensten Bereichen, wie z. B. der Herstellung von alternativen Biomaterialien sowie der Entdeckung und Entwicklung neuer Medikamente und Biofabrikationsstrategien.[2-8] Die derzeit in der Gewebezüchtung und regenerativen Medizin angewandten Therapien können in drei Hauptansätze unterteilt werden: A) Klassische Gewebezüchtung bzw. Stammzelltherapie, B) Einsatz von Gerüsten (*Scaffolds*), die durch traditionelle oder additive Fertigungsverfahren hergestellt werden. Die Trägermatrices werden dabei entweder ohne oder mit Zellen implantiert und C) die Implantation von zellbeladenen dreidimensionalen (3D-) Konstrukten, die mit Hilfe der Biofabrikation hergestellt werden (Abb. 1).

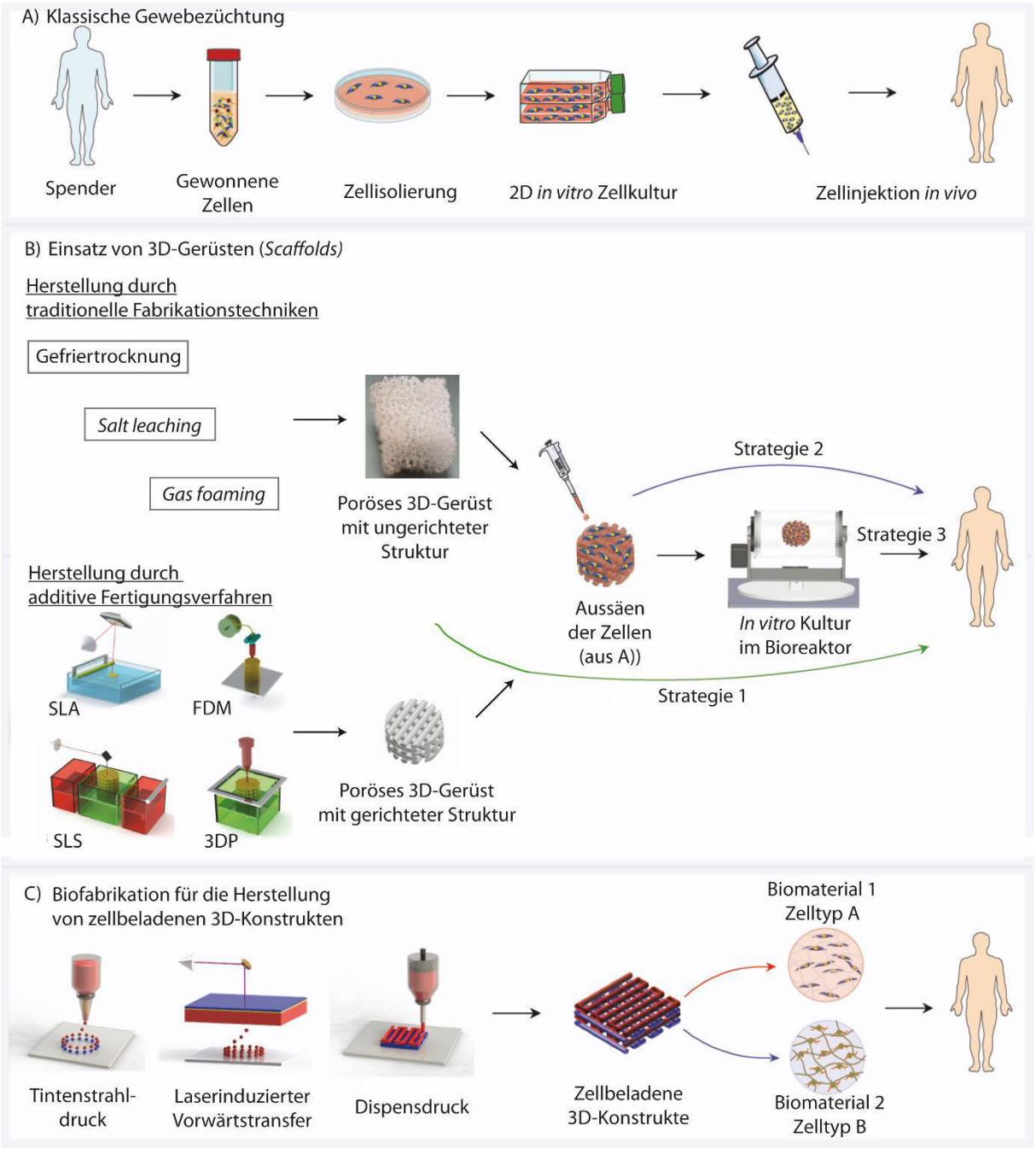

Abbildung 1. Ansätze der Gewebezüchtung und regenerativen Medizin. A) Klassische Gewebezüchtung bzw. Stammzelltherapie; B) Einsatz von Gerüsten (*Scaffolds*), die durch traditionelle Fabrikationstechniken oder additive Fertigungsverfahren hergestellt werden. Die Trägermatrices werden dabei entweder ohne Zellen (Strategie 1), nach dem Aussäen der Zellen (Strategie 2), oder nach der *in vitro* Kultivierung implantiert (Strategie 3); C) Biofabrikation für die Herstellung zellbeladener 3D-Konstrukte, die anschließend implantiert werden. SLA: Stereolithographie; SLS: selektives Lasersintern; FDM: *Fused Deposition Modeling* (Schmelzschichtung); 3DP: 3D-Druck. Modifiziert nach Pereira & Bártolo, *Engineering* 2015, 1(1): 90-112 mit freundlicher Genehmigung des Verlages Chinese Academy of Engineering & Higher Education Press.

In der klassischen Gewebezüchtung bzw. Stammzelltherapie werden die Zellen entweder vom Patienten selbst (autolog) oder von einem Donor (allogen, xenogen) gewonnen und verschiedenen Weiterverarbeitungsschritten unterzogen, bevor sie erneut in den Patienten

injiziert werden.[9] Bevor dies geschieht, werden die gewonnenen Zellen nach der Isolierung *in vitro* in einer 2D-Zellkultur gezüchtet. Dieser Therapieansatz ist relativ einfach durchführbar, allerdings haben in vielen Bereichen solche Verfahren trotz langjähriger Forschungen nicht zum Durchbruch geführt, weder für therapeutische Anwendungen noch für die Herstellung funktionaler humaner *ex vivo* Gewebeäquivalente. Die injizierten Zellen können oft nur schwer in einem klinisch relevanten Zeitraum ohne Abnahme der Zellvitalität in der gewünschten Position überleben. Eine Alternative wäre hingegen die Zellimmobilisierung in Vesikeln, so dass die Zellen länger im Zielgewebe verweilen können bevor eine neue natürliche extrazelluläre Matrix (EZM) aufgebaut ist.[10]

Für komplexe dreidimensionale Gewebe und schwerwiegendere Verletzungen werden vorgefertigte Trägermatrices mit Zellen besiedelt, die die Infiltration sowie Zelladhäsion, -migration, -proliferation und -differenzierung ermöglichen.[2, 11] Bereits in den frühen 70er Jahren wurde vermutet, dass mit Hilfe von neuen biokompatiblen Materialien Zellen in ein synthetisches Stützgerüst eingelagert werden können, so dass anschließend nach Implantation in einen Organismus die Synthese neuer EZM gefördert wird und schließlich ein neues, funktionelles Gewebe entsteht.[12] Nach der Herstellung der porösen 3D-*Scaffolds* werden diese über die gesamte Trägerstruktur mit Zellen besiedelt. Anschließend erfolgt ein Reifungsprozess, vorzugsweise in einem Bioreaktor, bei dem ein Zell-Material-Verbund gezüchtet wird, der als Gewebeersatz in den Patienten implantiert wird. Traditionelle Fabrikationstechniken, wie z. B. Gefriertrocknung, das Auslagen von Salz (*Salt leaching*) oder das Aufschäumen (*Gas foaming*), werden immer noch zur Herstellung dieser porösen Strukturen verwendet (Abb. 1B).[13-14] Der kontinuierliche Gebrauch ist vor allem auf die einfache Herstellungsweise und die geringen Kosten zurückzuführen. Allerdings ist ein entscheidender Nachteil, dass die innere Architektur (z. B. Porosität, Porengröße und Poreninterkonnektivität) nur schwer kontrolliert werden kann.[15] Im Gegensatz dazu können mit Hilfe additiver Fertigungsverfahren, wie beispielsweise Stereolithographie (SLA), selektives Lasersintern (SLS), Schmelzschichtung (*Fused Deposition Modeling*; FDM) und 3D-Druck (3DP) *Scaffolds* mit erhöhter Genauigkeit, Auflösung und Reproduzierbarkeit hergestellt werden (Abb. 1B).[2, 14]

Additives Manufacturing (AM), auch als *Rapid Prototyping* oder einfach dreidimensionales (3D-) Drucken bezeichnet, zeichnet sich dadurch aus, dass die gewünschte Struktur durch einen automatisierten computergesteuerten Prozess direkt Schicht-für-Schicht ohne eine externe Form aufgebaut wird und somit komplexe, heterogene *Scaffolds* geschaffen werden. Open-Source-Projekte wie RepRap und Fab@home haben *additives Manufacturing* für Privatanwender erschwinglich gemacht und führten somit zu einer hohen Akzeptanz des 3D-Druckens (Abb. 1B). Die entwickelten Desktopdrucker basieren auf der *Fused Deposition*

Modeling-Methode und können 3D-*Scaffolds* aus thermoplastischen Materialien mit einer Auflösung von 200-400 µm herstellen.[16] Andere Systeme wie selektives Lasersintern erlauben die Herstellung von sehr komplexen Strukturen mit einer Auflösung von 50-300 µm, werden allerdings hauptsächlich in der Industrie eingesetzt.[17] Sowohl FDM als auch SLS werden verwendet, um thermoplastische Polymere zu verarbeiten. Mittels hoher Temperaturen wird zunächst das Material geschmolzen. Anschließend werden 3D-Strukturen durch kontrolliertes Aushärten des Thermoplasts hergestellt. Alternative Technologien zur Verarbeitung von beispielsweise Hydrogelen, um komplexe 3D-*Scaffolds* herzustellen, sind u. a. die Zwei-Photonen-Polymerisation und die Stereolithographie. Sie nutzen Licht, um meist radikale Polymerisation räumlich begrenzt zu induzieren und somit definierte Strukturen zu erstellen. Obwohl die Konstruktgröße begrenzt ist, können durch die 2PP-Methode Konstrukte mit einer Auflösung kleiner als 100 nm hergestellt werden. Dies ist vor allem für die Analyse von Zell-Matrix-Interaktionen interessant.[18] Im Gegensatz zur Zwei-Photonen-Polymerisation können mit Hilfe der Stereolithographie Konstrukte im Zentimeter-Bereich hergestellt werden. Der größte Nachteil der licht-induzierten Prozesse ist die begrenzte Anzahl an prozesskompatiblen Materialien. Zudem ist beim Drucken von zellenthaltenen Hydrogelen entscheidend, dass der Photoinitiator nicht zytotoxisch ist (Abb. 1B).[19] Die Wahl der Methode hängt sowohl von dem zu druckenden Material als auch von der daraus resultierenden Struktur (Größe, Architektur, Auflösung) ab. Der Vorteil aller additiven Technologien ist die verbesserte Kontrolle über die Eigenschaften der 3D-*Scaffolds*. Allerdings ist der entscheidende Nachteil, dass die Zellbesiedlung nicht homogen über das Gerüst verteilt ist, und somit die Neubildung von Blutgefäßen, also die Vaskularisierung, unzureichend ist, wodurch das Gewebewachstum ungleichmäßig erfolgt.[20] Lebende Zellen und Signalmoleküle können nicht während des Herstellungsprozesses hinzugegeben werden, da die langwierige Produktion sowie die rauen Bedingungen und die schädlichen Lösungsmittel einen negativen Einfluss haben.[15]

Die Implantation von zellbeladenen Matrices, also die gleichzeitige Verarbeitung von Zellen und Biomaterialien, scheint eine vielversprechende Alternative darzustellen (Abb. 1C). In der Biomaterialforschung und Gewebezüchtung wird dieses Verfahren seit Beginn des Einsatzes additiver Fertigungsverfahren als Biofabrikation bzw. Biodrucken bezeichnet. Bei der Biofabrikation können Zellen, Signalmoleküle und Materialien direkt in gewebeartige Strukturen überführt werden. Dadurch kann bereits vor der biologischen Reifung in Kultur eine dem natürlichen Gewebe nachempfundene Struktur erzeugt werden und die notwendige Reifungszeit minimalisiert werden.

Um Zellen sowohl auf zwei- als auch auf dreidimensionalen Matrices züchten zu können, ist es wichtig, die Zell-Matrix-Interaktionen zu verstehen. Im folgenden Kapitel werden die

unspezifischen und spezifischen Interaktionen zwischen Zellen und der jeweiligen Matrix (EZM oder das eingesetzte Material) näher erläutert.

1.2 ZELL-MATRIX-INTERAKTIONEN

Trägermatrices, die in der Gewebezüchtung eingesetzt werden, müssen eine Vielzahl an Anforderungen erfüllen. Primäre Zellen benötigen eine Matrix, entweder die extrazelluläre Matrix oder ein Substrat, um ihre spezifischen Phänotypen zu entwickeln. Zell-Matrix-Interaktionen beeinflussen viele verschiedene Prozesse, wie z. B. morphologische Veränderung, Zellmigration, -proliferation und -differenzierung.[21] Die komplexen Interaktionen zwischen Zellen und der Materialoberfläche können sowohl durch unspezifische Interaktionen, wie z. B. Benetzbarkeit, Oberflächenladung, elektrische Leitfähigkeit und Oberflächentopographie, als auch durch spezifische Interaktionen, z. B. mittels Zelladhäsionsmotive, vermittelt werden (Abb. 2).[21-24]

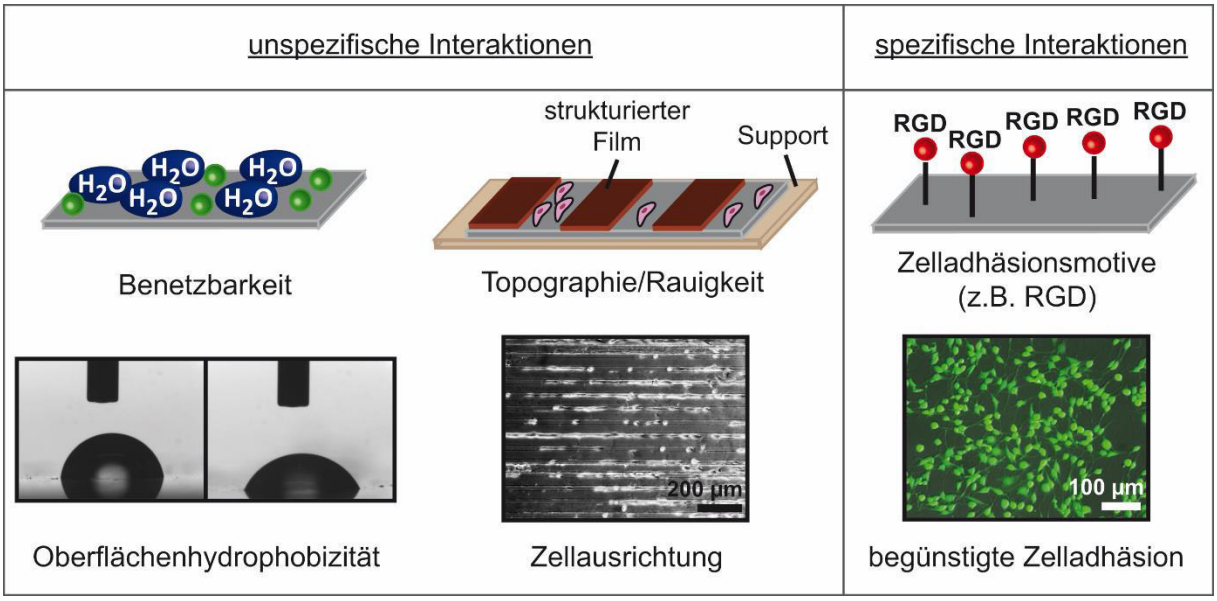

Abbildung 2. Übersicht über unspezifische Zell-Matrix-Interaktionen, wie z. B. Benetzbarkeit und Oberflächentopographie, sowie spezifische Interaktionen begünstigt durch Zelladhäsionsmotive. Modifiziert nach Schacht & Scheibel, *Current Opinion in Biotechnology* 2014, 29: 62-69, mit freundlicher Genehmigung des Verlages Elsevier.

Außer den Zellen des Blutes und des Immunsystems sind alle Zelllinien adhäsionsabhängig und besitzen Adhäsionsproteine (cell adhesion molecules, CAMs), wie z. B. Integrine und Cadherine, um mit der Oberfläche bzw. mit anderen Zellen zu interagieren. Viele Zellen

leiten ohne Matrix-Adhäsion den Zelltod (Apoptose) ein, wodurch es *in vivo* zur Abstoßung oder Einkapselung von Implantaten kommen kann.[25-26]

1.2.1 UNSPEZIFISCHE INTERAKTIONEN

Im Allgemeinen spielen Ladung, Benetzbarkeit und Topographie von Materialoberflächen eine entscheidende Rolle für die Zelladhäsion, wenn spezifische Zelladhäsionsdomänen (z. B. RGD) fehlen (Abb. 2).[21] Die Doppellipidschicht der Zellmembran und viele extrazelluläre Matrixproteine sind unter physiologischen Bedingungen negativ geladen, so dass die Zelladhäsion auf positiv geladenen Materialien durch die elektrostatische Anziehung begünstigt ist.[26-30] Zusätzlich erfolgt eine unspezifische Bindung von Proteinen durch elektrostatische Wechselwirkungen an dem Substrat, die wiederum die Zelladhäsion an der Oberfläche beeinflussen.[26, 31] Die Proteinadsorption und die Zelladhäsion können zudem durch die Benetzbarkeit bzw. Hydrophobizität der Oberfläche beeinflusst werden.[32] Es wurde beobachtet, dass die Proteinadsorption auf hydrophoben Materialoberflächen (Wasserkontaktwinkel > 65°) gegenüber hydrophilen erhöht ist.[33] Auf stark hydrophoben Oberflächen kommt es zu einer Konformationsänderung der Proteine und dadurch bedingt, vermutlich zu veränderten Zugänglichkeiten von z. B. Zelladhäsionsdomänen.[34-35] Dadurch ist die Zelladhäsion auf Oberflächen mit Hydrophobizität mittlerer Größenordnung (Wasserkontaktwinkel 55°) bevorzugt.[29, 35-37] Neben der Hydrophobizität der Oberfläche spielt deren Topographie bzw. Rauigkeit eine entscheidende Rolle bei der Zelladhäsion. Bereits 1911 zeigte Harrison, dass die Oberflächenstruktur einen Einfluss auf die Zellmorphologie, -migration und -ausrichtung adhärenter Zellen hat.[38] Zellen reagieren dabei auf Strukturen im Mikro- bis Nanometerbereich.[39-44] Es können somit je nach Anwendungsgebiet gezielt Oberflächeneigenschaften gesteuert werden, die entweder die Zelladhäsion begünstigen oder verhindern.

1.2.2 SPEZIFISCHE INTERAKTIONEN

Neben unspezifischen Interaktionen spielen spezifische Interaktionen zwischen Liganden und Zelladhäsionsmolekülen (CAMs), wie Integrinen und Cadherinen, eine wichtige Rolle bei der Zelladhäsion. Während Cadherine Zell-Zell-Interaktionen steuern, sind Integrine transmembrane Zell-Adhäsions-Glykoprotein-Rezeptoren, die die größte Klasse der CAMs darstellen und sowohl bei Zell-Zell- als auch bei Zell-Matrix-Interaktionen beteiligt sind.[45] Die

Integrine stellen die Verbindung zwischen extrazellulären und intrazellulären Prozessen dar und steuern die Struktur des Cytoskeletts, die Zellpolarität, -adhäsion, -migration, -proliferation, sowie den Aufbau der extrazellulären Matrix.[46-48] Integrin ist ein nicht-kovalent verbundenes Heterodimer, das aus einer α- und β-Untereinheit besteht und u. a. an das Tripeptid RGD, eine Erkennungssequenz, die zuerst in Fibronektin identifiziert wurde, bindet.[45, 49-51] Mittlerweile sind weitere, die Zelladhäsion fördernde Erkennungssequenzen, wie z. B. IKVAV und YIGSR bekannt.[52-55] IKVAV und YIGSR sind Erkennungssequenzen, die in der α1 bzw. β1 Kette von Laminin, einem weiteren Bestandteil der extrazellulären Matrix, vorkommen.[56-57] Dennoch ist RGD die am besten erforschte und am meisten eingesetzte Zelladhäsionssequenz für die Förderung von Zelladhäsion.

Zelladhäsion und somit die Biokompatibilität eines *Scaffolds* kann mit Hilfe von Zelladhäsionsdomänen entscheidend verbessert werden, indem die Materialien entweder direkt mit extrazellulären Matrixproteinen (z. B. Fibronektin) beschichtet oder genetisch bzw. chemisch mit entsprechenden Peptidsequenzen modifiziert werden (Abb. 3).[58]

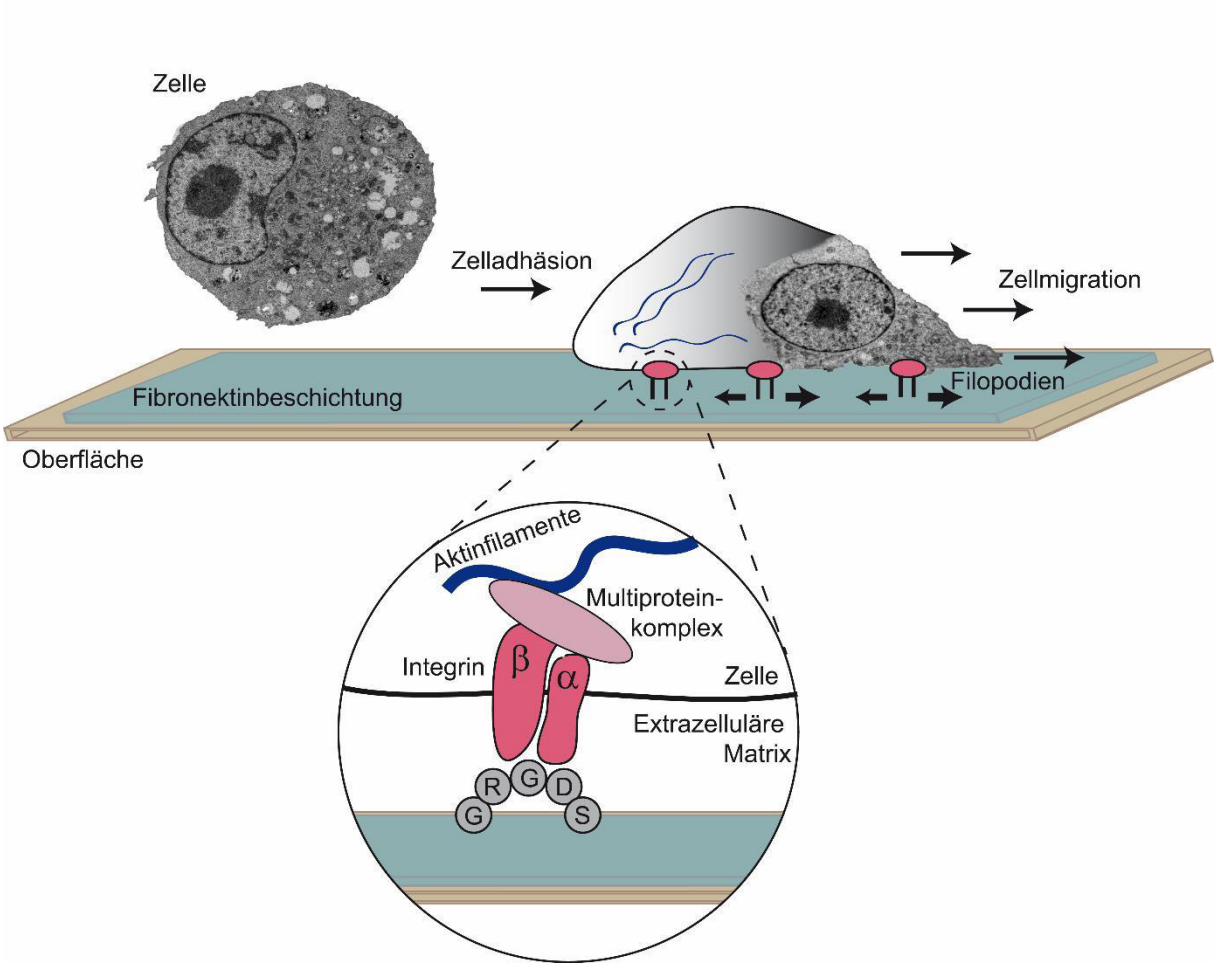

Abbildung 3. Integrin-vermittelte Zelladhäsion auf einer Oberfläche mit Fibronektin-beschichtung. Nach der Zellanhaftung und -ausbreitung wird das Cytoskelett über die Aktinfilamente und den Multiproteinkomplex organisiert und fokale Adhäsionen bilden sich aus. Die Zellmigration erfolgt über Filopodien.

Zum Beispiel wurde das Seidenraupenprotein Fibroin mit dem synthetischen Peptid GRGDS kovalent funktionalisiert und somit die Zelladhäsion entscheidend verbessert.[21, 59] Zudem wurden Adhäsionsdomänen (von Kollagen I oder Fibronektin III) in rekombinant hergestelltem *Bombyx mori*-Fibroin eingebracht, so dass anschließend die Adhäsion von Fibroblasten (BALB/3T3) auf Filmen aus dem modifizierten Protein gesteigert wurde.[60-62] Dieses Verhalten wurde ebenfalls bei Filmen aus rekombinant hergestellten Spinnenseidenproteinen, die entweder genetisch oder chemisch mit dem RGD-Peptid funktionalisiert wurden, festgestellt.[63]

1.3 DREIDIMENSIONALE GERÜSTE

1.3.1 ANFORDERUNGEN

In vitro Zellkulturanalysen erfolgen typischerweise in zweidimensionalen (2D-) Systemen (Abb. 4). Allerdings stimmt das Zellverhalten dort nicht mit dem Verhalten in natürlicher Umgebung überein. Deshalb sind dreidimensionale Gerüste von großem Interesse, die als Matrix in der Gewebezüchtung bzw. nach dem 3D-Drucken den Zellen als Leitstruktur dienen und somit die Adhäsion, Proliferation und Differenzierung fördern. Die 3D-*Scaffolds* ahmen dabei die natürliche zelluläre Mikroumgebung mit ihren mechanischen und biochemischen Eigenschaften nach.[11] Als Gerüst werden beispielsweise Vliesstoffe, poröse Schäume und Hydrogele eingesetzt, die somit als künstliche extrazelluläre Matrix dienen.[64-65]

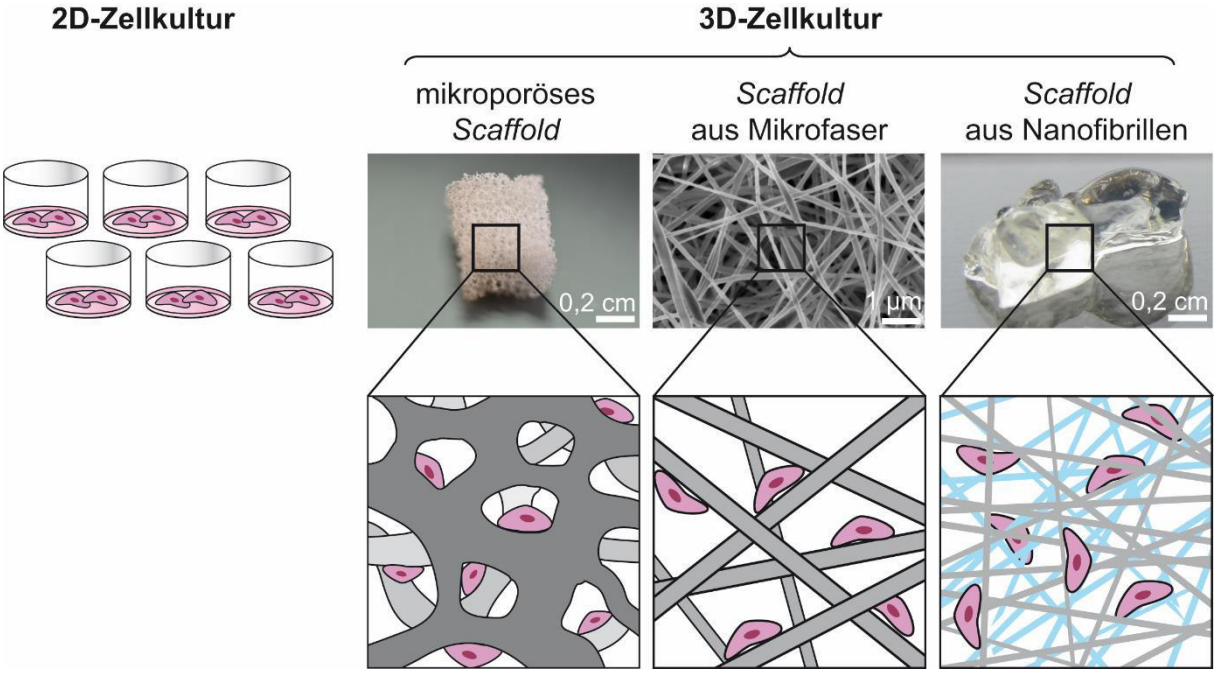

Abbildung 4. 2D-Zellkultur versus 3D-Zellkultur. 3D-*Scaffolds* sind beispielsweise Schäume (mikroporöse *Scaffolds*), Vliese, die aus Mikrofasern bestehen oder Hydrogele, die aus Nanofibrillen aufgebaut sind.

Wenn künstliche *Scaffolds* in der Zellkultur eingesetzt werden sollen, müssen verschiedene Parameter berücksichtigt und verschiedene Anforderungen erfüllt werden. Ein ideales Gerüst für die Gewebezüchtung sollten Zelladhäsion, -migration und -proliferation in dreidimensionaler Umgebung ermöglichen und fördern. Sowohl die Benetzbarkeit und Oberflächenladung als auch die Topographie des Gerüstes spielen eine entscheidende

Rolle. Porengröße, Porosität, mechanische Eigenschaften sowie Biokompatibilität und Bioabbaubarkeit der Gerüste sind wichtig bei der Kultivierung von Zellen *in vitro* und *in vivo*.

Studien haben gezeigt, dass das Zellverhalten in 3D-Strukturen unter anderem von der Porengröße, Porosität und deren Verteilung abhängt. Diese Parameter können u. a. durch das Herstellungsverfahren und die Polymerkonzentration stark beeinflusst werden.[66] Eine hohe Porosität ist ein wichtiger Faktor, da das hohe Oberflächen-Volumen-Verhältnis essentiell ist, um Platz für Zellkultivierung, -wachstum und EZM-Produktion zu schaffen.[22, 67-69] Außerdem muss die Diffusion von Nährstoffen, Sauerstoff und Abfallprodukten (Stoffwechselabfälle und Nebenprodukte des biologischen Abbaus) garantiert sein.[68-69] Die favorisierte Porengröße hängt zusätzlich vom Zelltyp ab.[70-71] Oh et al. haben beobachtet, dass Osteoblasten und Chondrozyten ein besseres Zellwachstum auf einem Poly-ε-Caprolacton (PCL)-*Scaffold* mit einer Porengröße zwischen 380 und 405 µm aufweisen, während Fibroblasten Porengrößen zwischen 186 und 200 µm bevorzugen.[70] Weitere Parameter, wie die Festigkeit des Materials, also die mechanischen Eigenschaften und die Stabilität des Gerüstes, spielen eine entscheidende Rolle beim Zellwachstum. Ein Gerüst für die Gewebezüchtung sollte temporär das Zellwachstum unterstützen und darf deshalb nicht *in vitro* oder nach der Implantation vorzeitig kollabieren.[13, 22] Außerdem sollte das Gerüst möglichst genau die mechanischen Eigenschaften des Zielgewebes nachahmen.[13] Zellen können die Festigkeit ihrer Umgebung in biologische Signale übersetzen (Mechanotransduktion) und anschließend in gewissem Maße darauf reagieren.[72-73] Die Elastizität der Matrix spielt eine wichtige Rolle bei der Proliferation und Differenzierung der Zellen.[74-75] Engler und seine Kollegen haben gezeigt, dass mesenchymale Stammzellen sich unterschiedlich differenzierten, je nachdem welche Festigkeit (0,1 – 40 kPa) die Matrix aufwies.[75] Gewebe und Organe des menschlichen Körpers zeigen, mit Ausnahme von Knochen, Elastizitätsmoduln (E-Moduln) zwischen 1 und 200 kPa.[75] Dementsprechend muss je nach Anwendungsgebiet die Festigkeit des Gerüstes angepasst werden, indem z. B. das Herstellungsverfahren, das Material selbst oder die Polymerkonzentration variiert werden.[21]

Neben der Porengröße, Porosität und den mechanischen Eigenschaften der Gerüste ist die Biokompatibilität des Materials entscheidend.[21] Eine gute Biokompatibilität des Materials ist zwingend erforderlich, da z. B. keine Abstoßungsreaktionen in umliegenden Geweben ausgelöst werden dürfen, die die Funktion des neuen Gewebes beeinträchtigen.[13, 22, 76] Das Material sollte nicht toxisch sein und keine allergische Reaktion oder Immunantwort auslösen, während es kontrolliert abgebaut wird.[13, 21, 24, 76] Generell lassen sich die Materialien für die Gewebezüchtung in zwei Gruppen einteilen. Zum einen die natürlichen Materialien, die sich wieder in autolog, allogen und xenogen einteilen lassen und zum anderen die synthetischen Materialien.[77] Der Vorteil synthetischer Polymere besteht darin,

dass unterschiedliche Strukturen preiswert und reproduzierbar hergestellt werden können. Zudem können ihre Eigenschaften, wie mechanische Festigkeit und Hydrophobizität, kontrolliert werden. Allerdings sind synthetische Polymere im Körper häufig nur sehr langsam abbaubar und sind toxisch bzw. verursachen entzündliche Reaktionen.[12] Im Gegensatz dazu sind natürliche Polymere, wie z. B. Chitosan, Alginat und Kollagen biokompatibel, ohne eine immunologische Reaktion auszulösen. Die physikomechanischen Eigenschaften dieser Polymere sind jedoch zum Teil eingeschränkt. Deshalb ist es wichtig, entweder ein natürliches, mechanisches stabiles Polymer zu finden, das in großen Mengen bei gleichbleibender Qualität produziert werden kann, oder ein synthetisches biokompatibles Polymer.[78]

1.3.2 SCHÄUME

Schäume werden in der Gewebezüchtung vor allem in der Knochen- und Knorpelregeneration eingesetzt. Beim Herstellungsprozess dürfen keine Zusatz- und Hilfsstoffe verwendet werden, die als toxische Rückstände im Schaum zurückbleiben können. Zudem dürfen hohe Temperaturen nicht die Eigenschaften des verwendeten Materials verändern. Der Prozess selbst muss eine optimale Porengröße und Verteilung bei optimaler Porosität liefern, um eine Strukturkompatibilität zu erreichen.[13] Eine Vielzahl an Herstellungsverfahren, wie Gefriertrocknung oder *Salt leaching*, wurde entwickelt um bioabbaubare und -resorbierbare Materialien in 3D-Polymer-*Scaffolds* mit einer hohen Porosität und Oberfläche zu produzieren.[79-81] Bei allen Methoden ist das Ziel reproduzierbare 3D-*Scaffolds* zu produzieren, die als Stütze dienen, bis das neue Gewebe ersetzt ist.

Die Gefriertrocknung bzw. Lyophilisation ist eine häufig eingesetzte Methode um poröse Zellträger für die Gewebezüchtung und andere biologische Anwendungen herzustellen.[82] Ein entscheidender Vorteil bei dieser Methode ist, dass als Lösungsmittel Wasser eingesetzt werden kann. Beim Entfernen des Lösungsmittels kommt es zu keinen Verunreinigungen, so dass keine langen Waschschritte benötigt werden. Bei Seidenfibroin-Gerüsten beispielsweise, die durch die Gefriertrocknung hergestellt wurden, wurde beobachtet, dass verschiedene Porenmorphologien und Nanostrukturen sowohl durch die Proteinkonzentration als auch die Gefrier-Parameter während der Herstellung beeinflusst werden können.[83] *Salt leaching* wurde bereits für Gerüste aus z. B. Kollagen oder Polylactiden, genutzt.[69, 84] Diese Technik wird oft eingesetzt, da sie eine effiziente und leichte Verarbeitung darstellt. Die Porengröße und Porosität der Gerüste wird reguliert, indem

granulare Salzpartikel (Porogene) mit unterschiedlichen Größen (60-1200 µm) zu der Polymerlösung hinzugegeben werden (Abb. 5).[81, 85-88]

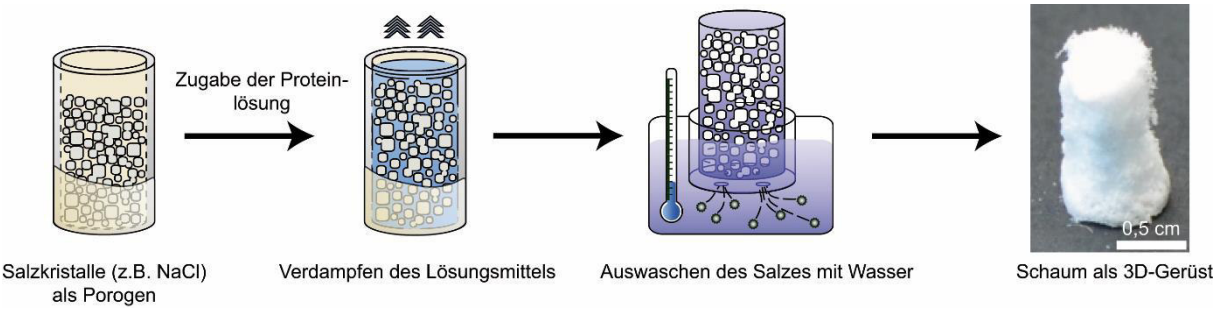

Abbildung 5. Herstellung von Schäumen mit Hilfe der *Salt leaching*-Methode. Für die Herstellung der 3D-Gerüste werden Salzkristalle als Porenbildner (Porogene) verwendet. Nach dem Verdampfen des Lösungsmittels wird das Porogen herausgewaschen, sodass ein poröser Schaum entsteht.

Freed et al. und Mikos et al. produzierten poröse Poly-L-Lactid (PLLA) Gerüste durch Lösen des Polymers in Chloroform und Zugabe von NaCl-Kristallen mit definierter Größe in einem bestimmten Salz-Polymer-Verhältnis. Die Dispersion wurde anschließend in eine Form gegossen und das Lösungsmittel verdampft. Im nächsten Schritt wurde das Salz mit Wasser ausgewaschen und die poröse Polymermatrix getrocknet, so dass ein Schaum entstand.[67] Schäume, die durch *Salt leaching* hergestellt wurden, zeigen oft an der Grenzfläche eine dichte und wenig poröse Schicht, die die Zelladhäsion und -migration *in vitro*, sowie das Einwachsen des Gewebes nach der Implantation *in vivo* behindern.[13] Zusätzlich sind die Makroporen teilweise schlecht vernetzt, was zu einer ungleichmäßigen Verteilung der Zellen und einer verminderten Lebensfähigkeit führt.[89] In der *Salt leaching*-Methode wird das Porogen als Platzhalter für die späteren Poren verwendet. Beim *Gas foaming* hingegen bilden sich die Poren durch ein Hochdruckgas, z. B. CO_2, welches als Schaummittel dient.[13] Die Porosität und Porenstruktur hängen von der Menge an Gas, der Art der Bläschenbildung und der Diffusionsrate der Gasmoleküle durch das Polymer ab. Oftmals ist das durch *Gas foaming* hergestellte Gerüst jedoch zu kompakt für die Zellen.[90] Deshalb werden oft *Gas foaming* und *Salt leaching* kombiniert. In diesem Fall dient Ammoniumhydrogencarbonat als Porogen und nur die Menge an Salzpartikeln und deren Größe bestimmen die Porosität und Porengröße.[91] Nam et al. haben PLLA mit Ammoniumhydrogencarbonat gemischt. Das Lösungsmittel Dichlormethan wurde verdampft und durch Vakuum oder Immersion in heißem Wasser (~90 °C) anschließend die Schaumbildung induziert. Die entstandenen Gerüste zeigten eine zusammenhängende Makroporenstruktur ohne eine kompakte Schicht und ohne Poren an der Oberfläche der Gerüste.[89]

Durch die unterschiedlichen Herstellungsverfahren können Schäume mit verschiedenen Eigenschaften je nach Anwendungsgebiet produziert werden. Im Vergleich zu Hydrogelen

zeigen Schäume eine stabilere und offenporigere Struktur, was die Zelladhäsion unterstützt und fördert. Allerdings können sie aufgrund ihrer starren Struktur schwer in einen Patienten injiziert werden. Besser dafür geeignet sind Hydrogele, die als Wirkstoffdepot bzw. im Bereich der Wundheilung als injizierbares System zum Einsatz kommen.

1.3.3 HYDROGELE

Bereits seit mehreren Jahren werden Hydrogele aufgrund ihrer dreidimensionalen Struktur, der hydrophilen Eigenschaften und der potentiellen Biokompatibilität in der Gewebezüchtung eingesetzt, da sie verschiedene Merkmale der natürlichen Umgebung von Zellen vereinen und eine homogene Zellverteilung gewährleisten.[65, 92-93] Hydrogele sind dreidimensionale vernetzte hydrophile Polymernetzwerke, die bis zu 99 % (w/w) ihres Trockengewichtes an Wasser aufnehmen und physikalisch quellen ohne sich zu lösen.[94-98] Hydrogele für biomedizinische Anwendungen wurden bereits aus einer Vielzahl von synthetischen und natürlichen Polymeren, wie z. B. Polylactid (PLA), Polyglykolsäure (PGA), Polyethylenglykol (PEG) und Poly-ε-Caprolacton (PCL), Kollagen, Alginat, Agarose, Fibrin, Chitosan und Seide, hergestellt.[98-100] Hydrogele können in folgende zwei Gruppen eingeteilt werden: molekulare und selbstassemblierende Hydrogele. Molekulare Hydrogele basieren auf einzelnen Molekülen als Grundbausteine. Durch eine chemische oder physikalische Vernetzung der langkettigen Polymere entstehen Hydrogele. Die chemischen bzw. permanenten Hydrogele bilden ein kovalentes Netzwerk, das nicht in wässrigen Systemen gelöst werden kann, ohne die kovalenten Bindungen zu brechen.[16, 101] Die chemischen Hydrogele können beispielsweise durch Radiation (z. B. Bestrahlung von Polyethylenoxid (PEO) in Wasser), chemische Quervernetzer (z. B. Behandlung von Kollagen mit Glutaraldehyd) oder Copolymerisierung von einem Monomer und Quervernetzer in Lösung (z. B. Hydroxyethylmethacrylat (HEMA) + Ethylenglycoldimethacrylat (EGDMA)) synthetisiert werden.[102] Im Gegensatz zu den chemischen Hydrogelen sind die physikalisch quervernetzten Hydrogele dynamisch und reversibel durch nicht-kovalente Interaktionen (z. B. hydrophobe, elektrostatische und ionische Wechselwirkungen, sowie durch Wasserstoffbrückenbindungen) quervernetzt (Abb. 6).[16, 102]

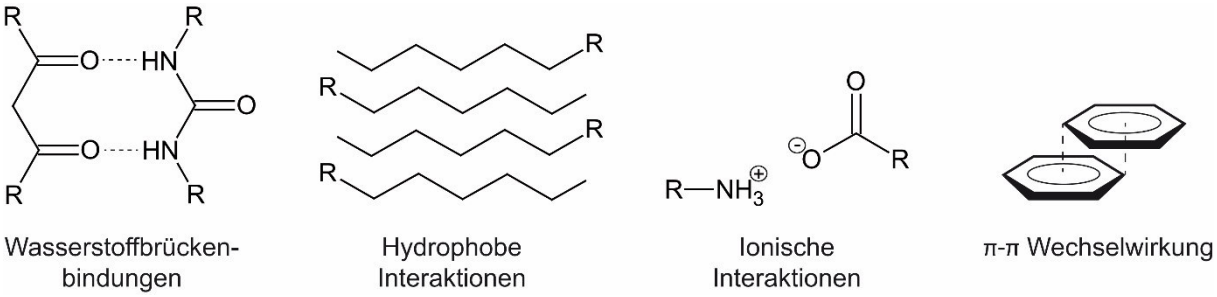

Abbildung 6. Grundlegende molekulare Interaktionen, die an der physikalischen Gelbildung beteiligt sind.

Wenn beispielsweise Polyelektrolyte mit multivalenten Ionen der gegensätzlichen Ladung inkubiert werden, kann ein physikalisches bzw. ionotropes Hydrogel entstehen. Ein Beispiel für diese Art der Hydrogele ist Alginat. Die Gelbildung hängt dabei von der Konzentration der Komponenten, der Ionenstärke und dem pH-Wert der Lösung ab.[103] Ein weiteres Beispiel sind Agarose oder Gelatine, die durch die Abkühlung der Polymerlösung ein physikalisches Hydrogel bilden.[102] Physikalisch quervernetzte Hydrogele zeigen vielversprechende Eigenschaften für den Einsatz in der Gewebezüchtung, da die Gelbildung angepasst werden kann und oftmals keine chemischen Quervernetzer nötig sind, die das Zellverhalten beeinträchtigen könnten.[16]

Die zweite Gruppe umfasst Hydrogele, die aus selbstassemblierenden Strukturen, wie z. B. Fibrillen oder Mizellen, bestehen. Dabei wandeln sich spontan die ungeordneten Grundbausteine in große und komplexere supramolekulare Einheiten um.[104-105] Die Umorganisation der Grundbausteine in geordnete Strukturen erfolgt aufgrund spezifischer Erkennungssequenzen, unterstützt durch eine Kombination aus vielen verschiedenen nicht-kovalenten Interaktionen (Abb. 6).[106] Als Grundbausteine dienen vor allem Proteine und Peptide. Kollagen aus der Haut kann z. B. solch ein makroskopisch strukturelles Element darstellen. Bei dem Strukturprotein der extrazellulären Matrix lagern sich drei linksgängige Helices zu einer rechtsgängigen Superhelix durch Wasserstoffbrückenbindungen zusammen. Ein weiteres Beispiel sind Amyloid-Fibrillen. Die in Lösung intrinsisch ungeordnet vorliegenden Proteine bzw. Peptide können sich unter bestimmten Bedingungen in β-Faltblattstrukturen umwandeln, die in *cross*-β–Konformation vorliegen. Amyloid-β-Peptide sind ein typisches Beispiel für fibrillenformende Peptide. Das charakteristische Röntgenbeugungsmuster für *cross*-β–Strukturen zeigt, dass die Stränge der dicht gepackten β-Faltblätter senkrecht zur Faserachse verlaufen.[107-108] Die Zwischenprodukte (z. B. Oligomere und Protofibrillen) während der Fibrillenbildung werden mit einer Vielzahl an Krankheiten, wie z. B. Alzheimer und Parkinson, in Verbindung gebracht.[109-110] Allerdings können auch andere Proteine, die keine Krankheiten auslösen, amyloidähnliche Fibrillen

ausbilden.[111] Untersuchungen haben gezeigt, dass die Seidenproteine Fibroin (von *Bombyx mori*) und das rekombinante Spinnenseidenprotein eADF4(C16) spontan Hydrogele bilden, die auf Fibrillen basieren (Abb. 7).[95, 112-114]

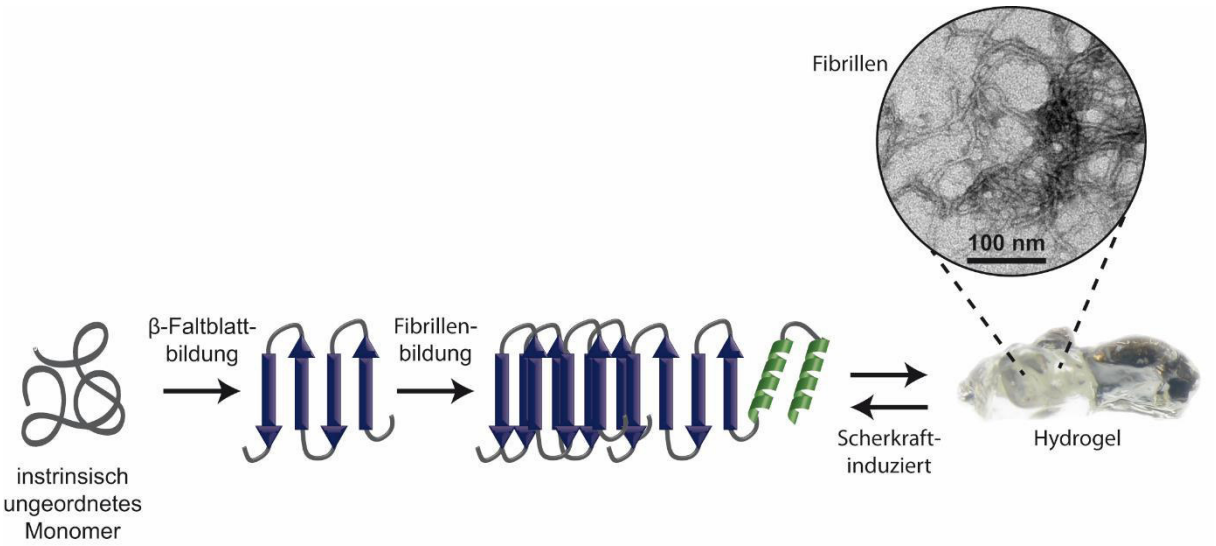

Abbildung 7. Hydrogelbildung durch Selbstassemblierung. In dem intrinsisch ungeordneten Monomer kommt es durch eine strukturelle Umlagerung zu β-Faltblattstrukturen. Bei einer kritischen Größe von Monomeren bzw. Oligomeren bildet sich ein Nukleationskeim. Anschließend erfolgt durch Anlagerung von weiteren Monomeren oder Oligomeren das Fibrillenwachstum.[95, 115-118] Durch eine physikalische Vernetzung (z. B. hydrophobe Interaktionen, Verschlaufung) der Fibrillen kommt es zur Hydrogelbildung.

Die Seidenproteine sind amphiphil, da sich hydrophobe und hydrophile Bereiche in der repetitiven Sequenz abwechseln. Die räumliche Umlagerung von hydrophoben und hydrophilen Grenzflächen verursacht die Selbstassemblierung der Seidenproteine in Nanofibrillen.[117] Die Fibrillenassemblierung der Seidenproteine beinhaltet zwei Phasen, die typisch für *cross*-β-Fibrillen sind:[119-121] Die Anfangsphase beinhaltet die Umwandlung von ungeordneten Monomeren zu antiparallen β-Faltblättern, die durch Wasserstoffbrücken-bindungen und intramolekulare Interaktionen stabilisiert werden.[118] Die hydrophoben Interaktionen initiieren eine Oligomerisierung und schließlich die Bildung eines Nukleationskeims. Die Wachstumsphase startet nach der Keimbildung, wenn sich weitere Monomere oder Oligomere anlagern und die Fibrillen wachsen.[117-118] Die Umwandlung zu Fibrillen kann durch hohe Proteinkonzentrationen, hohe Temperaturen, niedrigen pH-Wert und bivalente Ionen erfolgen.[95, 113-114]

Die Vorteile von Hydrogelen als Trägermatrix in der Gewebezüchtung sind, dass die wässrige Umgebung Zellen und anfällige Wirkstoffe (z. B. Peptide, Proteine, DNA) schützen kann und ein guter Transport von Nährstoffen und Abfallprodukten zu sowie von den Zellen weg erfolgen kann. Die Nachteile sind allerdings, dass die Hydrogele oftmals schlechtere

mechanische Eigenschaften aufweisen und es schwer ist, unter sterilen Bedingungen zu arbeiten.[102, 122] Dennoch zählen Hydrogele zu den vielversprechendsten Kandidaten in der Biofabrikation und Wundheilung. Im folgenden Kapitel wird der Einsatz von Hydrogelen in der Biofabrikation näher erläutert.[16]

1.4 BIOFABRIKATION IN DER GEWEBEZÜCHTUNG

In der Gewebezüchtung und regenerativen Medizin ist die Biofabrikation eine innovative Technologie, die nicht nur auf die Herstellung von Gerüsten durch additive Fertigungsverfahren beschränkt ist.[123] Anders als in klassischen, additiven Fertigungsverfahren zur Herstellung biomedizinischer Implantate und *Scaffolds* mit anschließender Zellbesiedlung, zielt die Biofabrikation zur gleichzeitigen Verarbeitung von Materialien und Zellen auf die Nutzung automatisierter Prozesse ab. Dadurch werden Zell-Biomaterial-Konstrukte hergestellt, die durch ihre innere und äußere räumliche Anordnung in funktionale Gewebe reifen können. Der Begriff Biofabrikation wurde erstmals 2009 von Mironov et al. als „die Produktion von komplexen lebenden und nicht lebenden biologischen Produkten aus Rohmaterialien wie lebenden Zellen, Molekülen, extrazellulärer Matrix und Biomaterialien“[124] definiert. Vor kurzem wurde von der Internationalen Gesellschaft für Biofabrikation eine aktualisierte Definition veröffentlicht.[123] In dieser heißt es, dass „Biofabrikation [ist] die automatisierte Herstellung biologisch funktionaler Produkte mit struktureller Organisation aus lebenden Zellen, Zellaggregaten wie Mikrogeweben, hybriden Gewebekonstrukten, bioaktiven Molekülen oder Biomaterialien durch Biodrucken oder Bioassemblierung und nachfolgender Reifungsprozesse“[123] sei. Biodruck (*Bioprinting*) und Bioassemblierung sind zwei Hauptstrategien der Biofabrikation. Wenn lebende einzelne Zellen, bioaktive Moleküle, Biomaterialien oder Zellaggregate klein genug sind und gedruckt werden können, können die Konstrukte durch den Biodruck hergestellt werden.[125] Im Biodruck ist die minimale Herstellungseinheit auf molekularer Ebene. Im Gegensatz dazu sind bei der zweiten Strategie, der Bioassemblierung, die minimale Fertigungseinheit Bausteine aus vorgeformten Zellkomplexen, die für die automatisierte Assemblierung groß genug sind. Bei der Bioassemblierung werden Zellaggregate, Zellstränge, Zellschichten oder komplexere Strukturen, wie Organoide oder Mikrogewebe, bestehend aus Zellen und deren extrazellulärer Matrix, für die Herstellung von 2D- oder 3D-Konstrukten verwendet.[126] Die Bildung dieser vielzelligen Strukturen erfolgt durch zellgetriebene Selbstorganisation.[123] Im Folgenden werden Fabrikationssysteme und etablierte druckbare Materialien für den Biodruck beschrieben.

1.4.1 FABRIKATIONSSYSTEME

Wenn Zellen gedruckt werden sollen, können viele additive Fertigungstechniken, die in Kapitel 1 beschrieben wurden, aufgrund der extremen Bedingungen (z. B. hohe Temperaturen) nicht eingesetzt werden. Die Anforderungen an die Biofabrikationsprozesse und die dafür verwendeten Materialien, die sogenannten Biotinten, sind wesentlich höher als beim Drucken von klassischen Werkstoffen ohne Zellen. Der Herstellungsprozess muss unter zellfreundlichen Bedingungen, wie z. B. mit wässrigen Lösungsmitteln, bei physiologischen Temperaturen und mit niedrigen mechanischen Scherkräften ablaufen. Zudem müssen die eingesetzten Materialien, bei denen Hydrogele derzeit die vielversprechendsten Kandidaten sind, zellkompatibel sein. Dabei müssen durch den Druckprozess mechanisch belastbare sowie formstabile 3D-Strukturen, die das Überleben der Zellen gewährleisten, erzielt werden. Durch diese Voraussetzungen liegt eine begrenzte Anzahl an geeigneten Technologien und Materialien vor. Nur wenige 3D-Druckverfahren sind hierfür geeignet. In den nachfolgenden Kapiteln werden die wichtigsten und am besten etablierten Technologien (Tintenstrahldruck, Dispensdruck und laserinduzierter Vorwärtstransfer) für das Drucken von Hydrogelen unter zellfreundlichen Bedingungen im Detail und vergleichend dargestellt (Tab. 1).[16]

Tabelle 1. Vergleich der wichtigsten und am besten etablierten additiven Fertigungstechniken in der Biofabrikation, deren Eigenschaften und besonderen Merkmale. Modifiziert nach Jungst et al., *Chemical Reviews* 2015, **DOI:** 10.1021/acs.chemrev.5b00303, mit freundlicher Genehmigung des Verlages American Chemical Society und nach Malda et al., *Advanced Materials* 2013, 25(36): 5011–5028, mit freundlicher Genehmigung des Verlages John Wiley and Sons.

Eigenschaften	Tintenstrahldruck	Dispensdruck	Laserinduzierter Vorwärtstransfer (LIFT)	Ref.
	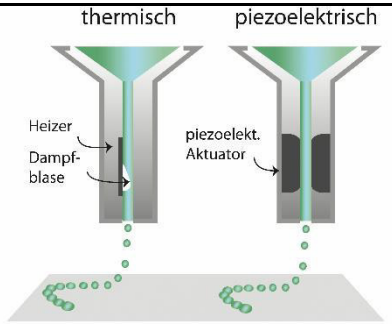	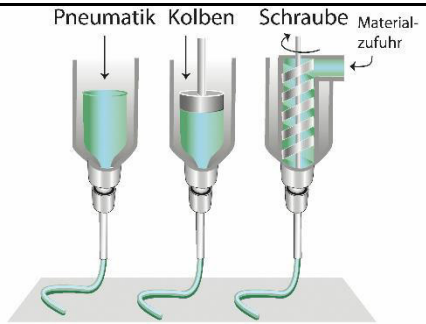	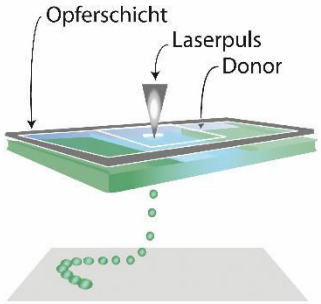	127
Materialviskositäts-bereich	3.5 – 12 mPa·s	30 - (6 x 10^7) mPa·s	1 – 300 mPa·s	128-132
Mechanische/strukturelle Integrität	niedrig	hoch	niedrig	133
Auflösung	~ 75 µm	100 µm bis mm-Bereich	10 – 100 µm	134-137
Arbeitsprinzip	kontaktfrei	Kontakt	kontaktfrei	
Nadelgröße	20 – 150 µm	20 µm bis mm-Bereich	ohne Nadel	137-138
Beladungsvolumen	ml - Bereich	ml - Bereich	> 500 nl	134
Günstiges/einfaches auswechselbares Reservoir	nein (wenn kommerziell erhältliche Kartuschen verwendet werden)	ja	ja	
Fabrikationszeit	mittel bis lang	kurz	lang	16
Kommerziell verfügbar	ja	ja	nein	133
Kosten des Druckers	niedrig	mittel	hoch	131
Vorteile	hohe Auflösung, hohe Zellvitalität, kommerziell erhältlich, kosteneffizient	breite Viskositätsspanne der Materialien, Aufbau klinisch relevanter Konstruktgrößen möglich, kommerziell erhältlich	hohe Auflösung, hohe Zellvitalität	133-134
Nachteile	limitierter Viskositätsbereich	limitierte Auflösung	limitierte Konstruktgrößen, nicht kommerziell erhältlich, hohe Kosten	133-134

1.4.1.1 TINTENSTRAHLDRUCK

Beim Tintenstrahldruck wurden zunächst handelsübliche Tintenstrahldrucker umgebaut, indem die Kartuschen entleert, gereinigt und mit dem zu druckenden Material-Zell-Gemisch wieder befüllt wurden.[139] Im Laufe der Jahre wurden neue Systeme entwickelt und neben thermischen auch piezoelektrische Druckköpfe eingesetzt (Tab. 1). Bei thermischen Tintenstrahldruckern wird die Erzeugung von Tropfen durch elektrische Impulse ausgelöst, die zu einem Temperaturanstieg im Heizer führen und anschließend von der Tintenverdampfung und dem Materialausstoß begleitet werden.[127] In den thermischen Tintenstrahldruckern werden Temperaturen von bis zu 300 °C erreicht.[140] Es konnte allerdings gezeigt werden, dass mit diesen Druckern selbst bei diesen Temperaturen vitale Zellen gedruckt werden können.[140-142] Es wird angenommen, dass der kurze Temperaturimpuls im Millisekundenbereich nur zu einem kleinen Temperaturanstieg (wenige Grad Celsius) des Materials führt und somit keinen Einfluss auf die Zellvitalität hat.[142] Allerdings verwenden die meisten Forscher, die mit Tintenstrahldruckern arbeiten, piezoelektrische Drucksysteme für biomedizinische Anwendungen. Bei dem piezoelektrischen Druckkopf wird das Material aus dem Reservoir mit Hilfe eines piezoelektrischen Aktuators ausgestoßen. Die angelegte Spannung führt zu einer Deformation des piezoelektrischen Kristalls und somit zu einem Materialausstoß.[16] Durch die Deformation kann die ausgestoßene Materialmenge und die Geschwindigkeit des gedruckten Tropfens gesteuert werden, so dass dieses Verfahren flexibel ist und an die Materialeigenschaften angepasst werden kann.[143]

Der Tintenstrahldruck als kontaktfreie Druckmethode mit einem typischen Arbeitsabstand von 1-3 mm kann in drei entscheidende Schritte eingeteilt werden: (1) Materialausstoß, (2) Tropfenbildung im Flug sowie (3) Aufprall und Wechselwirkung des Tropfens auf dem Substrat.[144] Typischerweise weisen die Nadeln am Druckkopf einen Durchmesser von 20-30 µm auf, so dass nur Materialien mit Viskositäten unter 20 mPa·s gedruckt werden können.[128, 140] Beim Tintenstrahldruck sollte im Idealfall jeder Druckimpuls einen individuellen Tropfen erzeugen. Allerdings kann sich während des Fluges der Tropfen in kleinere Satelittentropfen teilen, so dass die Auflösung reduziert wird.[145] Abhängig von der Aufprallgeschwindigkeit (~ 5-10 $m \cdot s^{-1}$) und den Materialeigenschaften wird der Tropfen auf der Substratoberfläche seine Form behalten oder sich ausbreiten.[145] Typischerweise nimmt die Oberfläche des Tropfens beim Aufprall zu, wodurch die Auflösung der Methode auf ca. 75 µm für das Drucken mit Zellen begrenzt ist.[135]

Um Linien oder 3D-Strukturen zu erzeugen ist es notwendig, dass die Tropfen überlappen und miteinander wechselwirken. Dabei ist die Oberflächenspannung entscheidend, die stabil genug sein muss, um die Geometrie bis zur Verfestigung zu erhalten.[144] Zusammengefasst

sind die Vorteile des Tintenstrahldruckers der geringe Materialverbrauch, die hohe Überlebensrate von Zellen sowie die hohe Auflösung der Strukturen von etwa 75 µm.[135, 144] Vor allem weil die Drucker kommerziell erhältlich sind, ist dieses Verfahren zudem kosteneffizient. Eines der Hauptnachteile dieses Verfahrens hingegen ist, dass sich hiermit nur niedrigviskose Materialien verarbeiten lassen.[128, 140]

1.4.1.2 DISPENSDRUCK

Der Dispensdruck ist möglicherweise die vielversprechendste Methode im Bereich der Biofabrikation, da 3D-Konstrukte mit klinisch relevanten Abmessungen in einer für die praktische Anwendung geeigneten Zeitspanne gefertigt werden können (Tab. 1).[16] Im Gegensatz zum Tintenstrahldruck, bei dem einzelne Tropfen gedruckt werden, wird beim Dispensdruck ein kontinuierliches Filament abgelegt, so dass die strukturelle Integrität der gedruckten Konstrukte erhöht wird (Abb. 8).[127]

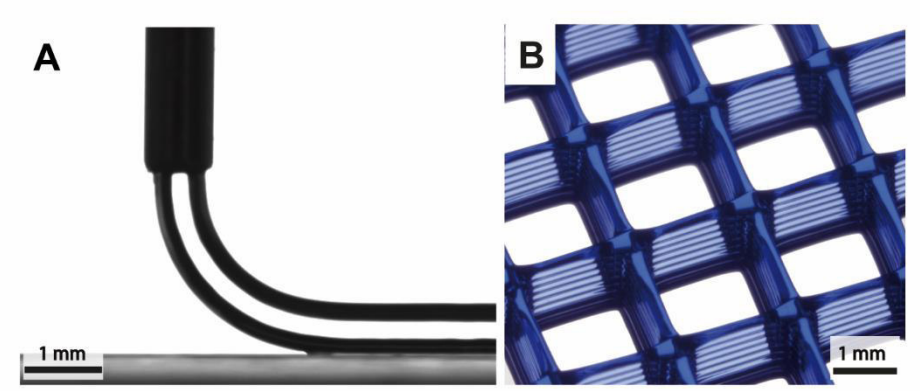

Abbildung 8. Dispensdruck. A) Computergesteuerter Dispensdruck, bei dem das Material aus der Nadel fließt und auf der Substratoberfläche abgelegt wird. B) Stereomikroskopische Aufnahme eines mehrlagigen, gedruckten Pluronic® F127 Konstruktes. Modifiziert nach Jungst et al., *Chemical Reviews* 2015, **DOI:** 10.1021/acs.chemrev.5b00303, mit freundlicher Genehmigung des Verlages American Chemical Society.

Beim Dispensdrucken wird das zu verdruckende Material in eine Kartusche gefüllt. Mit Hilfe eines Kontrollsystems kann die Kartusche computergesteuert bewegt und Schicht-für-Schicht eine 3D-Struktur aufgebaut werden. Der Mechanismus des Dosierens kann entweder pneumatisch oder mechanisch erfolgen (Tab. 1). Bei der am häufigsten vorkommenden pneumatischen Dosierung steuert ein Ventil den Materialausstoß. Die mechanisch betriebene Dosierung basiert meist auf einem Kolben oder einer Schraube mit deren Hilfe das Material, wie bei der pneumatischen Dosierung, durch eine feine Nadel gedrückt wird.[127] Dementsprechend bestimmt der Nadeldurchmesser die Auflösung (100 µm bis mm-Bereich) des Prozesses.[129] Aufgrund der verschiedenen Dosierungssysteme ist

dieses Verfahren besonders variabel in Bezug auf die Viskosität des zu verdruckenden Materials (30 – ($6x10^7$) mPa·s). Das auf einer Schraube basierende System kann Materialien mit den höchsten Viskositäten verarbeiten, da während des Ausstoßens hohe Drücke erzielt werden.[129] Allerdings ist es auch das Verfahren mit dem kompliziertesten Aufbau. Im Gegensatz dazu weist die pneumatische Dosierung einen einfacheren Aufbau auf und im Vergleich zum Kolben getriebenen System können hier aufgrund der variablen Drücke höhere Viskositäten verdruckt werden.[129] Der größte Nachteil dieses Verfahrens ist die Verwendung von Druckluft, da das komprimierte Gas zu einer Verzögerung zwischen dem Start bzw. Stopp des Materialflusses und dem Start/Stopp der letztendlichen Dosierung führt. Dieses Problem kann behoben werden, indem entweder eine Zeitverzögerung einkalkuliert wird, so dass die eigentliche Druckposition erst anschließend angefahren wird, oder indem unmittelbar vor der Öffnung des Druckkopfes ein Ventil eingesetzt wird.[16] Allerdings ist im Hinblick auf das eingesetzte Material der Dispensdruck das vielseitigste Verfahren. Dadurch, dass Nadeln mit unterschiedlichen Durchmessern verwendet werden können, können diese einfach an die Viskositäten des zu verdruckenden Materials angepasst werden. Außerdem können Konstrukte im Millimeterbereich in kurzer Fabrikationszeit hergestellt werden, worunter allerdings die Auflösung leidet.[137] Mit dieser Methode können jedoch, sofern die Auflösung nicht entscheidend ist, große Konstrukte, wie z. B. klinisch relevante Implantate, gedruckt werden.[127]

1.4.1.3 LASERINDUZIERTER VORWÄRTSTRANSFER (LIFT)

Das additive Fertigungsverfahren mit der höchsten Auflösung (10 – 100 µm), das sogar ein kontrolliertes Verdrucken einzelner Zellen erlaubt, ist der laserinduzierte Vorwärtstransfer (LIFT) (Tab. 1).[146] Hierbei wird ein gepulster Laser auf den sogenannten Donor, bestehend aus einem lichtdurchlässigen Trägermaterial, einer Opferschicht und dem zu druckenden Material, gerichtet. Der Laser verdampft die Opferschicht lokal und führt damit zu einem Ausstoß des Materials. Werden der Donor und/oder das Substrat kontrolliert bewegt, können durch die Materialtröpfchen 2D- und 3D-Strukturen aufgebaut werden.[130, 132, 147-150] Da ein Laser als treibende Kraft verwendet wird, ist die Auflösung bei der LIFT-Technik hauptsächlich von der Laserenergie und Dauer des Laserpulses abhängig. Zusätzlich sind die Materialeigenschaften und die Dicke der Donorschicht entscheidend für das ausgestoßene Materialvolumen. Durch den Laserpuls wird Material im Donor verdampft, so dass eine Blase entsteht. Diese Dampfblase muss sich bis zum Substrat ausbreiten, damit Material ausgestoßen werden kann. Ist die Laserfluenz jedoch zu niedrig, kollabiert die Blase. Ist die Fluenz zu hoch, produziert die Blase ungerichtete submikrometergroße

Tropfen.[151-154] Die Materialeigenschaften sind dementsprechend entscheidend, da sie einen Einfluss auf die Blasenbildung haben. Zusätzlich beeinflussen die viskoelastischen Eigenschaften des Materials die Weitergabe des Gasdruckes und somit das Ausstoßen des Materials. Der laserinduzierte Vorwärtstransfer schließt die Lücke im Viskositätsbereich zwischen dem Tintenstrahldruck und Dispensdruck (1 – 300 mPa·s).[132] Zudem ist dieses Verfahren, wie der Tintenstrahldruck, eine kontaktfreie Druckmethode bei dem ein Arbeitsabstand von 1-3 mm vorliegt, so dass auch raue Oberflächen bedruckt werden können.[16] Zum Drucken wird auf der einen Seite nur wenig Material (einige 100 nl) benötigt, auf der anderen Seite wird der schnelle Aufbau größerer Strukturen dadurch erschwert.[134] Zudem sind derzeit keine kommerziell erhältlichen Drucksysteme verfügbar und die hohe Auflösung des Prozesses erfordert teure, hochpräzise Aktuatoren.[133]

1.4.2 BIOTINTEN

In der Biofabrikation beschreibt der Begriff Biotinte druckbare Biomaterialien mit integrierten Zellen. Da die Anforderungen an die gewählten Materialien sehr hoch sind, stellen Biotinten oft den limitierenden Faktor in der Biofabrikation dar (Abb. 9).

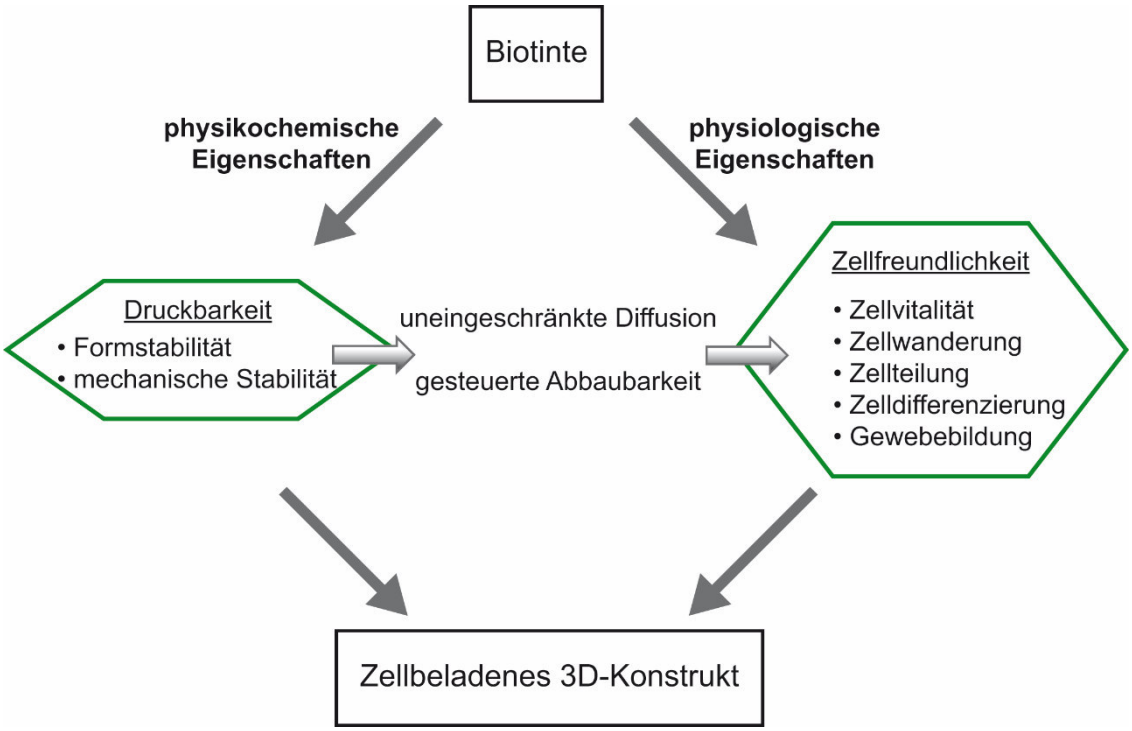

Abbildung 9. Physikochemische und physiologische Anforderungen an Biotinten. Die physikochemischen Eigenschaften beinhalten die Druckbarkeit des Materials und die Form- und mechanische Stabilität des gedruckten Konstruktes. Das 3D-Konstrukt soll zusätzlich in einem adäquaten Zeitraum abgebaut werden können und die Diffusion von Nährstoffen und Abfallprodukten ermöglichen. Dies wiederum steht in engem Zusammenhang mit der Zellfreundlichkeit. Die eingeschlossenen Zellen müssen migrieren, sich teilen und differenzieren können, so dass es zu einer Gewebeneubildung kommen kann. Eine ideale Biotinte vereint all diese Eigenschaften. Modifiziert nach DeSimone et al., *Pure and Applied Chemistry* 2015, 87(8): 737-749, mit freundlicher Genehmigung des Verlages De Gruyter.

Neben der Druckbarkeit und Zellfreundlichkeit des Materials muss das gedruckte 3D-Konstrukt eine hohe Formstabilität aufweisen.[127] Idealerweise sollte das Konstrukt selbsttragend sein, so dass keine Nachbehandlung für die mechanische Stabilisierung nötig ist.[16] Das Konstrukt soll anschließend die Eigenschaften des Zielgewebes so gut wie möglich nachahmen. Viele Studien haben gezeigt, dass Hydrogele aufgrund ihres hydrophilen Charakters und da sie eine zellfreundliche Umgebung gewähren, derzeit die erfolgversprechendsten Ausgangsmaterialien für Biotinten sind.[127, 134] Die wichtigste physikalische Eigenschaft, die ein Hydrogel für den 3D-Druck auszeichnet, ist dessen rheologisches Verhalten.[16, 127, 155] Vor dem Druck darf es nicht zu einer Sedimentation der eingekapselten Zellen kommen und während des Druckens muss die Biotinte gleichmäßig fließen und anschließend auf der Substratoberfläche schnell aushärten bzw. gelieren. Wenn die Biotinte bereits vor dem Drucken geliert, darf der Druckprozess keine irreversiblen Schäden des Gelnetzwerks verursachen.[156] Wenn die Polymere nicht selbstassemblieren, werden sowohl physikalische als auch chemische Quervernetzungen verwendet, um formstabile 3D-Kontrukte zu erzielen. Die physikalische Quervernetzung ist zwar eine

zellfreundliche Methode, allerdings wird oft nur ein schwaches Netzwerk ausgebildet und der Abbau der Konstrukte erfolgt unkontrolliert.[16, 155] Aus diesem Grund müssen viele derart vernetzte Hydrogele durch chemische Quervernetzer (z. B. Enzyme oder Photoinitiatoren) nachbehandelt werden. Diese wiederum dürfen keine toxische Wirkung auf die immobilisierten Zellen haben.

Die durch die Fertigungsverfahren bedingten Anforderungen an Biotinten stehen oft im Konflikt mit den biologischen. Die eingekapselten Zellen müssen im gedruckten Konstrukt migrieren, proliferieren und sich differenzieren können. Das verwendete Material muss dies nicht nur zulassen, sondern sogar fördern.[157] Zusätzlich muss das Biomaterialgerüst in einem Zeitraum abgebaut werden, in dem sich neues Gewebe bildet und das *Scaffold* ersetzt, ohne dass schädliche Abbauprodukte entstehen.[155] Da Biopolymere oft Komponten der extrazellulären Matrix sind oder makromolekulare Eigenschaften ähnlich zu der natürlichen EZM aufweisen, kommen darauf basierende Biotinten in Form von injizierbaren und druckbaren Hydrogelen verstärkt zum Einsatz.[134]

1.4.2.1 BIOPOLYMERE FÜR DEN 3D-DRUCK

Natürliche Polymere werden, trotz ihrer Nachteile gegenüber synthetischen Polymeren, oft als Biotinten eingesetzt. Vor allem durch die fehlende Reproduzierbarkeit der Grundstoffe und somit die Kontrolle der Prozessparameter sowie die oftmals limitierten mechanischen Eigenschaften weisen natürliche Polymere eine bessere Bioaktivität als synthetische Polymere auf.[158-160] Weder die Biopolymere selbst noch deren Abbauprodukte sind toxisch für den Körper und oft wird keine Immunantwort ausgelöst. In einigen natürlichen Proteinen fördern spezifische Signalmoleküle, wie z. B. die Zelladhäsionsdomäne RGD, die Zelladhäsion und –proliferation beim Kontakt mit der Hydrogelmatrix.[127] Proteine, wie Kollagen, dessen Derivat Gelatine und Fibrin, werden ebenso wie eine Reihe von Polysacchariden, wie Alginat, Agarose und Hyaluronsäure, für den 3D-Druck eingesetzt (Tab. 2).[16, 161] Oftmals werden Biopolymere kombiniert, um optimale materialspezifische Eigenschaften hinsichtlich der Zellantwort bzw. der mechanischen Stabilität, Porosität, Viskosität und chemischen Zusammensetzung in einem Hydrogel zu vereinen.[134, 161]

Tabelle 2. Natürliche Polymere, die als druckbare Hydrogele in der Biofabrikation eingesetzt werden. Modifiziert nach Jungst et al., *Chemical Reviews* 2015, **DOI:** 10.1021/acs.chemrev.5b00303, mit freundlicher Genehmigung des Verlages American Chemical Society.

Biopolymer	Additives Fertigungsverfahren	Anwendungsbereich	Ref.
Polysaccharide			
Agar/Agarose	Dispensdruck	Geweberegeneration (Knorpel), Nervenregeneration	159, 162-167
Alginat	Dispensdruck, Laserinduzierter Vorwärtstransfer, Tintenstrahldruck	Geweberegeneration (Herzmuskel), Nervenregeneration, Transportsysteme (Wirkstoffe, Proteine, Zellen, Gene), Wundheilung	130, 136, 141, 148, 164, 168-171
Cellulose	Dispensdruck	Geweberegeneration (Knorpel), Wundheilung	164, 172-173
Gellan	Tintenstrahldruck	Geweberegeneration (Knorpel), Wirkstofftransportsystem	174-177
Hyaluronsäure	Dispensdruck	Geweberegeneration (Knorpel, Gehirn, Blutgefäße)	168, 178-183
Proteine			
Fibrin/Fibrinogen	Tintenstrahldruck	Geweberegeneration (Nerven, Blutgefäße, Haut, Sehnen, Bänder, Leber, Augen), Transportsysteme (Wirkstoffe, Proteine, Gene), Wundheilung	74, 168, 171, 184
Gelatine	Dispensdruck	Geweberegeneration (Knorpel), Transportsysteme (Wachstumsfaktoren, Zellen), Wundheilung	168, 171, 185-189
Kollagen	Dispensdruck, Tintenstrahldruck	Geweberegeneration (Haut, Leber, Blutgefäße, Dünndarm), Transportsysteme (Wirkstoffe, Proteine, Zellen)	137, 190-192
Seide	Tintenstrahldruck	Geweberegeneration (Knochen, Knorpel), Wirkstofftransportsystem	157, 193-195
Gemisch			
Matrigel	Dispensdruck	Geweberegeneration (Leber)	196

Polysaccharide

Die meisten Polysaccharide sind in der Lage Hydrogele zu bilden, die entweder auf Wasserstoffbrückenbindungen (z. B. Agarose) oder intermolekularen, elektrostatischen Interaktionen (z. B. Alginat) basieren. Es wurde bereits eine Vielzahl an injizierbaren und biologisch abbaubaren Hydrogelen aus natürlich vorkommenden Polysacchariden, wie Hyaluronsäure, Alginat und Agarose, für biomedizinische Anwendungen entwickelt und getestet. Im Folgenden werden die Polysaccharide Alginat und Agarose, die bereits in der Biofabrikation eingesetzt werden, näher beschrieben.

Alginat, als ein wichtiger und häufig verwendeter Vertreter der natürlichen Polymere im 3D-Druck, zeichnet sich durch eine gute Biokompatibilität aus. Es wird aus Braunalgen gewonnen und besitzt eine lineare Block-Copolymer Struktur, die aus 1,4-glycosidisch verknüpften α-L-Guluronsäuren und β-D-Mannuronsäuren besteht.[165] Hydrogele aus Alginat können durch die Gelierung mit bivalenten Kationen (Ca^{2+}) hergestellt werden.[103] Die ionische Quervernetzung ist ein milder und zellfreundlicher Prozess, da im Vergleich zur Photopolymerisation beispielsweise kein Energieeintrag stattfindet. Alginat zeigt zudem (wie z. B. Zahnpasta) ein scherverdünnendes Verhalten. Dadurch fließt die Biotinte durch die angelegten Scherkräfte im Druckkopf während des Druckens und härtet sofort aus, wenn anschließend die feinen Gerüststrukturen auf der Oberfläche abgelegt werden.[127] Da die Viskosität über die Konzentration eingestellt werden kann, ist Alginat für die meisten Prozesstechniken in der Biofabrikation geeignet. Es konnte gezeigt werden, dass Alginat mit menschlichen adipösen Stammzellen gedruckt werden konnte, ohne dass im Anschluss die strukturelle Integrität beeinflusst wurde.[169] Allerdings ist der Abbau von auf Alginat-basierten Biotinten nur schwer zu steuern und es konnte nachgewiesen werden, dass die mechanische Stabilität von gedruckten Konstrukten nach kurzer Zeit (ca. 40 % in 9 Tagen) verloren geht. Zudem besitzt Alginat keine Zelladhäsionsdomänen.[169-170, 197] Zur Verbesserung der Zellantwort und thermischen und mechanischen Stabilität wird Alginat mit zahlreichen Proteinen modifiziert, indem beispielsweise oxidiertes Alginat über eine kovalente Bindung mit Gelatine verbunden wird.[198]

Agarose, eine Hauptkomponente des Agars, wird vor allem aus den Rotalgengattungen *Gelidium* und *Gracillaria* gewonnen und besteht aus D-Galaktose und 3,6-Anhydro-L-Galaktose, die glycosidisch miteinander verbunden sind, sowie ionisierten Sulfatgruppen.[199] Agarose geliert durch die Bildung von intermolekularen Wasserstoffbrückenbindungen bei Abkühlung.[200] Die viskoelastischen Eigenschaften der Hydrogele aus Agarose hängen vom Molekulargewicht und der Konzentration ab. Die einstellbaren Elastizitätsmoduln der physikalisch vernetzten Hydrogele liegen zwischen < 1 kPa und einigen tausend Kilopascal und somit im Bereich von natürlichen Geweben und

Organen (Knochen ausgenommen).[75, 201] Maher und Kollegen haben 2009 3D-*Scaffolds* aus thermoreversiblen Agarose-Hydrogelen mit Hilfe eines pneumatischen Dispensdruckers hergestellt.[162] Dabei wurde Agarose in ein Gelatineenthaltendes Bad gedruckt. Gelatine diente nicht als Quervernetzer, sondern als Unterstützung, um das gedruckte Konstrukt zu stabilisieren. Ohne dieses Bad verschmolzen die einzelnen Lagen und in den meisten Fällen kollabierte das *Scaffold.*[202] Zudem wurden Hydrogele aus Agarose mit eingekapselten mesenchymalen Stammzellen mit Hilfe eines Fluorkohlenstoffbads gedruckt. Die eingekapselten Zellen waren mindestens 21 Tage vital und die zellbeladenen Hydrogele waren mehr als sechs Monate stabil.[163]

Neben Polysacchariden, die aus Pflanzen und Algen gewonnen werden, werden auch bakterielle extrazelluläre Polysaccharide (EPS) im Bereich des 3D-Druckens eingesetzt. Kürzlich wurde Gellan, ein Vertreter der EPS, als Biotinte mit verschiedenen Zelltypen verdruckt.[174] Gellan ist ein Vielfachzucker, der mittels Fermentation von Kohlenhydraten hergestellt wird und als Zusatzstoff in der Lebensmittelindustrie als Verdickungsmittel eingesetzt wird.[203] Die linearen Moleküle von Gellan liegen bei Temperaturen um 30 °C ungeordnet vor und transformieren bei niedrigeren Temperaturen zu Doppelhelices. Bei hohen Konzentrationen (> 2 % w/v) wandeln sich die Doppelhelices in längliche Aggregate um und bilden ein makroskopisch stabiles Gel.[204] Es wurde gezeigt, dass das Gel aus Gellan eine Sedimentation und Aggregation der Zellen verhindert sowie ein kontinuierliches Fließen während des Druckprozesses erlaubt.[174]

Obwohl Polysaccharide eine Vielzahl an vorteilhaften Eigenschaften für Biotinten aufweisen, sind vor allem deren schwache mechanische Stabilität und ihr Quellverhalten von entscheidendem Nachteil. Proteine stellen eine vielversprechende Alternative dar.

Proteine

Proteine, wie Kollagen, Gelatine, Fibrin und Fibroin, wurden bereits als Biotinte für die Herstellung von 3D-Konstrukten eingesetzt.[127]

Kollagen ist mit einem Anteil von 20-30 % der Gesamtproteine das am häufigsten vorkommende Protein in Säugetieren und deshalb von besonderem Interesse in der Gewebezüchtung.[181, 205] Die Hauptfunktionen von Kollagen sind die mechanische Stabilisierung der extrazellulären Matrix sowie die Kontrolle der Zelladhäsion, -migration und Wundheilung.[206] Kollagene bestehen aus drei linksgängigen Helices, die wiederum über Wasserstoffbrückenbindungen zu einer rechtsgängigen Superhelix angeordnet sind. Kollagen ist bioabbaubar, bioverträglich und kann einfach gewonnen und modifiziert

werden.[207] Allerdings zeigen kollagenbasierte Biotinten chargenabhängige Variationen und schwache mechanische Eigenschaften (Elastizitätsmoduln: ~ 1 kPa).[137, 208] Gelatine ist die denaturierte Form von fibrillärem Kollagen und wird oft als Biotinte eingesetzt, weil es eine schwächere immunogene Reaktion als Kollagen zeigt.[209] Gelatine ist wasserlöslich, bioabbaubar, biokompatibel und enthält das natürliche Zelladhäsionsmotif Arg-Gly-Asp (RGD).[178, 185, 189-190, 210-211] Allerdings basiert die Gelbildung auf physikalischen intermolekularen Wechselwirkungen der Gelatinemoleküle, so dass die entstehenden Gele unter physiologischen Temperaturen nicht stabil sind.[212] Aus diesem Grund werden oft Mischungen aus den zuvor beschriebenen Biopolymeren beim 3D-Druck eingesetzt sowie Quervernetzungsmethoden angewendet. Beispielsweise wurde eine Biotinte aus Alginat, Gelatine und Fibrinogen hergestellt, die anschließend mit Ca^{2+} quervernetzt wurde.[171] Alternativ wurde Gelatine mit Alginat gemischt und zweifach quervernetzt (thermisch und ionisch).[186-187] Kirchmajer und Panhuis zeigten kürzlich, dass stabile Hydrogele aus Gelatine und Gellan mit Calciumionen und Genipin, eine chemische Komponente, die aus der Gardenia Frucht gewonnen wird, vernetzt und die Eigenschaften durch die Zusammensetzung gesteuert werden können.[213]

Fibrin, ein weiteres extrazelluläres Matrixprotein, ist ebenfalls für Anwendungen in der Biofabrikation geeignet. Fibrin wird mit Hilfe des Enzyms Thrombin aus Fibrinogen gebildet, das so aggregiert, dass ein fibrilläres Netzwerk entsteht. All diese Faktoren sind maßgeblich an der Wundheilung beteiligt.[214-215] Fibrin geliert schnell, ist biokompatibel und bioabbaubar; Hydrogele aus Fibrin werden ohne fibrinolytischen Inhibitor innerhalb von zwei Wochen enzymatisch abgebaut.[216-217] Vor kurzem wurde Fibrin als druckbares Hydrogel beim Tintenstrahldruck eingesetzt, um 3D-Nervenkonstrukte herzustellen. Die Konstrukte wurden erstellt, indem abwechselnd Fibringele und neuronale Vorläuferzellen gedruckt wurden.[184] Obwohl Fibrinogen und Thrombin einfach aus dem Blut gewonnen werden können, weisen Fibrinhydrogele als Biotinten einen Nachteil auf: die gedruckten Konstrukte aus Fibrin zeigten inadäquate mechanische Eigenschaften und zerfielen schnell. Die Fibrinhydrogele mit der vielversprechendsten mechanischen Integrität waren für nur 3 Wochen stabil.[218-220]

Seiden sind natürliche Proteinfasern, die von Arthropoden (Spinnen & Insekten) produziert werden. Seide ist von großem Interesse in biomedizinischen Anwendungen und der Biofabrikation, da sie biokompatibel ist, langsam abgebaut wird und außergewöhnliche mechanische Eigenschaften zeigt.[21, 58, 157, 221] Kürzlich wurde die Herstellung von strukturierten Substraten aus Seidenfibroin (*Bombyx mori*) durch Tintenstrahldruck etabliert.[195] Schicht-für-Schicht wurden Tropfen aus ionomeren Seidenproteinen, die chemisch mit Poly(L)-Lysin und Poly(L)-Glutaminsäure Seitenketten modifiziert wurden, produziert. Die sogenannten Seidennester dienten als Plattform für die Immobilisierung von

Escherichia coli (*E. coli*) Zellen, die weder ihre Zellmorphologie noch Funktion verloren. Durch diesen Fabrikationsprozess konnten biokompatible *Scaffolds* innerhalb eines geeigneten Zeitraums hergestellt werden, die beispielsweise als Biosensoren verwendet werden könnten.[195] Jedoch wurde festgestellt, dass eine Seidenfibroinlösung ohne Zugabe anderer Polymere häufig zu einer Nadelverstopfung, aufgrund der scherinduzierten β-Faltblattkristallisation während des Druckens, führt.[194] Deshalb wurde Fibroin kürzlich in Kombination mit Gelatine als Biotinte für die Herstellung von 3D-Gewebekonstrukten eingesetzt und es wurde gezeigt, dass die *in situ* Quervernetzung und der Druckprozess zellfreundlich sind, da eingekapselte Vorläuferzellen überlebten.[157]

Die Verwendung von natürlichen Proteinen als Biotinte ist hauptsächlich aufgrund ihrer variierenden Reinheit sowie durch das mögliche Auslösen von unerwünschten biologischen Antworten begrenzt. Da Säugetiergewebe die Hauptquelle für Proteine, wie z. B. Kollagen, Gelatine und Fibrin, sind, bestehen weitere Bedenken hinsichtlich Krankheitsübertragungen und immunogenen Reaktionen.[78, 222]

1.4.2.2 Rekombinant hergestellte Biopolymere

Heutzutage können durch molekularbiologische Methoden neue Biopolymere entworfen und entwickeln werden, die in dieser Komplexität und Funktionalität nicht natürlich vorkommen. Die rekombinante Herstellung von künstlichen Proteinen ermöglicht es, die Materialeigenschaften, wie Mechanik, Abbau, Porosität, Zell-Material-Interaktionen und Zytokompatibilität, anzupassen bzw. einzustellen (Abb. 10).[16, 223]

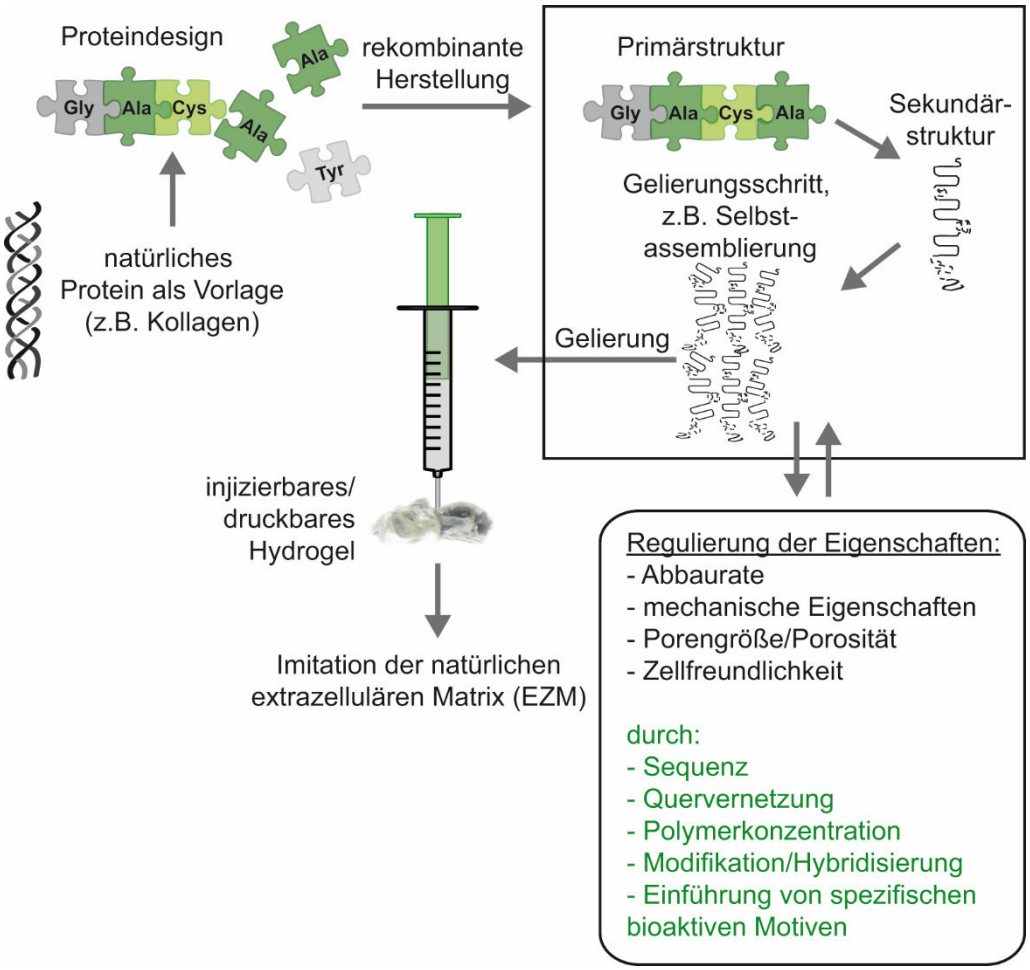

Abbildung 10. Schematisches Modell, das den Weg vom natürlichen Protein über das Proteindesign bis hin zum injizierbaren bzw. druckbaren Hydrogel aus rekombinanten Proteinen aufzeigt. Modifiziert nach Jungst et al., *Chemical Reviews* 2015, **DOI:** 10.1021/acs.chemrev.5b00303, mit freundlicher Genehmigung des Verlages American Chemical Society.

Rekombinante Proteine sind viel leichter mit einer definierten Molekülstruktur herzustellen als synthetische und natürliche Materialien.[54, 224-227] Durch das spezifische Design von rekombinanten Proteinen, wie z. B. der Kopplung von funktionellen Gruppen an Strukturproteine wie Kollagen, Elastin oder Seide, können biologische Aktivitäten ähnlich der natürlichen extrazellulären Matrix geschaffen werden. Beispielsweise können verschiedene funktionelle Domänen von natürlichen Proteinen, z. B. Zell-Material-Interaktions-Domänen, mit strukturellen Domänen in einem neu designten Protein (z. B. Fusionsprotein) kombiniert werden. Alternativ können rekombinante Proteine leicht mit kurzen Peptidsequenzen, wie z. B. RGD oder IKVAV, die spezifische Liganden für Zellrezeptoren sind und Zelladhäsion steuern, modifiziert werden.[58]

Es ist wichtig zu erwähnen, dass zum einen nicht alle Polypeptide und Proteine rekombinant hergestellt werden können und zum anderen nicht alle Proteine mit nicht-peptidischen

Motiven kombiniert werden können, ohne eine chemische Modifikation nach der Herstellung. Wenn eine rekombinante Produktion möglich ist, besteht die Herausforderung meistens in der Gewinnung von ausreichenden Ausbeuten für den industriellen Maßstab. Dies hängt vom gewählten Wirtsorganismus, dem Fermentationsprozess und dem Protein selbst ab. Bislang gibt es nur wenige rekombinante Proteine, die in ausreichenden Mengen hergestellt werden können. In Tabelle 3 sind die rekombinant hergestellten Proteine, die entweder bereits beim 3D-Druck eingesetzt wurden oder zu injizierbaren Hydrogelen verarbeitet werden können, aufgelistet.

Tabelle 3. Rekombinant produzierte Proteine, die als injizierbare bzw. druckbare Hydrogele eingesetzt werden können. Modifiziert nach Jungst et al., *Chemical Reviews* 2015, DOI: 10.1021/acs.chemrev.5b00303, mit freundlicher Genehmigung des Verlages American Chemical Society.

Rekombinante Proteine	Vorteilhafte Eigenschaften	Anwendungsbereiche	Ref.
Kollagen	Bioabbaubar, biokompatibel	Geweberegeneration (kornealer Ersatz, Nerven), Wirkstofftransportsysteme	207, 228-230
Elastin	Elastomere Eigenschaften, biokompatibel, hohe Löslichkeit	Geweberegeneration (Knorpel, Blutgefäße), Weichgewebeersatz, Wirkstofftransportsysteme	231-235
Resilin	Geringe Festigkeit, hohe Elastizität, reversible Dehnbarkeit	Geweberegeneration (Knorpel, Blutgefäße)	236-238

Nahezu jedes Expressionssystem, wie Bakterien, Hefen, transgene Tabakpflanzen, Insektenzellen, Säugetierzellen, Seidenraupen und transgene Mäuse, wurde genutzt, um rekombinantes Kollagen oder ausgewählte Domänen herzustellen.[207, 228, 230, 239] Im Vergleich zum natürlichen Kollagen hat das rekombinant Hergestellte die Vorteile, dass es z. B. unbedenklich hinsichtlich Krankheitsübertragungen ist und mit Zelladhäsionsdomänen funktionalisiert werden kann.[78, 222, 230] Die rekombinante Produktion von Kollagen ist sehr komplex, da häufig posttranslationale Modifikationen eingeführt werden müssen, um die quervernetzten und helikalen Strukturen zu stabilisieren. Deshalb erfordert die Biosynthese von Kollagen spezifische Enzyme wie Prolyl-4-Hydroxylase. Ohne Prolyl-4-Hydroxylase entstehen keine rechtsgängigen Superhelices, sondern funktionslose Kollagenmoleküle, die unter physiologischen Bedingungen nicht stabil und somit für biomedizinische Anwendungen ungeeignet sind.[240] Von den getesteten Wirtsorganismen produzieren nur Säugetierzellen

Kollagen mit einem identischen L-4-Hydroxyprolingehalt wie das natürliche Kollagen. Allerdings können damit nur geringe Mengen (0,6 – 20 mg/l) Protein hergestellt werden.[241] In Wirtsorganismen wie *E. coli* und Hefen ist eine Multigenexpression nötig, um der Abwesenheit des Enzyms Prolyl-4-Hydroxylase entgegenzuwirken.[241] Mit Hilfe der Multigenexpression konnte Kollagen Typ I, II und III mit dem gleichen Gehalt an L-4-Hydroxyprolin wie im nativen Protein und einem Titer von 0,2 – 0,6 g/l hergestellt werden.[242] Bislang wurde der Gebrauch von Hydrogelen aus rekombinant hergestelltem Kollagen als Biotinte noch nicht veröffentlicht.

Elastin ist eine Komponente der extrazellulären Matrix, die in elastischen Geweben vorkommt und für die Flexibilität der Gewebe verantwortlich ist. Die elastomeren Eigenschaften von Elastin haben die Herstellung von Elastin-ähnlichen Polypeptiden (ELPs) unterstützt.[11, 233] ELPs zeigen ein thermosensitives Verhalten, so dass die Übergangstemperatur durch die Hydrophobizität, das Molekulargewicht und die Konzentration der Polypeptide kontrolliert werden kann.[233, 243] Zudem kann der komplette reversible Phasenübergang durch verschiedene Umgebungsbedingungen, wie Temperatur, Ionenstärke, Redoxzustand und pH, gesteuert werden.[232, 234] ELPs sind unterhalb der charakteristischen Übergangstemperatur wasserlöslich. Steigt die Temperatur allerdings über die charakteristische Temperatur, kommt es zu einem Phasenübergang und die ELPs aggregieren, was zu einem physikalisch-vernetzten Netzwerk führt.[232, 244] Materialien, die aus diesen ELPs hergestellt wurden, zeigen exzellente mechanische Eigenschaften (ähnlich zu natürlichen Elastin), sind biokompatibel und weisen eine minimale Immunantwort nach der Implantation auf.[235, 245-246] Gelenkknorpelzellen wurden bereits erfolgreich in Hydrogele aus ELPs eingekapselt, die anschließend injiziert wurden, um einen unregelmäßig geformten Knorpeldefekt zu füllen bis eine Integration in das umliegende Gewebe erfolgte.[231, 234, 247] Das ELP Netzwerk unterstützte sowohl die Zellvitalität und Infiltration als auch die Knorpelmatrixsynthese.

Natürliches Resilin ist ein elastomeres Protein mit außergewöhnlichen mechanischen Eigenschaften, mit geringer Steifigkeit und hoher Elastizität. Es ist in speziellen Regionen der Insektencuticula vorhanden und spielt eine entscheidende Rolle beim Insektenflug, im Sprungmechanismus von Flöhen und der Stimmgebung von Zikaden.[248] Kürzlich wurden Hydrogele aus rekombinant hergestellten Resilin-ähnlichen Polypeptiden (RLPs) hergestellt, die gute mechanische Eigenschaften (1 – 25 kPa) für die Gewebezüchtung aufzeigten.[236] Es konnte gezeigt werden, dass das isotrope dreidimensionale Netzwerk sich wie ein ideales Gummi mit einer nahezu perfekten reversiblen Elastizität verhält.[238] RLP Hydrogele können mit Tris[(hydroxymethyl)-phosphin] schnell gebildet werden und es konnte gezeigt werden,

dass die mechanische Integrität während des Quervernetzens aufrechterhalten bleibt und eingekapselte primäre mesenchymale Stammzellen (MSCs) überleben.[237]

1.5 SPINNENSEIDE

1.5.1 NATÜRLICHE SPINNENSEIDE

Catherine Craig hat 1997 den Begriff Seide folgendermaßen definiert: „Seiden sind Proteine mit einer hochrepetitiven Aminosäuresequenz, die im flüssigen Zustand gespeichert und durch Scherung oder Verspinnen zu einer Faser werden.“[249] Seiden werden ausschließlich von den zu den Gliederfüßern (Arthropoda) gehörenden Klassen der Spinnentiere (*Arachnida*), Insekten (*Insecta*) und Tausendfüßer (*Myriapoda*) in speziellen Drüsen für unterschiedliche Aufgaben produziert.[249] Spinnenseide zählt, zusammen mit der Seide des Seidenspinners *Bombyx mori*, zur bekanntesten Seide. Spinnenseide fasziniert Wissenschaftler vor allem aufgrund ihrer außergewöhnlichen mechanischen Eigenschaften.[250] Seidenfasern sind extrem stabil und dehnbar, so dass sie eine Zähigkeit aufweisen, die keine andere natürliche oder synthetische Faser erreicht.[251] Zusätzlich ist Spinnenseide biokompatibel, biologisch abbaubar und löst keine Entzündungs- bzw. allergischen Reaktionen aus.[221] Deshalb wurden Spinnennetze bereits seit Jahrhunderten als Wundverband für Hautverletzungen verwendet.[252]
Vor kurzem wurde Spinnenseide als künstliches *Scaffold* für die Nervenregeneration eingesetzt.[253-254] Defekte der peripheren Nerven können durch ein artifizielles Nervenimplantat aus dezellularisierten Venen, Spinnenseidenfasern und Schwann-Zellen in einem Matrigel repariert werden. In einem adulten Schaf konnte gezeigt werden, dass die Spinnenseide die Schwann-Zell Migration, das Neuwachsen von Axonen und die Remyelinisierung in einem 6 cm großen Defekt des *Nervus tibialis* (Schienbeinnerv) förderte.[255] Außerdem wurden natürliche Spinnenseidenfasern als mikrochirurgisches Nahtmaterial getestet, um herkömmlich verwendete Materialien in der Mikro- und Neurochirurgie zu ersetzen.[256-257] Dabei wurde gezeigt, dass die mechanischen Eigenschaften der geflochtenen Spinnenseidenfäden im Vergleich zu Nylon, dem gegenwärtigen klinischen Standard, verbessert waren. Zusammen mit der Biokompatibilität der Spinnenseide könnten die Mikrofäden für die Nervenregeneration eingesetzt werden.[257]

Spinnenseide ist ein vielseitiges Material, da Spinnen, im Gegensatz zu anderen Gliedertieren, verschiedene Arten von Seiden für unterschiedliche Aufgaben produzieren

können (für einen detaillierten Überblick siehe Heidebrecht & Scheibel, 2013).[258] Ungefähr die Hälfte aller derzeit bekannten Spinnenarten verwenden Netze zum Beutefang.[259] Neben Trichter- und Baldachinnetzen finden Radnetze die weiteste Verbreitung. Weibliche Radnetzspinnen, zu denen die europäische Gartenkreuzspinne *Araneus diadematus* und die goldene Seidenspinne *Nephila clavipes* zählen, produzieren sieben verschiedene Seiden (Abb. 11).[258, 260]

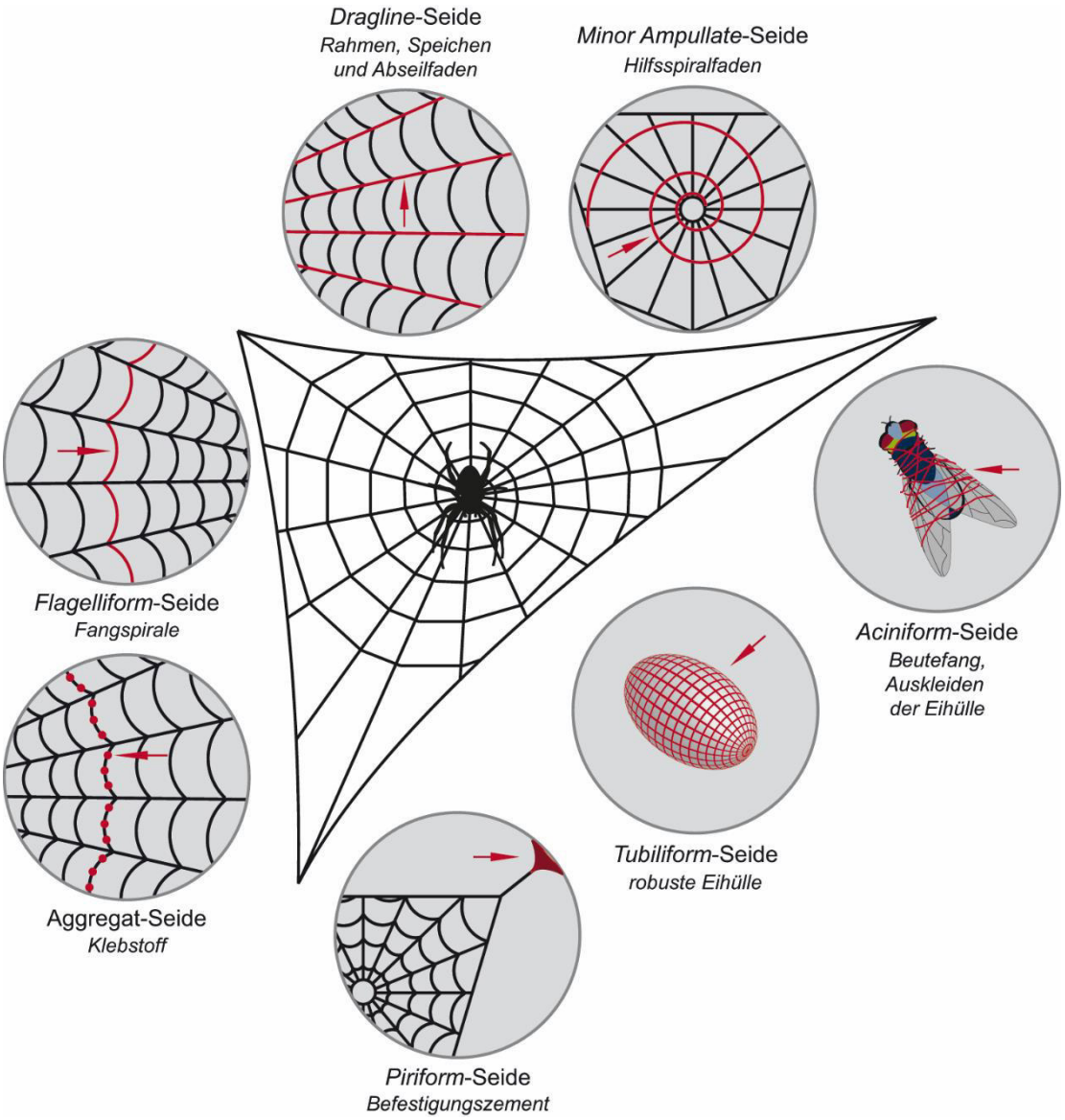

Abbildung 11. Übersicht der sieben verschiedenen Seidenarten, die von weiblichen Radnetzspinnen, wie z. B. der Gartenkreuzspinne (*Araneus diadematus*), produziert werden. Modifiziert nach Heidebrecht & Scheibel, *Advances in Applied Microbiology* 2013, 82: 115-153, mit freundlicher Genehmigung des Verlages Elsevier.

Die Seidenarten sind benannt nach der Drüse, in der sie gebildet werden, und unterscheiden sich zum einen in ihrer Zusammensetzung und zum anderen in ihren mechanischen Eigenschaften.[261] Die am besten charakterisierte Spinnenseide ist die *Dragline*-Seide (engl. *dragline* = Schleppseil), die sowohl die Rahmenkonstruktion und Speichen des Netzes und

als auch den Abseilfaden bildet und dem Netz Stabilität verleiht.[258, 262] Die Seide besitzt, wie die *Flagelliform*-Seide, eine außergewöhnlich hohe Zähigkeit, so dass sie, bezogen auf den Durchmesser der Faser, mehr Energie aufnehmen kann als viele andere Seidenarten, bevor sie reißt.[251] Die außergewöhnlichen mechanischen Eigenschaften basieren auf der molekularen Struktur und auf dem hierarchischen Aufbau des Spinnenseidenfadens (Abb. 12).[258, 263-264]

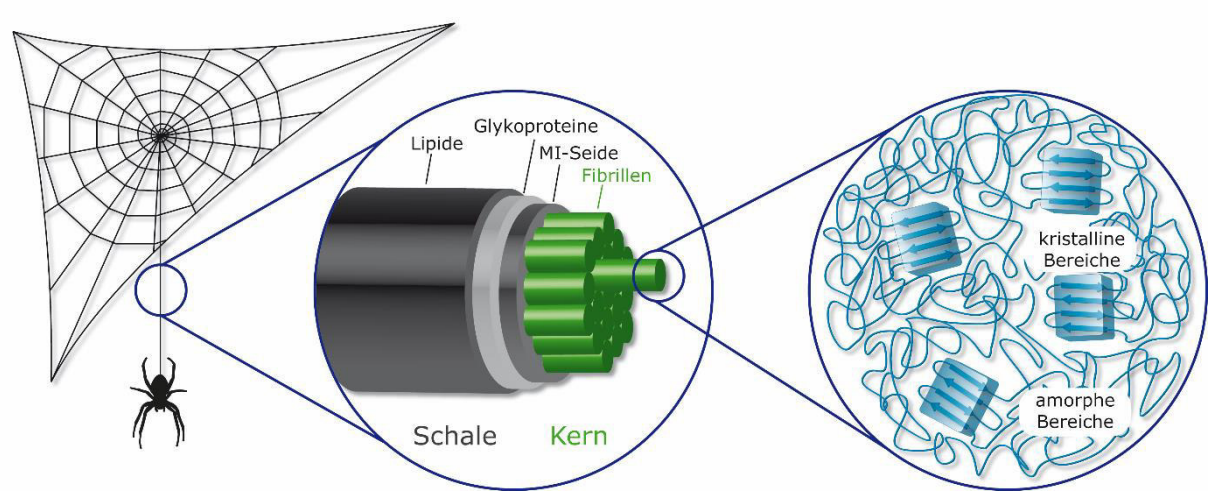

Abbildung 12. Kern-Schale Struktur der *Dragline*-Seide. Der Kern des Fadens besteht aus Fibrillen, die entlang der Faserachse angeordnet sind. Auf molekularer Ebene beinhalten die Fibrillen kristalline Bereiche, die je nach Aminosäurezusammensetzung in einer amorphen Matrix eingebettet sind. Der Kern wird von einer Schale aus drei Lagen, *Minor Ampullate* (MI)-Seide, Glykoproteinen und Lipiden, umschlossen. Modifiziert nach Heidebrecht & Scheibel, *Advances in Applied Microbiology* 2013, 82: 115-153, mit freundlicher Genehmigung des Verlages Elsevier.

Die hierarchische Struktur der *Dragline*-Seide besteht aus einer Kern-Schale Struktur. Die Schale beinhaltet Lipide, Glykoproteine und *Minor Ampullate*-Seide und dient als Schutz vor Austrocknung und Bakterien.[265-267] Der Kern hingegen besteht aus Nano- und Mikrofibrillen-bündeln, die entlang der Faserachse angeordnet sind.[258, 268] Diese Fibrillen bestehen aus hochgeordneten nanokristallinen Bereichen, die in einer amorphen Matrix eingebettet sind.[269-270] Die alaninreichen, kristallinen Bereiche dienen als Quervernetzer und sind somit für die Reißfestigkeit der *Dragline*-Seide verantwortlich, während die glycinreichen, amorphen GGX und GPGXX Motive für die Elastizität des Spinnenseidenfadens sorgen.[271-274]

Der Kern des *Dragline*-Fadens besteht mindestens aus den zwei Hauptproteinkomponenten MaSp1 (*Major Ampullate* Spidroin 1) und MaSp2 (*Major Ampullate* Spidroin 2), die beide einen hohen Anteil (~ 60 %) der unpolaren, hydrophoben Aminosäuren Glycin und Alanin aufweisen und in der großen Ampullendrüse (*Major Ampullate*) produziert werden.[258] Sie unterscheiden sich nur in ihrem Prolingehalt und der Hydrophobizität.[275] Alle *Major Ampullate* Spidroine besitzen eine hoch repetitive Kernsequenz mit alaninreichen, hydrophoben und

glycinreichen, hydrophileren Regionen, die von nicht-repetitiven, gefalteten Termini flankiert werden.[271] Die repetitiven Einheiten bestehen aus etwa 20-40 Aminosäuren, welche 90 % der Gesamtproteinsequenz darstellen und in dem natürlichen Seidenprotein bis zu hundertmal hintereinander wiederholt werden.[275] Die terminalen, ca. 120-140 Aminosäuren langen, hochkonservierten Domänen spielen eine wichtige Rolle bei der Speicherung der hochkonzentrierten Proteinlösung in der Spinndrüse sowie bei der korrekten Ausrichtung der Moleküle während der Fadenassemblierung im Spinnkanal. Beide Termini sind dimerisierungsfähige, globuläre Domänen, die aus fünf α-Helices bestehen.[276-279]
Bei der Gartenkreuzspinne *Araneus diadematus* werden die Hauptkomponenten der *Dragline*-Seide ADF3 und ADF4 (*Araneus diadematus* Fibroin) genannt.[261] Beide Seidenproteine weisen im Gegensatz zu den bekannten MaSp-Proteinen einen hohen Prolingehalt von ca. 16 % auf.[261, 280] Aus diesem Grund können sie als MaSp2-Analoga betrachtet werden.[281] Wie bei den MaSp-Proteinen existieren bei ADF3 und ADF4 Unterschiede bezüglich ihrer Hydrophobizität. ADF3 ist hydrophiler und somit besser löslich in wässrigen Systemen, während ADF4 hydrophober ist und dadurch leicht zu fibrillären Strukturen assembliert.[282-283]

1.5.2 Herstellung rekombinanter Spinnenseide

Aufgrund der herausragenden mechanischen und physiologischen Eigenschaften von Spinnenseide ist diese in den Fokus der Forschung gerückt, wodurch die Gewinnung und Produktion von Spinnenseide im großen Maßstab nötig wurde. Im Gegensatz zum Seidenspinner *B. mori* können Spinnen nicht gezüchtet werden, da sie ein kannibalistisches und territoriales Verhalten zeigen.[284] Außerdem ist die Gewinnung der natürlichen Seide sehr zeitaufwändig. Da die Seidenqualität durch Umwelteinflüsse, wie z. B. die Nahrung, beeinflusst wird, stellen Qualitätsschwankungen ein weiteres Problem dar.[259, 285-286] Deshalb wurde eine biotechnologische Herstellung von rekombinanten Spinnenseidenproteinen etabliert, so dass Proteine mit gleichbleibender Zusammensetzung und Qualität in ausreichenden Mengen produziert werden können.[258, 287]

Verschiedene prokaryotische und eukaryotische Wirtsorganismen wurden getestet, um Spinnenseidenproteine rekombinant herzustellen. Eine detaillierte Zusammenfassung wurde kürzlich von Heidebrecht und Scheibel veröffentlicht.[258] Dabei kann die Anzahl, der sich wiederholenden Module, verschiedenen Motive und Abstände zwischen ihnen, variiert werden.[258, 282, 288-289] Für eine effiziente Produktion in Prokaryoten wurde die abgeleitete Konsensussequenz der natürlichen Spinnenseidenproteine durch reverse Translation unter Berücksichtigung der bakteriellen *codon usage* in eine Nukleotidsequenz übersetzt.[281] Die

Konsensussequenz wurde anschließend durch eine nahtlose Klonierungsstrategie multimerisiert und in einen Expressionsvektor transformiert.[282] Die designten Gene konnten im Anschluss in *E. coli* exprimiert und die Proteine durch Hochzelldichtefermentation in großen Mengen produziert werden.[287] Obwohl die so hergestellten Proteine in Bezug auf Aminosäuresequenz und Größe den natürlichen Seidenproteinen nicht identisch sind, weisen sie dennoch deren wesentliche Merkmale auf, wie z. B. intrinsisch entfaltete lösliche Strukturen, β-Faltblattreiche unlösliche Formen und Selbstassemblierung. Mit Hilfe der biotechnologischen Herstellung können nun die Hauptkomponenten der *Dragline*-Seide der Gartenkreuzspinnen in ausreichenden Mengen produziert werden. eADF3 und eADF4 (*engineered A. diadematus* Fibroin 3 und 4) sind abgeleitete Varianten der natürlichen Spinnenseidenproteine ADF3 und ADF4.[282] In dieser Arbeit wurde das rekombinante Spinnenseidenprotein eADF4(C16) und dessen modifizierte Variante eADF4(C16)-RGD verwendet (Abb. 13).

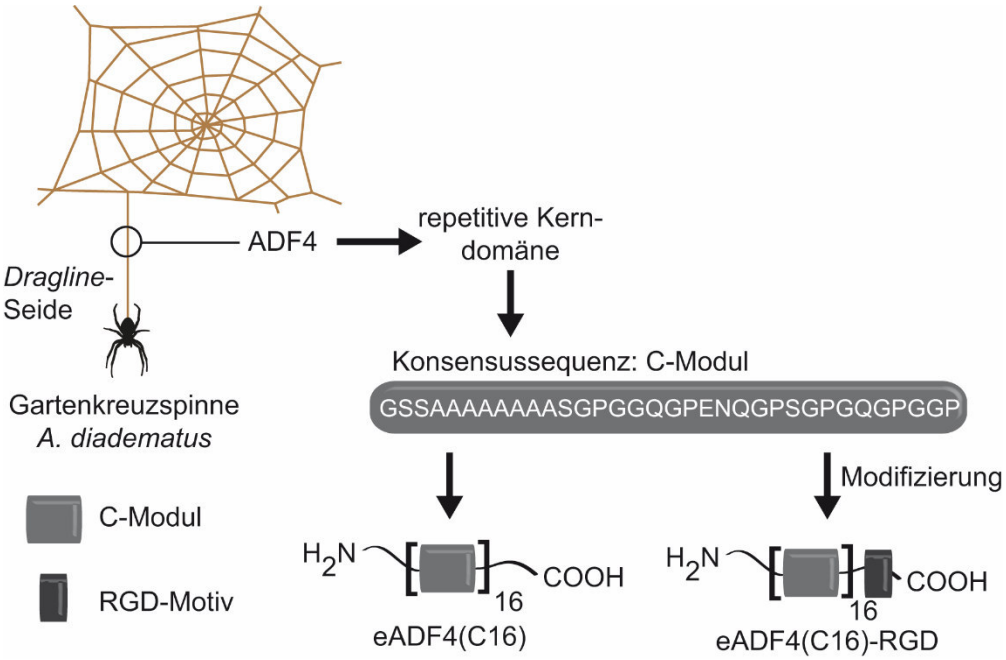

Abbildung 13. Die rekombinanten Spinnenseidenproteine eADF4(C16) und eADF4(C16)-RGD bestehen aus 16 C-Modulen. Das C-Modul ist die Konsensussequenz der repetitiven Kerndomäne von *Araneus diadematus* Fibroin 4 (ADF4). Das Protein ADF4 ist eine der Hauptkomponenten der *Dragline*-Seide, die wiederum den Rahmen des Spinnennetzes bildet und als Abseilfaden der Gartenkreuzspinne (*A. diadematus*) dient. eADF4(C16)-RGD ist die genetisch mit der Zelladhäsionsdomäne RGD modifizierte Variante von eADF4(C16). Modifiziert nach DeSimone et al., *Pure and Applied Chemistry* 2015, 87(8): 737-749, mit freundlicher Genehmigung des Verlages DeGruyter.

eADF4(C16) entspricht einer artifiziellen Variante des repetitiven Kernbereichs von ADF4 ohne terminale Domänen. Dabei wurde die Konsensussequenz (C-Modul) 16-mal wiederholt.[282] Bei der rekombinanten Herstellung können in artifiziellen

Spinnenseidenproteinen durch genetische Modifikation entweder gezielt einzelne Aminosäuren mutiert oder funktionelle Gruppen eingeführt werden.[58, 63, 290-292] Die Spinnenseidenproteine können dadurch für diverse Anwendungen spezifisch funktionalisiert werden. Die einfachste genetische Modifikation ist die Einführung von einzelnen Aminosäuren mit spezifischen, chemischen Seitenketten, wie z. B. Cysteinreste mit ihren Thiolgruppen. An jene Gruppen können anschließend z. B. Peptide, Enzyme oder Partikel kovalent gekoppelt werden.[63, 292] In dieser Arbeit wurde neben dem rekombinanten Spinnenseidenprotein eADF4(C16) mit eADF4(C16)-RGD gearbeitet, bei dem über eine Linkersequenz (GGSG) eine lineare RGD Sequenz (GRGDSPG) am C-Terminus genetisch eingeführt wurde, um die Zelladhäsion zu verbessern (Abb. 13).[63]

Rekombinante Spinnenseidenproteine können nicht nur zu Fäden, sondern auch zu anderen Morphologien, wie Filme, Hydrogele, Partikel, Schäume oder Vliese für diverse Anwendungen, verarbeitet werden.[23, 114, 116, 291-293]

1.5.3 Spinnenseidenproteine für biomedizinische Anwendungen

Aufgrund der Biokompatibilität und vollständigen biologischen Abbaubarkeit rekombinanter Spinnenseide sowie durch deren Prozessierbarkeit in unterschiedliche Morphologien gibt es vielfältige Anwendungsmöglichkeiten. Neben einem Einsatz der Seidenproteine in neuartigen Hochleistungsfasern, z. B. als Nahtmaterial, sind Einsätze in Wundverbänden, im gerichteten Wirkstofftransport oder in *Scaffolds* in der Gewebezüchtung vorstellbar (Abb. 14).[24, 221, 251, 287, 294-295]

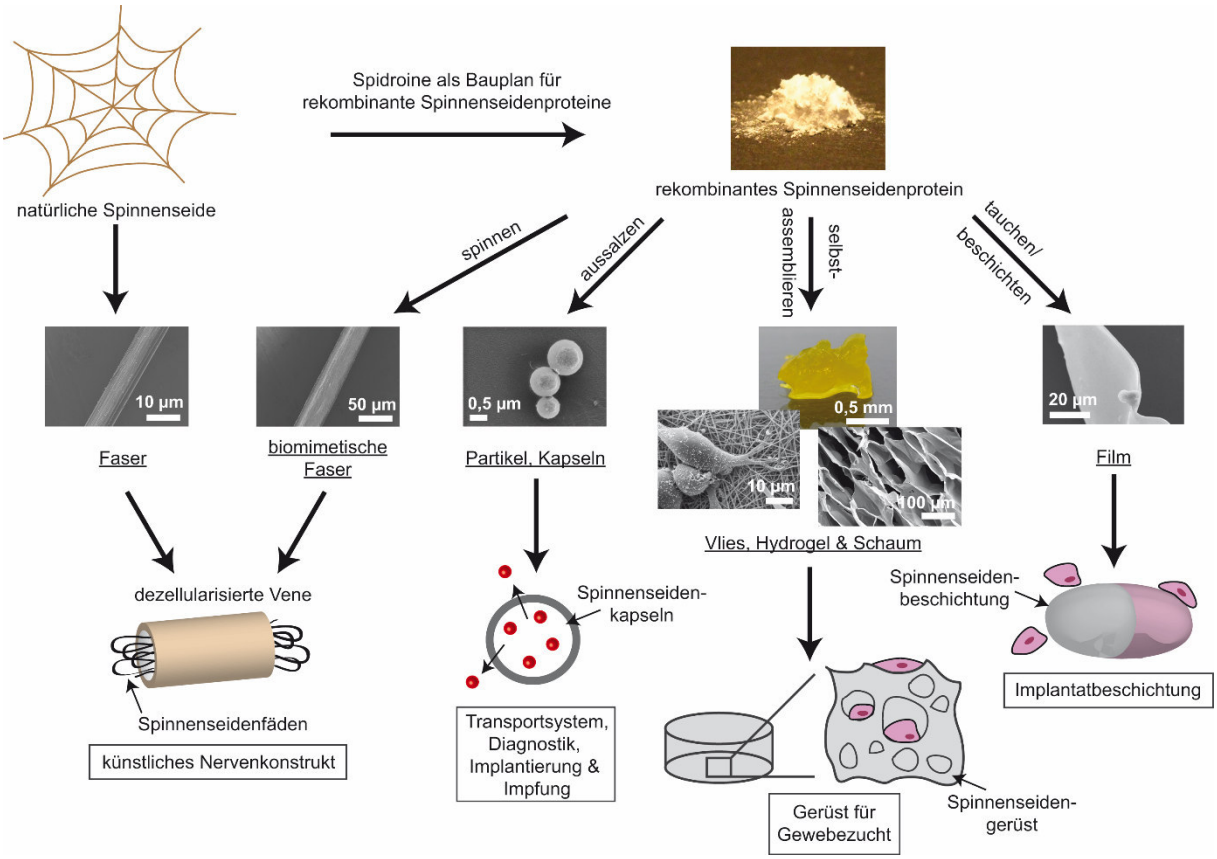

Abbildung 14. Biomedizinische Anwendungen von Spinnenseide. Rekombinante Spinnenseidenproteine können in verschiedene Morphologien, wie Fasern, Partikel, Kapseln, Vliese, Hydrogele, Schäume und Filme, weiter verarbeitet werden. Modifiziert nach Schacht & Scheibel, *Current Opinion in Biotechnology* 2014, 29: 62-69, mit freundlicher Genehmigung des Verlages Elsevier.

Es wurden bereits dreidimensionale Gerüste (z. B. Schäume und Hydrogele) aus rekombinanten Spinnenseidenproteinen für die Gewebezüchtung hergestellt und deren Biokompatibilität getestet. Schäume wurden aus dem rekombinanten Spinnenseidenprotein rS1/9 (basierend auf MaSp1 von *Nephila clavipes*) durch *Salt leaching* hergestellt. *In vitro* Studien haben gezeigt, dass Mausfibroblasten auf Schäumen aus rS1/9 adhärieren und proliferieren. Innerhalb einer Woche migrierten die Zellen in die porösen *Scaffolds*.[296] Auch *in vivo* konnte beobachtet werden, dass eine Vaskularisierung und das Einwachsen in das umliegende Gewebe sowie das Ausbilden von Nervenfasern bei den rS1/9 *Scaffolds* acht Wochen nach der subkutanen Implantation erfolgte.[297] Schäume und fasernbasierte Matrizen aus dem rekombinanten Spinnenseidenprotein 4RepCT (basierend auf *Major Ampullate* Spidroin 1 von *Euprosthenops australis*) unterstützten ebenfalls Wachstum, Adhäsion und Kollagen Typ I Produktion bei menschlichen primären Fibroblasten.[298-299] Zusätzlich waren makroskopische 4RepCT-Fasern nach der subkutanen Implantation in Ratten gut verträglich. Im Gegensatz zur Kontrollgruppe mit Fasern des Seidenspinners (MersilkTM) unterstützten

4RepCT-Fasern das Einwachsen von Fibroblasten und die Bildung von Kapillaren im Zentrum der Faserbündel.[298-299]

2 ZIELSETZUNG

In der Biomedizin wird angestrebt, Trägermatrices (*Scaffolds*) herzustellen, die die Zelladhäsion, -migration, -proliferation und -differenzierung ermöglichen. Die Entwicklung von neuen biokompatiblen Materialien, welche nach der Implantation zunächst den Zellen als künstliches Stützgerüst dienen, ist entscheidend. Die Materialien müssen anschließend nach und nach abgebaut und durch neue extrazelluläre Matrix ersetzt werden, bis ein neues, funktionelles Gewebe entsteht. Spinnenseide ist aufgrund ihrer hervorragenden Biokompatibilität und Bioabbaubarkeit ein Material für vielseitige biomedizinische Anwendungen. Die biotechnologische Herstellung von Spinnenseidenproteinen erlaubt eine Produktion im industriellen Maßstab mit gleichbleibender Qualität. Zudem ist es möglich, die rekombinanten Spinnenseidenproteine gentechnisch, z. B. mit Zelladhäsionsdomänen, zu modifizieren und somit die biologischen Eigenschaften des Materials zu steuern. In dieser Arbeit wurde mit den rekombinanten Spinnenseidenproteinen eADF4(C16) und der RGD-modifizierten Variante eADF4(C16)-RGD gearbeitet, deren Sequenzen von der *Dragline*-Seide der Gartenkreuzspinne (*A. diadematus*) abgeleitet wurden. Die rekombinanten Spinnenseidenproteine können in verschiedene Morphologien, wie z. B. Schäume und Hydrogele, überführt werden. Eine Fabrikationstechnik für die Herstellung von Schäumen stellt das *Salt leaching* dar. Diese Methode wurde in der Arbeit angewendet, um poröse Strukturen aus rekombinanten Spinnenseidenproteinen für den Einsatz als 3D-*Scaffolds* herzustellen. Zunächst sollten die Porengrößen, Porosität und strukturellen Eigenschaften der Schäume sowie deren mechanische und katalytische Eigenschaften wie auch deren Abbaueigenschaften analysiert werden. Im Anschluss sollte die Biokompatibilität dieser 3D-*Scaffolds* mit Hilfe von Adhäsions- und Proliferationstests untersucht werden. Darüber hinaus sollten Hydrogele aus rekombinanten Spinnenseidenproteinen, wie die Schäume, als Trägermatrix für diverse Zelllinien (Fibroblasten, Keratinozyten, Myoblasten, Osteoblasten, HeLa) untersucht werden. Mit Hilfe der Biofabrikation bzw. dem 3D-Drucken können 3D-Strukturen Schicht-für-Schicht aus Material/Hydrogel-Zell-Mischungen computergesteuert aufgebaut werden. Im Gegensatz zur klassischen Gewebezüchtung können gewebeähnliche 3D-Konstrukte mit isotrop verteilten Zellen hergestellt werden, die eine direkte Versorgung mit Nährstoffen garantieren. Sowohl an den Herstellungsprozess als auch an die verwendeten Materialien, die sogenannten Biotinten, werden hohe Anforderungen gestellt. Da Biotinten einerseits druckbar und andererseits zellkompatibel sein müssen, stellen diese oft den limitierenden Faktor in der Biofabrikation dar. In dieser Arbeit sollte zunächst untersucht werden, ob Hydrogele aus rekombinanten Spinnenseidenproteinen mit eingekapselten Fibroblasten als Biotinte im 3D-Druck eingesetzt

werden können. Dabei ist zunächst die Druckbarkeit der Hydrogele entscheidend, so dass formstabile 3D-Konstrukte hergestellt werden können. Zusätzlich sollte analysiert werden, ob die eingekapselten Zellen sowohl die Gelbildung als auch den Druckprozess überleben und im Anschluss innerhalb der 3D-Konstrukte migrieren und proliferieren können. Um die Zellvitalität und Überlebensrate sowie die Proliferationsrate der eingekapselten Zellen zu erhöhen, sollte der physikalische Gelbildungsprozess der Hydrogele aus eADF4(C16) optimiert und funktionelle Gruppen, wie z. B. RGD, eingebracht werden.

3 SYNOPSIS

Obwohl die klassische Gewebezüchtung, bei der isolierte Zellen *in vitro* in der 2D-Zellkultur gezüchtet werden, relativ unkompliziert ist, können komplexe 3D-Strukturen mit dieser Methode nicht aufgebaut werden. Die injizierten Zellen können oft nur schwer in einem klinisch relevanten Zeitraum in der gewünschten Position überleben, ohne dass die Zellvitalität abnimmt.[9, 14] Deshalb werden für schwerwiegendere Verletzungen und komplexere, dreidimensionale Gewebe entweder vorgefertigte Trägermatrices (*Scaffolds*) vor der Implantation mit Zellen besiedelt oder die Zellen direkt mit dem Material gemischt, bevor komplexe 3D-Konstrukte Schicht-für-Schicht aufgebaut werden.[2, 11, 14, 300] Die vorliegende Arbeit umfasst drei Publikationen, die in Kapitel 7 dargestellt sind und die Herstellung von 3D-*Scaffolds* aus rekombinanten Spinnenseidenproteinen für die Gewebezüchtung umfassend diskutieren (Abb. 15).

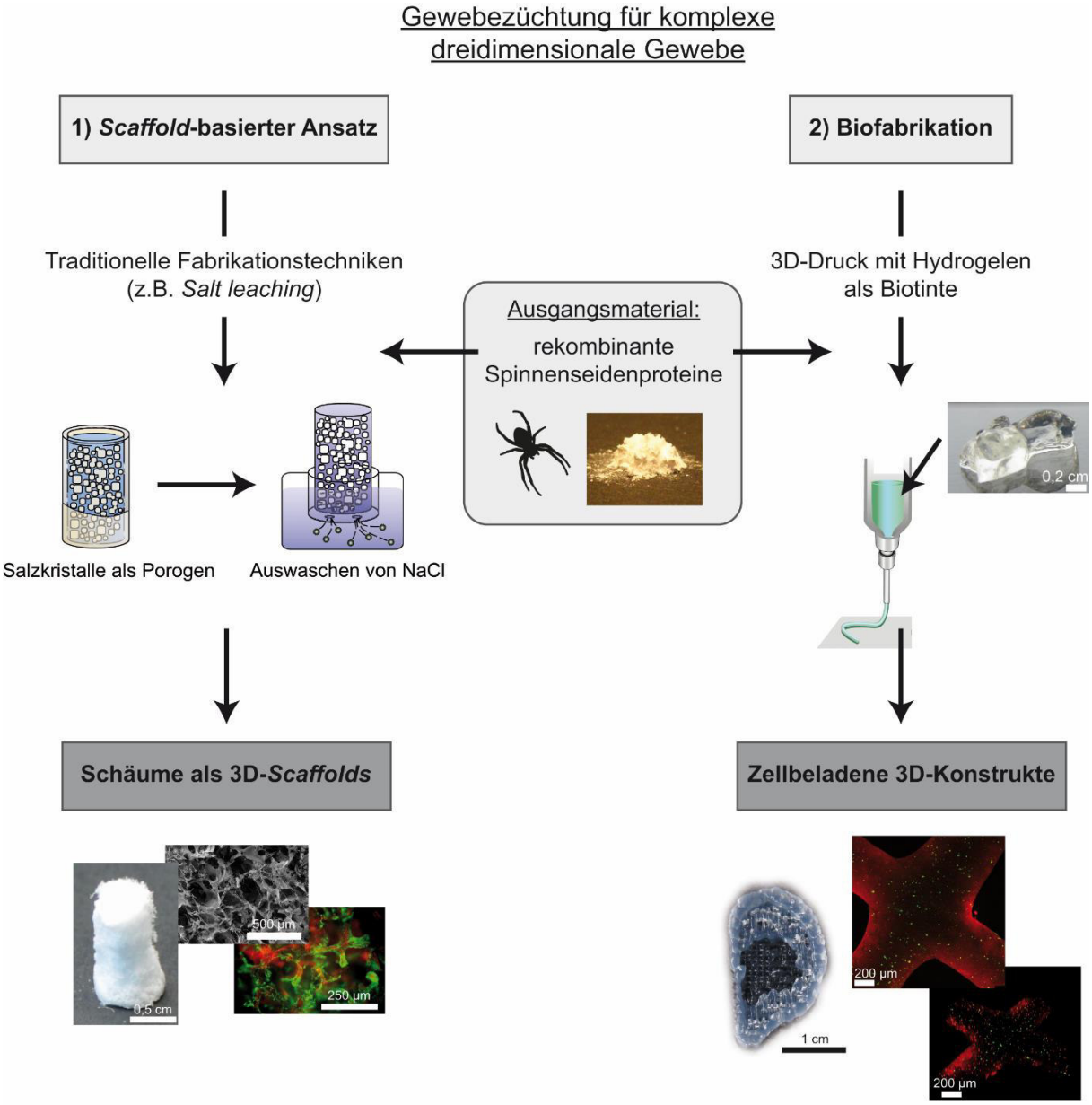

Abbildung 15. Verschiedene Herstellungswege von dreidimensionalen *Scaffolds* für die Gewebezüchtung. 3D-*Scaffolds* können z. B. durch traditionelle Fabrikationsverfahren, wie *Salt leaching*, hergestellt werden. Dabei wird die Trägermatrix (z. B. Schäume) nach dessen Herstellung mit Zellen besiedelt. Es können aber auch zellbeladene 3D-Konstrukte mittels 3D-Druck für die Gewebezüchtung von komplexen Geweben verwendet werden. Dabei werden oftmals Hydrogele als Biotinte eingesetzt. Als Ausgangsmaterial dienen rekombinante Spinnenseidenproteine.

Eine vielversprechende Methode zur Herstellung von porösen Schäumen aus den rekombinanten Spinnenseidenproteinen eADF4(C16) und der RGD-modifizierten Variante eADF4(C16)-RGD stellt das *Salt leaching* dar (Teilarbeit I, Kapitel 7). Die daraus resultierenden porösen 3D-Strukturen wiesen mechanische Eigenschaften im Bereich von Weichgeweben auf. Die Porengrößen und Porosität der Schäume konnte durch die Salzkristallgrößen individuell eingestellt werden. Neben den strukturellen und mechanischen

Eigenschaften, die das Zielgewebe so gut wie möglich nachahmen sollen, müssen die 3D-*Scaffolds* biokompatibel sein und die Zelladhäsion, -proliferation und -differenzierung unterstützen.[25, 75, 81] Fibroblasten konnten auf den oben beschriebenen Schäumen aus eADF4(C16)-RGD adhärieren und proliferieren, während die Zellen auf den unmodifizierten eADF4(C16) Schäumen schlecht adhärierten. Dennoch stellt die schwierige Kontrolle über die innere Architektur (z. B. Porosität, Porengröße) beim *Salt leaching* einen entscheidenden Nachteil dar. Durch einen automatisierten Prozess können 3D-*Scaffolds* mit erhöhter Genauigkeit und Reproduzierbarkeit hergestellt werden. Dadurch können die Konstrukte direkt in hierarchische gewebeartige Strukturen überführt werden. Deshalb wurden im zweiten Teil der Dissertation in Zusammenarbeit mit Prof. Dr. Jürgen Groll und Tomasz Jüngst (Universität Würzburg) Hydrogele aus den rekombinanten Spinnenseidenproteinen eADF4(C16) und eADF4(C16)-RGD als neue Biotinte im 3D-Druck eingesetzt (Teilarbeit II, Kapitel 7). Erstmals konnten zellbeladene Spinnenseidenhydrogele mittels Dispensdruck ohne zusätzliche Quervernetzer in formstabile Konstrukte gedruckt werden. Zusätzlich konnten die eingekapselten Fibroblasten mindestens sieben Tage in den gedruckten *Scaffolds* überleben. Die genetische Einführung der RGD-Sequenz hat den Vorteil, dass es zudem möglich ist, die Zell-Material-Interaktionen zu steuern. Da bereits ein Drittel der Zellen vor dem Druckprozess durch die Einkapselung der Zellen starben, war das anschließende Ziel, die Überlebens- und Proliferationsrate der eingeschlossenen Zellen zu erhöhen (Teilarbeit III, Kapitel 7). Da die Zellen Zellkulturmedium zum Überleben brauchen, wurde zunächst der Einfluss des Mediums auf die Hydrogelbildung und mechanischen Eigenschaften untersucht (Teilarbeit III, Kapitel 7). Mono- und bivalente Kationen, die im Zellkulturmedium enthalten sind, beeinflussten den Selbstassemblierungsprozess der Spinnenseidenproteine sowie die Gelbildungskinetik und Festigkeit der Hydrogele entscheidend. Bemerkenswerterweise konnten sowohl Fibroblasten als auch Myoblasten langfristig (über 15 Tage) durch die Einführung der funktionellen Gruppe RGD spreiten und letztendlich proliferieren.

3.1 MITTELS *SALT LEACHING* HERGESTELLTE SCHÄUME ALS 3D-*SCAFFOLDS*

Eine Vielzahl an Herstellungsverfahren wurde entwickelt, um 3D-*Scaffolds* mit einer hohen Porosität und großen Oberfläche aus biokompatiblen und bioabbaubaren Materialien für die Gewebezüchtung zu produzieren. Es ist jeweils das Ziel, reproduzierbare 3D-*Scaffolds* herzustellen, die eine gewisse Zeit (bis das neue Gewebe ersetzt ist) im Körper den Zellen als Stütze dienen. Eine traditionell angewendete Technik zur Herstellung dieser 3D-*Scaffolds* ist das *Salt leaching*, bei der die Porengröße und Porosität der Gerüste durch die Größe von

granularen Salzkristallen (Porogen) reguliert wird (Abb. 5).[79-81, 85-88] Diese vielversprechende Methode wurde bereits für die Herstellung von Gerüsten aus diversen Polymeren, wie z. B. Kollagen oder Polylactiden, angewendet.[69, 84] In dieser Arbeit wurden 3D-*Scaffolds* aus den rekombinanten Spinnenseidenproteinen eADF4(C16) und eADF4(C16)-RGD durch die *Salt leaching*-Methode hergestellt. Durch den Porenbildner NaCl entstanden mechanisch stabile Schäume, die nicht zusätzlich mit Lösungsmitteln, wie z. B. Methanol oder Ethanol, nachbehandelt werden mussten. Dies ist ein großer Unterschied zu *Salt leaching*-Schäumen aus Fibroin Seide vom Seidenspinner *B. mori* (Teilarbeit I, Tabelle 1). Schäume, die durch *Salt leaching* hergestellt werden, zeigen oft eine dichte und wenig poröse Schicht an der Grenzfläche, die die Zellmigration *in vitro* sowie das Einwachsen des Gewebes nach der Implantation behindert.[13] Hier konnte allerdings gezeigt werden, dass die Schäume hoch porös (> 91 %) mit verbundenen Poren waren (Teilarbeit I, Abbildung 2A und Tabelle 2). Durch die Salzkristallgröße konnte die Porengröße gesteuert werden, so dass Schäume mit Porengrößen von 30-440 µm hergestellt werden konnten, die damit in einem für eine effiziente Zelladhäsion optimalen Bereich liegen (Teilarbeit I, Abbildung 1 und Tabelle 2). Neben der Porengröße und Porosität der 3D-*Scaffolds* sind die mechanischen Eigenschaften wichtig für die Zelladhäsion und -proliferation.[74] Deshalb wurde mit Hilfe von Drucktests die mechanische Stabilität der Schäume untersucht (Teilarbeit I, Abbildung 2B). Die Druckfestigkeit stieg von 0,94 auf 3,24 kPa mit zunehmender Proteinkonzentration (4 %-8 % w/v) an. Im Gegensatz zu *Salt-leaching*-Schäumen aus Fibroin liegen damit die mechanischen Eigenschaften im Bereich von sehr weichem Gewebe.[75, 81, 85-86] Weiche Matrices mit einem Elastizitätsmodul im Bereich des Elastizitätsmoduls von Gehirn (~ 0,1-1 kPa) fördert die Differenzierung von Stammzellen in neuronale Zellen, während Stammzellen auf festeren Matrices im Bereich von Muskeln (E-Modul ~ 8-17 kPa) sich in myogene Zellen differenzieren.[75] Interessanterweise zeigten alle Spinnenseidenschäume ein geringes Quellverhalten (3-9 %) (Teilarbeit I, Tabelle S1). Im Gegensatz dazu zeigten *Salt leaching*-Schäume aus Fibroin eine Quellung von 20-55 %. Möglicherweise ist dies durch die unterschiedliche Hydrophobizität der zwei Proteine zu erklären.[85]

Die 3D-*Scaffolds* müssen allerdings nicht nur mechanisch stabil sein, sondern auch nach und nach durch die natürliche extrazelluläre Matrix ersetzt werden und somit bioabbaubar sein.[81] Es konnte anhand der Modellproteasen Kollagenase Typ IA (CHC) aus *Clostridium histolyticum* und Protease Mix XIV (PXIV) aus *Streptomyces griseus* eindrucksvoll gezeigt werden, dass die Schäume aus rekombinanten Spinnenseidenproteinen abbaubar sind. In Anwesenheit von Protease Mix XIV erfolgte der Abbau innerhalb von vier Tagen, während die Schäume über einen untersuchten Zeitraum von 15 Tage in Anwesenheit von Kollagenase nur zu 20 % abgebaut wurden (Teilarbeit I, Abbildung 3).

Um die Biokompatibilität der Schäume zu analysieren, wurde zunächst die Zellvitalität und Morphologie von Mausfibroblasten nach sieben Tagen Inkubation detektiert (Teilarbeit I, Abbildung 4). Die Zelladhäsion auf Schäumen aus eADF4(C16) war schwach; die Zellen zeigten eine runde Morphologie. Zudem konnten Zellaggregate beobachtet werden. Da eADF4(C16) kein Zelladhäsionsmotiv besitzt, wird die Zelladhäsion vor allem durch die Hydrophobizität, Oberflächenladung und Topographie beeinflusst.[23-24, 63, 301] Wie bereits für Filme aus rekombinanten Spinnenseidenproteinen gezeigt[63], konnte die Zelladhäsion auf eADF4(C16)-RGD Schäumen aufgrund der Zelladhäsionsdomäne RGD entscheidend verbessert werden (Abbildung 16 und Teilarbeit I, Abbildung 5). Quantitativ wurde das Adhäsions- und Proliferationsverhalten der Fibroblasten mittels Alamar-Blau-Assay analysiert.

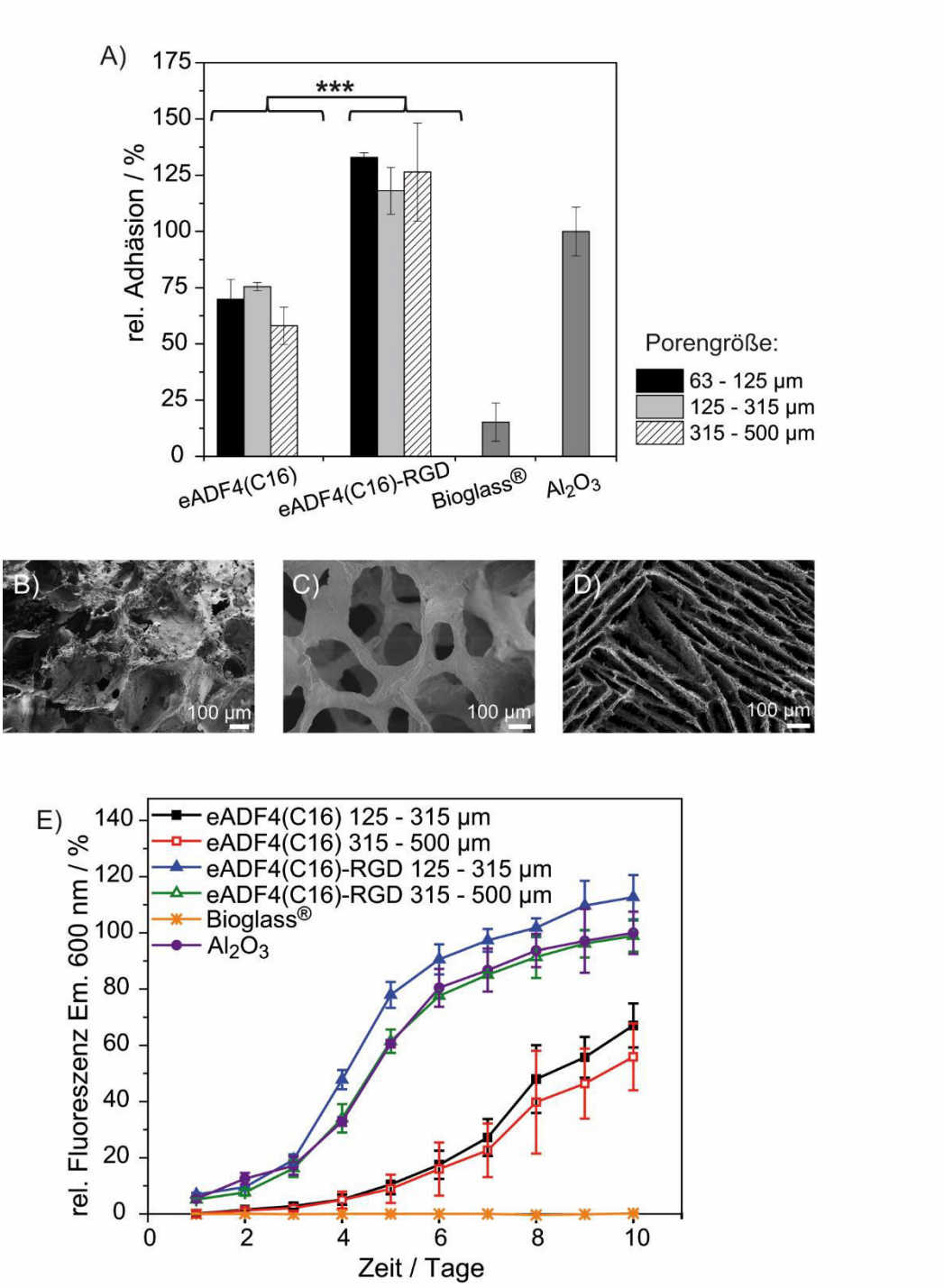

Abbildung 16. Kultivierung von BALB/3T3 Mausfibroblasten auf 8 % (w/v) eADF4(C16) und eADF4(C16)-RGD Schäumen mit verschiedenen Porengrößen (wie angegeben). 45S5 Bioglass® und Al_2O_3 Schäume wurden als Kontrollen verwendet. A) Adhäsionstest nach 24 h, quantifiziert durch den Alamar-Blau-Assay und normiert zur Adhäsion auf Al_2O_3 Schäumen (Positivkontrolle). Im Vergleich zu eADF4(C16) Schäumen war die Adhäsion auf allen eADF4(C16)-RGD Schäumen signifikant (***p<0,0001) verbessert. B-D) Rasterelektronenmikroskopische Aufnahmen von 8 % (w/v) eADF4(C16) (B), 45S5 Bioglass® (C) und Al_2O_3 (D) *Scaffolds*. E) Analyse der Proliferation von Fibroblasten auf Seidenschäumen und Kontrollschäumen. Die Proliferation wurde durch den Alamar-Blau-Assay quantifiziert und gegen die Proliferation auf Al_2O_3 *Scaffolds* nach zehn Tagen normiert.

Die Ergebnisse der quantitativen Analyse der Zelladhäsion korrelierten mit den Ergebnissen der morphologischen Untersuchungen. Durch die Offenporigkeit waren die Fibroblasten im Schaum gleichmäßig verteilt und das gesamte Gerüst war innerhalb von sieben Tagen bewachsen (Teilarbeit I, Abbildung S5). Interessanterweise hatte die Porengröße bei allen Schäumen keinen entscheidenden Einfluss auf die Zellmorphologie. Im Gegensatz dazu konnte dieser Einfluss im Proliferationstest über zehn Tage festgestellt werden. Auf beiden Schaumarten (eADF4(C16) & eADF4(C16)-RGD) proliferierten die Zellen auf den *Scaffolds* mit mittleren Porengrößen (125-315 µm) schneller als auf den *Scaffolds* mit den größeren Poren (315-500 µm). Dies ist bedingt durch die Kombination aus gutem Nährstoff- und Abfallprodukttransport und großer Oberfläche. Die Proliferation war prinzipiell langsamer auf Schäumen ohne RGD-Domäne.

Die Ergebnisse zeigten, dass Spinnenseidenschäume mit kontrollierbaren Eigenschaften (z. B. Porengröße, mechanische Eigenschaften, Zelladhäsion sowie –proliferation) hergestellt werden können, die neue Perspektiven der *3D-Scaffolds* im Bereich des Weichgewebeersatzes eröffnen.

3.2 Spinnenseidenhydrogele als neue Biotinte für den 3D-Druck

In früheren Studien wurde bereits gezeigt, dass aus den rekombinanten Spinnenseidenproteinen eADF4(C16) und eADF4(C16)-RGD durch Selbstassemblierung physikalisch quervernetzte Hydrogele hergestellt werden können (Abb. 7).[95, 114] Die Morphologie und Porengröße dieser Hydrogele hängt von der Proteinkonzentration ab und wird zudem durch die Funktionalisierung des Proteins und die chemische Quervernetzung beeinflusst.[114] Mit zunehmender Proteinkonzentration nimmt die Porengröße von 200 µm auf 10 µm ab und die Festigkeit der Hydrogele zu. Durch eine chemische Quervernetzung wird die dreidimensionale Struktur der Hydrogele zusätzlich stabilisiert. Die Elastizitätsmoduln lagen je nach Proteinkonzentration und Vernetzungsgrad zwischen 0,1 und 110 kPa und somit im Bereich von natürlichen Weichgeweben und Organen und in einem optimalen Bereich für eine effiziente Zelladhäsion.[75, 114] Durch die regulierbaren Eigenschaften der Hydrogele aus rekombinanten Spinnenseidenproteinen zeigen diese ein großes Potential für verschiedene biomedizinische Anwendungen. Deshalb wurde in dieser Arbeit zunächst die Zytokompatibilität der Hydrogele aus den rekombinanten Spinnenseidenproteinen eADF4(C16) und eADF4(C16)-RGD analysiert. Wie bereits auf Filmen und Schäumen aus eADF4(C16) gezeigt (Teilarbeit I),[63] war die Zelladhäsion sowie -proliferation von BALB/3T3 Fibroblasten gering (Teilarbeit II, Abbildung 1). Auf den eADF4(C16)-RGD Hydrogelen

hingegen konnten nicht nur Fibroblasten, sondern auch alle weiteren getesteten Zelllinien, wie Myoblasten, Osteoblasten, Keratinozyten und HeLa Zellen, signifikant verbessert adhärieren und proliferieren. Aufgrund dieser Ergebnisse wurde anschließend das Potential dieser Hydrogele als neue Biotinte evaluiert, weil Hydrogele zu den vielversprechendsten Biotinten-Kandidaten für die Biofabrikation zählen. Da Biotinten nicht nur druckbar, sondern auch zellfreundlich sein müssen, stellen geeignete Materialien für den 3D-Druck oftmals die größte Herausforderung dar.[127, 155]

Für die Herstellung der Hydrogele wurde eine 3 % (w/v) eADF4(C16) und eADF4(C16)-RGD Lösung über Nacht bei 37 °C inkubiert. Die Analyse mittels Fourier Transform-Infrarot-Spektroskopie zeigte, dass sich der β-Faltblattgehalt der Proteine während der Gelbildung verdoppelte und somit intermolekulare β-Faltblatt-Interaktionen die treibende Kraft bei der Gelierung sind (Teilarbeit II, Tabelle S1). Erstmalig ist es gelungen, dass Hydrogele aus rekombinanten Spinnenseidenproteinen gedruckt werden konnten (Teilarbeit II, Abbildung 2). Aufgrund ihres scherverdünnenden Verhaltens und der schnellen und reversiblen supramolekularen Wechselwirkungen zwischen den Proteinen konnte im Gegensatz zu Hydrogelen aus Fibroin ohne weitere Komponenten direkt gedruckt werden (Teilarbeit II, Abbildung S2 A & B).[157, 194]

Die während des Druckens im Druckkopf entstehenden Scherkräfte ließen das Hydrogel fließen. Sobald die Gerüststrukturen auf der Oberfläche abgelegt wurden, härtete das Hydrogel sofort aus. Dadurch konnten formstabile 3D-Konstrukte aus mehr als zehn Lagen mit einer Höhe von ca. 3 mm hergestellt werden (Teilarbeit II, Abbildung 2 und S3). Bemerkenswerterweise konnten die Spinnenseidenkonstrukte ohne zusätzliche Quervernetzer oder Nachbehandlung für die mechanische Stabilisierung gedruckt werden. Im Gegensatz dazu müssen viele etablierte Biotinten, wie beispielsweise Alginat, mit Quervernetzern (Ca^{2+} etc.) nachbehandelt werden, um die Druckgenauigkeit zu erhöhen.[103]

Um zellbeladene Konstrukte zu drucken, wurden humane Fibroblasten vor der Gelbildung mit den hochkonzentrierten Spinnenseidenlösungen gemischt (Abbildung 17A und Teilarbeit II, Abbildung 2 &3).

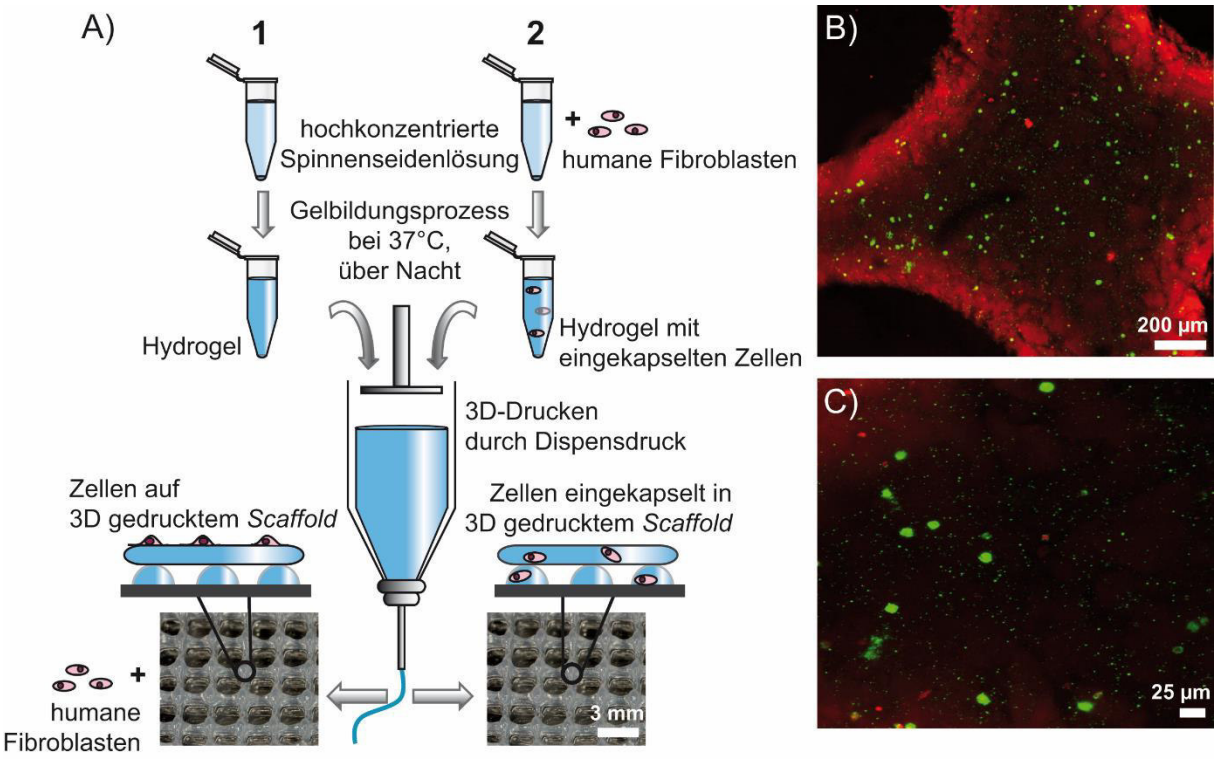

Abbildung 17. 3D-Druck von Spinnenseidenhydrogelen durch Dispensdruck. A) Schematische Darstellung des 3D-Druckens. Die Zellen wurden entweder auf den Konstrukten nach dem Drucken kultiviert (1) oder vor dem Druckprozess eingekapselt (2). B & C) Konfokale Laser-Scanning-Mikroskopie Aufnahmen von humanen Fibroblasten, die vor dem Druck in eADF4(C16) Hydrogele eingekapselt wurden. Die gedruckten Konstrukte bestanden aus zwei Lagen und die Lebend/Tot-Färbung (lebende Zellen: grün; tote Zellen: rot) erfolgte 48 h nach dem Drucken.

Die Zugabe der Zellen zur Biotinte hatte weder einen Einfluss auf die Selbstassemblierung des Hydrogels noch die Druckbarkeit des Materials. Zusätzlich war entscheidend, dass die Zellen den Druckprozess überlebten und mittels Lebend/Tot-Färbung gezeigt werden konnte, dass sie über mindestens sieben Tage vital waren (Abbildung 17B &C, sowie Teilarbeit II, Abbildung 3 & S4). 48 Stunden nach dem Drucken konnte eine durchschnittliche Vitalität der Zellen von 70,1 ± 7,6 % quantifiziert werden. Dies ist identisch zu nicht gedruckten Hydrogelen aus rekombinanter Spinnenseide, was verdeutlicht, dass der Druckprozess die Zellvitalität nicht negativ beeinflusst. Die Ergebnisse dieser Arbeit zeigten, dass Hydrogele aus rekombinanten Spinnenseidenproteinen vor allem aufgrund ihrer Formstabilität und Biokompatibilität eine vielversprechende Grundlage für die Herstellung von Biotinten und eine attraktive Alternative zu etablierten Biotinten darstellen.

3.3 Optimierung der Überlebensrate von eingekapselten Zellen in der Biotinte

Wie bereits in Teilarbeit II gezeigt, konnten 3D-Konstrukte aus eADF4(C16) und eADF4(C16)-RGD Hydrogelen mittels Dispensdruck hergestellt werden. Die Überlebensrate der eingeschlossenen humanen Fibroblasten lag nach 48 Stunden bei den gedruckten eADF4(C16) Hydrogelen bei 97 % im Vergleich zu nicht gedruckten Hydrogelen. Allerdings starben bereits ~ 30 % der Fibroblasten vor dem Druckprozess während der Gelbildung. Außerdem zeigten die eingeschlossenen Zellen eine runde Zellmorphologie. Aus diesem Grund wurde in dieser Arbeit erforscht, wie die Überlebens- und Proliferationsrate der eingekapselten Zellen erhöht werden kann (Teilarbeit III). Da die Zellen Zellkulturmedium zum Überleben benötigen, erfolgte die Zugabe der Zellen in 15 % (w/v) Zellkulturmedium zur hochkonzentrierten Spinnenseidenlösung. Im Zellkulturmedium sind eine Vielzahl an Salzen, Zuckern und Proteinen enthalten, die die Interaktionen und Wechselwirkungen zwischen den Seidenproteinen beeinflussen können. Es konnte bereits gezeigt werden, dass Salze, wie z. B. $CaCl_2$, NaCl und KCl, eine wichtige Rolle bei der Fadenbildung im Spinnentrakt spielen.[277-279, 302] In dieser Arbeit wurde der Einfluss des Zellkulturmediums auf die Sekundärstruktur und Hydrogelbildung der Seidenproteine sowie die mechanischen Eigenschaften der Hydrogele untersucht (Teilarbeit III, Kapitel 7). Die mono- und bivalenten Kationen des Zellkulturmediums beeinflussten den Selbstassemblierungsprozess der Spinnenseidenproteine entscheidend. Obwohl die Zugabe von Zellkulturmedium zu den Spinnenseidenhydrogelen keinen Effekt auf die Sekundärstruktur zeigte, konnte ein signifikanter Effekt bei der Gelierungskinetik festgestellt werden (Abbildung 18A und Teilarbeit III, Tabelle 1 & Abbildung 1).

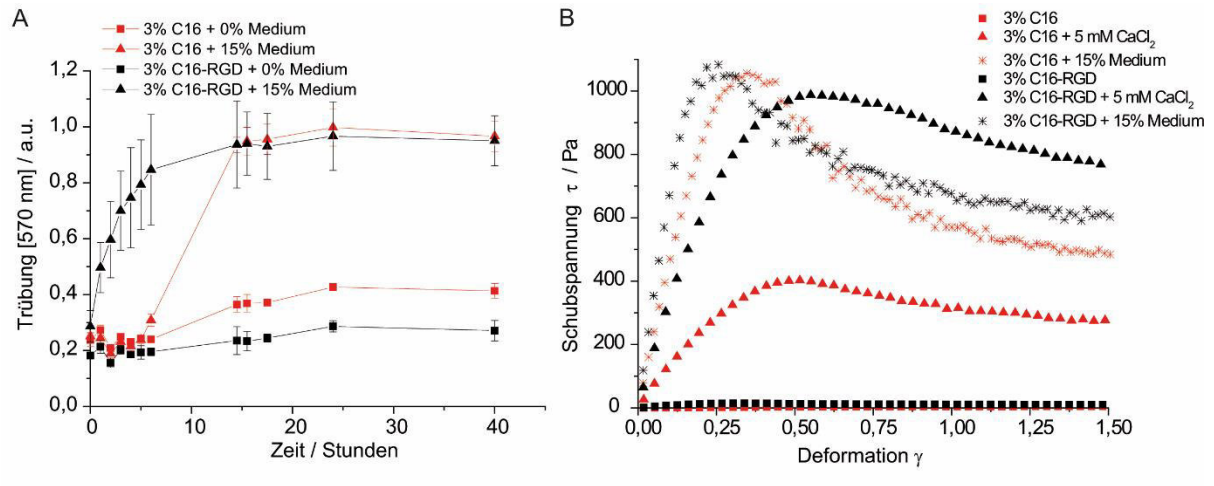

Abbildung 18. Einfluss von Zellkulturmedium auf die Hydrogelbildung (A) und rheologischen Eigenschaften (B) von 3 % (w/v) eADF4(C16) und eADF4(C16)-RGD Hydrogelen. A) Zeitabhängige Gelierungskinetik von eADF4(C16) und eADF4(C16)-RGD Lösungen in An- und Abwesenheit von Zellkulturmedium (15 % w/v) bei 37 °C. Mittels Trübungsmessungen (bei 570 nm) wurde auf Bildung von Nanofibrillen geschlossen. B) Rheologische Charakterisierung von eADF4(C16) und eADF4(C16)-RGD Hydrogelen in der An- und Abwesenheit von 5 mM $CaCl_2$ und Zellkulturmedium (15 % w/v).

Die Hydrogele gelierten sehr viel schneller in Anwesenheit von Zellkulturmedium als ohne. Der Bildungprozess von 3 % (w/v) eADF4(C16)-RGD Hydrogelen mit Zellkulturmedium begann direkt nach der Dialyse und war nach ca. zehn Stunden abgeschlossen. Interessanterweise zeigten im Gegensatz dazu Hydrogele aus eADF4(C16) eine fünfstündige Verzögerungsphase und der gesamte Gelbildungsprozess dauerte ca. 15 Stunden. Generell hatte das Zellkulturmedium einen größeren Einfluss auf die Hydrogelbildung bei eADF4(C16)-RGD Hydrogelen. Mittels rheologischer Messungen wurden die mechanischen Eigenschaften der Spinnenseidenhydrogele in An- und Abwesenheit von $CaCl_2$ und des Zellkulturmediums bestimmt (Abbildung 18B). Durch die Zugabe von 5 mM $CaCl_2$ änderten sich die mechanischen Eigenschaften der Hydrogele entscheidend. Bei eADF4(C16)-RGD Hydrogelen nahm die Schubspannung bei gleicher Deformation um das 1000-fache im Vergleich zu getesteten Hydrogelen bei Abwesenheit von $CaCl_2$ zu. Durch die bivalenten Ionen werden die abstoßenden, elektrostatischen Wechselwirkungen reduziert und die Kräfte für die intermolekularen Reaktionen können überwiegen.[303] Zudem führten die ionischen Interaktionen zwischen den bivalenten Kationen und COO^- Seitenketten der Spinnenseidenproteine zu einem Anstieg in der Festigkeit der Hydrogele. In Anwesenheit von $CaCl_2$ waren eADF4(C16)-RGD Hydrogele 2,5-fach fester als eADF4(C16) Hydrogele. Dieses Phänomen ist derzeit nicht komplett verstanden, da durch die Zelladhäsionsdomäne RGD diese Hydrogele lediglich eine weitere Carboxylgruppe besitzen. Da das Zellkulturmedium eine hochkomplexe elektrolytische Lösung ist, wurden durch die Zugabe von Zellkulturmedium die ionischen Wechselwirkungen verstärkt. Obwohl

die Hydrogele durch die Zugabe von Zellkulturmedium fester waren, wiesen die Hydrogele immer noch ein scherverdünnendes Verhalten auf, was entscheidend für den 3D-Druckprozess ist (Teilarbeit III, Abbildung 3). Es kann zusammengefasst werden, dass Kationen die Vernetzung, Bildung und Festigkeit von Hydrogelen aus Spinnenseide beeinflussen, so dass dadurch die Einkapselung der Zellen reguliert werden kann. Zudem konnte gezeigt werden, dass durch die Variation der Proteinkonzentration und die Einführung der funktionellen Gruppe RGD die Überlebens- und Proliferationsraten signifikant erhöht werden (Abbildung 19).

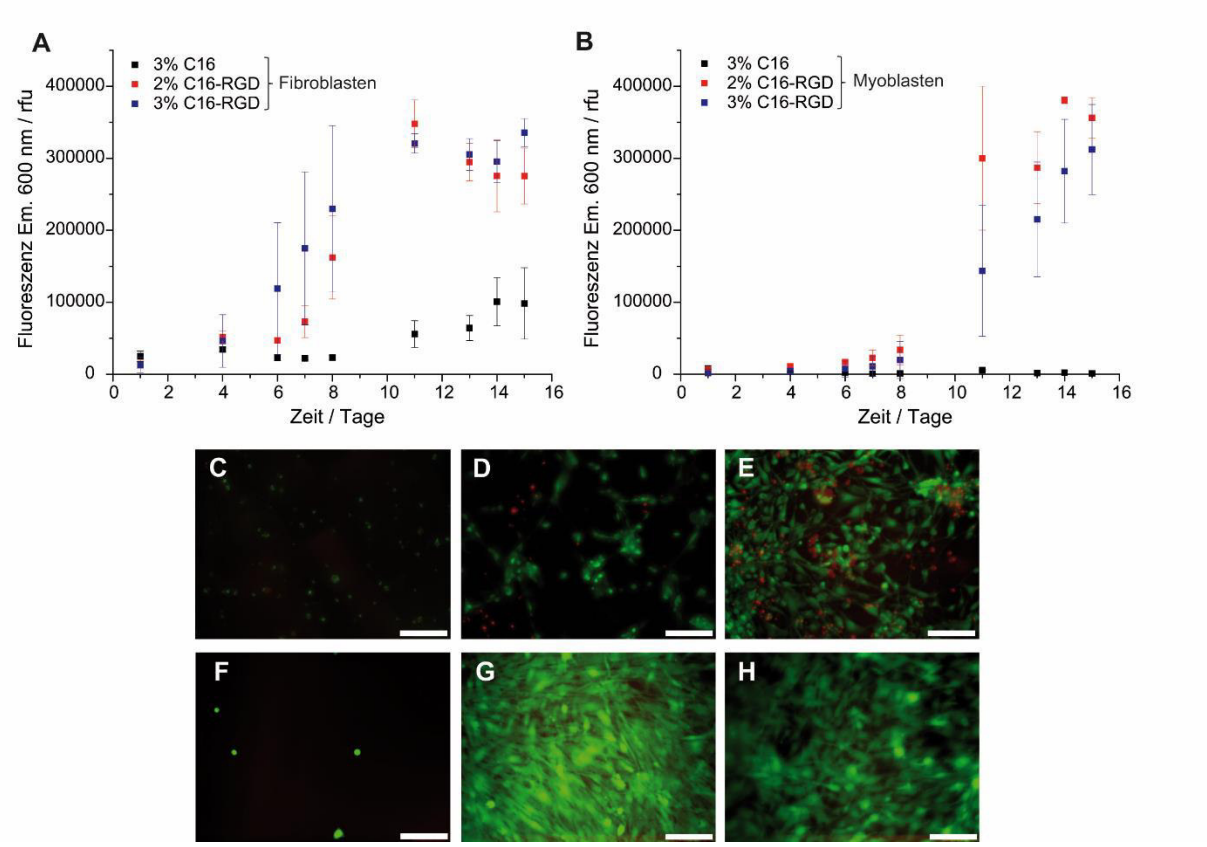

Abbildung 19. Kultivierung von BALB/3T3 Fibroblasten und C2C12 Myoblasten eingekapselt in 2 % und 3 % (w/v) eADF4(C16) und eADF4(C16)-RGD Hydrogelen. Proliferationstest über 15 Tage mit Fibroblasten (A) und Myoblasten (B), quantifiziert durch den Alamar-Blau-Assay. Im Vergleich zu eADF4(C16) Hydrogelen war die Proliferation auf eADF4(C16)-RGD verbessert. C-H) Fluoreszenzmikroskopische Aufnahmen von Fibroblasten (C-E) und Myoblasten (F-H), die in eADF4(C16) und eADF4(C16)-RGD Hydrogele eingekapselt wurden. Die Lebend/Tot-Färbung erfolgte nach 20 Tagen Inkubation. C, F) 3 % (w/v) eADF4(C16); D, G) 2 % (w/v) eADF4(C16)-RGD; E, H) 3 % (w/v) eADF4(C16)-RGD. Maßstab: 250 µm.

Im Gegensatz zu den in Teilarbeit II gezeigten Ergebnissen konnte erstaunlicherweise nach ca. sechs Tagen detektiert werden, dass sowohl Fibroblasten als auch Myoblasten in eADF4(C16)-RGD Hydrogelen spreiten und proliferieren. Dies war für beide Zelllinien in Hydrogelen ohne funktionelle Gruppe nicht möglich. Interessanterweise bevorzugten die

Fibroblasten eine Proteinkonzentration von 3 % (w/v) eADF4(C16)-RGD, während die Myoblasten bevorzugt in 2 % (w/v) eADF4(C16)-RGD Hydrogelen proliferierten. Wie bereits erwähnt, reagieren unterschiedliche Zelllinien auch unterschiedlich auf verschiedene Matrixelastizitäten, die in diesen Hydrogelen durch die Proteinkonzentration reguliert werden können.[75]

In dieser Arbeit konnte gezeigt werden, dass mit dem gleichen Material und damit der gleichen chemischen Zusammensetzung die mechanischen Eigenschaften, Gelierungskinetik und Biokompatibilitäten ohne den Einsatz von weiteren Materialien oder Quervernetzern gesteuert werden können. Dies eröffnet ein breites Anwendungsspektrum für die Gewebezüchtung und regenerative Medizin, wie z. B. in der Knorpelregeneration, Wundheilung oder als Wirkstofftransportsystem.

4 LITERATURVERZEICHNIS

[1] Langer, R.; Vacanti, J. P. Tissue Engineering. *Science* **1993,** *260* (5110), 920-926.

[2] Melchels, F. P. W.; Domingos, M. A. N.; Klein, T. J.; Malda, J.; Bartolo, P. J.; Hutmacher, D. W. Additive manufacturing of tissues and organs. *Prog Polym Sci* **2012,** *37* (8), 1079-1104.

[3] Khademhosseini, A.; Langer, R.; Borenstein, J.; Vacanti, J. P. Microscale technologies for tissue engineering and biology. *P Natl Acad Sci USA* **2006,** *103* (8), 2480-2487.

[4] Tuan, R. S.; Boland, G.; Tuli, R. Adult mesenchymal stem cells and cell-based tissue engineering. *Arthritis Res Ther* **2003,** *5* (1), 32-45.

[5] Newman, D. J.; Cragg, G. M. Natural Products As Sources of New Drugs over the 30 Years from 1981 to 2010. *J Nat Prod* **2012,** *75* (3), 311-335.

[6] Ma, P. X. Biomimetic materials for tissue engineering. *Adv Drug Deliver Rev* **2008,** *60* (2), 184-198.

[7] Pereira, R. F.; Barrias, C. C.; Granja, P. L.; Bartolo, P. J. Advanced biofabrication strategies for skin regeneration and repair. *Nanomedicine-Uk* **2013,** *8* (4), 603-621.

[8] Wegst, U. G. K.; Bai, H.; Saiz, E.; Tomsia, A. P.; Ritchie, R. O. Bioinspired structural materials. *Nat Mater* **2015,** *14* (1), 23-36.

[9] Passier, R.; van Laake, L. W.; Mummery, C. L. Stem-cell-based therapy and lessons from the heart. *Nature* **2008,** *453* (7193), 322-329.

[10] Kirsner, R. S.; Marston, W. A.; Snyder, R. J.; Lee, T. D.; Cargill, D. I.; Slade, H. B. Spray-applied cell therapy with human allogeneic fibroblasts and keratinocytes for the treatment of chronic venous leg ulcers: a phase 2, multicentre, double-blind, randomised, placebo-controlled trial. *Lancet* **2012,** *380* (9846), 977-985.

[11] Jia, X. Q.; Kiick, K. L. Hybrid Multicomponent Hydrogels for Tissue Engineering. *Macromol Biosci* **2009,** *9* (2), 140-156.

[12] Krukemeyer, M. G.; Spiegel, H.-U., *Chirurgische Forschung*. Georg Thieme Verlag KG: Stuttgart, 2005.

[13] Hutmacher, D. W. Scaffolds in tissue engineering bone and cartilage. *Biomaterials* **2000,** *21* (24), 2529-2543.

[14] Pereira, R. F.; Bártolo, P. J. 3D Photo-Fabrication for Tissue Engineering and Drug Delivery. *Engineering* **2015,** *1*, 90-112.

[15] Bajaj, P.; Schweller, R. M.; Khademhosseini, A.; West, J. L.; Bashir, R. 3D Biofabrication Strategies for Tissue Engineering and Regenerative Medicine. *Annu Rev Biomed Eng* **2014,** *16*, 247-276.

[16] Jungst, T.; Smolan, W.; Schacht, K.; Scheibel, T.; Groll, J. Strategies and Molecular Design Criteria for 3D Printable Hydrogels. *Chem Rev* **2016,** *116* (3), 1496-1539.

[17] Vaezi, M.; Seitz, H.; Yang, S. F. A review on 3D micro-additive manufacturing technologies. *Int J Adv Manuf Tech* **2013,** *67* (5-8), 1721-1754.

[18] Raimondi, M. T.; Eaton, S. M.; Nava, M. M.; Lagana, M.; Cerullo, G.; Osellame, R. Two-photon laser polymerization: from fundamentals to biomedical application in tissue engineering and regenerative medicine. *J Appl Biomater Func* **2012,** *10* (1), 56-66.

[19] Melchels, F. P. W.; Feijen, J.; Grijpma, D. W. A review on stereolithography and its applications in biomedical engineering. *Biomaterials* **2010,** *31* (24), 6121-6130.

[20] Mironov, V.; Visconti, R. P.; Kasyanov, V.; Forgacs, G.; Drake, C. J.; Markwald, R. R. Organ printing: Tissue spheroids as building blocks. *Biomaterials* **2009,** *30* (12), 2164-2174.

[21] Leal-Egana, A.; Scheibel, T. Silk-based materials for biomedical applications. *Biotechnol Appl Bioc* **2010,** *55*, 155-167.

[22] Cima, L. G.; Ingber, D. E.; Vacanti, J. P.; Langer, R. Hepatocyte Culture on Biodegradable Polymeric Substrates. *Biotechnol Bioeng* **1991,** *38* (2), 145-158.

[23] Leal-Egana, A.; Lang, G.; Mauerer, C.; Wickinghoff, J.; Weber, M.; Geimer, S.; Scheibel, T. Interactions of Fibroblasts with Different Morphologies Made of an Engineered Spider Silk Protein. *Adv Eng Mater* **2012,** *14* (3), B67-B75.

[24] Leal-Egana, A.; Scheibel, T. Interactions of cells with silk surfaces. *J Mater Chem* **2012,** *22* (29), 14330-14336.

[25] Reddig, P. J.; Juliano, R. L. Clinging to life: cell to matrix adhesion and cell survival. *Cancer Metast Rev* **2005,** *24* (3), 425-439.

[26] Leal-Egana, A.; Diaz-Cuenca, A.; Boccaccini, A. R. Tuning of Cell-Biomaterial Anchorage for Tissue Regeneration. *Advanced Materials* **2013,** *25* (29), 4049-4057.

[27] Healy, K. E.; Thomas, C. H.; Rezania, A.; Kim, J. E.; McKeown, P. J.; Lom, B.; Hockberger, P. E. Kinetics of bone cell organization and mineralization on materials with patterned surface chemistry. *Biomaterials* **1996,** *17* (2), 195-208.

[28] Szabo, I.; Brutsche, S.; Tombola, F.; Moschioni, M.; Satin, B.; Telford, J. L.; Rappuoli, R.; Montecucco, C.; Papini, E.; Zoratti, M. Formation of anion-selective channels in the cell plasma membrane by the toxin VacA of Helicobacter pylori is required for its biological activity. *Embo J* **1999,** *18* (20), 5517-5527.

[29] Anselme, K. Osteoblast adhesion on biomaterials. *Biomaterials* **2000,** *21* (7), 667-681.

[30] Kim, J.; Kim, D. H.; Lim, K. T.; Seonwoo, H.; Park, S. H.; Kim, Y. R.; Kim, Y.; Choung, Y. H.; Choung, P. H.; Chung, J. H. Charged Nanomatrices as Efficient Platforms for Modulating Cell Adhesion and Shape. *Tissue Eng Part C-Me* **2012,** *18* (12), 913-923.

[31] Roach, P.; Eglin, D.; Rohde, K.; Perry, C. C. Modern biomaterials: a review-bulk properties and implications of surface modifications. *Journal of Materials Science-Materials in Medicine* **2007,** *18* (7), 1263-1277.

[32] Wohlrab, S.; Spiess, K.; Scheibel, T. Varying surface hydrophobicities of coatings made of recombinant spider silk proteins. *J Mater Chem* **2012,** *22* (41), 22050-22054.

[33] Muller, C.; Luders, A.; Hoth-Hannig, W.; Hannig, M.; Ziegler, C. Initial Bioadhesion on Dental Materials as a Function of Contact Time, pH, Surface Wettability, and Isoelectric Point. *Langmuir* **2010,** *26* (6), 4136-4141.

[34] Hlady, V.; Buijs, J. Protein adsorption on solid surfaces. *Current Opinion in Biotechnology* **1996,** *7* (1), 72-77.

[35] Lensen, M. C.; Schulte, V. A.; Salber, J.; Diez, M.; Menges, F.; Moller, M. Cellular responses to novel, micropatterned biomaterials. *Pure and Applied Chemistry* **2008,** *80* (11), 2479-2487.

[36] Ruardy, T. G.; Schakenraad, J. M.; Vandermei, H. C.; Busscher, H. J. Adhesion and Spreading of Human Skin Fibroblasts on Physicochemically Characterized Gradient Surfaces. *J Biomed Mater Res* **1995,** *29* (11), 1415-1423.

[37] Lee, J. H.; Khang, G.; Lee, J. W.; Lee, H. B. Interaction of different types of cells on polymer surfaces with wettability gradient. *J Colloid Interf Sci* **1998,** *205* (2), 323-330.

[38] Harrison, R. G. On the Stereotropism of Embryonic Cells. *Science* **1911,** *34* (870), 279-281.

[39] Meyle, J.; Gultig, K.; Nisch, W. Variation in Contact Guidance by Human-Cells on a Microstructured Surface (Vol 29, Pg 81, 1995). *J Biomed Mater Res* **1995,** *29* (7), 905-905.

[40] Wojciak-Stothard, B.; Curtis, A.; Monaghan, W.; Macdonald, K.; Wilkinson, C. Guidance and activation of murine macrophages by nanometric scale topography. *Exp Cell Res* **1996,** *223* (2), 426-435.

[41] Teixeira, A. I.; Abrams, G. A.; Bertics, P. J.; Murphy, C. J.; Nealey, P. F. Epithelial contact guidance on well-defined micro- and nanostructured substrates. *J Cell Sci* **2003,** *116* (10), 1881-1892.

[42] Fraser, S. A.; Ting, Y. H.; Mallon, K. S.; Wendt, A. E.; Murphy, C. J.; Nealey, P. F. Sub-micron and nanoscale feature depth modulates alignment of stromal fibroblasts and corneal epithelial cells in serum-rich and serum-free media. *Journal of Biomedical Materials Research Part A* **2008,** *86A* (3), 725-735.

[43] Anselme, K.; Bigerelle, M. Role of materials surface topography on mammalian cell response. *Int Mater Rev* **2011,** *56* (4), 243-266.

[44] Jeffries, E. M.; Wang, Y. D. Incorporation of parallel electrospun fibers for improved topographical guidance in 3D nerve guides. *Biofabrication* **2013,** *5* (3), 1-8.
[45] Luo, B. H.; Carman, C. V.; Springer, T. A. Structural basis of integrin regulation and signaling. *Annu Rev Immunol* **2007,** *25*, 619-647.
[46] Giancotti, F. G.; Ruoslahti, E. Transduction - Integrin signaling. *Science* **1999,** *285* (5430), 1028-1032.
[47] Hynes, R. O. Integrins - Versatility, Modulation, and Signaling in Cell-Adhesion. *Cell* **1992,** *69* (1), 11-25.
[48] Wang, F.; Li, Y. Y.; Shen, Y. Q.; Wang, A. M.; Wang, S. L.; Xie, T. The Functions and Applications of RGD in Tumor Therapy and Tissue Engineering. *Int J Mol Sci* **2013,** *14* (7), 13447-13462.
[49] Pierschbacher, M. D.; Ruoslahti, E. Cell Attachment Activity of Fibronectin Can Be Duplicated by Small Synthetic Fragments of the Molecule. *Nature* **1984,** *309* (5963), 30-33.
[50] Ruoslahti, E.; Pierschbacher, M. D. New Perspectives in Cell-Adhesion - Rgd and Integrins. *Science* **1987,** *238* (4826), 491-497.
[51] Hynes, R. O. Cell adhesion: old and new questions. *Trends Biochem Sci* **1999,** *24* (12), M33-M37.
[52] Plow, E. F.; Pierschbacher, M. D.; Ruoslahti, E.; Marguerie, G. A.; Ginsberg, M. H. The Effect of Arg-Gly-Asp-Containing Peptides on Fibrinogen and Von Willebrand Factor Binding to Platelets. *P Natl Acad Sci USA* **1985,** *82* (23), 8057-8061.
[53] Hubbell, J. A.; Massia, S. P.; Desai, N. P.; Drumheller, P. D. Endothelial Cell-Selective Materials for Tissue Engineering in the Vascular Graft Via a New Receptor. *Bio-Technol* **1991,** *9* (6), 568-572.
[54] Ranieri, J. P.; Bellamkonda, R.; Bekos, E. J.; Vargo, T. G.; Gardella, J. A.; Aebischer, P. Neuronal Cell Attachment to Fluorinated Ethylene-Propylene Films with Covalently Immobilized Laminin Oligopeptides Yigsr and Ikvav .2. *J Biomed Mater Res* **1995,** *29* (6), 779-785.
[55] Ruoslahti, E. RGD and other recognition sequences for integrins. *Annu Rev Cell Dev Bi* **1996,** *12*, 697-715.
[56] Grant, D. S.; Tashiro, K.; Segui-Real, B.; Yamada, Y.; Martin, G. R.; Kleinman, H. K. Two different laminin domains mediate the differentiation of human endothelial cells into capillary-like structures in vitro. *Cell* **1989,** *58* (5), 933-943.
[57] Graf, J.; Iwamoto, Y.; Sasaki, M.; Martin, G. R.; Kleinman, H. K.; Robey, F. A.; Yamada, Y. Identification of an Amino-Acid-Sequence in Laminin Mediating Cell Attachment, Chemotaxis, and Receptor-Binding. *Cell* **1987,** *48* (6), 989-996.
[58] Schacht, K.; Scheibel, T. Processing of recombinant spider silk proteins into tailor-made materials for biomaterials applications. *Current Opinion in Biotechnology* **2014,** *29*, 62-69.
[59] Sofia, S.; McCarthy, M. B.; Gronowicz, G.; Kaplan, D. L. Functionalized silk-based biomaterials for bone formation. *J Biomed Mater Res* **2001,** *54* (1), 139-148.
[60] Yanagisawa, S.; Zhu, Z. H.; Kobayashi, I.; Uchino, K.; Tamada, Y.; Tamura, T.; Asakura, T. Improving cell-adhesive properties of recombinant Bombyx mori silk by incorporation of collagen or fibronectin derived peptides produced by transgenic silkworms. *Biomacromolecules* **2007,** *8* (11), 3487-3492.
[61] Morgan, A. W.; Roskov, K. E.; Lin-Gibson, S.; Kaplan, D. L.; Becker, M. L.; Simon, C. G. Characterization and optimization of RGD-containing silk blends to support osteoblastic differentiation. *Biomaterials* **2008,** *29* (16), 2556-2563.
[62] Yang, M.; Tanaka, C.; Yamauchi, K.; Ohgo, K.; Kurokawa, M.; Asakura, T. Silklike materials constructed from sequences of Bombyx mori silk fibroin, fibronectin, and elastin. *Journal of Biomedical Materials Research Part A* **2008,** *84A* (2), 353-363.
[63] Wohlrab, S.; Muller, S.; Schmidt, A.; Neubauer, S.; Kessler, H.; Leal-Egana, A.; Scheibel, T. Cell adhesion and proliferation on RGD-modified recombinant spider silk proteins. *Biomaterials* **2012,** *33* (28), 6650-6659.

[64] Yoshimoto, H.; Shin, Y. M.; Terai, H.; Vacanti, J. P. A biodegradable nanofiber scaffold by electrospinning and its potential for bone tissue engineering. *Biomaterials* **2003,** *24* (12), 2077-2082.
[65] Tibbitt, M. W.; Anseth, K. S. Hydrogels as Extracellular Matrix Mimics for 3D Cell Culture. *Biotechnol Bioeng* **2009,** *103* (4), 655-663.
[66] Gerecht-Nir, S.; Cohen, S.; Ziskind, A.; Itskovitz-Eldor, J. Three-dimensional porous alginate scaffolds provide a conducive environment for generation of well-vascularized embryoid bodies from human embryonic stem cells. *Biotechnol Bioeng* **2004,** *88* (3), 313-320.
[67] Mikos, A. G.; Sarakinos, G.; Leite, S. M.; Vacanti, J. P.; Langer, R. Laminated three-dimensional biodegradable foams for use in tissue engineering. *Biomaterials* **1993,** *14* (5), 323-330.
[68] Mikos, A. G.; Sarakinos, G.; Lyman, M. D.; Ingber, D. E.; Vacanti, J. P.; Langer, R. Prevascularization of Porous Biodegradable Polymers. *Biotechnol Bioeng* **1993,** *42* (6), 716-723.
[69] Agrawal, C. M.; Ray, R. B. Biodegradable polymeric scaffolds for musculoskeletal tissue engineering. *J Biomed Mater Res* **2001,** *55* (2), 141-150.
[70] Oh, S. H.; Park, I. K.; Kim, J. M.; Lee, J. H. In vitro and in vivo characteristics of PCL scaffolds with pore size gradient fabricated by a centrifugation method. *Biomaterials* **2007,** *28* (9), 1664-1671.
[71] Zeltinger, J.; Sherwood, J. K.; Graham, D. A.; Mueller, R.; Griffith, L. G. Effect of pore size and void fraction on cellular adhesion, proliferation, and matrix deposition. *Tissue Eng* **2001,** *7* (5), 557-572.
[72] Vogel, V. Mechanotransduction involving multimodular proteins: Converting force into biochemical signals. *Annu Rev Bioph Biom* **2006,** *35*, 459-488.
[73] Vogel, V.; Sheetz, M. P. Cell fate regulation by coupling mechanical cycles to biochemical signaling pathways. *Curr Opin Cell Biol* **2009,** *21* (1), 38-46.
[74] Janmey, P. A.; Winer, J. P.; Weisel, J. W. Fibrin gels and their clinical and bioengineering applications. *J R Soc Interface* **2009,** *6* (30), 1-10.
[75] Engler, A. J.; Sen, S.; Sweeney, H. L.; Discher, D. E. Matrix elasticity directs stem cell lineage specification. *Cell* **2006,** *126* (4), 677-689.
[76] Liu, X. H.; Ma, P. X. Polymeric scaffolds for bone tissue engineering. *Ann Biomed Eng* **2004,** *32* (3), 477-486.
[77] Shevchenko, R. V.; James, S. L.; James, S. E. A review of tissue-engineered skin bioconstructs available for skin reconstruction. *J R Soc Interface* **2010,** *7* (43), 229-258.
[78] Langer, R.; Tirrell, D. A. Designing materials for biology and medicine. *Nature* **2004,** *428* (6982), 487-492.
[79] Deville, S. Freeze-Casting of Porous Biomaterials: Structure, Properties and Opportunities. *Materials* **2010,** *3* (3), 1913-1927.
[80] Hacker, M.; Tessmar, J.; Neubauer, M.; Blaimer, A.; Blunk, T.; Gopferich, A.; Schulz, M. B. Towards biomimetic scaffolds: Anhydrous scaffold fabrication from biodegradable amine-reactive diblock copolymers. *Biomaterials* **2003,** *24* (24), 4459-4473.
[81] Nazarov, R.; Jin, H. J.; Kaplan, D. L. Porous 3-D scaffolds from regenerated silk fibroin. *Biomacromolecules* **2004,** *5* (3), 718-726.
[82] Lv, Q.; Feng, Q. L. Preparation of 3-D regenerated fibroin scaffolds with freeze drying method and freeze drying/foaming technique. *Journal of Materials Science-Materials in Medicine* **2006,** *17* (12), 1349-1356.
[83] Oliveira, A. L.; Sun, L.; Kim, H. J.; Hu, X.; Rice, W.; Kluge, J.; Reis, R. L.; Kaplan, D. L. Aligned silk-based 3-D architectures for contact guidance in tissue engineering. *Acta Biomater* **2012,** *8* (4), 1530-1542.
[84] Maquet, V.; Blacher, S.; Pirard, R.; Pirard, J. P.; Jerome, R. Characterization of porous polylactide foams by image analysis and impedance spectroscopy. *Langmuir* **2000,** *16* (26), 10463-10470.

[85] Kim, U. J.; Park, J.; Kim, H. J.; Wada, M.; Kaplan, D. L. Three-dimensional aqueous-derived biomaterial scaffolds from silk fibroin. *Biomaterials* **2005,** *26* (15), 2775-2785.
[86] Rajkhowa, R.; Gil, E. S.; Kluge, J.; Numata, K.; Wang, L. J.; Wang, X. D.; Kaplan, D. L. Reinforcing Silk Scaffolds with Silk Particles. *Macromol Biosci* **2010,** *10* (6), 599-611.
[87] Griffith, L. G.; Naughton, G. Tissue engineering - Current challenges and expanding opportunities. *Science* **2002,** *295*, 1009-1014.
[88] Yao, D. Y.; Dong, S.; Lu, Q.; Hu, X.; Kaplan, D. L.; Zhang, B. B.; Zhu, H. S. Salt-Leached Silk Scaffolds with Tunable Mechanical Properties. *Biomacromolecules* **2012,** *13* (11), 3723-3729.
[89] Nam, Y. S.; Yoon, J. J.; Park, T. G. A novel fabrication method of macroporous biodegradable polymer scaffolds using gas foaming salt as a porogen additive. *J Biomed Mater Res* **2000,** *53* (1), 1-7.
[90] Mooney, D. J.; Baldwin, D. F.; Suh, N. P.; Vacanti, L. P.; Langer, R. Novel approach to fabricate porous sponges of poly(D,L-lactic-co-glycolic acid) without the use of organic solvents. *Biomaterials* **1996,** *17* (14), 1417-1422.
[91] Ikada, Y., *Tissue Engineering: Fundamentals and Applications*. Elsevier Ltd: Oxford UK, 2006; Vol. 1.
[92] Wichterle, O.; Lim, D. Hydrophilic Gels for Biological Use. *Nature* **1960,** *185* (4706), 117-118.
[93] Lim, F.; Sun, A. M. Microencapsulated Islets as Bioartificial Endocrine Pancreas. *Science* **1980,** *210* (4472), 908-910.
[94] Buenger, D.; Topuz, F.; Groll, J. Hydrogels in sensing applications. *Prog Polym Sci* **2012,** *37* (12), 1678-1719.
[95] Rammensee, S.; Huemmerich, D.; Hermanson, K. D.; Scheibel, T.; Bausch, A. R. Rheological characterization of hydrogels formed by recombinantly produced spider silk. *Appl Phys a-Mater* **2006,** *82* (2), 261-264.
[96] Yan, H.; Saiani, A.; Gough, J. E.; Miller, A. F. Thermoreversible protein hydrogel as cell scaffold. *Biomacromolecules* **2006,** *7* (10), 2776-2782.
[97] Hu, X.; Kaplan, D.; Cebe, P. Determining beta-sheet crystallinity in fibrous proteins by thermal analysis and infrared spectroscopy. *Macromolecules* **2006,** *39* (18), 6161-6170.
[98] Drury, J. L.; Mooney, D. J. Hydrogels for tissue engineering: scaffold design variables and applications. *Biomaterials* **2003,** *24* (24), 4337-4351.
[99] Armentano, I.; Dottori, M.; Fortunati, E.; Mattioli, S.; Kenny, J. M. Biodegradable polymer matrix nanocomposites for tissue engineering: A review. *Polym Degrad Stabil* **2010,** *95* (11), 2126-2146.
[100] Kamath, K. R.; Park, K. Biodegradable Hydrogels in Drug-Delivery. *Adv Drug Deliver Rev* **1993,** *11* (1-2), 59-84.
[101] Peppas, N. A.; Hilt, J. Z.; Khademhosseini, A.; Langer, R. Hydrogels in biology and medicine: From molecular principles to bionanotechnology. *Advanced Materials* **2006,** *18* (11), 1345-1360.
[102] Hoffman, A. S. Hydrogels for biomedical applications. *Adv Drug Deliver Rev* **2002,** *54* (1), 3-12.
[103] Draget, K. I.; SkjakBraek, G.; Smidsrod, O. Alginate based new materials. *Int J Biol Macromol* **1997,** *21* (1-2), 47-55.
[104] Berl, V.; Huc, I.; Khoury, R. G.; Krische, M. J.; Lehn, J. M. Interconversion of single and double helices formed from synthetic molecular strands. *Nature* **2000,** *407* (6805), 720-723.
[105] Schneider, H.-J., *Supramolecular Systems in Biomedical Fields*. Royal Society of Chemistry: Cambridge UK, 2013; Vol. 13.
[106] Gazit, E. Self-assembled peptide nanostructures: the design of molecular building blocks and their technological utilization. *Chem Soc Rev* **2007,** *36* (8), 1263-1269.
[107] Bouchard, M.; Zurdo, J.; Nettleton, E. J.; Dobson, C. M.; Robinson, C. V. Formation of insulin amyloid fibrils followed by FTIR simultaneously with CD and electron microscopy. *Protein Sci* **2000,** *9* (10), 1960-1967.

[108] Serpell, L. C. Alzheimer's amyloid fibrils: structure and assembly. *Bba-Mol Basis Dis* **2000,** *1502* (1), 16-30.
[109] Caughey, B.; Lansbury, P. T. Protofibrils, pores, fibrils, and neurodegeneration: Separating the responsible protein aggregates from the innocent bystanders. *Annu Rev Neurosci* **2003,** *26*, 267-298.
[110] Nelson, R.; Sawaya, M. R.; Balbirnie, M.; Madsen, A. O.; Riekel, C.; Grothe, R.; Eisenberg, D. Structure of the cross-beta spine of amyloid-like fibrils. *Nature* **2005,** *435* (7043), 773-778.
[111] Kenney, J. M.; Knight, D.; Wise, M. J.; Vollrath, F. Amyloidogenic nature of spider silk. *European Journal of Biochemistry* **2002,** *269* (16), 4159-4163.
[112] Vepari, C.; Kaplan, D. L. Silk as a biomaterial. *Prog Polym Sci* **2007,** *32* (8-9), 991-1007.
[113] Kim, U. J.; Park, J. Y.; Li, C. M.; Jin, H. J.; Valluzzi, R.; Kaplan, D. L. Structure and properties of silk hydrogels. *Biomacromolecules* **2004,** *5* (3), 786-792.
[114] Schacht, K.; Scheibel, T. Controlled Hydrogel Formation of a Recombinant Spider Silk Protein. *Biomacromolecules* **2011,** *12*, 2488–2495.
[115] Slotta, U.; Hess, S.; Spiess, K.; Stromer, T.; Serpell, L.; Scheibel, T. Spider silk and amyloid fibrils: A structural comparison. *Macromol Biosci* **2007,** *7* (2), 183-188.
[116] Slotta, U. K.; Rammensee, S.; Gorb, S.; Scheibel, T. An engineered spider silk protein forms microspheres. *Angew Chem Int Edit* **2008,** *47* (24), 4592-4594.
[117] Humenik, M.; Scheibel, T. Self-assembly of nucleic acids, silk and hybrid materials thereof. *J Phys-Condens Mat* **2014,** *26* (50), 1-12.
[118] Humenik, M.; Magdeburg, M.; Scheibel, T. Influence of repeat numbers on self-assembly rates of repetitive recombinant spider silk proteins. *J Struct Biol* **2014,** *186* (3), 431-437.
[119] Cohen, S. I. A.; Vendruscolo, M.; Dobson, C. M.; Knowles, T. P. J. From Macroscopic Measurements to Microscopic Mechanisms of Protein Aggregation. *J Mol Biol* **2012,** *421* (2-3), 160-171.
[120] Morris, A. M.; Watzky, M. A.; Agar, J. N.; Finke, R. G. Fitting neurological protein aggregation kinetic data via a 2-step, Minimal/"Ockham's Razor" model: The Finke-Watzky mechanism of nucleation followed by autocatalytic surface growt. *Biochemistry* **2008,** *47* (8), 2413-2427.
[121] Crick, S. L.; Ruff, K. M.; Garai, K.; Frieden, C.; Pappu, R. V. Unmasking the roles of N- and C-terminal flanking sequences from exon 1 of huntingtin as modulators of polyglutamine aggregation. *P Natl Acad Sci USA* **2013,** *110* (50), 20075-20080.
[122] Hutmacher, D. W. Scaffold design and fabrication technologies for engineering tissues--state of the art and future perspectives. *J Biomater Sci Polym Ed* **2001,** *12* (1), 107-124.
[123] Groll, J.; Boland, T.; Blunk, T.; Burdick, J. A.; Cho, D. W.; Dalton, P. D.; Derby, B.; Forgacs, G.; Li, Q.; Mironov, V. A.; Moroni, L.; Nakamura, M.; Shu, W.; Takeuchi, S.; Vozzi, G.; Woodfield, T. B.; Xu, T.; Yoo, J. J.; Malda, J. Biofabrication: reappraising the definition of an evolving field. *Biofabrication* **2016,** *8* (1), 1-5.
[124] Mironov, V.; Trusk, T.; Kasyanov, V.; Little, S.; Swaja, R.; Markwald, R. Biofabrication: a 21st century manufacturing paradigm. *Biofabrication* **2009,** *1* (2), 1-16.
[125] Guillemot, F.; Mironov, V.; Nakamura, M. Bioprinting is coming of age: report from the International Conference on Bioprinting and Biofabrication in Bordeaux (3B'09). *Biofabrication* **2010,** *2* (1), 1-7.
[126] Onoe, H.; Okitsu, T.; Itou, A.; Kato-Negishi, M.; Gojo, R.; Kiriya, D.; Sato, K.; Miura, S.; Iwanaga, S.; Kuribayashi-Shigetomi, K.; Matsunaga, Y. T.; Shimoyama, Y.; Takeuchi, S. Metre-long cell-laden microfibres exhibit tissue morphologies and functions. *Nat Mater* **2013,** *12* (6), 584-590.
[127] Malda, J.; Visser, J.; Melchels, F. P.; Jüngst, T.; Hennink, W. E.; Dhert, W. J. A.; Groll, J.; Hutmacher, D. W. 25th Anniversary Article: Engineering Hydrogels for Biofabrication. *Adv Mater* **2013,** *25* (36), 5011-5028.

[128] Kim, J. D.; Choi, J. S.; Kim, B. S.; Choi, Y. C.; Cho, Y. W. Piezoelectric inkjet printing of polymers: Stem cell patterning on polymer substrates. *Polymer* **2010,** *51* (10), 2147-2154.
[129] Chang, C. C.; Boland, E. D.; Williams, S. K.; Hoying, J. B. Direct-write bioprinting three-dimensional biohybrid systems for future regenerative therapies. *J Biomed Mater Res B* **2011,** *98B* (1), 160-170.
[130] Guillotin, B.; Souquet, A.; Catros, S.; Duocastella, M.; Pippenger, B.; Bellance, S.; Bareille, R.; Remy, M.; Bordenave, L.; Amedee, J.; Guillemot, F. Laser assisted bioprinting of engineered tissue with high cell density and microscale organization. *Biomaterials* **2010,** *31* (28), 7250-7256.
[131] Murphy, S. V.; Atala, A. 3D bioprinting of tissues and organs. *Nat Biotechnol* **2014,** *32* (8), 773-785.
[132] Guillemot, F.; Souquet, A.; Catros, S.; Guillotin, B.; Lopez, J.; Faucon, M.; Pippenger, B.; Bareille, R.; Remy, M.; Bellance, S.; Chabassier, P.; Fricain, J. C.; Amedee, J. High-throughput laser printing of cells and biomaterials for tissue engineering. *Acta Biomater* **2010,** *6* (7), 2494-2500.
[133] Dababneh, A. B.; Ozbolat, I. T. Bioprinting Technology: A Current State-of-the-Art Review. *J Manuf Sci E-T Asme* **2014,** *136* (6).
[134] Wust, S.; Muller, R.; Hofmann, S. Controlled Positioning of Cells in Biomaterials-Approaches Towards 3D Tissue Printing. *J Funct Biomater* **2011,** *2* (3), 119-154.
[135] Campbell, P. G.; Miller, E. D.; Fisher, G. W.; Walker, L. M.; Weiss, L. E. Engineered spatial patterns of FGF-2 immobilized on fibrin direct cell organization. *Biomaterials* **2005,** *26* (33), 6762-6770.
[136] Khalil, S.; Nam, J.; Sun, W. Multi-nozzle deposition for construction of 3D biopolymer tissue scaffolds. *Rapid Prototyping J* **2005,** *11* (1), 9-17.
[137] Smith, C. M.; Stone, A. L.; Parkhill, R. L.; Stewart, R. L.; Simpkins, M. W.; Kachurin, A. M.; Warren, W. L.; Williams, S. K. Three-dimensional bioassembly tool for generating viable tissue-engineered constructs. *Tissue Eng* **2004,** *10* (9-10), 1566-1576.
[138] Sobral, J. M.; Caridade, S. G.; Sousa, R. A.; Mano, J. F.; Reis, R. L. Three-dimensional plotted scaffolds with controlled pore size gradients: Effect of scaffold geometry on mechanical performance and cell seeding efficiency. *Acta Biomater* **2011,** *7* (3), 1009-1018.
[139] Wilson, W. C.; Boland, T. Cell and organ printing 1: Protein and cell printers. *Anat Rec Part A* **2003,** *272A* (2), 491-496.
[140] Calvert, P. Inkjet printing for materials and devices. *Chem Mater* **2001,** *13* (10), 3299-3305.
[141] Boland, T.; Xu, T.; Damon, B.; Cui, X. Application of inkjet printing to tissue engineering. *Biotechnol J* **2006,** *1* (9), 910-917.
[142] Xu, T.; Jin, J.; Gregory, C.; Hickman, J. J.; Boland, T. Inkjet printing of viable mammalian cells. *Biomaterials* **2005,** *26* (1), 93-99.
[143] Derby, B. Inkjet Printing of Functional and Structural Materials: Fluid Property Requirements, Feature Stability, and Resolution. *Annu Rev Mater Res* **2010,** *40*, 395-414.
[144] Saunders, R. E.; Derby, B. Inkjet printing biomaterials for tissue engineering: bioprinting. *Int Mater Rev* **2014,** *59* (8), 430-448.
[145] Martin, G. D.; Hoath, S. D.; Hutchings, I. M. Inkjet printing - the physics of manipulating liquid jets and drops. *Journal of Physics: Conference Series* **2008,** *105*, 1-14.
[146] Barron, J. A.; Krizman, D. B.; Ringeisen, B. R. Laser printing of single cells: Statistical analysis, cell viability, and stress. *Ann Biomed Eng* **2005,** *33* (2), 121-130.
[147] Gruene, M.; Pflaum, M.; Hess, C.; Diamantouros, S.; Schlie, S.; Deiwick, A.; Koch, L.; Wilhelmi, M.; Jockenhoevel, S.; Haverich, A.; Chichkov, B. Laser Printing of Three-Dimensional Multicellular Arrays for Studies of Cell-Cell and Cell-Environment Interactions. *Tissue Eng Part C-Me* **2011,** *17* (10), 973-982.

[148] Koch, L.; Deiwick, A.; Schlie, S.; Michael, S.; Gruene, M.; Coger, V.; Zychlinski, D.; Schambach, A.; Reimers, K.; Vogt, P. M.; Chichkov, B. Skin tissue generation by laser cell printing. *Biotechnol Bioeng* **2012,** *109* (7), 1855-1863.
[149] Michael, S.; Sorg, H.; Peck, C. T.; Koch, L.; Deiwick, A.; Chichkov, B.; Vogt, P. M.; Reimers, K. Tissue Engineered Skin Substitutes Created by Laser-Assisted Bioprinting Form Skin-Like Structures in the Dorsal Skin Fold Chamber in Mice. *PLoS One* **2013,** *8* (3), 1-12.
[150] Nahmias, Y.; Schwartz, R. E.; Verfaillie, C. M.; Odde, D. J. Laser-guided direct writing for three-dimensional tissue engineering. *Biotechnol Bioeng* **2005,** *92* (2), 129-136.
[151] Duocastella, M.; Fernandez-Pradas, J. M.; Serra, P.; Morenza, J. L. Jet formation in the laser forward transfer of liquids. *Appl Phys a-Mater* **2008,** *93* (2), 453-456.
[152] Lin, Y. F.; Huang, Y.; Chrisey, D. B. Droplet formation in matrix-assisted pulsed-laser evaporation direct writing of glycerol-water solution. *J Appl Phys* **2009,** *105* (9), 1-6.
[153] Mezel, C.; Hallo, L.; Souquet, A.; Breil, J.; Hebert, D.; Guillemot, F. Self-consistent modeling of jet formation process in the nanosecond laser pulse regime. *Phys Plasmas* **2009,** *16* (12), 1-12.
[154] Young, D.; Auyeung, R. C. Y.; Pique, A.; Chrisey, D. B.; Dlott, D. D. Plume and jetting regimes in a laser based forward transfer process as observed by time-resolved optical microscopy. *Appl Surf Sci* **2002,** *197*, 181-187.
[155] DeSimone, E.; Schacht, K.; Jüngst, T.; Groll, J.; Scheibel, T. Biofabrication of 3D Constructs: Related Techniques and Silk Proteins as Bioinks. *Pure and Applied Chemistry* **2015,** *87* (8), 737-749.
[156] Loh, Q. L.; Choong, C. Three-Dimensional Scaffolds for Tissue Engineering Applications: Role of Porosity and Pore Size. *Tissue Eng Pt B-Rev* **2013,** *19* (6), 485-502.
[157] Das, S.; Pati, F.; Choi, Y.-J.; Rijal, G.; Shim, J.-H.; Kim, S. W.; Ray, A. R.; Cho, D.-W.; Ghosh, S. Bioprintable, cell-laden silk fibroin-gelatin hydrogel supporting multilineage differentiation of stem cells for fabrication of 3D tissue constructs. *Acta Biomater* **2014,** *11*, 233-246.
[158] Yu, L.; Ding, J. D. Injectable hydrogels as unique biomedical materials. *Chem Soc Rev* **2008,** *37* (8), 1473-1481.
[159] Awad, H. A.; Wickham, M. Q.; Leddy, H. A.; Gimble, J. M.; Guilak, F. Chondrogenic differentiation of adipose-derived adult stem cells in agarose, alginate, and gelatin scaffolds. *Biomaterials* **2004,** *25* (16), 3211-3222.
[160] Tan, H. P.; Gong, Y. H.; Lao, L. H.; Mao, Z. W.; Gao, C. Y. Gelatin/chitosan/hyaluronan ternary complex scaffold containing basic fibroblast growth factor for cartilage tissue engineering. *Journal of Materials Science-Materials in Medicine* **2007,** *18* (10), 1961-1968.
[161] Billiet, T.; Vandenhaute, M.; Schelfhout, J.; Van Vlierberghe, S.; Dubruel, P. A review of trends and limitations in hydrogel-rapid prototyping for tissue engineering. *Biomaterials* **2012,** *33* (26), 6020-6041.
[162] Maher, P. S.; Keatch, R. P.; Donnelly, K.; Mackay, R. E.; Paxton, J. Z. Construction of 3D biological matrices using rapid prototyping technology. *Rapid Prototyping J* **2009,** *15* (3), 204-210.
[163] Campos, D. F. D.; Blaeser, A.; Weber, M.; Jakel, J.; Neuss, S.; Jahnen-Dechent, W.; Fischer, H. Three-dimensional printing of stem cell-laden hydrogels submerged in a hydrophobic high-density fluid. *Biofabrication* **2013,** *5* (1), 1-11.
[164] Fedorovich, N. E.; Dewijn, J. R.; Verbout, A. J.; Alblas, J.; Dhert, W. J. A. Three-dimensional fiber deposition of cell-laden, viable, patterned constructs for bone tissue printing. *Tissue Eng Pt A* **2008,** *14* (1), 127-133.
[165] Lee, K. Y.; Mooney, D. J. Alginate: Properties and biomedical applications. *Prog Polym Sci* **2012,** *37* (1), 106-126.
[166] Landers, R.; Hubner, U.; Schmelzeisen, R.; Mulhaupt, R. Rapid prototyping of scaffolds derived from thermoreversible hydrogels and tailored for applications in tissue engineering. *Biomaterials* **2002,** *23* (23), 4437-4447.

[167] Mauck, R. L.; Soltz, M. A.; Wang, C. C. B.; Wong, D. D.; Chao, P. H. G.; Valhmu, W. B.; Hung, C. T.; Ateshian, G. A. Functional tissue engineering of articular cartilage through dynamic loading of chondrocyte-seeded agarose gels. *J Biomech Eng-T Asme* **2000,** *122* (3), 252-260.

[168] Li, Y. L.; Rodrigues, J.; Tomas, H. Injectable and biodegradable hydrogels: gelation, biodegradation and biomedical applications. *Chem Soc Rev* **2012,** *41* (6), 2193-2221.

[169] Jia, J.; Richards, D. J.; Pollard, S.; Tan, Y.; Rodriguez, J.; Visconti, R. P.; Trusk, T. C.; Yost, M. J.; Yao, H.; Markwald, R. R.; Mei, Y. Engineering alginate as bioink for bioprinting. *Acta Biomater* **2014,** *10* (10), 4323-4331.

[170] Fedorovich, N. E.; Schuurman, W.; Wijnberg, H. M.; Prins, H. J.; van Weeren, P. R.; Malda, J.; Alblas, J.; Dhert, W. J. A. Biofabrication of Osteochondral Tissue Equivalents by Printing Topologically Defined, Cell-Laden Hydrogel Scaffolds. *Tissue Engineering, Part C: Methods* **2012,** *18* (1), 33-44.

[171] Zhao, Y.; Yao, R.; Ouyang, L. L.; Ding, H. X.; Zhang, T.; Zhang, K. T.; Cheng, S. J.; Sun, W. Three-dimensional printing of Hela cells for cervical tumor model in vitro. *Biofabrication* **2014,** *6* (3), 1-10.

[172] Mano, J. F.; Silva, G. A.; Azevedo, H. S.; Malafaya, P. B.; Sousa, R. A.; Silva, S. S.; Boesel, L. F.; Oliveira, J. M.; Santos, T. C.; Marques, A. P.; Neves, N. M.; Reis, R. L. Natural origin biodegradable systems in tissue engineering and regenerative medicine: present status and some moving trends. *J R Soc Interface* **2007,** *4* (17), 999-1030.

[173] Czaja, W. K.; Young, D. J.; Kawecki, M.; Brown, R. M. The future prospects of microbial cellulose in biomedical applications. *Biomacromolecules* **2007,** *8* (1), 1-12.

[174] Ferris, C. J.; Gilmore, K. J.; Beirne, S.; McCallum, D.; Wallace, G. G.; Panhuis, M. I. H. Bio-ink for on-demand printing of living cells. *Biomater Sci-Uk* **2013,** *1* (2), 224-230.

[175] Du, H. W.; Hamilton, P.; Reilly, M.; Ravi, N. Injectable in situ Physically and Chemically Crosslinkable Gellan Hydrogel. *Macromol Biosci* **2012,** *12* (7), 952-961.

[176] Oliveira, J. T.; Martins, L.; Picciochi, R.; Malafaya, I. B.; Sousa, R. A.; Neves, N. M.; Mano, J. F.; Reis, R. L. Gellan gum: A new biomaterial for cartilage tissue engineering applications. *Journal of Biomedical Materials Research Part A* **2009,** *93A* (3), 852-863.

[177] Matricardi, P.; Cencetti, C.; Ria, R.; Alhaique, F.; Coviello, T. Preparation and Characterization of Novel Gellan Gum Hydrogels Suitable for Modified Drug Release. *Molecules* **2009,** *14* (9), 3376-3391.

[178] Schuurman, W.; Levett, P. A.; Pot, M. W.; van Weeren, P. R.; Dhert, W. J. A.; Hutmacher, D. W.; Melchels, F. P. W.; Klein, T. J.; Malda, J. Gelatin-Methacrylamide Hydrogels as Potential Biomaterials for Fabrication of Tissue-Engineered Cartilage Constructs. *Macromol Biosci* **2013,** *13* (5), 551-561.

[179] Skardal, A.; Zhang, J. X.; Prestwich, G. D. Bioprinting vessel-like constructs using hyaluronan hydrogels crosslinked with tetrahedral polyethylene glycol tetracrylates. *Biomaterials* **2010,** *31* (24), 6173-6181.

[180] Zhang, T.; Yan, Y. N.; Wang, X. H.; Xiong, Z.; Lin, F.; Wu, R. D.; Zhang, R. J. Three-dimensional gelatin and gelatin/hyaluronan hydrogel structures for traumatic brain injury. *Journal of bioactive and compatible polymers* **2007,** *22* (1), 19-29.

[181] Tan, H. P.; Marra, K. G. Injectable, Biodegradable Hydrogels for Tissue Engineering Applications. *Materials* **2010,** *3* (3), 1746-1767.

[182] Tan, H. P.; Rubin, J. P.; Marra, K. G. Injectable in situ forming biodegradable chitosan-hyaluronic acid based hydrogels for adipose tissue regeneration. *Organogenesis* **2010,** *6* (3), 173-180.

[183] Burdick, J. A.; Prestwich, G. D. Hyaluronic Acid Hydrogels for Biomedical Applications. *Advanced Materials* **2011,** *23* (12), H41-H56.

[184] Xu, T.; Gregory, C. A.; Molnar, P.; Cui, X.; Jalota, S.; Bhaduri, S. B.; Boland, T. Viability and electrophysiology of neural cell structures generated by the inkjet printing method. *Biomaterials* **2006,** *27* (19), 3580-3588.

[185] Hoch, E.; Hirth, T.; Tovar, G. E. M.; Borchers, K. Chemical tailoring of gelatin to adjust its chemical and physical properties for functional bioprinting. *J Mater Chem B* **2013,** *1* (41), 5675-5685.
[186] Duan, B.; Hockaday, L. A.; Kang, K. H.; Butcher, J. T. 3D Bioprinting of heterogeneous aortic valve conduits with alginate/gelatin hydrogels. *Journal of Biomedical Materials Research Part A* **2013,** *101* (5), 1255-1264.
[187] Wust, S.; Godla, M. E.; Muller, R.; Hofmann, S. Tunable hydrogel composite with two-step processing in combination with innovative hardware upgrade for cell-based three-dimensional bioprinting. *Acta Biomater* **2014,** *10* (2), 630-640.
[188] Cheng, E. J.; Li, Y. L.; Yang, Z. Q.; Deng, Z. X.; Liu, D. S. DNA-SWNT hybrid hydrogel. *Chem Commun* **2011,** *47* (19), 5545-5547.
[189] Hersel, U.; Dahmen, C.; Kessler, H. RGD modified polymers: biomaterials for stimulated cell adhesion and beyond. *Biomaterials* **2003,** *24* (24), 4385-4415.
[190] Lee, K. Y.; Mooney, D. J. Hydrogels for tissue engineering. *Chem Rev* **2001,** *101* (7), 1869-1879.
[191] Parenteau-Bareil, R.; Gauvin, R.; Berthod, F. Collagen-Based Biomaterials for Tissue Engineering Applications. *Materials* **2010,** *3* (3), 1863-1887.
[192] Shim, J. H.; Kim, J. Y.; Park, M.; Park, J.; Cho, D. W. Development of a hybrid scaffold with synthetic biomaterials and hydrogel using solid freeform fabrication technology. *Biofabrication* **2011,** *3* (3), 1-9.
[193] Kundu, B.; Rajkhowa, R.; Kundu, S. C.; Wang, X. G. Silk fibroin biomaterials for tissue regenerations. *Adv Drug Deliver Rev* **2013,** *65* (4), 457-470.
[194] Das, S.; Pati, F.; Chameettachal, S.; Pahwa, S.; Ray, A. R.; Dhara, S.; Ghosh, S. Enhanced Redifferentiation of Chondrocytes on Microperiodic Silk/Gelatin Scaffolds: Toward Tailor-Made Tissue Engineering. *Biomacromolecules* **2013,** *14* (2), 311-321.
[195] Suntivich, R.; Drachuk, I.; Calabrese, R.; Kaplan, D. L.; Tsukruk, V. V. Inkjet Printing of Silk Nest Arrays for Cell Hosting. *Biomacromolecules* **2014,** *15* (4), 1428-1435.
[196] Snyder, J. E.; Hamid, Q.; Wang, C.; Chang, R.; Emami, K.; Wu, H.; Sun, W. Bioprinting cell-laden matrigel for radioprotection study of liver by pro-drug conversion in a dual-tissue microfluidic chip. *Biofabrication* **2011,** *3* (3), 1-9.
[197] Shoichet, M. S.; Li, R. H.; White, M. L.; Winn, S. R. Stability of hydrogels used in cell encapsulation: An in vitro comparison of alginate and agarose. *Biotechnol Bioeng* **1996,** *50* (4), 374-381.
[198] Zehnder, T.; Sarker, B.; Boccaccini, A. R.; Detsch, R. Evaluation of an alginate-gelatine crosslinked hydrogel for bioplotting. *Biofabrication* **2015,** *7* (2), 1-12.
[199] Arnott, S.; Fulmer, A.; Scott, W. E.; Dea, I. C. M.; Moorhouse, R.; Rees, D. A. Agarose Double Helix and Its Function in Agarose-Gel Structure. *J Mol Biol* **1974,** *90* (2), 269-284.
[200] Velasco, D.; Tumarkin, E.; Kumacheva, E. Microfluidic Encapsulation of Cells in Polymer Microgels. *Small* **2012,** *8* (11), 1633-1642.
[201] Normand, V.; Lootens, D. L.; Amici, E.; Plucknett, K. P.; Aymard, P. New insight into agarose gel mechanical properties. *Biomacromolecules* **2000,** *1* (4), 730-738.
[202] Draget, K. I.; Stokke, B. T.; Yuguchi, Y.; Urakawa, H.; Kajiwara, K. Small-angle x-ray scattering and rheological characterization of alginate gels. 3. Alginic acid gels. *Biomacromolecules* **2003,** *4* (6), 1661-1668.
[203] Jansson, P. E.; Lindberg, B.; Sandford, P. A. Structural Studies of Gellan Gum, an Extracellular Polysaccharide Elaborated by Pseudomonas-Elodea. *Carbohyd Res* **1983,** *124* (1), 135-139.
[204] Miyoshi, E.; Takaya, T.; Nishinari, K. Gel-Sol Transition in Gellan Gum Solutions .1. Rheological Studies on the Effects of Salts. *Food Hydrocolloid* **1994,** *8* (6), 505-527.
[205] Thiele, J.; Ma, Y. J.; Bruekers, S. M. C.; Ma, S. H.; Huck, W. T. S. 25th Anniversary Article: Designer Hydrogels for Cell Cultures: A Materials Selection Guide. *Advanced Materials* **2014,** *26* (1), 125-148.
[206] Kadler, K. E.; Baldock, C.; Bella, J.; Boot-Handford, R. P. Collagens at a glance. *J Cell Sci* **2007,** *120* (12), 1955-1958.

[207] Gomes, S.; Leonor, I. B.; Mano, J. F.; Reis, R. L.; Kaplan, D. L. Natural and genetically engineered proteins for tissue engineering. *Prog Polym Sci* **2012,** *37* (1), 1-17.
[208] Sheu, M. T.; Huang, J. C.; Yeh, G. C.; Ho, H. O. Characterization of collagen gel solutions and collagen matrices for cell culture. *Biomaterials* **2001,** *22* (13), 1713-1719.
[209] Tan, H. P.; Huang, D. J.; Lao, L. H.; Gao, C. Y. RGD Modified PLGA/Gelatin Microspheres as Microcarriers for Chondrocyte Delivery. *J Biomed Mater Res B* **2009,** *91B* (1), 228-238.
[210] Choi, Y. S.; Hong, S. R.; Lee, Y. M.; Song, K. W.; Park, M. H.; Nam, Y. S. Study on gelatin-containing artificial skin: I. Preparation and characteristics of novel gelatin-alginate sponge. *Biomaterials* **1999,** *20* (5), 409-417.
[211] Young, S.; Wong, M.; Tabata, Y.; Mikos, A. G. Gelatin as a delivery vehicle for the controlled release of bioactive molecules. *J Control Release* **2005,** *109* (1-3), 256-274.
[212] Sisson, K.; Zhang, C.; Farach-Carson, M. C.; Chase, D. B.; Rabolt, J. F. Evaluation of Cross-Linking Methods for Electrospun Gelatin on Cell Growth and Viability. *Biomacromolecules* **2009,** *10* (7), 1675-1680.
[213] Kirchmajer, D. M.; Panhuis, M. I. H. Robust biopolymer based ionic-covalent entanglement hydrogels with reversible mechanical behaviour. *J Mater Chem B* **2014,** *2* (29), 4694-4702.
[214] Smith, G. F. Fibrinogen-Fibrin Conversion - Mechanism of Fibrin-Polymer Formation in Solution. *Biochem J* **1980,** *185* (1), 1-11.
[215] Zhao, W.; Jin, X.; Cong, Y.; Liu, Y. Y.; Fu, J. Degradable natural polymer hydrogels for articular cartilage tissue engineering. *J Chem Technol Biot* **2013,** *88* (3), 327-339.
[216] Drinnan, C. T.; Zhang, G.; Alexander, M. A.; Pulido, A. S.; Suggs, L. J. Multimodal release of transforming growth factor-beta 1 and the BB isoform of platelet derived growth factor from PEGylated fibrin gels. *J Control Release* **2010,** *147* (2), 180-186.
[217] Lee, Y. B.; Polio, S.; Lee, W.; Dai, G. H.; Menon, L.; Carroll, R. S.; Yoo, S. S. Bio-printing of collagen and VEGF-releasing fibrin gel scaffolds for neural stem cell culture. *Exp Neurol* **2010,** *223* (2), 645-652.
[218] Eyrich, D.; Brandl, F.; Appel, B.; Wiese, H.; Maier, G.; Wenzel, M.; Staudenmaier, R.; Goepferich, A.; Blunk, T. Long-term stable fibrin gels for cartilage engineering. *Biomaterials* **2007,** *28* (1), 55-65.
[219] Wang, X. H.; Yan, Y. N.; Zhang, R. J. Recent Trends and Challenges in Complex Organ Manufacturing. *Tissue Eng Pt B-Rev* **2010,** *16* (2), 189-197.
[220] Xu, W.; Wang, X.; Yan, Y.; Zheng, W.; Xiong, Z.; Lin, F.; Wu, R.; Zhang, R. Rapid Prototyping Three-Dimensional Cell/Gelatin/Fibrinogen Constructs for Medical Regeneration. *Journal of bioactive and compatible polymers* **2007,** *22*, 363-377.
[221] Altman, G. H.; Diaz, F.; Jakuba, C.; Calabro, T.; Horan, R. L.; Chen, J. S.; Lu, H.; Richmond, J.; Kaplan, D. L. Silk-based biomaterials. *Biomaterials* **2003,** *24* (3), 401-416.
[222] Romano, N. H.; Sengupta, D.; Chung, C.; Heilshorn, S. C. Protein-engineered biomaterials: Nanoscale mimics of the extracellular matrix. *Bba-Gen Subjects* **2011,** *1810* (3), 339-349.
[223] Meyer, D. E.; Chilkoti, A. Genetically encoded synthesis of protein-based polymers with precisely specified molecular weight and sequence by recursive directional ligation: Examples from the elastin-like polypeptide system. *Biomacromolecules* **2002,** *3* (2), 357-367.
[224] Arul, V.; Gopinath, D.; Gomathi, K.; Jayakumar, R. Biotinylated GHK peptide incorporated collagenous matrix: A novel biomaterial for dermal wound healing in rats. *J Biomed Mater Res B Appl Biomater* **2005,** *73* (2), 383-391.
[225] Jun, H. W.; West, J. L. Modification of polyurethaneurea with PEG and YIGSR peptide to enhance endothelialization without platelet adhesion. *J Biomed Mater Res B Appl Biomater* **2005,** *72* (1), 131-139.

[226] Matsuda, A.; Kobayashi, H.; Itoh, S.; Kataoka, K.; Tanaka, J. Immobilization of laminin peptide in molecularly aligned chitosan by covalent bonding. *Biomaterials* **2005,** *26* (15), 2273-2279.
[227] Wong, J. Y.; Weng, Z. P.; Moll, S.; Kim, S.; Brown, C. T. Identification and validation of a novel cell-recognition site (KNEED) on the 8th type III domain of fibronectin. *Biomaterials* **2002,** *23* (18), 3865-3870.
[228] Koide, T. Triple helical collagen-like peptides: Engineering and applications in matrix biology. *Connect Tissue Res* **2005,** *46* (3), 131-141.
[229] Liu, W.; Merrett, K.; Griffith, M.; Fagerholm, P.; Dravida, S.; Heyne, B.; Scaiano, J. C.; Watsky, M. A.; Shinozaki, N.; Lagali, N.; Munger, R.; Li, F. Recombinant human collagen for tissue engineered corneal substitutes. *Biomaterials* **2008,** *29* (9), 1147-1158.
[230] Werkmeister, J. A.; Ramshaw, J. A. M. Recombinant protein scaffolds for tissue engineering. *Biomed Mater* **2012,** *7* (1), 1-29.
[231] Betre, H.; Ong, S. R.; Guilak, F.; Chilkoti, A.; Fermor, B.; Setton, L. A. Chondrocytic differentiation of human adipose-derived adult stem cells in elastin-like polypeptide. *Biomaterials* **2006,** *27* (1), 91-99.
[232] Chilkoti, A.; Christensen, T.; MacKay, J. A. Stimulus responsive elastin biopolymers: applications in medicine and biotechnology. *Curr Opin Chem Biol* **2006,** *10* (6), 652-657.
[233] Urry, D. W. Physical chemistry of biological free energy transduction as demonstrated by elastic protein-based polymers. *J Phys Chem B* **1997,** *101* (51), 11007-11028.
[234] McHale, M. K.; Setton, L. A.; Chilkoti, A. Synthesis and in vitro evaluation of enzymatically cross-linked elastin-like polypeptide gels for cartilaginous tissue repair. *Tissue Eng* **2005,** *11* (11-12), 1768-1779.
[235] Testera, A. M.; Girotti, A.; de Torre, I. G.; Quintanilla, L.; Santos, M.; Alonso, M.; Rodriguez-Cabello, J. C. Biocompatible elastin-like click gels: design, synthesis and characterization. *J Mater Sci: Mater Med* **2015,** *26* (2), 1-13.
[236] Li, L.; Kiick, K. L. Resilin-Based Materials for Biomedical Applications. *Acs Macro Lett* **2013,** *2* (8), 635-640.
[237] Li, L. Q.; Tong, Z. X.; Jia, X. Q.; Kiick, K. L. Resilin-like polypeptide hydrogels engineered for versatile biological function. *Soft Matter* **2013,** *9* (3), 665-673.
[238] McGann, C. L.; Levenson, E. A.; Kiick, K. L. Resilin-Based Hybrid Hydrogels for Cardiovascular Tissue Engineering. *Macromol Chem Phys* **2013,** *214* (2), 203-213.
[239] Ramshaw, J. A.; Werkmeister, J. A.; Dumsday, G. J. Bioengineered collagens: emerging directions for biomedical materials. *Bioengineered* **2014,** *5* (4), 227-233.
[240] Frank, S.; Kammerer, R. A.; Mechling, D.; Schulthess, T.; Landwehr, R.; Bann, J.; Guo, Y.; Lustig, A.; Bachinger, H. P.; Engel, J. Stabilization of short collagen-like triple helices by protein engineering. *J Mol Biol* **2001,** *308* (5), 1081-1089.
[241] Olsen, D.; Yang, C. L.; Bodo, M.; Chang, R.; Leigh, S.; Baez, J.; Carmichael, D.; Perala, M.; Hamalainen, E. R.; Jarvinen, M.; Polarek, J. Recombinant collagen and gelatin for drug delivery. *Adv Drug Deliver Rev* **2003,** *55* (12), 1547-1567.
[242] Myllyharju, J.; Nokelainen, M.; Vuorela, A.; Kivirikko, K. I. Expression of recombinant human type I-III collagens in the yeast Pichia pastoris. *Biochem Soc T* **2000,** *28*, 353-357.
[243] Li, B.; Alonso, D. O. V.; Daggett, V. The molecular basis for the inverse temperature transition of elastin. *J Mol Biol* **2001,** *305* (3), 581-592.
[244] Meyer, D. E.; Chilkoti, A. Quantification of the effects of chain length and concentration on the thermal behavior of elastin-like polypeptides. *Biomacromolecules* **2004,** *5* (3), 846-851.
[245] Urry, D. W. Elastic molecular machines in metabolism and soft-tissue restoration. *Trends Biotechnol* **1999,** *17* (6), 249-257.
[246] Urry, D. W.; Pattanaik, A.; Xu, J.; Woods, T. C.; McPherson, D. T.; Parker, T. M. Elastic protein-based polymers in soft tissue augmentation and generation. *J Biomater Sci Polym Ed* **1998,** *9* (10), 1015-1048.

[247] Betre, H.; Setton, L. A.; Meyer, D. E.; Chilkoti, A. Characterization of a genetically engineered elastin-like polypeptide for cartilaginous tissue repair. *Biomacromolecules* **2002,** *3* (5), 910-916.
[248] Bracalello, A.; Santopietro, V.; Vassalli, M.; Marletta, G.; Del Gaudio, R.; Bochicchio, B.; Pepe, A. Design and Production of a Chimeric Resilin-, Elastin-, and Collagen-Like Engineered Polypeptide. *Biomacromolecules* **2011,** *12* (8), 2957-2965.
[249] Craig, C. L. Evolution of arthropod silks. *Annu Rev Entomol* **1997,** *42*, 231-267.
[250] Gerritsen, V. B. The tiptoe of an airbus. *Protein Spotlight, Swiss Prot* **2002,** *24*, 1-2.
[251] Gosline, J. M.; Guerette, P. A.; Ortlepp, C. S.; Savage, K. N. The mechanical design of spider silks: From fibroin sequence to mechanical function. *J Exp Biol* **1999,** *202* (23), 3295-3303.
[252] Bon, M. A discourse upon the usefulness of the silk of spiders. *Philos Trans R Soc Lond B Biol Sci* **1710,** *27*, 2-16.
[253] Allmeling, C.; Jokuszies, A.; Reimers, K.; Kall, S.; Choi, C. Y.; Brandes, G.; Kasper, C.; Scheper, T.; Guggenheim, M.; Vogt, P. M. Spider silk fibres in artificial nerve constructs promote peripheral nerve regeneration. *Cell Prolif* **2008,** *41* (3), 408-420.
[254] Allmeling, C.; Jokuszies, A.; Reimers, K.; Kall, S.; Vogt, P. M. Use of spider silk fibres as an innovative material in a biocompatible artificial nerve conduit. *J Cell Mol Med* **2006,** *10* (3), 770-777.
[255] Radtke, C.; Allmeling, C.; Waldmann, K. H.; Reimers, K.; Thies, K.; Schenk, H. C.; Hillmer, A.; Guggenheim, M.; Brandes, G.; Vogt, P. M. Spider Silk Constructs Enhance Axonal Regeneration and Remyelination in Long Nerve Defects in Sheep. *PLoS One* **2011,** *6* (2), 1-10.
[256] Hennecke, K.; Redeker, J.; Kuhbier, J. W.; Strauss, S.; Allmeling, C.; Kasper, C.; Reimers, K.; Vogt, P. M. Bundles of Spider Silk, Braided into Sutures, Resist Basic Cyclic Tests: Potential Use for Flexor Tendon Repair. *PLoS One* **2013,** *8* (4), 1-10.
[257] Kuhbier, J. W.; Reimers, K.; Kasper, C.; Allmeling, C.; Hillmer, A.; Menger, B.; Vogt, P. M.; Radtke, C. First investigation of spider silk as a braided microsurgical suture. *J Biomed Mater Res B* **2011,** *97B* (2), 381-387.
[258] Heidebrecht, A.; Scheibel, T. Recombinant production of spider silk proteins. *Adv Appl Microbiol* **2013,** *82*, 115-153.
[259] Vollrath, F. Biology of spider silk. *Int J Biol Macromol* **1999,** *24* (2-3), 81-88.
[260] Vollrath, F.; Knight, D. P. Liquid crystalline spinning of spider silk. *Nature* **2001,** *410* (6828), 541-548.
[261] Guerette, P. A.; Ginzinger, D. G.; Weber, B. H. F.; Gosline, J. M. Silk properties determined by gland-specific expression of a spider fibroin gene family. *Science* **1996,** *272* (5258), 112-115.
[262] Aprhisiart, A.; Vollrath, F. Design-Features of the Orb Web of the Spider, Araneus-Diadematus. *Behavioral Ecology* **1994,** *5* (3), 280-287.
[263] Nova, A.; Keten, S.; Pugno, N. M.; Redaelli, A.; Buehler, M. J. Molecular and Nanostructural Mechanisms of Deformation, Strength and Toughness of Spider Silk Fibrils. *Nano Lett* **2010,** *10* (7), 2626-2634.
[264] Lintz, E. S.; Scheibel, T. R. Dragline, Egg Stalk and Byssus: A Comparison of Outstanding Protein Fibers and Their Potential for Developing New Materials. *Adv Funct Mater* **2013,** *23* (36), 4467-4482.
[265] Frische, S.; Maunsbach, A. B.; Vollrath, F. Elongate cavities and skin-core structure in Nephila spider silk observed by electron microscopy. *J Microsc-Oxford* **1998,** *189*, 64-70.
[266] Liu, Y.; Shao, Z. Z.; Vollrath, F. Relationships between supercontraction and mechanical properties of spider silk. *Nat Mater* **2005,** *4* (12), 901-905.
[267] Sponner, A.; Vater, W.; Monajembashi, S.; Unger, E.; Grosse, F.; Weisshart, K. Composition and Hierarchical Organisation of a Spider Silk. *PLoS One* **2007,** *2* (10), 1-8.
[268] Augsten, K.; Muhlig, P.; Herrmann, C. Glycoproteins and skin-core structure in Nephila clavipes spider silk observed by light and electron microscopy. *Scanning* **2000,** *22* (1), 12-15.

[269] van Beek, J. D.; Hess, S.; Vollrath, F.; Meier, B. H. The molecular structure of spider dragline silk: Folding and orientation of the protein backbone. *P Natl Acad Sci USA* **2002,** *99* (16), 10266-10271.
[270] Papadopoulos, P.; Solter, J.; Kremer, F. Hierarchies in the structural organization of spider silk-a quantitative model. *Colloid Polym Sci* **2009,** *287* (2), 231-236.
[271] Ayoub, N. A.; Garb, J. E.; Tinghitella, R. M.; Collin, M. A.; Hayashi, C. Y. Blueprint for a High-Performance Biomaterial: Full-Length Spider Dragline Silk Genes. *PLoS One* **2007,** *2* (6), 1-13.
[272] Andersen, S. O. Amino Acid Composition of Spider Silds. *Comp Biochem Physiol* **1970,** *35* (3), 705-711.
[273] Kummerlen, J.; van Beek, J. D.; Vollrath, F.; Meier, B. H. Local structure in spider dragline silk investigated by two-dimensional spin-diffusion nuclear magnetic resonance. *Macromolecules* **1996,** *29* (8), 2920-2928.
[274] Hayashi, C. Y.; Shipley, N. H.; Lewis, R. V. Hypotheses that correlate the sequence, structure, and mechanical properties of spider silk proteins. *Int J Biol Macromol* **1999,** *24* (2-3), 271-275.
[275] Hinman, M. B.; Lewis, R. V. Isolation of a clone encoding a second dragline silk fibroin. Nephila clavipes dragline silk is a two-protein fiber. *The Journal of biological chemistry* **1992,** *267* (27), 19320-19324.
[276] Askarieh, G.; Hedhammar, M.; Nordling, K.; Saenz, A.; Casals, C.; Rising, A.; Johansson, J.; Knight, S. D. Self-assembly of spider silk proteins is controlled by a pH-sensitive relay. *Nature* **2010,** *465* (7295), 236-239.
[277] Eisoldt, L.; Smith, A.; Scheibel, T. Decoding the secrets of spider silk. *Mater Today* **2011,** *14* (3), 80-86.
[278] Hagn, F.; Eisoldt, L.; Hardy, J. G.; Vendrely, C.; Coles, M.; Scheibel, T.; Kessler, H. A conserved spider silk domain acts as a molecular switch that controls fibre assembly. *Nature* **2010,** *465* (7295), 239-244.
[279] Hagn, F.; Thamm, C.; Scheibel, T.; Kessler, H. pH-Dependent Dimerization and Salt-Dependent Stabilization of the N-terminal Domain of Spider Dragline Silk-Implications for Fiber Formation. *Angew Chem Int Edit* **2011,** *50* (1), 310-313.
[280] Gatesy, J.; Hayashi, C.; Motriuk, D.; Woods, J.; Lewis, R. Extreme diversity, conservation, and convergence of spider silk fibroin sequences. *Science* **2001,** *291* (5513), 2603-2605.
[281] Scheibel, T. Spider silks: recombinant synthesis, assembly, spinning, and engineering of synthetic proteins. *Microb Cell Fact* **2004,** *3*, 1-10.
[282] Huemmerich, D.; Helsen, C. W.; Quedzuweit, S.; Oschmann, J.; Rudolph, R.; Scheibel, T. Primary structure elements of spider dragline silks and their contribution to protein solubility. *Biochemistry* **2004,** *43* (42), 13604-13612.
[283] Huemmerich, D.; Scheibel, T.; Vollrath, F.; Cohen, S.; Gat, U.; Ittah, S. Novel assembly properties of recombinant spider dragline silk proteins. *Curr Biol* **2004,** *14* (22), 2070-2074.
[284] Fox, L. R. Cannibalism in Natural-Populations. *Annu Rev Ecol Syst* **1975,** *6*, 87-106.
[285] Madsen, B.; Shao, Z. Z.; Vollrath, F. Variability in the mechanical properties of spider silks on three levels: interspecific, intraspecific and intraindividual. *Int J Biol Macromol* **1999,** *24* (2-3), 301-306.
[286] Craig, C. L.; Riekel, C.; Herberstein, M. E.; Weber, R. S.; Kaplan, D.; Pierce, N. E. Evidence for diet effects on the composition of silk proteins produced by spiders. *Mol Biol Evol* **2000,** *17* (12), 1904-1913.
[287] Römer, L.; Scheibel, T. Grundlage für neue Materialien Spinnenseidenproteine. *Chem. Unserer Zeit* **2007,** *41*, 306-314.
[288] Heidebrecht, A.; Eisoldt, L.; Diehl, J.; Schmidt, A.; Geffers, M.; Lang, G.; Scheibel, T. Biomimetic fibers made of recombinant spidroins with the same toughness as natural spider silk. *Advanced materials* **2015,** *27* (13), 2189-2194.
[289] Vendrely, C.; Scheibel, T. Biotechnological production of spider-silk proteins enables new applications. *Macromol Biosci* **2007,** *7* (4), 401-409.

[290] Wohlrab, S.; Thamm, C.; Scheibel, T., *The Power of Recombinant Spider Silk Proteins*. Springer: Netherland, 2014; Vol. 5.
[291] Hardy, J. G.; Romer, L. M.; Scheibel, T. R. Polymeric materials based on silk proteins. *Polymer* **2008,** *49* (20), 4309-4327.
[292] Spiess, K.; Wohlrab, S.; Scheibel, T. Structural characterization and functionalization of engineered spider silk films. *Soft Matter* **2010,** *6* (17), 4168-4174.
[293] Hermanson, K. D.; Huemmerich, D.; Scheibel, T.; Bausch, A. R. Engineered microcapsules fabricated from reconstituted spider silk. *Advanced Materials* **2007,** *19* (14), 1810-1815.
[294] Heim, M.; Keerl, D.; Scheibel, T. Spider Silk: From Soluble Protein to Extraordinary Fiber. *Angew Chem Int Edit* **2009,** *48* (20), 3584-3596.
[295] Müller-Herrmann, S.; Scheibel, T. Enzymatic Degradation of Films, Particles, and Nonwoven Meshes Made of a Recombinant Spider Silk Protein. *Biomaterials Science & Engineering* **2015,** *1*, 247-259.
[296] Agapov, I. I.; Pustovalova, O. L.; Moisenovich, M. M.; Bogush, V. G.; Sokolova, O. S.; Sevastyanov, V. I.; Debabov, V. G.; Kirpichnikov, M. P. Three-dimensional scaffold made from recombinant spider silk protein for tissue engineering. *Dokl Biochem Biophys* **2009,** *426* (1), 127-130.
[297] Moisenovich, M. M.; Pustovalova, O.; Shackelford, J.; Vasiljeva, T. V.; Druzhinina, T. V.; Kamenchuk, Y. A.; Guzeev, V. V.; Sokolova, O. S.; Bogush, V. G.; Debabov, V. G.; Kirpichnikov, M. P.; Agapov, I. I. Tissue regeneration in vivo within recombinant spidroin 1 scaffolds. *Biomaterials* **2012,** *33* (15), 3887-3898.
[298] Widhe, M.; Bysell, H.; Nystedt, S.; Schenning, I.; Malmsten, M.; Johansson, J.; Rising, A.; Hedhammar, M. Recombinant spider silk as matrices for cell culture. *Biomaterials* **2010,** *31* (36), 9575-9585.
[299] Fredriksson, C.; Hedhammar, M.; Feinstein, R.; Nordling, K.; Kratz, G.; Johansson, J.; Huss, F.; Rising, A. Tissue Response to Subcutaneously Implanted Recombinant Spider Silk: An in Vivo Study. *Materials* **2009,** *2* (4), 1908-1922.
[300] Gibson, I.; Rosen, D. W.; Stucker, B., *Additive Manufacturing Technologies. 3D Printing, Rapid Prototyping, and Direct Digital Manufacturing*. Springer: New York, 2010; Vol. 2.
[301] Bauer, F.; Wohlrab, S.; Scheibel, T. Controllable cell adhesion, growth and orientation on layered silk protein films. *Biomater Sci-Uk* **2013,** *1* (12), 1244-1249.
[302] Eisoldt, L.; Thamm, C.; Scheibel, T. Review the role of terminal domains during storage and assembly of spider silk proteins. *Biopolymers* **2012,** *97* (6), 355-361.
[303] Klement, K.; Wieligmann, K.; Meinhardt, J.; Hortschansky, P.; Richter, W.; Fandrich, M. Effect of different salt ions on the propensity of aggregation and on the structure of Alzheimer's A beta(1-40) amyloid fibrils. *J Mol Biol* **2007,** *373* (5), 1321-1333.

5 DARSTELLUNG DES EIGENANTEILS

Die in der vorliegenden Dissertation vorgestellten Ergebnisse wurden in Zusammenarbeit mit Kooperationspartnern erzielt. Nachfolgend werden die einzelnen Beiträge aller Autoren zu den jeweiligen Veröffentlichungen genau dargestellt.

> I. **Schacht, K.***, Vogt, J.*, und Scheibel, T. (2015). "Foams made of Engineered Recombinant Spider Silk Proteins as Optimized 3D Scaffolds for Cell Growth." Biomaterials Science and Engineering 2: 514-525.

Die Veröffentlichung ist im Rahmen der Masterarbeit von Jessica Vogt, die von Thomas Scheibel und mir betreut wurde, entstanden. Die Experimente wurden von Jessica Vogt unter meiner Betreuung und Anleitung durchgeführt. Dabei wurde eADF4(C16)-RGD von Andreas Schmidt bzw. Johannes Diehl fermentiert und gereinigt. Das Manuskript wurde zu weiten Teilen von mir verfasst. Thomas Scheibel war in wissenschaftliche Diskussionen involviert und an der Fertigstellung des Manuskripts beteiligt.

> II. **Schacht, K.***, Jungst, T.*, Schweinlin, M., Ewald, A., Groll, J., und Scheibel, T. (2015). "Biofabrication of Cell-Loaded 3D Spider Silk Constructs." Angewandte Chemie Int. Ed. 54: 2816-2820.

Die Veröffentlichung ist in Zusammenarbeit mit dem Lehrstuhl für Funktionswerkstoffe der Medizin und der Zahnheilkunde der Universität Würzburg entstanden. eADF4(C16)-RGD wurde von Andreas Schmidt bzw. Johannes Diehl fermentiert und gereinigt. Die Hydrogelherstellung und sämtliche Zellkulturexperimente wurden von mir durchgeführt. Die FTIR-Messungen, Fourier-Selbstdekonvolution, rheologischen Messungen und Diffusionstests wurden von mir durchgeführt. Der 3D-Druck der Hydrogele wurde von Tomasz Jungst durchgeführt. Die stereomikroskopischen und fluoreszenzmikroskopischen Bilder wurden von Tomasz Jungst und mir aufgenommen. Die Konfokal-Laser-Scanning-mikroskopischen Aufnahmen hat Matthias Schweinlin durchgeführt. Andrea Ewald hat mich im Zellkulturlabor der Universität Würzburg unterstützt. Das Manuskript wurde von mir verfasst. Thomas Scheibel und Jürgen Groll betreuten das Projekt. Tomasz Jungst, Jürgen Groll und Thomas Scheibel waren an wissenschaftlichen Diskussionen und der Fertigstellung des Manuskripts beteiligt.

III. DeSimone, E.*, **Schacht, K.*** und Scheibel, T. (2016). ”Cations influence the cross-linking of hydrogels made of recombinant, polyanionic spider silk proteins.“ Materials Letters 183: 101-104.

Das Konzept der Veröffentlichung ist von Elise DeSimone und mir entwickelt worden. eADF4(C16)-RGD wurde von Andreas Schmidt bzw. Johannes Diehl fermentiert und gereinigt. Die FTIR-Messungen und Fourier-Selbstdekonvolution sind von mir durchgeführt worden. Die Herstellung der Hydrogele erfolgte durch Elise DeSimone und mir. Deformations-Schubspannungskurven und die Gelierungskinetiken wurden von Elise DeSimone und mir aufgenommen. Die rheologischen Messungen mit zunehmender Scherrate, sowie die Transmissionselektronenmikroskopie Aufnahmen wurden von mir durchgeführt. Das Manuskript wurde von Elise DeSimone und mir in Zusammenarbeit verfasst. Thomas Scheibel betreute das Projekt und war an der Fertigstellung des Manuskripts beteiligt.

IV. **Schacht, K.** und Scheibel, T. (2014). “Processing of recombinant spider silk proteins into tailor-made materials for biomaterials applications.“ Current Opinion in Biotechnology 29: 62-69.

Die Konzeption des Artikels wurde von Thomas Scheibel und mir erarbeitet. Das Manuskript wurde von mir verfasst. Thomas Scheibel war in wissenschaftliche Diskussionen eingebunden und an der Fertigstellung des Manuskripts beteiligt.

V. DeSimone, E.*, **Schacht, K.***, Jungst, T., Groll, J., und Scheibel, T. (2015). “Biofabrication of 3D Constructs: Fabrication Technologies and Spider Silk Proteins as Bioinks.” Pure and Applied Chemistry 87(8): 737-749.

Das Konzept der Veröffentlichung ist von Elise DeSimone, Thomas Scheibel und mir entwickelt worden. Das Manuskript wurde von Elise DeSimone und mir verfasst. Tomasz Jungst, Jürgen Groll und Thomas Scheibel waren an wissenschaftlichen Diskussionen und an der Fertigstellung des Manuskripts beteiligt.

VI. Jungst, T.*, Smolan, W.*, **Schacht, K.**, Scheibel, T., und Groll, J. (2016). “Strategies and Molecular Design Criteria for 3D Printable Hydrogels.“ Chemical Reviews 116(3):1496-1539.

Die Konzeption des Artikels wurde von Tomasz Jungst, Willi Smolan und Jürgen Groll erarbeitet. Die Kapitel “Naturally occurring biopolymers used for hydrogel formation” und

“Biotechnological approaches towards bioinks” wurden von mir geschrieben. Die anderen Kapitel des Manuskripts wurden von Tomasz Jungst, Willi Smolan und Jürgen Groll verfasst. Alle Autoren waren an wissenschaftlichen Diskussionen und an der Fertigstellung des Manuskripts beteiligt.

VII. **Schacht, K.**, Jungst, T., Zehnder, T., Boccaccini, A.R., Groll, J. und Scheibel, T. (2016). “Zellgewebe aus dem Drucker.“ Nachrichten aus der Chemie 64: 13-16.

Die Konzeption der Veröffentlichung wurde von Thomas Scheibel und mir erarbeitet. Das Manuskript wurde von Tomasz Jungst, Tobias Zehnder und mir verfasst. Aldo Boccaccini, Jürgen Groll und Thomas Scheibel waren an wissenschaftlichen Diskussionen und der Fertigstellung des Manuskripts beteiligt.

* gleichberechtigte Co-Autorenschaft

6 PUBLIKATIONSLISTE

I. Schacht, K.*, Vogt, J.*, und Scheibel, T. (2016). “Foams made of Engineered Recombinant Spider Silk Proteins as Optimized 3D Scaffolds for Cell Growth.” Biomaterials Science and Engineering 2: 517-525.

II. **Schacht, K.***, Jungst, T.*, Schweinlin, M., Ewald, A., Groll, J., und Scheibel, T. (2015). “Biofabrication of Cell-Loaded 3D Spider Silk Constructs.“ Angewandte Chemie Int. Ed. 54: 2816-2820.

III. DeSimone, E.*, **Schacht, K.*** und Scheibel, T. (2016). ”Cations influence the cross-linking of hydrogels made of recombinant, polyanionic spider silk proteins.“ Materials Letters 183: 101-104.

IV. **Schacht, K.** und Scheibel, T. (2014). “Processing of recombinant spider silk proteins into tailor-made materials for biomaterials applications.“ Current Opinion in Biotechnology 29: 62-69.

V. DeSimone, E.*, **Schacht, K.***, Jungst, T., Groll, J., und Scheibel, T. (2015). “Biofabrication of 3D Constructs: Fabrication Technologies and Spider Silk Proteins as Bioinks.” Pure and Applied Chemistry 87(8): 737-749.

VI. Jungst, T.*, Smolan, W.*, **Schacht, K.**, Scheibel, T., und Groll, J. (2016). “Strategies and Molecular Design Criteria for 3D Printable Hydrogels.“ Chemical Reviews 116(3): 1496-1539.

VII. **Schacht, K.**, Jungst, T., Zehnder, T., Boccaccini, A.R., Groll, J. und Scheibel, T. (2016). “Zellgewebe aus dem Drucker.“ Nachrichten aus der Chemie 64: 13-16.

* gleichberechtigte Co-Autorenschaft

7 TEILARBEITEN

TEILARBEIT I

Die Ergebnisse dieses Kapitels wurden bereits in *Biomaterials Science and Engineering* veröffentlicht als:

> "Foams made of Engineered Recombinant Spider Silk Proteins as Optimized 3D Scaffolds for Cell Growth." Schacht, K.*, Vogt, J.* und Scheibel, T..

* gleichberechtigte Co-Autorenschaft

ACS Biomaterials SCIENCE & ENGINEERING

Article

pubs.acs.org/journal/abseba

Foams Made of Engineered Recombinant Spider Silk Proteins as 3D Scaffolds for Cell Growth

Kristin Schacht,[†,‡] Jessica Vogt,[†,‡,§] and Thomas Scheibel[*,‡,⊥,∥,#,△]

[‡]Lehrstuhl Biomaterialien, [⊥]Bayreuther Zentrum für Kolloide und Grenzflächen (BZKG), [∥]Institut für Bio-Makromoleküle (bio-mac), [#]Bayreuther Zentrum für Molekulare Biowissenschaften (BZMB), and [△]Bayreuther Materialzentrum (BayMAT), Universität Bayreuth, Universitätsstraße 30, D-95447 Bayreuth, Germany

Supporting Information

ABSTRACT: Materials for tissue engineering have to be biocompatible and have to support cell adhesion, proliferation and differentiation. Additionally, in case of soft tissue engineering the mechanical properties have to accommodate that of the tissue with mechanical integrity until the artificial scaffold is replaced by natural extracellular matrix. In case of artificial 3D scaffolds, it is of critical importance to be able to tune the mechanical properties, the inner free volume (i.e., pore size) and degradation behavior of the employed biomaterial. Here, the potential of recombinant spider silk proteins was evaluated concerning their processing into and application as 3D scaffolds for soft tissue engineering. Highly porous foams made of the recombinant spider silk protein eADF4(C16) and a variant containing an RGD motif were fabricated by salt leaching yielding mechanically robust scaffolds. In contrast to other salt-leached silk scaffolds, the swelling behavior of these scaffolds was low, and the mechanical properties in the range of soft tissues. The pore size and porosity of the foams could be adjusted by the salt crystal size. Fibroblasts adhered and proliferated well in foams made of the spider silk RGD variant but not in the foams of the nonmodified one.

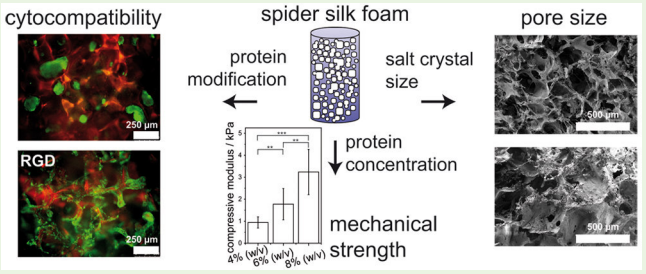

KEYWORDS: *recombinant spider silk proteins, salt leaching, foams, porous scaffolds, biomedical applications, tissue engineering*

INTRODUCTION

An ideal scaffold for tissue engineering should enable cell adhesion, migration, proliferation, and differentiation in three dimensions based on a high porosity with suitable pore sizes.[1−6] Moreover, the used material should be biocompatible, nontoxic, nonimmunogenic as well as biodegradable at a rate that allows the formation of new natural tissue.[7] On the other hand the scaffold has to be mechanically stable, with properties in the range of the natural soft tissue (Elastic modulus ∼1 kPa) to be replaced.[3] Matrix stiffness is increasingly appreciated as an important mediator of cell behavior to regulate cell signaling, effecting growth, survival, and motility, and it has been shown that tissue-specific cells like fibroblasts sense matrix stiffness to regulate the formation and maintenance of tissues.[8−10]

A broad range of synthetic polymers, like polylactic acid (PLA) and polyglycolic acid (PGA), as well as natural polymers such as collagen, alginate and silk, have been utilized for biomedical applications in the form of 3D scaffolds. In spite of the processability of synthetic ones, naturally occurring polymers are generally considered more promising in this field due to their biodegradability and biocompatibility. In recent years, silkworm silk fibroin has been explored as scaffold material for different biomedical applications, due to its biocompatibility, biodegradability and mechanical properties upon processing.[11−14] It could be detected that fibroin scaffolds can act as matrices for cells supporting their adhesion, migration and proliferation. Silk fibroin scaffolds were also shown to sustain for over 1 year in rats without significant degradation.[15] A number of methods have been used to prepare silk-based 3D scaffolds.[1,16−19] Salt leaching is a widely used technique due to its efficiency and ease of processing.[1,20−22] However, salt-leached fibroin scaffolds generally are stiff caused by the adopted silk conformation (β-sheet-rich), which restricts their use in some soft tissue applications.[1,20,21] Salt leached fibroin scaffolds show compressive moduli between 100 and 790 kPa depending on the porogen content, being comparable with other polymeric biomaterial scaffolds commonly used in tissue engineering such as in regeneration of cortical bone.[1,20] Also foams of recombinant silks based on the major ampullate spidroin 1 from the spider *Euprosthenops australis* were tested for the growth behavior of neural stem cells, which were shown to retain their differentiation potential into acstrocytes.[23] Fibroblasts showed a slightly less growth on such foams compared to other scaffolds made of this silk protein, such as films and fibers.[24,25]

Here, recombinant spider silk proteins based on the repetitive core sequence of ADF4, one out of at least two major ampullate spidroins of the European garden spider

Received: November 12, 2015
Accepted: March 3, 2016
Published: March 4, 2016

DOI: 10.1021/acsbiomaterials.5b00483
ACS Biomater. Sci. Eng. 2016, 2, 517−525

Araneus diadematus, were employed, because materials made of the engineered variant eADF4(C16) can be easily processed into various morphologies with adjustable properties.[26,27] In this study, the polyanion eADF4(C16) were prepared as foams and thus acted as an optimized control of the material and scaffold properties. Additionally, we used a genetically modified variant of eADF4(C16) with the cell binding motif RGD.[28] Salt leaching was used to fabricate such three-dimensional porous foams, and the structure, pore size, porosity, and swelling behavior of the salt leached foams were controlled by the salt crystals.

MATERIALS AND METHODS

Materials. The recombinant spider silk protein eADF4(C16) consists of 16 repeats of a consensus sequence, named C-module (GSSAAAAAAAASGPGGYGPENQGPSGPGGY GPGGP), mimicking the core domain of one dragline silk protein of the European garden spider (*Araneus diadematus*). Recombinant production of eADF4(C16) and of the genetically modified variant eADF4(C16)-RGD in *Escherichia coli* as well as their purification were performed as described previously.[26,28] Briefly, for the purification of eADF4(C16) and eADF4(C16)-RGD, *E. coli* cells were incubated in 50 mM Tris/HCl + 100 mM NaCl buffer, pH 7.5 and 0.2 mg/mL lysozyme at 4 °C for 30 min and lysed by ultrasonication. After centrifugation of cell fragments, soluble *E. coli* proteins were precipitated by heat denaturation at 80 °C for 20 min and removed by centrifugation. The remaining silk proteins were salted out with 20% ammonium sulfate at room temperature (RT).[26,28]

Preparation of Recombinant Spider Silk Foams, Films and Hydrogels. The standard conditions for the foam preparation are summarized in Table 1.

Table 1. Standard Conditions for Foam Preparation

protein concentration (eADF4(C16)) w/v %	salt crystal size (μm) range I: 63−125	range II: 125−315	range III: 315−500	salt-to-protein ratio w/w ≙ low ratio	salt-to-protein ratio w/w ≙ high ratio
4	4-I	4-II	4-III	75:1	125:1
6	6-I	6-II	6-III	50:1	85:1
8	8-I	8-II	8-III	37.5:1	60:1

For foam preparation, the lyophilized recombinant spider silk proteins were dissolved in 1,1,1,3,3,3-Hexafluoro-2-propanol (HFIP) (Alfa Aesar) at final concentrations of 4, 6 and 8% (w/v). Crystals of sodium chloride (NaCl, Carl Roth) were used as porogen. NaCl was grinded using a Mortar Grinder RM 200 (Retsch) and sieved using a Sieve Shaker KS 1000 (Retsch) yielding NaCl crystals in the ranges of 63−125 μm, 125−315 μm or 315−500 μm. In a 75:1 (4% (w/v)), 50:1 (6% (w/v)), and 37.5:1 (8% (w/v)) (w/w) salt/protein ratio, the protein solution was cast on the salt crystals in cylindrical molds (Figure S1). The solvent was evaporated for at least 48 h, and the NaCl was leached out in milli-Q water for 24 h upon 6−8 water changes. Until usage, the scaffolds were either stored in milli-Q water at room temperature or freeze-dried using a Lyophilizer (alpha 1−2 LD plus, Christ).

For film preparation, the silk protein solutions (4, 6 and 8% (w/v) eADF4(C16) in HFIP) were cast in cylindrical molds without salt crystals. After evaporation of the solvent the films were either stored untreated or incubated in 6 M NaCl solution for 4 h to induce β-sheet formation rendering silk films water insoluble.[29]

The recombinant spider silk hydrogels were prepared by dialysis of 4 mg/mL soluble eADF4(C16) against aqueous buffer (10 mM Tris/HCl, pH 7.5) and concentrated by dialysis against polyethylene glycol (PEG 20,000, Carl Roth), which induces water removal as described previously.[30] The final protein concentration was adjusted to 3% (w/v). The gelation occurred overnight at 37 °C. Until usage, the hydrogels were stored at room temperature.

Fourier Transform Infrared (FTIR) Spectroscopy. Analysis of the secondary structure of freeze-dried eADF4(C16) foams, as well as untreated and post-treated (NaCl) HFIP-derived eADF4(C16) films was performed using a Bruker Tensor 27 spectrometer (Bruker, Germany). Spectra were measured by attenuated total reflection (ATR) with a resolution of 4 cm^{-1}, and 60 scans were averaged. Analysis of the amide I band (1590−1720 cm^{-1}) was performed by Fourier self-deconvolution (FSD) to determine individual secondary structure elements (Figure S2B−D). Band assignments were made according to Hu et al.[31] Minimum 3 spots per sample were tested of each composition.

Pore Size and Porosity. To analyze the morphology of the salt leached scaffolds, they were fractured in liquid nitrogen using a razor blade. Freeze-dried samples were sputter coated (2 nm) with platinum, and scanning electron microscopy (SEM) images were taken using a 1450EsB Cross Beam (Zeiss, Germany) at an accelerated voltage of 3 kV. To determine the pore size, light microscopy images of wet and freeze-dried foams were evaluated graphically. The area and lateral length of the pores were analyzed using ImageJ 1.48v (Wayne Rasband, National Institute of Health).

The density and porosity of freeze-dried eADF4(C16) foams were determined by gravimetry.[32] For the analysis of the influence of the salt-to-protein ratio, foams were prepared at different salt-to-protein ratios (low ratio: 75:1 (4% (w/v)), 50:1 (6% (w/v)), and 37.5:1 (8% (w/v)); high ratio: 125:1 (4% (w/v)), 85:1 (6% (w/v)), and 60:1 (8% (w/v)) (w/w) salt/protein ratio). The density of eADF4(C16) protein ($\varsigma_{protein}$) and of the foams (ς_{foam}) was measured with a density scale AG245 (Mettler Toledo). Freeze-dried foams and untreated HFIP-derived eADF4(C16) films were weighed in air (m_a) at room temperature and afterward submerged in a liquid of known density (ς_b) and weighed again in liquid (m_b). The density of the samples, ς, is expressed as

$$\varsigma = m_a/(m_a - m_b)\varsigma_b \quad (1)$$

To determine $\varsigma_{protein}$, ethanol was used as medium. To determine ς_{foam}, 86% (v/v) glycerol (Carl Roth) was used. The porosity of a foam, Π, was expressed as

$$\Pi(\%) = (1 - \varsigma_{foam}/\varsigma_{protein})100\% \quad (2)$$

Mechanical Properties. The compressive moduli were analyzed with an open-sided/confined method using an ElectroForce 3220 (Bose), equipped with a 0.49 N load cell. Four to five samples were evaluated for each composition. Round foams (Ø 12 mm) with a height of 4−5 mm were prepared in polystyrene well plates with 12 mm in diameter (Thermo Fisher Scientific) and stored in milli-Q water until testing. To compress the wet foams, a cylindrical Teflon stamp of 8 mm in diameter was moved onto the foams until a prepressure of 2 mN was reached. With a velocity of 0.01 mm/min the stamp was moved 0.3 mm into the foam. After the reduction of the pressure to 0 N, the foam was compressed for a second time. The stress−strain curves were recorded, and the elastic compressive moduli were determined by the slope of the initial linear section of the curve.[33,34] For statistical analysis, an unpaired two-tailed *t*-test was performed for groups with similar variances. No difference could be detected between different salt crystal sizes, and therefore the samples were averaged for statistical analysis ($n \geq 11$).

Enzymatic Degradation. The in vitro degradation experiment was performed as described previously by Müller-Hermann and Scheibel.[35] For the degradation experiment, 8% (w/v) eADF4(C16) foams (125−315 μm salt crystal size) and 3% (w/v) eADF4(C16) hydrogels were analyzed. The scaffolds were incubated in the presence of 87.5 μg protease per 1 mg scaffold for 15 days under controlled atmosphere (30% humidity) at 25 °C. Collagenase type IA from *Clostridium histolyticum* (CHC, Sigma-Aldrich) and protease mix type XIV from *Streptomyces griseus* (PXIV, Sigma-Aldrich) were used. Control experiments without enzymes were performed in TCNB buffer (50 mM Tris, 10 mM $CaCl_2$, 150 mM, NaCl, 0.05% Brij 35, pH

DOI: 10.1021/acsbiomaterials.5b00483
ACS Biomater. Sci. Eng. 2016, 2, 517−525

Table 2. Secondary Structure Elements of Freeze-Dried Salt Leached Foams in Comparison to That of Untreated Films, Salt-Treated (NaCl) Films, and 100% Methanol-Treated Films Made of eADF4(C16)[b]

		secondary structure content (%)			
secondary structure	wavenumber range (cm^{-1})[a]	untreated film	film treated with 6 M NaCl	film treated with 100% methanol	salt (NaCl) leached foam
α-helices	1656−1662	14.2 ± 1.4	9.3 ± 1.3	9.1 ± 1.3	9.3 ± 1.8
β-sheets	1616−1637	22.5 ± 1.8	44.6 ± 1.8	46.6 ± 1.0	42.4 ± 2.0
	1697−1703				
random coils	1638−1655	45.2 ± 3.1	23.9 ± 0.5	22.5 ± 0.3	25.2 ± 1.1
β-turns	1663−1696	18.2 ± 2.9	22.2 ± 0.5	21.9 ± 0.6	23.1 ± 1.6

[a]Peak assignment taken from refs 30 and 39. [b]Structural contents were calculated using Fourier self-deconvolution (FSD) of the amide I bands.

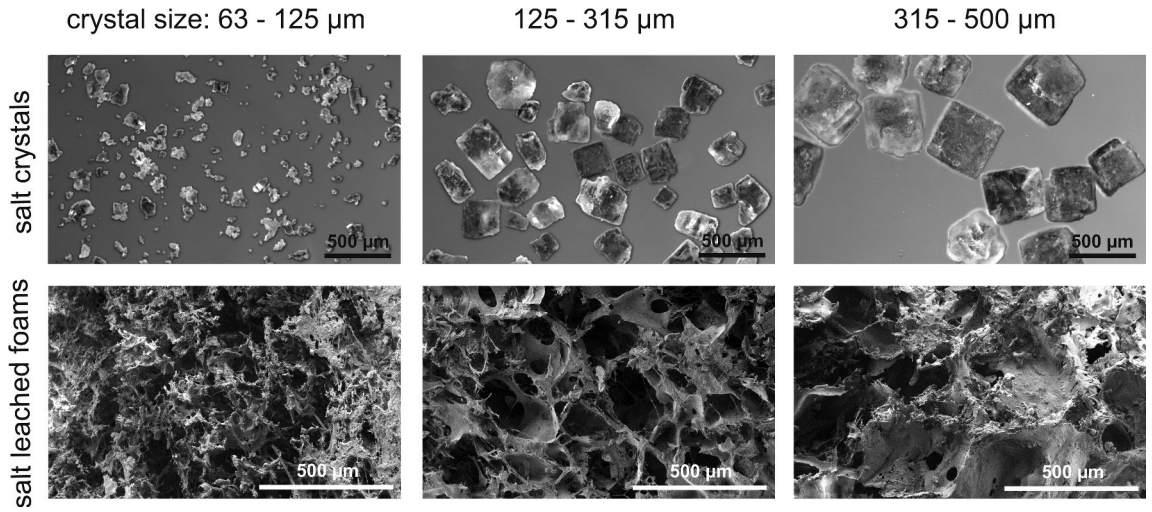

Figure 1. Top panel: light microscopy images of salt crystals used in the salt leaching process; bottom panel, scanning electron microscopy images of the cross-section of 8% (w/v) eADF4(C16) salt leached foams, respectively.

7.5). Buffers or enzyme solutions were changed every 24 h. The experiments were performed in triplicates.

Cell Line Cultivation. BALB/3T3 mouse fibroblasts (European Collection of Cell Cultures) were cultivated in Dulbecco's Modified Eagle Medium (DMEM, Biochrom) supplemented with 10% fetal bovine serum (Biochrom), 1% (v/v) GlutaMAX (Gibco), and 0.1% (v/v) gentamicin sulfate (Sigma-Aldrich) in a controlled atmosphere of 5% CO_2, 95% humidity and at 37 °C. Viability and number of cells were analyzed using trypan blue (Sigma-Aldrich) in a Neubauer chamber (Laboroptik, UK).

Calcein A/M Staining. 8% (w/v) recombinant spider silk foams were prepared in 8-well μ-slides with a glass bottom (Ibidi, Germany) and incubated for 30 min in the presence of a final concentration of 150 μM Rhodamin-B (Carl Roth). Porous Al_2O_3 and 45S5 Bioglass scaffolds were used as controls. All scaffolds were washed twice with phosphate buffered saline (PBS) (Sigma-Aldrich) and once with DMEM before adding cells; 143 000 or 714 000 cells per cm^3 scaffold were seeded and cultivated up to 7 days. The foams had a volume of 0.07 cm^3. Cell culture medium was changed every day. For the Calcein A/M staining cells were incubated in the presence of 0.4 mM calcein acetoxymethyl ester (Calcein A/M, Invitrogen) for 20 min at 37 °C. After washing with PBS twice, the cells within the scaffolds were visualized using a LeicaDFC3000 G fluorescence microscope (Leica). Fluorescence microscopy images were deconvoluted with the no-Neighbor method using the LASX software from Leica.

Adhesion and Proliferation Assay. 8% (w/v) recombinant spider silk scaffolds were prepared in hanging cell culture inserts for 24-well plates (Merck Millipore). Porous Al_2O_3 and 45S5 Bioglass scaffolds were used as controls. All scaffolds had a volume of 0.14 cm^3 and were washed twice with PBS and once with DMEM. For the adhesion test 714,000 cells/cm^3 were seeded on the scaffolds. Additionally, for controlling the cell behavior under standard conditions, 50,000 cells/cm^2 were seeded on untreated or treated 24-well plates. In the adhesion assay the cells were cultivated for 24 h at 37 °C. After washing with PBS twice, the scaffolds were incubated in 10% CellTiter-Blue (Promega) in DMEM for 4 h at 37 °C. Every hour the solution was mixed by pipetting. Cell adhesion was quantified by determining the fluorescence intensity of resorufin (λ_{ex} 530 nm; λ_{em} 590 nm) by using a plate reader (Mithras LB940, Berthold). All cell adhesion experiments were repeated three times with three replicates each time. For statistical analysis an unpaired two-tailed t test was performed for groups with similar variances. The sample number was ≥8 (for all samples).

For cell proliferation analysis, 71 400 cells/cm^3 were seeded on the scaffolds and as controls 5,000 cells/cm^2 on untreated and treated 24-well plates, each. The cells were cultivated for 10 days at 37 °C. Every day, the samples were washed twice with PBS and then incubated in 10% CellTiter-Blue in DMEM for 4 h at 37 °C. Every hour the solution was mixed by pipetting. After measurement of the fluorescence intensity the samples were washed twice with PBS, and fresh DMEM was added.

RESULTS AND DISCUSSION

Foam Preparation and Protein Secondary Structure determination. Porous foams were fabricated using a salt leaching technique, as previously used for other biopolymers such as fibroin, collagen and polylactic acid (Figure S1).[1,20,36−38] After mixing of the porogen salt (sodium chloride (NaCl)) with the recombinant spider silk protein in 1,1,1,3,3,3-hexafluoro-2-propanol (HFIP) and evaporation of the solvent, the salt was removed in water yielding a highly porous mechanically stable protein scaffold.

The secondary structure of the freeze-dried foams was analyzed using Fourier transform infrared (FTIR) spectroscopy and Fourier self-deconvolution (FSD) analysis of the amide I

DOI: 10.1021/acsbiomaterials.5b00483
ACS Biomater. Sci. Eng. 2016, 2, 517−525

band (Figure S2, Table 2). As control, untreated HFIP-derived eADF4(C16) films were analyzed showing mainly α-helical and random coil structures.[29,39] Previously it has been shown that treatment of spider silk films with alcohols (e.g., methanol, ethanol) or potassium phosphate leads to a conversion of the α-helical and random coil to β-sheet-rich structures, accompanied by a gain of water insolubility and a higher chemical stability against denaturing agents.[29,39] Spider silk films treated with 6 M NaCl solution showed also an increase in β-sheet content (44.6 ± 1.8%), which is in the same range as seen for films post-treated with methanol (46.6 ± 1.0%).[39] Similar to treated films, salt-leached, HFIP-derived foams displayed 42.4 ± 2.0% β-sheet, 9.3 ± 1.8% α-helix, 25.2 ± 1.1% random coil, and 23.1 ± 1.6% β-turn structures. In both cases, the NaCl crystals acted as structure-conversion nuclei.[20] Because of the high β-sheet content induced by NaCl, an additional post-treatment of the salt leached foams with, e.g., methanol or ethanol was not necessary, simplifying the fabrication process, which reflected a clear difference to the process of making salt-leached silkworm fibroin foams.[1]

Pore Size and Porosity. Pore size, interconnectivity, and porosity of the scaffolds are critical for tissue engineering, because cell migration, as well as the transport of nutrients and waste products has to be guaranteed. Additionally, the cells should be able to attach to the scaffold walls, and cell−cell interactions have to be enabled. The pore sizes of the freeze-dried spider silk foams were analyzed using scanning electron (SEM) and light microscopy (Figure 1, Figure S3). The SEM images showed interconnected and porous morphologies. The porogen particles used for salt leaching were sieved to obtain pore sizes in a defined regime and, therefore, scaffolds with specific properties. Not surprisingly, the salt crystal size had a significant influence on the pore size of the salt leached foams with increased pore sizes upon increased salt crystal size. Generally, scaffolds with interconnected pores with diameters >100 μm are considered as a minimum requirement for tissue engineering.[32,36,40] Here, the analyzed foams showed pore sizes between 31 and 437 μm depending on the used salt crystal sizes (Figure 1 and Table 3).

Table 3. Theoretical and Analyzed Salt Crystal Size, As Well As Pore Size and Porosity of 8% (w/v) eADF4(C16) Foams

	size range		
	I	II	III
theoretical salt crystal size (μm)	63−125	125−315	315−500
analyzed salt crystal size (μm)	45−158	121−320	319−514
pore size (μm)	31−172	59−248	129−437
porosity (%)	91.0 ± 0.5	93.0 ± 0.9	93.7 ± 0.1

Quantitative analysis of the salt crystal and pore sizes showed that the pore sizes deviated between 10 and 60% from the size of the original salt crystals used to form the pores. In most cases the pore sizes were smaller than the size of the NaCl salt crystals (Table 2) reflecting the partial dissolution of the salt crystal surface during the foam-building process. Differences in pore sizes between wet and freeze-dried foams could not be detected (Figure S3).

The porosity of freeze-dried eADF4(C16) foams was determined by gravimetry, showing only a slight increase of porosity with increasing salt crystal size (from 91.0 ± 0.5% to 93.0 ± 0.9% and 93.7 ± 0.1%), respectively, whereas neither the protein concentration nor the ratio between the used volume of salt and protein solution had an apparent influence on the porosity of the salt leached spider silk foams (Table 3, Figure 2A). In contrast, the porosities of salt leached silkworm fibroin foams varied between 84 and 98% depending on the porogen ratio of 10:1 w/w and 20:1 w/w porogen to silk.[1]

Mechanical Properties. Besides pore size and porosity of the scaffolds, their mechanical properties are highly important for cell survival, adhesion, and proliferation.[41] Application of salt-leached silk scaffolds in soft tissue regeneration can be encumbered with excessive stiffness, since salt-leached silkworm fibroin silk scaffolds generally have a relatively high silk II (β-sheet-rich) content, resulting in the observed high stiffness.[1,20,22,42,43] Nazarov et al. prepared HFIP-derived salt leached fibroin foams with compressive moduli between 100 and 790 kPa, and water-derived foams showed even higher compressive moduli (70−3330 kPa).[1,20] Additionally, the stiffness increased upon raising the concentration of silk fibroin from 4 to 10 wt %.[20]

The compressive moduli of the salt leached spider silk foams in a hydrated state raised from 0.94 ± 0.26 kPa to 3.24 ± 1.03 kPa with increasing protein concentration from 4% (w/v) to 8% (w/v) (Figure 2B). The elastic moduli of the salt leached foams were in the range of soft tissues, and the determined compressive moduli were in the range of scaffolds derived from low-concentrated fibroin solutions.[3,22] This feature is important because Engler et al. had examined the influence of matrix elasticity on the differentiation of human mesenchymal stem cells, where soft matrices with an elastic modulus in the range of that of brain (~0.1−1 kPa) favored differentiation of mesenchymal stem cells into neuronal-like cells.[3]

The swelling behavior of the salt leached foams was determined using a Discovery V20 stereomicroscope (Zeiss) (n = 6) (Figure S3, Table S1). Sizes of the foams were analyzed in a dry state using the stereomicroscope software (ZEN2012 blue edition). Afterward, the foams were incubated in 50 μL milli-Q water for 2 min. The water was removed and size of the foams was measured again. All foams (4−8% (w/v)) revealed a low swelling characteristic, scaffolds swelled 3−9% depending on the porogen size. In contrast to the spider silk foams, aqueous-derived fibroin scaffolds showed a swelling of 20−55%, likely due to the differences in hydrophilicity of the two proteins.[20] Spider silk foams prepared in the presence of smaller salt particles showed a higher swelling behavior (e.g., 8% (w/v) 8.9 ± 2.5%) than foams prepared with 315−500 μm salt crystals (8% (w/v) 3.2 ± 1.1). It was assumed that foams with a higher surface-to-volume area can absorb a higher amount of water.

Proteolytic Degradation. Materials for tissue engineering applications have not only to be mechanically stable to support cell adhesion and proliferation without collapsing, but they also need to be replaced gradually by native extracellular matrix and, therefore, have to be (slowly) biodegradable.[1]

All foams and hydrogels were stable in TCNB buffer, and upon incubation no significant hydrolysis or dissolution thereof was detected for 15 days (Figure 3). To test the biodegradation of the scaffolds, we employed collagenase IA (CHC) and protease mix XIV (PXIV), because they have been previously established as good model proteases for degradation studies of silk protein scaffolds.[35,44−46] The collagenase type IA is a mixture of several enzymes, including type I and type II collagenase, acting as a model enzyme cocktail representative for wound proteases.[47] The protease mix XIV is a mixture of at least ten proteases with broad substrate specificity. Although

DOI: 10.1021/acsbiomaterials.5b00483
ACS Biomater. Sci. Eng. 2016, 2, 517−525

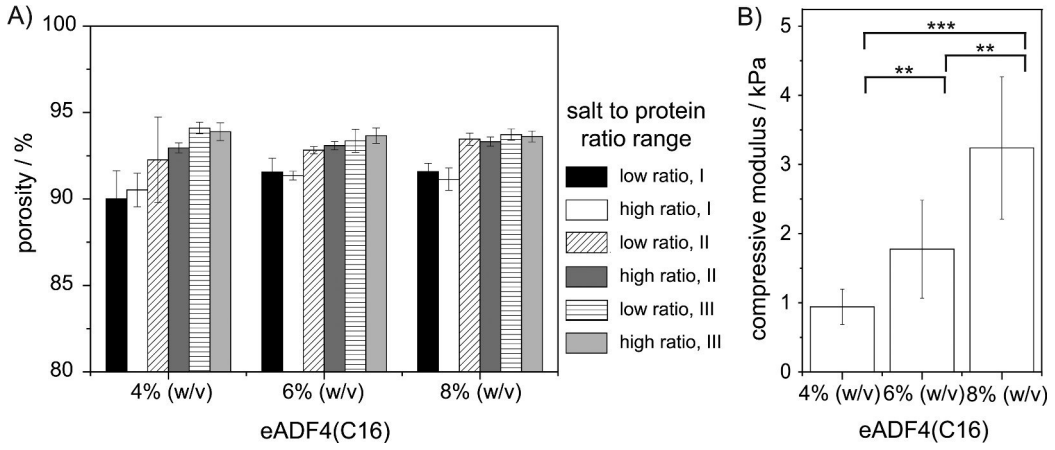

Figure 2. (A) Porosity of 4% (w/v), 6% (w/v), and 8% (w/v) eADF4(C16) foams with different salt-to-protein ratios (low ratio: 75:1 (4%), 50:1 (6%), and 37.5:1 (8%); high ratio: 125:1 (4%), 85:1 (6%), and 60:1 (8%) (w/w) salt/protein ratio) and salt particle size ranges as indicated (I, 63−125; II, 125−315; III, 315−500). (B) Compressive moduli of 8% foams were significantly higher in comparison to 4% and 6% foams at low salt-to-protein ratios (75:1 (4%), 50:1 (6%), and 37.5:1 (8%)) (**$p \leq 0.001$, ***$p < 0.0001$). The samples were averaged over all salt crystal sizes, because no difference could be detected.

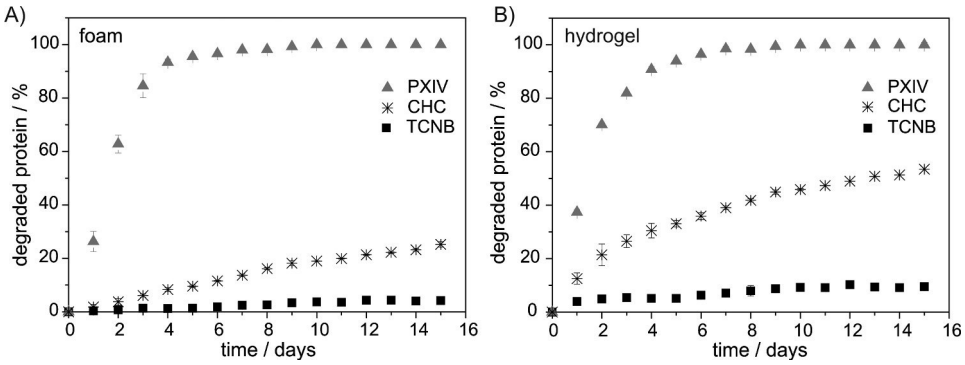

Figure 3. Percentage of degraded eADF4(C16) after incubation of (A) 8% (w/v) eADF4(C16) salt leached foams (125−315 μm porogen size) and (B) 3% (w/v) eADF4(C16) hydrogels in TCNB buffer in the presence or absence of PXIV (digestive enzyme model) (465 μg/mL) or Collagenase (CHC) (wound protease model) (465 μg/mL) over 15 days under controlled atmosphere (30% humidity) at 25 °C, respectively.

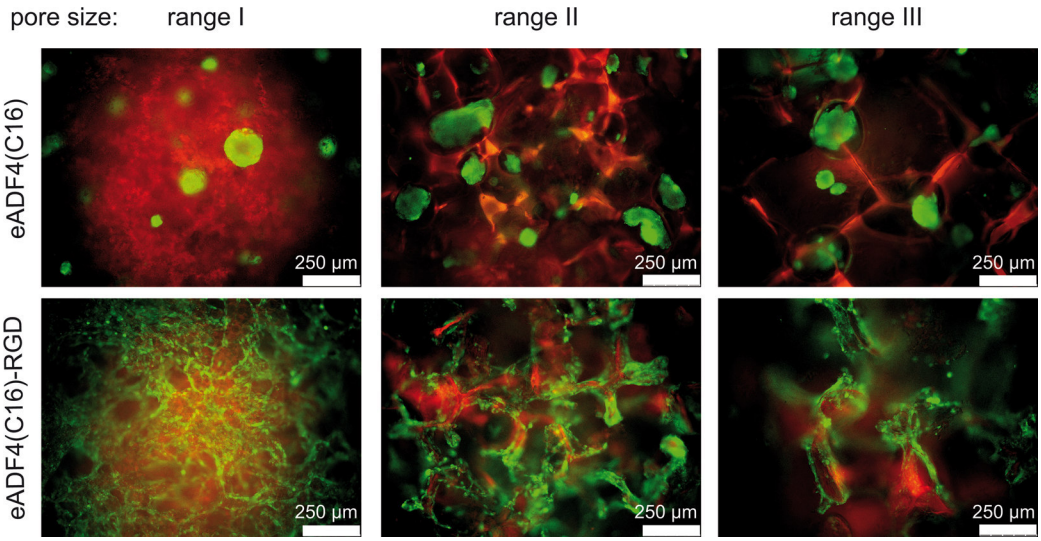

Figure 4. Fluorescence microscopy images of BALB/3T3 fibroblasts cultivated on 8% (w/v) eADF4(C16) and 8% (w/v) eADF4(C16)-RGD foams with different pore sizes and >91% porosity after 7 days of incubation. The cells were stained with Calcein A/M (green). The scaffolds were stained with Rhodamin-B.

PXIV is more likely a suitable model for digestive enzymes, it was here used as an additional model enzyme to allow comparison with previously published data.[48,49] In correspondence to previous degradation experiments of other eADF4-

DOI: 10.1021/acsbiomaterials.5b00483
ACS Biomater. Sci. Eng. 2016, 2, 517−525

(C16) morphologies (particles, films and nonwoven meshes) with PXIV and CHC the total amount of 87.5 μg protease per 1 mg scaffold was kept constant, resulting in a concentration of 465 μg/mL, which is a factor of 1300 higher than the naturally occurring 351 ng/mL of wound proteases.[35] Degradation experiments were not feasible at lower protease concentrations, due to the slow kinetics and to the extremely low concentration of degradation products (being below the detection limit). Therefore, it should be kept in mind that degradation in vivo might be much slower than the here detected degradation in vitro.

Similar to previously published results with hydrogels made of *B. mori* fibroin, in the presence of PXIV the 3D-scaffolds degraded quickly within 4 days (remaining hydrogel: 9.25 wt %; remaining foam: 6.62 wt %), whereas in the presence of CHC less degradation could be detected even after 15 days (remaining hydrogel: 46.55 wt %; remaining foam: 74.75 wt %), confirming the high proteolytic activity of PXIV for silk materials.[45,46,50,51]

Compared to the degradation of other morphologies made of recombinant spider silk, the hydrogels and foams degraded relatively quickly in the presence of CHC. Only particles degraded faster (93% in 15 days), while films and nonwoven meshes degraded only up to 13% and 5% within 15 days, respectively.[35] This phenomenon can be explained by the high surface-to-volume ratio, based on the high porosity of the salt-leached foams. However, it has to be noted that the protease concentration was 3 times higher in the experiments with foams and hydrogels (465 μg/mL) in comparison to experiments with particles, films and nonwoven meshes (175 μg/mL).[35]

Cell Viability and Morphology. To analyze the biocompatibility of the scaffolds, BALB/3T3 mouse fibroblasts were cultivated on foams made of 8% (w/v) eADF4(C16) and eADF4(C16)-RGD with different pore sizes over 7 days (Figure 4, Figure S5).

The cell adhesion was weak on eADF4(C16) foams independent of the pore size. The cells showed a round morphology, and cell aggregates were detected. Rounded morphology and cell aggregates of mouse fibroblasts could be also observed on hydrogels and films made of eADF4(C16) under various cell culture conditions.[28] Because of the lack of cell binding motifs in eADF4(C16), adhesion is mostly influenced by hydrophobicity, surface charge and topography of the scaffold.[28,52,53] However, the cells were viable over at least 1 week in such spider silk foams. Adhesion of cells was improved on foams made of eADF4(C16)-RGD compared to those made of eADF4(C16). The cells attached to the strands of the porous structures and showed spread morphology. Furthermore, the cells were homogeneously distributed inside the eADF4(C16)-RGD scaffolds and covered almost the entire scaffold within 7 days, without an apparent influence of the pore size (Figure S5). The improved cell adhesion on eADF4(C16)-RGD foams correlates well with results obtained from experiments performed on hydrogels and films.[28,54] However, whereas fibroblasts encapsulated in hydrogels showed a round shape due to the dense fibrillary network, the open-cell interconnetive and porous structure of the foams obviously rendered these scaffolds more attractive for the cells.[54]

Adhesion and Proliferation. To evaluate cytocompatibility of the spider silk foams, we quantified adhesion and proliferation of fibroblasts using the cell-titer blue assay. Cell seeding densities and efficiencies were calculated after 24 h of incubation (Table S2).

Porous scaffolds made of 45S5 Bioglass (Figure 5C) and aluminum oxide (Al_2O_3) (Figure 5D) were used as 3D

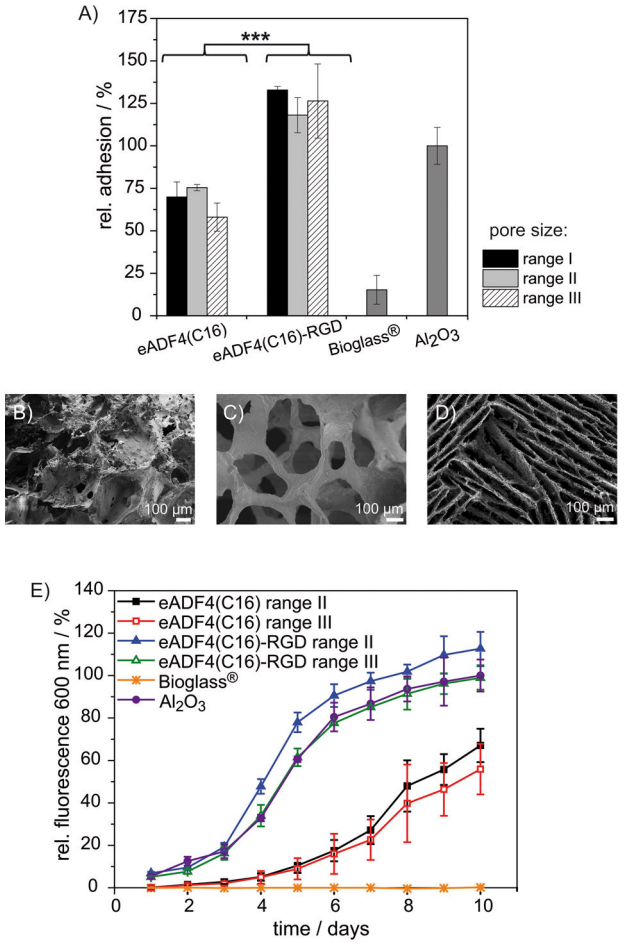

Figure 5. Cultivation of BALB/3T3 fibroblasts on 8% (w/v) eADF4(C16) and 8% (w/v) eADF4(C16)-RGD foams with different pore sizes (as indicated) and >91% porosity. 45S5 Bioglass and Al_2O_3 foams were used as controls. (A) Adhesion was quantified after 24 h of incubation by using the cell-titer blue assay and normalized to adhesion on Al_2O_3 scaffolds (positive control). The adhesion of all tested samples was significantly improved (***$p < 0.0001$) on eADF4(C16)-RGD foams compared to that on eADF4(C16) foams. (B–D) Scanning electron microscopy images of 8% (w/v) eADF4-(C16) (B), 45S5 Bioglass (C) and Al_2O_3 (D) scaffolds. E) Analysis of the proliferation of BALB/3T3 fibroblasts on 8% (w/v) eADF4(C16), 8% eADF4(C16)-RGD, 45S5 Bioglass, and Al_2O_3 scaffolds in a controlled atmosphere of 5% CO_2, 95% humidity and at 37 °C. Proliferation was quantified by using the cell-titer blue assay and normalized to proliferation on Al_2O_3 scaffolds (positive control) at day 10.

controls. 45S5 Bioglass is a highly porous and brittle bioactive ceramic material with a porosity of ~90%, pore sizes between 200 and 500 μm, and compressive and bending strengths in the range of 0.3–0.5 MPa.[6,55] The freeze-cast aluminum scaffolds showed an aligned honeycomb structure with pore sizes of 100–500 μm, porosity of 40–85% and a compressive strength in the range of 10–95 MPa (Figure 5D).[56−59]

Figure 5A shows the adhesion of fibroblasts on the scaffolds after 24 h of incubation. All values were normalized to adhesion on Al_2O_3 scaffolds (positive control). Even after 24 h of intensive washing of the scaffolds with water, PBS or DMEM

DOI: 10.1021/acsbiomaterials.5b00483
ACS Biomater. Sci. Eng. 2016, 2, 517−525

before seeding of the cells, the 45S5 Bioglass scaffolds released alkaline substances hampering the viability of the cells resulting in a low adhesion of only 15 ± 9% relative to the fluorescence intensity of Al_2O_3 scaffolds. The release was observed using the pH indicator phenol red in the cell culture medium. In correlation with the results of the Calcein A/M staining, the fibroblasts showed a significantly improved adhesion on eADF4(C16)-RGD foams compared to that on eADF4(C16) ones. The relative adhesion was determined to be 70 ± 9% (63−125 μm), 75 ± 2% (125−315 μm) and 58 ± 8% (315−500 μm) for foams made of eADF4(C16) in comparison to that on the positive control. On scaffolds made of eADF4(C16)-RGD the fibroblasts adhered with 133 ± 2% (63−125 μm), 118 ± 10% (125−315 μm), and 126 ± 22% (315−500 μm) of the adhesion on the positive control, showing the strong influence of the type of protein, as well as in this case the low impact of the pore size at the given size ranges on cell adhesion.

Next, the proliferation of fibroblasts was tested on the scaffolds over 10 days (Figure 5E). Fibroblasts could not grow on 45S5 Bioglass scaffolds, but proliferated well on Al_2O_3 scaffolds. All values were normalized to proliferation on Al_2O_3 scaffolds (positive control) at day 10. On eADF4(C16)-RGD foams, the cells showed a very similar growth rate compared to that on Al_2O_3 scaffolds, whereas the cell proliferation was significantly decreased on foams made of eADF4(C16). After 10 days of incubation, almost twice the amount of cells were detected on eADF4(C16)-RGD foams (113 ± 8%, 125−315 μm and 99 ± 6%, 315−500 μm, relative to the fluorescence intensity of the positive control) when compared to scaffolds made of eADF4(C16) (67 ± 8%, 125−315 μm and 56 ± 12%, 315−500 μm). While fibroblasts reached the plateau phase of growth on the eADF4(C16)-RGD foams after 10 days, the cells on the eADF4(C16) foams were still growing in the exponential growth phase at that time point. Interestingly, an influence of the pore size was detectable on cell proliferation. On both foams, made of eADF4(C16) and eADF4(C16)-RGD, the cells proliferated faster on the scaffolds with pores sizes between 125 and 315 μm, compared to scaffolds with bigger pores (315−500 μm). Foams with smaller pore sizes between 63 and 125 μm could not be used, because it was particularly difficult to wash these foams in order to remove residues of the cell-titer blue assay, which interfered with the measurements leading to data misinterpretation.

In summary, the results showed an improved adhesion and proliferation of BALB/3T3 fibroblasts on foams made of eADF4(C16)-RGD compared to ones made of eADF4(C16), which is due to the presence of the cell recognition motif RGD.[28,54] In accordance with this finding, matrices (e.g., fibers, foams and films) made of the RGD-modified 4RepCT showed significantly improved cell adhesion in comparison to unmodified 4RepCT matrices.[60] The spider silk matrices with the cell binding motif RGD promoted early adherence of all tested cells types (fibroblasts, keratinocytes, endothelial and Schwann cells) which formed stress fibers and distinct focal adhesion points.[60] The adhesion and proliferation of the cells on RGD-modified spider silk scaffolds was even better than on Bioglass and Al_2O_3 scaffolds. Both Bioglass and Al_2O_3 scaffolds are generally fabricated as scaffolds for bone tissue engineering.[56] Fibroblasts prefer softer materials instead of osteoblast-like cells, however, explaining the observed results. Additionally, salt leached spider silk scaffolds showed a higher porosity and smaller pore sizes than both ceramic scaffolds. Oh et al. evaluated the optimal pore size for fibroblasts growing on cylindrical PCL scaffolds, in which fibroblasts preferred a smaller pore size range (186−200 μm) compared to chondrocytes (380−405 μm), because of the higher surface area for cell attachment and signaling.[61]

CONCLUSION

Salt-leached foams of the recombinant spider silk proteins eADF4(C16) and eADF4(C16)-RGD were fabricated with tunable properties. NaCl crystals allowed the production of β-sheet-rich scaffolds with a porosity of at least 91% without the need of additives or cross-linkers for mechanical stabilization. The mechanical properties of the foams were simply adjusted by the protein concentration. The compressive moduli were in the range of soft tissue, rendering the spider silk foams suitable scaffolds for soft tissue engineering, as well as wound dressings. The proteolytic degradation of the spider silk foams in the presence of a model protease mix for wound healing proteases confirmed the biodegradability of recombinant spider silk proteins. In cell adhesion assays, fibroblasts showed a round morphology and weak adhesion on salt leached foams made of eADF4(C16), but cell adhesion and proliferation was significantly improved on foams made of eADF4(C16)-RGD. Fibroblasts proliferated best in foams with a middle pore size, because of the combination of good nutrient and waste product transport and a high surface area. Compared to other porous scaffolds such as Al_2O_3 and Bioglass, cell adhesion and proliferation was slightly better on eADF4(C16)-RGD foams. The results indicate that spider silk foams with controllable properties can be used as scaffolds for tissue repair and soft tissue engineering.

ASSOCIATED CONTENT

Supporting Information

The Supporting Information is available free of charge on the ACS Publications website at DOI: 10.1021/acsbiomaterials.5b00483.

Detailed information about the fabrication of foams made of recombinant spider silk proteins by salt leaching; Fourier transform infrared spectra of foams and films and their Fourier self-deconvolution spectra; as well as swelling analysis, cell seeding efficiencies, and confocal scanning microscopy images (PDF)

AUTHOR INFORMATION

Corresponding Author

*E-mail: thomas.scheibel@bm.uni-bayreuth.de. Tel.: +49 (0) 921 55 7361. Fax: +49 (0) 921 55 7346.

Present Address

[§]J.V. is currently at RESORBA Medical GmbH, Am Flachmoor 16, D-90475 Nürnberg, Germany

Author Contributions

[†]These authors contributed equally. The manuscript was written through contributions of all authors. All authors have given approval to the final version of the manuscript.

Notes

The authors declare no competing financial interest.

ACKNOWLEDGMENTS

We thank Dr. Hendrik Bargel for scanning electron microscopy, Prof. Dr. Gregor Lang for experimental help

DOI: 10.1021/acsbiomaterials.5b00483
ACS Biomater. Sci. Eng. 2016, 2, 517−525

with tensile testing, Elena Doblhofer for experimental help with FTIR and FSD, and Aniela Heidebrecht for proof reading and discussions. The sintered 45S5 Bioglass® scaffolds, fabricated by the replication method, were produced at the Department of Biomaterials, University Erlangen-Nuremberg, supervised by Prof. Dr. Aldo R. Boccaccini. The freeze-cast aluminum oxide (Al_2O_3) scaffolds were prepared at the Thayer School of Engineering at Dartmouth, supervised by Prof. Dr. Ulrike Wegst. This work was supported by the Deutsche Forschungsgemeinschaft (SFB 840 TPA8).

■ ABBREVIATIONS

ADF4, *Araneus diadematus* fibroin 4
eADF4, engineered *Araneus diadematus* fibroin 4
Al_2O_3, aluminum oxide
HFIP, 1,1,1,3,3,3-hexafluoro-2-propanol
w/v, weight/volume
NaCl, sodium chloride
Tris/HCl, Tris(hydroxymethyl)aminomethane hydrochloride
p.a, *pro analysi*
PEG, polyethylene glycol
FTIR, Fourier transform infrared
ATR, attenuated total reflection
FSD, Fourier self-deconvolution
SEM, scanning electron microscopy
v/v, volume/volume
TCNB, Tris/$CaCl_2$/NaCl/Brij 35
PXIV, protease type XIV from *Streptomyces griseus*
CHC, collagenase type IA from *Clostridium histolyticum*
$CaCl_2$, calcium chloride
DMEM, Dulbecco's Modified Eagle Medium
PBS, phosphate buffered saline
Calcein A/M, calcein acetoxymethyl ester

■ REFERENCES

(1) Nazarov, R.; Jin, H. J.; Kaplan, D. L. Porous 3-D scaffolds from regenerated silk fibroin. *Biomacromolecules* **2004**, *5* (3), 718−726.
(2) Lutolf, M. P.; Hubbell, J. A. Synthetic biomaterials as instructive extracellular microenvironments for morphogenesis in tissue engineering. *Nat. Biotechnol.* **2005**, *23* (1), 47−55.
(3) Engler, A. J.; Sen, S.; Sweeney, H. L.; Discher, D. E. Matrix elasticity directs stem cell lineage specification. *Cell* **2006**, *126* (4), 677−689.
(4) Engler, A. J.; Humbert, P. O.; Wehrle-Haller, B.; Weaver, V. M. Multiscale Modeling of Form and Function. *Science* **2009**, *324* (5924), 208−212.
(5) Reddig, P. J.; Juliano, R. L. Clinging to life: cell to matrix adhesion and cell survival. *Cancer Metastasis Rev.* **2005**, *24* (3), 425−439.
(6) Chen, Q. Z. Z.; Thompson, I. D.; Boccaccini, A. R. 45S5 Bioglass (R)-derived glass-ceramic scaffolds for bone tissue engineering. *Biomaterials* **2006**, *27* (11), 2414−2425.
(7) Griffith, L. G.; Naughton, G. Tissue engineering - Current challenges and expanding opportunities. *Science* **2002**, *295* (5557), 1009−1014.
(8) Wells, R. G. The role of matrix stiffness in regulating cell behavior. *Hepatology* **2008**, *47* (4), 1394−1400.
(9) Saez, A.; Ghibaudo, M.; Buguin, A.; Silberzan, P.; Ladoux, B. Rigidity-driven growth and migration of epithelial cells on microstructured anisotropic substrates. *Proc. Natl. Acad. Sci. U. S. A.* **2007**, *104* (20), 8281−8286.
(10) Discher, D. E.; Janmey, P.; Wang, Y. L. Tissue cells feel and respond to the stiffness of their substrate. *Science* **2005**, *310* (5751), 1139−1143.
(11) Jin, H. J.; Park, J.; Valluzzi, R.; Cebe, P.; Kaplan, D. L. Biomaterial films of Bombyx mori silk fibroin with poly(ethylene oxide). *Biomacromolecules* **2004**, *5* (3), 711−717.
(12) Jiang, C. Y.; Wang, X. Y.; Gunawidjaja, R.; Lin, Y. H.; Gupta, M. K.; Kaplan, D. L.; Naik, R. R.; Tsukruk, V. V. Mechanical properties of robust ultrathin silk fibroin films. *Adv. Funct. Mater.* **2007**, *17* (13), 2229−2237.
(13) Liu, H. F.; Fan, H. B.; Toh, S. L.; Goh, J. C. H. A comparison of rabbit mesenchymal stem cells and anterior cruciate ligament fibroblasts responses on combined silk scaffolds. *Biomaterials* **2008**, *29* (10), 1443−1453.
(14) Vepari, C.; Kaplan, D. L. Silk as a biomaterial. *Prog. Polym. Sci.* **2007**, *32* (8−9), 991−1007.
(15) Wang, Y.; Rudym, D. D.; Walsh, A.; Abrahamsen, L.; Kim, H. J.; Kim, H. S.; Kirker-Head, C.; Kaplan, D. L. In vivo degradation of three-dimensional silk fibroin scaffolds. *Biomaterials* **2008**, *29* (24−25), 3415−3428.
(16) Lv, Q.; Feng, Q. L. Preparation of 3-D regenerated fibroin scaffolds with freeze drying method and freeze drying/foaming technique. *J. Mater. Sci.: Mater. Med.* **2006**, *17* (12), 1349−1356.
(17) Tamada, Y. New process to form a silk fibroin porous 3-D structure. *Biomacromolecules* **2005**, *6* (6), 3100−3106.
(18) Zhang, X. H.; Baughman, C. B.; Kaplan, D. L. In vitro evaluation of electrospun silk fibroin scaffolds for vascular cell growth. *Biomaterials* **2008**, *29* (14), 2217−2227.
(19) Lu, Q.; Zhang, X. H.; Hu, X.; Kaplan, D. L. Green Process to Prepare Silk Fibroin/Gelatin Biomaterial Scaffolds. *Macromol. Biosci.* **2010**, *10* (3), 289−298.
(20) Kim, U. J.; Park, J.; Kim, H. J.; Wada, M.; Kaplan, D. L. Three-dimensional aqueous-derived biomaterial scaffolds from silk fibroin. *Biomaterials* **2005**, *26* (15), 2775−2785.
(21) Rajkhowa, R.; Gil, E. S.; Kluge, J.; Numata, K.; Wang, L. J.; Wang, X. D.; Kaplan, D. L. Reinforcing Silk Scaffolds with Silk Particles. *Macromol. Biosci.* **2010**, *10* (6), 599−611.
(22) Yao, D. Y.; Dong, S.; Lu, Q.; Hu, X.; Kaplan, D. L.; Zhang, B. B.; Zhu, H. S. Salt-Leached Silk Scaffolds with Tunable Mechanical Properties. *Biomacromolecules* **2012**, *13* (11), 3723−3729.
(23) Lewicka, M.; Hermanson, O.; Rising, A. U. Recombinant spider silk matrices for neural stem cell cultures. *Biomaterials* **2012**, *33* (31), 7712−7717.
(24) Widhe, M.; Bysell, H.; Nystedt, S.; Schenning, I.; Malmsten, M.; Johansson, J.; Rising, A.; Hedhammar, M. Recombinant spider silk as matrices for cell culture. *Biomaterials* **2010**, *31* (36), 9575−9585.
(25) Hedhammar, M.; Rising, A.; Grip, S.; Martinez, A. S.; Nordling, K.; Casals, C.; Stark, M.; Johansson, J. Structural properties of recombinant nonrepetitive and repetitive parts of major ampullate spidroin 1 from Euprosthenops australis: Implications for fiber formation. *Biochemistry* **2008**, *47* (11), 3407−3417.
(26) Huemmerich, D.; Helsen, C. W.; Quedzuweit, S.; Oschmann, J.; Rudolph, R.; Scheibel, T. Primary structure elements of spider dragline silks and their contribution to protein solubility. *Biochemistry* **2004**, *43* (42), 13604−13612.
(27) Hardy, J. G.; Romer, L. M.; Scheibel, T. R. Polymeric materials based on silk proteins. *Polymer* **2008**, *49* (20), 4309−4327.
(28) Wohlrab, S.; Muller, S.; Schmidt, A.; Neubauer, S.; Kessler, H.; Leal-Egana, A.; Scheibel, T. Cell adhesion and proliferation on RGD-modified recombinant spider silk proteins. *Biomaterials* **2012**, *33* (28), 6650−6659.
(29) Huemmerich, D.; Slotta, U.; Scheibel, T. Processing and modification of films made from recombinant spider silk proteins. *Appl. Phys. A: Mater. Sci. Process.* **2006**, *82* (2), 219−222.
(30) Schacht, K.; Scheibel, T. Controlled Hydrogel Formation of a Recombinant Spider Silk Protein. *Biomacromolecules* **2011**, *12* (7), 2488−2495.
(31) Hu, X.; Kaplan, D.; Cebe, P. Determining beta-sheet crystallinity in fibrous proteins by thermal analysis and infrared spectroscopy. *Macromolecules* **2006**, *39* (18), 6161−6170.

DOI: 10.1021/acsbiomaterials.5b00483
ACS Biomater. Sci. Eng. 2016, 2, 517−525

(32) Hu, Y. H.; Grainger, D. W.; Winn, S. R.; Hollinger, J. O. Fabrication of poly(alpha-hydroxy acid) foam scaffolds using multiple solvent systems. *J. Biomed. Mater. Res.* **2002**, *59* (3), 563−572.
(33) Cappella, B.; Dietler, G. Force-distance curves by atomic force microscopy. *Surf. Sci. Rep.* **1999**, *34* (1−3), 1−104.
(34) Neubauer, M. P.; Blum, C.; Agostini, E.; Engert, J.; Scheibel, T.; Fery, A. Micromechanical characterization of spider silk particles. *Biomater. Sci.* **2013**, *1* (11), 1160−1165.
(35) Muller-Herrmann, S.; Scheibel, T. Enzymatic Degradation of Films, Particles, and Nonwoven Meshes Made of a Recombinant Spider Silk Protein. *ACS Biomater. Sci. Eng.* **2015**, *1*, 247−259.
(36) Agrawal, C. M.; Ray, R. B. Biodegradable polymeric scaffolds for musculoskeletal tissue engineering. *J. Biomed. Mater. Res.* **2001**, *55* (2), 141−150.
(37) Maquet, V.; Blacher, S.; Pirard, R.; Pirard, J. P.; Jerome, R. Characterization of porous polylactide foams by image analysis and impedance spectroscopy. *Langmuir* **2000**, *16* (26), 10463−10470.
(38) Lee, S. B.; Kim, Y. H.; Chong, M. S.; Lee, Y. M. Preparation and characteristics of hybrid scaffolds composed of beta-chitin and collagen. *Biomaterials* **2004**, *25* (12), 2309−2317.
(39) Slotta, U.; Tammer, M.; Kremer, F.; Koelsch, P.; Scheibel, T. Structural analysis of spider silk films. *Supramol. Chem.* **2006**, *18* (5), 465−471.
(40) Hollinger, J. O.; Leong, K. Poly(alpha-hydroxy acids): Carriers for bone morphogenetic proteins. *Biomaterials* **1996**, *17* (2), 187−194.
(41) Janmey, P. A.; Winer, J. P.; Murray, M. E.; Wen, Q. The Hard Life of Soft Cells. *Cell Motil. Cytoskeleton* **2009**, *66* (8), 597−605.
(42) Zhang, X. H.; Cao, C. B.; Ma, X. L.; Li, Y. A. Optimization of macroporous 3-D silk fibroin scaffolds by salt-leaching procedure in organic solvent-free conditions. *J. Mater. Sci.: Mater. Med.* **2012**, *23* (2), 315−324.
(43) Yan, L. P.; Oliveira, J. M.; Oliveira, A. L.; Caridade, S. G.; Mano, J. F.; Reis, R. L. Macro/microporous silk fibroin scaffolds with potential for articular cartilage and meniscus tissue engineering applications. *Acta Biomater.* **2012**, *8* (1), 289−301.
(44) Zhao, C. X.; Wu, X. F.; Zhang, Q. A.; Yan, S. Q.; Li, M. Z. Enzymatic degradation of Antheraea pernyi silk fibroin 3D scaffolds and fibers. *Int. J. Biol. Macromol.* **2011**, *48* (2), 249−255.
(45) Li, M. Z.; Ogiso, M.; Minoura, N. Enzymatic degradation behavior of porous silk fibroin sheets. *Biomaterials* **2003**, *24* (2), 357−365.
(46) Brown, J.; Lu, C. L.; Coburn, J.; Kaplan, D. L. Impact of silk biomaterial structure on proteolysis. *Acta Biomater.* **2015**, *11*, 212−221.
(47) Wolters, G. H. J.; Vosscheperkeuter, G. H.; Lin, H. C.; Vanschilfgaarde, R. Different Roles of Class-I and Class-Ii Clostridium-Histolyticum Collagenase in Rat Pancreatic-Islet Isolation. *Diabetes* **1995**, *44* (2), 227−233.
(48) Bauer, C. A.; Lofqvist, B.; Pettersson, G. Studies on the catalytic mechanism of a serine protease from Streptomyces griseus. *Eur. J. Biochem.* **1974**, *41* (1), 45−9.
(49) Bauer, C. A.; Pettersson, G. Effect of pH on the catalytic activity of Streptomyces griseus protease 3. *Eur. J. Biochem.* **1974**, *45* (2), 469−72.
(50) Pritchard, E. M.; Valentin, T.; Boison, D.; Kaplan, D. L. Incorporation of proteinase inhibitors into silk-based delivery devices for enhanced control of degradation and drug release. *Biomaterials* **2011**, *32* (3), 909−918.
(51) Arai, T.; Freddi, G.; Innocenti, R.; Tsukada, M. Biodegradation of Bombyx mori silk fibroin fibers and films. *J. Appl. Polym. Sci.* **2004**, *91* (4), 2383−2390.
(52) Leal-Egana, A.; Scheibel, T. Interactions of cells with silk surfaces. *J. Mater. Chem.* **2012**, *22* (29), 14330−14336.
(53) Bauer, F.; Wohlrab, S.; Scheibel, T. Controllable cell adhesion, growth and orientation on layered silk protein films. *Biomater. Sci.* **2013**, *1* (12), 1244−1249.
(54) Schacht, K.; Jungst, T.; Schweinlin, M.; Ewald, A.; Groll, J.; Scheibel, T. Biofabrication of Cell-Loaded 3D Spider Silk Constructs. *Angew. Chem., Int. Ed.* **2015**, *54* (9), 2816−2820.
(55) Chen, Q. Z.; Efthymiou, A.; Salih, V.; Boccaccinil, A. R. Bioglass (R)-derived glass-ceramic scaffolds: Study of cell proliferation and scaffold degradation in vitro. *J. Biomed. Mater. Res., Part A* **2008**, *84A* (4), 1049−1060.
(56) Deville, S. Freeze-Casting of Porous Biomaterials: Structure, Properties and Opportunities. *Materials* **2010**, *3* (3), 1913−1927.
(57) Wegst, U. G. K.; Schecter, M.; Donius, A. E.; Hunger, P. M. Biomaterials by freeze casting. *Philos. Trans. R. Soc., A* **2010**, *368* (1917), 2099−2121.
(58) Yoon, B. H.; Choi, W. Y.; Kim, H. E.; Kim, J. H.; Koh, Y. H. Aligned porous alumina ceramics with high compressive strengths for bone tissue engineering. *Scr. Mater.* **2008**, *58* (7), 537−540.
(59) Deville, S.; Saiz, E.; Tomsia, A. P. Ice-templated porous alumina structures. *Acta Mater.* **2007**, *55* (6), 1965−1974.
(60) Widhe, M.; Johansson, U.; Hillerdahl, C. O.; Hedhammar, M. Recombinant spider silk with cell binding motifs for specific adherence of cells. *Biomaterials* **2013**, *34* (33), 8223−8234.
(61) Oh, S. H.; Park, I. K.; Kim, J. M.; Lee, J. H. In vitro and in vivo characteristics of PCL scaffolds with pore size gradient fabricated by a centrifugation method. *Biomaterials* **2007**, *28* (9), 1664−1671.

DOI: 10.1021/acsbiomaterials.5b00483
ACS Biomater. Sci. Eng. 2016, 2, 517−525

SUPPORTING INFORMATION

Foams made of engineered recombinant spider silk proteins as 3D scaffolds for cell growth

Kristin Schacht[‡], Jessica Vogt[‡] and Thomas Scheibel

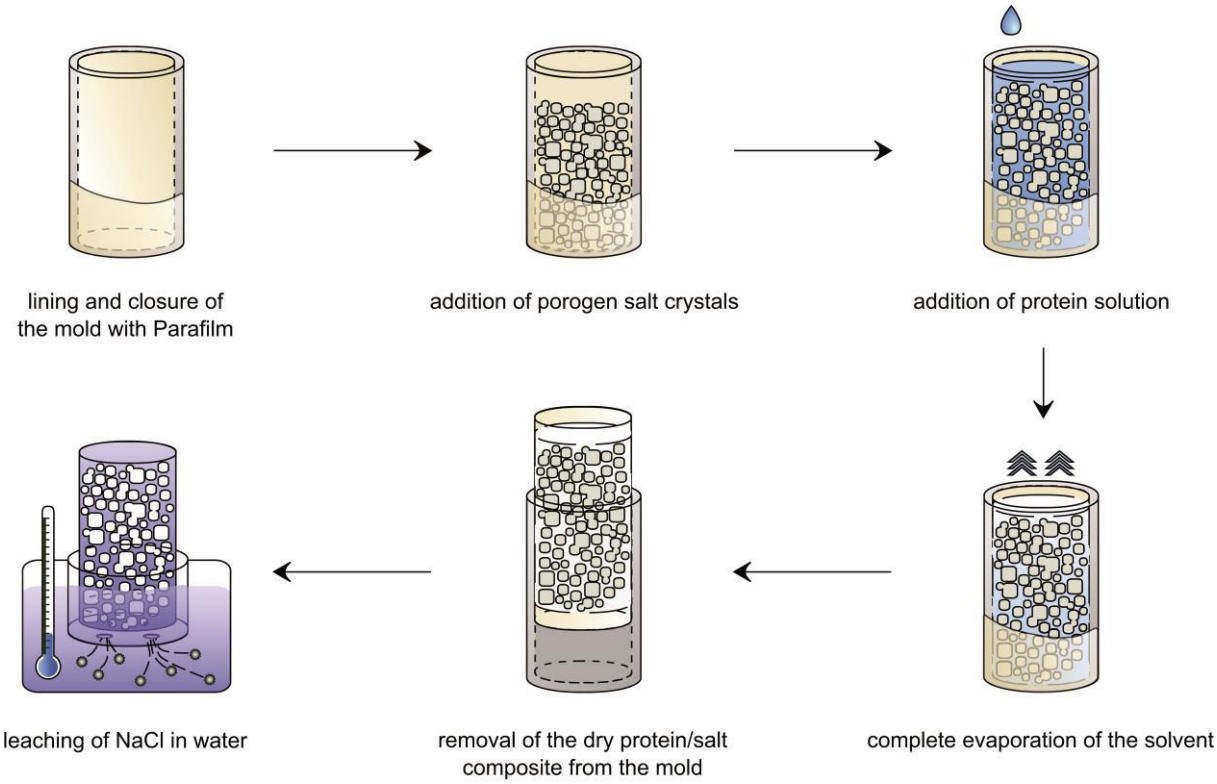

Figure S1. Foam preparation by the salt leaching technique. For the foam preparation, lyophilized recombinant spider silk proteins were dissolved in 1,1,1,3,3,3-Hexafluoro-2-propanol (HFIP) (Alfa Aesar) at final concentrations of 4, 6 and 8% (w/v). Sodium chloride crystals (NaCl) were used as porogen. NaCl crystals were sieved to achieve size ranges of 63-125 µm, 125-315 µm or 315-500 µm. A protein solution was cast on the salt crystals in cylindrical molds at a 75:1 (4% (w/v)), 50:1 (6% (w/v)), and 37.5:1 (8% (w/v)) (w/w) salt/protein ratio. The solvent was evaporated for at least 48 h, and NaCl was leached out in milli-Q water for 24 h upon 6-8 water changes.

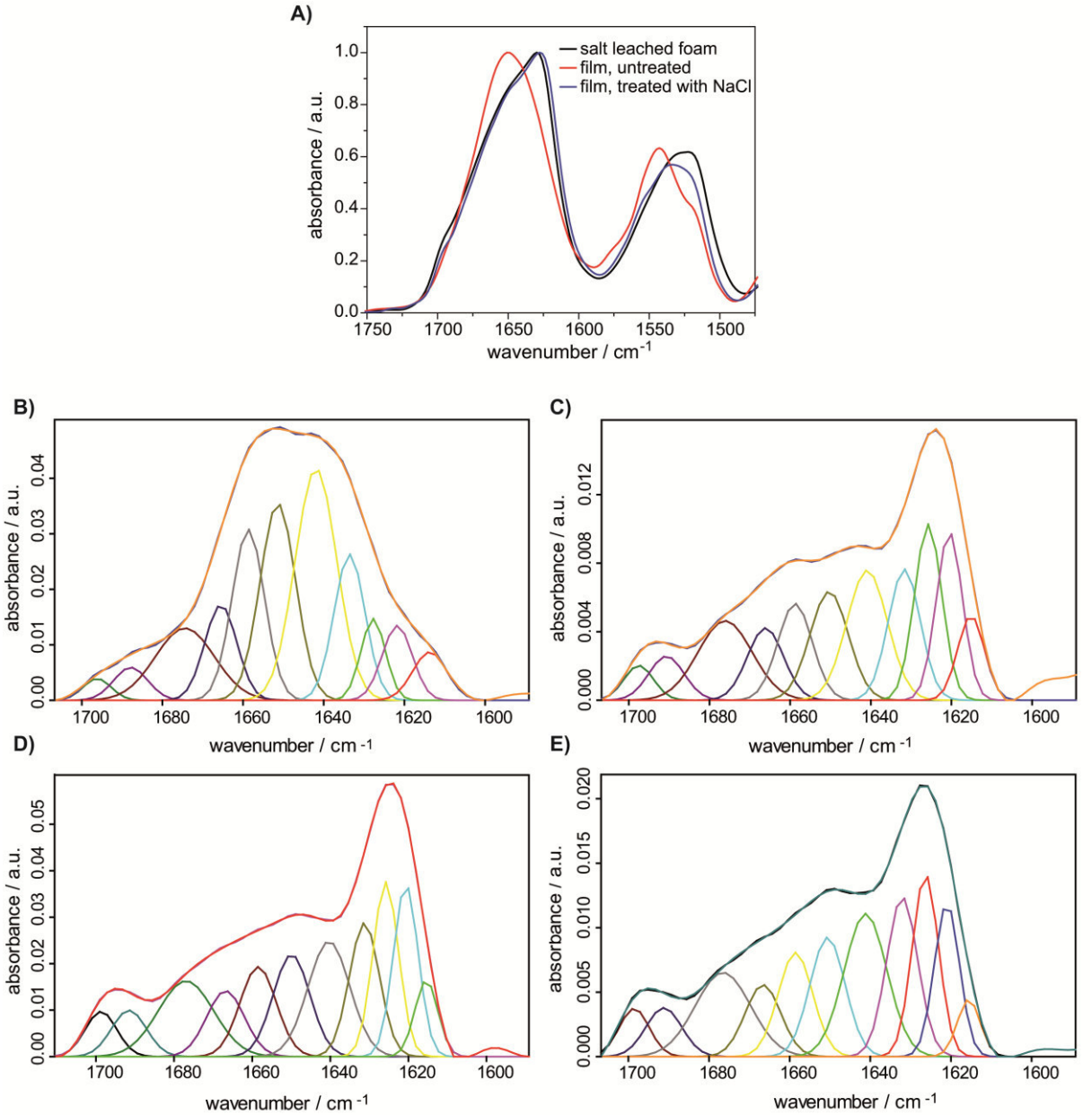

Figure S2. FTIR (1750 – 1475 cm^{-1}) (A) and Fourier self-deconvolution (FSD) spectra (1720 – 1590 cm^{-1}) (B-E) of salt leached foams (E) in comparison to that of untreated films (B), salt-treated (C), and 100% methanol-treated (D) films made of eADF4(C16). For film preparation, the silk protein solutions (4, 6 and 8% (w/v) eADF4(C16) in HFIP) were cast in cylindrical molds without salt crystals. After evaporation of the solvent the films were either stored untreated or they were post-treated upon incubation in 6 M NaCl solution or 100% methanol for 4 h to induce β-sheet formation rendering silk films water insoluble.

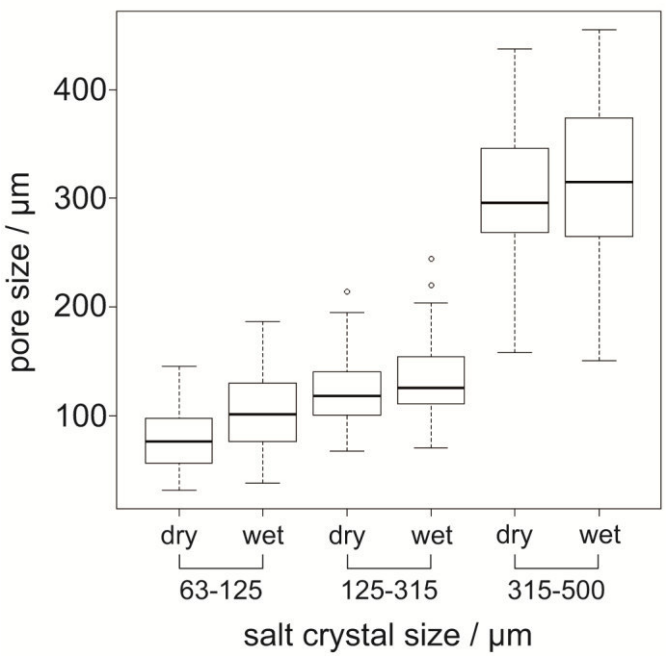

Figure S3. Pore sizes of salt leached foams made of 8% (w/v) eADF4(C16) with different salt particle sizes have been analyzed in a freeze-dried state.

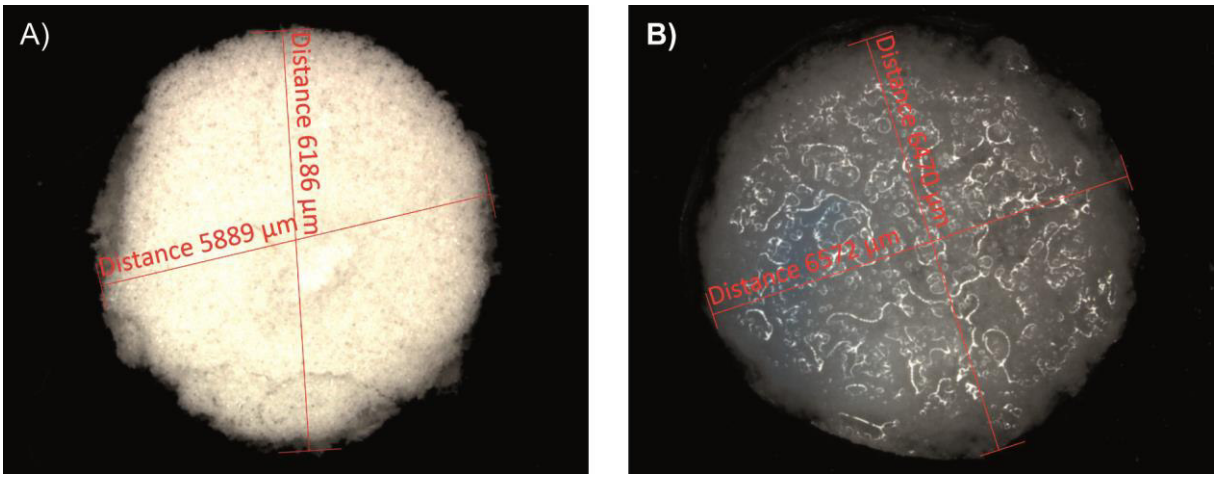

Figure S4. Stereomicroscope measurements to determine the swelling ratio of 8% (w/v) salt-leached eADF4(C16) foams with 63-125 µm salt crystal size. A) Dry state; B) Wet state.

Table S1. Swelling percentage of salt leached foams made of eADF4(C16) as analyzed by stereomicroscopy.

	spider silk concentration / (w/v) %		
	4	**6**	**8**
salt crystal size / µm	**swelling / %**		
63 – 125	6.1 ± 1.8	7.4 ± 0.5	8.9 ± 2.5
125 – 315	4.9 ± 2.2	4.5 ± 0.3	4.0 ± 2.2
315 – 500	4.3 ± 1.1	2.7 ± 1.0	3.2 ± 1.1

Table S2. Cell seeding densities used in the adhesion test with BALB/3T3 fibroblasts after 24 hours of incubation. The data were normalized to the treated cell culture plate.

		Al_2O_3	Bioglass®	eADF4(C16)			eADF4(C16)-RGD		
				range I	range II	range III	range I	range II	range III
cell seeding density / %	*cell culture plate*	0 ± 0.1	0 ± 0.1	18 ± 16.5	20 ± 3.3	49 ± 13.3	27 ± 45	11 ± 13.3	31 ± 3.0
	scaffold	69 ± 10	81 ± 21	48 ± 8	52 ± 2	40 ± 8	92 ± 2	82 ± 10	87 ± 20
cell seeding efficiency / %		**100**	**100**	**73**	**72**	**45**	**78**	**88**	**74**

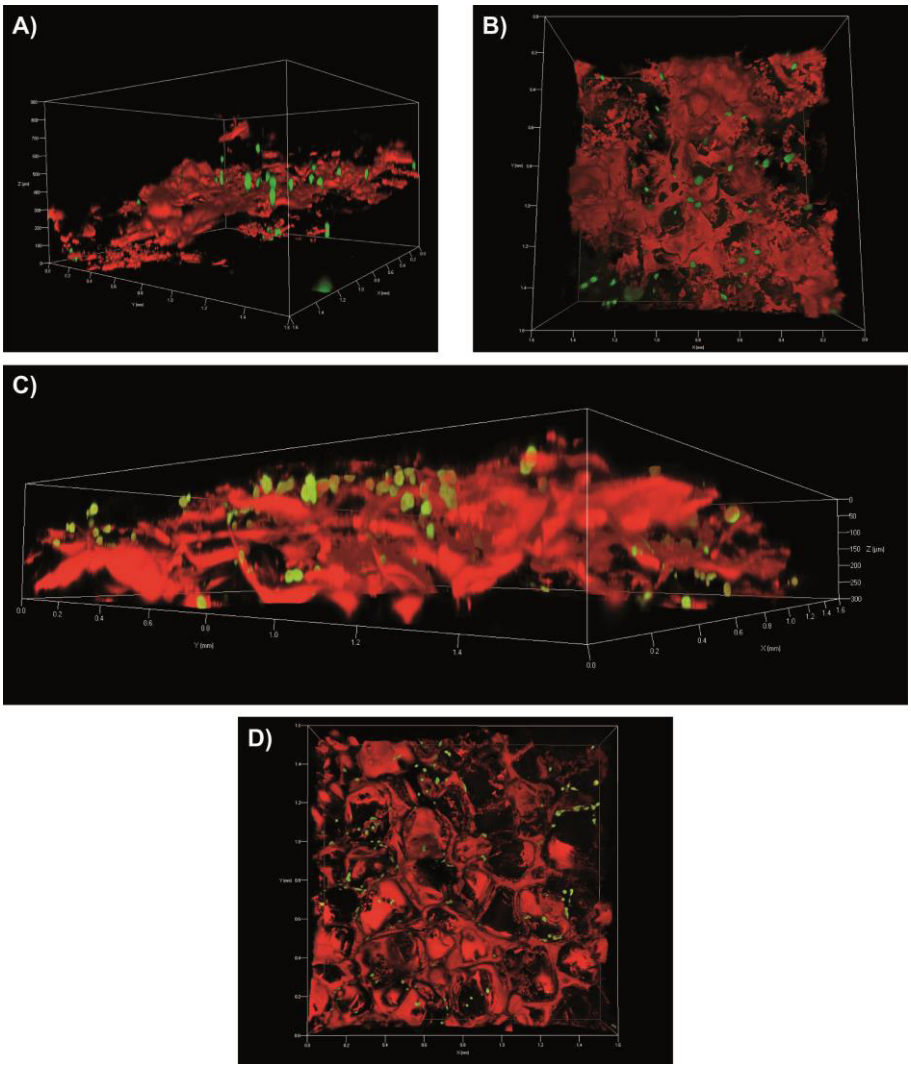

Figure S5. Confocal scanning microscopy images of BALB/3T3 fibroblasts cultivated on 8% (w/v) eADF4(C16) (A & B) and 8% (w/v) eADF4(C16)-RGD (C & D) foams with 125-315 µm salt particle size after 24 hours of incubation. The cells were stained with Calcein A/M (green) and the scaffolds with Rhodamin-B.

TEILARBEIT II

Die Ergebnisse dieses Kapitels wurden bereits in *Angewandte Chemie* veröffentlicht als:

> "Biofabrication of Cell-Loaded 3D Spider Silk Constructs " Schacht, K.*, Jungst, T.*, Schweinlin, M., Ewald, A., Groll, J. und Scheibel, T..

Reproduziert aus *Angewandte Chemie* **2015**, 54: 2816-2820 mit freundlicher Genehmigung des Verlages John Wiley and Sons.

* gleichberechtigte Co-Autorenschaft

Biofabrication

DOI: 10.1002/anie.201409846

Biofabrication of Cell-Loaded 3D Spider Silk Constructs**

Kristin Schacht, Tomasz Jüngst, Matthias Schweinlin, Andrea Ewald, Jürgen Groll, and Thomas Scheibel**

Abstract: *Biofabrication is an emerging and rapidly expanding field of research in which additive manufacturing techniques in combination with cell printing are exploited to generate hierarchical tissue-like structures. Materials that combine printability with cytocompatibility, so called bioinks, are currently the biggest bottleneck. Since recombinant spider silk proteins are non-immunogenic, cytocompatible, and exhibit physical crosslinking, their potential as a new bioink system was evaluated. Cell-loaded spider silk constructs can be printed by robotic dispensing without the need for crosslinking additives or thickeners for mechanical stabilization. Cells are able to adhere and proliferate with good viability over at least one week in such spider silk scaffolds. Introduction of a cell-binding motif to the spider silk protein further enables fine-tuned control over cell–material interactions. Spider silk hydrogels are thus a highly attractive novel bioink for biofabrication.*

Research in tissue engineering is traditionally focused on the seeding of cells into porous material scaffolds in order to generate a three-dimensional (3D) cell–material construct. By using biodegradable materials with optimized scaffold porosity, generated for example by additive manufacturing (AM) techniques, promising results have been achieved in the context of the repair and/or regeneration of tissues.[1] One current focus of research is on seeding and culturing various cell types in 3D environments that closely mimic the native extracellular matrix (ECM).[2] This is based on the fact that scaffolds must support cellular adhesion, growth, proliferation, migration, and, in case of progenitor cells, differentiation.[3] Recently, a rapidly growing number of studies have focused on biomimicry beyond the ECM and the generation of cell-loaded tissue-like hierarchical structures.[4] To achieve this goal, it is important to choose materials with properties and functions which mimic the tissue that needs to be replaced on the macroscopic scale.[5] Moreover, such morphologies cannot be reached by seeding cells on prefabricated scaffolds; they are only achievable through the combined 3D printing of cells and materials.

In addition to cytocompatibility, the printed materials (so called "bioinks") must show distinct physicochemical properties. For example, they should exhibit viscous fluid behavior within the printing head but polymerize shortly after extrusion. In contrast to other AM techniques, robotic dispensing enables the printing of clinically relevant scaffolds containing biologically active substances and even cells. This technique also allows the simultaneous processing of multiple materials, which enables reproduction of the zonal structures of tissues.[6] However, only few materials have so far been developed for this purpose, with hydrogels as the most promising candidates.[7] Hydrogels are well established for applications in tissue regeneration.[8] They are usually based on a variety of synthetically derived polymers, such as poly(acrylic acid) (PAA), poly(ethylenglycol) (PEG), and poly-(ethylene oxide) (PEO), as well as naturally derived polymers such as agarose, alginate, chitosan, collagen, or silk.[8a,9] Concerning silk, in previous works, an inkjet printing process was developed for the fabrication of microscopic arrays of silkworm silk "nests" capable of hosting live cells for prospective biosensors.[10] Spider silk materials are particularly interesting for biomedical use since they show an absence of toxicity, slow degradation, little or no immunogenicity, wide pore-size distribution, and elastic properties.[11] Hydrogels made of recombinant spider silk proteins are physically crosslinked by β-sheet structures, hydrophobic interactions, and entanglement. The morphology and pore sizes of spider silk hydrogels depend on protein concentration and can be further influenced through functionalization of the protein.[12]

In this study, hydrogels of recombinant spider silk proteins were produced and used as a new bioink for the automatized generation of 3D cell-loaded constructs. The recombinant spider silk protein eADF4(C16) and a variant containing an RGD motif were applied and assessed with regard to their printability, the possibility to encapsulate cells, and finally the generation of cell-loaded 3D hydrogel constructs through the printing of cells suspended in spider silk protein solutions.[13]

[*] K. Schacht,[+] Prof. Dr. T. Scheibel
Lehrstuhl Biomaterialien, Universität Bayreuth
Universitätsstraße 30, 95447 Bayreuth (Germany)
E-mail: thomas.scheibel@bm.uni-bayreuth.de
T. Jüngst,[+] Dr. A. Ewald, Prof. Dr. J. Groll
Lehrstuhl für Funktionswerkstoffe der Medizin
und der Zahnheilkunde, Universitätsklinikum Würzburg
Pleicherwall 2, 97070 Würzburg (Germany)
E-mail: juergen.groll@fmz.uni-wuerzburg.de
M. Schweinlin
Lehrstuhl für Tissue Engineering und Regenerative Medizin
Universitätsklinikum Würzburg
Röntgenring 11, 97070 Würzburg (Germany)
[+] These authors contributed equally to this work.

[**] We would like to thank Andreas Schmidt for fermentation and purification of the proteins; Martin Humenik, Kathrin Hahn, Simone Werner, Florian Gisdon, and Jan Scheler for experimental help; Stefanie Wohlrab, Elise DeSimone, Kiran Pawar, Martina Elsner, and Martin Humenik for proof reading and discussions; and Joschka Bauer for discussions and technical support in creating the artwork. Funding was obtained from the DFG (SCHE 603/9-1) and the European Union's Seventh Framework Programm (FP7/2007-2013) under grant agreement no. 309962 (project HydroZones).

Supporting information for this article is available on the WWW under http://dx.doi.org/10.1002/anie.201409846.

Like most concentrated polymer networks, hydrogels made of spider silk proteins demonstrate viscoelastic behavior, with stress changes proportional to linearly increasing strain (Figure S1 in the Supporting Information).[14] The elastic modulus of the eADF4(C16) hydrogel (3 % w/v) was approximately 0.02 kPa, and that of the eADF4(C16)-RGD hydrogel (3 % w/v) was approximately 0.2 kPa, which is in the range of soft human tissues and organs.[11] Shear thinning of the gels was analyzed through oscillating measurements with an oscillating stress of 10 Pa (Figure S2). The storage moduli (G′) exceeded the loss moduli (G″) over the whole angular frequency range, and both moduli were slightly dependent on frequency. In these hydrogels, elastic behavior dominates over viscous behavior, with low-viscosity flow behavior and good form stability. Additionally, eADF4 hydrogels showed shear-thinning (non-Newtonian) behavior, with high viscosity at low angular frequencies and a decrease in viscosity at higher frequencies (Figure S2B).

One important feature of hydrogels as cell scaffolds is sufficient diffusion of nutrients, oxygen, and waste products during cultivation. 5(6)-carboxyfluorescein or fluorescein isothiocyanate (FITC)-conjugated dextrans were used as model compounds for diffusion. It was shown that the transport of nutrients and waste products through both eADF4(C16) and eADF4(C16)-RGD hydrogels is possible, even for the high-molecular-weight FITC-dextran (500 kDa), although its diffusion was limited (Figure S2C,D).

To evaluate general cytocompatibility, cell adhesion of BALB/3T3 mouse fibroblasts to the eADF4(C16) and eADF4(C16)-RGD hydrogels was tested. The cell adhesion of mouse fibroblasts was weak on eADF4(C16) hydrogels, as shown by a round shape and cell aggregation (Figure 1 A,B,E). Owing to the lack of cell adhesion motifs in eADF4(C16), adhesion is mostly influenced by surface charge, as well as the hydrophobicity and topography of the scaffold.[13c,15] On eADF4(C16)-RGD hydrogels, mouse fibroblasts were well spread and showed filopodia, a result consistent with previous observations of mouse fibroblasts growing on films and non-woven meshes made of eADF4-(C16)-RGD (Figure 1 C).[13c,15a] For all of the tested cell lines (fibroblasts, myoblasts, HeLa cells, osteoblasts, and keratinocytes), cell adhesion on eADF4(C16)-RGD hydrogels was significantly improved in comparison to unmodified eADF4-(C16) hydrogels (Figure 1).

Interestingly, the adhesion of osteoblasts is much better on eADF4(C16) hydrogels compared to the other cell lines. This osteoblast-specific phenomenon is not yet fully understood. In addition to improved adhesion, the proliferation of fibroblasts was better on eADF4(C16)-RGD hydrogels in comparison to eADF4(C16) hydrogels. Based on these findings, eADF4 hydrogels were printed by using robotic dispensing (Figure 2 A). Initial attempts to print with a printhead that dispenses material based on a time–pressure principle failed owing to inconsistent filament diameter. Ultimately, we used a printhead with an electromagnetic valve in combination with a 0.3 mm nozzle to print meshes with a filament center-to-center distance of 2 mm. With this printhead, the hydrogels were process compatible and had high shape fidelity, based on the β-sheet transformation during gelation and the shear thinning behavior (Table S1, Figure S2A,B). The ultrastructural integrity was also evaluated. It was possible to print up to 16 layers on top of each other with a construct depth of approximately 3 mm without structural collapse (Figure 2 B–D and Figure S3).

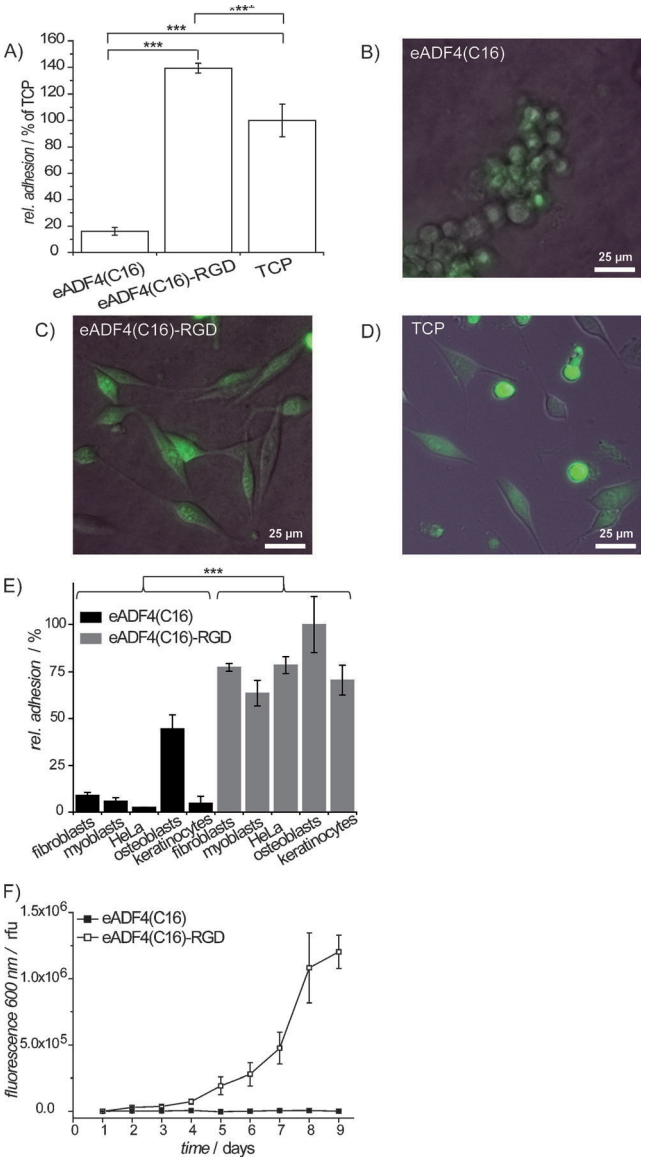

Figure 1. Cultivation of different cell lines on hydrogels made of 3 % eADF4(C16) or 3 % eADF4(C16)-RGD. A) BALB/3T3 fibroblast adhesion was quantified by using the cell-titer blue assay and normalized to adhesion onto treated tissue culture plates (TCP) as the 100 % value. The adhesion of fibroblasts was significantly (***$p < 0.001$) higher on eADF4(C16)-RGD hydrogels than eADF4(C16) hydrogels and TCP. B–D) Live-cell microscopy of BALB/3T3 mouse fibroblasts cultivated on eADF4(C16) (B) and eADF4(C16)-RGD (C) hydrogels and treated tissue culture plates (D) after 24 h of incubation. The cells were stained with the Vybrant CFDA SE Cell Tracer Kit. Scale bars: 50 µm. E) Adhesion of different cell lines to respective hydrogels. Adhesion of osteoblasts to eADF4(C16)-RGD hydrogels was set to 100 %. The adhesion of all of the tested cell lines was significantly improved (***$p < 0.001$) on eADF4(C16)-RGD hydrogels compared to eADF4(C16) hydrogels. F) Proliferation of fibroblasts was quantified by using the cell-titer blue assay.

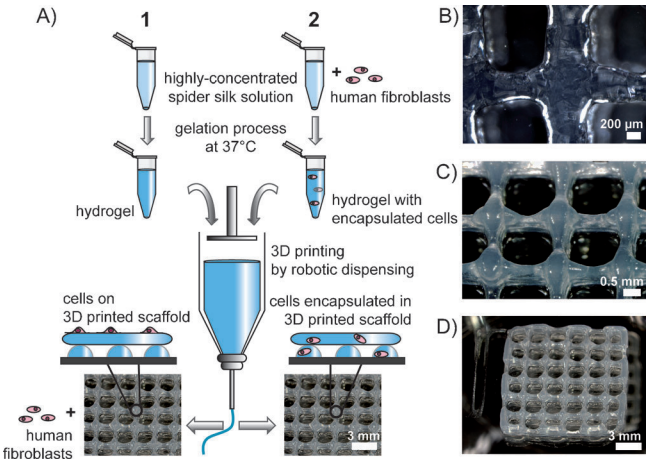

Figure 2. 3D printing of spider silk scaffolds by robotic dispensing. A) Schematic representation of 3D-printing. Cells were either cultivated on the 3D-scaffold (1) or encapsulated during processing (2). Stereomicroscopy and digital images of 2-layer eADF4(C16) (B) and 8-layer eADF4(C16) scaffolds (C, D) are shown.

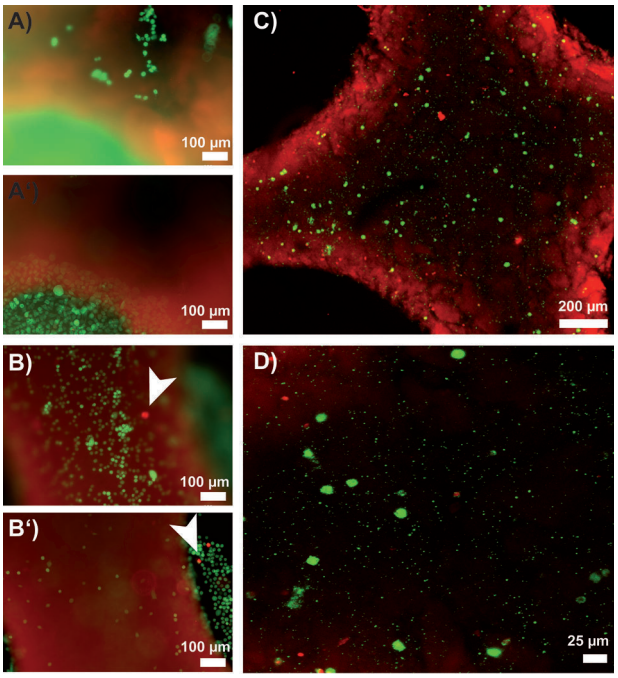

Figure 3. Human fibroblasts cultivated on printed 2-layer eADF4(C16) (A) and eADF4(C16)-RGD (B) hydrogels after 24 h of incubation. Fluorescence microscopy images of cells stained with calcein A/M (live cells: green) and ethidium homodimer I (dead cells; red). Ethidium homodimer I also stained the printed scaffolds. A, B) Focus on the hydrogel. A′, B′) Focus on the well-plate. White arrow: dead cells. (The corresponding confocal laser scanning microscopy images are included in Figure S4A,B). C, D) Confocal laser scanning microscopy images of human fibroblasts encapsulated in a printed 2-layer eADF4(C16) hydrogel after 48 h of incubation (corresponding fluorescence microscopy images are included in Figure S4C–F).

In a first approach, human fibroblasts were seeded on the scaffolds directly after printing. Human fibroblasts adhered weakly on the surface of printed eADF4(C16) hydrogels after 24 h, while the cells spread on scaffolds made of eADF4-(C16)-RGD (Figure 3 and Figure S4A,B). These results correlate well with the experiments performed on the respective hydrogels prepared conventionally and indicate that robotic dispensing does not negatively alter the cell–material interactions of the spider silk proteins. No structural changes occur during the printing process and the shear stress during printing does not influence the cell behavior (Table S1).

Given these results, the next step was to mix human fibroblasts with highly concentrated 3% w/v eADF4(C16) silk solution before gelation in an incubator at 37°C. The addition of cells to the bioink did not influence the printability of the material. The printing parameters only needed minor modifications compared to cell-free inks: an increase of the barrel pressure from 1.0 bar to 1.1 bar and a delay of the valve opening time from 700 microseconds to 900 microseconds. All other parameters could be kept constant without reducing printing fidelity. Cell viability was evaluated at 24, 48, 72 h, and 7 days after printing by live/dead staining. It was confirmed that, when encapsulated in eADF4(C16) hydrogels, the human fibroblasts survived the printing process and were viable for at least seven days in situ, even in the absence of cell adhesion domains (Figure 3 C,D and Figure S4C–F). We quantified viability according to the live/dead assays and detected an average viability of $70.1 \pm 7.6\%$ after 48 h of incubation. However, in this context it is important to note that reference samples with cells incubated in the spider silk hydrogels without printing showed almost identical survival rates, so that the relative survival rate of cells in printed versus non printed gels is 97%. Hence, although cell viability in the spider silk constructs is lower when compared to established bioinks such as alginate (usually 90%) and gelatin (usually 98%), we could show that the printing procedure does not affect viability.[16] Most importantly, and in contrast to the mentioned established systems, our spider silk offers the possibility to biotechnologically and thus precisely tune the biochemical properties in terms of cell adhesion and proliferation, which will in future studies be performed and optimized for printing. Given these results, as well the the low batch-to-batch variations of the material and high reproducibility of the printing, we are confident that recombinant spider silk can be established as a bioink system for biofabrication. The cells were spherical in shape and were homogeneously distributed within the constructs. Cell density did not seem to differ between the constructs, thus leading to the conclusion that cells were distributed homogeneously within the syringe and no sedimentation occurred during gelation. The cells were spherical in shape because movement of the cells was hindered by the dense nanofibrillar matrix. Cellular mobility can be dependent on microenvironmental conditions, such as morphology, space, substrate stiffness, and hydrophobicity.[17] Accordingly, the spherical shape was also detected for primary dermal fibroblasts encapsulated in alginate or fibrin hydrogels.[18]

In conclusion, it could be demonstrated that recombinant spider silk proteins can be used as bioink for 3D printing without the need for additional components or post-processing. By contrast, alginate, which is one of the most frequently

used bioinks for 3D printing, shows less pronounced shear thinning behavior than the silk used in this study. Therefore, post-processing with a crosslinker (calcium ions) or the addition of thickeners is necessary to increase the printing fidelity of alginate, whereas the recombinant spider silk hydrogels can be printed without additives or additional crosslinking.[19] In the case of recombinant spider silk proteins, cells can be directly added to the printing solution, thus resulting in 3D printed cell-loaded constructs with high cell viability for at least seven days. The introduction of a cell-adhesion motif in the spider silk protein also enables control over the cell–material interactions. This is thus a powerful new system that significantly broadens the material spectrum within the field of biofabrication.

Experimental Section

Hydrogel preparation: The recombinant spider silk protein eADF4(C16) consists of 16 repeats of module C (sequence: GSSAAAAAAAASGPGGYG PENQGPSGPGGYGPGGP), which mimics the repetitive core sequence of dragline silk fibroin 4 (ADF4) of the European garden spider *Araneus diadematus*.[13a,b] eADF4(C16) (MW: 47698 g mol^{-1}) and eADF4(C16)-RGD (MW: 48583 g mol^{-1}) were produced and purified as described previously.[13a,c] 30 mg mL^{-1} (3% w/v) eADF4(C16) and eADF4(C16)-RGD solutions were prepared as described previously[12e] (see the Supporting Information). Gels were formed overnight at 37°C and 95% relative humidity.[12e] Recombinant spider silk protein eADF4(C16) and its variants can be produced under good manufacturing practice (GMP) conditions and printing was performed in a biosafety cabinet in a cell culture laboratory, with sterile conditions and media. For the in vitro assays performed in this study, no further additional sterilization was performed and we did not encounter any problems with contamination. Nevertheless, for further long term studies and in vivo investigations, sterilization methods (e.g., autoclaving, sterile filtration, or γ-irradiation) have already been developed for the recombinant spider silks.[20]

Cell culture experiments: For details of the cell lines and their cultivation and preparation before the experiments, see the Supporting Information. For all cell culture experiments, hydrogels were washed twice with cell culture medium before seeding the cells. For cell morphology analysis, BALB/3T3 mouse fibroblasts were seeded on eADF4(C16) and eADF4(C16)-RGD hydrogels with an initial cell density of 47000 cells cm^{-2}. As a positive control, the (well-adhering) cells were seeded on commercially available treated tissue culture plates (TCP; Nunc). Cells were stained with carboxyfluorescein diacetate succinimidyl ester [Vybrant CFDA SE Cell Tracer Kit (Life Technologies GmbH)], and after 24 h of incubation they were visualized with a live-cell microscope (Leica). For cell adhesion tests, 3% w/v eADF4(C16) and 3% w/v eADF4(C16)-RGD solutions were placed in Millicell inserts with 8 μm pore diameter, and the hydrogels were formed overnight at 37°C. The next day, 75000 cells cm^{-2} were seeded on the hydrogels for 2.5 h. After cultivation, the hydrogels were washed twice with phosphate-buffered saline (PBS; Sigma Aldrich) to remove non-attached or dead cells, followed by the addition of fresh medium. After incubation for 4 h with 10% v/v CellTiter-Blue reagent (Promega), cell adhesion was quantified by determining the fluorescence intensity of resorufin (λ_{ex} 530 nm; λ_{em} 590 nm) by using a plate reader (Mithras LB 940). All cell adhesion experiments were repeated three times with three replicates each time. The statistical analyses were performed with the software package STATISTICA 12.0 (StatSoft Inc). An independent Student's *t*-test (two-tailed) was performed on the absolute values of the adhesion tests. Prior to the *t*-test, the homogeneity of variances was tested with Levene's test. The sample variances were considered equal if the *p*-value of the Levene's test was greater than 0.05. For cell proliferation analysis, 5000 cells cm^{-2} were cultivated on eADF4(C16) and eADF4(C16)-RGD hydrogels for 9 days. Once every 24 h, the samples were washed with PBS and the cells quantified by using the CellTiter-Blue assay. The samples were then washed twice with medium and incubated in fresh medium under controlled atmosphere until the next day. The proliferation experiments were repeated twice with three replicates per experiment. For analysis of the printed 2-layer eADF4(C16) and eADF4(C16)-RGD scaffolds, human fibroblasts were cultivated on the scaffolds with a cell seeding density of 75000 cells cm^{-2}. Cells and scaffolds were stained with Calcein acetoxymethyl ester (Calcein A/M) and Ethidium Homodimer I (Invitrogen; see the Supporting Information). Live and dead cells, as well as the scaffolds, were visualized with a fluorescence microscope (Carl Zeiss Axio Observer.Z1) and a confocal scanning microscope (Leica TCS SP8 STED). Confocal laser scanning microscopy images of human fibroblasts encapsulated in a printed 2-layer eADF4(C16) hydrogel were made at a cell density of 1200000 cells mL^{-1} after 48 h of incubation.

3D printing through robotic dispensing: Robotic dispensing was performed by using a Bioplotter (regenHU) in a laminar-flow hood. The printhead (CF-300N/H cell-friendly printhead for contact dispensing) operated in the *y*,*z* plane and the collector along the *x* axis. Before printing, the spider silk solutions were pre-gelled overnight at 37°C and 95% relative humidity (Figure 2A).[12e] During printing, the material was stored at room temperature in a pressurized 3cc syringe (Nordson EFD). Precise dispensing was achieved by using an electromagnetic valve positioned in front of a nozzle with an inner diameter of 0.3 mm, with a resulting strand width of 626 ± 8 μm. The valve opening time was 700–900 μs and the flow was regulated by pressure (1.0–1.1 bar). The printed constructs were analyzed with a stereomicroscope (Carl Zeiss SteREO Discovery.V20).

Received: October 7, 2014
Revised: November 21, 2014
Published online: January 13, 2015

Keywords: biofabrication · cell encapsulation · fibroblasts · hydrogels · spider silk

[1] S. J. Hollister, *Nat. Mater.* **2005**, *4*, 518–524.
[2] a) X. Q. Jia, K. L. Kiick, *Macromol. Biosci.* **2009**, *9*, 140–156; b) V. A. Schulte, K. Hahn, A. Dhanasingh, K. H. Heffels, J. Groll, *Biofabrication* **2014**, *6*, 024106.
[3] a) M. P. Lutolf, J. A. Hubbell, *Nat. Biotechnol.* **2005**, *23*, 47–55; b) A. J. Engler, S. Sen, H. L. Sweeney, D. E. Discher, *Cell* **2006**, *126*, 677–689; c) A. J. Engler, P. O. Humbert, B. Wehrle-Haller, V. M. Weaver, *Science* **2009**, *324*, 208–212; d) P. J. Reddig, R. L. Juliano, *Cancer Metastasis Rev.* **2005**, *24*, 425–439.
[4] B. Derby, *Science* **2012**, *338*, 921–926.
[5] a) J. H. Shim, S. E. Kim, J. Y. Park, J. Kundu, S. W. Kim, S. S. Kang, D. W. Cho, *Tissue Eng. Part A* **2014**, *20*, 1980–1992; b) B. Duan, L. A. Hockaday, K. H. Kang, J. T. Butcher, *J. Biomed. Mater. Res. Part A* **2012**, *101*, 1255–1264; c) F. P. W. Melchels, W. J. A. Dhert, D. W. Hutmacher, J. Malda, *J. Mater. Chem. B* **2014**, *2*, 2282–2289.
[6] a) W. Schuurman, P. A. Levett, M. W. Pot, P. R. van Weeren, W. J. A. Dhert, D. W. Hutmacher, F. P. W. Melchels, T. J. Klein, J. Malda, *Macromol. Biosci.* **2013**, *13*, 551–561; b) P. Bajaj, R. M. Schweller, A. Khademhosseini, J. L. West, R. Bashir, *Annu. Rev. Biomed. Eng.* **2014**, *16*, 247–276; c) W. Schuurman, V. Khristov, M. W. Pot, P. R. van Weeren, W. J. A. Dhert, J. Malda, *Biofabrication* **2011**, *3*, 021001.
[7] J. Malda, J. Visser, F. P. Melchels, T. Jungst, W. E. Hennink, W. J. A. Dhert, J. Groll, D. W. Hutmacher, *Adv. Mater.* **2013**, *25*, 5011–5028.

[8] a) J. L. Drury, D. J. Mooney, *Biomaterials* **2003**, *24*, 4337 – 4351; b) M. W. Tibbitt, K. S. Anseth, *Biotechnol. Bioeng.* **2009**, *103*, 655 – 663; c) O. Wichterle, D. Lim, *Nature* **1960**, *185*, 117 – 118; d) K. R. Kamath, K. Park, *Adv. Drug Delivery Rev.* **1993**, *11*, 59 – 84.

[9] a) I. Armentano, M. Dottori, E. Fortunati, S. Mattioli, J. M. Kenny, *Polym. Degrad. Stab.* **2010**, *95*, 2126 – 2146; b) K. Y. Lee, D. J. Mooney, *Chem. Rev.* **2001**, *101*, 1869 – 1879.

[10] R. Suntivich, I. Drachuk, R. Calabrese, D. L. Kaplan, V. V. Tsukruk, *Biomacromolecules* **2014**, *15*, 1428 – 1435.

[11] A. Leal-Egaña, T. Scheibel, *Biotechnol. Appl. Biochem.* **2010**, *55*, 155 – 167.

[12] a) S. Rammensee, D. Huemmerich, K. D. Hermanson, T. Scheibel, A. R. Bausch, *Appl. Phys. A* **2006**, *82*, 261 – 264; b) U. J. Kim, J. Y. Park, C. M. Li, H. J. Jin, R. Valluzzi, D. L. Kaplan, *Biomacromolecules* **2004**, *5*, 786 – 792; c) A. Matsumoto, J. Chen, A. L. Collette, U. J. Kim, G. H. Altman, P. Cebe, D. L. Kaplan, *J. Phys. Chem. B* **2006**, *110*, 21630 – 21638; d) X. Q. Wang, J. A. Kluge, G. G. Leisk, D. L. Kaplan, *Biomaterials* **2008**, *29*, 1054 – 1064; e) K. Schacht, T. Scheibel, *Biomacromolecules* **2011**, *12*, 2488 – 2495.

[13] a) D. Huemmerich, C. W. Helsen, S. Quedzuweit, J. Oschmann, R. Rudolph, T. Scheibel, *Biochemistry* **2004**, *43*, 13604 – 13612; b) C. Vendrely, T. Scheibel, *Macromol. Biosci.* **2007**, *7*, 401 – 409; c) S. Wohlrab, S. Muller, A. Schmidt, S. Neubauer, H. Kessler, A. Leal-Egaña, T. Scheibel, *Biomaterials* **2012**, *33*, 6650 – 6659.

[14] F. C. Mackintosh, J. Kas, P. A. Janmey, *Phys. Rev. Lett.* **1995**, *75*, 4425 – 4428.

[15] a) A. Leal-Egaña, G. Lang, C. Mauerer, J. Wickinghoff, M. Weber, S. Geimer, T. Scheibel, *Adv. Eng. Mater.* **2012**, *14*, B67 – B75; b) F. Bauer, S. Wohlrab, T. Scheibel, *Biomater. Sci.* **2013**, *1*, 1244 – 1249.

[16] a) J. Jia, D. J. Richards, S. Pollard, Y. Tan, J. Rodriguez, R. P. Visconti, T. C. Trusk, M. J. Yost, H. Yao, R. R. Markwald, Y. Mei, *Acta Biomater.* **2014**, *10*, 4323 – 4331; b) T. Billiet, E. Gevaert, T. De Schryver, M. Cornelissen, P. Dubruel, *Biomaterials* **2014**, *35*, 49 – 62.

[17] a) L. Moroni, L. P. Lee, *J. Biomed. Mater. Res. A* **2009**, *88A*, 644 – 653; b) B. M. Gillette, J. A. Jensen, B. X. Tang, G. J. Yang, A. Bazargan-Lari, M. Zhong, S. K. Sia, *Nat. Mater.* **2008**, *7*, 636 – 640; c) T. Yeung, P. C. Georges, L. A. Flanagan, B. Marg, M. Ortiz, M. Funaki, N. Zahir, W. Y. Ming, V. Weaver, P. A. Janmey, *Cell Motil. Cytoskeleton* **2005**, *60*, 24 – 34; d) J. C. M. Teo, R. R. G. Ng, C. P. Ng, A. W. H. Lin, *Acta Biomater.* **2011**, *7*, 2060 – 2069.

[18] C. M. Hwang, B. Ay, D. L. Kaplan, J. P. Rubin, K. G. Marra, A. Atala, J. J. Yoo, S. J. Lee, *Biomed. Mater.* **2013**, *8*, 014105.

[19] S. Wüst, M. E. Godla, R. Muller, S. Hofmann, *Acta Biomater.* **2014**, *10*, 630 – 640.

[20] a) D. N. Rockwood, R. C. Preda, T. Yucel, X. Q. Wang, M. L. Lovett, D. L. Kaplan, *Nat. Protoc.* **2011**, *6*, 1612 – 1631; b) E. S. Gil, S. H. Park, X. Hu, P. Cebe, D. L. Kaplan, *Macromol. Biosci.* **2014**, *14*, 257 – 269.

Angewandte Chemie
Eine Zeitschrift der Gesellschaft Deutscher Chemiker

Supporting Information

69451 Weinheim, Germany

Biofabrication of Cell-Loaded 3D Spider Silk Constructs**

Kristin Schacht, Tomasz Jüngst, Matthias Schweinlin, Andrea Ewald, Jürgen Groll, and Thomas Scheibel**

anie_201409846_sm_miscellaneous_information.pdf

Hydrogel preparation

Lyophilized eADF4(C16) and eADF4(C16)-RGD were dissolved in 6 M guanidinium thiocyanate at 4 mg/mL and dialyzed against 10 mM Tris/HCl, pH 7.5 overnight at room temperature using dialysis membranes with a molecular weight cutoff of 6,000-8,000 Da. Subsequent dialysis against 20% w/v poly(ethylenglycol) (PEG, 20,000 g/mol) with a volume extent of PEG between 50 and 400 was used to adjust 30 mg/mL (3% w/v) silk solutions as described previously.[1]

Cell culture experiments

Cell line cultivation

BALB/3T3 mouse fibroblasts (European Collection of Cell Cultures), C2C12 mouse myoblasts (CLS, cell lines service), MC3T3-E1 mouse osteoblasts (Leibniz Institute DSMZ-German Collection of Microorganisms and Cell Cultures), HaCaT keratinocytes (CLS, cell lines service) and HeLa human epithelial cells (Leibniz Institute DSMZ-German Collection of Microorganisms and Cell Cultures) were cultivated in Dulbecco's Modified Eagle Medium (DMEM) (Biochrom, Berlin, Germany) supplemented with 10% v/v fetal bovine serum (Biochrom, Berlin, Germany), 1% v/v GlutaMAX (Gibco, Grand Island, USA) and 0.1% v/v gentamicin sulphate (Sigma-Aldrich, Seelze, Germany) in controlled atmosphere of 5% CO_2, 95% relative humidity and 37°C. Human fibroblasts (patient dermal fibroblast cells, G12660) were cultivated in Dulbecco's Modified Eagle Medium (DMEM) (Invitrogen, Eugene, USA) supplemented with 10% v/v fetal bovine serum (Invitrogen, Eugene, USA), 1% v/v Streptomycin (Invitrogen, Eugene, USA) and 100 I.U./mL v/v penicillin (Invitrogen, Eugene, USA). Viability and number of cells were analyzed using trypan blue (Sigma-Aldrich, Ayrshire, UK) or accutase (PAN Biotech

GmbH, Aidenbach, Germany) and a cell counter (CASY TT-Cell Counter, Roche AG, Penzberg, Germany).

Live/dead assay

For the live/dead assay cells and scaffolds were stained with Calcein acetoxymethyl ester (Calcein A/M) and Ethidium Homodimer I (Invitrogen, Eugene, USA). Calcein A/M was added to the medium at a final concentration of 0.3 µM, Ethidium Homodimer I was added to the medium at a final concentration of 0.1 µM and incubated for 20 minutes. The samples were washed once with PBS, followed by addition of fresh PBS. Live and dead cells as well as scaffolds were visualized using a fluorescence microscope (Carl Zeiss Axio Observer.Z1, Oberkochen, Germany) and a confocal scanning microscope (Leica TCS SP8 STED, Wetzlar, Germany).

FTIR Spectroscopy

Infrared-spectra were detected on a Bruker Tensor 27 (Bruker, Germany) spectrometer equipped with an AquaSpec Flow Cell (microbiolytics GmbH, Germany) for analyzing FTIR spectra in aqueous buffers. eADF4(C16) solutions (before gelation, after gelation and after 3D printing) were suspended in 10 mM Tris/HCl, pH 7.5 to a final concentration of 2 mg/mL and measured. Absorption spectra were detected after accumulation of 128 scans from 900 to 4000 cm^{-1}. All spectral transformations were performed using OPUS software (version 6.5, Bruker Optik GmbH). Fourier self-deconvolution (FSD) of the Amid I region (1595-1705 cm^{-1}) was performed as described previously.[2]

Rheological measurements

Flow measurements

Stress-strain curves of 3% w/v eADF4(C16) and 3% w/v eADF4(C16)-RGD were measured using the Rheometer AR-G2 (TA Instruments, New Castle, DE, USA) with a 25 mm plate-plate geometry with a 0.5 mm gap and a sample volume of 600 µL at room temperature (Figure S1). A solvent trap with a wet sponge was used to minimize evaporation. Shear (G) and elastic (E) moduli were calculated according to Hooke's law using the Poisson's ratio (0.43) published by Urayama *et al.*, 1993 and Johnson *et al.*, 2004.[3] Each measurement was repeated three times.

Oscillating measurements

Oscillating measurements of 3% w/v eADF4(C16) and 3% w/v eADF4(C16)-RGD hydrogels were performed as described above (Figure S2). Shear stress amplitude and frequency sweeps were measured with a 0.5 mm gap and a sample volume of 600 µL. Stress amplitude sweeps were measured at a constant angular frequency of 10 rad/s. Afterwards dynamic frequency spectra were recorded in the linear viscoelastic regime (constant oscillating stress: 10 Pa, as determined by shear stress amplitude sweeps). Each measurement was repeated three times.

Diffusion test

Time-dependent tests of diffusion through eADF4(C16) and eADF4(C16)-RGD hydrogels were performed using 5(6)-carboxyfluorescein (376 g/mol) (Sigma-Aldrich, Seelze, Germany) or fluorescein isothiocyanate-dextrans (FITC-dextrans) (Sigma-Aldrich, St. Louis, USA) with different molecular weights (3-5 kDa, 40 kDa, 150 kDa and 500 kDa) (Figure S2). Spider silk solutions (3% w/v) were placed in Millicell® inserts with 8 µm pore diameter (Merck Millipore, Billerica, MA, USA), and hydrogels were formed overnight at 37°C and 95% relative humidity. 1 mM of the fluorescence dyes, solved in 10 mM Tris/HCl, pH 7.5, were pipetted on the hydrogels and incubated at room temperature. After 3-4 h of incubation the amount of dye in the flow-through was quantified determining fluorescence intensity (λ_{ex} 485 nm; λ_{em} 530 nm) using a plate reader (Mithras LB 940, Berthold, Bad Wildbad, Germany). Each measurement was repeated three times.

Table S1. Secondary structure elements eADF4(C16) before gelation, after gelation and after 3D printing. Structural contents were calculated using Fourier self-deconvolution (FSD) of the Amide I bands.

		***secondary structure content* / %**		
secondary structure*	***wavenumber range* / cm^{-1}**	**before gelation**	**after gelation**	**after 3D printing**
α-helices	1656-1662	12.6	7.5	7.5
β-sheets	1616-1637, 1697-1703	20.4	41.2	41.5
random coils	1638-1655	35.8	24.9	23.6
turns	1663-1696	27.0	18.2	19.0
side chains	1595-1615	4.2	8.2	8.4

* Peak assignment taken from literature.[2a, 4]

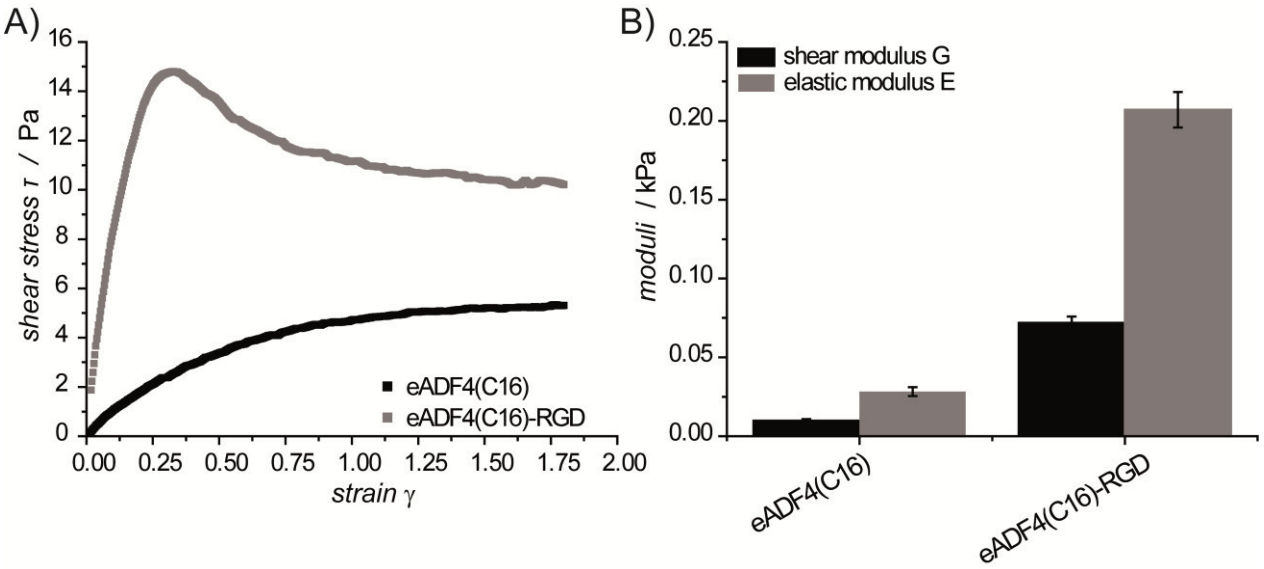

Figure S1. Stress-strain curves (A), shear moduli G and elastic moduli E (B) of 3% eADF4(C16) and 3% eADF4(C16)-RGD hydrogels.

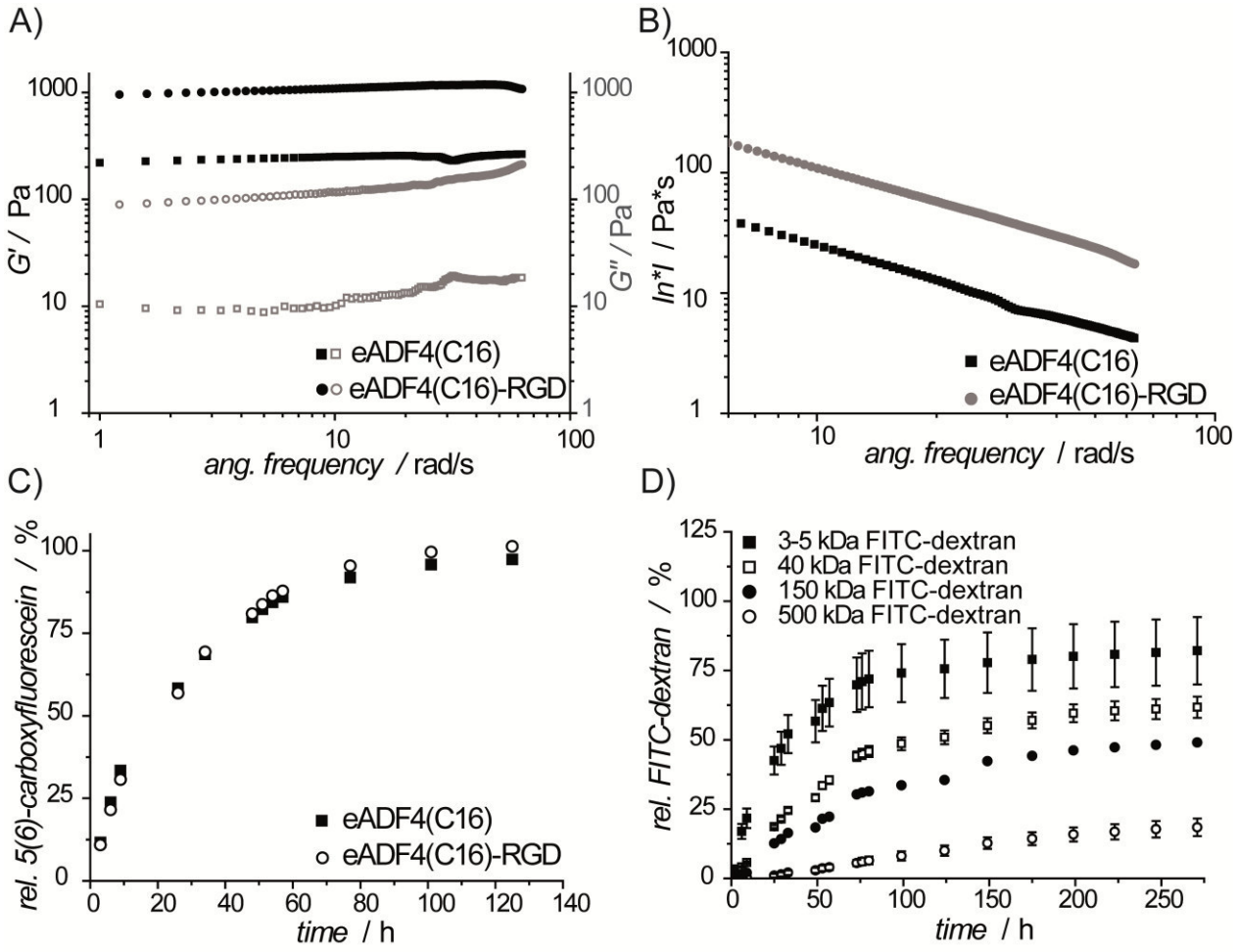

Figure S2. Oscillating rheological measurements (A,B) and time-dependent tests of diffusion (C,D) through 3% eADF4(C16) and 3% eADF4(C16)-RGD hydrogels. A) Dynamic frequency spectra were conducted in the linear viscoelastic regime of the hydrogels, as determined by dynamic stress sweeps (data not shown); full symbols: G', empty symbols: G''. B) The complex viscosity In*I is plotted as a function of angular (ang.) frequency. G' = shear storage moduli; G'' = shear loss moduli. C) Diffusion of 5(6)-carboxyfluorescein through hydrogels in relation to the amount of loaded dye. D) Diffusion of FITC-dextrans with different molecular weights (as indicated) through eADF4(C16) hydrogels.

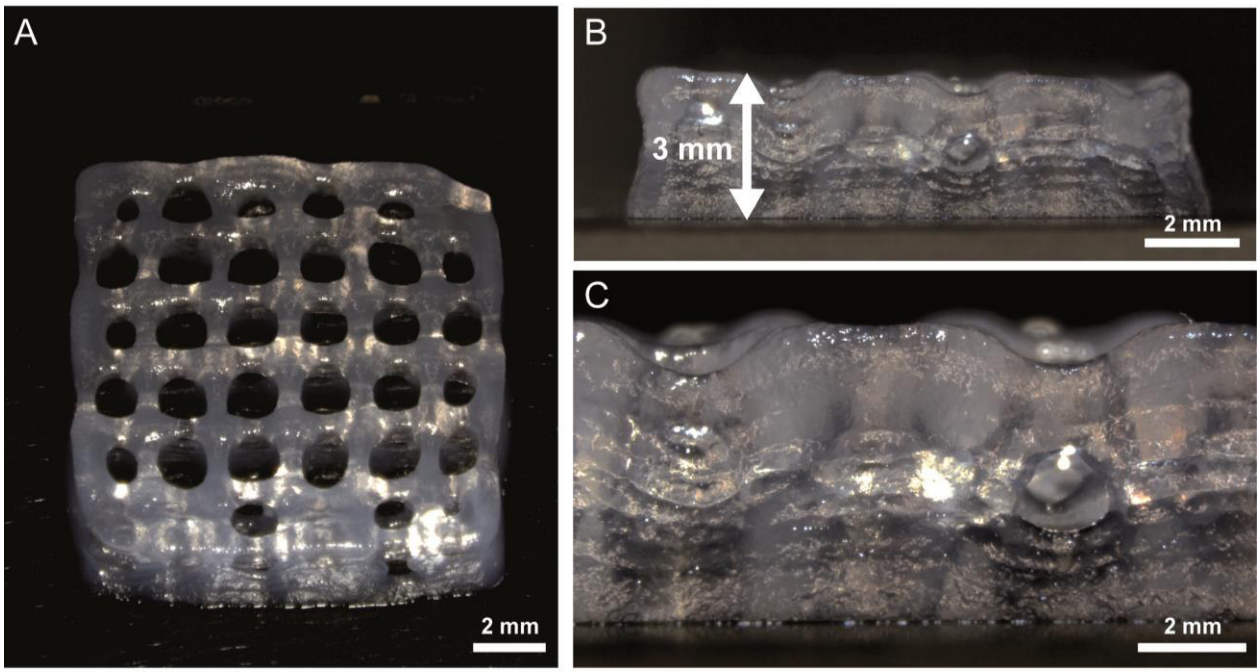

Figure S3. Stereomicroscopy images of printed 16-layer eADF4(C16)-RGD scaffolds with a construct depth of ~3 mm.

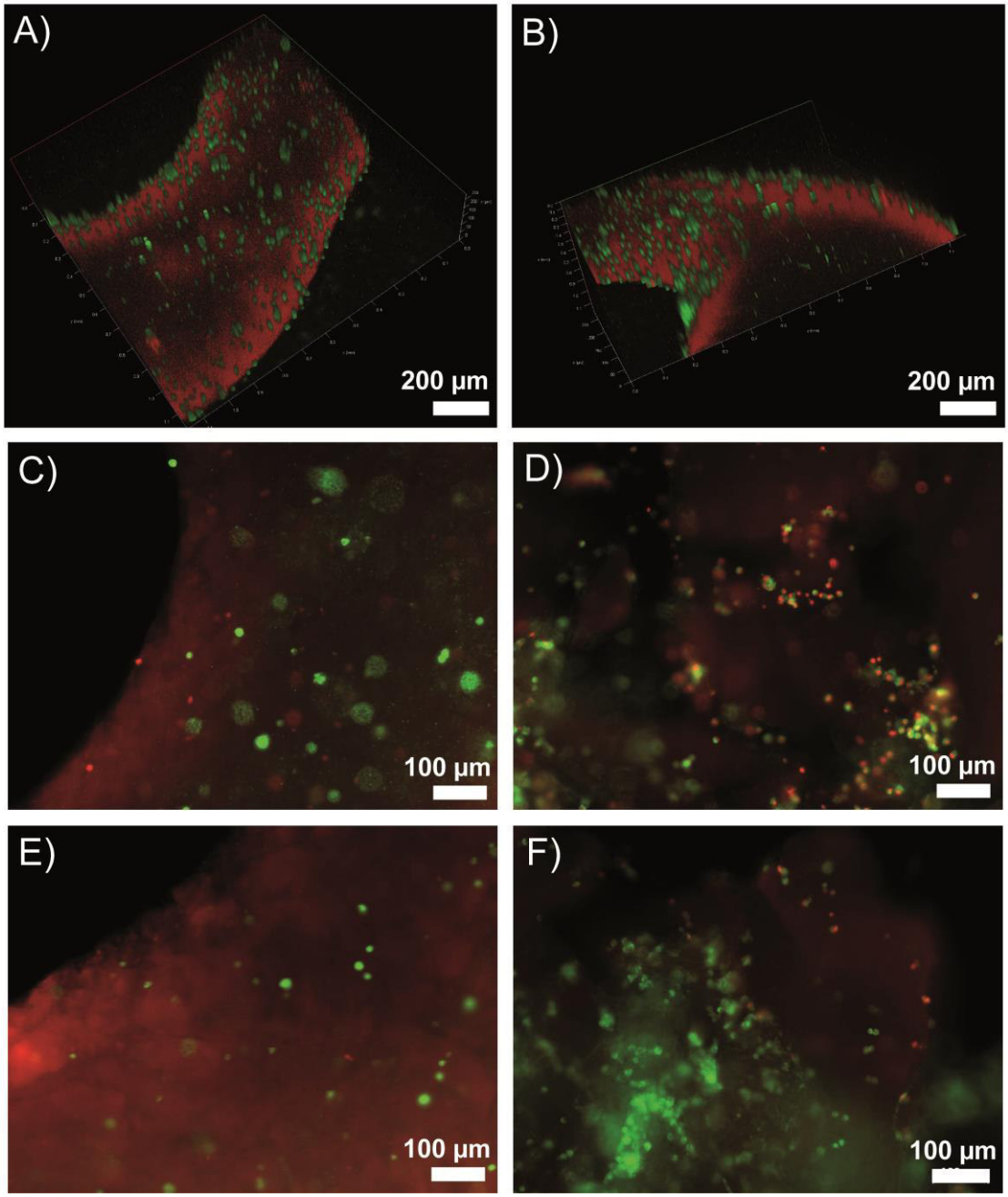

Figure S4. A,B) Confocal laser scanning microscopy of human fibroblasts cultivated on a printed 1-layer eADF4(C16)-RGD scaffold after 48 h of incubation. C-F) Fluorescence microscopy images of human fibroblasts encapsulated in a printed 2-layer eADF4(C16) hydrogel after 48 h (C) and 7 days (E) of incubation. (D,F) Non-printed eADF4(C16) hydrogel as reference to (C) and (E). Cells were stained with calcein A/M (live cells: green) and Ethidium Homodimer I (dead cells: red). Ethidium Homodimer I stained also the printed scaffolds.

[1] K. Schacht, T. Scheibel, *Biomacromolecules* **2011**, *12*, 2488-2495.

[2] a) X. Hu, D. Kaplan, P. Cebe, *Macromolecules* **2006**, *39*, 6161-6170; b) A. S. Lammel, X. Hu, S. H. Park, D. L. Kaplan, T. R. Scheibel, *Biomaterials* **2010**, *31*, 4583-4591; c) K. Spiess, R. Ene, C. D. Keenan, J. Senker, F. Kremer, T. Scheibel, *J. Mater. Chem.* **2011**, *21*, 13594-13604; d) M. Humenik, T. Scheibel, *Acs Nano* **2014**, *8*, 1342-1349.

[3] a) B. D. Johnson, D. J. Beebe, W. Crone, *Materials Science & Engineering* **2004**, *24*, 575-581; b) K. Urayama, T. Takigawa, T. Masuda, *Macromolecules* **1993**, *26*, 3092-3096.

[4] A. Nova, S. Keten, N. M. Pugno, A. Redaelli, M. J. Buehler, *Nano Lett.* **2010**, *10*, 2626-2634.

TEILARBEIT III

Die Ergebnisse dieses Kapitels wurden bereits in *Materials Letters* veröffentlicht als:

> "Cations influence the cross-linking of hydrogels made of recombinant, polyanionic spider silk proteins." DeSimone, E.*, Schacht, K.* und Scheibel, T..

Reproduziert aus *Materials Letters* **2016**, 183: 101-104 mit freundlicher Genehmigung des Verlages Elsevier.

* gleichberechtigte Co-Autorenschaft

Materials Letters 183 (2016) 101–104

Contents lists available at ScienceDirect

Materials Letters

journal homepage: www.elsevier.com/locate/matlet

Cations influence the cross-linking of hydrogels made of recombinant, polyanionic spider silk proteins

Elise DeSimone [1], Kristin Schacht [1], Thomas Scheibel *

Lehrstuhl Biomaterialien, Universität Bayreuth, Universitätsstraße 30, 95447 Bayreuth, Germany

ARTICLE INFO

Article history:
Received 23 December 2015
Received in revised form
29 June 2016
Accepted 10 July 2016
Available online 11 July 2016

Keywords:
Bioinks
Biofabrication
3D Bioprinting
Recombinant spider silk protein
Physical crosslinking
Spidroin

ABSTRACT

Hydrogels made of polyanionic recombinant spider silk proteins (spidroins) were prepared either in the presence or the absence of Dulbecco's Modified Eagle Medium (DMEM). Mono- and divalent cations present in DMEM severely affected the self-assembly process of the spidroins. Although the addition of DMEM had no apparent effect on secondary structure formation, there was a significant effect on the kinetics as well as on the hydrogel network; in the presence of DMEM, gelation occurred more rapidly. Additionally, the hydrogels were stiffer; however, the hydrogels were still shear-thinning. In summary, it can be concluded that there is a significant impact of ionic cross-linking on recombinant spidroin-based hydrogels.

1. Introduction

Traditional tissue engineering techniques have a significant disadvantage: the placement of different components which are used to prepare tissue-like constructs (cells, biomaterials and biochemical factors) is imprecise [1,2]. To overcome this disadvantage, researchers have developed several techniques which allow for co-processing of cells and biomaterials into specific structures; this sub-type of tissue engineering is referred to as biofabrication [3,4]. Of these techniques, one of the most promising is 3D bioprinting; layer-by-layer manufacturing of cell-encapsulating biomaterials into 3D scaffolds [5]. Natural biomaterials which have been used in 3D bioprinting are collagen, gelatin and alginate; however, all of these have some sort of disadvantage i.e. poor mechanical properties [1–3,6–14]. As an alternative to these common bioinks, the recombinant spider silk protein (spidroin) eADF4(C16) and its modified variant eADF4(C16)-RGD have been recently introduced [15].

The polyanionic spidroin eADF4(C16) consists of 16 repeats of module C (sequence: GSSAAAAAAAASGPGGYG PENQGPSGPG-GYGPGGP), which mimics the consensus sequence of the repetitive core of the European garden spider *Araneus diadematus* dragline silk fibroin 4 (ADF4) [16,17]. The RGD variant thereof contains an RGD integrin-binding motif introduced by genetic engineering at the C-terminus, which was previously shown to enhance mammalian cell attachment on spider silk films [18]. These proteins can self-assemble from a disordered structure in solution into β-sheet rich fibrils [19]. Self-assembly is triggered by temperature, kosmotropic phosphate ions and increased protein concentration [20,21].

Bioinks naturally require the use of cell culture media in the fabrication process. As various ions severely affect the self-assembly process [22], the aim of this research was to characterize the material properties of the hydrogel prepared in the presence of cell culture media. Through various assays, stages of the network formation were observed: basic protein structure (FTIR), fibril morphology and association (TEM), hydrogel network formation kinetics (turbidimetry). Additionally, an effect of the formed network on a critical bulk property (i.e. mechanics) of the hydrogel was also observed (rheology).

2. Experimental

2.1. Transmission electron microscopy (TEM)

For TEM analysis, 3% w/v eADF4(C16) and 3% w/v eADF4(C16)-RGD hydrogels, in the presence or absence of 15% v/v DMEM, were diluted to 1 mg/mL. 5 μL of the diluted hydrogel was scattered on 100-mesh Formvar-coated copper TEM grids (Plano GmbH, Germany), incubated for 10 min, washed two times using 5 μL of double distilled water (ddH_2O), and fibrils were negatively stained

* Corresponding author.
E-mail address: thomas.scheibel@bm.uni-bayreuth.de (T. Scheibel).
[1] First authors.

http://dx.doi.org/10.1016/j.matlet.2016.07.044
0167-577X/

using 5 μL 2% uranyl acetate solution. Samples were allowed to dry for at least 24 h at ambient temperature before imaging. TEM imaging of dry samples was performed with a JEM-2100 transmission electron microscope (JEOL, Tokyo, Japan) operated at 80 kV and equipped with a 4000 × 4000 charge-coupled device camera (UltraScan 4000; Gatan, Pleasanton, CA).

2.2. Analysis of gelation kinetics

For gelation analysis, 100 μL of concentrated eADF4(C16) and eADF4(C16)-RGD solutions in the presence or absence of 15% v/v Dulbecco's Modified Eagle Medium (DMEM) without phenol red (Life Technologies, USA) were added to 96-well plates (Nunc, Germany). Phenol red-free DMEM was used to prevent false measurement or background noise that might be introduced by this pH indicator. The hydrogels were incubated at 37 °C and analyzed at various time points for changes in turbidity. Turbidity changes upon gelation were monitored at 570 nm using a Microplate Reader (Mithras LB 940, Berthold Technologies, Germany) in absorbance mode. A sample number of 4 (n=4) was used for each experimental group.

2.3. Fourier-Transform Infrared (FTIR) spectroscopy

Secondary structure content of the eADF4(C16) and eADF4(C16)-RGD hydrogels in the presence or absence of 15% v/v DMEM (Biochrom, Berlin, Germany) was evaluated after freeze-drying hydrogel samples with a Bruker Tensor 27 spectrometer (Bruker, Germany). Spectra were detected by attenuated total reflection (ATR) with a resolution of 4 cm^{-1}, and 120 scans were averaged. Analysis of the amide I band (1595–1705 cm^{-1}) was performed by Fourier self-deconvolution (FSD) to determine individual secondary structure elements as described previously [23–26]. A sample number of 3 (n=3) was used for each experimental group.

2.4. Rheology

Stress-strain curves of eADF4(C16) and eADF4(C16)-RGD in the presence of different ions were measured using a flow measurement mode at the Rheometer AR-G2 (TA Instruments, New Castle, DE, USA) with a 25 mm plate-plate geometry and a 0.5 mm gap and a sample volume of 600 μL at room temperature. The shear rate was kept constant at 3.0^{-3} 1/s. To analyze the influence of 15% v/v DMEM on the viscosity behavior of these hydrogels, the hydrogels were measured using additionally the steady state flow measurement mode. Here, the shear rate was increased from 0.1 to 100 s^{-1}. For all measurements a solvent trap with a wet sponge was used to minimize evaporation. All rheological measurements were performed with pre-formed hydrogels. The highly concentrated spider silk solutions were gelled for 24 h at 37 °C before rheological measurements. A sample number of 2–3 (n=2–3) was used for each experimental group and one representative curve shown per group.

3. Results and discussions

3.1. Concentration of relevant ions in hydrogel formulations

Dulbecco's Modified Eagle Medium (DMEM) contains numerous salts, sugars and proteins, which could influence the charge-charge interactions between the proteins. In this context, salts like $CaCl_2$, NaCl and KCl have already been identified as important in the formation of spider silk threads in nature, and are therefore of particular interest for the hydrogel formation as well [27]. These ions are classified as either kosmotropic or chaotropic [28]: Ions such as Ca^{2+}, are highly chaotropic, Cl^- is neither kosmotropic of chaotropic, and K^+ and Na^+ are kosmotropic, with K+ being slightly more kosmotropic.

In the final formulation of the eADF4(C16) and eADF4(C16)-RGD hydrogels prepared with DMEM, the molarity is 16.43 mM for NaCl, 0.80 mM for KCl, and 0.27 mM for $CaCl_2$. An example calculation for NaCl is shown below in Eq. (1). The entire value is multiplied by 0.15 to account for the fact that the final concentration of DMEM is 15% v/v.

$$6.4g/L/58.44g/mol*1000\ mM/1\ M*0.15 = 16.43\ mM\ \ NaCl \quad (1)$$

3.2. Structural characterization of eADF4(C16) and eADF4(C16)-RGD hydrogels

The consensus motif (C-module) comprises 35 amino acids with one $(Ala)_8$ stretch able to form β-sheets as well as glycine/proline rich GPGXY repeats remaining disordered or helical in solution [26,29,30]. When the protein converts from the soluble to the insoluble state, there is an increase in the amount of β-sheet rich structures [21,26]. Therefore, the gelation process of eADF4(C16) and eADF4(C16)-RGD can be characterized by the formation of nanofibrils accompanied by this change in secondary structure. Here, it was investigated if the presence of 15% v/v cell culture media influences the secondary structure of eADF4(C16) and eADF4(C16)-RGD hydrogels using FTIR spectroscopy. Fourier self-deconvolution (FSD) of the amide I band allowed assignment of individual secondary structure elements (Table 1) [23–26].

The hydrogels fabricated in the absence or presence of DMEM were indistinguishable concerning their secondary structure composition; all hydrogels showed an overall β-sheet content between 45% and 47%.

3.3. Morphological analysis of the fibrillary network

The morphology of the fibrils and fibrillary network of the 3% w/v eADF4(C16) and eADF4(C16)-RGD hydrogels in presence of cell culture media were evaluated using transmission electron microscopy (TEM) (Fig. 1A and B).

3% w/v eADF4(C16) hydrogels were organized by nanofibrils with a diameter of around 10 nm as shown previously, while 3% w/v eADF4(C16)-RGD hydrogels showed slightly thinner nanofibrils with a diameter of around 7 nm [32]. In addition, the fibrillary network of eADF4(C16)-RGD hydrogels was more densely packed in comparison to that of eADF4(C16) hydrogels. However, the presence of DMEM had no apparent influence on the gross morphology of the hydrogels; although there appeared to be a change in opacity, as confirmed by turbidity measurements, likely originating from the slightly denser packing.

Table 1
Secondary structure elements of 3% eADF4(C16) and 3% eADF4(C16)-RGD made in the absence or the presence of DMEM (15% v/v). Structural contents were calculated using Fourier self-deconvolution (FSD) of the amide I bands.

		Secondary structure content/%			
Secondary structure[a]	*Wavenumber range/* cm^{-1}	3% C16	3% C16, 15% DMEM	3% C16-RGD	3% C16-RGD, 15% DMEM
α-helices	1656–1662	8.9 ± 0.3	8.5 ± 0.1	8.7 ± 0.6	7.5 ± 1.1
β-sheets	1616–1637, 1697–1703	44.7 ± 1.3	47.1 ± 1.8	45.1 ± 0.8	46.1 ± 2.5
Random coils	1638–1655	22.5 ± 0.9	21.7 ± 0.3	23.0 ± 0.2	21.9 ± 0.2
Turns	1663–1696	21.3 ± 0.4	21.4 ± 0.5	20.7 ± 0.6	21.9 ± 0.7
Side chains	1595–1615	2.6 ± 1.1	1.3 ± 2.2	2.5 ± 0.4	2.6 ± 1.0

[a] Peak assignment taken from literature [23,31].

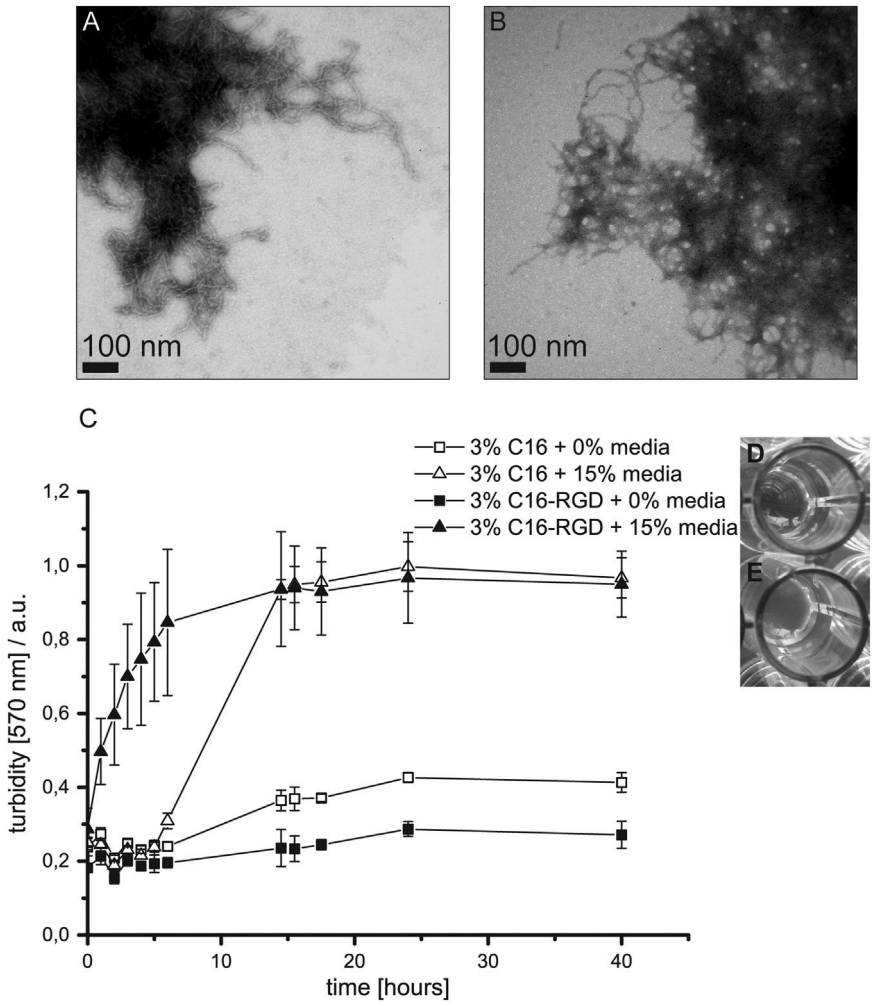

Fig. 1. (A, B) TEM images of hydrogels made of self-assembled recombinant spider silk fibrils. (A) 3% eADF4(C16), (B) 3% eADF4(C16)-RGD. (C-E) Time-dependent turbidity changes (indicative of nanofibril formation) [21] of 3% eADF4(C16) and 3% eADF4(C16)-RGD solutions in the absence and presence of DMEM (15% v/v) as indicated at 37 °C. (C) Changes in turbidity were quantified at 570 nm and normalized to the highest value. Each data point is averaged from three independent samples. 3% eADF4(C16) hydrogels in the absence of DMEM (D) and presence of DMEM (15% v/v) (E) after 2 h of incubation at 37 °C.

3.4. Effects of cell culture media on the gelation process

Physical crosslinking in recombinant spider silk protein hydrogels occurs due to the formation of inter- and intramolecular interactions among the proteins based on hydrogen bonds and hydrophobic interactions [22]. To analyze the impact of the ions and the ionic strength of the DMEM on the assembly rate of the network, the turbidity of each sample was monitored at 570 nm in a time-dependent manner (Fig. 1C).

Hydrogel formation in the presence of DMEM exhibited more rapid gelation in comparison to that without DMEM. For 3% w/v eADF4(C16)-RGD hydrogels, the gelation process began immediately after dialysis and was completed after around 10–15 h. Formation of hydrogels made of 3% eADF4(C16) had a 5 h lag-phase and took overall longer to complete. It was also observed that DMEM had a significantly greater influence on the rate of hydrogel formation of eADF4(C16)-RGD compared to that of eADF4 (C16). This could be due to the additional charge residues on the RGD sequence for ionic bonding.

3.5. Rheological characterization of eADF4(C16) and eADF4(C16)-RGD hydrogels

Previously it has been shown that eADF4(C16) hydrogels demonstrate elastic moduli similar to most polymers, within the regime of most human tissues and organs, with the exception of bone tissue [21,33–35]. To determine the effects of cations (exemplary Ca^{2+} was tested) and DMEM on the mechanical properties of spider silk hydrogels, their stiffness was determined using rheology (Fig. 2).

The addition of 5 mM $CaCl_2$ to 3% w/v eADF4(C16)-RGD hydrogels resulted in a 1000 × increase of shear stress, while the shear stress of 3% w/v eADF4(C16) hydrogels increased just 400 × at the same applied strain. Divalent ions decrease repulsive electrostatic interactions, and forces that favor intermolecular association reactions can prevail [36]. Additionally, COO^- ions of amino acid side chains in the spidroins by ionic interactions, and therefore result in a significant increase in the mechanical stiffness. Interestingly, the effect of DMEM was more significant than $CaCl_2$ alone. As DMEM is a highly complex electrolyte solution, there is most likely multiple types of ionic bonding.

Previously it was shown that hydrogels made of 3% w/v eADF4 (C16) exhibit shear thinning behavior, in contrast to hydrogels made of silk fibroin [15,37]. To analyze the impact of DMEM on the shear-thinning behavior of the spider silk hydrogels, they were characterized using a steady state flow mode (Fig. 3).

All analyzed samples showed shear thinning behavior, with high viscosity at low angular frequencies and a decrease in viscosity at higher frequencies. However, the addition of DMEM lead to higher viscosities at low shear rates. Interestingly, no

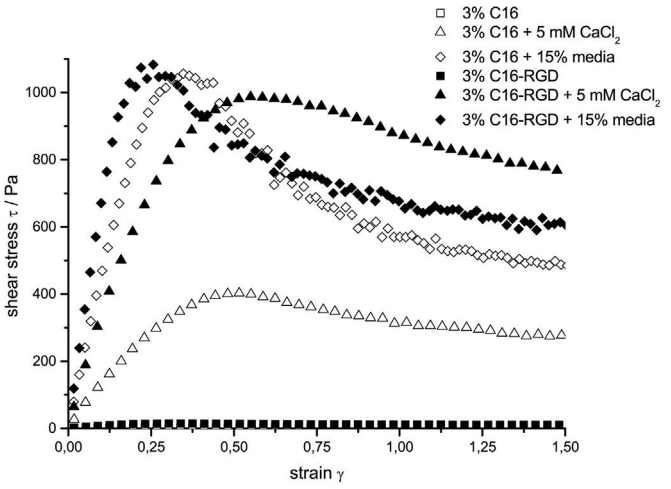

Fig. 2. Rheological characterization of hydrogels made of recombinant spider silk proteins. Stress-strain curves of 3% w/v eADF4(C16) and 3% w/v eADF4(C16)-RGD hydrogels in the absence and presence of 5 mM $CaCl_2$ and DMEM (15% v/v).

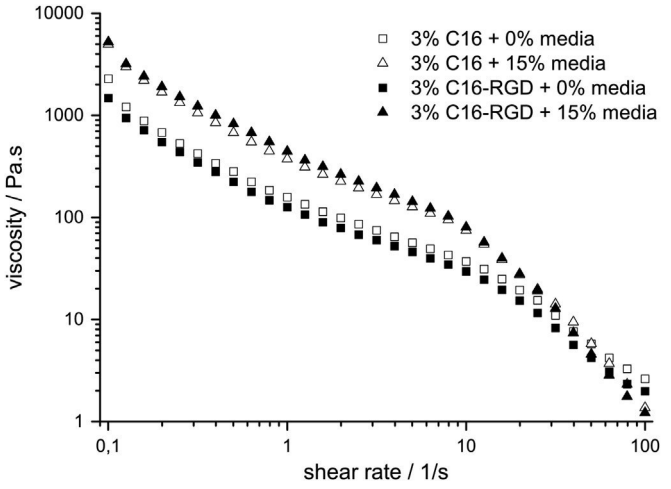

Fig. 3. Viscosity measurements with increasing shear rate of 3% w/v eADF4(C16) and 3% w/v eADF4(C16)-RGD hydrogels in the absence and presence of DMEM (15% v/v).

differences in viscosity between 3% w/v eADF4(C16) and 3% w/v eADF4(C16)-RGD was observed.

4. Conclusion

In this work, recombinant spider silk protein-based hydrogels were characterized in the presence or absence of Dulbecco's Modified Eagle Medium (DMEM). The formulation of DMEM contains many ions which are identified as important for the self-assembly process of spider silk proteins [27]. Data showed similar secondary structures and fibril formation, regardless of the addition of DMEM, and therefore differences seen in the hydrogel's stiffness, viscosity, or turbidity can be related instead to the formation of additional physical crosslinks to the presence of monovalent and bivalent cations [22,38]. However, which is an important property for 3D printing, the shear thinning behavior is maintained, this being important for applications of spider silk hydrogels as bioinks.

Acknowledgements

Funding was obtained from the Deutsche Forschungsgemeinschaft SFB 840 TP A8.

Appendix A

Hydrogel preparation: eADF4(C16) (MW: 47698 g mol^{-1}) and eADF4(C16)-RGD (MW: 48583 g mol^{-1}) were produced and purified as described previously [16,18]. Lyophilized eADF4(C16) and eADF4(C16)-RGD were dissolved in 6 M guanidinium thiocyanate at 4 mg/mL and dialyzed against 10 mM Tris/HCl, pH 7.5 overnight at room temperature using dialysis membranes with a molecular weight cutoff of 6000–8000 Da. Subsequent dialysis against 25% w/v poly(ethylenglycol) (PEG, 20,000 g mol^{-1}) with a volume extent of PEG between 50 and 400 was used to adjust 30 mg/mL (3% w/v) silk solutions as described previously [21]. Hydrogels were formed overnight at 37 °C and 95% relative humidity [21].

References

[1] E. DeSimone, K. Schacht, T. Jungst, J. Groll, T. Scheibel, Pure Appl. Chem. 87 (2015) 737.
[2] S.V. Murphy, A. Atala, Nat. Biotechnol. 32 (2014) 773.
[3] J. Malda, J. Visser, F.P. Melchels, T. Jungst, W.E. Hennink, W.J. Dhert, J. Groll, D. W. Hutmacher, Adv. Mater. 25 (2013) 5011.
[4] V. Mironov, T. Trusk, V. Kasyanov, S. Little, R. Swaja, R. Markwald, Biofabrication 1 (2009) 022001.
[5] B. Berman, Bus. Horiz. 55 (2012) 155.
[6] J. Jia, D.J. Richards, S. Pollard, Y. Tan, J. Rodriguez, R.P. Visconti, T.C. Trusk, M. J. Yost, H. Yao, R.R. Markwald, Y. Mei, Acta Biomater. 10 (2014) 4323.
[7] Q.L. Loh, C. Choong, Tissue Eng. Part B: Rev. 19 (2013) 485.
[8] B.S. Kim, D.J. Mooney, Trends Biotechnol. 16 (1998) 224.
[9] S. Moon, S.K. Hasan, Y.S. Song, F. Xu, H.O. Keles, F. Manzur, S. Mikkilineni, J. W. Hong, J. Nagatomi, E. Haeggstrom, A. Khademhosseini, U. Demirci, Tissue Eng. Part C: Methods 16 (2010) 157.
[10] X. Wang, Y. Yan, R. Zhang, Tissue Eng. Part B: Rev. 16 (2010) 189.
[11] C.M. Smith, A.L. Stone, R.L. Parkhill, R.L. Stewart, M.W. Simpkins, A. M. Kachurin, W.L. Warren, S.K. Williams, Tissue Eng. 10 (2004) 1566.
[12] R. Parenteau-Bareil, R. Gauvin, F. Berthod, Materials 3 (2010) 1863.
[13] U. Hersel, C. Dahmen, H. Kessler, Biomaterials 24 (2003) 4385.
[14] E. Hoch, T. Hirth, G.E.M. Tovar, K. Borchers, J. Mater. Chem. B 1 (2013) 5675.
[15] K. Schacht, T. Jungst, M. Schweinlin, A. Ewald, J. Groll, T. Scheibel, Angew. Chem. Int. Ed. Engl. 54 (2015) 2816.
[16] D. Huemmerich, C.W. Helsen, S. Quedzuweit, J. Oschmann, R. Rudolph, T. Scheibel, Biochemistry 43 (2004) 13604.
[17] C. Vendrely, T. Scheibel, Macromol. Biosci. 7 (2007) 401.
[18] S. Wohlrab, S. Muller, A. Schmidt, S. Neubauer, H. Kessler, A. Leal-Egana, T. Scheibel, Biomaterials 33 (2012) 6650.
[19] U. Slotta, S. Hess, K. Spiess, T. Stromer, L. Serpell, T. Scheibel, Macromol. Biosci. 7 (2007) 183.
[20] U.K. Slotta, S. Rammensee, S. Gorb, T. Scheibel, Angew. Chem. Int. Ed. Engl. 47 (2008) 4592.
[21] K. Schacht, T. Scheibel, Biomacromolecules 12 (2011) 2488.
[22] U.J. Kim, J. Park, C. Li, H.J. Jin, R. Valluzzi, D.L. Kaplan, Biomacromolecules 5 (2004) 786.
[23] X. Hu, D. Kaplan, P. Cebe, Macromolecules 39 (2006) 6161.
[24] A.S. Lammel, X. Hu, S.H. Park, D.L. Kaplan, T.R. Scheibel, Biomaterials 31 (2010) 4583.
[25] K. Spiess, R. Ene, C.D. Keenan, J. Senker, F. Kremer, T. Scheibel, J. Mater. Chem. 21 (2011) 13594.
[26] M. Humenik, M. Drechsler, T. Scheibel, Nano Lett. 14 (2014) 3999.
[27] L. Eisoldt, C. Thamm, T. Scheibel, Biopolymers 97 (2012) 355.
[28] J.J. Grigsby, H.W. Blanch, J.M. Prausnitz, Biophys. Chem. 91 (2001) 231.
[29] K. Spiess, A. Lammel, T. Scheibel, Macromol. Biosci. 10 (2010) 998.
[30] T. Lefevre, S. Boudreault, C. Cloutier, M. Pezolet, J. Mol. Biol. 405 (2011) 238.
[31] A. Nova, S. Keten, N.M. Pugno, A. Redaelli, M.J. Buehler, Nano Lett. 10 (2010) 2626.
[32] M. Humenik, T. Scheibel, ACS Nano 8 (2014) 1342.
[33] A. Leal-Egana, T. Scheibel, Biotechnol. Appl. Biochem. 55 (2010) 155.
[34] F.C. MacKintosh, J. Kas, P.A. Janmey, Phys. Rev. Lett. 75 (1995) 4425.
[35] A.J. Engler, S. Sen, H.L. Sweeney, D.E. Discher, Cell 126 (2006) 677.
[36] K. Klement, K. Wieligmann, J. Meinhardt, P. Hortschansky, W. Richter, M. Fandrich, J. Mol. Biol. 373 (2007) 1321.
[37] T. Jungst, W. Smolan, K. Schacht, T. Scheibel, J. Groll, Chem. Rev. (2015).
[38] A. Ochi, K.S. Hossain, J. Magoshi, N. Nemoto, Biomacromolecules 3 (2002) 1187.

TEILARBEIT IV

Die Ergebnisse dieses Kapitels wurden bereits in *Current Opinion in Biotechnology* veröffentlicht als:

> "Processing of recombinant spider silk proteins into tailor-made materials for biomaterials applications." Schacht, K. und Scheibel, T..

Reproduziert aus *Current Opinion in Biotechnology* **2014**, 29: 62-69 mit freundlicher Genehmigung des Verlages Elsevier.

Available online at www.sciencedirect.com

ScienceDirect

Current Opinion in Biotechnology

Processing of recombinant spider silk proteins into tailor-made materials for biomaterials applications

Kristin Schacht[1] and Thomas Scheibel[1,2,3,4,5]

Spider silk has extraordinary mechanical properties, is biocompatible and biodegradable, and therefore an ideal material for biomedical applications. However, a drawback for any application is the inhomogeneity of spider silk, as seen for other natural materials, as well as the low availability due to the cannibalism of most spiders. Recently, developed recombinant spider silk proteins ensure constant material properties, as well as scalable production, and further the processing into morphologies other than fibres. Biotechnology enables genetic modification, broadening the range of applications, such as implant coatings, scaffolds for tissue engineering, wound dressing devices as well as drug delivery systems.

Addresses
[1] Lehrstuhl Biomaterialien, Fakultät für Ingenieurwissenschaften, Universität Bayreuth, Universitätsstraße 30, Bayreuth 95440, Germany
[2] Bayreuther Zentrum für Kolloide und Grenzflächen (BZKG), Universität Bayreuth, Universitätsstraße 30, Bayreuth 95440, Germany
[3] Institut für Bio-Makromoleküle (bio-mac), Universität Bayreuth, Universitätsstraße 30, Bayreuth 95440, Germany
[4] Bayreuther Zentrum für Molekulare Biowissenschaften (BZMB), Universität Bayreuth, Universitätsstraße 30, Bayreuth 95440, Germany
[5] Bayreuther Materialzentrum (BayMAT), Universität Bayreuth, Universitätsstraße 30, Bayreuth 95440, Germany

Corresponding author: Scheibel, Thomas (Thomas.Scheibel@uni-bayreuth.de)

Current Opinion in Biotechnology 2014, **29**:62–69

This review comes from a themed issue on **Cell and pathway engineering**

Edited by **Tina Lütke-Eversloh** and **Keith EJ Tyo**

Available online XXX

0958-1669/$ – see front matter,

http://dx.doi.org/10.1016/j.copbio.2014.02.015

Introduction

Spider silk fibres fascinate scientists especially due to their extraordinary mechanical properties [1]. The combination of strength and elasticity provides a toughness no other natural or synthetic fibre can achieve [2]. Additionally, spider silk is biocompatible, biodegradable and shows hypoallergenic properties suitable for biomedical applications [3,4].

Importantly, spider silk reflects an entire class of materials with different properties, since spiders can produce several types of silk (for an overview see Heidebrecht and Scheibel [5••]). The best characterised spider silk is the *Major Ampullate* (MA)/Dragline silk, constituting the outer frame of orb webs, serving also as a lifeline for the spider and which will be exclusively discussed herein [6]. Two classes of *Major Ampullate* spidroins have been identified in dragline fibres, called MaSp1 and MaSp2, which differ in proline content and hydrophobicity [7]. All *Major Ampullate* spidroins consist of a highly repetitive core domain, flanked by non-repetitive termini [8]. In the core domain distinct amino acid motifs (glycine-rich repeats and polyalanine blocks) enable secondary structures (random coil/helical and β-sheet) accounting for the mechanical properties of the fibre [8–11]. The terminal domains play an important role during storage of spidroins as a spinning dope in the gland and during the initiation of fibre assembly in the spinning duct [12–15].

For centuries, spider's webs have been successfully used to stop bleeding and to promote wound healing [16]. Recently, spider silk has been used as an artificial support for nerve regeneration [17,18]. Defects of peripheral nerves can be repaired by a composite nerve graft made of acellularized veins, spider silk fibres and Schwann cells (SC) mixed with matrigel (a solubilized tissue basement membrane matrix rich in extracellular matrix proteins). In adult sheep, spider silk enhanced Schwann cell migration, axonal-regrowth and remyelination including electrophysiological recovery in a 6.0 cm tibial nerve defect [19••]. Further, native spider silk fibres were tested as a braided microsurgical suture to substitute conventional materials in microsurgery and neurosurgery [20,21]. It was shown that the mechanical properties of braided spider silk sutures were superior to those of nylon, the current clinical gold-standard [21]. However, one major drawback of natural spider silk sutures is the inhomogeneity of the fibres, as seen with other natural materials, since differences in silk properties occur between individual spiders and even within single individuals upon environmental changes. Another drawback is the low availability of natural material due to problems in farming based on the cannibalistic behaviour of spiders [22,23].

Biotechnological production of spider silk proteins, as well as the development of silk processing techniques enabled the supply of engineered silk materials for biomedical applications, such as implant coatings, drug delivery systems or scaffolds for tissue engineering, which are reviewed herein.

Figure 1

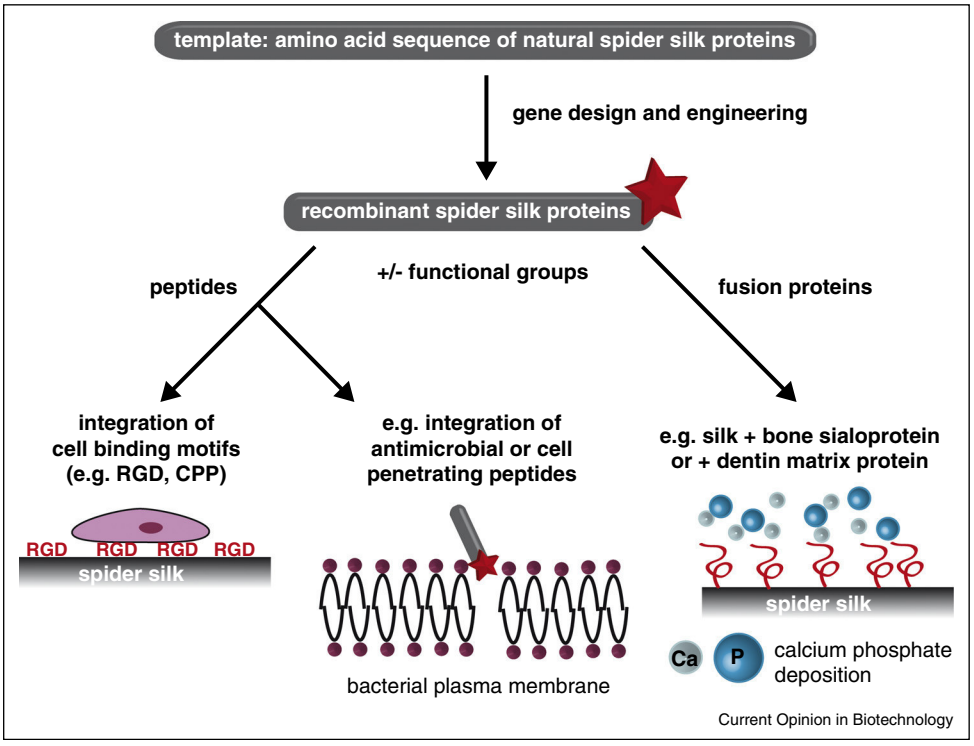

Genetic engineering to achieve functional spider silk proteins.

Recombinant production of engineered spider silk proteins

In the last decades, several prokaryotic and eukaryotic hosts have been tested concerning recombinant production of spider silk proteins, as recently summarized in Heidebrecht and Scheibel [5••].

The benefits of recombinant spider silk proteins (RSSP) are the homogeneity of the starting material as well as the controllable processability into different morphologies, like films, hydrogels, particles or non-woven meshes for various applications [24–29]. Further, biotechnology enables genetic engineering to directly incorporate functional groups into the RSSPs (Figure 1) [24,25,30•].

The simplest genetic modification is the incorporation of individual amino acid residues with chemically specific side chains, like cysteine residues comprising thiol groups. A cysteine variant of the RSSP eADF4(C16) (based on the dragline silk protein ADF4 of *A. diadematus*) allowed the covalent coupling of peptides, enzymes or particles before and after silk processing into materials, demonstrating its potential for a broad range of applications [25,30•].

Engineered spider silk proteins comprising functional peptide sequences

For biomaterials applications, specific interactions between cells and the surface of a material are essential. Spider silk proteins can be exemplarily modified with cell adhesive peptides to improve cell binding, such as the integrin-binding motif RGD (Arg-Gly-Asp) (Figure 1) [28,30•,31,32]. Films made of eADF4(C16)-RGD showed a significantly improved attachment and proliferation of fibroblasts (BALB/3T3) in comparison to unmodified eADF4(C16) films [30•]. Another RSSP, 4RepCT, genetically functionalized with RGD or the cell binding peptides IKVAV, naturally found in the laminin α1 chain, or YIGSR, present in the β1 chain, were processed into fibres, foams and films [33,34]. The adhesion of all tested cell types (fibroblasts, keratinocytes, endothelial and Schwann cells) was significantly improved on RGD-modified in comparison to unmodified 4RepCT films. While only Schwann cells adhered better on matrices comprising the IKVAV-motif, no clear effect of YIGSR could be detected on any of the selected cell types [35].

Functionalizing spider silk proteins or silk hybrids with antimicrobial peptides could be a new approach to

achieve multifunctional biomaterials in order to suppress infections in combination with for example, supporting cell growth. Recently, the human antimicrobial peptides human neutrophil defensin 2 (HNP-2), human neutrophil defensin 4 (HNP-4) and hepcidin were fused to an RSSP 6mer, based on the sequence of MaSp1 from *Nephila clavipes* (*N. clavipes*) (Figure 1). The silk hybrids were processed into films showing antimicrobial activity against Gram negative *E. coli* and Gram positive *S. aureus*. In addition, *in vitro* cell culture studies (cytotoxicity/proliferation) with a human osteosarcoma cell line (SaOs-2) demonstrated the compatibility of these films with mammalian cells [36]. *In vivo* studies in mice showed that the silk-hepcidin protein was highly biocompatible, causing a mild to low inflammatory reaction [37]. In a similar approach, a hybrid between spider silk and a silver binding peptide was produced, which could be processed into films. These films nucleated silver ions from a solution of silver nitrate and inhibited afterwards microbial growth of Gram positive as well as Gram negative bacteria *in vitro* [38].

Silica binding peptides were fused to a consensus sequence of *N. clavipes* MaSp1 introducing silicifying properties [39]. Films thereof promoted osteoblast development with the upregulation of key markers associated with bone formation [40,41].

Other peptides, such as cell penetrating and cell membrane destabilizing peptides (CPPs) are useful candidates, for example, for promoting gene transfer. In this context, recombinant spider silk–polylysine fusions with a ppTG1 peptide, a lysine-rich cell membrane destabilizing peptide to bind plasmid DNA (pDNA), were designed as a highly efficient gene carrier. The newly generated fusion proteins showed useful transfection efficiency, comparable to the transfection reagent Lipofectamine 2000, and at the same time the possibility to control gene release by controlling enzymatic degradation rates of the complexes [42].

Engineering of chimeric spider silk proteins

Chimeric proteins consisting of the RSSP 6mer and the bone sialoprotein (BSP) were processed into films as a support for bone regeneration. Compared to the control (6mer silk films), the Young's modulus of films made of the chimeric silk protein was significantly increased. Furthermore, the chimeric protein retained the ability to form supramolecular aggregates, and in the presence of Ca^{2+} ions these aggregates generated networks [43–45]. *In vitro* studies have demonstrated that human mesenchymal stem cells proliferated and differentiated into the osteogenic lineage on 6mer + BSP films. The presence of cell binding domains in BSP (such as RGD) may be responsible for the cell response when compared to silk alone. For the plain 6mer films, osteoblast-like morphology was not as evident, and a reduction on viability/proliferation was observed after 3, 7 and 14 days in osteogenic medium [46,47].

Chimeric proteins based on *N. clavipes* MaSp1, and the dentin matrix protein 1 (CDMP1), which provides controlled nucleation and crystallization of hydroxyapatite, targeted self-assembled silk structures with controlled hydroxyapatite (HA) mineralization. Upon processing into films, mineralization was initiated using simulated body fluids (SBF) [48]. Mineralized silk films mediated and promoted bone regeneration around wounds and promoted osteoblastic differentiation in a three dimensional scaffold [49–52].

Processing of engineered spider silk proteins for biomedical applications

Spider silk proteins can be processed into coatings which can be used to improve the biocompatibility and the surface properties of biomaterials, such as medical grade silicone implants. Silicones are highly resistant against hydrolytic and enzymatic degradation, otherwise they are considerably hydrophobic. Thus, adhesion of unspecific proteins and cells as well as proliferation of inflammatory and pro-fibrotic cells is promoted, all of which trigger foreign body-associated fibrosis [53,54]. The most frequently identified complication is capsular fibrosis, which occurs in up to 27% of the patients in the first year after surgery, and no modification of the silicone surface tested showed beneficial effects so far [55–57]. Coatings of eADF4(C16) yielded reduced fibrosis and contraction upon implantation in rats, since the silk coating inhibited fibroblast adhesion, proliferation and collagen I synthesis. Additionally, significant reduction in capsule thickness, post-operative inflammation and re-modeling of extracellular matrix were observed for silk coated implants in comparison to uncoated ones [58•].

Non-woven meshes made of natural (e.g. collagen, fibroin) or synthetic (e.g. PLGA, PCL) polymers have a great potential as an artificial extracellular matrix (ECM) useful for wound healing and tissue engineering [59]. Electrospinning of eADF4(C16) yielded a mesh enabling the adhesion of fibroblasts (BALB/3T3) as well as their proliferation [28]. In contrast, fibroblasts did not adhere and proliferate on flat films indicating that the topography of a silk scaffold influences cell-matrix interactions [32]. Therefore, structured films were analysed to learn more about the influence of topographies on cell attachment [32,60]. Patterned silk films were made of two different silk proteins (RSSP and recombinant lacewing silk protein) using a Polydimethylsiloxan (PDMS) stamp. Both, fibroblasts (BALB/3T3) and myoblasts (C2C12), preferably adhered and aligned on the ground layer (RSSP) and not on the ridges (recombinant lacewing silk protein) [60]. In general, it can be stated that in the absence of specific cell adhesion domains (such as RGD), charge, wettability and topography of a surface

Figure 2

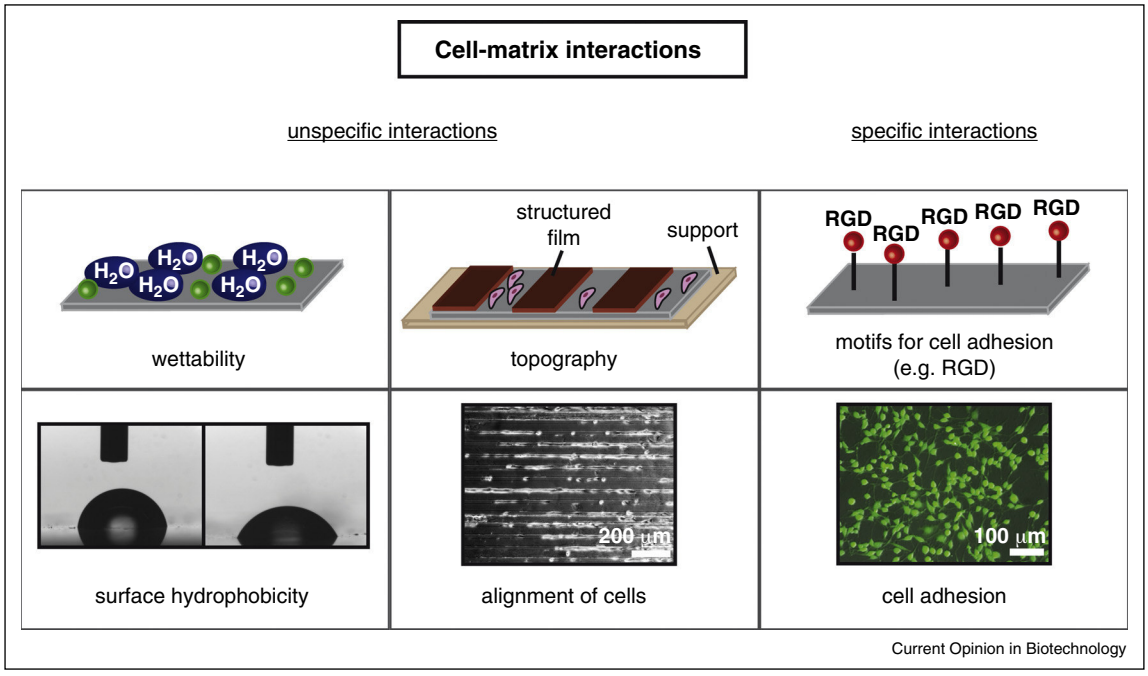

Overview of unspecific cell–matrix interactions determined by wettability and topography, as well as specific cell–matrix interactions mediated by motifs for cell adhesion.

Figure 3

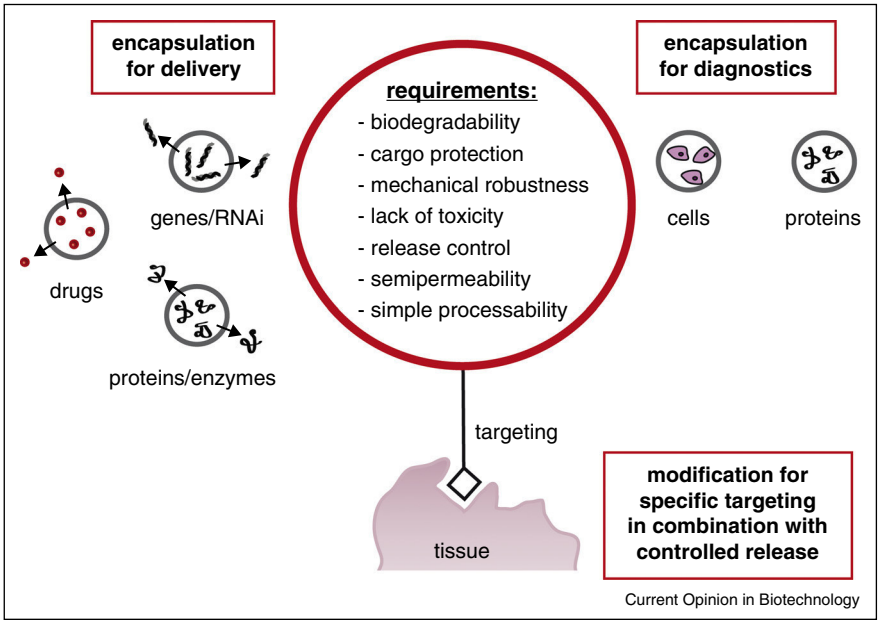

Processing of recombinant spider silk proteins into colloidal systems for various biomaterials applications, such as drug, gene or enzyme delivery or cell and protein encapsulation for diagnostics.

Figure 4

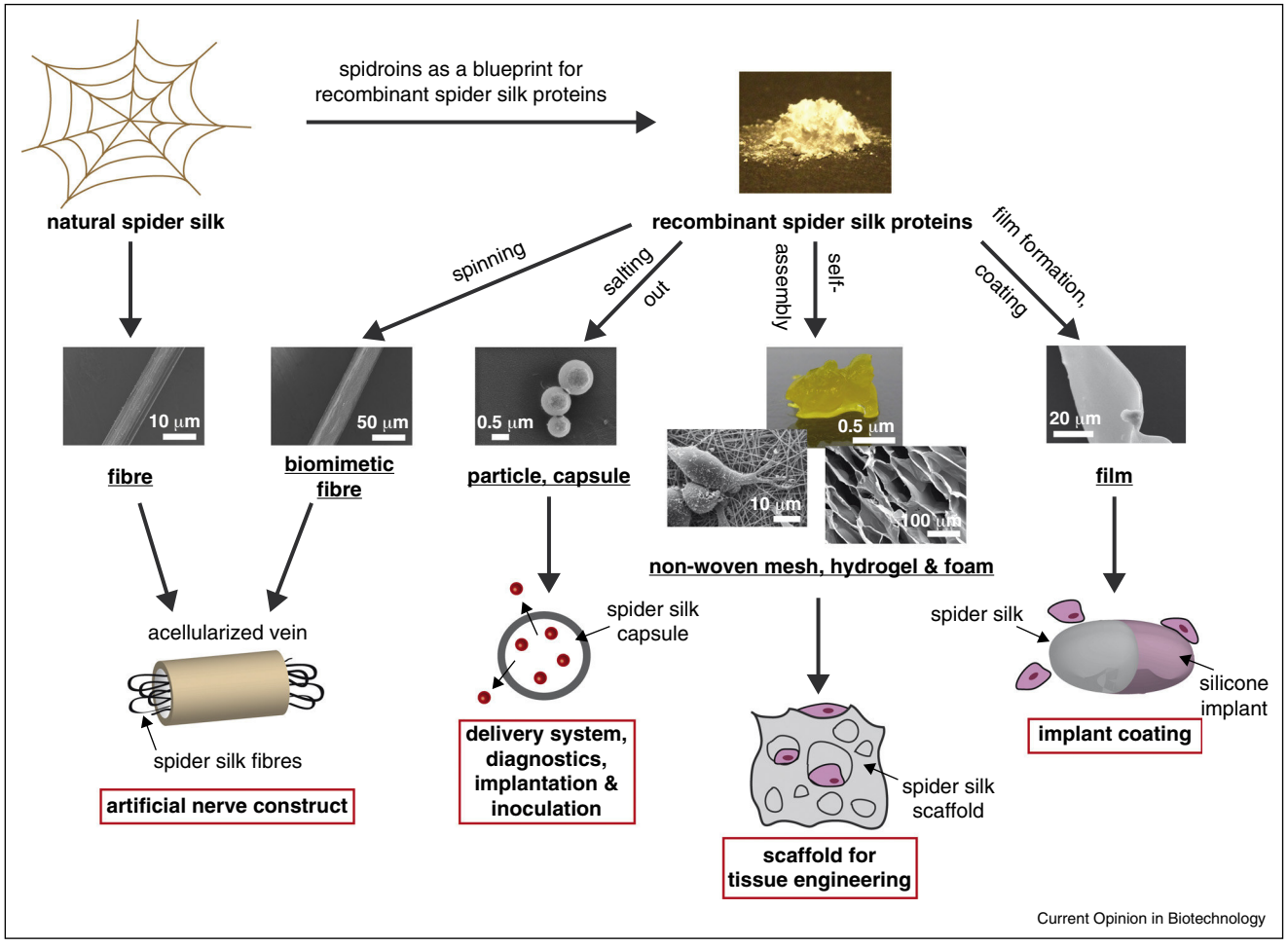

Possible applications of spider silk materials in biomedicine. Recombinant spider silk proteins can be processed into morphologies other than fibres, broadening the spectrum of possible applications.

play an important role for cell attachment (Figure 2) [28,32]. Interestingly, in case of the patterned silk films the presence of the RGD-cell binding motif did not significantly improve cell binding, indicating the importance of topography [60].

In vitro studies demonstrated that three-dimensional porous scaffolds made of the RSSP rS1/9 allowed mouse fibroblast adhesion and proliferation. Within one week, cells migrated into the deeper layers of the porous scaffolds [61]. Next, porous scaffolds made of rS1/9 and natural silkworm fibroin were compared concerning microstructure and physiological behaviour. There was a detectable difference in the microstructure with the walls of the rS1/9 scaffolds being thicker and containing specific micropores in contrast to fibroin-based ones [62••]. The vascularization and intergrowth of the connective tissue, penetrated with nerve fibres, was more prominent in Balb/c mice 8 weeks after subcutaneous implantation using the rS1/9 scaffolds. Further, after implantation into bone defects of Wistar rats, the regeneration, accounting the number of macrophages and multinuclear giant cells, was better in case of the rS1/9 scaffolds.

Foams and fibre-based matrices made of 4RepCT supported growth, attachment and collagen type I production of human primary fibroblast. Further, macroscopic 4RepCT fibres were well tolerated when implanted subcutaneously in rats. In contrast to the control using silkworm silk (Mersilk^{TM}) fibres, 4RepCT-fibres supported ingrowth of fibroblasts and formation of capillaries in the centre of 4RepCT fibre bundles, indicating that 4RepCT is superior in supporting the physiological migration of fibroblasts and angioblasts [63,64]. Yang et al., 2010 used supersaturated simulated body fluids to deposit calcium phosphate coatings on 4RepCT spider silk fibre bundles, yielding a homogeneous and thick crystalline calcium phosphate (CaP) layer, which was a perfect template for bone marrow-derived hMSCs [65].

RSSP can further be used to encapsulate active ingredients including drugs, proteins, genes and cells for delivery or diagnostics (Figure 3) [66–68]. Low molecular weight drugs as well as proteins can be loaded into eADF4(C16) particles, which makes these slowly biodegradable particles a promising drug carrier system, with uptake and release of water-soluble substances being controlled by processing conditions and crosslinking [66–68].

Spider silk particles can also be used as gene carriers for tumour cell-specific delivery. Importantly, pDNA complexes of RSSP containing poly(L-lysine) and the tumour-homing peptides (THPs) F3 and CGKRK showed significantly higher target specificity to tumour cells and transfection efficiency in comparison to pDNA complexes of recombinant spider silk proteins without THP [69••,70].

Microcapsules made of eADF4(C16) resemble an enclosed reaction chamber with a semipermeable membrane, in which reactions can be initiated from outside. Further, the capsules can protect the enzyme (β-galactosidase was used as a model) against proteolysis. Recently established eADF4(C16) capsules are therefore promising tunable as well as protective enzyme reaction containers for technical and medical applications [71•].

Conclusion

In the past five years, the establishment of engineered recombinant spider silk proteins has led to a steadily increasing number of putative applications of spider silk materials (Figure 4).

The benefits of recombinantly produced spider silk proteins include the high quality and homogeneity of the raw material. Biotechnological production is further easily scalable, and processing as well as functionalization through genetic engineering are controllable. By incorporation of individual amino acids, functional peptide sequences or even proteins, novel spider silk hybrid proteins can be designed with a combination of natural and non-natural silk features, opening the road towards novel multifunctional (bio-) materials.

Acknowledgements

This work was supported by DFG SCHE 603/4.

We would like to thank Dr. Martin Humenik and Martina Elsner for discussions and technical support in creating the artwork and Aniela Heidebrecht, Stefanie Wohlrab and Christian Borkner for providing images.

References and recommended reading

Papers of particular interest, published within the period of review, have been highlighted as:

- • of special interest
- •• of outstanding interest

1. Gerritsen VB: **The tiptoe of an airbus**. *Protein Spotlight Swiss Prot* 2002, **24**:1-2.

2. Gosline JM, Guerette PA, Ortlepp CS, Savage KN: **The mechanical design of spider silks: from fibroin sequence to mechanical function**. *J Exp Biol* 1999, **202**:3295-3303.

3. Altman GH, Diaz F, Jakuba C, Calabro T, Horan RL, Chen JS, Lu H, Richmond J, Kaplan DL: **Silk-based biomaterials**. *Biomaterials* 2003, **24**:401-416.

4. Vollrath F, Barth P, Basedow A, Engström W, List H: **Local tolerance to spider silks and protein polymers in vivo**. *In Vivo* 2002, **16**:229-234.

5. •• Heidebrecht A, Scheibel T: **Recombinant production of spider silk proteins**. *Adv Appl Microbiol* 2013, **82**:115-153.
The review summarizes on one hand different types of spider silk and their properties in a web as well as the natural spinning process, and on the other hand the recombinant production of spider silk proteins by different host organisms, such as bacteria, yeast, plants, insect and mammalian cells.

6. Aprhisiart A, Vollrath F: **Design-features of the orb web of the spider, Araneus-diadematus**. *Behav Ecol* 1994, **5**:280-287.

7. Hinman MB, Lewis RV: **Isolation of a clone encoding a 2nd dragline silk fibroin – Nephila-clavipes dragline silk is a 2-protein fiber**. *J Biol Chem* 1992, **267**:19320-19324.

8. Ayoub NA, Garb JE, Tinghitella RM, Collin MA, Hayashi CY: **Blueprint for a high-performance biomaterial: full-length spider dragline silk genes**. *PLoS ONE* 2007, **2**:e514.

9. Andersen SO: **Amino acid composition of spider silds**. *Compar Biochem Physiol* 1970, **35**:705-711.

10. Kummerlen J, van Beek JD, Vollrath F, Meier BH: **Local structure in spider dragline silk investigated by two-dimensional spin-diffusion nuclear magnetic resonance**. *Macromolecules* 1996, **29**:2920-2928.

11. Hayashi CY, Shipley NH, Lewis RV: **Hypotheses that correlate the sequence, structure, and mechanical properties of spider silk proteins**. *Int J Biol Macromol* 1999, **24**:271-275.

12. Askarieh G, Hedhammar M, Nordling K, Saenz A, Casals C, Rising A, Johansson J, Knight SD: **Self-assembly of spider silk proteins is controlled by a pH-sensitive relay**. *Nature* 2010, **465**:236-239.

13. Eisoldt L, Smith A, Scheibel T: **Decoding the secrets of spider silk**. *Mater Today* 2011, **14**:80-86.

14. Hagn F, Eisoldt L, Hardy J, Vendrely C, Coles M, Scheibel T, Kessler H: **A highly conserved spider silk domain acts as a molecular switch that controls fibre assembly**. *Nature* 2010, **465**:239-242.

15. Hagn F, Thamm C, Scheibel T, Kessler H: **pH-dependent dimerization and salt-dependent stabilization of the N-terminal domain of spider dragline silk-implications for fiber formation**. *Angew Chem Int Ed* 2011, **50**:310-313.

16. Bon M: **A discourse upon usefulness of the silk of spiders**. *Philos Trans* 1710, **27**:2-16.

17. Allmeling C, Jokuszies A, Reimers K, Kall S, Choi CY, Brandes G, Kasper C, Scheper T, Guggenheim M, Vogt PM: **Spider silk fibres in artificial nerve constructs promote peripheral nerve regeneration**. *Cell Prolif* 2008, **41**:408-420.

18. Allmeling C, Jokuszies A, Reimers K, Kall S, Vogt PM: **Use of spider silk fibres as an innovative material in a biocompatible artificial nerve conduit**. *J Cell Mol Med* 2006, **10**:770-777.

19. •• Radtke C, Allmeling C, Waldmann KH, Reimers K, Thies K, Schenk HC, Hillmer A, Guggenheim M, Brandes G, Vogt PM: **Spider silk constructs enhance axonal regeneration and remyelination in long nerve defects in sheep**. *PLoS ONE* 2011, **6**:e16990.
Spider silk fibres together with an acellularized vein and Schwann cells embedded in a matrigel were used as guidance material for nerve regeneration. It was demonstrated that spider silk enhances Schwann cell migration, axonal regrowth and remyelination including electrophysiological recovery in a long-distance peripheral nerve gap in rats.

20. Hennecke K, Redeker J, Kuhbier JW, Strauss S, Allmeling C, Kasper C, Reimers K, Vogt PM: **Bundles of spider silk, braided into sutures, resist basic cyclic tests: potential use for flexor tendon repair**. *PLoS ONE* 2013, **8**:e61100.

21. Kuhbier JW, Reimers K, Kasper C, Allmeling C, Hillmer A, Menger B, Vogt PM, Radtke C: **First investigation of spider silk as a braided microsurgical suture**. *J Biomed Mater Res B Appl Biomater* 2011, **97**:381-387.

22. Madsen B, Shao ZZ, Vollrath F: **Variability in the mechanical properties of spider silks on three levels: interspecific, intraspecific and intraindividual**. *Int J Biol Macromol* 1999, **24**:301-306.

23. Fox LR: **Cannibalism in natural-populations**. *Annu Rev Ecol System* 1975, **6**:87-106.

24. Hardy JG, Romer LM, Scheibel TR: **Polymeric materials based on silk proteins**. *Polymer* 2008, **49**:4309-4327.

25. Spiess K, Wohlrab S, Scheibel T: **Structural characterization and functionalization of engineered spider silk films**. *Soft Matter* 2010, **6**:4168-4174.

26. Schacht K, Scheibel T: **Controlled hydrogel formation of a recombinant spider silk protein**. *Biomacromolecules* 2011, **12**:2488-2495.

27. Slotta UK, Rammensee S, Gorb S, Scheibel T: **An engineered spider silk protein forms microspheres**. *Angew Chem Int Ed* 2008, **47**:4592-4594.

28. Leal-Egana A, Lang G, Mauerer C, Wickinghoff J, Weber M, Geimer S, Scheibel T: **Interactions of fibroblasts with different morphologies made of an engineered spider silk protein**. *Adv Eng Mater* 2012, **14**:B67-B75.

29. Hermanson KD, Huemmerich D, Scheibel T, Bausch AR: **Engineered microcapsules fabricated from reconstituted spider silk**. *Adv Mater* 2007, **19**:1810-1815.

30. • Wohlrab S, Muller S, Schmidt A, Neubauer S, Kessler H, Leal-Egana A, Scheibel T: **Cell adhesion and proliferation on RGD-modified recombinant spider silk proteins**. *Biomaterials* 2012, **33**:6650-6659.

The engineered spider silk protein eADF4(C16) was modified with the integrin recognition sequence RGD both by a genetic and a chemical approach. After film processing it could be demonstrated that adhesion and proliferation of fibroblasts were significantly improved on films made of both RGD-modified proteins.

31. Bini E, Foo CWP, Huang J, Karageorgiou V, Kitchel B, Kaplan DL: **RGD-functionalized bioengineered spider dragline silk biomaterial**. *Biomacromolecules* 2006, **7**:3139-3145.

32. Leal-Egana A, Scheibel T: **Interactions of cells with silk surfaces**. *J Mater Chem* 2012, **22**:14330-14336.

33. Grant DS, Tashiro K-I, Segui-Real B, Yamada Y, Martin G, Kleinman H: **Two different laminin domains mediate the differentiation of human endothelial cells into capillary-like structures in vitro**. *Cell* 1989, **58**:933-943.

34. Graf J, Iwamoto Y, Sasaki M, Martin G, Kleinman H, Robey F, Yamada Y: **Identification of an amino acid sequence in laminin mediating cell attachment, chemotaxis, and receptor binding**. *Cell* 1987, **48**:989-996.

35. Widhe M, Johansson U, Hillerdahl CO, Hedhammar M: **Recombinant spider silk with cell binding motifs for specific adherence of cells**. *Biomaterials* 2013, **34**:8223-8234.

36. Gomes SC, Leonor IB, Mano JF, Reis RL, Kaplan DL: **Antimicrobial functionalized genetically engineered spider silk**. *Biomaterials* 2011, **32**:4255-4266.

37. Gomes S, Gallego-Llamas J, Leonor IB, Mano JF, Reis RL, Kaplan DL: **Biological responses to spider silk–antibiotic fusion protein**. *J Tissue Eng Regener Med* 2011, **6**:356-368.

38. Currie HA, Deschaume O, Naik RR, Perry CC, Kaplan DL: **Genetically engineered chimeric silk-silver binding proteins**. *Adv Funct Mater* 2011, **21**:2889-2895.

39. Foo CWP, Patwardhan SV, Belton DJ, Kitchel B, Anastasiades D, Huang J, Naik RR, Perry CC, Kaplan DL: **Novel nanocomposites from spider silk-silica fusion (chimeric) proteins**. *Proc Natl Acad Sci U S A* 2006, **103**:9428-9433.

40. Mieszawska AJ, Fourligas N, Georgakoudi I, Ouhib NM, Belton DJ, Perry CC, Kaplan DL: **Osteoinductive silk–silica composite biomaterials for bone regeneration**. *Biomaterials* 2010, **31**:8902-8910.

41. Belton DJ, Mieszawska AJ, Currie HA, Kaplan DL, Perry CC: **Silk–silica composites from genetically engineered chimeric proteins: materials properties correlate with silica condensation rate and colloidal stability of the proteins in aqueous solution**. *Langmuir* 2012, **28**:4373-4381.

42. Numata K, Kaplan DL: **Silk-based gene carriers with cell membrane destabilizing peptides**. *Biomacromolecules* 2010, **11**:3189-3195.

43. Gomes S, Numata K, Leonor IB, Mano JF, Reis RL, Kapan DL: **AFM study of morphology and mechanical properties of a chimeric spider silk and bone sialoprotein protein for bone regeneration**. *Biomacromolecules* 2011, **12**:1675-1685.

44. Mizuno M, Imai T, Fujisawa R, Tani H, Kuboki Y: **Bone sialoprotein (BSP) is a crucial factor for the expression of osteoblastic phenotypes of bone marrow cells cultured on type I collagen matrix**. *Calcif Tissue Int* 2000, **66**:388-396.

45. Valverde P, Zhang J, Fix A, Zhu J, Ma WL, Tu QS, Chen J: **Overexpression of bone sialoprotein leads to an uncoupling of bone formation and bone resorption in mice**. *J Bone Miner Res* 2008, **23**:1775-1788.

46. Gomes S, Leonor IB, Mano JF, Reis RL, Kaplan DL: **Spider silk-bone sialoprotein fusion proteins for bone tissue engineering**. *Soft Matter* 2011, **7**:4964-4973.

47. Gomes S, Gallego-Llamas J, Leonor IB, Mano JF, Reis RL, Kaplan DL: **In vivo biological responses to silk proteins functionalized with bone sialoprotein**. *Macromol Biosci* 2013, **13**:444-454.

48. Huang J, Wong C, George A, Kaplan DL: **The effect of genetically engineered spider silk-dentin matrix protein 1 chimeric protein on hydroxyapatite nucleation**. *Biomaterials* 2007, **28**:2358-2367.

49. Yan WQ, Nakamura T, Kawanabe K, Nishigochi S, Oka M, Kokubo T: **Apatite layer-coated titanium for use as bone bonding implants**. *Biomaterials* 1997, **18**:1185-1190.

50. Li PJ: **Biomimetic nano-apatite coating capable of promoting bone ingrowth**. *J Biomed Mater Res A* 2003, **66A**:79-85.

51. Barrere F, van der Valk CM, Meijer G, Dalmeijer RAJ, de Groot K, Layrolle P: **Osteointegration of biomimetic apatite coating applied onto dense and porous metal implants in femurs of goats**. *J Biomed Mater Res B Appl Biomater* 2003, **67**:655-665.

52. Chou YF, Dunn JCY, Wu BM: **In vitro response of MC3T3-E1 preosteoblasts within three-dimensional apatite-coated PLGA scaffolds**. *J Biomed Mater Res B Appl Biomater* 2005, **75**:81-90.

53. Pajkos A, Deva AK, Vickery K, Cope C, Chang L, Cossart YE: **Detection of subclinical infection in significant breast implant capsules**. *Plast Reconstruct Surg* 2003, **111**:1605-1611.

54. Hezi-Yamit A, Sullivan C, Wong J, David L, Chen MF, Cheng PW, Shumaker D, Wilcox JN, Udipi K: **Impact of polymer hydrophilicity on biocompatibility: implication for DES polymer design**. *J Biomed Mater Res A* 2009, **90**:133-141.

55. Henriksen TF, Fryzek JP, Holmich LR, McLaughlin JK, Kjoller K, Hoyer AP, Olsen DH, Friis S: **Surgical intervention and capsular contracture after breast augmentation – a prospective study of risk factors**. *Ann Plast Surg* 2005, **54**:343-351.

56. Dancey A, Nassimizadeh A, Levick P: **Capsular contracture – what are the risk factors? A 14 year series of 1400 consecutive augmentations**. *J Plast Reconstruct Aesth Surg* 2012, **65**:213-218.

57. Zeplin PH, Larena-Avellaneda A, Jordan M, Laske M, Schmidt K: **Phosphorylcholine-coated silicone implants effect on inflammatory response and fibrous capsule formation**. *Ann Plast Surg* 2010, **65**:560-564.

58. • Zeplin PH, Maksimovikj NC, Jordan MC, Nickel J, Lang G, Leimer AH, Römer L, Scheibel T: **Spider silk coatings as a bioshield to reduce periprosthetic fibrous capsule formation**. *Adv Funct Mater* 2014 http://dx.doi.org/10.1002/adfm20130281.

Silk coating of medical grade silicone was shown to yield reduced major post-operative complications, such as capsule formation and contraction.

59. Sell SA, Wolfe PS, Garg K, McCool JM, Rodriguez IA, Bowlin GL: **The use of natural polymers in tissue engineering: a focus on electrospun extracellular matrix analogues**. *Polymers* 2010, **2**:522-553.

60. Bauer F, Wohlrab S, Scheibel T: **Controllable cell adhesion, growth and orientation on layered silk protein films**. *Biomater Sci* 2013, **1**:1244-1249.

61. Agapov II, Pustovalova OL, Moisenovich MM, Bogush VG, Sokolova OS, Sevastyanov VI, Debabov VG, Kirpichnikov MP: **Three-dimensional scaffold made from recombinant spider silk protein for tissue engineering**. *Doklady Biochem Biophys* 2009, **426**:127-130.

62. •• Moisenovich MM, Pustovalova O, Shackelford J, Vasiljeva TV, Druzhinina TV, Kamenchuk YA, Guzeev VV, Sokolova OS, Bogush VG, Debabov VG *et al.*: **Tissue regeneration in vivo within recombinant spidroin 1 scaffolds**. *Biomaterials* 2012, **33**:3887-3898.

Two porous scaffolds made from different silk proteins (fibroin of *B. mori* and the recombinant spider silk protein rS1/9) by salt leaching were compared concerning microstructure and biocompatibility. Especially the matrices derived from the recombinant rS1/9 protein were favourable for tissue engineering due to their internal microstructures.

63. Widhe M, Bysell H, Nystedt S, Schenning I, Malmsten M, Johansson J, Rising A, Hedhammar M: **Recombinant spider silk as matrices for cell culture**. *Biomaterials* 2010, **31**:9575-9585.

64. Fredriksson C, Hedhammar M, Feinstein R, Nordling K, Kratz G, Johansson J, Huss F, Rising A: **Tissue response to subcutaneously implanted recombinant spider silk: an in vivo study**. *Materials* 2009, **2**:1908-1922.

65. Yang LA, Hedhammar M, Blom T, Leifer K, Johansson J, Habibovic P, van Blitterswijk CA: **Biomimetic calcium phosphate coatings on recombinant spider silk fibres**. *Biomed Mater* 2010, **5**:1-10.

66. Lammel A, Schwab M, Hofer M, Winter G, Scheibel T: **Recombinant spider silk particles as drug delivery vehicles**. *Biomaterials* 2011, **32**:2233-2240.

67. Hofer M, Winter G, Myschik J: **Recombinant spider silk particles for controlled delivery of protein drugs**. *Biomaterials* 2012, **33**:1554-1562.

68. Blüm C, Scheibel T: **Control of drug loading and release properties of spider silk sub-microparticles**. *BioNanoSci* 2012, **2**:67-74.

69. •• Numata K, Mieszawska-Czajkowska AJ, Kvenvold LA, Kaplan DL: **Silk-based nanocomplexes with tumor-homing peptides for tumor-specific gene delivery**. *Macromol Biosci* 2012, **12**:75-82.

The authors designed nanoscale complexes of recombinant silk molecules containing tumour-homing peptides with DNA as less cytotoxic and highly target-specific gene carriers. The silk-based block copolymers showed relatively high target specificity and transfection efficiency.

70. Numata K, Reagan MR, Goldstein RH, Rosenblatt M, Kaplan DL: **Spider silk-based gene carriers for tumor cell-specific delivery**. *Bioconjug Chem* 2011, **22**:1605-1610.

71. • Blüm C, Nichtl A, Scheibel T: **Spider silk capsules as protective reaction containers for enzymes**. *Adv Funct Mater* 2014, **24**:763-768.

Microcapsules made of the recombinant spider silk protein eADF4(C16) can be used as a container for high molecular weight compounds such as enzymes. The capsules constitute small enclosed reaction chambers with a semi-permeable membrane.

TEILARBEIT V

Die Ergebnisse dieses Kapitels wurden bereits in *Pure and Applied Chemistry* veröffentlicht als:

> "Biofabrication of 3D Constructs: Fabrication Technologies and Spider Silk Proteins as Bioinks." DeSimone, E.*, Schacht, K.*, Jungst, T., Groll, J. und Scheibel, T..

Reproduziert aus *Pure and Applied Chemistry* **2015**, 87(8): 737-749 mit freundlicher Genehmigung des Verlages De Gruyter.

* gleichberechtigte Co-Autorenschaft

Conference paper

Elise DeSimone[a], Kristin Schacht[a], Tomasz Jungst, Jürgen Groll and Thomas Scheibel*

Biofabrication of 3D constructs: fabrication technologies and spider silk proteins as bioinks

DOI 10.1515/pac-2015-0106

Abstract: Despite significant investment in tissue engineering over the past 20 years, few tissue engineered products have made it to market. One of the reasons is the poor control over the 3D arrangement of the scaffold's components. Biofabrication is a new field of research that exploits 3D printing technologies with high spatial resolution for the simultaneous processing of cells and biomaterials into 3D constructs suitable for tissue engineering. Cell-encapsulating biomaterials used in 3D bioprinting are referred to as bioinks. This review consists of: (1) an introduction of biofabrication, (2) an introduction of 3D bioprinting, (3) the requirements of bioinks, (4) existing bioinks, and (5) a specific example of a recombinant spider silk bioink. The recombinant spider silk bioink will be used as an example because its unmodified hydrogel format fits the basic requirements of bioinks: to be printable and at the same time cytocompatible. The bioink exhibited both cytocompatible (self-assembly, high cell viability) and printable (injectable, shear-thinning, high shape fidelity) qualities. Although improvements can be made, it is clear from this system that, with the appropriate bioink, many of the existing faults in tissue-like structures produced by 3D bioprinting can be minimized.

Keywords: biofabrication; bioink; biomaterials; biomedical applications; 3D bioprinting; biotechnology; NICE-2014; spider silk.

Biofabrication

In 1907, a protocol was first described for maintaining the viability of isolated tissue outside of an organism [1]. This technique, called *in vitro* tissue culture, catalyzed a boom of biologically-based technology and debate over the possibilities and implications of this development. One of the most exciting technologies which emerged is tissue engineering. Traditionally, tissue engineering is the modular assembly of biomateri-

Article note: A collection of invited papers based on presentations at the 2nd International Conference on Bioinspired and Biobased Chemistry and Materials: Nature Inspires Chemical Engineers (NICE-2014), Nice, France, 15–17 October 2014.

[a]The authors contributed equally to this work.

***Corresponding author: Thomas Scheibel,** Lehrstuhl Biomaterialien, Universität Bayreuth, Universitätsstraße 30, 95447 Bayreuth, Germany, e-mail: thomas.scheibel@bm.uni-bayreuth.de; Bayreuther Zentrum für Kolloide und Grenzflächen (BZKG), Universität Bayreuth, Universitätsstraße 30, 95440 Bayreuth, Germany; Institut für Bio-Makromoleküle (bio-mac), Universität Bayreuth, Universitätsstraße 30, 95440 Bayreuth, Germany; Bayreuther Zentrum für Molekulare Biowissenschaften (BZMB), Universität Bayreuth, Universitätsstraße 30, 95440 Bayreuth, Germany; and Bayreuther Materialzentrum (BayMAT), Universität Bayreuth, Universitätsstraße 30, 95440 Bayreuth, Germany

Elise DeSimone and Kristin Schacht: Lehrstuhl Biomaterialien, Universität Bayreuth, Universitätsstraße 30, 95447 Bayreuth, Germany

Tomasz Jungst and Jürgen Groll: Lehrstuhl für Funktionswerkstoffe der Medizin und der Zahnheilkunde, Universität Würzburg, Pleicherwall 2, 97070 Würzburg, Germany

als, cells and biochemical factors into tissue-like constructs [2]. Most accept the premise that in order to do this successfully one must, to some degree, mimic the properties of the target tissue. These constructs are immediately implanted or incubated *in vitro* prior to implantation. Relevant applications of tissue engineering include, but are not limited to: implants for regenerative medicine [3], *in vitro* models [4], biobots [5], and alternative food-sources [6]. Although tissue engineering has shown promise towards these applications, few have been approved for consumer use.

The high attrition rates of tissue engineered products are often hypothesized to be due to the modularity of the approach. It results in high variability in the spatial arrangement of the different components (biomaterials, cells, soluble and insoluble biochemical entities). This is problematic for presentation of factors to cells, which direct their behavior, as well as the architecture-dependent mechanical properties of these materials [7]. Due to the intimate relationship between structure and function in biological systems, which is observed across size scales, the success of tissue engineering is thereby limited by this poor control over hierarchical structures and their assembly [8, 9]. To overcome these limits, novel technologies have been established: cell-sheet technology, embedding or molding, centrifuge casting, dielectrophoresis, magnetic-force driven cell-motion, micro-fluidics, biospraying and 3D bioprinting (Table 1). Of these, perhaps the most interesting is the process of 3D bioprinting (3DBP). In this context, biofabrication can be defined as the automated,

Table 1: Published techniques in biofabrication and their basic, generalized process.

Technique	Basic process	References
Embedding or molding	1. Suspension of cells in polymer solution 2. Addition of crosslinker or induction of crosslinking conditions 3. Encapsulation of cells in crosslinked polymer solution, typically within a vessel which results in a defined 3D shape 4. Removal of construct from mold if necessary	[10, 11]
Centrifuge casting	1. Suspension of cells in polymer solution 2. Addition of crosslinker or induction of crosslinking conditions 3. Cell-polymer solution transferred to vessel with defined 3D shape 4. Centrifugation during polymerization of construct 5. Removal of construct from mold if necessary	[12]
Dielectrophoresis	1. Suspension of cells in a viscous polymer solution 2. Application of spatially non-uniform electric field 3. Movement of cells, depending on the set-up, towards low or high field intensities 4. Rapid polymerization of the solution, and encapsulation of cells	[13]
Magnetic-force driven cell-motion	1. Labeling of cells with magnetic nanoparticles 2. Cells cultured under magnetic field until monolayer formation 3. Repositioning of cell monolayer onto a magnetized, positive mold 4. Removal of cell-based constructs from mold	[14]
Micro-fluidics	1. Pre-fabrication of cell-laden constructs as 'building blocks' 2. Flowing of constructs through microfluidic channels to a collection site 3. Fusion of the constructs at the collection site	[15, 16]
Cell sheet	1. Culture cells on a 'smart polymer' surface until monolayer formation; many cultures are done in parallel 2. Release of an undisrupted monolayer from the polymer's surface upon external stimulus (e.g. UV) 3. Layering of monolayers to create 3D constructs	[17]
Biospraying	1. Suspension of cells in polymer solution 2. Placement of polymer solution into a chamber with a nozzle 3. Application of pressure resulting in a controlled spray of the material	[18, 19]
3D bioprinting	1. Generation of 3D image 2. Dissection of image into 2D layers 3. Translation of data to 3D printer 4. Layer-by-layer printing until construct completion 5. Post-processing if necessary	[20–22]

additive assembly of a biological construct by 3D patterning of cells and biomaterials in one processing step [23, 24]. Although each of the named methods has unique advantages, 3DBP is often considered the most valuable technique for tissue engineering/biofabrication due to it having the best spatial control over specific components of the system.

The purpose of this review is to give the theoretical framework of 3DBP, and based on this framework to critically evaluate the recent success of the technology with a particular focus on its use in printing silk-based bioinks; bioinks are materials which are compatible with the 3DBP process.

3D bioprinting (3DBP)

3D printing, first patented by Charles W. Hull in 1986, is rapid fabrication of physical, three-dimensional morphologies [25]. The process can be divided into five steps: (1) generation of a 3D image, (2) re-definition of the 3D image into a stack of 2D layers by an user-demarcated thickness, (3) interfacing this data with the printer, (4) printing a layer of the previously defined thickness one-by-one until the construct is complete, and (5) any necessary post-processing of the material [26–29]. The last step, post-processing, will be discussed in greater detail in later sections, as this is dependent on the material which is used. Although this process applies to most of the existing 3D printers, it should be said that this is a general description: there are many types of 3D printing. As such, the nomenclature for this field is broad, and there is great variety depending on the subfield. For example, some are based on the use of solid or liquid materials in the printing process, while others are based on how the 3D object is created, for example, by adding material a layer at a time (additive manufacturing) [30].

3D printing fitting the definition of biofabrication is referred to as 3D bioprinting (3DBP). Its anatomical elements include: the print head, the material cartridge, the actuator, the nozzle, the working area, and the print stage. The print head is the part which connects precise, motor-controlled movement with actuation of the material. The material cartridge holds the biomaterial and the cells to be printed under user-specified conditions. The actuator is some element which applies pressure to cause material deposition. The nozzle is the orifice, frequently a blunt needle, from which material is ejected. The print stage is the surface which the 3D scaffold is printed onto, and in many set-ups also provides further motor-control. The working area is the volume of space available for the construct. 3D bioprinters are most commonly classified based on their mechanism of material deposition: extrusion, inkjet, or laser-assisted bioprinting (LAB).

Extrusion 3DBP, sometimes referred to as direct-write printing, is a set-up where the mechanical or pneumatic pressure is applied to a cartridge of material to extrude a continuous solution [31]. In the case of inkjet 3DBP, heat or acoustic energy is used to propel droplets of solution; the pressure in the cartridge is kept constant with compressed gas [32]. In LAB, a high energy density beam is directed through a glass slide onto an energy absorbing layer, typically gold or titanium, and the focused energy causes the formation of a concave pocket in the material layer, and subsequently droplets or a jet being propelled towards a collector [33, 34]. Generally, the final printed volume is composed of single droplets; therefore they are correspondingly depicted in Fig. 1. Each of these actuation mechanisms has direct and indirect effects. The direct, downstream effects are on the materials which can be printed and on the shape of the volume which is printed (Fig. 1).

In order to be suitable for biofabrication, the most critical characteristics of a 3DBP process are that it is (1) cell-friendly, (2) reproducible and practical, (3) it allows for printing complex physical and chemical gradients, and (4) geometric structures. The performance of printers is typically evaluated by cell density and viability (fulfills requirement 1), process speed, resolution and accuracy (fulfills requirement 2), and the range of printable materials (fulfills requirement 3 and 4). How well these different printer set-ups generally perform will now be discussed based on these requirements.

Extrusion printing

From this basic set-up there are many interesting variations, for example coaxial needle design [37] or complex robotic joints to increase the degree of geometric freedom [38]. In biofabrication the resolution of

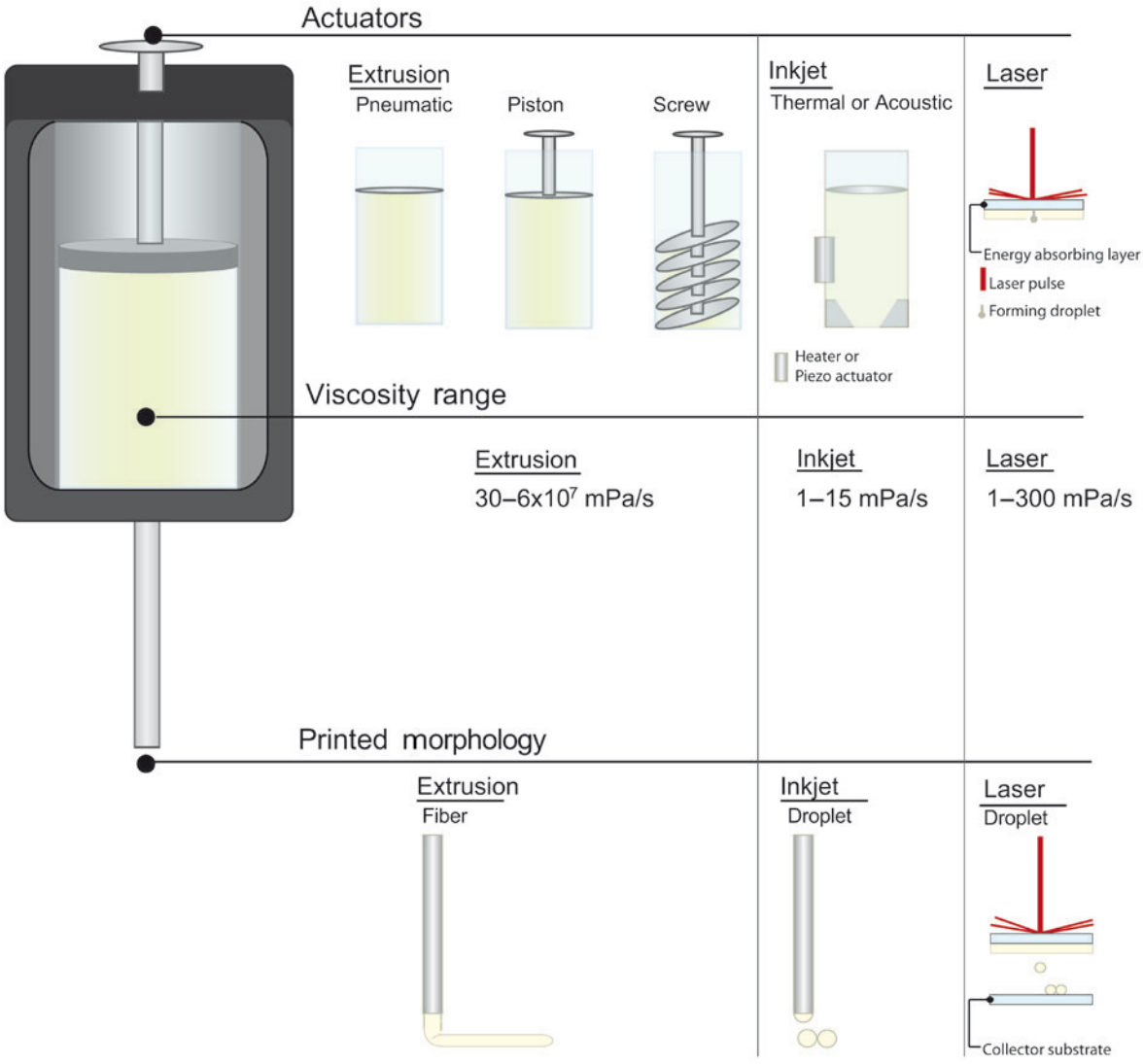

Fig. 1: The different types of 3D bioprinting set-ups. They are defined based on their mechanism of material deposition, the viscosity range of printable materials, and the morphology of the printed volume (i.e. fiber or droplet). These definitions are given in relation to a representation of a print head which shows the actuator, the housing, the material cartridge, and the nozzle (needle) [26, 32, 35, 36].

this technique is mainly limited by requirement 1 mentioned in the chapter above. Cell-free inks enable fiber diameters, and thus resolutions of this method, to be as small as 10 μm [39]. Using cell-loaded bioinks limits the nozzle diameter and leads to a decrease in resolution to dimensions in the range of 200 μm. This limitation in resolution is accompanied by an increase in fabrication speed, as such extrusion printing enables generating 3D structures of clinically-relevant sizes in a reasonable period of time [29]. In terms of the effects on cells, cells can be printed at densities of several million/mL, and there is a wide potential for cell viability post-printing; the cell viability ranges from as low as 40 % to as high as 97 % post-printing [26, 40]. Based on this broad range, which is also compared across similar processing conditions (temperature and shear stress), it is reasonable to conclude that cell viability is significantly affected by the bioink which is used. Further, the attractiveness of this type of system is the wide-range of printable materials. In general, providing printable, biocompatible materials is a greater challenge in the field than the printing technology itself, as will be discussed in the later section, Bioinks.

Inkjet printing

Inkjet systems are the next most commonly used technique for 3DBP. The variables considered for the printed volume (size, shape, speed) are pressure in the material cartridge, rate of nozzle opening and nozzle size. Its performance allows cell viability of ~85 % and a resolution of 50 μm [26]. Compared to the other methods discussed in this review inkjet printing based on commercially available inkjet printers suffers from the lowest cell density (typically <1 million cells/mL) which can be printed [26]. Inkjet printing is also limited to a narrow range of low material viscosities to avoid nozzle clogging or application of cell-damaging forces. There have been, however, some adaptations used to prevent these problems, for example, nozzle-free ejection [26].

Laser-assisted bioprinting (LAB)

LAB is the least commonly used technique due to the complexity of the set-up, and the fabrication systems not being commercially available. However, this should not indicate that it is not a valuable technique. A distinct advantage of LAB is the absence of nozzle clogging, allowing a wide-range of rheological material properties, although the non-dynamic viscosity range is limited compared to extrusion printing [36]. LAB has exceptional resolution in the 10-micron range without affecting the cell viability as compared to the other techniques. The process reliably has cell viabilities above 95 %, and can be used with cell densities of up to 10^8 cells/mL [26]. Unfortunately, in spite of these attractive features from the technical point of view, LAB alone is unable to reach clinically-relevant construct volumes in a reasonable timeframe. This is because of the low volume of printing material in the donor layer as well as of printed droplets. Therefore, LAB might be limited in its practical applications in tissue engineering in the future.

Bioinks

In 3D bioprinting (3DBP) the term “bioinks” is used to describe cell-encapsulating material-matrices which combine printability with cytocompatibility. These demands are quite high and often result in contradicting requirements, making bioinks one great challenge in biofabrication. An ideal bioink can be printed, has high shape-fidelity upon printing, is cytocompatible, and is tailored to its target tissue. Amongst studied bioinks, hydrogels have had the greatest tendency towards success [29].

The major physicochemical parameters determining the printability of a hydrogel are their viscosity and their rheological properties. During 3DBP, the bioink should extrude smoothly and undergo a rapid gelation after printing. If the bioink is already pre-gelled, then the printing process should not result in irreversible damage of the polymer network. Adequate mechanical properties, which can be tailored by polymer concentration or crosslinking of the hydrogel, are necessary to retain the designed and fabricated shape up to clinically-relevant sizes [41]. As previously stated, the requirements imposed by the technique for the bioinks tend to conflict with the biological requirements imposed by the cellular components. The final constructs should allow migration, proliferation and support targeted differentiation of encapsulated cells, which typically calls for a soft substrate. Additionally, the gelation process should be mild and cell friendly [20]. Finally, once the hydrogel precursors have been printed and the cells have survived, the scaffold must degrade at a pre-determined rate when exposed to physiological conditions found in the target tissue [42]. Refer to Fig. 2 for representation of these requirements.

Established bioinks

Existing bioinks include natural (e.g. alginate, fibrin, collagen and gelatin) and synthetic [e.g. poly(ethylenglycol) (PEG), polylactic acid (PLA)], polymers as well as modified versions of these polymers. The most commonly

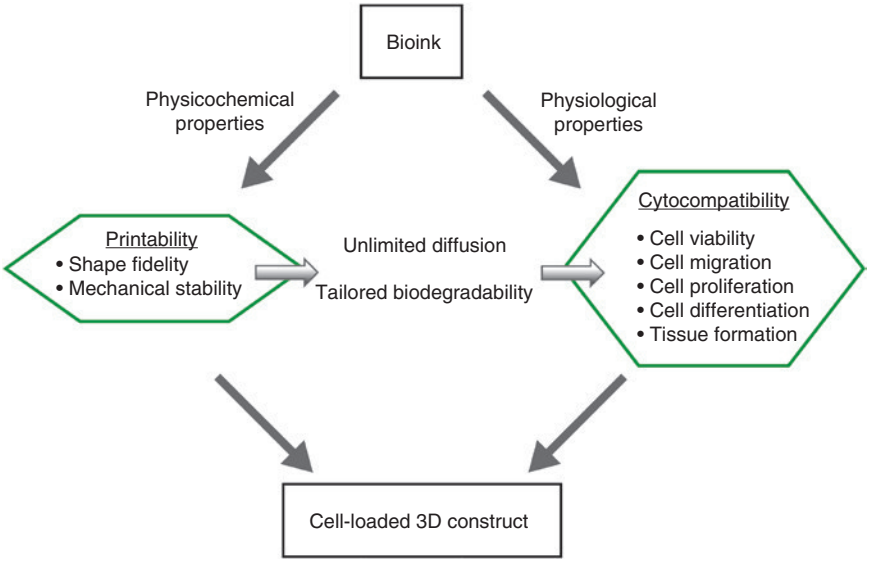

Fig. 2: Physicochemical and physiological requirements of the bioink. Physicochemical properties are related to the printability by the viscosity and macromolecular structure of the material. The printed construct should also allow for diffusion, relating the printed architecture to the cytocompatibility. The physiological activity is related to cytocompatibility by the degradation products, the behavior under physiological conditions, and the biological activity (e.g. cell binding motifs). The final product, the cell-loaded construct, should seamlessly combine these qualities.

used bioinks are the unmodified, natural polymers processed as hydrogels, and will therefore be the focus of this discussion; natural polymers are the only biomaterials whose fabrication process can be directly used for 3DBP [43, 44]. For more detailed information, refer to Table 2 and to Malda et al. [29].

Alginate is one of the most commonly used materials for 3DBP. As a biomaterial in general, alginate has been confirmed to be beneficial for cell viability and differentiation [42], as well as drug delivery [43, 45]. However, alginate-based bioinks also degrade rapidly, translate poorly when used with human-derived cells, and have a limited amount of bioactive binding sites [42, 43, 46]. The next most commonly used bioink is fibrin which has been used due to its success when cultured with neurons [22, 47] and the ability for autologous sourcing [48]. However, fibrin hydrogels possess poor mechanical properties for most applications and degrade before construct maturation [49, 50]. The last most commonly used hydrogel is collagen and its derivative, gelatin. Collagen possesses a major advantage in being biodegradable, biocompatible, easily available and highly versatile [32]. However, collagen-based bioinks show batch-to-batch variations, contraction of constructs, poor mechanical properties, are difficult to sterilize, and have poor water solubility [32, 51, 52]. In an attempt to maintain some of the positive biological activities while reducing these disadvantages, gelatin has also been developed as a bioink [53–55]. Although gelatin shows improvement of the water solubility and viscosity, the gel formation is solely based on physical intermolecular interaction of the gelatin molecules, and the resulting gels are not stable under physiological temperature. Additionally, these gels are also highly variable from batch-to-batch.

In order to expand the range of usable bioinks, there have been many modifications made to these polymers. The most common modifications are chemical ones or polymer blending [35]. Some examples of chemical functionalization include: methacrylation and acetylation of gelatin (modifies degradation) [54, 56], oxidation of alginate (modifies degradation) [42, 64], and synthesis of a block co-polymer comprised of poly(N-(2-hydroxypropyl)methacrylamide lactate) [p(HPMAm-lactate)] and PEG (improves biodegradability) [62]. Some examples of blends include fibrin and alginate (improves biological activity) [22, 54, 61, 65, 66], alginate and gelatin, alginate and gelatin in modified and unmodified forms [55], alginate, gelatin and hydroxyapatite (optimized for bone tissue engineering) [58], thermoresponsive poly(*N*-isopropylacrylamide) grafted hyaluronan (HA-pNIPAAM) blended with methacrylated hyaluronan (HAMA) (to improve printability)

Table 2: Overview of existing bioinks, their gelation method, and their advantages and disadvantages.

Bioink	Gelation method	Advantages	Disadvantages	References
Alginate	Ionic	Biocompatible; supports cellular function and differentiation	Rapid degradation; lack of cell binding motifs	[42, 43, 45, 46]
Fibrin	Enzymatic	Biodegradable; rapid gelation; easy purification process	Poor mechanical properties; fast disintegration	[22, 47–50]
Collagen	Thermal	Biodegradable; biocompatible; availability; versatile	Limited sterilization techniques; batch-to-batch variations; poor mechanical properties	[32, 51, 52]
Gelatin	Thermal	Biodegradable; biocompatible; water soluble	Unstable at body temperature	[53–55]
Gelatin methacrylamide	Thermal/photo	Mechanically stable; biodegradable; biocompatible; water soluble	–	[54, 56]
Fibroin	Self-assembly	Biocompatible; biodegradable; robust mechanical properties	Lack of cell binding motifs or enzyme degradation sites; does not degrade under physiological conditions	[20, 57]
Recombinant spider silk	Self-assembly	Biocompatible; biodegradable; robust mechanical properties	Lack of enzyme degradation sites; does not degrade under physiological conditions	[40]
Bioinks optimized for specific applications by blending				
Alginate/gelatin/ hydroxyapatite	Thermal/ionic/ chemical/	Biocompatible; biodegradable; robust mechanical properties	–	[58]
Gelatin methacrylamide/ hyaluronic acid	Thermal/photo	Mechanically stable; biodegradable; biocompatible; water soluble	–	[55]
Gelatin methacrylamide/ gellan gum	Ionic/thermal/ photo	Mechanically stable; biodegradable; biocompatible; water soluble	–	[59, 60]
Fibroin/gelatin	Enzymatic/ thermal	Biocompatible; biodegradable; robust mechanical properties	–	[20, 57]
Fully synthetic bioinks				
Poly(ethylene glycol) dimethacrylate	Photo	Mechanically stable; cartilage applications	Low cytocompatibility	[61]
p(HPMAm-lactate)-PEG	Thermal/photo	Biodegradable; mechanically stable	Low cytocompatibility	[62]
Glycosaminoglycan-based	Thermal	Chondrogenic	Low viscosity; slow gelation; poor printing properties	[63]
HA-pNIPAAM-HAMA	Thermal/photo	Cytocompatible; fast, reversible gelation; structural fidelity	–	[63]

[63], gelatin with hyaluronic acid or gellan gum (to improve cell behavior towards bone tissue engineering, mechanical properties and printability) [55, 59, 60, 67]. However, even with these modifications, there is an urgent need for further development of bioinks to improve the mechanical properties, gelation process, cytocompatibility, degradation rate, tissue specificity, and adaptability to clinical set-ups.

Silk materials are particularly interesting for technical and biomedical use since they show absence of toxicity, slow degradation, low or absence of immunogenicity, and extraordinary mechanical properties [40, 68–70]. Silk-based biomaterials have been used for medical sutures and breast implant coatings [70–72], biosensing applications [73], and enzyme immobilization [74–76]. Recently, a silk-gelatin blend was used as a bioink [20, 57]. This composite was cytocompatible, crosslinked, showed improved mechanical properties (to gelatin alone), improved cell viability and differentiation (to gelatin, alginate and silk alone), and improved degradation rates (to alginate and gelatin) [20, 43]. However, it was impossible to print silk fibroin without additives; deposition of plain silk fibroin solutions leads to frequent clogging due to shear-induced β-sheet crystallization [57]. In contrast, compared to silk fibroin scaffolds, spider silk bioink can flow through the nozzle without clogging facilitating scaffold manufacturing [40]. This is due to the fact that hydrogels made of recombinant spider silk proteins are physically crosslinked by β-sheet structures and hydrophobic interactions and entanglements, which allows for reversible gelation upon shear-thinning [40, 77]. Further, due to the biotechnological production of recombinant spider silk proteins they can be genetically modified, e.g. with the cell binding motif RGD improving cell attachment [40, 78]. The combination of these mechanical and biological properties raises the number of applications of recombinant spider silk as a novel bioink.

Post-processing and crosslinking

Without delving into complex macromolecular chemistry, it is important to briefly discuss some of the options for solidifying materials in 3DBP when materials do not self-assemble. The basic requirements for a crosslinking process are that it must be rapid for shape-fidelity as well as non-toxic to cells. There are two basic types of crosslinking which can be used: physical or chemical. In the case of physical crosslinking, the most common approach is to maintain the conditions which stabilize the liquid phase in the material cartridge and the conditions which push it towards gelation in the working volume or a tandem print head. An example of this principle is printing a temperature-sensitive hydrogel onto a heated print stage [55]. The advantage of physical crosslinking is that it is often cell-friendly; the disadvantage is that the networks formed are typically weak and their degradation difficult to control. Due to these disadvantages most physically crosslinked hydrogels must be post-processed by chemical crosslinking, and this results in newly formed covalent bonds [29]. This is particularly true for inkjet printing, where the necessity of a low viscosity material mandates some type of post-processing. Some interesting examples of chemical crosslinking techniques include the use of enzymes or UV light [31, 47]. An example of a versatile method for generating UV-crosslinkable hydrogels is by functionalizing 2-hydroxyethyl methacrylate (HEMA) with a photoinitiator. HEMA is a polymeric monomer which can be coupled at hydroxyl groups, making it compatible with many other polymers [79]. However, these types of crosslinking techniques often require synthetic chemistry, making them impractical. Wet-chemical crosslinking allows for predictable, stable network formation, however, the used crosslinking agents may be harmful to cells, and it requires a precise control of crosslinking kinetics to avoid nozzle clogging [29].

3D bioprinting with recombinant spider silk proteins

Recently, the recombinant spider silk protein eADF4(C16) and a variant containing an RGD-motif were established as bioinks. eADF4(C16) consists of 16 repeats of a module C mimicking the repetitive core sequence of dragline silk *Araneus diadematus* fibroin 4 (ADF4) of the European garden spider (Fig. 3a) [81, 82]. The

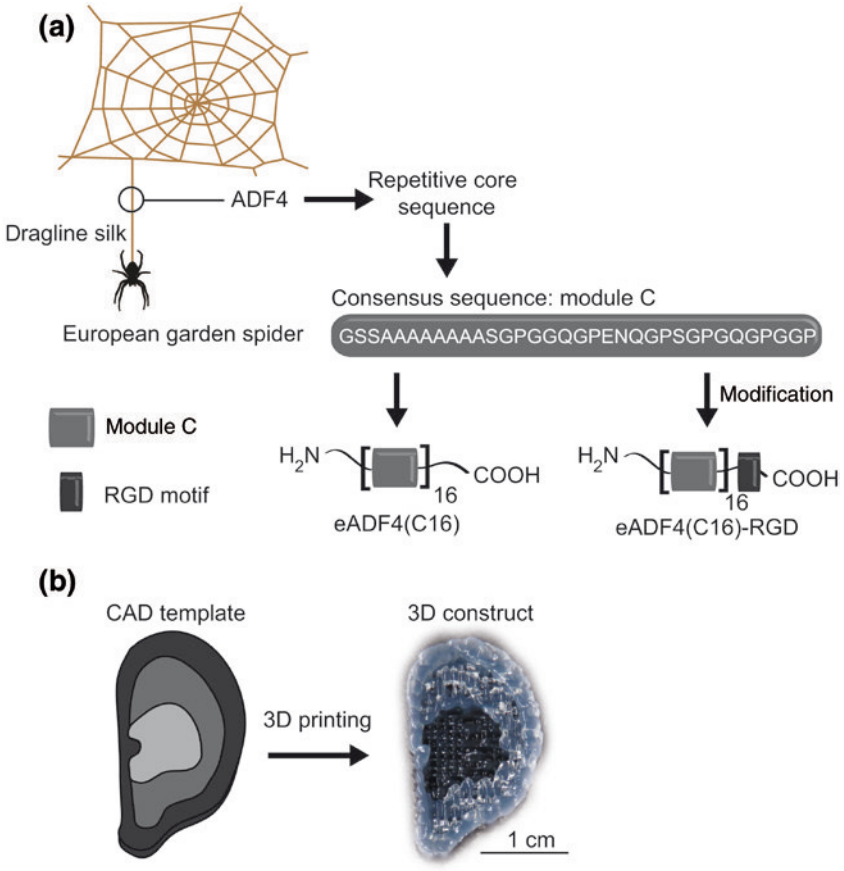

Fig. 3: (a) eADF4(C16) and eADF4(C16)-RGD are made of 16 C modules. The C-module reflects the consensus sequence of the repetitive core sequence of *Araneus diadematus* fibroin 4 (ADF4), one of the main components of the dragline silk of the European garden spider (*A. diadematus*). Dragline silk is the best characterized spider silk, constituting the outer frame of orb webs and serving as a lifeline for the spider [80]. (b) Going from a CAD template (left) to a 3DBP recombinant spider silk construct (right). Recombinant eADF4(C16) was printed by robotic dispensing. In the CAD template, the different shades of gray represent thickness with darker shades representing multiple layers. In the image of the construct it can be qualitatively observed that the construct has the same shape as the CAD file, and the printed strands made of spider silk also have high shape fidelity without the use of post-processing, crosslinking or thickeners.

recombinant spider silk proteins were assessed regarding their printability [40], and spider silk constructs could be printed by robotic dispensing using a print head with an electromagnetic valve. The hydrogels were process-compatible and had high shape fidelity (Fig. 3b). The printability is based on the β-sheet transformation of the proteins during gelation and shear thinning behavior of the hydrogels (Fig. 4).

It was shown that recombinant spider silk proteins can be used as bioink for 3D printing without the need of additional components or post-processing [40]. In contrast, alginate and fibroin need post-processing with crosslinkers or thickeners added to the solution to increase the printing fidelity [20, 58]. For more detailed information of other bioinks, refer to [29] and Table 2.

To produce cell-loaded 3D hydrogel constructs, cells were encapsulated within a highly concentrated silk solution before gelation. The addition of cells to the bioink did not influence the self-assembly into a hydrogel or the printability of the material [40]. The cells survived the printing process and were viable at least 7 days *in situ*. The viability within the spider silk hydrogel could be quantified with 70.1 ± 7.6 %. Although the cell viability in the spider silk constructs is lower when compared to established bioinks such as alginate (~90 %) and gelatin (~98 %), it could be shown that the printing procedure did not significantly affect viability, since after printing 97 % of the cells survived [40, 42, 83].

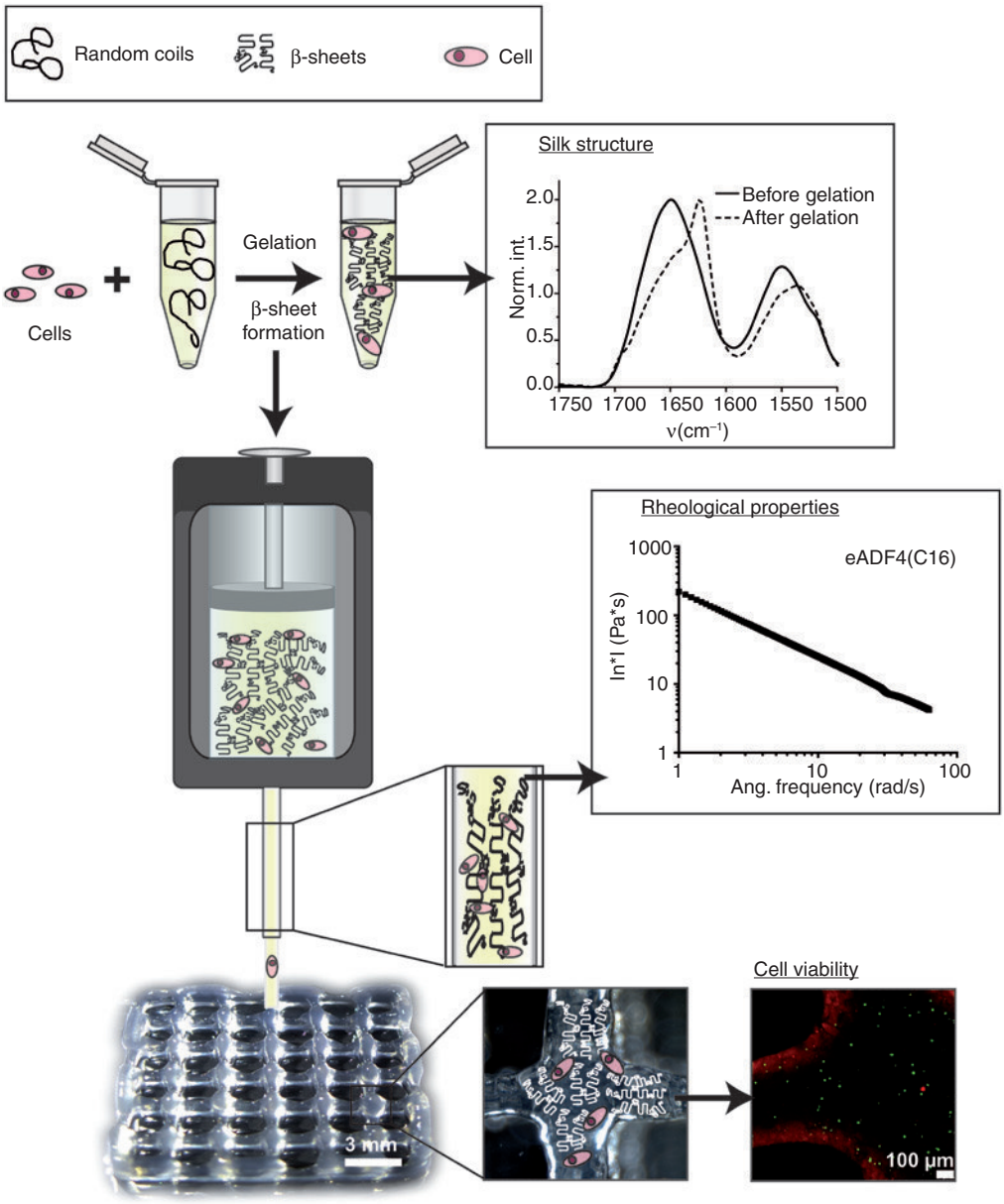

Fig. 4: Printing process for a physically crosslinked recombinant spider silk bioink. Cell-loaded spider silk constructs were printed by robotic dispensing, as mentioned in Fig. 3. The process begins with preparation of the hydrogel from a cell-loaded solution. The corresponding Fourier-transformed infrared spectroscopy (FTIR) structure data shows a peak shift corresponding to β-sheet formation which occurred during self-assembly of the hydrogel. The next step in the process represents the printing of the hydrogel accompanied by alignment of β-sheets under shear-stress, and this corresponds to the given rheological behavior with increasing angular frequency leading to a decrease in complex viscosity, which is called shear-thinning. The final construct is represented by a stereoscope image of the layered structure. The right-hand image represents the presence of viable cells (redlines reflect auto-fluorescence of spider silk; red stained cells are dead and green stained ones viable).

Conclusion and future perspectives

In conclusion, 3D bioprinting (3DBP) techniques hold potential to overcome the current, process-based challenges faced in tissue engineering: high variability and low control over the placement of different scaffold components. Of the different types of 3DBP, it seems as though extrusion printing will be one excellent option for the future of biofabrication, despite some of its drawbacks (nozzle clogging, resolution). Extrusion

printing allows for fabrication of clinically-relevant constructs (size, cell density) and greater ease in bioink development. Additionally, these advantages outweigh the disadvantages. For example, bioinks are critical in cell viability after printing (physicochemical properties) and cell behavior throughout construct maturation (physiological properties). Current bioinks tend to be better in either the "cell friendliness" (e.g. fibrin, gelatin) or printability (recombinant spider silk protein). Future work will most likely focus on polymer blends such that advantages are conserved or enhanced, and the disadvantages minimized or eliminated.

In terms of cell viability after printing, it is reasonable to hypothesize that cell viability is directly correlated with the mechanical stress that the cells are exposed to. In the optimal viscosity range for extrusion printing, there seems to be some protection to shear stress which is absent in inkjet printing; in LAB there are virtually no shear forces on the bioink, due to the nozzle-free set-up. However, LAB is incompatible with higher viscosity ranges, due to the incompability of cells with certain wavelengths and energy densities. Thereby, due to the greater flexibility in bioink development, it seems as though extrusion bioprinting will be the technology that shows the greatest potential in the future. However, it is also possible to imagine future developments will also focus on combining the different types of 3D bioprinting in order to further optimize the process.

Acknowledgments: This work was supported by the Deutsche Forschungsgemeinschaft (SCHE 603/9-1) and the European Union's Seventh Framework Program (FP7/2007-2013) under grant agreement no. 309962 (project HydroZones).

References

[1] R. G. Harrison, M. J. Greenman, F. P. Mall, C. M. Jackson. *Anat. Rec.* **1**, 116 (1907).
[2] R. Langer, J. P. Vacanti. *Science* **260**, 920 (1993).
[3] T. Aberle, K. Franke, E. Rist, K. Benz, B. Schlosshauer. *PLoS One* **9**, e86740 (2014).
[4] M. A. Lancaster, J. A. Knoblich. *Nat. Protoc.* **9**, 2329 (2014).
[5] A. Bozkurt, F. Gilmour R Jr., A. Lal. *IEEE Trans. Biomed. Eng.* **56**, 2304 (2009).
[6] M. J. Post. *Meat Sci.* **92**, 297 (2012).
[7] J. H. Shim, S. E. Kim, J. Y. Park, J. Kundu, S. W. Kim, S. S. Kang, D. W. Cho. *Tissue Eng. Part A* **20**, 1980 (2014).
[8] J. J. Mancuso, J. Cheng, Z. Yin, J. C. Gilliam, X. Xia, X. Li, S. T. Wong. *Front. Neuroanat.* **8**, 130 (2014).
[9] A. Wittinghofer, I. R. Vetter. *Annu. Rev. Biochem.* **80**, 943 (2011).
[10] D. D. Allison, K. R. Braun, T. N. Wight, K. J. Grande-Allen. *Acta Biomater.* **5**, 1019 (2009).
[11] M. D. Tang-Schomer, J. D. White, L. W. Tien, L. I. Schmitt, T. M. Valentin, D. J. Graziano, A. M. Hopkins, F. G. Omenetto, P. G. Haydon, D. L. Kaplan. *Proc. Natl. Acad. Sci. USA* **111**, 13811 (2014).
[12] V. A. Kasyanov, J. Hodde, M. C. Hiles, C. Eisenberg, L. Eisenberg, L. E. De Castro, I. Ozolanta, M. Murovska, R. A. Draughn, G. D. Prestwich, R. R. Markwald, V. Mironov. *J. Mater. Sci. Mater. Med.* **20**, 329 (2009).
[13] D. R. Albrecht, R. L. Sah, S. N. Bhatia. *Biophys. J.* **87**, 2131 (2004).
[14] A. Ito, K. Ino, M. Hayashida, T. Kobayashi, H. Matsunuma, H. Kagami, M. Ueda, H. Honda. *Tissue Eng.* **11**, 1553 (2005).
[15] G. Y. Huang, L. H. Zhou, Q. C. Zhang, Y. M. Chen, W. Sun, F. Xu, T. J. Lu. *Biofabrication* **3**, 012001 (2011).
[16] Y. Ling, J. Rubin, Y. Deng, C. Huang, U. Demirci, J. M. Karp, A. Khademhosseini. *Lab. Chip.* **7**, 756 (2007).
[17] I. Elloumi-Hannachi, M. Yamato, T. Okano. *J. Intern. Med.* **267**, 54 (2010).
[18] A. Abeyewickreme, A. Kwok, J. R. McEwan, S. N. Jayasinghe. *Integr. Biol.* **1**, 260 (2009).
[19] N. K. Pakes, S. N. Jayasinghe, R. S. Williams. *J. R. Soc., Interface* **8**, 1185 (2011).
[20] S. Das, F. Pati, Y.-J. Choi, G. Rijal, J.-H. Shim, S. W. Kim, A. R. Ray, D.-W. Cho, S. Ghosh. *Acta Biomater.* **11**, 233 (2014).
[21] L. Koch, M. Gruene, C. Unger, B. Chichkov. *Curr. Pharm. Biotechnol.* **14**, 91 (2013).
[22] T. Xu, C. A. Gregory, P. Molnar, X. Cui, S. Jalota, S. B. Bhaduri, T. Boland. *Biomaterials* **27**, 3580 (2006).
[23] P. Bajaj, R. M. Schweller, A. Khademhosseini, J. L. West, R. Bashir. *Annu. Rev. Biomed. Eng.* **16**, 247 (2014).
[24] V. Mironov, T. Trusk, V. Kasyanov, S. Little, R. Swaja, R. Markwald. *Biofabrication* **1**, 022001 (2009).
[25] C. J. Luo, S. D. Stoyanov, E. Stride, E. Pelan, M. Edirisinghe. *Chem. Soc. Rev.* **41**, 4708 (2012).
[26] S. V. Murphy, A. Atala. *Nat. Biotechnol.* **32**, 773 (2014).
[27] J. S. Miller. *PLoS Biol.* **12**, e1001882 (2014).
[28] A. Pfister, R. Landers, A. Laib, U. Hubner, R. Schmelzeisen, R. Mulhaupt. *J. Polym. Sci., Part A: Polym. Chem.* **42**, 624 (2004).

[29] J. Malda, J. Visser, F. P. Melchels, T. Jüngst, W. E. Hennink, W. J. A. Dhert, J. Groll, D. W. Hutmacher. *Adv. Mater.* **25**, 5011 (2013).
[30] R. Nayaran, Ed. *Rapid Prototyping of Biomaterials: Principles and Applications*. Woodhead Publishing, Philadelphia (2014).
[31] L. A. Hockaday, K. H. Kang, N. W. Colangelo, P. Y. Cheung, B. Duan, E. Malone, J. Wu, L. N. Girardi, L. J. Bonassar, H. Lipson, C. C. Chu, J. T. Butcher. *Biofabrication* **4**, 035005 (2012).
[32] S. Moon, S. K. Hasan, Y. S. Song, F. Xu, H. O. Keles, F. Manzur, S. Mikkilineni, J. W. Hong, J. Nagatomi, E. Haeggstrom, A. Khademhosseini, U. Demirci. *Tissue Eng., Part C* **16**, 157 (2010).
[33] M. Duocastella, J. M. Fernandez-Pradas, P. Serra, J. L. Morenza. *Appl. Phys. A: Mater. Sci. Process.* **93**, 453 (2008).
[34] C. Mézel, L. Hallo, A. Souquet, J. Breil, D. Hebert, F. Guillemot. *Phys. Plasmas* **16**, 123112 (2009).
[35] C. J. Ferris, K. G. Gilmore, G. G. Wallace, M. I. H. Panhuis. *Appl. Microbiol. Biotechnol.* **97**, 4243 (2013).
[36] S. Catros, B. Guillotin, M. Bacakova, J. C. Fricain, F. Guillemot. *Appl. Surf. Sci.* **257**, 5142 (2011).
[37] R. Cornock, S. Beirne, B. Thompson, G. G. Wallace. *Biofabrication* **6**, 025002 (2014).
[38] I. T. Ozbolat, H. Chen, Y. Yu. *Robotics and Computer-Integrated Manufacturing* **30**, 295 (2014).
[39] J. N. H. Shepherd, S. T. Parker, R. F. Shepherd, M. U. Gillette, J. A. Lewis, R. G. Nuzzo. *Adv. Funct. Mater.* **21**, 47 (2011).
[40] K. Schacht, T. Jüngst, M. Schweinlin, A. Ewald, J. Groll, T. Scheibel. *Angew. Chem., Int. Ed.* **54**, 2816 (2015).
[41] Q. L. Loh, C. Choong. *Tissue Eng. Part B, Rev.* **19**, 485 (2013).
[42] J. Jia, D. J. Richards, S. Pollard, Y. Tan, J. Rodriguez, R. P. Visconti, T. C. Trusk, M. J. Yost, H. Yao, R. R. Markwald, Y. Mei. *Acta Biomater.* **10**, 4323 (2014).
[43] N. E. Fedorovich, J. Alblas, J. R. de Wijn, W. E. Hennink, A. J. Verbout, W. J. A. Dhert. *Tissue Eng.* **13**, 1905 (2007).
[44] B. Derby. *Science* **338**, 921 (2012).
[45] B. S. Kim, D. J. Mooney. *Trends Biotechnol.* **16**, 224 (1998).
[46] N. E. Fedorovich, W. Schuurman, H. M. Wijnberg, H. J. Prins, P. R. van Weeren, J. Malda, J. Alblas, W. J. A. Dhert. *Tissue Eng., Part C* **18**, 33 (2012).
[47] J. C. Schense, J. A. Hubbell. *Bioconjug. Chem.* **10**, 75 (1999).
[48] C. L. Cummings, D. Gawlitta, R. M. Nerem, J. P. Stegemann. *Biomaterials* **25**, 3699 (2004).
[49] W. Xu, X. Wang, Y. Yan, W. Zheng, Z. Xiong, F. Lin, R. Wu, R. Zhang. *J. Bioact. Compat. Polym.* **22**, 363 (2007).
[50] X. Wang, Y. Yan, R. Zhang. *Tissue Eng. Part B, Rev.* **16**, 189 (2010).
[51] C. M. Smith, A. L. Stone, R. L. Parkhill, R. L. Stewart, M. W. Simpkins, A. M. Kachurin, W. L. Warren, S. K. Williams. *Tissue Eng.* **10**, 1566 (2004).
[52] R. Parenteau-Bareil, R. Gauvin, F. Berthod. *Materials* **3**, 1863 (2010).
[53] U. Hersel, C. Dahmen, H. Kessler. *Biomaterials* **24**, 4385 (2003).
[54] E. Hoch, T. Hirth, G. E. M. Tovar, K. Borchers. *J. Mater. Chem. B* **1**, 5675 (2013).
[55] W. Schuurman, P. A. Levett, M. W. Pot, P. R. van Weeren, W. J. A. Dhert, D. W. Hutmacher, F. P. W. Melchels, T. J. Klein, J. Malda. *Macromol. Biosci.* **13**, 551 (2013).
[56] E. Hoch, C. Schuh, T. Hirth, G. E. M. Tovar, K. Borchers. *J. Mater. Sci. Mater. Med.* **23**, 2607 (2012).
[57] S. Das, F. Pati, S. Chameettachal, S. Pahwa, A. R. Ray, S. Dhara, S. Ghosh. *Biomacromolecules* **14**, 311 (2013).
[58] S. Wust, M. E. Godla, R. Muller, S. Hofmann. *Acta Biomater.* **10**, 630 (2014).
[59] F. P. W. Melchels, W. J. A. Dhert, D. W. Hutmacher, J. Malda. *J. Mater. Chem. B* **2**, 2282 (2014).
[60] R. Levato, J. Visser, J. A. Planell, E. Engel, J. Malda, M. A. Mateos-Timoneda. *Biofabrication* **6**, 035020 (2014).
[61] X. F. Cui, K. Breitenkamp, M. G. Finn, M. Lotz, D. D. D'Lima. *Tissue Eng. Part A* **18**, 1304 (2012).
[62] R. Censi, W. Schuurman, J. Malda, G. di Dato, P. E. Burgisser, W. J. A. Dhert, C. F. van Nostrum, P. di Martino, T. Vermonden, W. E. Hennink. *Adv. Funct. Mater.* **21**, 1833 (2011).
[63] M. Kesti, M. Muller, J. Becher, M. Schnabelrauch, M. D'Este, D. Eglin, M. Zenobi-Wong. *Acta Biomater.* **11**, 162 (2015).
[64] K. Y. Lee, D. J. Mooney. *Prog. Polym. Sci.* **37**, 106 (2012).
[65] P. Kesari, T. Xu, T. Boland. *Mater. Res. Soc. Symp. Proc.* **845**, 111 (2005).
[66] X. F. Cui, T. Boland. *Biomaterials* **30**, 6221 (2009).
[67] J. Visser, B. Peters, T. J. Burger, J. Boomstra, W. J. A. Dhert, F. P. W. Melchels, J. Malda. *Biofabrication* **5**, 035007 (2013).
[68] G. H. Altman, F. Diaz, C. Jakuba, T. Calabro, R. L. Horan, J. S. Chen, H. Lu, J. Richmond, D. L. Kaplan. *Biomaterials* **24**, 401 (2003).
[69] A. Leal-Egaña, T. Scheibel. *Biotechnol. Appl. Biochem.* **55**, 155 (2010).
[70] K. Schacht, T. Scheibel. *Curr. Opin. Biotechnol.* **29**, 62 (2014).
[71] P. H. Zeplin, N. C. Maksimovikj, M. C. Jordan, J. Nickel, G. Lang, A. H. Leimer, L. Roemer, T. Scheibel. *Adv. Funct. Mater.* **24**, 2658 (2014).
[72] P. H. Zeplin, A.-K. Berninger, N. C. Maksimovikj, P. van Gelder, T. Scheibel, H. Walles. *Handchir. Mikrochir. Plast. Chir.* **46**, 336 (2014).
[73] H. Mori, M. Tsukada. *J. Biotechnol.* **74**, 95 (2000).
[74] Y. Q. Zhang, W. D. Shen, R. A. Gu, J. Zhu, R. Y. Xue. *Anal. Chim. Acta* **369**, 123 (1998).
[75] I. Drachuk, O. Shchepelina, S. Harbaugh, N. Kelley-Loughnane, M. Stone, V. V. Tsukruk. *Small* **9**, 3128 (2013).
[76] C. Blum, A. Nichtl, T. Scheibel. *Adv. Funct. Mater.* **24**, 763 (2014).
[77] K. Schacht, T. Scheibel. *Biomacromolecules* **12**, 2488 (2011).

[78] S. Wohlrab, S. Muller, A. Schmidt, S. Neubauer, H. Kessler, A. Leal-Egana, T. Scheibel. *Biomaterials* **33**, 6650 (2012).
[79] L. Pescosolido, W. Schuurman, J. Malda, P. Matricardi, F. Alhaique, T. Coviello, P. R. Weeren, W. J. Dhert, W. E. Hennink, T. D. Vermonden. *Biomacromolecules* **12**, 1831 (2011).
[80] A. Aprhisiart, F. Vollrath. *Behav. Ecol.* **5**, 280 (1994).
[81] D. Huemmerich, C. W. Helsen, S. Quedzuweit, J. Oschmann, R. Rudolph, T. Scheibel. *Biochemistry-Us* **43**, 13604 (2004).
[82] C. Vendrely, T. Scheibel. *Macromol. Biosci.* **7**, 401 (2007).
[83] T. Billiet, E. Gevaert, T. De Schryver, M. Cornelissen, P. Dubruel. *Biomaterials* **35**, 49 (2014).

TEILARBEIT VI

Die Ergebnisse dieses Kapitels wurden bereits in *Chemical Reviews* veröffentlicht als:

> "Strategies and Molecular Design Criteria for 3D Printable Hydrogels." Jungst, T.*, Smolan, W.*, Schacht, K., Scheibel, T. und Groll, J..

Reproduziert aus *Chemical Reviews* **2016**, 116(3): 1496-1539 mit freundlicher Genehmigung des Verlages American Chemical Society.

* gleichberechtigte Co-Autorenschaft

CHEMICAL REVIEWS

Review

pubs.acs.org/CR

Strategies and Molecular Design Criteria for 3D Printable Hydrogels

Tomasz Jungst,[†,§] Willi Smolan,[†,§] Kristin Schacht,[‡] Thomas Scheibel,[‡] and Jürgen Groll*[,†]

[†]Department for Functional Materials in Medicine and Dentistry, University of Würzburg, Pleicherwall 2, 97070 Würzburg, Germany

[‡]Chair of Biomaterials, Faculty of Engineering Science, University of Bayreuth, Universitätsstrasse 30, 95447 Bayreuth, Germany

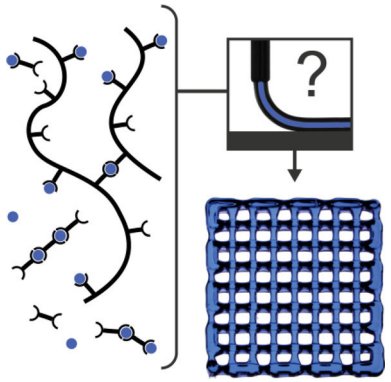

CONTENTS

1. Introduction 1496
2. Fabrication Systems 1498
2.1. Laser-Induced Forward Transfer 1498
2.2. Inkjet Printing 1499
2.3. Robotic Dispensing 1501
2.4. Comparison of the Fabrication Methods 1502
3. Rheological Considerations 1502
3.1. Rheology of Non-Newtonian Liquids 1503
3.2. Important Aspects of the Printing Process 1503
3.3. Underlying Molecular Concepts: Colloidal Solutions 1504
3.4. Underlying Molecular Concepts: Polymer Solutions 1505
3.5. Characterization of Rheological Properties 1505
4. Chemical Cross-Linking 1506
4.1. Post- and Prefabrication Cross-Linking 1506
4.2. Application of Dynamic Covalent Bonds for Printing 1507
5. Molecular Physical Gels 1507
5.1. Supramolecular Approaches 1508
5.1.1. Ionic Interactions and Coordination Bonds 1508
5.1.2. Hydrogen Bonds 1509
5.1.3. Host–Guest and Aromatic Donor–Acceptor Interactions 1509
5.1.4. Low Molecular Weight Gelator 1510
5.2. Macromolecular Gels 1511
5.2.1. Naturally Occurring Biopolymers Used for Hydrogel Formation 1511
5.2.2. Synthetic Peptides and Proteins 1514
5.2.3. Host–Guest Interaction 1515
5.2.4. Ionic Interactions and Coordination Chemistry 1517
5.2.5. Hydrogen Bonds 1518
5.3. Colloidal Systems 1518
5.3.1. Silica Nanoparticles and Laponite-Based Hydrogels 1518
5.3.2. Carbon-Nanotube- and Graphene-Sheet-Rich Compounds 1519
5.3.3. Metal-Based Gels 1521
6. Biotechnological Approaches toward Bioinks 1521
6.1. Designable Biopolymers: Recombinantly Produced Proteins 1522
6.1.1. Methods for Recombinant Protein Production 1522
6.1.2. Silk-like Proteins 1523
6.1.3. Recombinant Collagen/Collagen-like Proteins 1523
6.1.4. Elastin-like Polypeptides 1524
6.1.5. Resilin-like Polypeptides 1524
6.1.6. Hybrid Proteins 1524
6.2. Designable Biopolymers: Polynucleotides 1525
7. Conclusions and Outlook 1525
Author Information 1526
Corresponding Author 1526
Author Contributions 1526
Notes 1526
Biographies 1526
Acknowledgments 1527
References 1527

1. INTRODUCTION

Additive manufacturing (AM), also referred to as rapid prototyping, solid free-form fabrication, or simply three-dimensional (3D) printing, comprises a number of technologies that allow the direct generation of objects in a layer-by-layer fashion through computer-aided design (CAD) and/or computer-aided manufacturing (CAM).[1] With these processing technologies, objects can be generated without the need for molds, enabling a high degree of freedom in design and allowing the direct production of structures that cannot be fabricated using classical subtractive manufacturing techniques. AM technologies have been primarily used in the engineering and fabrication community[2] for decades but have matured into high-precision (e.g., via electron beam melting) or low-cost (e.g., fused deposition modeling, FDM) printers. AM is increasingly relied upon for certain industrial production processes, for example, in the case of laser sintering for titanium hip implants, and is regarded as the next industrial or manufacturing revolution.[3]

Special Issue: Frontiers in Macromolecular and Supramolecular Science

Received: May 18, 2015
Published: October 23, 2015

DOI: 10.1021/acs.chemrev.5b00303
Chem. Rev. 2016, 116, 1496–1539

The high degree of automation and reproducibility in AM, together with the precise control over where different components can be placed in a 3D model, renders AM particularly interesting for tissue engineering (TE), which aims for the full restoration of damaged or degenerated tissues and organs. Traditionally, the three main components of TE (cells, prefabricated scaffolds, and growth factors) are combined to form a construct that can be either directly implanted or incubated in vitro for maturation prior to implantation.[4] AM techniques have predominantly been applied for the fabrication of scaffolds for such TE approaches.[5−8] Seeding of cells onto such prefabricated scaffolds usually results in a nonordered and random distribution of cells which does not reflect the complex hierarchical organization of functional tissue.

However, recapitulating the hierarchical complexity of native tissues in cell-loaded constructs is a highly attractive strategy for the creation of functional tissue equivalents. Therefore, cells, biomaterials, and bioactive compounds have to be processed simultaneously, and AM technologies are regarded as a method to achieve this.[9] This relatively young approach is termed biofabrication and can be defined as the creation of biological structures for TE, pharmacokinetic, or basic cell biology studies (including disease models) by a computer-aided transfer process for patterning and assembling living and nonliving materials with a prescribed 3D organization.[10] This research field holds the promise to overcome some of the most urgent challenges of TE, such as the direct generation of large constructs including vessel-like structures for initial nutrient and oxygen supply of the embedded cells.

Biofabrication research has rapidly developed over the past decade and has very recently been addressed by several excellent review papers.[11−14] It places high demands on the AM process and the materials used for it, including so-called "bioinks", cell loadable and printable formulations that solidify after printing for shape fidelity of the desired structure. The entire manufacturing must produce defined structures using cell-compatible conditions such as buffered aqueous solution and a narrow temperature range and with limited mechanical shear forces. Also, the materials and chemistry used for printing have to be cytocompatible. This significantly limits the variety of applicable AM technologies and suitable materials, with hydrogels as predetermined candidates for bioinks. Hydrogels are three-dimensionally cross-linked hydrophilic polymer networks that swell without dissolution up to 99% (w/w) water of their dry weights.[15] These materials are particularly attractive for biomedical applications as they recapitulate several features of the natural environment of cells, the so-called extracellular matrix (ECM),[16] and allow for efficient and homogeneous cell seeding in a highly hydrated mechanically supportive 3D environment. Depending on the type of cross-linking, hydrogels can be divided into two classes: (i) chemically cross-linked hydrogels (also termed chemical hydrogels) and (ii) physically cross-linked hydrogels (also termed physical hydrogels). Chemical hydrogels are formed by covalent networks and cannot dissolve in water without breakage of covalent bonds. Physical hydrogels are, however, formed by dynamic and reversible cross-linking of synthetic or natural building blocks based on noncovalent interactions such as hydrophobic and electrostatic interaction or hydrogen bridges. Hence, physical hydrogels exhibit promising properties for bioink development since they can rapidly retain their shape after printing. Some recent reviews give a comprehensive overview on the design and application of hydrogels for biomedical applications,[17−19] TE,[20] and regenerative medicine.[21]

There has been intensive research with regard to injectable hydrogel formulations based on the fact that the gelation behavior of hydrogels can be adjusted so that a hydrogel precursor solution can be prepared and injected into a mold or cavity and subsequently gelate and form a hydrogel after injection.[22−24] This can, for example, be achieved through shear thinning properties leading to a viscosity decrease with increasing shear stress accompanied by the injection through a cannula.[25] However, for 3D printing of cell-containing hydrogels, the prerequisites are even more stringent than for injectable hydrogels. For printing, the cell-loaded bioink formulation has to be stable in the reservoir for the time of the printing procedure (typically at least several minutes, depending on the size and complexity of the structure to be printed) with rheological properties imposed by the fabrication process and with a homogeneous three-dimensional distribution of the cells. To achieve reasonable resolutions, the nozzle diameters are also significantly lower in printing than for simple injection, and after printing, the (re)gelation needs to be rapid enough to ensure shape stability of the printed construct. Ideally, the resulting structure is self-supporting, and no postprocessing treatment is needed for mechanical stabilization. The lack of geometrical constraints and the need for rapid gelation to ensure shape fidelity is the most significant and at the same time the most challenging difference of injectable versus printable hydrogels.

As biofabrication eventually aims at delivering human tissue models for biomedical research and eventually as a therapeutic treatment option, it is important to keep in mind that a general suitability for clinical translation should be taken into account for the development of a new bioink. Generally, the materials have to be sterile when entering the fabrication process, either through sterile production or through conformity with a sterilization method. Moreover, the materials should ideally be endotoxin free but definitely cannot exceed the limits set by regulation, which may be a more critical point for biopolymers than for synthetic systems. These few but important general considerations should therefore always be taken into account for bioink development.

Bioprinting and biofabrication originated from the technology- and application-oriented (bio)engineering community and did not evolve from chemistry or materials science. Hence, the field has for long worked with established hydrogel systems available in quantities that are necessary for the processes. The vast majority of bioprinting and biofabrication studies thus use alginate- and gelatin-based bioink formulations. Although this has allowed achieving some remarkable successes, it has recently become evident that the lack of a bigger variety of printable hydrogel systems is one major drawback that hampers progress of the complete field.[26−28]

Hence, the scope of this review paper is neither to simply recapitulate and summarize established printing methods and printable hydrogels nor to summarize the achievements obtained with the present biofabrication approaches toward the construction of complex cellular arrangements or tissue-like structures and their evaluation in vitro and in vivo. For this information, we refer the reader to several excellent and most recent review papers.[11−14,26−28] The main objective of this paper is to complement this information with a material-focused but integral summary of the most important rheological aspects relevant for printing together with an overview on the most important printing techniques. Core part of the paper is an interdisciplinary overview of possibilities to create tailored

DOI: 10.1021/acs.chemrev.5b00303
Chem. Rev. 2016, 116, 1496−1539

(macro)molecular building blocks for printable hydrogels. This overview comprises existing strategies in related research fields such as supramolecular chemistry for self-assembly strategies or biotechnological approaches for bioinspired building blocks. Our aim is to deliver a comprehensive set of information to be used as a toolbox for polymer chemists and material scientists with a basic set of fundamental design criteria for the rational development of novel strategies toward bioinks.

In this review, we first introduce the most common 3D printing techniques for hydrogel printing, followed by the rheological demands on printable hydrogel systems with respect to the different techniques and the additional limitation of cytocompatibility during printing. We then briefly summarize the role of chemical cross-linking, so far mainly used for pre-cross-linking of the hydrogel building blocks before printing or postfixing of printed structures, but also introduce dynamic chemical bonds as a new and promising option for printing. We then summarize the physical cross-linking possibilities potentially exploitable for hydrogel printing, divided into supramolecular systems, functionalized polymers, and other strategies such as particulates. Finally, we outline the potential of biotechnological processes for the production of tailored biomolecules for bioink development and review the most promising biotechnologically produced systems.

2. FABRICATION SYSTEMS

Open source projects such as RepRap and Fab@home made AM affordable for private users and led to increased popularity of 3D printing. The developed desktop printers are based on FDM and enable fabrication of 3D constructs from thermoplastic materials in a layer-by-layer fashion with resolutions of about 200−400 μm. A constantly growing number of users can experience the benefits of AM and appreciate the new freedom of designing printable objects. Other processes such as selective laser sintering (SLS) allow production of very complex structures with high resolution of 50−300 μm but are still mainly limited to industry use.[29] Both methods—FDM and SLS—can be used to process polymers. They generate heat to melt the material and create structures by controlled solidification of the thermoplasts. Due to the thermal conditions during printing, they do not allow for hydrogel processing, but there are a variety of technologies that enable structuring hydrogels into 3D constructs.

Two very interesting processes capable of fabricating complex 3D objects from hydrogels are two-photon polymerization (2PP) and stereolithography (SLA). They use light to induce spatially limited polymerization and can be used to create well-defined structures. For both processes the construct is mainly generated by light-induced radical polymerization within a monomer reservoir or light-induced cross-linking of a photopolymer. In 2PP a femtosecond laser is focused onto a spot within this reservoir, releasing radicals from a photoinitiator on its path. These radicals start a polymerization/cross-linking reaction leading to solidification of material along the laser track. Usually a drop of material, enclosed between two microscopy glass coverslips with spacers in the millimeter range defining the construct thickness, is used as the reservoir. Relating the reservoir size to coverslips and taking into account that prints usually are much smaller than the overall size of the slips gives an indication of the producible sample size. Although the object size is limited, 2PP offers the possibility to produce constructs with spatial resolutions as small as 100 nm and is thus especially interesting for analyzing cell−construct interactions.[30] SLA enables the size limitations of 2PP prints to be easily overcome, generating constructs with dimensions in the centimeter range. Although compared to that of 2PP the resolution is decreased, it still is as high as 80−125 μm.[31] In SLA the objects are produced in a layer-by-layer fashion. The most frequently applied setup is the bottom-up system where a laser scans and solidifies the top layer of a reservoir. After one layer is created, a movable platform lowers the construct further into the resin, covering it with the next material layer. Print speeds can be increased using digital light projectors, instead of scanning lasers, illuminating and solidifying the whole layer at the same time. Another setup of SLA is top-down systems where the construct is stepwise pulled out of the resin after irradiation of one plane.[32] A new version of top-down SLA using digital light projectors that has recently attracted attention is continuous liquid interface production (CLIP).[33] In contrast to other SLA systems, CLIP utilizes an oxygen-permeable window delivering oxygen to the glass−resin interface. The oxygen inhibits the polymerization reaction, creating a persistent liquid interface, allowing—in combination with precise process timing—print speeds to be further increased. CLIP enables the production of structures at hundreds of millimeters per hour and thus is much faster than traditional SLA techniques. Further research needs to be carried out to confirm if the high print speeds can be realized for biomedical applications. The main disadvantage of the light-induced processes introduced in this section is the limited number of suitable resins. Especially when printing structures from cell-containing hydrogels, a special focus needs to be put on the cytotoxicity of the photoinitiator.[32]

As this short introduction shows, there is a large selection of fabrication systems available. The choice of the method mainly depends on the material that shall be processed and on the structure (size, architecture, resolution) that needs to be created. As we will discuss, each method has limitations, and none of the approaches can be considered better than another one. For some applications, also the combination of different processes might be beneficial. Fabrication systems are also still developed further, and new technologies do arise. However, as this review focuses on exploring material strategies that have been and/or can be exploited for bioprinting and biofabrication, we focus here on the three most important and best established technologies for printing of hydrogels under cell-friendly conditions: laser-induced forward transfer, inkjet printing, and robotic dispensing. These techniques will be described in detail and compared to each other in the following sections.

2.1. Laser-Induced Forward Transfer

The reviews of Chrisey et al.,[34] Ringeisen et al.,[35] and Schiele et al.[36] give excellent summaries of laser-induced forward transfer (LIFT) techniques used for cell printing and also show examples of structures being produced with these methods. For biomedical applications, mostly modified LIFT techniques are applied. Generally, all these systems have the same setup in common and are comprised of three main components. The first is a pulsed laser, the second is a donor slide (ribbon) from which the material is propelled, and the third is a receiving substrate. The laser is focused onto a laser-absorbing layer, evaporating the material and thus generating a high gas pressure propelling material toward the substrate. By controlled movement of the donor and/or substrate, it is possible to build up 2D and 3D structures from material droplets.[37−42] For processing biological materials, two different versions of modified LIFT are utilized: matrix-assisted pulsed laser evaporation direct writing (MAPLE-DW) and absorbing film-assisted laser-induced forward transfer

DOI: 10.1021/acs.chemrev.5b00303
Chem. Rev. 2016, 116, 1496−1539

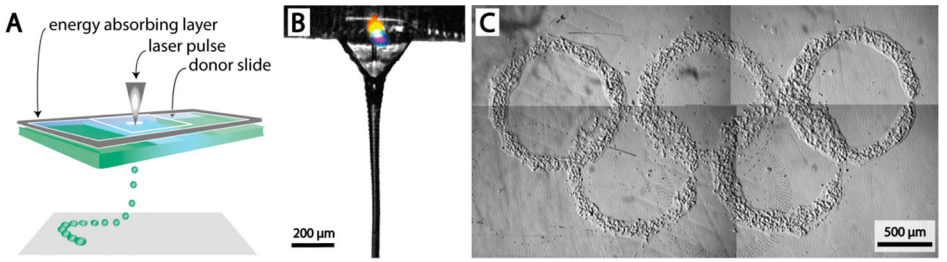

Figure 1. Laser-induced forward transfer (LIFT). (A) Schematic drawing of the process. Reprinted in part with permission from ref 27. Copyright 2013 John Wiley and Sons. (B) Close-up view of the jet generated by the incident laser pulse. Adapted with permission from ref 44. Copyright 2011 Springer. (C) Cell pattern printed with LIFT. Reprinted in part with permission from ref 39. Copyright 2010 Elsevier.

(AFA-LIFT). The main difference between those two techniques can be found in the donor slide setup. In the most frequently used MAPLE-DW setups, the donor slide comprises two different layers—a laser transparent support layer and a laser absorption layer. If the printing material itself is not absorbing light efficiently, it needs to be mixed with a matrix that will adsorb light and transfer the energy. In the case of cell printing, this matrix usually is a hydrogel, cell culture medium with addition of glycerol, or an extracellular matrix.[35] In contrast to that in AFA-LIFT and its related versions such as biological laser printing (BioLP), the donor contains three different layers—a laser transparent support layer, a laser absorption layer, and a layer with the deposition material (Figure 1A). The laser adsorption layer in general is a thin (about 100 nm) metal coating that absorbs the laser light, leading to evaporation of the coating. This evaporation leads to a high-pressure bubble expanding toward the surface and finally to material deposition. Although not obligatory,[43] the receiving substrate in modified LIFT processes for biomedical applications is mainly coated with a thin (20−40 μm) hydrogel layer that prevents the deposited material from drying and in the case of printing cells cushions the impact.[35] In the following section, we compare AFA-LIFT and MAPLE-DW in regard to printing hydrogels for biomedical applications.[36]

As discussed, the main difference between MAPLE-DW and AFA-LIFT is the ribbon. In MAPLE-DW the light-absorbing matrix is mixed with the biomedical material. The heating within this layer and the irradiation with light might cause problems when printing sensitive materials, but as many researchers could confirm, it did not seem to have a negative effect on the cell viability.[45−47] AFA-LIFT and BioLP use an additional light-absorption layer mainly from Au, Ti, or TiO_2.[40,48,49] This layer protects the underlying biological layer from radiation-induced damage, but upon its evaporation the printed material will be contaminated. It could be shown that by using an energy conversion layer the reproducibility and resolution are enhanced (Figure 1C shows a 2D pattern printed with LIFT). Furthermore, this additional layer increases the selection of possible printing materials.[35]

After having commented on the differences between the setups, we now briefly point out special demands on the material accompanied by the LIFT process. Using a laser as the driving force, the resolution of the LIFT techniques is mainly influenced by the laser energy and laser pulse duration, but also the material properties and the thickness of the deposition material layer will influence the propelled material volume. The laser pulse will evaporate material at the donor slide, leading to a vapor bubble. This bubble needs to expand toward the surface, finally leading to material ejection. As discussed by several groups,[50−54] there is a distinct laser fluence leading to material jetting (jetting regime; see Figure 1B). If the fluence is too small, the bubble will collapse (subthreshold regime), and if the laser pulse energy is too high, the bubble will generate undirected submicrometer droplets (plume regime). For a given laser fluence, the material properties will influence the bubble expansion. The thickness of the biological layer on the donor slide will influence the energy of the jetted material. The thicker the layer, the lower the amount of kinetic energy that will be transferred to the jet. In addition, the viscoelastic properties of the material will influence the propagation of the gas pressure. Finally, also the surface tension will determine material ejection.

2.2. Inkjet Printing

The process of inkjet printing is well-known from desktop applications. Many private users have printed 2D graphical printouts and maybe even refilled cartilages unwittingly, gaining experiences potentially useful for biofabrication. The first printers used modified setups and especially have cleaned and reused cartilages originally produced for desktop applications.[55] This straightforward approach in combination with the accessibility of printers led to a profound understanding of the inkjet printing process for biomedical applications. In the following section, we give a basic overview of the different setups. For a more detailed discussion of inkjet printing, we refer the reader to a variety of excellent reviews dealing with the inkjet technology and material properties for inkjet printing.[56−63]

Inkjet printing can generally be operated in two modes. In continuous inkjet (CIJ) processes, the ongoing generation of drops creates a jet. Usually these drops are individually charged and deflected by a second pair of electrodes for printing. Droplets that are not needed for printing are collected in a gutter and can be reused. CIJ is primarily used as a fast process for marking and coding of products. The second inkjet printing mode is drop-on-demand (DOD) printing. Here drops are only generated when needed for printing. DOD is the setup well-known from consumer inkjet printers used for 2D graphical printouts. The working principle is based on an actuator generating triggered pulses, leading to the ejection of a defined material volume from a reservoir. Ideally, on its way to the substrate, the ejected material will transform into a single drop being collected on a predefined position on the substrate. As shown in Figure 2A, there are mainly two possible driving forces for pulse generation applied for DOD printing. In thermal inkjet printers, a heater is used to evaporate its surrounding ink, generating a vapor bubble that leads to ejection of material. Simply put, the droplet generation is triggered by an electrical pulse leading to a temperature increase in the heater accompanied by ink evaporation and material ejection. Material is also expelled from the reservoir using piezoelectric actuators. Here the applied voltage will generate a distortion of a piezoelectric crystal, leading to triggered ejection of material. In the next two sections, we discuss the benefits and

DOI: 10.1021/acs.chemrev.5b00303
Chem. Rev. 2016, 116, 1496−1539

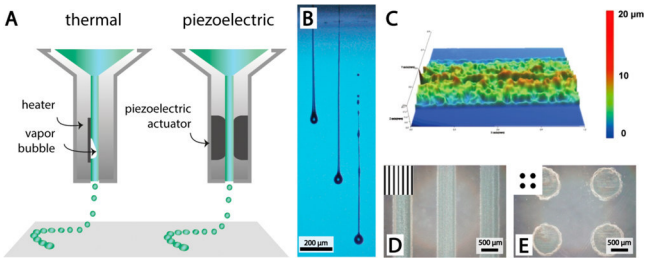

Figure 2. Inkjet printing. (A) Schematic drawing of the process. Reprinted in part with permission from ref 27. Copyright 2013 John Wiley and Sons. (B) Example for propelled material after ejection at different time points using a drop-on-demand printer. Adapted with permission from ref 61. Copyright 2008 IOP Publishing. (C) Surface profile of a linear pattern printed with inkjet-printed poly(lactic acid-*co*-glycolic acid) (PLGA). (D, E) Different patterns of PLGA printed with a piezoelectric inkjet. Panels C–E adapted with permission from ref 64. Copyright 2010 Elsevier.

disadvantages of the different inkjet printing methods described above with a focus on hydrogel printing for biomedical applications.

The main disadvantage of CIJ for laboratory-scale and biomedical applications is the high material throughput accompanied by the continuous stream of drops. Compared to other printing methods used for these applications, more material is needed, and concerns regarding sterility and potential material property changes due to processing might arise when the material is reused. In contrast, the DOD process uses material very efficiently and can also handle small batch sizes, making it highly interesting for small-scale and nonindustrial applications. In addition, the spatial resolution of DOD inkjet printers is higher than for CIJ systems.[60]

In thermal inkjet printers, the temperature of the heated resistor can reach about 300 °C.[57] Nevertheless, Xu et al.[65] and other groups—as reviewed by Boland[56]—were able to print viable cells using thermal DOD printers. It is believed that the short duration of heating pulses in the range of several microseconds only leads to a slight temperature increase (a few degrees) of the bulk material, not negatively influencing the cell viability.[65] Setti et al.[66] could also print enzymes with negligible loss of activity using a thermal inkjet. As pointed out by Saunders et al.,[62] further research on the influence of thermal damage while printing biomolecules needs to be undertaken to establish thermal inkjet printing in the field of biomedicine. Due to this concern, most researchers working with inkjet printers for biomedical application use piezoelectric DOD inkjet systems to avoid ink property changes by heat exposure. Another important benefit of piezoelectric actuators in contrast to thermal actuators is that they allow for an easy change of the piezoelectric crystal distortion and thus in the pulsing. This again enables controlling the ejected material volume and velocity of the created drop, making the process more flexible to parameter adjustment depending on the material characteristics.[60]

We now analyze inkjet printing from a material scientist's perspective and thus focus on the material properties that are decisive for this method. Inkjet printing as a noncontact printing method with typical working distances of 1–3 mm[62] can be divided into three crucial steps: (1) ink ejection, (2) drop formation during flight, (3) impact and interaction of drops after collection on the substrate. The ink ejection and possible expelling mechanisms have already been discussed. It has to be taken into account that typical nozzle sizes are in the range of 20–30 μm.[57] This limits the viscosity of ink used for biomedical applications to values that are typically below 20 mPa s^{-1}. In addition to the viscosity, the ejection may be influenced by the wetting behavior and thus for a given nozzle by the surface tension of the ink, as wetting of the nozzle may lead to spray formation rather than jet formation.[58] Surface tension is also critical for the second step and is typically in the range of 20–70 mJ m^{-2} for graphical prints.[62] In inkjet printing, each pressure pulse should ideally generate an individual droplet, but the dispensed material is initially composed of a leading drop accompanied by a tail that can break up into satellite drops (see Figure 2B) during flight,[61] decreasing the resolution. Drop formation in inkjet processes is complex and cannot be discussed in detail in context of this work. Interested readers are referred to the work of Fromm,[67] Reis et al.,[68] and Jang et al.[69] Briefly, these works used a dimensionless number defined as the ratio between the Reynolds number and the square root of the Webber number. They used this to determine printable materials for DOD inkjet printing. Further research investigating drop formation with a focus on bioprinting was done by Xu et al.[70] The third crucial step during inkjet printing is the impact and interaction of drops after collection on the substrate. Depending on the droplet velocity (typically in the range of 5–10 m s^{-1} [61]) and material properties, the drop will splash or keep its shape after impact (examples for different patterns fabricated with inkjet printing are shown in Figure 2 C–E).[60] Typically, inks spread on surfaces and increase their size, limiting the resolution of the method to approximately 75 μm for bioprinting applications.[71] As shown by Sirringhaus et al.[72] for inkjet-printed polymer transistors, substrate surface energy patterning can further increase the resolution. Also changing the surface charge can increase the printing resolution as shown by Cobas et al.[73] These surface modifications can be applied on 2D constructs when printing dots or lines. When printing lines or structures, drop overlap is needed and interaction between the droplets

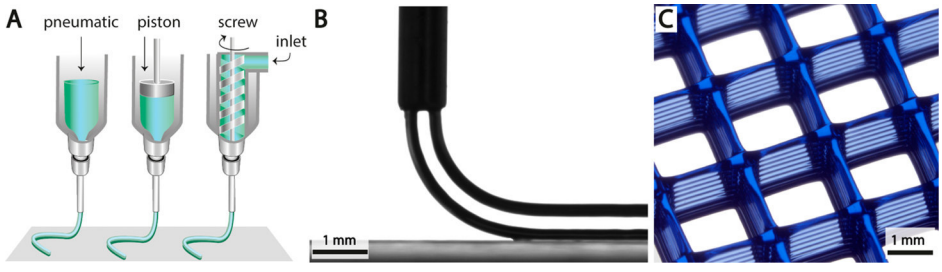

Figure 3. Robotic dispensing. (A) Schematic drawing of robotic dispensing showing the different mechanisms of ejection. Reprinted in part with permission from ref 27. Copyright 2013 John Wiley and Sons. (B) Magnified view showing material dispensing from the needle and collection onto a substrate. (C) Stereomicroscopic image of a printed Pluronic F127 construct.

DOI: 10.1021/acs.chemrev.5b00303
Chem. Rev. 2016, 116, 1496–1539

Table 1. Comparison of Fabrication Systems

feature	modified LIFT	inkjet	robotic dispensing	refs
material viscosity range	1−300 mPa·s	3.5−12 mPa·s	30 − 6 × 10^7 mPa·s	14, 38, 64, 76, 82
mechanical/structural integrity	low	low	high	77
resolution	10−100 μm	∼75 μm	100 μm to mm range	31, 71, 83, 84
working principle	noncontact	noncontact	contact	
nozzle size	nozzle free	20−150 μm	20 μm to mm range	84−86
load volume	>500 nL	mL range	mL range	31
cheap/easily interchangeable reservoirs	yes	no (if using commercial printer cartridges)	yes	
fabrication time	long	long to medium	short	
preparation time	medium to high	low to medium	low to medium	14
commercially available	no	yes	yes	77
costs for printer	high	low	medium	14
advantages	accuracy	affordable, versatile	printing of large constructs in cm range	31, 77
disadvantages	ribbon fabrication, not suitable for constructs in mm range	nozzle clogging	accuracy	31, 77

must be considered. The surface energy is crucial for those interactions, and they need to be stable enough to keep their geometry previous to solidification.[62] To generate uniform lines, the spacing between the drops has to be adapted.[74,75] In cases where inkjet printing is used for 3D printing, surface modification methods cannot be applied because droplets need to be collected on top of each other. Here interactions between the droplets are even more important than for generating 2D structures with droplet overlap,[74] making creation of 3D structures highly dependent on droplet solidification.

2.3. Robotic Dispensing

Especially during the past few years, a large number of great reviews dealing with technologies applied in biofabrication have been published.[11,12,14,26,27,76−78] All of these reviews also discuss the process of robotic dispensing, displaying how promising this comparatively new technique is for the field of biofabrication. This is mainly due to the fact that robotic dispensing allows production of 3D objects with sizes and dimensions relevant for biomedical applications in short processing times. In the following section, we will give an introduction to the different setups (Figure 3A) used for biomedical applications termed robotic dispensing.

Robotic dispensing is mainly used for printing 3D constructs from continuous filaments. Material is loaded into a reservoir and dispensed through a nozzle. By automated movement of the nozzle relative to the build plate, constructs can be generated in a layer-by-layer fashion. The driving mechanism of dispensing can generally be either pneumatic or mechanical. In the most frequent pneumatically driven setup, the valve triggering material ejection sits between the inlet of the pressurized air and the material. Mechanically driven dispensing is mainly screw- or piston-based. Piston-based systems eject material triggered by controlling the linear displacement of a plunger. The displacement of the piston can directly be related to the dispensed volume. In screw-driven systems, rotation of the screw transports the material to the nozzle and is thus responsible for dispensing. The material feed can be controlled not only by the screw rotation speed but also by the screw design.[27] All robotic dispensing systems have in common that material is dispensed through a fine nozzle determining the resolution of the process.[76] As known from industrial dispensing applications, the design of the nozzle has a big effect on the dispensing homogeneity. Because most printer setups for biomedical application use disposable and interchangeable needles, it is important to choose the right needle with respect to the given ink properties. In their latest review, Dababneh et al.[77] pointed out that further improving the nozzle design might be necessary in the field of bioprinting. Combining the fundamentals of the work of Yan et al.,[79] who mathematically modeled the forces cells experience during printing, with nozzle-design-dependent shear stress analysis during dispensing might help to improve cell survival. In the next section, we compare the different robotic dispensing modes explained above and again focus on processing of hydrogels for biomedical applications.

Utilizing a concept known from thermopolymer extrusion, screw-driven systems are the method of choice when it comes to processing high-viscosity materials because they are able to generate high pressures for material dispensing. Tailoring the screw design helps to adjust the process in regard to the feed rate and dispensing homogeneity. Having the most complicated setup in addition to being able to generate the highest shear stresses makes screw-driven systems the least applied approach in biofabrication. From an engineering point of view, pneumatically driven systems have the easiest setup. Nevertheless, applying high pressure typically makes them more suitable for processing higher viscosity materials than piston-driven systems.[76] Being able to deal with a broad range of pressures and thus with a broad range of material viscosities makes pneumatic dispensing the most versatile robotic dispensing mode. Using pressurized gas to apply a dispensing force at the same time implies its biggest disadvantage. The gas used for dispensing is compressible, which will result in a delay between the material flow start/stop signal and actual dispensing start/stop. This problem can be addressed either by applying a time delay before reaching the printing position and a vacuum to stop dispensing or by using a valve sitting just in front of the orifice. Piston-driven systems have the most direct control over dispensing. As described above, the linear piston displacement directly leads to material ejection. Because most printers use disposable syringes made from plastics, the maximum dispensing pressure is limited by the stability of the piston and the quality of the sealing between the piston and barrel. Taking into account that at the laboratory scale dealing with small batch sizes might be necessary, piston and pneumatic systems using disposable barrels that can be emptied nearly entirely will be preferential to screw-driven systems where material will remain in the system.

DOI: 10.1021/acs.chemrev.5b00303
Chem. Rev. 2016, 116, 1496−1539

Just as the other fabrication techniques, robotic dispensing also puts specific demands on material properties. In contrast to inkjet printing where single droplets are required in robotic dispensing, collection of a continuous strand is crucial (Figure 3). The material properties need to be designed in a way that avoids strut breakup.[78] Schuurman et al.[80] could influence drop formation of low-viscous gelatin methacrylamide solutions by introducing high molecular weight hyaluronic acid. Using 20% (w/v) gelatin methacrylamide solutions resulted in drop formation at the needle tip. Adding 2.4% (w/v) hyaluronic acid changed the viscoelastic properties of the ink, and strands could be generated, highly improving the printing fidelity. As mentioned by Lewis,[81] printing functional 3D structures using robotic dispensing places high demands on the inks. Ideally, the inks should even self-support when spanning features need to be printed. When it comes to building a 3D construct layer-by-layer, the interaction of the substrate and the first layer is crucial and the wetting behavior needs to be adjusted. This can be done by choosing the right material combination or the right ink composition[80] or by surface modification as mentioned in section 2.2.

2.4. Comparison of the Fabrication Methods

Now that the different fabrication systems for biomedical applications have been described, we compare those techniques with regard to hydrogel processing. Table 1 shows a comparison of the main differences and features of the printing methods. For more detailed information, the reader is referred to a variety of reviews.[14,27,31,77] These reviews will also offer a good overview of the applications and give an excellent insight into the state-of-the art research and latest developments in the field of biofabrication. Some further excellent reviews focus on material systems for biofabrication and connect bioink to the fabrication techniques and applications.[27,28,31]

In the following paragraph, the fabrication processes will be investigated and compared from three different aspects: (i) material and structural, (ii) processing, and (iii) economical. From a material and structural point of view, robotic dispensing is the most versatile process. It enables generation of constructs from a wide range of material viscosities displayed in Table 1. Robotic dispensing mainly uses interchangeable needles and thus allows the nozzle diameter to be easily adjusted to the dispensed material's viscosity. In contrast to the other processes, it deposits a material filament instead of a single droplet and thus increases the structural integrity. For many applications, the most important processing aspect is the resolution. Modified LIFT processes offer the highest resolution followed by inkjet printing. The process with the lowest resolution is robotic dispensing. Inkjet printing and LIFT as noncontact techniques allow deposition of material with jetting distances of about 1−3 mm. The benefit of noncontact deposition is that it allows printing onto surfaces that do not need to be smooth. Ovsianikov et al., for example, used BioLP to print cells into a 3D scaffold fabricated with two-photon polymerization.[87] From a material research point of view, the amount of material needed for the process and material throughput are important—especially when materials are synthesized on the laboratory scale. The methods where the least material is needed are LIFT-based processes. Here, usually very small material amounts in the range of several hundred nanoliters are processed. The disadvantage that accompanies this small material demand is of course that this process only allows the building up of small-scale constructs.[31] Even though high-throughput versions of modified LIFT techniques have been developed for tissue engineering applications,[38] they still have the lowest material throughput of all discussed techniques. Robotic dispensing allows fabrication of constructs on the millimeter scale in a reasonable time, but depending on the nozzle diameter can easily generate throughputs in the range of milliliters per minute. From an economical point of view, we first compare the processes with regard to fabrication and preparation time. Of course, fabrication time goes along with resolution. If high resolution is not needed and big constructs such as clinically relevant implants are to be fabricated, robotic dispensing is the method of choice. In robotic dispensing and inkjet printing, the preparation times are low, and preparation mainly consists of filling a reservoir that can be as big as several milliliters. In modified LIFT techniques, a thin film of material needs to be applied to the ribbon, and when the material is used (one ribbon usually contains several hundred nanoliter volumes of material), a new ribbon needs to be prepared, increasing the preparation time. From a different point of view, using ribbons can also be beneficial. On one hand, the preparation is time-consuming, but on the other hand, the material cost for the ribbon—it mainly consists of a glass coverslip—is very low. Just as the needles, in robotic dispensing, the reservoirs are disposables and can be easily purchased from industrial or medical supply companies. Although the trend is changing—more and more specialized systems are available—most researchers use modified desktop inkjet printers for biomedical applications. Using off-the-shelf printers is accompanied by high costs for new printheads compared to those of the other techniques. Even if cartridges are reused, the preparation is time-consuming. Of course, the benefit of using modified printers also needs to be taken into account. They are cheap and available and can easily be fixed. In robotic dispensing, scientists also started to use modified low-cost open source printers. Nevertheless, there are commercially available systems that are adapted to the special needs of material dispensing for biomedical applications, and most researchers prefer this more expensive alternative. Contrary to the other methods for modified LIFT techniques, there are no commercially available printing systems available[77] to date. The high resolution of the process further necessitates using expensive high-precision actuators.

3. RHEOLOGICAL CONSIDERATIONS

After having discussed the different fabrication systems and the demands put on the inks by these techniques in the last section, we now take a closer look at rheological aspects important for designing printable hydrogels for nozzle-based dispensing. This section can only introduce the topic generally, since the variety of different hydrogel inks and their molecular properties (molecular architecture, molecular interaction, ink formulation, ion strength, colloidal components, reactive processes, etc.) have a strong influence on the respective individual behaviors. However, the information given in this section is intended as a basis and starting point for bioink design and development.

From a rheological point of view, printing using nozzle-based systems can be considered as material flow through a contraction followed by tube flow. After the material is ejected and deposited onto the collector, it needs to undergo a fast phase transition obligatory to preserve the shape and thus enabling fabrication of 3D structures. As highlighted in the Introduction, the rate of this process is crucial for printing and is one of the biggest differences in demands between injectable and printable hydrogel systems. After discussing some fundamentals of liquid dynamics in the

DOI: 10.1021/acs.chemrev.5b00303
Chem. Rev. 2016, 116, 1496−1539

next sections, we will subsequently increase the complexity of the regarded models, approaching toward printable inks highlighted with examples of applied ink systems. For further review on liquid dynamics and polymer rheology, we refer the reader to a, by far not complete, list of excellent literature dealing with this topic.[88−93]

3.1. Rheology of Non-Newtonian Liquids

Liquids can generally be divided into two categories: Newtonian and non-Newtonian. For Newtonian fluids, the viscosity is independent of the shear rate, whereas, for non-Newtonian liquids, the viscosity tensor exhibits a shear-rate-dependent behavior (Figure 4). This dependence can be used to separate non-Newtonian liquids mainly into the following types: shear thinning, shear thickening, thixotropic, and rheopectic. A complete list with example systems developing the different properties can be found elsewhere.[90] As shown in Figure 4, shear thinning materials show a decrease of viscosity with increasing shear rates. Despite very low molecular weight materials, most polymer solutions show this behavior. Polymeric liquids further usually depict a linear plateau at low shear rates called zero shear viscosity (also low shear viscosity or first Newtonian plateau). This linear plateau is, in the literature, often set on a level with yield stress, but there is a difference between those two phenomena that can, for example, be observed at low shear. By definition, yield stress materials will not flow—also taking into account the very long time scales—until a critical stress, the so-called yield stress, is exceeded. In contrast to that, the majority of the systems discussed in this review will flow—even at observable shorter time scales—under shears beneath the shear stress plateau. This led to an ongoing[94] debate about the yield stress concept.[95−97] For practical applications this discussion seems to be somewhat excessive and most researchers stick to the concept.[98] Nevertheless, it is important to be aware of the difference as this may, under certain circumstances, have an impact on printing. Although not displayed in Figure 4 non-Newtonian polymeric liquids usually evolve a second plateau called high-shear viscosity or second Newtonian plateau.[91] Since in most cases, this plateau is only slightly higher than the solvent viscosity, the second Newtonian plateau is not relevant for printing processes.

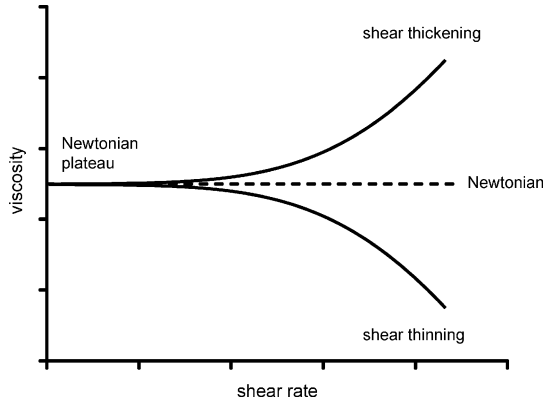

Figure 4. Viscosity against shear rate for Newtonian and different non-Newtonian fluids.

Another interesting phenomenon observed for non-Newtonian fluids is thixotropy. Especially when analyzing only limited shear rate ranges, viscosity against shear rate plots of thixotropic materials are often similar to those of shear thinning materials, but there is a very distinct difference: thixotropy is time-dependent, whereas shear thinning is not. This becomes obvious when the viscosity is plotted against time for a constant shear rate. For shear thinning fluids, the viscosity will be constant, but for thixotropic materials, it will decrease with time. A detailed discussion of thixotropy and also the hysteresis that can be examined by measuring material properties during increasing and decreasing shear rates is not within the scope of this paper and is described elsewhere.[99,100] In terms of printing, the time-dependent viscosity thixotropic materials depict is important and must be considered as it might lead to inhomogeneous dispensing.

Shear thickening (see Figure 4) is the opposite of shear thinning and is characterized by an increase of viscosity with increasing shear rates. Also, just as shear thinning has shear thickening as its counterpart, rheopectic materials evolve characteristics opposite thixotropy. It is obvious that these both behaviors are not favorable for printing applications.

3.2. Important Aspects of the Printing Process

For printability of non-Newtonian fluids, it is important to take into account flow phenomena known from other technical applications such as injection molding as summarized briefly by Larson et al.[101] and Irgens[102] and detailed in the papers of Barnes[91] and Shenoy.[90] In accordance with the rheological discussion above, especially the phenomenon of extrudate swell—also known as the Barus effect—is of interest. The practical observation accompanied by this phenomenon is the increase of the jet diameter after material exits the orifice of the tube it was flowing through. This observation is mainly limited to elastic materials such as polymer solutions[91] and can in simple terms be explained as follows: Flowing through the tube, the material is compressed by the given confinement, and the polymer chains are stretched. After the material is ejected, it will expand due to the elasticity of the chains and their partial relaxation, so that the diameter of the jet will increase. Extrudate swell especially needs to be taken into account for high-resolution printing using robotic dispensing. Usually, by adjusting the process parameters—mainly the deposition speed—it is possible to compensate this effect at least to some extent.

As mentioned above, a very important property for printable hydrogels and thus a crucial parameter to take into account during ink development is the recovery rate of transition to the solid state after printing. To achieve shape fidelity, the material must undergo a rapid structural change and keep its shape after dispensing. The faster the material gelifies after ejection the higher the resolution of the resulting structure. In the case of recovering materials, the interactions between the molecules will strongly influence the transition and the time it takes after flow stops. Although the aspect of solidification is important for injectable materials too—for that reason we will take this class of materials into account in the following sections—the conditions are much more stringent for printable systems, as the nozzle diameters used for printing are smaller and the time acceptable for gelation is shorter.

Summarizing this discussion, from a rheological point of view, an ideal ink for hydrogel printing combines the following characteristics:

- Physical gel formation before printing with a shear thinning but not thixotropic behavior down to a viscosity that allows printing with the selected technology.

DOI: 10.1021/acs.chemrev.5b00303
Chem. Rev. 2016, 116, 1496−1539

- Rapid regelation after printing for shape fidelity at high resolution.
- No or little pronounced extrudate swell.

If cells are part of the formulation, the viscosity before printing must allow mixing and homogeneous 3D distribution of cells throughout the printing process without affecting the viability. Cell sedimentation that might lead to nozzle clogging and/or uncontrolled inhomogeneous cell distribution through the printed construct must be avoided. Also, shear forces cannot exceed limits tolerable for cell survival.[79,103] Hence, cell aggregation during the time frame of printing is usually not beneficial as it affects the shear-rate sensitivity.

In practice, a combination of these parameters is hard to achieve. Especially the regelation rate after printing remains a challenge. Hence, printed hydrogel structures usually have to be stabilized if real 3D structures are to be obtained. One strategy is to double print with a Thermoplast, resulting in a 3D interdigitating structure of hydrogel and Thermoplast, thus mechanically reinforcing the construct.[104,105] Most commonly, the printed hydrogels are stabilized by postfabrication treatment, increasing the cross-linking density of the network, for example, by incubation in a solution that contains physical or chemical cross-linker molecules, or by UV illumination if hydrogel components are equipped with photopolymerizable groups. These strategies are in principle undesired necessities for suboptimal inks and will briefly be summarized and discussed in section 4.

3.3. Underlying Molecular Concepts: Colloidal Solutions

In the following sections, we introduce some basic particular and molecular concepts that comply with the terminology and the ideas gained from discussing non-Newtonian fluids. One of the simplest models able to depict non-Newtonian fluid behavior is a so-called hard-sphere system. This can be considered as a monodisperse suspension of spherical particles in a Newtonian fluid not experiencing interparticle and particle−liquid interactions. Although there are only a few real model systems showing all necessary properties,[106,107] there is some general knowledge one can gain from that model, such as the fact that non-Newtonian characteristics will only be developed when concentrations are high enough.

When interparticle interactions are additionally taken into account, these interactions are manifold and will strongly influence the rheological properties of the particulate systems, inducing suspensions to be able to depict all known non-Newtonian behavior.[107] The general character of interparticle interactions can be distinguished using the concept of interaction potential energy,[106] which helps to describe the resulting forces and relevant length scales. Roughly, these interactions can be separated into electrostatic, steric, electrosteric, and structural. Mentioning the relevant length scales of these interactions underlines why the properties of suspensions will be concentration-dependent. At low solid loadings, the particles will not alter the linearity of the Newtonian fluid because the distances between particles are much bigger than the length scales of the interactions. Increasing the loading, interactions will more likely appear. If interparticle interactions dominate over Brownian motions, so-called rest structures can form.[91] In the case of repulsive interactions, this will result in pseudolattice structures, whereas, in the case of attractive interactions, the particles will aggregate. When shear is applied to those systems and is slowly increased, these structures will first withstand the generated forces and then will be rearranged due to the reversible character of the interactions. Depending on the interaction properties, this can lead to a macroscopic shear response comparable to a first Newtonian plateau or even induce yield stress. A further increase in shearing results in permanent disintegration of the aggregates and nonrestored arbitrary particle distribution after shearing. The shear-induced velocity gradient leads to an orientation of the particles that enables them to move over each other more freely. This in turn leads to shear thinning or in the case of attractive interactions also to thixotropy.[108] Generally, such systems will depict a second Newtonian plateau if all particles show the orientation and, by disruption of those layer orientations, show shear thickening with further increasing shear rates. If shearing stops, the particles will return to a rest structure.[91] Of course, these descriptions are very pictorial, and there are theoretical models that represent the properties of the suspension more adequately.[91,109−111] Furthermore, scientific descriptions of colloidal suspensions are also discussed in specialized literature.[106,108] In the next section, we give an example of how colloidal systems can be exploited for ink development.

As described, particle interactions are crucial for the properties of suspensions and thus need to be considered when designing colloidal inks as shown by the Lewis laboratory. Jennifer Lewis and co-workers transferred knowledge from ceramics science to develop concentrated colloidal gel-based inks for direct-writing applications.[112] Over the past few years, they have generated inspiring work,[113−115] continuously improving their inks by analyzing and controlling interparticle forces. Here, we use one of their earlier systems[116] as it comprises a model system containing monodisperse silica microspheres that displays their meticulous scientific work on developing printable colloidal inks. Coating the colloids with poly(ethylene imine), they exploited the concept of electrosteric[106] interparticle forces to tailor the viscoelastic properties of the system. Electrostatic interactions between negatively charged silica particles and positively charged poly(ethylene imine) induced strong ionic interactions between the two species. In addition, changing the pH of the solution, they were able to vary the ζ potential of the coated particles and found the point of zero charge to be at a pH of about 10. At this pH, the absence of electrostatic repulsion between the colloids led to a system strongly flocculated by van der Waals forces and thus to a fluid-to-gel transition. Finally, they added cellulose as a thickening agent to increase the ink viscosity and reduce the flocculation kinetics, even enabling fabrication of unsupported spanning structures that are considered to be the most difficult structures to print using robotic dispensing systems.

In describing ceramic colloid systems to a nonexpert, it might seem strange that there are only a few real systems displaying the properties of the hard-sphere model. However, due to surface charges, even uncoated rigid ceramic particles will depict an interaction potential energy longing for a classification as soft-sphere systems.[106] Taking into account that spheres can also be deformable will be the next step approaching toward the description of polymeric systems. As outlined before, low concentrations of hard spheres in a solution will not change the Newtonian character of the liquid they are suspended in. Nevertheless, they will increase the viscosity by deviating the fluid flow lines.[91] By shear-induced shape adaptation, deformable particles will lead to less deviation and thus to a less pronounced viscosity increase considering shear.[107] For higher concentrations, this will further result in more pronounced shear thinning. This effect contributes to the extraordinary properties of blood.[117] Under shear, red blood cells will deform,[118] enabling

DOI: 10.1021/acs.chemrev.5b00303
Chem. Rev. 2016, 116, 1496−1539

blood to flow even through the tiniest capillaries in the human body. For synthetic systems, the particle elasticity also has a major impact on the rheological properties as reviewed by Vlassopoulos et al.[119] They pointed out that colloid elasticity has an impact not only on flow-induced material response but also on the zero shear viscosity of colloidal suspensions and that the decrease of zero shear viscosity with increasing particle deformability is generally more pronounced at higher volume fractions. The models they considered for their review contained polymer coils and star polymers evolving the lowest elasticity of the discussed systems. Singh et al.[120] performed computer simulations of ultrasoft colloids under linear shear flow, showing that star polymers deform due to shearing. Furthermore, Huang et al.[121,122] used simulations calculating that linear polymers will depict shear-induced decoiling and stretching accompanied by orientation along the flow direction. Huber et al.[123] could visualize the tumbling dynamics of semiflexible polymers under shear conditions by imaging fluorescently labeled actin molecules.

3.4. Underlying Molecular Concepts: Polymer Solutions

Polymer solutions are commonly used as model systems for soft colloids which lead to the field of polymer solutions. Just as for the hard-sphere model, the concentration will be crucial for the rheological response of such systems. At very low volume fractions, the distance between the chains will be larger than their size. These systems are called dilute. As already discussed for hard and deformable spheres, at very low concentrations, the solvent properties will not be altered significantly. Increasing the concentration results in coil overlap and leads to semidilute solutions. Although the solvent will occupy most of the volume, the coils will overlap and have a considerable impact on the rheological properties. Being able to overlap clearly distinguishes polymeric systems from the suspensions discussed before. Raising the solid loading further will lead to concentrated solutions dominated by coil interactions.[89] Printable hydrogels will usually depict concentrations in either the semidilute or concentrated regime, and thus, for the following discussions, only these systems will be considered. Even early models describing semidilute systems, not taking into account interactions other than topological, had to deal with coil overlap and with the concept of entanglements.[124] Although used in one context, it is important to mention that overlap and entanglement should not be put on one level. Semidilute and concentrated solutions are defined by coil overlap but do not need to be entangled.[107] For the chains to entangle, they will need to be long and flexible enough. Experimental results could show that there is a critical molecular weight for the formation of entanglements that depends on the flexibility of the polymer backbone.[91,107] Entanglement can, however, only occur in semidilute or concentrated solutions. If chains are separated from each other, they will not be able to interact. To some extent, these findings are connected to each other. The longer the chains, the bigger their interaction potential and the higher the number of entanglements at the same concentration. Connecting the entanglement density to rheological properties, the concept of entanglements drastically changed the scientific understanding of polymers. Accompanied by the model of reptation, researchers were able to relate macroscopic polymer properties to the microscopic behavior of single molecules. Due to that, the concept of entanglements is an excellent example of how theoretical models can enrich and evolve general understanding. As we will not focus on models here, we refer the interested reader to excellent reviews dealing with this topic[101,125] and continue our argumentation describing general factors influencing the properties of semidilute and concentrated polymer solutions.

Aside from entanglements and the movement of polymer chains within semidilute/concentrated solutions, intermolecular interactions have to be taken into account. In general, an increase of concentration will increase the amount of interactions, and thus, polymer concentrations in solutions will have an influence on the rheological properties. As shown in Figure 5, a general observation dealing with polymer solutions is that with increasing concentration the zero shear viscosity is raised and the onset of shear thinning is shifted toward lower values.[110] With increasing load volume, the viscoelastic properties will be more pronounced and lead to a bigger difference between first and second Newtonian plateau values.[91] Another aspect is the influence of the molecular weight distribution on the rheological properties of polymeric liquids. Generally, it can be observed[107] that increased polydispersity influences the transition from Newtonian to non-Newtonian behavior. Solutions with a broader molecular weight distribution will evolve non-Newtonian properties at lower shear rates, but shear thinning will not be as pronounced, and the decrease of viscosity against shear rate will be broadened.

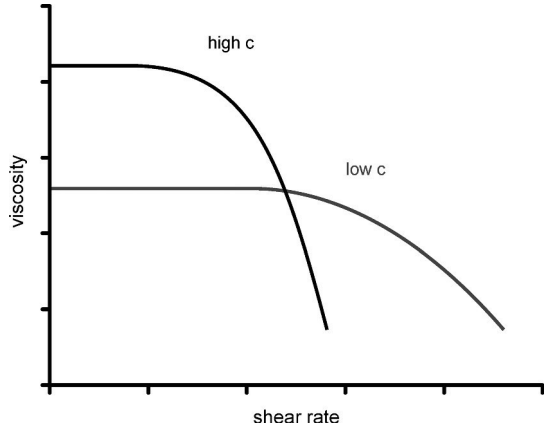

Figure 5. Viscosity against shear rate for high and low polymer concentrations (c) of a homopolymer solution in a good solvent.

Recently, researchers have exploited this concept for designing printable materials. Although using materials with a broader molecular weight distribution was not the only aspect influencing the rheological behavior of the inks, they could tune the flow properties of their systems either by mixing batches of different molecular weight distributions of identical materials[115] or by combining two types of materials with different distributions.[126] These examples show that modern inks usually are—from a rheological point of view—complex systems. The complexity is mainly introduced by interactions between the molecules and by molecule−liquid interactions. Due to the huge number of interactions, a closer rheological discussion is outside the scope of this review. We rather intended to present and discuss simplified basic views of rheological concepts aiming for a more generalized understanding of the possible system variations allowing control of the rheological properties.

3.5. Characterization of Rheological Properties

Although it is not the main focus of this paper, we briefly introduce some general aspects of rheological hydrogel analysis

DOI: 10.1021/acs.chemrev.5b00303
Chem. Rev. 2016, 116, 1496−1539

before moving on to the next sections. Rheological characterization is often underestimated in terms of hydrogel design for biomedical applications.[27,127] The spectrum of rheological characterization methods for hydrogels is nearly as manifold as the gels themselves, which sometimes makes comparability difficult, which contributes to delaying general systematic progress, especially for ink development. An excellent book describing rheological concepts and explaining the different characterization methods was provided by Malkin et al.[128] For a short overview focusing on hydrogel rheology, the interested reader is also referred to less detailed reviews.[127,129]

As described, non-Newtonian fluids have shear-rate-dependent properties. Furthermore, their characteristics will be dependent on the kinetics and the magnitude of deformation. This needs to be considered when choosing the test parameters. They should be adapted to the processing and application conditions as closely as possible. In terms of biofabrication, we can roughly divide the measurement conditions into those that are adjusted for the fabrication step or, postfabrication, for the demands of the application. Due to the cellular component usually present in TE applications, postfabrication characterization is mainly limited to analysis of the linear viscoelastic properties of the printed hydrogels in the zero shear viscosity region under static or dynamic conditions. In contrast, fabrication conditions in the case of nozzle-based systems mainly long for characterizations of the shear thinning region and the recovery of the hydrogel after printing. Rheological measurements with alternating shear rates are a helpful tool to analyze the important recovery rate of printable materials. Eventually, the correct set of characterization method and conditions has to be selected for each ink system taking into account the envisioned application. Independent of the fabrication method and application, we nonetheless highlight the importance of rheology and underline that taking into account rheological considerations from the beginning is crucial for a rational and successful development of a printable hydrogel formulation.

This section has underlined how crucial the rheological properties of an ink are for successful printability. Before presenting the different strategies to induce intermolecular interaction and to design molecular components for printable hydrogels which will be discussed in sections 5 and 6, the following section will focus on the limitation of using chemical cross-linking for 3D printing and its potential and common use for postfabrication stabilization of constructs.

4. CHEMICAL CROSS-LINKING

As already introduced in section 1, hydrogels can be classified according to the mechanism of their formation in chemical and physical hydrogels. Physical hydrogels rely on noncovalent interactions between their building blocks for network formation. This makes the gels dynamic and endows them with self-healing properties;[130] however, this is often accompanied by low mechanical strength and stability, which is undesired in 3D printing for the final printed construct. Chemical hydrogels in contrast are formed through chemical reactions and the formation of covalent bonds that constitute the network. Hence, these networks are less dynamic but stable until forces are big enough to irreversibly break the covalent bonds. Such properties are ideal for generation of mechanically stable constructs. However, for the application of covalent cross-linking during 3D printing of hydrogels, an ongoing chemical reaction imposes a number of demands. A general challenge is noncontinuous printing with stop−go phases, since the chemical reaction should not continue in the stop phase. Throughout the printing procedure, no or only very limited cross-linking should occur for the formulation remaining printable and also not significantly changing its behavior over time during printing, which would lead to structural inhomogeneity in the printed object. During or immediately after printing, the cross-linking should occur rapidly to ensure shape fidelity. These two demands are best met by two-component systems that rapidly react upon mixing. Such approaches have already been followed more than 10 years ago in work by Mülhaupt et al., who used isophorone diisocyanate for the cross-linking of poly(ethylene glycol) (PEG) and glycerin during 3D plotting, an approach which they termed "reactive plotting".[131] However, they did not plot a hydrogel but did create a water-swellable 3D hydrogel construct, and the chemistry used is not cytocompatible and would definitely not allow printing in the presence of cells.

Nonetheless, various in situ gelations via chemical cross-linking methods such as polymerization, classical organic reactions (e.g., Michael addition, click reactions), redox reactions, and enzyme-driven reactions were used for the generation of injectable hydrogels,[132−134] and numerous cytocompatible cross-linking reactions for hydrogels are known and have been used for encapsulation of cells within hydrogels.[135] Moreover, a number of hydrogels have been developed that chemically cross-link via peptide sequences which are substrates for matrix-remodeling enzymes (so-called matrix metalloproteases, or MMPs),[136] so that chemical cross-linking can be combined with tailored specific biodegradability. However, a most critical challenge for printing cells containing covalently cross-linked two-component hydrogels remains the mixing step, as cells are sensitive toward shear rates, but on the other side, homogeneous mixing of the formulation has to be ensured in a short time.

4.1. Post- and Prefabrication Cross-Linking

In accordance to the discussion above, the main application of chemical cross-linking for hydrogel printing is postfabrication stabilization of the printed constructs. Therefore, the hydrogel precursors are endowed with chemically reactive groups, mostly photopolymerizable groups such as acrylates, and the printed construct is illuminated by UV light immediately after plotting. Examples for this approach are numerous, and the most common precursors used are poly(ethylene glycol) methacrylate,[137] poly(ethylene glycol) diacrylate,[138] polydiacetylene/poly(ethylene glycol) acrylate,[139] poly(2-hydroxyethyl methacrylate)/2-hydroxyethyl methacrylate,[115] succinimidyl valerate (SVA)−poly(ethylene glycol)/gelatin/gelatin methacrylate/fibrinogen/poly(ethylene glycol) amine/atelocollagen,[140] hyaluronic acid/hydroxyethyl methacrylate-derivatized dextran,[141] gelatin methacrylate,[142,143] poly(ethylene glycol) diacrylate/alginate,[144] and GRGDS (Gly-Arg-Gly-Asp-Ser) acrylate/matrix metalloproteinase-sensitive peptide acrylate/poly(ethylene glycol) methacrylate/gelatin methacrylate.[145]

Hyaluronic acid methacrylate/gelatin methacrylate[146] was chemically cross-linked before and after printing to tune the formulation properties for the printing process and stabilize the printed structure afterward. Combination of photoinitiated and thermal cross-linking after printing was also used to adjust the properties of gelatin methacrylamide/hyaluronic acid,[80] Lutrol,[147] and poly(*N*-(2-hydroxypropyl)methacrylamide lactate)−poly(ethylene glycol).[148] Finally, in some studies chemical cross-linking was solely performed prior to printing, for example, applying photopolymerization for poly(ethylene glycol) dia-

DOI: 10.1021/acs.chemrev.5b00303
Chem. Rev. 2016, 116, 1496−1539

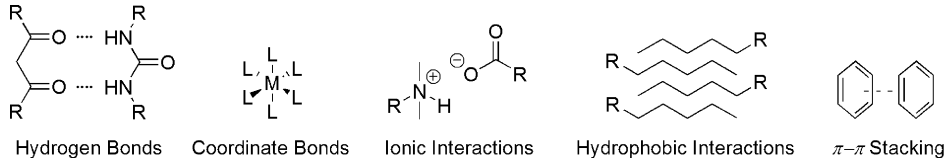

Figure 6. Basic physical molecular interactions exploitable for physical gel formation.

crylate,[149] gelatin methacrylate,[150] or Michael-type addition between thiolated hyaluronic acid/thiolated gelatin/four-armed poly(ethylene glycol) acrylate.[151]

Also combinations of different intermolecular interactions (ionic interaction and thermoswitchable hydrophobic interaction plus photochemical cross-linking) have been exploited for optimizing the formulation properties for poly(*N*-isopropylacrylamide)/*N*,*N*′-methylenebis(acrylamide)/poly(ethylene glycol) dimethacrylate before printing.[152] The same strategy to combine different interaction types was also exploited with chemical reaction as the fixation step of the structure after printing. Examples comprise gelatin,[153] a gelatin/hyaluronic acid mixture,[154] a formulation containing gelatin, alginate, and fibrinogen,[155,156] a mixture of gelatin and chitosan,[157] a fibrinogen/collagen formulation,[158] a collagen/agarose/chitosan system,[159] and a gelatin methacrylamide/gellan/alginate formulation.[160] Finally, systems containing alginate acrylamide/*N*,*N*′-methylenebis(acrylamide)/ethylene glycol and Ca^{2+} ions[161] as well as alginate/poly(ethylene glycol) diacrylate/laponite and Ca^{2+} ions[162] were ionically tuned for printability before and structurally stabilized through irradiation after the printing process.

4.2. Application of Dynamic Covalent Bonds for Printing

Some chemical bonds exhibit dynamic character after they have been formed, meaning that they are stable under some conditions but labile under others, or that they are in a constant equilibrium between two states. Examples of dynamic chemical bonds from nature are the switching of disulfides or thioester exchanges in biosynthetic processes. For a detailed and comprehensive presentation and discussion of such reversible and dynamic chemical bonds, we refer to excellent reviews on that topic.[163,164] Chemical cross-linking toward networks that are covalently built up by such dynamic bonds is possible prior to the printing procedure and would allow, under the conditions necessary for the respective bond, reversibility of the cross-linked network during and after the printing, similar to the healing phenomenon in physically cross-linked systems. One example that has recently been exploited for hydrogel printing is the dynamic chemistry of imines.[165] Imine chemistry has been used for preparation of injectable hydrogels for several years, for example, through mixing of oxidized hyaluronic acid with chitosan. Gelation in this system was attributed to the reaction between aldehydes in the oxidized hyaluronic acid and amines of the chitosan.[166] A dynamic chemically cross-linked hydrogel system for bioplotting was prepared along this cross-linking rationale by cross-linking partially oxidized alginate with gelatin.[167] Imine formation resulted in gelation before plotting, but the gel could be printed using a robotic dispensing setup. The viscosity of the system facilitated good printability and sufficient stability of the printed structure so that the chemical cross-linking could further stabilize the construct. As a beneficial byproduct, gelatin improved the cytocompatibility of the system, and cells could be plotted with this system. In another example of a dynamic chemical bond, Meng et al.[168] used boronic ester formation for supramolecular hydrogels based on boronic acid-modified alginate and poly(vinyl alcohol) under basic conditions. Step strain measurements show shear thinning behavior, e.g., at low strain $G' \approx 10^3$ Pa/$G'' \approx 500$ Pa, and at high strain $G' \approx 400$ Pa/$G'' \approx 600$ Pa with recovery properties. This combination of reversible chemical cross-linking with shear thinning and self-healing properties is very promising for printing applications. Furthermore, disulfide cross-linked hydrogels have been prepared from thiolated star-shaped PEG molecules and linear polygylcidols. Disulfide formation and thus gelation could be achieved and controlled under mild and cytocompatible conditions either by using alloxan as the catalyst[169] or by exploiting horseradish peroxidase without the need to add hydrogen peroxide.[170] The dynamic equilibrium between thiols and disulfides presents another attractive example of dynamic covalent bonds with potential application for printable hydrogel systems.

5. MOLECULAR PHYSICAL GELS

We now focus on physically cross-linked hydrogels. As highlighted in section 3, such gels inherently possess beneficial properties for the printing procedure due to the dynamic and reversible nature of their cross-links. Some of the established printable systems, most prominently alginate, belong to this group, and these will be included in this review for completion. However, our main focus here is to summarize fundamental principles for molecular assembly that have been developed in polymer chemistry and especially supramolecular chemistry, a very diverse field introduced by Jean-Marie Lehn,[171] and outline their possible exploitation for the development of 3D printable hydrogels. These strategies all rely on a small number of basic and well-known interaction mechanisms such as hydrogen bonds, complex formation or coordination bonds, $\pi-\pi$ stacking, and hydrophobic and ionic interactions (Figure 6). These mechanisms found widespread application in different fields of research and, before entering a detailed discussion about promising examples for 3D printing, we give an overview on recent review papers and briefly summarize their contents.

Supramolecular polymer networks are a new class of materials which basically can be categorized into two kinds of macromolecular systems and are compared with respect to their formation, structure, and dynamics in a review by Sprakel and Seiffert:[172] The first one is the "noncovalently bound monomer-based polymer" consisting of small units which interact physically and form a polymer network. The second is the "covalently bound monomer-based polymer" with "noncovalent chain interconnection" whose polymer backbone is covalently fixed, and the polymer possesses side chain functionalities for inter- and intramolecular interactions. A variety of functionalities for supramolecular systems with broad properties and numerous applications have been reviewed extensively by several research groups. Schalley and Qi[173] reported on macrocycles for functional supramolecular gels, including, e.g., crown ethers, cyclodextrins, and spiroborate cyclophanes, and highlighted different stabilization and gel−sol transition methods via

DOI: 10.1021/acs.chemrev.5b00303
Chem. Rev. 2016, 116, 1496−1539

environmental stimuli. Rim-bound/appended macrocycles and host−guest complexes form stable gels and can be transferred into solutions via temperature/pH change or addition of competitive hosts or guests, e.g., applicable for the host−guest formation of crown ethers and secondary positively charged amines. Furthermore, they can be used for pressure-responsive materials which can recover back to their initial form. Qiao and co-workers[174] gave a deeper insight into cyclodextrin-based supramolecular assemblies and hydrogels. The variety of host−guest interactions with cyclodextrins is an interesting flexible cross-linking method for building blocks, e.g., polyrotaxanes, molecular tubes, and capsules. The different cavity sizes of the cyclodextrins (CDs), α-CD, β-CD, and γ-CD, allow binding of appropriate guest moieties such as poly(ethylene glycol), poly(caprolactone), and phenyl and adamantyl groups. The host−guest formation was used for reversible sol−gel transition triggered by light and redox reaction. The morphology of host−guest-based supramolecular structures can be tuned via their overall amphiphilic character and was reviewed by Huang and co-workers.[175] Nanosheets, nanotubes, vesicles, and micelles can be formed in this way for different applications. Hereby, the molecular geometry and amount of hydrophilic and hydrophobic functionalities play an important role in the shape formation. Furthermore, organic compounds possessing π-systems form supramolecular gels via $\pi-\pi$ interactions in solutions, so-called low molecular weight gelators. Ajayaghosh and co-workers[176] reported on π-gelators with functional groups which can also form different shapes via stacking, such as nanofibers, columns, and helices. Percec and co-workers[177] presented several complex systems based on dendron-mediated self-assembly. Depending on the molecular geometry, the solvent, and the amount of generations and functionalities, the formed supramolecular structures, such as nanocapsules and columns, can be controlled and are stabilized through $\pi-\pi$ interactions and hydrogen bonds. With this wide pool of chemical functionalities and interactions, it is possible to tailor materials with new properties. Zhang and co-workers[178] reported on supramolecular polymers and highlighted the four most common interactions in this field with respect to historical development, preparation, characterization, and function. These are metal coordination bonds, multiple hydrogen bonds, and host−guest and donor−acceptor interactions. The dynamic nature of functional supramolecular polymers opens a wide field of applications in medicine and electronics for this new class of materials.[179] The design and use of these functionalities for supramolecular polymer gels was reported by Matushita and co-workers,[180] who explain some physical properties depending on the functionalities within the gel. Huang and co-workers[181] gave further insight into the stimulus responsiveness of these materials induced, e.g., via light, temperature, and concentration. Self-healing supramolecular gels (Figure 7) were recently focused on and were reviewed with

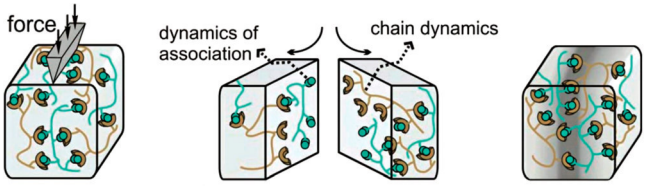

Figure 7. Concept of self-healing materials relying on the reversibility of physical interactions. Reprinted with permission from ref 183. Copyright 2013 John Wiley and Sons.

respect to the influence of basic molecular interactions within the material on its properties. For example, Hayes and co-workers[182] and Binder and co-workers[183] reported on healable supramolecular polymers based on a variety of hydrogen bonds, donor−acceptor interactions, ionic interactions, and metal coordination, which allow the materials to recover after being damaged. Self-healing is also possible via constitutional dynamic chemistry and was reported by Chen and co-workers.[184] They gave an overview of physical and also chemical self-healing with a variety of healing conditions and efficiencies.

A variety of injectable hydrogels were reviewed by Li et al.,[185] who gave an overview of natural and synthetic polymers with a focus on gelation, biodegradation, and biomedical applications. Guvendiren et al.[25] summarized shear thinning hydrogels also for biomedical applications, such as peptides and synthetic polymers, and explained the criteria for these properties which are necessary for injection. Also, the necessity of reversible linkages in adaptable hydrogel networks for cell encapsulation was reviewed by Wang and Heilshorn.[186]

This brief overview underlines the richdom of literature and the multiple applications that rely on (supra)molecular interaction mechanisms. All these basic physical molecular interactions will be reviewed in the following section with respect to their chemical design and possible use for printable hydrogels. Therefore, we categorized them into four systems which will be explained in the following order: supramolecular polymer, supramolecular (low molecular weight gelators), macromolecular, and colloidal (solid particles, also in combination with the aforementioned systems) as depicted in Figure 8.

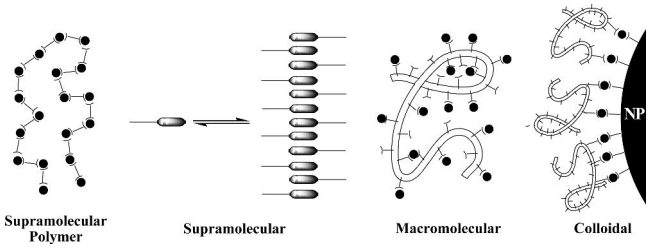

Figure 8. Supramolecular, macromolecular, and colloidal strategies for hydrogel formation.

5.1. Supramolecular Approaches

5.1.1. Ionic Interactions and Coordination Bonds.

Dupin and co-workers developed a hydrogel containing chain-end-dithiolated PEG ($PEG(SH)_2$) possessing 0.8 eq of Au^+ as a zigzag cross-linker.[187] A double-chamber syringe system with solutions of the components was used for the hydrogel formation during the injection. As the thiol's nucleophilic character depended on the pH value, the hydrogel's properties varied with this as well. For example, at pH 11, the thiol groups possessed a strong nucleophilic character and therefore led to a thiolate/Au−S exchange which made the hydrogel dynamically flow up to a frequency of 0.9 Hz, after which the storage modulus G' became higher than the loss modulus G''. In contrast, at pH 3.1, the nucleophilic character of the thiols was weaker, causing less thiolate/Au−S exchange, and therefore, the hydrogel was more stable. Grande and co-workers used glutathione as a binding component to Au^+ with its thiol functionality.[188] Hereby, the pH value was varied to switch between the gel and sol states, which could be an interesting application for the pH-controlled gelation process. Mecerreyes and co-workers synthesized a

DOI: 10.1021/acs.chemrev.5b00303
Chem. Rev. 2016, 116, 1496−1539

variety of polymer gels based on ionic interactions. They used (di/tri)carboxylic acids (e.g., citric acid) and (di/tri)alkylamines (e.g., *N,N′,N″,N‴*-tetramethyl-1,3-propanediamine) which formed supramolecular polymers after a proton transfer.[189] Their storage modulus G' and loss modulus G'' were temperature-dependent, and G'' became higher than G' after the gel−sol transition temperature, which varied from 20 to 60 °C on the basis of the used monomers. Rowan and co-workers[190] used 2,6-bis(1′-methylbenzimidazolyl)-4-oxypyridine for complexation of Zn^{2+} and La^{3+}, which formed shear thinning gels in acetonitrile. They could also be transformed to solutions via addition of acid or by heating. Generally, coordination bonds possess high binding constants and could be used with various metals and ligands for gel stabilization (Table 2).

Table 2. Examples of Metal-Coordination-Based Supramolecular Polymers[a]

Ligand Type	Metal	K_a	Solvent/Counterion
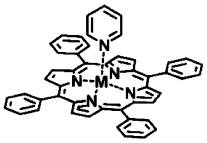	Zn^{2+}	4.1×10^3 M^{-1}	$CHCl_3$/-
	Co^{2+}	1.0×10^6 M^{-1}	Pyridine/OAc^-
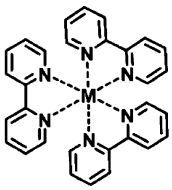	Zn^{2+}	$\sim 10^{13}$ M^{-1}	Aqueous KNO_3
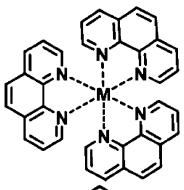	Zn^{2+}	1×10^{17} M^{-1}	Aqueous KNO_3
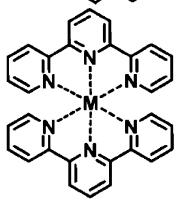	Zn^{2+}	2×10^{14} M^{-2}	CH_3CN/ClO_4^- /TBAPF
	Fe^{2+}	$\sim 10^{21}$ M^{-2}	Water
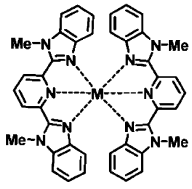	Zn^{2+}	$\sim > 10^6$ M^{-2}	$CHCl_3/CH_3CN/ClO_4^-$
	Fe^{2+}	$\sim 10^{14}$ M^{-2}	

[a]Adapted with permission from ref 178. Copyright 2015 American Chemical Society.

5.1.2. Hydrogen Bonds. Meijer and co-workers developed ureidopyrimidinone (UPy)/urea-end-functionalized poly(caprolactone) for binding with UPy/urea-end-functionalized peptides. Due to the strong association constant via quadruple hydrogen bonding ($K_a = 10^7$ M^{-1} in $CHCl_3$), the supramolecular polymer was very stable but also very flexible at the same time. The polymer was processed in a melt just below 80 °C, where the polymer possessed a low viscosity, and was used to produce fibers via electrospinning, films via solvent casting, and scaffolds via fused deposition modeling.[191] Further supramolecular gels based on interactions via hydrogen bonds were obtained by the same group.[192] The dodecane-based monomer possessed UPy and urea functionalities on both chain ends and formed a supramolecular polymer in chloroform via stirring. Mechanically induced gelation is thermoreversible and could be transferred back into the monomer solution via an increase of the temperature. It showed shear thinning properties, whereas the loss modulus G'' became higher than the storage modulus G' in repeatable cycles. A pH-switchable and self-healing supramolecular hydrogel for injection was also investigated by Dankers and co-workers.[193] End-functionalized PEG possessed at both chain ends urea and UPy functionalities for hydrogel formation via multiple hydrogen bonds which could be controlled by the pH value. UPy groups could be deprotonated at pH 8.5 lowering the strength of the hydrogen bonds, and this led to a solution. The material also showed shear thinning properties in a neutral state and a basic state, where in both cases the loss modulus G'' became higher than the storage modulus G'. Repeatable dynamic strain amplitude tests of hydrogels containing 10 wt % UPy−polymer also showed self-healing behavior over four cycles. Binder and co-workers[194] synthesized end-functionalized poly(isobutylene) with barbituric acid groups and the Hamilton wedge with six hydrogen bonds which formed a gel with self-healing properties. Table 3 shows hydrogen donor−acceptor systems possessing different geometries, binding constants, and amounts of hydrogen bonds which could be used for gel stabilization.

5.1.3. Host−Guest and Aromatic Donor−Acceptor Interactions. Crown ethers interact with compounds containing protonated secondary amines via hydrogen bonds[195] by forming host−guest complexes and were used by several research groups as building blocks for supramolecular polymeric gels. For example, Huang and co-workers synthesized two complementary homoditopic compounds, one containing a crown ether and the other a protonated alkylammonium group.[196,197] The formation of a supramolecular polymer via host−guest interaction was investigated at different concentrations in acetonitrile and chloroform. $[PdCl_2(PhCN)_2]$ was added as a cross-linker whose Pd^{2+} formed a complex with the triazole groups. The formed gel showed interesting properties: It could be transferred back to a solution by an external stimulus such as pH, temperature, or cations. Additionally, it showed shear thinning and self-healing properties. A gel containing 100 mM equimolar monomers with 60% cross-linker possessed a $G' \approx 10^4$ Pa and $G'' \approx 10^3$ Pa at low strain rates and reached its gel−sol transition at ∼100% strain. Strain sweep measurements from 0.1% to 200% showed how the network could be destroyed and recovered back to the initial cross-linked gel. Zheng and co-workers synthesized a series of amphiphilic heteroditopic building blocks with the same functional groups for host−guest interaction as described before and additionally varied the crown ether group, alkylammonium group, or spacer.[198] The gelation process was investigated in water, acetonitrile, and DMSO, and the minimum gelation concentration varied from 0.6 to 4.3 wt % with different functional groups. It might be interesting to transfer a viscous solution into a gel via changing the concentration during printing. Similar supramolecular polymeric gels were investigated by Yin and co-workers, who incorporated additional terpyridine groups for complex formation with Zn^{2+}.[199] The material showed self-healing properties and reversible gel−sol transition via heating/cooling and addition of base/acid, ligands/Pd^{2+}, and Zn^{2+}.

DOI: 10.1021/acs.chemrev.5b00303
Chem. Rev. 2016, 116, 1496−1539

Table 3. Examples of Donor and Acceptor Hydrogen Bonds[a]

Type	Example
Triple	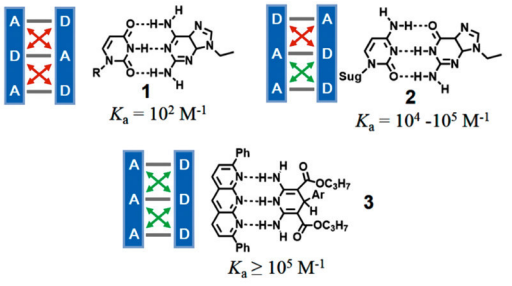
Quadruple	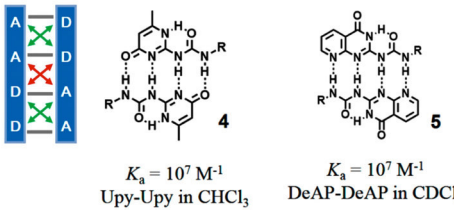
Sextuple	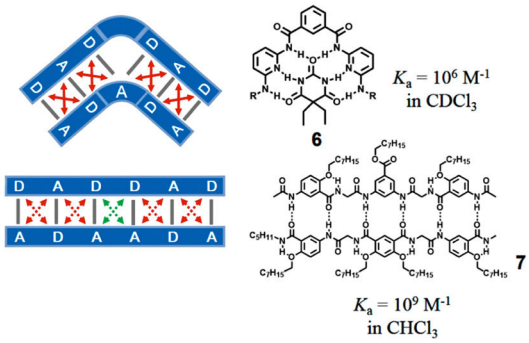

[a]Adapted with permission from ref 178. Copyright 2015 American Chemical Society.

Pillararene-based supramolecular polymer gels are novel materials stabilized via host–guest interactions. Wei and co-workers used copillar[5]arenes which possessed four 1,4-dimethoxybenzene units and either one 1-methoxy-4-dodecylbenzene (COP5–12) or one 1-methoxy-4-cetylbenzene (COP5–16) unit, forming supramolecular polymers via self-assembly in acetonitrile.[200] Thereby, the hydrophobic alkyl chain interacted with the aromatic benzenes via CH···π interactions, and the formed gels showed reversible gel–sol transition via a temperature change (68 °C for COP5–16 and 52 °C for COP5–12). Additionally, the gels possessed self-healing properties; e.g., a gel (20 wt % COP5–16 in acetonitrile) returned back to its initial form after being torn apart for 1 mm within 45 min. To get a hydrophilic supramolecular pillarene-based gel, Yao and co-workers introduced four 1,4-bis((2-ethyloxy)-trimethylammonium)benzene units and one 1-methoxy-4-cetylbenzene unit.[201] The self-assembly in water was also driven by CH···π interaction of the alkyl chain with the benzene units. The rodlike fiber network also showed a gel–sol transition via temperature. Zheng and co-workers developed amphiphilic calix[4]arenes by acylization of the amino groups of the calix[4]arene with dicarboxylic anhydrides which formed supramolecular hydrogels.[202] As the gel was not completely stable in water, at least 5% (v/v) ethanol was needed to be added to the solution. They investigated the gel stability from 5% to 25% (v/v) ethanol and showed that with a higher amount of ethanol the suspension–gel temperature and gel stability increased. These amphiphilic compounds are interesting for forming hydrogels but could be improved as ethanol is harmful for cells and the sol–gel temperature might be tuned by addition of other compounds. Table 4 shows host molecules with associated guest molecules.

Table 4. Examples of Host–Guest Interactions[a]

Host Molecules	Molecular Structures	Typical Guest Molecules
β-Cyclodextrin	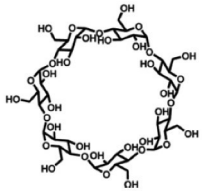	Adamantane, coumarin
Cucurbit[8]uril	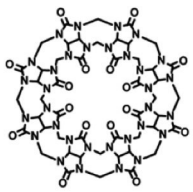	Methyl vologen, charged naphthalene, anthracene and alkene
Calixarene	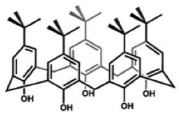	Charged alkane, viologen
Crown Ether	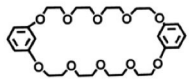	Viologen, charged amine
Pillarene	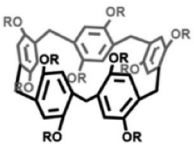	Charged imidazole and DABCO

[a]Adapted with permission from ref 178. Copyright 2015 American Chemical Society.

Rowan and co-workers[203] designed copolymers possessing π-electron-deficient naphthalenediimide units and π-electron-rich pyrenyl-end-capped polyamides which form self-healing supramolecular materials via π–π stacking. After damage, the aromatic groups were stretched and could interact again by heating to 87 °C with a recovery of 100% of the material. This concept of π–π stacking was mostly used for self-healing materials with different polymers and is summarized in Figure 9. Hayes and co-workers filed a patent[204] which described similar end-functionalized polymers with π–π stacking for inkjets.

5.1.4. Low Molecular Weight Gelator. Ravoo and co-workers developed tripeptides Fmoc-L-Cys(Acm)-L-His-L-Cys-OH (**1**) and Fmoc-L-Cys-L-His-L-Cys-OH (**2**) which formed supramolecular gels in water with shear thinning properties.[205] The Fmoc groups allow the π–π stacking for stabilization of the gel with a minimum gelation concentration of 1.5 wt % which possessed a storage modulus $G' \approx 10^3$ Pa at low strain decreasing

DOI: 10.1021/acs.chemrev.5b00303
Chem. Rev. 2016, 116, 1496–1539

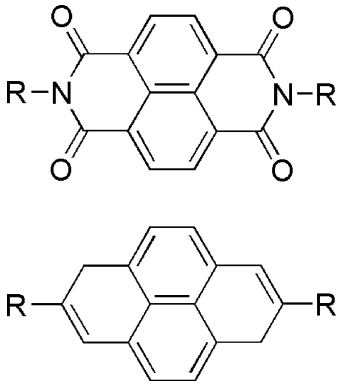

Figure 9. Examples of the two majorly used aromatic groups for donor−acceptor interactions.

to ∼1 Pa at 100% strain-amplitude sweep for peptide **1**. The viscosity decreased as well for peptide **1** by 6 orders of magnitude with increasing shear rate. Ulijn and co-workers explored the biocatalytic induction of supramolecular gel formation using Fmoc- and methyl ester-terminated dipeptides.[206] With these end groups, a solution was present, and just after addition of the hydrolytic enzyme from *Bacillus licheniformis*, which hydrolyzes the methyl ester, a gel was formed via self-assembly of the peptide. The subsequent hydrolysis was investigated with different concentrations of enzyme, and the gelation was confirmed via determination of the melting temperature. The greater the number of enzyme units added, the greater the amount of gel formed, and therefore, the melting temperature increased. The same group developed further interesting hydrogels based on Fmoc-functionalized short peptides.[207] The gel−sol/sol−gel transitions might be an interesting tool for printing and stabilizing hydrogels which can be tuned in different ways. Gelation of cyclic dipeptide derivates was induced by Feng and co-workers.[208] They used cyclo(L-Phe-L-Lys) and cyclo(L-Tyr-L-Lys) possessing *N*-acetylated D-(+)-gluconic acid for gel formation, which showed different sol−gel transition temperatures depending on the gelator concentration and perturbation. Further low molecular weight gelators containing aromatic groups for stabilization of gels via $\pi-\pi$ stacking and possessing thermoreversible properties were synthesized by the research group of Schmidt.[209−211] For example, they used 4-(octanoylamino)benzoic acid and 4-alkoxyanilines, which formed a gel upon addition of sodium hydroxide. Varying the ratio of the base led to different amounts of formed gels and therefore to different gel−sol transition temperatures. Zhang and co-workers[212] developed a naphthalene-based gelator which formed organogels with different gel−sol transition temperatures dependent on its amount. For example, a gel containing 0.5 wt % gelator possessed a gel−sol transition temperature of ∼42 °C, and a gel containing 2.0 wt % gelator possessed a gel−sol transition temperature of ∼58 °C. The group of Stupp[213] also used $\pi-\pi$ stacking for hydrogel formation with quinquethiophene−oligopeptide sequences at low concentrations. The thiophene groups were modified with amphiphilic peptide residues which improved the water solubility and in addition led to self-assembling via β-sheet formation. The gelation time was dependent on the concentration, e.g., 5 days for 1 wt % and 3−5 h for 3 wt %. While this appears to be too long for cell printing, the gelation time may significantly be optimized for bioink development, for example, by using a multivalent approach with functional polymers. Moreover, gelation times of several hours up to days are not per definition detrimental to biofabrication if the resulting network is dynamic as most recently demonstrated for 3D printing of cell-loaded recombinant spider silk protein hydrogels stabilized via β-sheet formation (see section 6.1.2).

5.2. Macromolecular Gels

5.2.1. Naturally Occurring Biopolymers Used for Hydrogel Formation. Biopolymers have frequently been used in biofabrication, especially since they exhibit excellent bioactivity.[24,214,215] A broad range of biopolymers has been investigated to assemble injectable/printable hydrogels for biomedical applications. This section summarizes the recent progress on biodegradable and injectable hydrogels fabricated from naturally occurring biopolymers such as polysaccharides

Table 5. Natural Biopolymers Used To Form Injectable or Printable Hydrogels for Biomedical Applications

biopolymer	3D printing technique	applications	refs
		Polysaccharides	
alginate	laser-induced forward transfer, inkjet, robotic dispensing, extrusion	tissue repair (myocardial), nerve regeneration, delivery system (drugs, proteins, cells, genes), wound healing	39, 40, 56, 83, 161, 162, 167, 185, 219,221−223, 225−241
chitosan	extrusion	tissue repair (cartilage, nerve), drug delivery, cancer therapy	185, 242, 243
agar/agarose	robotic dispensing	tissue repair (cartilage), nerve regeneration	138, 159, 214, 222, 236, 244−248
cellulose	robotic dispensing	tissue repair (cartilage), wound healing	222, 233, 249, 250
hyaluronic acid	robotic dispensing, extrusion	tissue repair (cartilage, brain, vascular constructs)	80, 141, 146, 151, 154, 166, 185, 242, 251, 252
chondroitin sulfate		tissue repair (cartilage), drug delivery, wound healing	185, 217, 242
gellan gum	inkjet	tissue repair (cartilage), drug delivery	253−256
		Proteins	
collagen	inkjet, robotic dispensing	tissue repair (skin, liver, blood vessels, small intestine), delivery systems (drugs, proteins, cells)	20, 84, 238, 257−261
gelatin	robotic dispensing	tissue repair (cartilage), delivery systems (growth factors, cells), wound healing	150, 185, 239−241, 243, 259, 262, 263
fibrin/fibrinogen	inkjet	tissue repair (nerves, blood vessels, skin, tendons, ligaments, liver, eyes), drug delivery systems (drugs, proteins, genes), wound healing	185, 239, 264−269
silk	robotic dispensing	tissue repair (bone, cartilage), drug delivery	270−274
		Mixture	
matrigel	robotic dispensing	tissue repair (liver)	275

DOI: 10.1021/acs.chemrev.5b00303
Chem. Rev. 2016, 116, 1496−1539

(alginate, agarose) and proteins (collagen, gelatin, fibrin, silk). A further overview of hydrogels based on biopolymers applicable for 3D printing is given by Kirchmajer et al.[216]

5.2.1.1. Polysaccharides. Polysaccharides consist of sugars linked via *O*-glycosidic bonds. Most of the polysaccharides are able to form hydrogels, on the basis of bonding (e.g., agarose) or intermolecular electrostatic interactions (e.g., alginate). A broad range of injectable and biodegradable hydrogels made of naturally occurring (or slightly modified) polysaccharides, such as chitosan, hyaluronic acid, alginate, and agarose, have been developed and tested for biomedical applications. For more detailed information, refer to Li et al.,[185] Thiele et al.,[217] and Table 5. Here, we focus on polysaccharides (alginate and agarose) already used in biofabrication.

Alginate is one of the most frequently used (bio)polymers for biofabrication due to its favorable biocompatibility and the capability to support cell survival and differentiation in culture. Alginate is a linear anionic polysaccharide containing homopolymeric blocks of 1,4-linked β-D-mannuronate and α-L-guluronate. Alginate hydrogels can form through different mechanisms. At pH values below 3, alginate self-assembles into acidic gels by the formation of intermolecular hydrogen bonds.[218] Furthermore, hydrogels can be formed by cooperative binding of divalent cations such as Ca^{2+} ions. Jia et al. have shown that alginate can be used as a bioink for bioprinting. The alginate-based bioinks were shown to be capable of modulating human adipose-derived stem cell functions without affecting their printability and structural integrity after cell culture.[219] In terms of alginate-based bioinks, unfortunately, the hydrogel's mechanical properties are quickly lost during in vitro culture (approximately 40% within 9 days). Further limitations are cellular responses differing dependent on the source of human and animal cells and the lack of bioactive binding sites.[219−221] Furthermore, alginate was prepared of different concentrations and was cross-linked via addition of Ca^{2+} ions.[39,40,56,83,105,222−232] Polymer concentrations and printing conditions were varied, leading to differences in the printing quality. For example, Guillotin et al.[39] used up to 1% (w/v) alginate solutions for printing and obtained well-defined constructs and high cell viability. Yan et al.[232] used alginate concentrations from 2% to 8% (w/v), but the higher it was, the more defined structures were obtained. Nanofibrillated cellulose/alginate[233] was also fabricated with subsequent cross-linking via Ca^{2+} ions in solution.

Agarose, one of the main components of agar, consists of (1→3)-β-D-galactopyranose-(1→4)-3,6-anhydro-α-L-galactopyranose as the basic unit and ionized sulfate groups.[276] Agarose gelates through the formation of intermolecular hydrogen bonds upon cooling, resulting in the aggregation of double helices by the entanglement of anhydro bridges.[277] The viscoelastic properties of agarose hydrogels depend on the molecular weight and solution concentration. The tunable elastic moduli of physical gels are between <1 kPa and a few thousand kilopascals, well in the stiffness range of natural tissues except bone.[278] Furthermore, agar was recently used with poly(acrylamide) and poly(stearyl methacrylate) to form double-network hydrogels with self-healing properties which exhibit potential for printing as well.[279] In 2009, Maher and co-workers produced 3D scaffolds made of thermoreversible agarose hydrogels by pneumatic robotic dispensing with a stainless steel cartridge which could be heated to 100 °C.[138] The agarose material was printed into a 3% (w/v) gelatin medium bath. The medium bath did not act as a cross-linking agent but merely as a construction support site. Dispensing of agarose without the incorporation into the gelatin medium bath resulted in the distortion of individual layers and in most cases caused the scaffolds to collapse.[138] Furthermore, human mesenchymal stem cells were encapsulated within agarose hydrogels and subsequently printed into 3D structures supported in high-density fluorocarbon. This high-density hydrophobic liquid mechanically supported the cell−hydrogel constructs during the printing process. Three-dimensional structures with various shapes and sizes were manufactured, and the resulting cell-laden hydrogel constructs remained stable for more than 6 months. Live/dead and 4′,6-diamidino-2-phenylindole (DAPI) staining showed viable cells 24 h after the printing process, as well as after 21 days in culture.[159] Thermal gelation was used for a variety of hydrogels after printing, such as agar,[244,246] agarose,[222,247,248] and methylcellulose.[222]

A large number of bacterial extracellular polysaccharides (EPSs) have been recently reported to be useful for biomedical applications. Compared to polysaccharides extracted from plants or algae, bacterial EPSs have improved physical properties.[280] Examples of reported bacterial EPSs for biomedical applications include xanthan gum, gellan gum, dextran, bacterial alginate, and bacterial cellulose. Although most bacterial EPSs are composed of repeating sugar units with varying sizes and degrees of ramification, some have an irregular structure, such as bacterial alginate. The properties of the EPSs are determined by their chemical composition, molecular structure, average molecular weight, and distribution.[281] Good examples for the correlation between chemical properties and functionality are gellan and xanthan gum. While xanthan gum forms double helices without creating a gel structure, gellan gum forms a macroscopic gel.[282] At high temperatures (∼30 °C), the linear molecules of gellan are in a disordered coiled state which turns into double helices upon cooling. At high concentrations (>2%, w/v), the double helices changed to thicker rodlike aggregates and formed the gel.[283] The final gel properties were dependent on the content of the acyl groups. In a highly acylated form, two acyl substituents such as D-acetate and D-glycerate were present. The acylated form produced thermoreversible, elastic, and flexible gels, whereas the deacetylated type formed hard, nonelastic, and brittle gels.[249] Recently, endotoxin-free low-acyl gellan gum has been used as a bioink for the reproducible printing of several cell types.[253] A commercial microvalve deposition system and many-nozzle piezoelectric inkjet printheads have been used for printing. The gellan gum kept cells stable in suspension, preventing the settling and aggregation of cells and showing stringent fluid properties during printing.[253] Additionally, deacetylated gellan gum was thiolated to prepare injectable gellan hydrogels which can be physically and chemically cross-linked in situ. The thiolation does not alter the hydrogel formation properties of gellan gum, but leads to a lower phase transition temperature under physiological conditions and to stable chemical cross-linking.[254]

5.2.1.2. Polypeptides/Proteins. Collagen is the most abundant protein in mammalian bodies, accounting for 20−30% of the total protein, and therefore, it is of interest to be used in biofabrication.[217,242,284] The main functions of collagen in tissues are to provide mechanical support and to control cell adhesion, cell migration, and tissue repair.[285] All fibrous collagens have a triple-helical structure with three parallel polypeptides, α-chains, coiling around each other and forming a right-handed triple-helical chain. Collagen is easy to process and modify, and its abundance, nonantigenicity, biodegradability, and biocompatibility render collagen a promising candidate for biofabrication.[286] Moon et al. developed a modified inkjet printer

DOI: 10.1021/acs.chemrev.5b00303
Chem. Rev. 2016, 116, 1496−1539

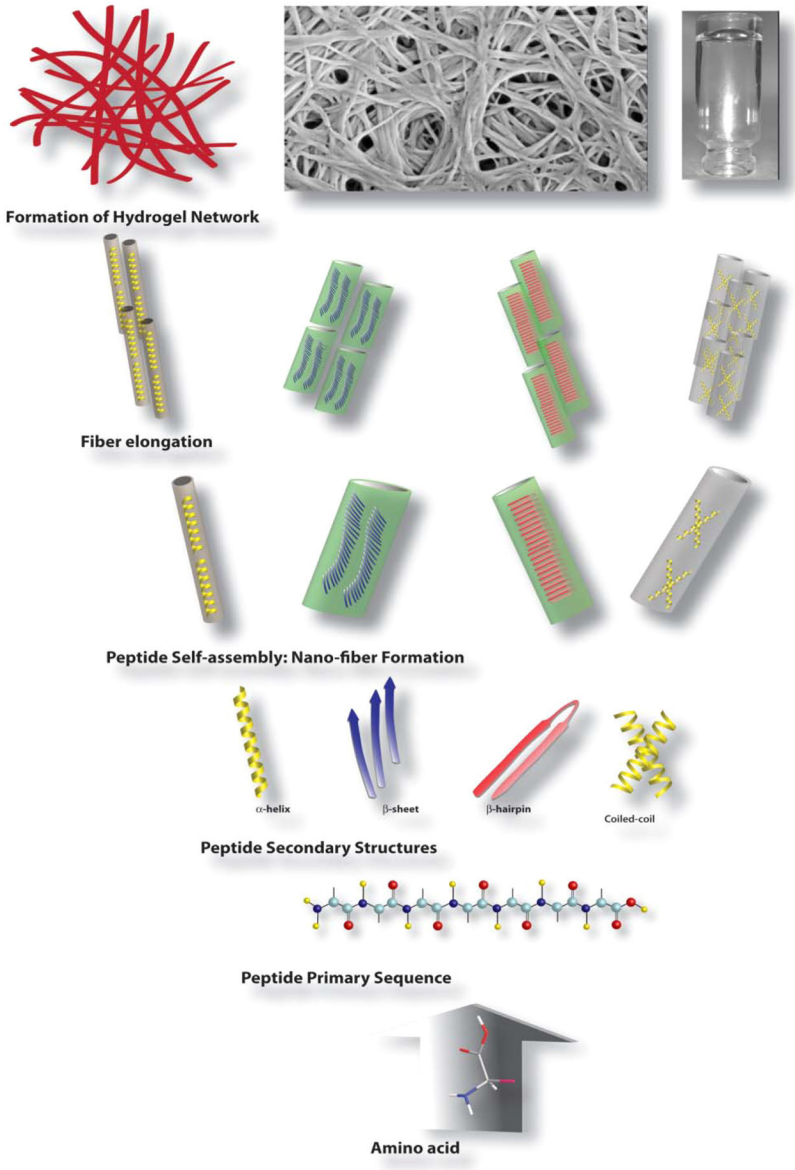

Figure 10. Stepwise formation from amino acids to hydrogel networks. Reprinted with permission from ref 311. Copyright 2013 Royal Society of Chemistry.

using mechanical valves for processing high-viscosity hydrogel precursors, such as collagen solutions, and prepared cell-laden collagen hydrogels using bladder smooth muscle cells.[257] However, collagen bioinks suffer from batch-to-batch variations, loss of shape and consistency due to shrinkage, and poor mechanical properties (elastic moduli around 1 kPa).[84,287] Additionally, it remains especially difficult to sterilize it without alterations of its structure.[258] Collagen type 1 was printed as well with subsequent cross-linking with sodium bicarbonate,[259,288] and a mixture of alginate/collagen type 1 was also reported for printing.[238]

Gelatin is partially denatured collagen.[289] Compared to collagen, gelatin is less immunogenic, and can be used as a bioink due to its biodegradability, biocompatibility, natural cell-adhesive Arg-Gly-Asp (RGD) motifs, and water solubility.[20,80,150,262,290,291] However, the gel formation is solely based on physical intermolecular interactions of the gelatin molecules, and the resulting gels are not stable under physiological temperature, but can be cross-linked.[292] A mixture of alginate/gelatin/fibrinogen[239] was fabricated with subsequent cross-linking via Ca^{2+} ions in solution. Thermal gelation was also used for gelatin,[259] acetocollagen,[260] collagen type 1,[261] collagen/gelatin,[259] matrigel,[275] and gelatin/chitosan.[243] Gelatin/alginate was also reported with a double-cross-linking method via temperature and ions.[240,241] A novel work by Kirchmajer and Panhuis[293] describes a very strong hydrogel based on gelatin/gellan gum cross-linked via genipin and Ca^{2+} ions whose properties can be tuned via the composition.

Fibrin is another example of a specialized extracellular matrix protein with potential applications in biofabrication. Fibrin is formed by thrombin-initiated aggregation of fibrinogen into a network of fibrils.[294,295] The mechanical properties are governed by the initial concentration of fibrinogen and/or thrombin.[296] Fibrin is biocompatible, cell adhesive, and biodegradable, and fibrin hydrogels undergo enzymatic degradation (through activated plasmin) within 2 weeks in cases where no fibrinolytic inhibitors, such as aprotinin, are added.[297,298] Recently, fibrin was used as a printable hydrogel for inkjet printing to build 3D neural

DOI: 10.1021/acs.chemrev.5b00303
Chem. Rev. 2016, 116, 1496−1539

constructs. 3D neural sheets were generated by alternate printing of fibrin gels and NT2 neuronal precursor cells.[264] Since fibrinogen and thrombin can both be easily purified from blood, they offer the opportunity of using an autologous source for making the scaffold.[266] However, there are also disadvantages for using fibrin hydrogels as bioink: some fibrin hydrogels possess poor mechanical properties and undergo fast disintegration.[267,268] The best fibrin hydrogels with mechanical integrity were transparent and stable for 3 weeks.[299]

Silks are natural protein fibers produced by Arthropoda such as spiders of the class Arachnida as well as insects of the order Lepidoptera. Native silk proteins are highly repetitive and are composed of crystalline domains periodically interrupted by helical or amorphous regions.[300,301] Due to the absence of toxicity, slow degradation, absence of immunogenicity, and extraordinary mechanical properties, silk is particularly of interest for biomedical applications and biofabrication.[271,302−305] The fabrication of patterned substrates from silk fibroin via inkjet printing was established[273] by successfully patterning silk arrays by layer-by-layer deposition of dots composed of ionomeric silk proteins chemically modified with poly(L-lysine) and poly(L-glutamic acid) side chains. These "locked-in" silk nests remained anchored to the substrate during incubation in cell growth medium to provide a biotemplated platform for printing-in, immobilization, encapsulation, and growth of *Escherichia coli* cells. Overall, this fabrication process shows potential for the universal and large-scale fabrication of biocompatible dot array templates within a practical processing time scale. The microscopic arrays could be used as prospective biosensors.[273] However, it could also be detected that a plain silk fibroin solution leads to frequent clogging of the needle due to shear-induced β-sheet crystallization.[270] Recently, Das et al. provided a strategy for fabrication of 3D tissue constructs using a novel silk−gelatin-based bioink encompassing living progenitor cells and in situ cross-linking through a cytocompatible gelation mechanism.[271]

The use of naturally derived proteins as bioinks is limited mainly due to their varying composition and purity, and they can elicit inconsistent or unwanted biological responses. Since mammalian tissues are the main source of proteins such as collagen, gelatin, and fibrin, further concerns exist regarding disease transmission and immunogenic responses.[306,307]

5.2.2. Synthetic Peptides and Proteins. A novel method of cross-linking using hydrogen bonds was reported recently where polypeptoids were functionalized with grafted single DNA strands, forming a shear thinning hydrogel after addition of the complementary DNA strand which was used for 3D printing[308] and injection.[309] Hauser et al.[310] developed bioinks consisting of trimer, tetramer, and hexamer peptides which self-assembled into nanofibers. The gelation time could be tuned via the solvent (deionized water versus phosphate-buffered saline, PBS), concentration, and amino acid sequences. Various peptide/protein-based hydrogels are also available via solid-phase synthesis. Dasgupta et al.[311] summarized the variety of peptide hydrogels and gave an overview of the relationship between molecular functionalization, conformation, and properties of the hydrogel. Condensation of amino acids first forms a primary peptide sequence which then forms secondary structures such as α-helix, β-sheet, β-hairpin, and coiled-coils. These peptides self-assemble into nanofibers and form a hydrogel network by elongation (Figure 10).

Apostolovic et al.[312] gave further insight into coiled coils in a review concerning their history and possible applications. Material properties and rheological measurements of different peptide- and protein-based hydrogels were summarized by Sathaye et al.,[313] and these hydrogels might be interesting inks for printing as they show shear thinning and rehealing properties based on their dynamic physical interactions. For example, Chen et al.[314] investigated a β-hairpin peptide hydrogel which was stabilized via hydrogen bonds within the amino acid units and showed shear thinning properties at the same time. They used different peptides with the sequences VKVKVKVKV^{D}PPTKVK-VKVKV-NH_2, IKIKVKVKV^{D}PPTKVKVKIKI-NH_2, VKVKI-KIKV^{D}PPTKIKIKVKV-NH_2, and IKIKIKIKV^{D}PPTKIKIKIKI-NH_2, where they varied the amount of L-valine and L-isoleucines in the peptide sequences. L-Isoleucine is more hydrophobic than L-valine and possesses a higher affinity to form β-sheets via hydrogen bonds. The hydrogel formation was triggered in a 4-(2-hydroxyethyl)-1-piperazineethanesulfonic acid (HEPES) solution containing 4 wt % peptide by adding Dulbecco's modified Eagle's medium (DMEM). Via dynamic frequency sweeps, it could be shown that with a higher amount of L-isoleucine the hydrogel formation was faster and the storage modulus G' and loss modulus G'' increased. Dynamic time sweep measurements of the peptide showed recovery to the initial G' value after removal of the strain. Schneider and co-workers[315−317] investigated the rheological properties and the kinetics of VKVKVKVKV^{D}PPTKVKVKVKV-NH_2/VKVKVKVKV^{D}P-PTKVEVKVKV-NH_2 hydrogels in more detail. These are biocompatible and injectable and can be used for the encapsulation of cells. For further stabilization, the peptide sequence KVKVKVKVKV^{D}P^{L}PTKVKVKVKVK was modified by the same group[318] to KVKVXVKVKV^{D}P^{L}PTKVKVXVKVK with X = lysyl sorbamide, which possessed double bonds for photochemical cross-linking. Bakota et al.[319] synthesized a peptide sequence called $E_2(SL)_6E_2$GRGDS which formed a hydrogel upon addition of Mg^{2+}. Its storage modulus G' was ∼480 Pa at low strain, which afterward decreased with higher strain like the loss modulus G'' at ∼80% strain. Step strain measurements were also performed and showed the material's shear thinning and recovery properties. It recovered over 75% within 15 s after strain was removed and up to 100% of its initial storage modulus within 10 min. A further temperature- and additionally ion-dependent shear thinning hydrogel was developed by Huang et al.,[320] who used the peptide sequence FLIVIGSIIGPGGDGPGGD cross-linked in Ca^{2+} solution or under acidic conditions. For example, a hydrogel containing H^+ possessed $G' \approx 4 \times 10^3$ Pa at 5 °C, $G' \approx 3 \times 10^3$ Pa at 50 °C, and a hydrogel with Ca^{2+} possessed $G' \approx 150$ Pa at 5 °C and $G' \approx 400$ Pa at 50 °C. This might be an interesting hydrogel whose properties could be tuned via ionic interactions and temperature. The same research group[321] investigated the hydrogel formation of this peptide sequence with Ca^{2+} in different DMSO/water ratios and showed that the gel's stability increases with higher Ca^{2+} concentration and water content.

Werner and co-workers developed a series of noncovalently cross-linked hydrogels based on biomimetic peptide−heparin or receptor−ligand interactions exhibiting properties potentially exploitable for 3D printing. For example, they used four-arm star PEG which was functionalized with positively charged oligopeptides derived from L-lysine/L-arginine. When these polymers were mixed with heparin, the peptides interacted with the negatively charged sulfate groups from heparin and thus formed a hydrogel.[322,323] Very low concentrations were sufficient for hydrogel formation (5 mM heparin, 2.5 or 5 mM star PEG−peptide conjugate), and the hydrogel's stability could be tuned

DOI: 10.1021/acs.chemrev.5b00303
Chem. Rev. 2016, 116, 1496−1539

through variation of the peptide sequences. Another physically cross-linked hydrogel based on a more specific protein−receptor interaction was prepared by the same group through functionalization of PEG with biotin and interaction with tetrameric avidin.[324] Biotin−avidin recognition resulted in hydrogel formation, and the receptor−ligand-stabilized hydrogel was investigated with respect to stiffness, swelling, and erosion in water and different PBS buffer concentrations.

Besides peptides/proteins, also synthetic biocompatible polymers such as poly(*N*-isopropylacrylamide)-*block*-poly(ethylene glycol)[325] and Lutrol F127[76,84,222] were printed and thermally stabilized. Physical cross-linking led to reversible interactions which ensured a constant viscosity during printing with a good biological compatibility.[27,132] There are still capacities in this field, especially in the macromolecular design. The materials were hardly varied, showing a limitation which might be extended by using novel building blocks and functionalizations described in more detail in the following sections.

5.2.3. Host−Guest Interaction. Many research groups developed functional polymers cross-linked via host−guest interaction showing shear thinning properties which could be interesting for printing. Chen and co-workers[326] synthesized poly(ethyl acrylate)-containing protonated dibenzylammonium moieties cross-linked with dibenzo-24-crown-8 bis(crown ether). The resulting gel was pH- and temperature-responsive and the gel−sol transition could be controlled via heating/cooling or by addition of base/acid. Additionally, it possessed self-healing properties, and strain amplitude sweep measurements showed that upon a strain of ∼30% the loss modulus G'' became higher than G'. Furthermore, step strain measurements confirmed the material's full recovery after removal of the strain. Huang and co-workers[327] used the same functionalities to produce gels but in the opposite way: They synthesized poly(methyl methacrylate) with pendant dibenzo[24]crown-8 ether groups and cross-linked them by addition of a secondary protonated bisammonium compound. This gel showed as well self-healing properties, pH responsiveness, and recovery after strain. Continuous step strain measurements displayed the repeatable changes of G' and G''; e.g., at a strain of 10^4%, $G' \approx 0.1$ Pa and $G'' \approx 5$ Pa, whereas, after the strain was decreased to 1%, $G' \approx 100$ Pa and $G'' \approx 10$ Pa.

The research group of Burdick developed a series of injectable hyaluronic acid-based hydrogels. They modified hyaluronic acid separately with adamantane and β-cyclodextrin at the side groups[328] in different ratios and investigated the influence of the degree of functionalization and ratio in water on the hydrogel formation, stability, and rheological properties. The storage modulus G', loss modulus G'', viscosity, and stability increased with higher amounts of functionalized hyaluronic acid in the hydrogel and with higher ratios of adamantane to β-cyclodextrin functionalities. For example, a hydrogel containing hyaluronic acid functionalized with 20% adamantane and 20% β-cyclodextrin each at 7.5 wt % in total possessed a yield stress at ∼60% where the viscosity started increasing drastically and G'' became higher than G'. Continuous step strain measurements of the same hydrogel showed full recovery after several cycles. In a further work, the same research group additionally introduced thiol and Michael acceptor groups for a secondary cross-linking via Michael addition to the same host−guest-functionalized hyaluronic acid.[329] In this work they investigated the effect of post-cross-linking on the stability of the hydrogel with different Michael acceptors, different pH values, and different amounts of functionalized hyaluronic acid. Finally, Burdick and co-workers used these materials for 3D printing.[252] A hydrogel based on a mixture of hyaluronic acid with 25% adamantane and 25% β-cyclodextrin functionalities was printed into a more stable support gel consisting of hyaluronic acid with 40% of the same functionalities. Further stabilization of the constructs was achieved by additional functionalization with methacrylate groups which were used for UV-induced cross-linking.

Ravoo and co-workers used adamantane-functionalized hydroxyethyl cellulose for hydrogel formation via host−guest interactions with amphiphilic β-cyclodextrin possessing *n*-dodecyl chains on the primary side and oligo(ethylene glycol) groups on the secondary side of the macrocycle.[330] These amphiphilic intermolecular cross-linked β-cyclodextrin vesicles are injectable and were investigated with respect to the storage modulus, loss modulus, viscosity, recovery, and different concentrations and host/guest ratios. The storage modulus and yield stress increased with higher amounts of host−guest functionalities in the hydrogel and could also be retransformed into solution by addition of free adamantane or β-cyclodextrin.

There are also other possible guest molecules for cyclodextrin, such as the linear PEG, which has been widely explored in this field. Ito and co-workers showed that the cyclodextrins threaded over PEG (rotaxanes) formed viscoelastic gels whereby two cyclodextrin units were connected with different groups, forming figure-eight cross-linkers.[331−333] These are interesting functionalities as they are pressure-responsive, and the cyclodextrin units slide over the PEG chain when pressure is applied. The gel therefore avoids the external stimulus to a greater extent compared to chemically fixed cross-linking units, which makes this concept attractive for functionalization of polymers for designing tunable shear thinning properties. For example, the following research groups have developed injectable hydrogels based on the host−guest interaction of PEG with particular α-cyclodextrins: Chen and co-workers[334] developed a reduction-sensitive supramolecular hydrogel based on [poly(ethylene glycol) monomethyl ether]-*graft*-[disulfide-linked poly(amidoamine)] with α-cyclodextrin with shear thinning properties. They investigated the influence of the added amount of dithiothreitol (DTT), which reduced disulfide bonds, on the storage modulus, loss modulus, and viscosity. For example, a gel without DTT possessed a viscosity at a low shear rate of ∼135 Pa·s, and a gel with DTT/disulfide bonds at a 5/1 ratio possessed a viscosity of ∼90 Pa·s, which both decreased upon a shear rate of 10 s^{-1} to the second Newtonian plateau, which is near 0 Pa·s. Zhang and Ma[335] prepared a polymeric prodrug (PEGylated indomethacin) which formed a supramolecular hydrogel by addition of α-cyclodextrin. They varied the amount of the host−guest compounds and investigated the influence on the storage modulus, loss modulus, and viscosity, which all decreased with lower host/guest ratios. A further series of host−guest-based supramolecular hydrogels was synthesized by Li et al.,[336] who compared the properties of the triblock copolymer poly[(*R*,*S*)-3-hydroxybutyrate]−poly(ethylene glycol)−poly[(*R*,*S*)-3-hydroxybutyrate] (5×10^3 g mol^{-1}) with those of the high molecular weight PEG (27×10^3 g mol^{-1}) and oligo(ethylene glycol) methyl ether (MPEG) (4.7×10^3 mol^{-1}) by threading with α-cyclodextrin. The poly[(*R*,*S*)-3-hydroxybutyrate] units of the triblock copolymer led to an additional stabilization of the hydrogel due to hydrophobic interactions, and the hydrogel possessed shear thinning properties with a higher yield stress than the other hydrogels containing PEG and MPEG.

DOI: 10.1021/acs.chemrev.5b00303
Chem. Rev. 2016, 116, 1496−1539

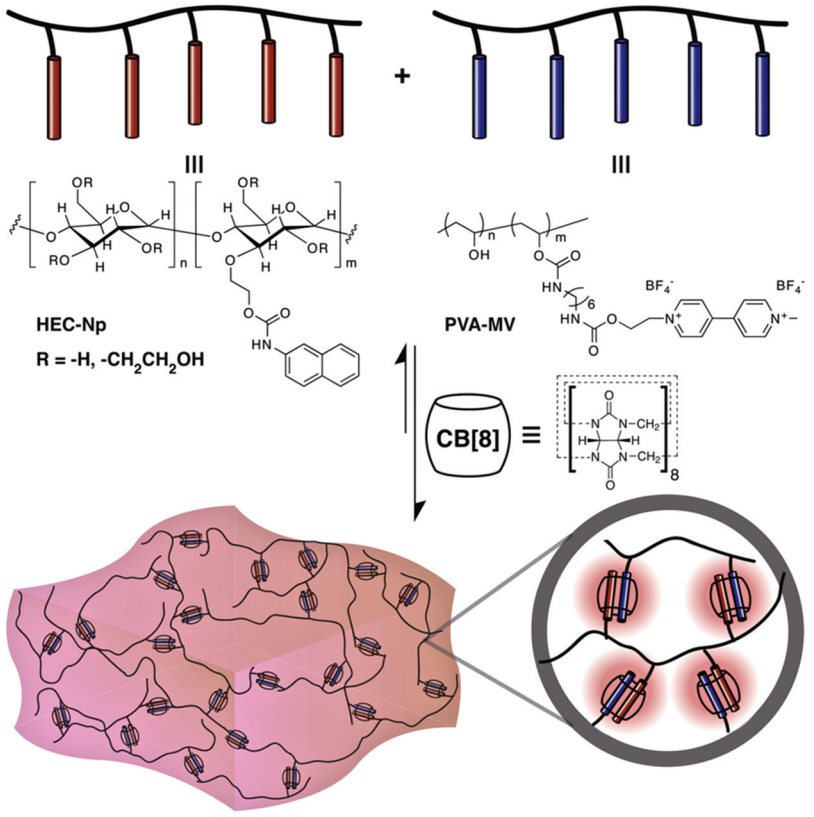

Figure 11. Supramolecular hydrogel with viologen/hydroxyethyl-functionalized cellulose and naphthalene-functionalized poly(vinyl alcohol) forming host−guest complexes with cucurbit[8]uril. Reprinted with permission from ref 343. Copyright 2012 American Chemical Society.

Tian et al.[337] developed an injectable and biodegradable poly(organophosphazene) with pendant MPEG and glycine ethyl ester side groups for supramolecular hydrogel formation with α-cyclodextrin. They varied the chain lengths/amount of MPEG, amount of α-cyclodextrin, and polymer concentration and investigated the influence on the gel formation and the rheological properties. Dynamic step strain measurements showed the hydrogels' shear thinning and recovery properties. For example, a gel containing 5×10^3 g mol^{-1} MPEG at the side functionalities possessed a storage modulus $G' \approx 10^5$ Pa and a loss modulus $G'' \approx 1.4 \times 10^3$ Pa at 1% strain and $G' \approx 6$ Pa and $G'' \approx 40$ Pa at 100% strain. Wu et al.[338] prepared an injectable electroactive supramolecular hydrogel. They used a copolymer based on ethylene glycol, sebacic acid, and xylitol with a carboxyl-capped aniline tetramer as a pendant side functionality whereby this and the ethylene glycol units formed host−guest complexes with γ-cyclodextrin dimers and led to hydrogel formation. It is interesting that the host−guest formation was conducted at the polymer backbone and at the side chain as well, which extends the possibility of functionalization and could be used for further tuning of the hydrogel's properties. As the aniline tetramer moiety is redox-active, this or other conducting groups might be used for further in situ modification of the hydrogel. Additionally, the reversible sol−gel transition can also be controlled via addition of 1-adamantanamine hydrochloride or γ-cyclodextrin dimer into the solution.

There are more compounds for host−guest interactions which were used for hydrogel formation showing controlled sol−gel transition. For example, Nakama et al.[339] modified hyaluronic acid with different amounts of PEG chains along the side groups and added α-cyclodextrin for supramolecular hydrogel formation. They investigated the effect of the degree of substitution and pH value on the gel melting temperature, which decreased with higher pH value/lower degree of substitution. Tomatsu et al.[340] developed a redox-responsive hydrogel based on dodecyl-modified poly(acrylic acid), β-cyclodextrin, and ferrocenecarboxylic acid. A hydrogel was formed only with the polymer itself due to the hydrophobic interactions of the long alkyl chains. Addition of β-cyclodextrin led to preferential formation of stronger intramolecular complexes with the alkyl chains, resulting in solutions that exhibited a lower viscosity with rising β-cyclodextrin content. Upon addition of ferrocenecarboxylic acid, its higher association constant with β-cyclodextrin released the alkyl chains from the complexes and thus induced re-establishment of intermolecular interaction and hydrogel formation. The subsequent oxidation of ferrocenecarboxylic acid retransformed the hydrogel into a solution as the oxidized species were too big for the host molecules, which could form complexes with the alkyl chains again.

Loh[341] described in his review the variety of supramolecular host−guest-based polymeric materials containing cyclodextrins, cucurbit[n]urils, and calix[n]arenes. Calix[n]arenes (see section 5.1) and cucurbit[n]urils have received more attention in this field and might be interesting for designing polymers for physical cross-linking which could be used for printing. Cucurbit[n]urils can interact with many different hosts such as diaminohexane/spermine-containing[342] and viologen/naphthalene-containing[343] polymers and form hydrogels. The latter work by Appel et al. described poly(vinyl alcohol)-containing viologen moieties and hydroxyethyl cellulose with naphthalene groups which formed host−guest complexes with cucurbit[8]uril (Figure 11). The hydrogels possessed very high water contents up to 99.7 wt

DOI: 10.1021/acs.chemrev.5b00303
Chem. Rev. 2016, 116, 1496−1539

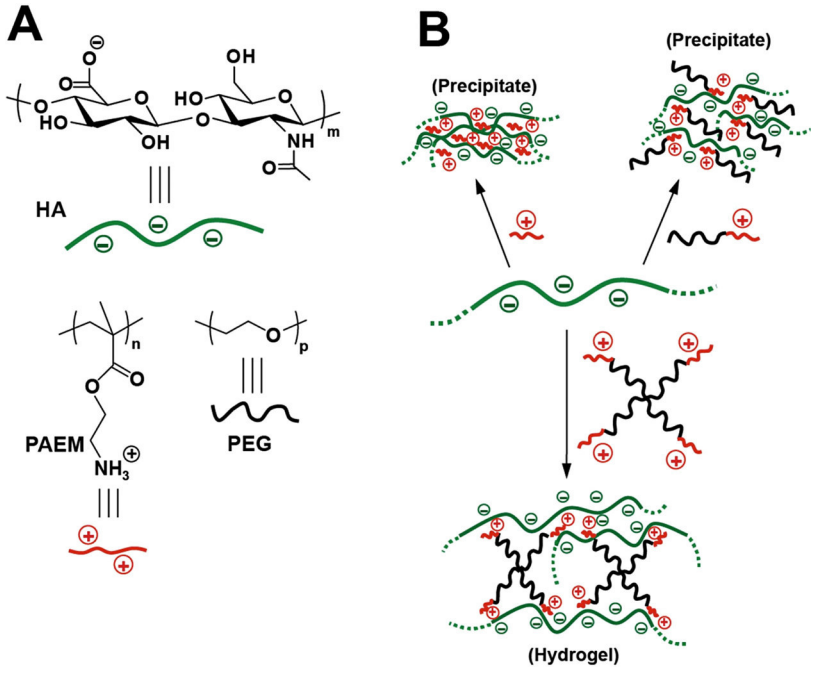

Figure 12. Hyaluronic acid- and PEG-based hydrogels. Adapted with permission from ref 344. Copyright 2015 John Wiley and Sons.

% and showed shear thinning properties and recovery after removal of the strain.

5.2.4. Ionic Interactions and Coordination Chemistry. Cross et al.[344] prepared injectable hybrid hydrogels based on negatively charged hyaluronic acid mixed with positively charged four-arm star poly(ethylene glycol)-*block*-poly(2-aminoethyl methacrylate) (Figure 12). Investigations were made concerning the influence of the star arm lengths, charge ratio, and osmolarity (pure water and phosphate buffer) on the gel formation; e.g., the most stable hydrogel was formed with $(PEG_{113}\text{-}b\text{-}PAEM_{12})_4$ and hyaluronic acid with a charge ratio of 1/1 in water. The star-shaped polymer acts as a cross-linker and has a positive influence on the hydrogel formation compared with the linear analogue, which led only to precipitations. Another PEG-based hydrogel stabilized via ionic interaction of charged side groups of the polymer was developed by Hunt et al.[345] In this work, PEG was used as a macroinitiator for ring-opening polymerization of allyl glycidyl ether, which was subsequently functionalized with sulfonate, carboxylate, or guanidinium groups via thiol−ene click chemistry. The hydrogel's stability could be tuned via the acidity and basicity of the groups, e.g., a 1/1 ratio of carboxylate/ammonium gave a solution, whereas 1/1 carboxylate/guanidinium yields a stable hydrogel at 10 wt %.

A further shear thinning gel based on positive and negative charge interaction was developed by Wang et al.[346] They synthesized poly(D,L-lactic acid-*co*-glycolic acid) nanoparticles coated either with poly(vinylamine) or with poly(ethylene-*co*-maleic acid) which formed a shear thinning network due to electrostatic interactions. If the polymer ratio and amount were decreased, the viscosity decreased as well, which could also be observed at high shear rates. For example, a gel containing 30% nanoparticles possessed a viscosity of ∼500 Pa·s and a gel with 20% nanoparticles possessed a viscosity of ∼175 Pa·s at a low shear rate, and both viscosities decreased significantly when a high shear rate was applied. Bünsow et al.[347] developed mechanoresponsive polyelectrolyte brushes consisting of cationic poly[2-(methacryloyloxy)ethyl]trimethylammonium chloride (PMETAC) brushes with a covalently attached fluorescent dye, 5(6)carboxyfluorescein. They investigated the pressure-dependent fluorescence quenching via atomic force microscopy, and upon application of force, the brushes were subsequently compressed due to the noncovalent electrostatic interaction. This might be an interesting approach for hydrogels functionalized with such groups to make them mechanoresponsive. The viscoelasticity and toughness of hydrogels could be controlled via the concentration of copolymers possessing cationic and anionic groups and the concentration of sodium chloride in the solution as shown by Gong and co-workers.[348,349] They investigated different ionic pairs with the monomers sodium *p*-styrenesulfonate, 2-acrylamido-2-methylpropanesulfonic acid, [3-[(meth)-acryloylamino]propyl]trimethylammonium chloride, [(acryloyloxy)ethyl]trimethylammonium chloride, and (*N*,*N*′-dimethylamino)ethyl acrylate and determined the swelling volume ratio, Young's modulus, the tensile/fracture stress, and the tearing energy of the materials. For example, a copolymer based on sodium *p*-styrenesulfonate and [3-(methacryloylamino)propyl]trimethylammonium chloride showed weak interactions at low concentrations of <1.6 M with swelling ratios up to ∼10-fold which afterward decreased with higher concentrations, and the Young's modulus increased at the same time, leading to a tougher hydrogel.

Gels can also be cross-linked via coordination chemistry, e.g., with palladium- and amine-based ligands, which was investigated by Xu et al.[350] to determine the effect on the gel's shear thinning/thickening properties[350] and on the zero shear viscosity.[351] They used poly(4-vinylpyridine) cross-linked with bis-Pd(II) compounds called [2,3,5,6-tetrakis{(dimethylamino)methyl}-phenylene-1,4-bis(palladium trifluoromethanesulfonate) or [2,3,5,6-tetrakis{(diethylamino)methy}phenylene-1,4-bis-(palladium trifluoromethanesulfonate)] in dimethyl sulfoxide or *N*,*N*′-dimethylformamide (DMF). The shear viscosity could be tuned via the temperature, polymer/cross-linker concentration, and kind of cross-linker that might be attractive for functional hydrogels with tunable properties. Jackson et al.[352,353] prepared

DOI: 10.1021/acs.chemrev.5b00303
Chem. Rev. 2016, 116, 1496−1539

metallopolymer films based on poly(butyl acrylate) containing 2,6-bis(1′-methylbenzimidazolyl)pyridine ligands for complexation of Cu^{2+}, Zn^{2+}, and Co^{2+} ions and tuning the material's mechanical stability. This approach might be used for stabilizing hydrogels via metal complexes.

5.2.5. Hydrogen Bonds. Polymers containing hydrogen bond side groups could be interesting for printing as these materials possess shear thinning properties. Lewis et al.[354] prepared poly(*n*-butyl acrylate) containing acrylamidopyridine, acrylic acid, carboxyethyl acrylate, or ureidopyrimidinone acrylate in different ratios which lead to higher glass transition temperatures, higher storage modulus G', and higher zero shear viscosities upon increased amount in the polymer. For example, a polymer with acrylic acid with a mole fraction of 6% possessed a zero shear viscosity of $\sim 2 \times 10^3$ Pa·s, and a polymer with acrylic acid with a mole fraction of 10% possessed a zero shear viscosity 10 times higher, $\sim 2 \times 10^4$ Pa·s. Vatankhah-Varnoosfaderani et al.[355] synthesized copolymers containing *N*-isopropylacrylamide and dopamine methacrylate, which formed a gel in dimethyl sulfoxide (DMSO) solution when sodium hydroxide was added. This led to deprotonation of the dopamine units, which could interact with each other and subsequently formed a gel within seconds, whereas the same process in alkaline water took several hours. The gel showed shear thinning properties whereby at room temperature at low shear rate $G' \approx 250$ Pa and $G'' \approx 19$ Pa and at 900% strain G'' became higher than G'.

Further poly(*N*-isopropylacrylamide) was used with hydrogen bond moieties for cross-linking by Hackelbusch et al.[356] They used diaminotriazine or cyanuric acid groups at the side chain and added the complementary bismaleimide or Hamilton wedge for gel formation in a methanol/chloroform (1/1) mixture. For example, a gel with the Hamilton wedge receptor with a polymer concentration of 200 mg mL^{-1} possessed a viscosity of ∼5.4 Pa·s at low shear rate and a yield stress of ∼0.9 s^{-1}. Hydrogen bond segments can also be used in the polymer backbone and thus form gels via α-helix and β-sheet formation such as the polypeptide-based organolator methoxypoly(ethylene glycol)-*block*-poly(γ-benzyl-L-glutamate-*co*-glycine) in DMF described by Fan et al.[357] The critical gelation concentration could be tuned via the monomer composition and the gel's properties via the α-helix/β-sheet ratio, which increases with higher amounts of glycine *N*-carboxyanhydride. Additionally, the gel was injectable and showed self-healing properties. Ji et al.[358] prepared a polymer possessing hydrogen bond and host−guest functionalities for gel formation. The polystyrene-based polymer contained 2,7-diamido-1,8-naphthyridine/dialkylammonium groups, and the poly(butyl methacrylate)-based polymer contained deazaguanosine/benzo-21-crown-7 groups, and both were separately dissolved in chloroform and formed a double-cross-linked gel by combination of the solutions.

5.3. Colloidal Systems

The scope of this section is systems containing solid particles as additives whose surface interacts in different ways with polymers or small organic molecules, thus yielding supramolecular hydrogels via self-assembly. Such strategies have so far been pursued using silica nanoparticles, laponite, carbon nanotubes, graphene sheets, titania sheets, and gold and silver nanoparticles as will be presented and discussed in detail. A most recent approach also demonstrated that interactions between latex particles or block copolymer micelles and polymers can lead to the formation of self-assembled hydrogels exhibiting shear thinning and self-healing properties.[359] All the systems containing solid particles described in this section show properties such as shear thinning, temperature/pH-induced reversible sol−gel transitions, or self-healing properties potentially exploitable for the design of printable hydrogels.

5.3.1. Silica Nanoparticles and Laponite-Based Hydrogels. The hydroxide-rich surface of silica nanoparticles allows covalent immobilization, e.g., of trimethoxysilyl compounds, via condensation reaction. Guo et al.[139] modified the silica's surface with β-cyclodextrin, which formed host−guest complexes with mono-end-functionalized PEG in aqueous solution. The addition of α-cyclodextrin led to inclusion complexes with the free PEG chain ends forming a viscoelastic hybrid hydrogel. Its storage modulus G' was around 4 times higher than that of the formed hydrogel without β-cyclodextrin-functionalized silica nanoparticles (native hydrogel). The hydrogel's viscosity, at low shear rates, was $\sim 1.3 \times 10^3$ Pa·s and was about 8 times higher than that of the native hydrogel, 157 Pa·s. The hybrid hydrogel showed pronounced shear thinning properties and reached the same viscosity (10 Pa·s) as the native hydrogel at a shear rate of 1 s^{-1}.

The silicium-rich compound laponite ($Na_{0.66}[Mg_{5.34}Li_{0.66}Si_8O_{20}(OH)_4]$) (clay nanosheet, CNS) was also investigated as an additive in hydrogels. Haraguchi et al.[360] copolymerized laponite with *N*,*N*′-dimethylacrylamide and *N*,*N*′-methylenebis(acrylamide) in different ratios and thus obtained hydrogels with tensile moduli ranging from 1.16 to 15.55 kPa, tensile strengths from 7 to 255.6 kPa, and water contents from 55.2% to 90.9%. Further insights into the shear thinning properties of those hydrogels were given by Aida and co-workers, who investigated the interaction between the clay nanosheets and polymers and dendrimers. Laponite contains oxyanions at the surface which can interact with cationic compounds, leading to a hydrogel formation via self-assembly. Additionally, sodium polyacrylate is necessary for disentanglement of the CNS in solution. For example, dendrimers of first, second, and third generation abbreviated as G1, G2, and G3 binders were synthesized.[361] They possessed a linear PEG core with esterified 2,2′-(ethylenedioxy)-bis(ethylamine) branches terminated with positively charged guanidinium functionalities. It could be shown that the hydrogel's storage modulus G' and loss modulus G'' increased with higher amounts of CNS and higher generation of the dendrimers and thus with increasing guanidinium content. Additionally, the formed hydrogels showed shear thinning properties; e.g., a hydrogel containing 5% CNS, 0.38% G3 binder, and 0.15% sodium polyacrylate possessed a critical strain region at 9% where the loss modulus G'' became higher than the storage modulus G' and thus the solid hydrogel transformed into a quasi-liquid state. The shear thinning behavior was also confirmed via continuous step strain measurements where the quasi-liquid and quasi-solid states could be obtained in change. The storage modulus decreased from 0.5 MPa to 5 kPa and tan δ increased from 0.4−0.5 to 3.0−4.0 when 100% oscillatory force was applied with a frequency of 1 Hz. By decreasing the amplitude to 0.1% at the same frequency, the hydrogel recovered and G' and tan δ reached their initial values. In a follow-up study, Aida and co-workers also compared the influence of linear molecular binders with different chain lengths and amounts of guanidinium functionalities with a dendritic molecular binder in CNS−hydrogels.[362] The linear molecular binders consisted of ABA triblock polymers with guanidinium-functionalized polyglycidol via thiol−ene click chemistry as A and polyethylene glycol as B. Dendritic molecular binder was a G3 binder as mentioned in the section before. Frequency sweep tests showed

DOI: 10.1021/acs.chemrev.5b00303
Chem. Rev. 2016, 116, 1496−1539

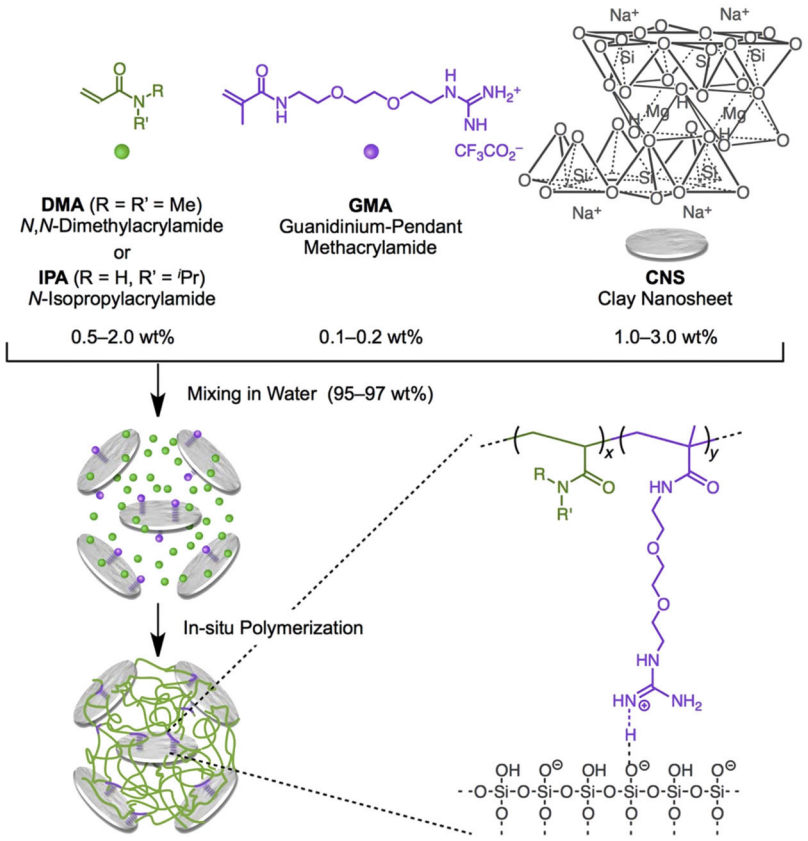

Figure 13. Schematic representation of CNS−polymer composite hydrogels reinforced by the incorporation of guanidinium pendant methacrylamide (GMA) in the polymer chains. Reprinted with permission from ref 363. Copyright 2013 John Wiley and Sons.

that with a higher amount of CNS and higher amount of guanidinium functionalities the storage modulus G' increased, which could also be observed for the loss modulus G'' but only up to a frequency of ∼10 rad s^{-1}. Shear thinning behavior of hydrogels was also shown via strain sweep tests at 0.05% and 100%, where the loss modulus G'' became higher than the storage modulus G' at a strain of 4%. Additionally, continuous step strain tests at 0.1% and 100% showed the reversibility between the quasi-solid and quasi-liquid states. The necessity of such cationic binders for the stabilization of CNS−hydrogels was further shown by the same research group in a follow-up study.[363] *N,N′*-Dimethylacrylamide (DMA)/*N*-isopropylacrylamide (NIPAAm) was copolymerized with guanidinium-pendant methacrylamide (GMA) monomer and clay nanosheets in water (Figure 13). The resultant hydrogels showed shear thinning properties; e.g., with 2% CNS, 0.5% DMA, and 0.1% GMA, the loss modulus G'' was larger than the storage modulus G' at 10% strain at 6.0 rad s^{-1} and the hydrogel changed from a quasi-solid state to a quasi-liquid one. Stress−strain experiments with different cationic amine side chain functionalities showed that the guanidinium side groups lead to the most stable hydrogels. In the case of no cationic compound in the hydrogel, it will lose its form, and therefore, the stabilization of CNS via charge interaction is necessary.

Gels were also prepared with a solid content between 3 and 10 wt % and CNS/gelatin ratio from 1/0 to 0/1.[364] Generally, the higher the CNS content, the larger the storage modulus, with a maximum of ∼1.4 × 10^3 Pa. Alternating high and low strains show the hydrogel's shear thinning properties and its ability to recover after strain.

5.3.2. Carbon-Nanotube- and Graphene-Sheet-Rich Compounds. Tan et al. synthesized an injectable supramolecular hydrogel based on single-walled carbon nanotubes (SWCNTs) with the bile salt sodium deoxycholate (NaDC).[365] The amphiphilic bile salt interacted through its hydrophobic steroid group with the carbon nanotube's surface, leading to self-assembly in aqueous solution due to the additional interaction of the carboxyl group with water. Shear thinning experiments revealed that, with a higher content of SWCNTs, the hydrogel had a greater shearing modulus and a higher shear stress. The content of NaDC was kept constant at 30%, and the amount of SWCNTs was varied from 1% to 3%. For example, with 1% SWCNTs, a shear modulus of 100 Pa (at a shear stress of 1 Pa) could be achieved, and with 2% SWCNTs, a shear modulus of even 10^4 Pa (shear stress of 80 Pa) could be achieved. An injectable supramolecular hydrogel based on multiwalled carbon nanotubes (MWCNTs) was investigated by Du et al. which is responsive to pH, temperature, and near-infrared (NIR) light showing self-healing properties.[366] MWCNTs were oxidized by treatment with a mixture of concentrated sulfuric and nitric acids, leading to a carboxylic acid-functionalized surface. The *N*-ethylamine-functionalized poly(ethylene imine) formed a hydrogel with the oxidized MWCNTs via hydrogen bonds ($COO^{-}\cdots$HN and NH···N), where the concentration of the polymer was varied from 25 to 75 wt % and that of the oxidized MWCNTS was varied from 0.015% to 0.5%. This system was sensitive to a variety of stimuli exploitable for printing. For example, the addition of HCl led to a protonation of the amine functionalities, which decreased the amount of hydrogen bonds, and therefore, a liquid was formed. After treatment with NaOH, the hydrogel retransformed by deprotonation of those amine groups. Gel−sol

DOI: 10.1021/acs.chemrev.5b00303
Chem. Rev. 2016, 116, 1496−1539

transition could also be controlled via exposure to NIR light or via a temperature change. The temperature sensitivity could be tuned linearly with the oxidized MWCNT content. For example, a hydrogel containing 0.1 wt % oxidized MWCNTs heated to 55 °C for 30 s transformed into a liquid and retransformed into a hydrogel after being cooled to 20 °C for 3 min. The self-healing behavior was confirmed after treatment of the hydrogel containing 0.5 wt % oxidized MWCNTs with a deformation stress of 200 or 800 Pa, and the storage modulus returned to 90% or 80% after recovery. Furthermore, interesting studies on the stability of hybrid hydrogels of amine-functionalized polymers and oxidized carbon nanotubes (CNTs) were performed by Hashmi et al.[367] They investigated poly(*N*-isopropylacrylamide) (PNIPAAm) and polymers with zwitterionic sulfobetaine functionalities with different ratios, CNT, and cross-linker in the hydrogel. SWCNTs were also used for supramolecular hydrogel formation via host−guest interactions. Wang and Chen[368] and Hui et al.[369] used Pluronic, whose hydrophobic poly(propylene oxide) (PPO) units interact with the SWCNTs' surface and whose hydrophilic poly(ethylene oxide) (PEO) units face into the hydrophilic solution after dispersion in water. Addition of α-CD led to a host−guest interaction with the PEO units and subsequently to hydrogel formation. For rheological measurements and comparison, a native hydrogel containing only Pluronic and α-CD was synthesized. In Wang's and Chen's work, surprisingly, the SWCNTs did not have a huge positive contribution to the storage modulus because all values were at least 1 order of magnitude smaller than those of the native hydrogel, and only the gel formation was accelerated by the addition of SWCNTs. The thermal reversibility and shear thinning properties of the hybrid hydrogel were retained. For example, at a shear rate of 0.01 s^{-1}, the native hydrogel possessed a viscosity of ~4.4 × 10^4 Pa·s, whereas the hybrid hydrogel's viscosity was only ~4 × 10^3 Pa·s. In Hui's work, the amount of α-CD was increased, yielding more stable hydrogels.

The following hydrogels could be interesting for printing as their sol−gel transition can be controlled. The interaction of pyrene-based compounds with the SWCNTs' surface via $\pi-\pi$ interaction was exploited for supramolecular hydrogel formation by Ogoshi et al.[370] They synthesized β-CD with a pyrene group which could be attached to the surface of the SWCNTs. After addition of poly(acrylic acid) containing 2 mol % dodecyl groups, host−guest complexes were formed by β-CD with the aliphatic side chains, and finally, a hydrogel was formed. The hydrogel could be transformed back to a solution either via addition of a competitive guest (sodium adamantine carboxylate) or by addition of a competitive host (α-CD). Yang et al.[371] used a one-pot hexacomponent system with $\pi-\pi$ stacking, Ugi reaction, and reversible addition fragmentation chain transfer (RAFT) polymerization for a polymer conjugation on carbon nanotubes. The polymer PNIPAAm interacted with its pyrene end group on the CNTs' surface and was functionalized with an MPEG at its other chain end. This formed host−guest complexes with α-CD and subsequently led to a transformation from a CNT dispersion to a supramolecular hydrogel. A further hydrogel formation via host−guest complexes of CNTs was investigated by Tamesue et al.[372] The polysaccharide curdlan was functionalized with β-CD at the side chains and could helically wrap around SWCNTs in water, exposing β-CD functionalities to the liquid surroundings. By adding poly(acrylic acid) containing pendant azobenzene groups, a photochemically reversible hydrogel was formed via host−guest interaction with β-CD under visible light (430 nm). This could be turned back into a solution by irradiation with UV light (365 nm) as the azobenzene group isomerized into the *trans*-conformation. A sol state could also be reached by adding a competitive host (α-CD) or a competitive guest (1,12-dodecanedicarboxylate sodium salt). Modified amino acid sequences possessing a long alkyl chain gelated in aqueous solution above the minimum gelation concentration (MGC). If they additionally possessed an aromatic group, they could interact with CNTs and were stabilized due to the $\pi-\pi$ interactions. Such supramolecular hydrogels were investigated by Mandal et al.[373] They varied the aromatic groups (imidazole, benzyl) and reached MGCs from 0.7% to 5.0% (w/v), enabling tunable gel-to-sol transition temperatures, e.g., with a fixed concentration of SWCNTs at 1.0% (w/v). In all cases, the hybrid hydrogel possessed a higher gel−sol transition temperature than the native hydrogel, and rheological measurements showed that in most cases the storage modulus G' increased with higher amounts of CNTs, which confirmed the stabilization via $\pi-\pi$ interactions.

First, supramolecular hydrogels based on a mixture of graphene and Pluronics did not show any improvement in mechanical features through addition of the graphene sheets compared to native Pluronic hydrogels.[374] A beneficial effect was observed by adding reduced graphene oxide (RGO) sheets into hydrogels based on short peptides as low molecular weight gelators.[375] They possessed [(fluorenylmethyl)oxy]carbonyl (Fmoc) and Tyr (**1**)/Phe (**2**) as functional aromatic groups which interacted with the graphene sheets via $\pi-\pi$ stacking and showed minimum gelation concentrations of 0.50% and 0.55% (w/v) for gelator peptides **1** and **2**. Furthermore, the storage modulus G' of the hydrogels increased with higher amounts of graphene sheets. As the hybrid hydrogels also showed thermoresponsiveness, the gel−sol transition could be used for the 3D printing process by transferring the gel to a solution via temperature change. Oxidized graphene sheets (graphene oxide, GO) with carboxyl and hydroxyl groups on the surface enabled the electrostatic interaction with compounds possessing protonated amine or other positively charged functionalities. On the basis of these interactions, a variety of stable supramolecular hydrogels with a very low minimum gelation concentration were prepared and could be useful tools for the 3D printing process by changing the gelator's concentration, transferring solutions into the gel state. For example, Adhikari et al.[376] used amino acids (L-arginine, L-tryptophan, L-histidine) with a minimum gelation concentration of 1.45% (w/v) and nucleosides (adenosine, guanosine, cytidine) with MGC = 2.0% (w/v) as gelators with GO. A nanofibrous robust 3D network structure was formed via self-assembly by heating the reaction solution above 100 °C and cooling it to room temperature afterward. Only a small amount of amino acids and nucleosides with respect to GO was needed (~2.21%, w/w), which confirmed their very good cross-linking ability between GO sheets. A hydrogel containing L-arginine possessed a very high storage modulus, $G' \approx 6 \times 10^4$ Pa, during the tested frequency range from 0.1 to 628 rad s^{-1}, displaying a positive effect on the hydrogel's stability. Similar experiments with polyamines (spermine, spermidine, tris(aminoethyl)amine) as incorporated cross-linkers in GO hydrogels were conducted by the same group.[377] Tao et al. used (dimethylguanyl)guanidine hydrochloride (metformin hydrochloride, MFH) as an amine-functional cross-linker for GO sheets which formed a hydrogel via electrostatic interactions and hydrogen bonds.[378] They investigated the hydrogel formation with respect to different cross-linkers: GO ratios need to be in the range of 1/13 to 1/10

DOI: 10.1021/acs.chemrev.5b00303
Chem. Rev. 2016, 116, 1496−1539

with 1 wt % GO content. Therefore, the necessary concentration of the cross-linker was very low with respect to GO at <10% (w/w). The pH value of the solution and thus the degree of protonation of MFH and the carboxylic acid groups on the GO surface played an important role as well in the hydrogel stability. For example, the strongest interaction was displayed at pH 3, where six kinds of hydrogen bonds were formed between GO's −OH/−COOH groups and MFH's =NH/—NH/—NH_2 groups along with electrostatic interaction of −COOH and =NH_2^+. In contrast, at pH 1, only four hydrogen bonds were available and caused the weakest interaction between GO and MFH. These results make materials interesting for 3D printing as the hydrogel's properties can be tuned via the concentration and the pH value, having an influence on the strength of cross-linking. Another pH-responsive graphene oxide-based hydrogel was investigated by Cong et al., who used poly(acryloyl-6-aminocaproic acid) and Ca^{2+} for cross-linking.[379] Ca^{2+} interacted with the carboxylic acid group of the polymer and with the graphene sheets' carboxylic acid groups on the surface, forming a highly porous hydrogel. Both components were varied from 1.0% to 9.5%, showing—with higher amounts—an increasing tensile stress of the hydrogel. In addition, it was stretchable, and in the case of ruptures, it showed self-healing properties at pH < 3. This pH range led to protonation of the carboxylic acid groups and therefore to a more flexible system which solidified at pH ≥ 7 reversibly. Yan and Han used chitosan as a cross-linker for GO, forming a hydrogel via electrostatic interactions.[380] It showed self-healing properties, and the gelation could be tuned via the temperature and concentration of GO as it possessed a very low sol−gel concentration. For example, a solution containing 8.0 wt % chitosan remained a solution at room temperature with 0.2 wt % GO and became a gel at room temperature with 0.3 wt % GO. With a higher amount of chitosan and GO, the storage modulus G' increased; e.g., at 20 °C, $G' \approx 70$ Pa for 0 wt % GO and $G' \approx 670$ Pa for 0.3 wt % GO. G' and G'' additionally showed a strong temperature dependency and decreased with higher temperature, weakening the electrostatic interactions within the hydrogel. The incorporation of thermoresponsive polymers as cross-linkers for GO is an ideal approach to tune the gelation via temperature and was performed by Jiang and co-workers.[381] They modified the GO surface with β-CD moieties and added the block copolymer azo-PDMA-*b*-PNIPAAm (PDMA = poly(*N*,*N*′-dimethylacrylamide)), which led to cross-linking due to the host−guest interaction of β-CD with the azophenyl group. Hydrogelation started when the temperature was above PNIPAAm's lower critical solution temperature (LCST) (29.3−39.9 °C), which varied with the degree of polymerization and composition within the block copolymer. The sol−gel transition was confirmed via measurement of the viscosity and storage/loss modulus over time with a temperature decrease of 1 °C min^{-1}. The hydrogel with host−guest-bound polymers on GO had significantly higher storage/loss moduli than the one with loosely bound GO without β-CD moieties and polymers which showed the strong effect of supramolecular interactions in the hydrogel. Another interesting method to increase the stability of hydrogel-containing graphene sheets is to control their orientation in a magnetic field. Wu et al. polymerized *N*,*N*′-dimethylacrylamide containing *N*,*N*′-methylenebis(acrylamide) as a cross-linker with GO and confirmed the anisotropic behavior via rheological measurements.[382] The storage modulus increased when the sheer force was orthogonal to the graphene sheets in the hydrogel due to higher resistance to an external influence compared to the parallel case. Such an external magnetic field during the 3D printing process could be used to control the hydrogels' properties.

5.3.3. Metal-Based Gels. *5.3.3.1. Titania Nanosheets.* Aida and co-workers controlled the orientation of titania nanosheets via an external magnetic field.[383,384] They used *N*,*N*′-dimethylacrylamide as a monomer and *N*,*N*′-methylenebis-(acrylamide) as a cross-linker for the UV-light induced polymerization. Thereby, titanium was used as the initiator which transfers an electron from the valence band to the conduction band upon exposure to UV light, which set free hydroxyl radicals in aquous solution and afterward initiated the polymerization. This experiment could be an interesting approach for in situ hydrogelation during 3D printing and for controlling the hydrogel's strength.

5.3.3.2. Gold and Silver Nanoparticles. Chen and co-workers[385] modified the gold's surface with monothiolated β-CD and used Pluronic as a cross-linker forming host−guest complexes between PEO moieties and β-CD, leading to a supramolecular hydrogel. The reversible transition to a solution could be conducted by adding 1-adamantanamine hydrochloride, which is a competitive guest for β-CD and destroyed the supramolecular network. Further insights into the mechanical properties of such host−guest formed hydrogels were given by Shi and co-workers.[386] They modified the gold nanoparticles' (AuNPs) and nanorods' (AuNRs) surfaces with monothiolated mPEG. Addition of α-CD yielded a supramolecular hydrogel that showed thermo- and mechanoresponsivity. AuNP hydrogels possessed a gel−sol transition at 60 °C, and AuNR hydrogels possessed a gel−sol transition at 70 °C. Both could be transformed into a gel upon cooling of the solutions reversibly. The storage modulus G' was higher than the loss modulus G'' over the whole frequency range, displaying a stable hydrogel doped with gold moieties. This gel also showed shear thinning properties. Das and co-workers used low molecular weight gelators (LMWGs) for the incorporation of gold salts and subsequently in situ reduction to gold nanoparticles.[387] The LMWGs consisted of dipeptides with a long aliphatic chain, different aromatic groups, and either a carboxylic acid or a sodium carboxylic group. The minimum gelation concentration of LMWGs was varied in water from 0.58% to 3% (w/v) and in aromatic solvents from 0.45% to 1.6% (w/v), which are very low contents. The in situ reduction and formation of AuNPs in the hydrogels increased their storage modulus G' and loss modulus G'' by around 1−2 orders of magnitude at low shear rates. Additionally, the supramolecular hydrogels showed shear thinning properties displayed by a change from the quasi-solid state to the quasi-liquid state with increasing oscillatory stress. Zhang and co-workers also synthesized supramolecular hydrogels based on low molecular weight gelators.[388] They used different derivates of bile acids with low concentrations between 25 and 100 mM and incorporated silver and gold salts with concentrations between 5 and 50 mM, which were reduced in situ via irradiation of light. Here, the G' and G'' of supramolecular hydrogels containing nanoparticles were 1 order of magnitude higher than those of the native hydrogels. They possessed shear thinning properties, and their yield stress was even lower than that of the native one.

6. BIOTECHNOLOGICAL APPROACHES TOWARD BIOINKS

Section 5 focused on chemical approaches to implement molecular interaction mechanisms in artificial materials. Nature has used and optimized such mechanisms throughout evolution,

DOI: 10.1021/acs.chemrev.5b00303
Chem. Rev. 2016, 116, 1496−1539

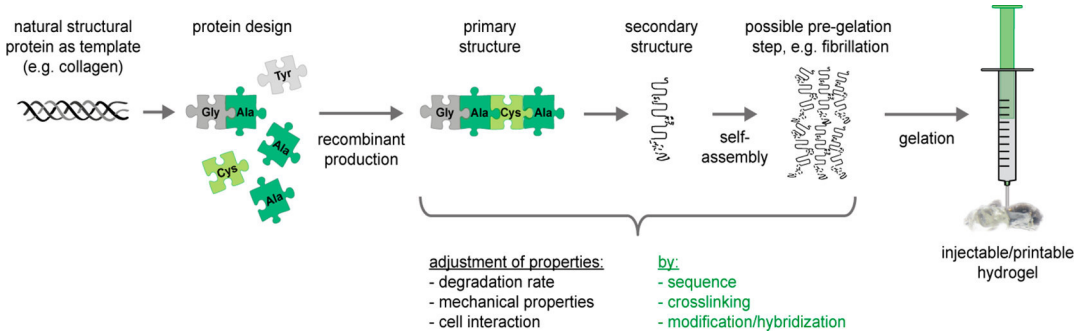

Figure 14. Schematic model of the steps along protein design to gain injectable/printable hydrogels.

together with a complex synthetic apparatus to synthesize the molecular building blocks with the highest precision. Nowadays, genetic engineering makes it possible to develop and design new biopolymers with a complexity and functionality not found in nature. Recombinant production of natural or artificial proteins allows tailoring of a material's properties such as mechanics, degradation, porosity, cell interaction, and cytocompatibility (Figure 14).[389] Genetically engineered recombinant proteins are much more accessible in a defined molecular structure than synthetically produced materials.[390−394] Specific design of functional groups along the constituent proteins (typically structural proteins such as collagen, elastin, or silk) allows biological activity similar to that of components of the natural ECM. One possibility is to combine different functional domains of natural proteins in one designed protein (e.g., a fusion protein), for example, merging cell interaction domains with structural ones. Alternatively, recombinant proteins can, by design, be easily modified with short peptide motifs such as RGD or IKVAV, which are unique ligands for cell receptors and mediate cell adhesion. In the context of this review, we will however primarily focus on (potential) printability.

Apart from the following exception, we will focus on recombinantly produced biopolymers as the main structural component of hydrogels, and not as a mediator or cross-linker for hydrogelation. Lu et al.[395] modified hyaluronic acid with peptide sequences as an anchoring domain which forms an injectable, shear thinning, and self-healing physical gel via the dock-and-lock principle after addition of recombinantly produced dimerized docking polypeptide sequences. The hydrogel possessed at low strain $G' \approx 250$ Pa/$G'' \approx 6$ Pa and at high strain $G' \approx 20$ Pa/$G'' \approx 50$ Pa, both of which were obtained in a repeatable way. Additionally, the hyaluronic acid was modified with methacrylate groups so that the hydrogel could be stabilized in a secondary step via photopolymerization. This approach is thus very promising as the initial step toward a printable hydrogel. For further details on the use of recombinant proteins as cross-linkers for hydrogelation, we refer to the review paper by Wang et al.[396]

It is important to mention that not all polypeptides and proteins can be recombinantly produced, nor can proteins be combined with nonpeptidic moieties, unless by chemical postproduction modification. In the case in which recombinant production is possible, receiving the proteins in sufficient yields is often challenging. This depends on the host organism selected for production, the fermentation process, and the protein itself. Especially the latter often creates certain unpredictability for the yield when a new process is initiated. Hence, so far there are not many recombinant protein materials available in sufficient amounts with properties such as shear thinning behavior and form stability, as well as cytocompatibility. However, biotechnology holds the promise of overcoming this drawback and expanding the field of bioinks for biofabrication, and the so far only and very recently published report on the use of a recombinant protein (based on spider silk sequences) without any additive for 3D printing and biofabrication underlines the great potential.[304]

In this section, we will briefly introduce the different possibilities for production of recombinant proteins and then give an overview over the so far reported recombinantly produced proteins (elastin-like polypeptide, resilin-like polypeptide, recombinant collagen, recombinant silk) with properties potentially exploitable for 3D printing. Furthermore, examples for peptide−polymer and protein−polymer hybrid materials and polynucleotides will be reviewed which show promising properties and may in the future be tailored for the demands of printing processes.

6.1. Designable Biopolymers: Recombinantly Produced Proteins

6.1.1. Methods for Recombinant Protein Production.

Different host organisms can be used for recombinant protein production such as bacteria, yeast, plants, insect and mammalian cells, or transgenic animals.[301] *E. coli* is often used as a host organism for recombinant protein production, since this Gram-negative enterobacterium is suitable for a fast and inexpensive large-scale production due to its simplicity, its well-known genetics, and the capability of fast high-density cultivation, in addition to the availability of different plasmids, fusion protein partners, and mutated strains.[397] Besides *E. coli*, other bacterial hosts have been employed for the recombinant production of proteins. In contrast to *E. coli*, the Gram-negative bacterium *Salmonella typhimurium*, for example, has the capability to secrete proteins, which simplifies the isolation of the target protein from the bacterial host proteins. Likewise, the Gram-positive bacterium *Bacillus subtilis* is able to secrete large quantities of recombinant proteins into the medium. The bacterial secretion systems are much simpler than those of yeasts and fungi, simplifying the efficient production.[398] Nevertheless, yeasts, such as *Saccharomyces cerevisiae* and *Pichia pastoris*, can be attractive alternatives to bacterial hosts because they are able to correctly process high molecular weight proteins including more complex post-translational modifications such as glycosylations,[399] and *P. pastoris* is even able to grow to high cell densities (>100 g L^{-1} dry cell mass).[400] To obtain large amounts of recombinant proteins, transgenic plants such as *Arabidopsis thaliana* and *Nicotiana tabacum* (tobacco) have also been used. Plants are capable of producing foreign proteins on a large scale and at lower costs in comparison to most other organisms.[401] Disadvantages of plant hosts are a more complicated genetic manipulation than for

DOI: 10.1021/acs.chemrev.5b00303
Chem. Rev. 2016, 116, 1496−1539

Table 6. Recombinantly Produced Proteins for Injectable/Printable Hydrogels

recombinant protein	3D printing technique	advantageous properties	applications	refs
collagen/collagen-like		biodegradability, biocompatibility	tissue repair (corneal substitutes), nerve regeneration, drug delivery	286, 407−410
silk-like	robotic dispensing	remarkable mechanical properties, biocompatibility, biodegradability	tissue repair, nerve regeneration, wound healing	304, 411
elastin-like		elastomeric properties, thermoresponsivebehavior, biocompatibility, high solubility	tissue repair (cartilage), vascular grafts, soft-tissue replacement, drug delivery	412−419
resilin-like		low stiffness, high resilience, reversible extensibility	tissue repair (cartilage, vascular grafts)	420−422

microbes and longer generation intervals.[402] Additionally, the production of large proteins can cause problems, because the underlying genes are prone to genetic rearrangements.[401]

Introducing foreign sequences and genes into animals can be achieved through different procedures, such as the integration of synthetic genes into the chromosomal DNA or by transporting a target DNA into cells, resulting in a transient expression.[403] The transformation efficiency is low using both approaches; viruses as transporters are in some cases much more promising because they are extraordinarily efficient in transferring their own genome into foreign cells. For example, baculovirus has been widely used as a vector of target genes for their expression in insect cells.[403] Using insect cells as expression hosts has advantages such as high-expression efficiencies, low feeding costs, the capability to secrete proteins, simplified purification, and possible post-translational modifications.[402,404] Disadvantages are more complex cloning procedures and longer generation times of the insect cell lines compared to bacteria.[405] Mammalian cells and even transgenic animals have also been used for recombinant protein production.[406] Using transgenic animals to produce recombinant proteins allows, e.g., the secretion into body fluids such as milk or urine, enabling protein production for long time intervals, thus gaining a higher protein yield.[301,402] Disadvantages of this system are that the creation of transgenic mammals is very time-consuming and complex. Additionally, as in the case of spider silk proteins that were secreted into the milk of goats and mice, the challenge is to separate the recombinant proteins from milk caseins, since several structural proteins and caseins show similar properties such as self-assembly, and especially mice only produce a small amount of milk.[267,402] Table 6 gives an overview of recombinantly produced proteins that have been used for 3D printing or as injectable hydrogels, or exhibit properties potentially exploitable for printing purposes. The different approaches will be presented and discussed in more detail in the following sections.

6.1.2. Silk-like Proteins. Due to spiders' aggressive territorial behavior and their cannibalism, their large-scale farming is not feasible. Therefore, several prokaryotic and eukaryotic hosts have been tested concerning recombinant production of spider silk proteins, as recently summarized by Heidebrecht et al.[301] Different silk-like polymers (SLPs) have been produced with varying numbers (i.e., repeats) of single sequence motifs, different types of motifs, and different spacings between them.[301,405,423,424] Spider silk offers a very high potential for biomedical applications due to the excellent mechanical properties of its fibers and the biocompatibility and biodegradation of materials processed from the underlying proteins.[302,402,425−427] Recombinant spider silk proteins can self-assemble into nanofibrillar networks triggered by high protein concentrations, salts, and temperature, and they form hydrogels.[428,429] Recently, it has been published that spider silk hydrogels can serve as a bioink for biofabrication.[304] In contrast to silk from *Bombyx mori*, the β-sheet-rich spider silk hydrogels showed moderate shear thinning behavior, with high viscosity at low angular frequencies and a decrease in viscosity at higher frequencies.[271] The elastic behavior dominated over the viscous behavior over the whole angular frequency range with a low-viscosity flow behavior and good form stability.[304,429] No structural changes occurred during the printing process, and the hydrogels solidified immediately after printing by robotic dispensing. Due to the form stability, it was possible to directly print up to 16 layers on top of each other with a construct depth of approximately 3 mm without structural collapse. Strikingly, cell-loaded spider silk constructs were printed without the need for additional cross-linker or thickener for mechanical stabilization. The encapsulated cells showed good viability over at least 1 week in such spider silk hydrogels.[304]

6.1.3. Recombinant Collagen/Collagen-like Proteins. Almost every possible type of expression system, such as bacteria, yeast, transgenic tobacco, insect cells, mammalian cells, silkworms, and transgenic mice, has been used for the recombinant expression of collagen, collagen-like proteins, and selected domains thereof.[286,407,410,430] Compared to native collagen, recombinantly produced collagens have the benefit of being biologically safe (no infectious contaminations) with useful self-assembly features, and they can be functionalized with bioinstructive domains such as cell adhesion motifs.[306,307,410] Recombinant expression of collagens is quite complex, since it can be necessary to introduce post-translational modifications important for cross-linking and helical stability. Therefore, biosynthesis of collagen might require specific enzymes, in particular prolyl 4-hydroxylase. In the absence of this enzyme, often non-triple-helical and nonfunctional collagen molecules are produced, which are unstable at physiological conditions and thus unsuitable for biomedical applications.[431] From the tested hosts, only mammalian cells produced collagen with an L-4-hydroxyproline content identical to that of natural collagen. However, this system yields only low levels of protein (0.6−20 mg L^{-1}). In *E. coli* and yeast, multigene expression is necessary to overcome the absence of the enzyme prolyl 4-hydroxylase.[409] On the basis of the multigene expression technology, collagen types I, II, and III were produced with an L-4-hydroxyproline content identical to that of the native human proteins and titers of 0.2−0.6 g L^{-1}.[432] Alternatively, peptide-based supramolecules mimicking the collagen structure and function have been tested. However, two critical issues arise for the development of peptide-based collagen-like supramolecules. One is the difficulty to generate a higher order structure to mimic the assembly (or gelation) property of natural collagen. The second is the not so easy incorporation of biologically relevant motifs into the material. Kaplan and co-workers designed collagen triblock peptides with the sequences $(Glu)_5$-(Gly-X-Hyp-Gly-Pro-Hyp)$_6$-$(Glu)_5$ which self-assembled into highly organized supramolecular structures forming a triple helix.[433,434] However,

DOI: 10.1021/acs.chemrev.5b00303
Chem. Rev. 2016, 116, 1496−1539

Table 7. New Hybrid Materials for Hydrogel Formation

fusion protein	expression system	hybrid system	refs
resilin−elastin−collagen-like (REC)	*Escherichia coli*	protein−protein	444
silk−elastin-like (SELP)	*Escherichia coli*	protein−protein	446, 447
silk−collagen-like ($C_2S^H{}_{48}C_2$)	*Pichia pastoris*	protein−protein	448
elastin-like polypeptide + polyethylene glycol (ELP−PEG)		protein−synthetic polymer	449
resilin-like polypeptide + polyethylene glycol (RLP−PEG)		protein−synthetic polymer	422

the physical properties of the collagen-like peptide supramolecules were far from those of native collagen hydrogels. Fusion proteins made of recombinant collagen and silk have also been developed, showing significantly enhanced cell viability and cell proliferation; see section 6.1.6.[435]

6.1.4. Elastin-like Polypeptides. Elastin is an abundant component of the extracellular matrix found in elastic tissues in the human body and is responsible for keeping the tissue flexible. The elastomeric properties of elastin materials provided major motivation for the design of mimetic elastin-like polypeptides (ELPs).[414,436] The study of ELPs was pioneered by Dan Urry, who synthesized a large number of polypeptides and studied their biophysical properties in solution and as cross-linked elastomeric materials.[414] The elastin-inspired sequence, derived from the hydrophobic domain of tropoelastin, is a pentapeptide repeat of VPGXG (where X is any residue except P), which is common in all ELPs.[413,414] Elastin shows thermoresponsive behavior, allowing control over its thermal transition temperature by changing the hydrophobicity, molecular weight, and concentration of the polypeptide.[414,437] The completely reversible phase transition can also be triggered by various environmental conditions such as temperature, ionic strength, redox state, and pH.[413,415] ELPs are water-soluble below their characteristic thermal transition temperature. However, when the temperature is increased above the transition temperature, the ELPs undergo a phase transition into an aggregated state which reveals a physically cross-linked network favorable for printing.[413,438] Materials made of elastin-like polypeptides show excellent mechanical properties (similar to those made of natural elastin), are biocompatible, and cause minimal cytotoxicity and immune response when implanted.[419,439,440] Nagapudi and coworkers found that upon T_t-triggered physical cross-linking block copolymers with the most hydrophilic inner blocks formed hydrogels with complex shear moduli ranging from 4.5 to 10.5 kPa. Decreasing the hydrophilicity of the inner block resulted in the formation of hydrogels with significantly greater shear moduli of up to 280 kPa.[441] The critical temperature of the phase transition can be varied by changing the "X" amino acid.[414,438] Therefore, depending on the guest residue, an ELP can be designed to be liquid at room temperature and to form a hydrogel in situ when the temperature is raised upon injection.

Using recombinant approaches allows incorporation of multiple physical or covalent cross-linking and reactive sites for specific mechanical properties and control.[442] For example, elastin-like polypeptides have been genetically designed, synthesized, and evaluated concerning enzyme-initiated covalent cross-links via tissue transglutaminase to form a network that sustains cartilage matrix synthesis and accumulation.[412,415,443] Articular chondrocytes were successfully encapsulated in the in situ cross-linked hydrogels, which were then injected to fill an irregularly shaped cartilage defect and to integrate into the surrounding tissue. The ELP network supported cell viability and infiltration, as well as cartilage matrix synthesis and accumulation. Whether the kinetics of enzymatic cross-linking can be adapted to be suitable for 3D printing remains an open question.

6.1.5. Resilin-like Polypeptides. Natural resilin is an elastomeric protein with remarkable mechanical properties. It is present in specialized regions of the insect cuticle and plays a key role in insect flight, the jumping mechanism of fleas, and vocalization of cicades.[444] Resilin possesses excellent mechanical properties such as low stiffness, high resilience, and effective energy storage. Recently, hydrogels made of recombinantly engineered resilin-like polypeptides (RLPs) have been produced with good mechanical (1−25 kPa) and cell-adhesive properties.[420] The polypeptide contained 12 repeats of the resilin consensus sequence and a single, distinct biologically active domain.[445] The approach allowed independent control over the concentration of cell-binding, MMP-sensitive, and polysaccharide-sequestration domains in hydrogels by mixing various RLPs. The RLP-based polypeptides exhibit a largely random coil conformation in solution and in the cross-linked hydrogels, on the basis of the repetitive motifs in the polypeptides. The randomly coiled, isotropic three-dimensional network has been shown to behave as an ideal rubber with near-perfect reversible long-range elasticity.[422] RLP hydrogels formed rapidly upon mixing with tris[(hydroxymethyl)phosphine], and they were able to maintain their mechanical integrity due to cross-linking as well as to allow the viability of encapsulated primary human mesenchymal stem cells (MSCs).[421]

6.1.6. Hybrid Proteins. Hybrid materials are made by fusing different bioactive domains or protein motifs that are not otherwise found in nature (Table 7). Injectable hydrogels made therefrom can benefit from the advantages of both components. For the same reason, hybrid materials made of natural polymers and synthetic polymers have been developed as injectable hydrogels.[242]

One example of hybrid proteins is the combination of silk repeat sequences and ELP sequences (SELPs).[447,450,451] By combining the silk-like and elastin-like blocks in various ratios and using different sequences, it is possible to produce a broad range of biomaterials with different material properties. The ELP blocks in the silk−elastin-like proteins influence the molecular chain properties of the protein.[452] The chimeric proteins were designed to retain the mechanical properties of silk, while incorporating the high solubility and environmental sensitivity of ELPs.[453−455] SELPs irreversibly undergo a two-step self-assembly process under physiological conditions to form hydrogels depending on the number of silk-like blocks in the repeat unit.[456] For example, increasing the number of silk-like blocks within a domain in a silk−elastin-like block copolymer increased the rate of gelation and decreased the rate of resorption of the polymer.[442,456,457] The first step in the gelation process is consistent with the crystallization of the silk-like domains via hydrogen-bond-mediated physical cross-linking.[456,457] The second assembly step is driven by the hydrophobic interaction between elastin blocks above a specific transition temperature, which leads to the ordered association of SELP molecules,

DOI: 10.1021/acs.chemrev.5b00303
Chem. Rev. 2016, 116, 1496−1539

indicating that the temperature-sensitive behavior of ELPs is even retained in ELP hybrids.[456] When hydrophobic residues were added to an otherwise hydrophilic SELP, the transition temperature was decreased.[454] Some SELPs were injected via syringes and then formed insoluble hydrogels at the injection site without any additional cross-linker.[446] It has been further demonstrated that genetically engineered SELPs (SELP-47 K) can be used to form injectable hydrogels for delivery of cell-based therapeutics.[447]

Hybrid materials made of silk and collagen blocks have also been designed, synthesized, and characterized.[448] The polymer ($C_2S^H{}_{48}C_2$) consists of a middle block ($S^H{}_{48}$) composed of 48 identical silk-like octapeptides in tandem and two end blocks (C_2), each of which is composed of two identical 99 amino acid long collagen-like sequences in tandem.[458] The hybrid protein formed nanofibrillar hydrogels exhibiting long-term stability, self-healing behavior, and tunable mechanical properties. Chimeric resilin-, elastin-, and collagen-like engineered polypetides (RECs) have been designed and produced.[444] The rubber-like proteins elastin and resilin exhibit a reversible deformation and very high resilience and elasticity. In combination with a collagen-like sequence, it has been shown that the material exhibits promising self-assembly properties potentially exploitable for printing.[444] Parisi-Amon et al.[459] reported on a mixing-induced two-component hydrogel for injection of stem cells which consists of two polymers called C7 and P9 possessing seven and nine repeating units of the CC43 WW domain (C) and the L-proline-rich peptide (P), respectively. Additionally, the C7 unit contains the cell-binding domain RGD. This system showed shear thinning and rehealing properties, cytocompatibility, and the ability to encapsulate cells at constant physiological conditions. Olsen et al.[409] investigated the rheological behavior of coiled-coil telechelic association domains (APQMLRE, LQETNAA, LQDVREL, LRQQVKE, ITFLKNT, VMESDAS) possessing linker domains ($[AGAGAGPEG]_n$), with n = 10 and 30, which show shear thinning properties.

In general, several peptide−polymer hybrid hydrogels exist, but they are usually built upon a synthetic polymer and peptide sequences produced by solid-phase synthesis (and not biotechnologically), which is not the focus here. For more detailed information thereon, we refer the reader, e.g., to the paper by Altbundas et al.[460] Recombinantly produced coiled-coil peptides have been combined with thermoresponsive polymers to yield thermoswitchable hydrogels. Therefore, a triblock copolymer[461] was prepared on the basis of the before mentioned peptides, such as APQMLRE, LQETNAA, LQDVREL, LRQQVKE, ITFLKNT, and VMESDAS, with n = 10, in the middle and two thiol−maleimide-conjugated PNIPAAm end blocks. Strain amplitude sweep measurements were performed at different temperatures and showed their influence on the storage modulus G' and loss modulus G''. Thereby, PNIPAAm's free polymer chains collapsed upon their lower critical solution temperature behavior, leading to higher values of the moduli but still maintaining their shear thinning property. One further example is the elastin-like polypeptide−polyethylene glycol (ELP−PEG) hydrogel system combining the tenability of ELP hydrogels with the distinct advantages of PEG hydrogels. The hybrid hydrogel enabled flexible and tailored tuning of the material stiffness and the cell-adhesive RGD ligand density.[449]

6.2. Designable Biopolymers: Polynucleotides

Recent progress in DNA nanotechnology has also facilitated the design of a variety of DNA-based nanosized structures useful for the generation of injectable hydrogels.[462−466] DNA has specific secondary structures, and stimulus-sensitive features can be incorporated to modulate such a specific structure on the nanoscale. First reported by Um et al.,[467] the connection of monomer (X-DNA) units resulted in the formation of DNA hydrogels. These hydrogels were biocompatible, biodegradable, inexpensive to fabricate, and easily molded into the desired shapes and sizes. In contrast to other bioinspired hydrogels (including alginate-based hydrogels), the gelation process of DNA hydrogels occurred under physiological conditions, and cell encapsulation was accomplished in situ. Drug molecules and even mammalian cells can be encapsulated in the liquid state, eliminating the cell loading step and also avoiding denaturing conditions.[467] In another study, the DNA sequence was replaced with one containing immunostimulatory cytosine−phosphate−guanine (CpG) motifs.[468] CpG-DNA induces the production of helper T-cell type 1 cytokines.[469−471] Nishikawa et al. developed a novel method to produce ligase-free, injectable, self-gelling, biodegradable DNA hydrogels using oligodeoxynucleotides.[472] Therefore, the single-stranded 5′-ends of polypod-like structured DNA were extended to hybridize under physiological conditions. The gelation of the DNA hydrogels occurred instantaneously after injection using a syringe with a fine needle because of a dissociation/association process. When the hydrogel was stressed, a fraction of the bonds dissociated, and the resulting free ends changed their partner and quickly reassociated through hydrogen bonds. Guo et al.[473] developed a pH-switchable DNA hydrogel which was stable at pH 5 and turned into a quasi-liquid at pH 8. This process is reversible and exhibited shape memory effects that would be interesting to assess regarding exploitability for 3D printing. In addition, it was shown that the DNA hydrogels can deliver tumor antigens (ovalbumin) for induction of antigen-specific immune responses.[472] Nevertheless, hydrogels formed by polynucleotides used for biomedical applications are still a challenge, since the carried genetic information might interfere with cellular function. Therefore, it remains to be seen whether they qualify as future bioinks.

7. CONCLUSIONS AND OUTLOOK

AM, often described as 3D printing in the popular media, has rapidly evolved into a very active field of research and is already used to produce medical implants. One strength of AM is the ability to fabricate hierarchical structures through the simultaneous printing of cells and supporting material in an approach termed biofabrication. In a holistic approach, materials for cell printing are predominantly limited to hydrogels, since the cells must be processed under cytocompatible conditions. We have presented and discussed the most prominent methods suitable for 3D hydrogel printing: (1) LIFT, (2) inkjet printing, and (3) robotic dispensing. While each method has its advantages and disadvantages, robotic dispensing is currently the only method that allows for the generation of clinically relevant constructs, albeit with lower resolutions than LIFT or inkjet printing. With our introduction into the rheological behavior of non-Newtonian liquids and other relevant flow phenomena, we developed general criteria that should be kept in mind for the development of a new bioink. The bioink formulation should have shear thinning properties (not being thixotropic) and should not show extrudate swell. If cells are part of the formulation, the viscosity before printing must allow mixing and homogeneous 3D distribution of the cells throughout the printing process without affecting the viability, and shear forces cannot exceed limits tolerable for cell survival. Most importantly, the bioink must

DOI: 10.1021/acs.chemrev.5b00303
Chem. Rev. 2016, 116, 1496−1539

rapidly gel after printing for good shape fidelity of the printing process.

These considerations underline the high demands that biofabrication imposes on the materials to be used for bioprinting. Hydrogels may generally be cross-linked either physically, through noncovalent molecular interactions, or chemically, through the formation of chemical bonds. Physical gels are dynamic due to the reversibility of the network-forming interaction, which is advantageous for the printing process, whereas their mechanical stability after printing is usually low. In contrast, chemically cross-linked gels are mechanically stronger but usually exhibit no reversibility once the network is formed. Dynamic chemical bonds are the exception to this rule and have in some most recent papers been successfully used for bioink development. However, the vast majority of studies which result in stable 3D printed cell loaded structures relies on a combination of both types of gel formation: a physical component for adjusting the rheological properties for printing and a postfabrication chemical cross-linking, often UV-mediated, for stabilizing the printed structure. This is also due to the fact that, since biofabrication originated from engineering and not from chemistry or materials science, most studies rely on established hydrogel systems for biomedical applications and rather optimize formulations than really develop new bioinks. Hence, we then summarized a number of strategies that have evolved in related fields of research, such as supramolecular chemistry and biotechnology, and selected studies that concern approaches potentially exploitable for 3D printing. This was intended to complete the toolbox for polymer chemists, materials researchers, and biotechnologists to be able to enter the field with a rational strategy for bioink development.

We believe that, for future bioink developments, a number of concepts from supramolecular chemistry can directly be transferred, for example, through multiple conjugation with polymers for multivalently interacting building blocks. Also, the concept of supramolecular polymers is a fascinating basis to assess the printability of such systems. Regarding chemical cross-linking of hydrogels in 3D printing, the concept of dynamic covalent bonds bears great potential for the development of novel bioinks. Also, stimulus-switchable chemical reactions, similar to the already used thermosensitive physically cross-linked hydrogels, may in the future be an option for printing hydrogels. Ideally, shear-stress-sensitive chemical bonds would be activated through the printing procedure and rapidly cross-link after the printing. Finally, biotechnology has evolved and is more and more able to produce bioinspired designer structures in yields that allow their use for materials science, and thus also for biofabrication. Further, this connection has just been initiated, and we are sure that this approach bears great potential for future bioink development, as the control over the primary sequence of recombinantly produced biomolecules exceeds the possibilities available in modern macromolecular chemistry, thus allowing for a far better control over structure−function relationships such as rheological properties. This outline for future developments shows the plethora of possibilities that arise for bioink development, especially through the convergence of strategies from related but different research fields.

AUTHOR INFORMATION

Corresponding Author

*E-mail juergen.groll@fmz.uni-wuerzburg.de.

Author Contributions

[§]T.J. and W.S. contributed equally to this work.

Notes

The authors declare no competing financial interest.

Biographies

Tomasz Jüngst was born in 1984 and studied nanostructural engineering in the Department of Physics at the University of Würzburg (Germany). After receiving his Dipl.-Ing. in 2011, he started working on his Ph.D. under the supervision of Jürgen Groll in the Department for Functional Materials in Medicine and Dentistry. During this time, he spent 3 months working at the Queensland University of Technology in Brisbane, Australia, with Dietmar W. Hutmacher and Paul D. Dalton, where he gained experience in the field of melt electrospinning writing granted by the DAAD (German Academic Exchange Service). His research is focused on three-dimensional structures for tissue engineering and biofabrication, where he is developing fabrication systems and processing materials.

Willi Smolan was born in 1989 and studied chemistry at the University of Göttingen (Germany) from 2008 to 2014, where he obtained his bachelor's and master's degrees. There he specialized in macromolecular chemistry and worked on several projects with functional polymers synthesized via RAFT polymerization. In 2011 and 2014, he worked with Martina Stenzel, Philipp Vana, and Peter Roth at the Centre for Advanced Macromolecular Design (Sydney, Australia) and in 2013 with David Fulton at the Chemical Nanoscience Laboratory (Newcastle upon Tyne, U.K.). During his studies, he also undertook industrial internships in the field of functional materials at ContiTECH AG (Northeim, Germany) in 2011 and at Merck KGaA (Darmstadt, Germany) in 2013/2014. Afterward, in 2014, he started his Ph.D. in the Department for Functional Materials in Medicine and Dentistry at the University of Würzburg (Germany), supervised by Jürgen Groll, working on biocompatible polymers for 3D printing.

DOI: 10.1021/acs.chemrev.5b00303
Chem. Rev. 2016, 116, 1496−1539

Kristin Schacht studied molecular biology and biochemistry at the Universität Bayreuth, where she received her M.Sc. in 2010. Afterward, she spent an $8^1/_2$ month research internship in the Department of Biomedical Materials and Regenerative Medicine at CSIRO Materials Science and Engineering, Melbourne, Australia. There, she was involved in the Bioscaffold Project, which contained the expression, purification, and characterization of novel designed collagen-like proteins in bacteria for biomedical applications. She is currently working on her Ph.D. thesis under the supervision of Prof. Dr. Thomas Scheibel at the Universität Bayreuth. Her research focuses on the preparation and characterization of three-dimensional scaffolds (hydrogels and foams) made of recombinant spider silk proteins for biomedical applications.

Thomas Scheibel is Chair of Biomaterials at the Universität Bayreuth in Germany since 2007. He received both his diploma of biochemistry (1994) and a Dr. rer. nat. (1998) from the Universität Regensburg in Germany, and his habilitation (2007) from the Technische Universität München in Germany. He was a Kemper Foundation postdoctoral fellow and a DFG postdoctoral fellow at the University of Chicago. He received the Junior Scientist Award of the Center of Competence for New Materials in 2004. His and his colleagues' work on spider silk proteins won the second prize in the Science4life Venture Cup 2006. He also gained the Biomimetics Award of the German Bundesministerium für Bildung and Forschung (BMBF) in 2006, and the Innovation by Nature Award of the BMBF in 2007. He is 1 of 10 recipients of the 2006 innovation tribute of the Bavarian prime minister, and received the Heinz-Maier-Leibnitz Medal in 2007, the Karl-Heinz-Beckurts Award in 2008, and the Dechema Award of the Max-Buchner Foundation in 2013. Since 2015 he is member of the German National Academy of Science and Engineering (acatech).

Jürgen Groll was born in 1976 and studied chemistry at the University of Ulm (Germany) from 1995 to 2000. He received his Ph.D., during which he spent a 6 month research internship with Virgil Percec (Philadelphia, PA), in 2004 from the RWTH Aachen (Germany) with summa cum laude honors after working under the guidance of Martin Möller. From 2005 to 2009, he worked for 4 years in industry at SusTech GmbH & Co. KG (Darmstadt, Germany) in the field of functional coatings and nanotechnology. In parallel, he built up a research group on polymeric biomaterials at the DWI Interactive Materials Research Institute in Aachen, Germany. Since August 2010, he has held the Chair for Functional Materials in Medicine and Dentistry at the University of Würzburg (Germany). His research interest comprises applied polymer chemistry, nanobiotechnology, biomimetic scaffolds, immunomodulatory materials, and biofabrication. He is the coordinator of the large-scale integrated European project HydroZONES (Contract No. 309962; www.hydrozones.eu) and was awarded an ERC consolidator grant (Design2Heal, Contract No. 617989). For his work, he has received a number of awards, such as the Henkel Innovation Award (2007), the Bayer Early Excellence in Science Award (2009), the Reimund-Stadler Award of the German Chemical Society—Section Macromolecular Chemistry (2010), and the Unilever Prize of the Polymer Networks Group (2014). He currently serves as an editorial board member of the journal *Biofabrication* and as a board member of the International Society for Biofabrication.

ACKNOWLEDGMENTS

We thank Paul D. Dalton for proofreading the manuscript. This research has received funding (J.G., T.J., W.S.) from the European Union's Seventh Framework Programme (FP7/2007-2013) under Grant Agreement No. 309962 (HydroZONES project) and the European Research Council (ERC) under Grant Agreement No. 617989 (Design2Heal project).

REFERENCES

(1) Gibson, I.; Rosen, D. W.; Stucker, B. *Additive Manufacturing Technologies. 3D Printing, Rapid Prototyping, and Direct Digital Manufacturing*; 2nd ed.; Springer: New York, 2010.
(2) Kruth, J.-P.; Leu, M.-C.; Nakagawa, T. Progress in Additive Manufacturing and Rapid Prototyping. *CIRP Ann.* **1998**, *47*, 525−540.
(3) Berman, B. 3-D Printing: The New Industrial Revolution. *Bus. Horizons* **2012**, *55*, 155−162.
(4) Langer, R.; Vacanti, J. Tissue Engineering. *Science* **1993**, *260*, 920−926.
(5) Leong, K. F.; Cheah, C. M.; Chua, C. K. Solid Freeform Fabrication of Three-Dimensional Scaffolds for Engineering Replacement Tissues and Organs. *Biomaterials* **2003**, *24*, 2363−2378.
(6) Hutmacher, D. W.; Sittinger, M.; Risbud, M. V. Scaffold-Based Tissue Engineering: Rationale for Computer-Aided Design and Solid Free-Form Fabrication Systems. *Trends Biotechnol.* **2004**, *22*, 354−362.

DOI: 10.1021/acs.chemrev.5b00303
Chem. Rev. 2016, 116, 1496−1539

(7) Yang, S.; Leong, K.-F.; Du, Z.; Chua, C.-K. The Design of Scaffolds for Use in Tissue Engineering. Part II. Rapid Prototyping Techniques. *Tissue Eng.* **2002**, *8*, 1−11.
(8) Yeong, W.-Y.; Chua, C.-K.; Leong, K.-F.; Chandrasekaran, M. Rapid Prototyping in Tissue Engineering: Challenges and Potential. *Trends Biotechnol.* **2004**, *22*, 643−652.
(9) Mironov, V.; Boland, T.; Trusk, T.; Forgacs, G.; Markwald, R. R. Organ Printing: Computer-Aided Jet-Based 3D Tissue Engineering. *Trends Biotechnol.* **2003**, *21*, 157−161.
(10) Guillemot, F.; Mironov, V.; Nakamura, M. Bioprinting is Coming of Age: Report from the International Conference on Bioprinting and Biofabrication in Bordeaux (3b′09). *Biofabrication* **2010**, *2*, 010201.
(11) Derby, B. Printing and Prototyping of Tissues and Scaffolds. *Science* **2012**, *338*, 921−926.
(12) Ferris, C. J.; Gilmore, K. G.; Wallace, G. G.; In het Panhuis, M. Biofabrication: An Overview of the Approaches used for Printing of Living Cells. *Appl. Microbiol. Biotechnol.* **2013**, *97*, 4243−4258.
(13) Melchels, F. P.; Domingos, M. A.; Klein, T. J.; Malda, J.; Bartolo, P. J.; Hutmacher, D. W. Additive Manufacturing of Tissues and Organs. *Prog. Polym. Sci.* **2012**, *37*, 1079−1104.
(14) Murphy, S. V.; Atala, A. 3D Bioprinting of Tissues and Organs. *Nat. Biotechnol.* **2014**, *32*, 773−785.
(15) Buenger, D.; Topuz, F.; Groll, J. Hydrogels in Sensing Applications. *Prog. Polym. Sci.* **2012**, *37*, 1678−1719.
(16) Tibbitt, M. W.; Anseth, K. S. Hydrogels as Extracellular Matrix Mimics for 3D Cell Culture. *Biotechnol. Bioeng.* **2009**, *103*, 655−663.
(17) Hoffman, A. S. Hydrogels for Biomedical Applications. *Adv. Drug Delivery Rev.* **2012**, *64*, 18−23.
(18) Seliktar, D. Designing Cell-Compatible Hydrogels for Biomedical Applications. *Science* **2012**, *336*, 1124−1128.
(19) Peppas, N. A.; Hilt, J. Z.; Khademhosseini, A.; Langer, R. Hydrogels in Biology and Medicine: From Molecular Principles to Bionanotechnology. *Adv. Mater.* **2006**, *18*, 1345−1360.
(20) Lee, K. Y.; Mooney, D. J. Hydrogels for Tissue Engineering. *Chem. Rev.* **2001**, *101*, 1869−1879.
(21) Annabi, N.; Tamayol, A.; Uquillas, J. A.; Akbari, M.; Bertassoni, L. E.; Cha, C.; Camci-Unal, G.; Dokmeci, M. R.; Peppas, N. A.; Khademhosseini, A. 25th Anniversary Article: Rational Design and Applications of Hydrogels in Regenerative Medicine. *Adv. Mater.* **2014**, *26*, 85−124.
(22) Patenaude, M.; Smeets, N. M.; Hoare, T. Designing Injectable, Covalently Cross-Linked Hydrogels for Biomedical Applications. *Macromol. Rapid Commun.* **2014**, *35*, 598−617.
(23) Van Tomme, S. R.; Storm, G.; Hennink, W. E. In Situ Gelling Hydrogels for Pharmaceutical and Biomedical Applications. *Int. J. Pharm.* **2008**, *355*, 1−18.
(24) Yu, L.; Ding, J. D. Injectable Hydrogels as Unique Biomedical Materials. *Chem. Soc. Rev.* **2008**, *37*, 1473−1481.
(25) Guvendiren, M.; Lu, H. D.; Burdick, J. A. Shear-Thinning Hydrogels for Biomedical Applications. *Soft Matter* **2012**, *8*, 260−272.
(26) Billiet, T.; Vandenhaute, M.; Schelfhout, J.; Van Vlierberghe, S.; Dubruel, P. A Review of Trends and Limitations in Hydrogel-Rapid Prototyping for Tissue Engineering. *Biomaterials* **2012**, *33*, 6020−6041.
(27) Malda, J.; Visser, J.; Melchels, F. P.; Jüngst, T.; Hennink, W. E.; Dhert, W. J. A.; Groll, J.; Hutmacher, D. W. 25th Anniversary Article: Engineering Hydrogels for Biofabrication. *Adv. Mater.* **2013**, *25*, 5011−5028.
(28) Skardal, A.; Atala, A. Biomaterials for Integration with 3-D Bioprinting. *Ann. Biomed. Eng.* **2015**, *43*, 730−746.
(29) Vaezi, M.; Seitz, H.; Yang, S. A Review on 3D Micro-Additive Manufacturing Technologies. *Int. J. Adv. Manuf. Technol.* **2013**, *67*, 1721−1754.
(30) Raimondi, M. T.; Eaton, S. M.; Nava, M. M.; Laganà, M.; Cerullo, G.; Osellame, R. Two-Photon Laser Polymerization: From Fundamentals to Biomedical Application in Tissue Engineering and Regenerative Medicine. *J. Appl. Biomater. Funct. Mater.* **2012**, *10*, 56−66.
(31) Wust, S.; Muller, R.; Hofmann, S. Controlled Positioning of Cells in Biomaterials-Approaches Towards 3D Tissue Printing. *J. Funct. Biomater.* **2011**, *2*, 119−154.
(32) Melchels, F. P.; Feijen, J.; Grijpma, D. W. A Review on Stereolithography and its Applications in Biomedical Engineering. *Biomaterials* **2010**, *31*, 6121−6130.
(33) Tumbleston, J. R.; Shirvanyants, D.; Ermoshkin, N.; Janusziewicz, R.; Johnson, A. R.; Kelly, D.; Chen, K.; Pinschmidt, R.; Rolland, J. P.; Ermoshkin, A.; et al. Continuous Liquid Interface Production of 3D Objects. *Science* **2015**, *347*, 1349−1352.
(34) Chrisey, D. B.; Pique, A.; McGill, R.; Horwitz, J.; Ringeisen, B.; Bubb, D.; Wu, P. Laser Deposition of Polymer and Biomaterial Films. *Chem. Rev.* **2003**, *103*, 553−576.
(35) Ringeisen, B. R.; Othon, C. M.; Barron, J. A.; Young, D.; Spargo, B. J. Jet-Based Methods to Print Living Cells. *Biotechnol. J.* **2006**, *1*, 930−948.
(36) Schiele, N. R.; Corr, D. T.; Huang, Y.; Raof, N. A.; Xie, Y.; Chrisey, D. B. Laser-Based Direct-Write Techniques for Cell Printing. *Biofabrication* **2010**, *2*, 032001.
(37) Gruene, M.; Pflaum, M.; Hess, C.; Diamantouros, S.; Schlie, S.; Deiwick, A.; Koch, L.; Wilhelmi, M.; Jockenhoevel, S.; Haverich, A.; et al. Laser Printing of Three-Dimensional Multicellular Arrays for Studies of Cell−Cell and Cell−Environment Interactions. *Tissue Eng., Part C* **2011**, *17*, 973−982.
(38) Guillemot, F.; Souquet, A.; Catros, S.; Guillotin, B.; Lopez, J.; Faucon, M.; Pippenger, B.; Bareille, R.; Remy, M.; Bellance, S.; et al. High-Throughput Laser Printing of Cells and Biomaterials for Tissue Engineering. *Acta Biomater.* **2010**, *6*, 2494−2500.
(39) Guillotin, B.; Souquet, A.; Catros, S.; Duocastella, M.; Pippenger, B.; Bellance, S.; Bareille, R.; Remy, M.; Bordenave, L.; Amedee, J.; et al. Laser Assisted Bioprinting of Engineered Tissue with High Cell Density and Microscale Organization. *Biomaterials* **2010**, *31*, 7250−7256.
(40) Koch, L.; Deiwick, A.; Schlie, S.; Michael, S.; Gruene, M.; Coger, V.; Zychlinski, D.; Schambach, A.; Reimers, K.; Vogt, P. M.; et al. Skin Tissue Generation by Laser Cell Printing. *Biotechnol. Bioeng.* **2012**, *109*, 1855−1863.
(41) Michael, S.; Sorg, H.; Peck, C. T.; Koch, L.; Deiwick, A.; Chichkov, B.; Vogt, P. M.; Reimers, K. Tissue Engineered Skin Substitutes Created by Laser-Assisted Bioprinting Form Skin-Like Structures in the Dorsal Skin Fold Chamber in Mice. *PLoS One* **2013**, *8*, e57741.
(42) Nahmias, Y.; Schwartz, R. E.; Verfaillie, C. M.; Odde, D. J. Laser-Guided Direct Writing for Three-Dimensional Tissue Engineering. *Biotechnol. Bioeng.* **2005**, *92*, 129−136.
(43) Koch, L.; Kuhn, S.; Sorg, H.; Gruene, M.; Schlie, S.; Gaebel, R.; Polchow, B.; Reimers, K.; Stoelting, S.; Ma, N.; et al. Laser Printing of Skin Cells and Human Stem Cells. *Tissue Eng., Part C* **2010**, *16*, 847−854.
(44) Gruene, M.; Unger, C.; Koch, L.; Deiwick, A.; Chichkov, B. Dispensing Pico to Nanolitre of a Natural Hydrogel by Laser-Assisted Bioprinting. *Biomed. Eng. Online* **2011**, *10*, 19.
(45) Barron, J. A.; Ringeisen, B. R.; Kim, H.; Spargo, B. J.; Chrisey, D. B. Application of Laser Printing to Mammalian Cells. *Thin Solid Films* **2004**, *453−454*, 383−387.
(46) Lin, Y.; Huang, G.; Huang, Y.; Tzeng, T.-R. J.; Chrisey, D. Effect of Laser Fluence in Laser-Assisted Direct Writing of Human Colon Cancer Cell. *Rapid Prototyping J.* **2010**, *16*, 202−208.
(47) Ringeisen, B. R.; Kim, H.; Barron, J. A.; Krizman, D. B.; Chrisey, D. B.; Jackman, S.; Auyeung, R.; Spargo, B. J. Laser Printing of Pluripotent Embryonal Carcinoma Cells. *Tissue Eng.* **2004**, *10*, 483−491.
(48) Barron, J. A.; Wu, P.; Ladouceur, H. D.; Ringeisen, B. R. Biological Laser Printing: A Novel Technique for Creating Heterogeneous 3-Dimensional Cell Patterns. *Biomed. Microdevices* **2004**, *6*, 139−147.
(49) Catros, S.; Guillotin, B.; Bačáková, M.; Fricain, J.-C.; Guillemot, F. Effect of Laser Energy, Substrate Film Thickness and Bioink Viscosity on Viability of Endothelial Cells Printed by Laser-Assisted Bioprinting. *Appl. Surf. Sci.* **2011**, *257*, 5142−5147.
(50) Duocastella, M.; Fernández-Pradas, J. M.; Serra, P.; Morenza, J. L. Jet Formation in the Laser Forward Transfer of Liquids. *Appl. Phys. A: Mater. Sci. Process.* **2008**, *93*, 453−456.

DOI: 10.1021/acs.chemrev.5b00303
Chem. Rev. 2016, 116, 1496−1539

(51) Guillemot, F.; Souquet, A.; Catros, S.; Guillotin, B. Laser-Assisted Cell Printing: Principle, Physical Parameters Versus Cell Fate and Perspectives in Tissue Engineering. *Nanomedicine* **2010**, *5*, 507−515.
(52) Lin, Y.; Huang, Y.; Chrisey, D. B. Droplet Formation in Matrix-Assisted Pulsed-Laser Evaporation Direct Writing of Glycerol-Water Solution. *J. Appl. Phys.* **2009**, *105*, 093111.
(53) Mézel, C.; Hallo, L.; Souquet, A.; Breil, J.; Hébert, D.; Guillemot, F. Self-Consistent Modeling of Jet Formation Process in the Nanosecond Laser Pulse Regime. *Phys. Plasmas* **2009**, *16*, 123112.
(54) Young, D.; Auyeung, R.; Pique, A.; Chrisey, D.; Dlott, D. Plume and Jetting Regimes in a Laser Based Forward Transfer Process as Observed by Time-Resolved Optical Microscopy. *Appl. Surf. Sci.* **2002**, *197-198*, 181−187.
(55) Wilson, W. C., Jr.; Boland, T. Cell and Organ Printing 1: Protein and Cell Printers. *Anat. Rec.* **2003**, *272A*, 491−496.
(56) Boland, T.; Xu, T.; Damon, B.; Cui, X. Application of Inkjet Printing to Tissue Engineering. *Biotechnol. J.* **2006**, *1*, 910−917.
(57) Calvert, P. Inkjet Printing for Materials and Devices. *Chem. Mater.* **2001**, *13*, 3299−3305.
(58) de Gans, B. J.; Duineveld, P. C.; Schubert, U. S. Inkjet Printing of Polymers: State of the Art and Future Developments. *Adv. Mater.* **2004**, *16*, 203−213.
(59) Derby, B. Bioprinting: Inkjet Printing Proteins and Hybrid Cell-Containing Materials and Structures. *J. Mater. Chem.* **2008**, *18*, 5717−5721.
(60) Derby, B. Inkjet Printing of Functional and Structural Materials: Fluid Property Requirements, Feature Stability, and Resolution. *Annu. Rev. Mater. Res.* **2010**, *40*, 395−414.
(61) Martin, G. D.; Hoath, S. D.; Hutchings, I. M. Inkjet Printing - the Physics of Manipulating Liquid Jets and Drops. *J.Phys.: Conf. Ser.* **2008**, *105*, 012001.
(62) Saunders, R. E.; Derby, B. Inkjet Printing Biomaterials for Tissue Engineering: Bioprinting. *Int. Mater. Rev.* **2014**, *59*, 430−448.
(63) Singh, M.; Haverinen, H. M.; Dhagat, P.; Jabbour, G. E. Inkjet Printing-Process and its Applications. *Adv. Mater.* **2010**, *22*, 673−685.
(64) Kim, J. D.; Choi, J. S.; Kim, B. S.; Choi, Y. C.; Cho, Y. W. Piezoelectric Inkjet Printing of Polymers: Stem Cell Patterning on Polymer Substrates. *Polymer* **2010**, *51*, 2147−2154.
(65) Xu, T.; Jin, J.; Gregory, C.; Hickman, J. J.; Boland, T. Inkjet Printing of Viable Mammalian Cells. *Biomaterials* **2005**, *26*, 93−99.
(66) Setti, L.; Fraleoni-Morgera, A.; Ballarin, B.; Filippini, A.; Frascaro, D.; Piana, C. An Amperometric Glucose Biosensor Prototype Fabricated by Thermal Inkjet Printing. *Biosens. Bioelectron.* **2005**, *20*, 2019−2026.
(67) Fromm, J. E. Numerical Calculation of the Fluid Dynamics of Drop-on-Demand Jets. *IBM J. Res. Dev.* **1984**, *28*, 322−333.
(68) Reis, N.; Derby, B. Ink Jet Deposition of Ceramic Suspensions: Modeling and Experiments of Droplet Formation. *MRS Online Proc. Libr.* **2000**, *625*, 117.
(69) Jang, D.; Kim, D.; Moon, J. Influence of Fluid Physical Properties on Ink-Jet Printability. *Langmuir* **2009**, *25*, 2629−2635.
(70) Xu, C.; Zhang, M.; Huang, Y.; Ogale, A.; Fu, J.; Markwald, R. R. Study of Droplet Formation Process During Drop-on-Demand Inkjetting of Living Cell-Laden Bioink. *Langmuir* **2014**, *30*, 9130−9138.
(71) Campbell, P. G.; Miller, E. D.; Fisher, G. W.; Walker, L. M.; Weiss, L. E. Engineered Spatial Patterns of FGF-2 Immobilized on Fibrin Direct Cell Organization. *Biomaterials* **2005**, *26*, 6762−6770.
(72) Sirringhaus, H.; Kawase, T.; Friend, R. H.; Shimoda, T.; Inbasekaran, M.; Wu, W.; Woo, E. P. High-Resolution Inkjet Printing of All-Polymer Transistor Circuits. *Science* **2000**, *290*, 2123−2126.
(73) Cobas, R.; Muñoz-Pérez, S.; Cadogan, S.; Ridgway, M. C.; Obradors, X. Surface Charge Reversal Method for High-Resolution Inkjet Printing of Functional Water-Based Inks. *Adv. Funct. Mater.* **2015**, *25*, 768−775.
(74) Soltman, D.; Subramanian, V. Inkjet-Printed Line Morphologies and Temperature Control of the Coffee Ring Effect. *Langmuir* **2008**, *24*, 2224−2231.
(75) Stringer, J.; Derby, B. Formation and Stability of Lines Produced by Inkjet Printing. *Langmuir* **2010**, *26*, 10365−10372.
(76) Chang, C. C.; Boland, E. D.; Williams, S. K.; Hoying, J. B. Direct-Write Bioprinting Three-Dimensional Biohybrid Systems for Future Regenerative Therapies. *J. Biomed. Mater. Res., Part B* **2011**, *98B*, 160−170.
(77) Dababneh, A. B.; Ozbolat, I. T. Bioprinting Technology: A Current State-of-the-Art Review. *J. Manuf. Sci., Trans. ASME* **2014**, *136*, 061016.
(78) Ozbolat, I. T.; Yu, Y. Bioprinting toward Organ Fabrication: Challenges and Future Trends. *IEEE Trans. Biomed. Eng.* **2013**, *60*, 691−699.
(79) Yan, K. C.; Nair, K.; Sun, W. Three Dimensional Multi-Scale Modelling and Analysis of Cell Damage in Cell-Encapsulated Alginate Constructs. *J. Biomech.* **2010**, *43*, 1031−1038.
(80) Schuurman, W.; Levett, P. A.; Pot, M. W.; van Weeren, P. R.; Dhert, W. J. A.; Hutmacher, D. W.; Melchels, F. P. W.; Klein, T. J.; Malda, J. Gelatin-Methacrylamide Hydrogels as Potential Biomaterials for Fabrication of Tissue-Engineered Cartilage Constructs. *Macromol. Biosci.* **2013**, *13*, 551−561.
(81) Lewis, J. A. Direct Ink Writing of 3D Functional Materials. *Adv. Funct. Mater.* **2006**, *16*, 2193−2204.
(82) Guillotin, B.; Guillemot, F. Cell Patterning Technologies for Organotypic Tissue Fabrication. *Trends Biotechnol.* **2011**, *29*, 183−190.
(83) Khalil, S.; Nam, J.; Sun, W. Multi-Nozzle Deposition for Construction of 3D Biopolymer Tissue Scaffolds. *Rapid Prototyping J.* **2005**, *11*, 9−17.
(84) Smith, C. M.; Stone, A. L.; Parkhill, R. L.; Stewart, R. L.; Simpkins, M. W.; Kachurin, A. M.; Warren, W. L.; Williams, S. K. Three-Dimensional Bioassembly Tool for Generating Viable Tissue-Engineered Constructs. *Tissue Eng.* **2004**, *10*, 1566−1576.
(85) Madou, M. J. *Fundamentals of Microfabrication: The Science of Miniaturization*; CRC Press: Boca Raton, FL, 2002.
(86) Sobral, J. M.; Caridade, S. G.; Sousa, R. A.; Mano, J. F.; Reis, R. L. Three-Dimensional Plotted Scaffolds with Controlled Pore Size Gradients: Effect of Scaffold Geometry on Mechanical Performance and Cell Seeding Efficiency. *Acta Biomater.* **2011**, *7*, 1009−1018.
(87) Ovsianikov, A.; Gruene, M.; Pflaum, M.; Koch, L.; Maiorana, F.; Wilhelmi, M.; Haverich, A.; Chichkov, B. Laser Printing of Cells into 3D Scaffolds. *Biofabrication* **2010**, *2*, 014104.
(88) Strobl, G. R. *The Physics of Polymers*; Springer: Berlin, 2007.
(89) Rubinstein, M.; Colby, R. H. *Polymer Physics*; Oxford University Press: Oxford, U.K., 2003.
(90) Shenoy, A. V. *Rheology of Filled Polymer Systems*; Kluwer Academic Publishers: Dordrecht, The Netherlands, 1999.
(91) Barnes, H. A.; Hutton, J. F.; Walters, K. *An Introduction to Rheology*; Elsevier: Amsterdam, 1989.
(92) Bird, R. B.; Armstrong, R. C.; Hassager, O. *Dynamics of Polymeric Liquids*; John Willey & Sons: New York, 1987.
(93) Ferry, J. D. *Viscoelastic Properties of Polymers*; John Wiley & Sons: New York, 1980.
(94) Møller, P. C. F.; Fall, A.; Bonn, D. Origin of Apparent Viscosity in Yield Stress Fluids Below Yielding. *Europhys. Lett.* **2009**, *87*, 38004.
(95) Barnes, H.; Walters, K. The Yield Stress Myth? *Rheol. Acta* **1985**, *24*, 323−326.
(96) Barnes, H. A. The Yield Stress—a Review or 'Παντα Ρει'—Everything Flows? *J. Non-Newtonian Fluid Mech.* **1999**, *81*, 133−178.
(97) Schurz, J. The Yield Stress—an Empirical Reality. *Rheol. Acta* **1990**, *29*, 170−171.
(98) Coussot, P. Yield Stress Fluid Flows: A Review of Experimental Data. *J. Non-Newtonian Fluid Mech.* **2014**, *211*, 31−49.
(99) Barnes, H. A. Thixotropy—a Review. *J. Non-Newtonian Fluid Mech.* **1997**, *70*, 1−33.
(100) Mewis, J.; Wagner, N. J. Thixotropy. *Adv. Colloid Interface Sci.* **2009**, *147−148*, 214−227.
(101) Larson, R. G.; Desai, P. S. Modeling the Rheology of Polymer Melts and Solutions. *Annu. Rev. Fluid Mech.* **2015**, *47*, 47−65.
(102) Irgens, F. *Rheology and Non-Newtonian Fluids*; Springer: Heidelberg, Germany, 2014.
(103) Aguado, B. A.; Mulyasasmita, W.; Su, J.; Lampe, K. J.; Heilshorn, S. C. Improving Viability of Stem Cells During Syringe Needle Flow

DOI: 10.1021/acs.chemrev.5b00303
Chem. Rev. 2016, 116, 1496−1539

through the Design of Hydrogel Cell Carriers. *Tissue Eng., Part A* **2012**, *18*, 806−815.
(104) Pati, F.; Jang, J.; Ha, D. H.; Kim, S. W.; Rhie, J. W.; Shim, J. H.; Kim, D. H.; Cho, D. W. Printing Three-Dimensional Tissue Analogues with Decellularized Extracellular Matrix Bioink. *Nat. Commun.* **2014**, *5*, 1−11.
(105) Schuurman, W.; Khristov, V.; Pot, M. W.; van Weeren, P. R.; Dhert, W. J. A.; Malda, J. Bioprinting of Hybrid Tissue Constructs with Tailorable Mechanical Properties. *Biofabrication* **2011**, *3*, 021001.
(106) Lewis, J. A. Colloidal Processing of Ceramics. *J. Am. Ceram. Soc.* **2000**, *83*, 2341−2359.
(107) Macosko, C. W. *Rheology: Principles, Measurements, and Applications*; Wiley-VCH: New York, 1994.
(108) Mewis, J.; Wagner, N. J. *Colloidal Suspension Rheology*; Cambridge University Press: Cambridge, U.K., 2012.
(109) Bergenholtz, J. Theory of Rheology of Colloidal Dispersions. *Curr. Opin. Colloid Interface Sci.* **2001**, *6*, 484−488.
(110) Goodwin, J. W.; Hughes, R. W. *Rheology for Chemists: An Introduction*; Royal Society of Chemistry: Cambridge, U.K., 2000.
(111) Krieger, I. M. Rheology of Monodisperse Latices. *Adv. Colloid Interface Sci.* **1972**, *3*, 111−136.
(112) Lewis, J. A. Direct-Write Assembly of Ceramics from Colloidal Inks. *Curr. Opin. Solid State Mater. Sci.* **2002**, *6*, 245−250.
(113) Ahn, B. Y.; Duoss, E. B.; Motala, M. J.; Guo, X.; Park, S.-I.; Xiong, Y.; Yoon, J.; Nuzzo, R. G.; Rogers, J. A.; Lewis, J. A. Omnidirectional Printing of Flexible, Stretchable, and Spanning Silver Microelectrodes. *Science* **2009**, *323*, 1590−1593.
(114) Ahn, B. Y.; Shoji, D.; Hansen, C. J.; Hong, E.; Dunand, D. C.; Lewis, J. A. Printed Origami Structures. *Adv. Mater.* **2010**, *22*, 2251−2254.
(115) Hanson Shepherd, J. N.; Parker, S. T.; Shepherd, R. F.; Gillette, M. U.; Lewis, J. A.; Nuzzo, R. G. 3D Microperiodic Hydrogel Scaffolds for Robust Neuronal Cultures. *Adv. Funct. Mater.* **2011**, *21*, 47−54.
(116) Smay, J. E.; Gratson, G. M.; Shepherd, R. F.; Cesarano, J.; Lewis, J. A. Directed Colloidal Assembly of 3D Periodic Structures. *Adv. Mater.* **2002**, *14*, 1279−1283.
(117) Schmid-Schönbein, H.; Wells, R.; Goldstone, J. Influence of Deformability of Human Red Cells Upon Blood Viscosity. *Circ. Res.* **1969**, *25*, 131−143.
(118) Winkler, R. G.; Fedosov, D. A.; Gompper, G. Dynamical and Rheological Properties of Soft Colloid Suspensions. *Curr. Opin. Colloid Interface Sci.* **2014**, *19*, 594−610.
(119) Vlassopoulos, D.; Cloitre, M. Tunable Rheology of Dense Soft Deformable Colloids. *Curr. Opin. Colloid Interface Sci.* **2014**, *19*, 561−574.
(120) Singh, S. P.; Chatterji, A.; Gompper, G.; Winkler, R. G. Dynamical and Rheological Properties of Ultrasoft Colloids under Shear Flow. *Macromolecules* **2013**, *46*, 8026−8036.
(121) Huang, C. C.; Sutmann, G.; Gompper, G.; Winkler, R. G. Tumbling of Polymers in Semidilute Solution under Shear Flow. *Europhys. Lett.* **2011**, *93*, 54004.
(122) Huang, C.-C.; Winkler, R. G.; Sutmann, G.; Gompper, G. Semidilute Polymer Solutions at Equilibrium and under Shear Flow. *Macromolecules* **2010**, *43*, 10107−10116.
(123) Huber, B.; Harasim, M.; Wunderlich, B.; Kröger, M.; Bausch, A. R. Microscopic Origin of the Non-Newtonian Viscosity of Semiflexible Polymer Solutions in the Semidilute Regime. *ACS Macro Lett.* **2014**, *3*, 136−140.
(124) De Gennes, P.; Leger, L. Dynamics of Entangled Polymer Chains. *Annu. Rev. Phys. Chem.* **1982**, *33*, 49−61.
(125) Watanabe, H. Viscoelasticity and Dynamics of Entangled Polymers. *Prog. Polym. Sci.* **1999**, *24*, 1253−1403.
(126) Melchels, F. P. W.; Dhert, W. J. A.; Hutmacher, D. W.; Malda, J. Development and Characterisation of a New Bioink for Additive Tissue Manufacturing. *J. Mater. Chem. B* **2014**, *2*, 2282−2289.
(127) Oyen, M. L. Mechanical Characterisation of Hydrogel Materials. *Int. Mater. Rev.* **2014**, *59*, 44−59.
(128) Malkin, A. Y.; Isayev, A. I. *Rheology: Concepts, Methods, and Applications*; ChemTec Publishing: Toronto, Canada, 2012.
(129) Picout, D. R.; Ross-Murphy, S. B. Rheology of Biopolymer Solutions and Gels. *Sci. World J.* **2003**, *3*, 105−121.
(130) Yang, Y.; Urban, M. W. Self-Healing Polymeric Materials. *Chem. Soc. Rev.* **2013**, *42*, 7446−7467.
(131) Pfister, A.; Landers, R.; Laib, A.; Hübner, U.; Schmelzeisen, R.; Mülhaupt, R. Biofunctional Rapid Prototyping for Tissue-Engineering Applications: 3D Bioplotting Versus 3D Printing. *J. Polym. Sci., Part A: Polym. Chem.* **2004**, *42*, 624−638.
(132) Ko, D. Y.; Shinde, U. P.; Yeon, B.; Jeong, B. Recent Progress of in Situ Formed Gels for Biomedical Applications. *Prog. Polym. Sci.* **2013**, *38*, 672−701.
(133) Yang, J.-A.; Yeom, J.; Hwang, B. W.; Hoffman, A. S.; Hahn, S. K. In Situ-Forming Injectable Hydrogels for Regenerative Medicine. *Prog. Polym. Sci.* **2014**, *39*, 1973−1986.
(134) Bakaic, E.; Smeets, N. M. B.; Hoare, T. Injectable Hydrogels Based on Poly(Ethylene Glycol) and Derivatives as Functional Biomaterials. *RSC Adv.* **2015**, *5*, 35469−35486.
(135) Nicodemus, G. D.; Bryant, S. J. Cell Encapsulation in Biodegradable Hydrogels for Tissue Engineering Applications. *Tissue Eng., Part B* **2008**, *14*, 149−165.
(136) Lutolf, M. P.; Hubbell, J. A. Synthetic Biomaterials as Instructive Extracellular Microenvironments for Morphogenesis in Tissue Engineering. *Nat. Biotechnol.* **2005**, *23*, 47−55.
(137) Cui, X.; Breitenkamp, K.; Finn, M. G.; Lotz, M.; D'Lima, D. D. Direct Human Cartilage Repair Using Three-Dimensional Bioprinting Technology. *Tissue Eng., Part A* **2012**, *18*, 1304−1312.
(138) Maher, P. S.; Keatch, R. P.; Donnelly, K.; Mackay, R. E.; Paxton, J. Z. Construction of 3D Biological Matrices using Rapid Prototyping Technology. *Rapid Prototyping J.* **2009**, *15*, 204−210.
(139) Guo, M.; Jiang, M.; Pispas, S.; Yu, W.; Zhou, C. Supramolecular Hydrogels Made of End-Functionalized Low-Molecular-Weight PEG and α-Cyclodextrin and their Hybridization with SiO_2 Nanoparticles through Host−Guest Interaction. *Macromolecules* **2008**, *41*, 9744−9749.
(140) Rutz, A. L.; Hyland, K. E.; Jakus, A. E.; Burghardt, W. R.; Shah, R. N. A Multimaterial Bioink Method for 3D Printing Tunable, Cell-Compatible Hydrogels. *Adv. Mater.* **2015**, *27*, 1607−1614.
(141) Pescosolido, L.; Schuurman, W.; Malda, J.; Matricardi, P.; Alhaique, F.; Coviello, T.; van Weeren, P. R.; Dhert, W. J. A.; Hennink, W. E.; Vermonden, T. Hyaluronic Acid and Dextran-Based Semi-IPN Hydrogels as Biomaterials for Bioprinting. *Biomacromolecules* **2011**, *12*, 1831−1838.
(142) Billiet, T.; Gevaert, E.; De Schryver, T.; Cornelissen, M.; Dubruel, P. The 3D Printing of Gelatin Methacrylamide Cell-Laden Tissue-Engineered Constructs with High Cell Viability. *Biomaterials* **2014**, *35*, 49−62.
(143) Gurkan, U. A.; El Assal, R.; Yildiz, S. E.; Sung, Y.; Trachtenberg, A. J.; Kuo, W. P.; Demirci, U. Engineering Anisotropic Biomimetic Fibrocartilage Microenvironment by Bioprinting Mesenchymal Stem Cells in Nanoliter Gel Droplets. *Mol. Pharmaceutics* **2014**, *11*, 2151−2159.
(144) Hockaday, L.; Kang, K.; Colangelo, N.; Cheung, P.; Duan, B.; Malone, E.; Wu, J.; Girardi, L.; Bonassar, L.; Lipson, H.; et al. Rapid 3D Printing of Anatomically Accurate and Mechanically Heterogeneous Aortic Valve Hydrogel Scaffolds. *Biofabrication* **2012**, *4*, 035005.
(145) Gao, G.; Yonezawa, T.; Hubbell, K.; Dai, G.; Cui, X. Inkjet-Bioprinted Acrylated Peptides and PEG Hydrogel with Human Mesenchymal Stem Cells Promote Robust Bone and Cartilage Formation with Minimal Printhead Clogging. *Biotechnol. J.* **2015**, DOI: 10.1002/biot.201400635.
(146) Skardal, A.; Zhang, J.; McCoard, L.; Xu, X.; Oottamasathien, S.; Prestwich, G. D. Photocrosslinkable Hyaluronan-Gelatin Hydrogels for Two-Step Bioprinting. *Tissue Eng., Part A* **2010**, *16*, 2675−2685.
(147) Fedorovich, N. E.; Swennen, I.; Girones, J.; Moroni, L.; van Blitterswijk, C. A.; Schacht, E.; Alblas, J.; Dhert, W. J. A. Evaluation of Photocrosslinked Lutrol Hydrogel for Tissue Printing Applications. *Biomacromolecules* **2009**, *10*, 1689−1696.
(148) Censi, R.; Schuurman, W.; Malda, J.; di Dato, G.; Burgisser, P. E.; Dhert, W. J. A.; van Nostrum, C. F.; di Martino, P.; Vermonden, T.;

DOI: 10.1021/acs.chemrev.5b00303
Chem. Rev. 2016, 116, 1496−1539

Hennink, W. E. A Printable Photopolymerizable Thermosensitive P(HPMAm-Lactate)-PEG Hydrogel for Tissue Engineering. *Adv. Funct. Mater.* **2011**, *21*, 1833−1842.
(149) Zhang, W.; Lian, Q.; Li, D.; Wang, K.; Hao, D.; Bian, W.; Jin, Z. The Effect of Interface Microstructure on Interfacial Shear Strength for Osteochondral Scaffolds Based on Biomimetic Design and 3D Printing. *Mater. Sci. Eng., C* **2015**, *46*, 10−15.
(150) Hoch, E.; Hirth, T.; Tovar, G. E. M.; Borchers, K. Chemical Tailoring of Gelatin to Adjust its Chemical and Physical Properties for Functional Bioprinting. *J. Mater. Chem. B* **2013**, *1*, 5675−5685.
(151) Skardal, A.; Zhang, J.; Prestwich, G. D. Bioprinting Vessel-Like Constructs using Hyaluronan Hydrogels Crosslinked with Tetrahedral Polyethylene Glycol Tetracrylates. *Biomaterials* **2010**, *31*, 6173−6181.
(152) Sasaki, J.-I.; Asoh, T.-A.; Matsumoto, T.; Egusa, H.; Sohmura, T.; Alsberg, E.; Akashi, M.; Yatani, H. Fabrication of Three-Dimensional Cell Constructs Using Temperature-Responsive Hydrogel. *Tissue Eng., Part A* **2010**, *16*, 2497−2504.
(153) Wang, X.; Yan, Y.; Pan, Y.; Xiong, Z.; Liu, H.; Cheng, J.; Liu, F.; Lin, F.; Wu, R.; Zhang, R.; et al. Generation of Three-Dimensional Hepatocyte/Gelatin Structures with Rapid Prototyping System. *Tissue Eng.* **2006**, *12*, 83−90.
(154) Zhang, T.; Yan, Y.; Wang, X.; Xiong, Z.; Lin, F.; Wu, R.; Zhang, R. Three-Dimensional Gelatin and Gelatin/Hyaluronan Hydrogel Structures for Traumatic Brain Injury. *J. Bioact. Compat. Polym.* **2007**, *22*, 19−29.
(155) Xu, M.; Wang, X.; Yan, Y.; Yao, R.; Ge, Y. An Cell-Assembly Derived Physiological 3D Model of the Metabolic Syndrome, Based on Adipose-Derived Stromal Cells and a Gelatin/Alginate/Fibrinogen Matrix. *Biomaterials* **2010**, *31*, 3868−3877.
(156) Li, S.; Xiong, Z.; Wang, X.; Yan, Y.; Liu, H.; Zhang, R. Direct Fabrication of a Hybrid Cell/Hydrogel Construct by a Double-Nozzle Assembling Technology. *J. Bioact. Compat. Polym.* **2009**, *24*, 249−265.
(157) Yan, Y.; Wang, X.; Pan, Y.; Liu, H.; Cheng, J.; Xiong, Z.; Lin, F.; Wu, R.; Zhang, R.; Lu, Q. Fabrication of Viable Tissue-Engineered Constructs with 3D Cell-Assembly Technique. *Biomaterials* **2005**, *26*, 5864−5871.
(158) Xu, T.; Binder, K. W.; Albanna, M. Z.; Dice, D.; Zhao, W.; Yoo, J. J.; Atala, A. Hybrid Printing of Mechanically and Biologically Improved Constructs for Cartilage Tissue Engineering Applications. *Biofabrication* **2013**, *5*, 015001.
(159) Campos, D. F. D.; Blaeser, A.; Weber, M.; Jakel, J.; Neuss, S.; Jahnen-Dechent, W.; Fischer, H. Three-Dimensional Printing of Stem Cell-Laden Hydrogels Submerged in a Hydrophobic High-Density Fluid. *Biofabrication* **2013**, *5*, 015003.
(160) Visser, J.; Peters, B.; Burger, T. J.; Boomstra, J.; Dhert, W. J. A.; Melchels, F. P. W.; Malda, J. Biofabrication of Multi-Material Anatomically Shaped Tissue Constructs. *Biofabrication* **2013**, *5*, 035007.
(161) Bakarich, S. E.; in het Panhuis, M.; Beirne, S.; Wallace, G. G.; Spinks, G. M. Extrusion Printing of Ionic−Covalent Entanglement Hydrogels with High Toughness. *J. Mater. Chem. B* **2013**, *1*, 4939−4946.
(162) Hong, S.; Sycks, D.; Chan, H. F.; Lin, S.; Lopez, G. P.; Guilak, F.; Leong, K. W.; Zhao, X. 3D Printing of Highly Stretchable and Tough Hydrogels into Complex, Cellularized Structures. *Adv. Mater.* **2015**, *27*, 4035−4040.
(163) Wilson, A.; Gasparini, G.; Matile, S. Functional Systems with Orthogonal Dynamic Covalent Bonds. *Chem. Soc. Rev.* **2014**, *43*, 1948−1962.
(164) Rowan, S. J.; Cantrill, S. J.; Cousins, G. R.; Sanders, J. K.; Stoddart, J. F. Dynamic Covalent Chemistry. *Angew. Chem., Int. Ed.* **2002**, *41*, 898−952.
(165) Belowich, M. E.; Stoddart, J. F. Dynamic Imine Chemistry. *Chem. Soc. Rev.* **2012**, *41*, 2003−2024.
(166) Tan, H.; Chu, C. R.; Payne, K. A.; Marra, K. G. Injectable in Situ Forming Biodegradable Chitosan−Hyaluronic Acid Based Hydrogels for Cartilage Tissue Engineering. *Biomaterials* **2009**, *30*, 2499−2506.
(167) Zehnder, T.; Sarker, B.; Boccaccini, A. R.; Detsch, R. Evaluation of an Alginate-Gelatine Crosslinked Hydrogel for Bioplotting. *Biofabrication* **2015**, *7*, 025001.
(168) Meng, H.; Xiao, P.; Gu, J.; Wen, X.; Xu, J.; Zhao, C.; Zhang, J.; Chen, T. Self-Healable Macro-/Microscopic Shape Memory Hydrogels Based on Supramolecular Interactions. *Chem. Commun.* **2014**, *50*, 12277−12280.
(169) Singh, S.; Zilkowski, I.; Ewald, A.; Maurell-Lopez, T.; Albrecht, K.; Möller, M.; Groll, J. Mild Oxidation of Thiofunctional Polymers to Cytocompatible and Stimuli-Sensitive Hydrogels and Nanogels. *Macromol. Biosci.* **2013**, *13*, 470−482.
(170) Singh, S.; Topuz, F.; Hahn, K.; Albrecht, K.; Groll, J. Embedding of Active Proteins and Living Cells in Redox-Sensitive Hydrogels and Nanogels through Enzymatic Cross-Linking. *Angew. Chem., Int. Ed.* **2013**, *52*, 3000−3003.
(171) Lehn, J.-M. From Supramolecular Chemistry Towards Constitutional Dynamic Chemistry and Adaptive Chemistry. *Chem. Soc. Rev.* **2007**, *36*, 151−160.
(172) Seiffert, S.; Sprakel, J. Physical Chemistry of Supramolecular Polymer Networks. *Chem. Soc. Rev.* **2012**, *41*, 909−930.
(173) Qi, Z.; Schalley, C. A. Exploring Macrocycles in Functional Supramolecular Gels: From Stimuli Responsiveness to Systems Chemistry. *Acc. Chem. Res.* **2014**, *47*, 2222−2233.
(174) Tan, S.; Ladewig, K.; Fu, Q.; Blencowe, A.; Qiao, G. G. Cyclodextrin-Based Supramolecular Assemblies and Hydrogels: Recent Advances and Future Perspectives. *Macromol. Rapid Commun.* **2014**, *35*, 1166−1184.
(175) Yu, G.; Jie, K.; Huang, F. Supramolecular Amphiphiles Based on Host−Guest Molecular Recognition Motifs. *Chem. Rev.* **2015**, *115*, 7240−7303.
(176) Babu, S. S.; Praveen, V. K.; Ajayaghosh, A. Functional π-Gelators and their Applications. *Chem. Rev.* **2014**, *114*, 1973−2129.
(177) Rosen, B. M.; Wilson, C. J.; Wilson, D. A.; Peterca, M.; Imam, M. R.; Percec, V. Dendron-Mediated Self-Assembly, Disassembly, and Self-Organization of Complex Systems. *Chem. Rev.* **2009**, *109*, 6275−6540.
(178) Yang, L.; Tan, X.; Wang, Z.; Zhang, X. Supramolecular Polymers: Historical Development, Preparation, Characterization, and Functions. *Chem. Rev.* **2015**, *115*, 7196−7239.
(179) Aida, T.; Meijer, E. W.; Stupp, S. I. Functional Supramolecular Polymers. *Science* **2012**, *335*, 813−817.
(180) Noro, A.; Hayashi, M.; Matsushita, Y. Design and Properties of Supramolecular Polymer Gels. *Soft Matter* **2012**, *8*, 6416−6429.
(181) Yan, X.; Wang, F.; Zheng, B.; Huang, F. Stimuli-Responsive Supramolecular Polymeric Materials. *Chem. Soc. Rev.* **2012**, *41*, 6042−6065.
(182) Hart, L. R.; Harries, J. L.; Greenland, B. W.; Colquhoun, H. M.; Hayes, W. Healable Supramolecular Polymers. *Polym. Chem.* **2013**, *4*, 4860−4870.
(183) Herbst, F.; Döhler, D.; Michael, P.; Binder, W. H. Self-Healing Polymers via Supramolecular Forces. *Macromol. Rapid Commun.* **2013**, *34*, 203−220.
(184) Wei, Z.; Yang, J. H.; Zhou, J.; Xu, F.; Zrinyi, M.; Dussault, P. H.; Osada, Y.; Chen, Y. M. Self-Healing Gels Based on Constitutional Dynamic Chemistry and their Potential Applications. *Chem. Soc. Rev.* **2014**, *43*, 8114−8131.
(185) Li, Y.; Rodrigues, J.; Tomas, H. Injectable and Biodegradable Hydrogels: Gelation, Biodegradation and Biomedical Applications. *Chem. Soc. Rev.* **2012**, *41*, 2193−2221.
(186) Wang, H.; Heilshorn, S. C. Adaptable Hydrogel Networks with Reversible Linkages for Tissue Engineering. *Adv. Mater.* **2015**, *27*, 3717−3736.
(187) Casuso, P.; Perez-San Vicente, A.; Iribar, H.; Gutierrez-Rivera, A.; Izeta, A.; Loinaz, I.; Cabanero, G.; Grande, H.-J.; Odriozola, I.; Dupin, D. Aurophilically Cross-Linked "Dynamic" Hydrogels Mimicking Healthy Synovial Fluid Properties. *Chem. Commun.* **2014**, *50*, 15199−15201.
(188) Odriozola, I.; Loinaz, I.; Pomposo, J. A.; Grande, H. J. Gold-Glutathione Supramolecular Hydrogels. *J. Mater. Chem.* **2007**, *17*, 4843−4845.
(189) Aboudzadeh, M. A.; Muñoz, M. E.; Santamaría, A.; Marcilla, R.; Mecerreyes, D. Facile Synthesis of Supramolecular Ionic Polymers that

DOI: 10.1021/acs.chemrev.5b00303
Chem. Rev. 2016, 116, 1496−1539

Combine Unique Rheological, Ionic Conductivity, and Self-Healing Properties. *Macromol. Rapid Commun.* **2012**, *33*, 314−318.
(190) Weng, W.; Beck, J. B.; Jamieson, A. M.; Rowan, S. J. Understanding the Mechanism of Gelation and Stimuli-Responsive Nature of a Class of Metallo-Supramolecular Gels. *J. Am. Chem. Soc.* **2006**, *128*, 11663−11672.
(191) Dankers, P. Y. W.; Harmsen, M. C.; Brouwer, L. A.; Van Luyn, M. J. A.; Meijer, E. W. A Modular and Supramolecular Approach to Bioactive Scaffolds for Tissue Engineering. *Nat. Mater.* **2005**, *4*, 568−574.
(192) Teunissen, A. J. P.; Nieuwenhuizen, M. M. L.; Rodríguez-Llansola, F.; Palmans, A. R. A.; Meijer, E. W. Mechanically Induced Gelation of a Kinetically Trapped Supramolecular Polymer. *Macromolecules* **2014**, *47*, 8429−8436.
(193) Bastings, M. M. C.; Koudstaal, S.; Kieltyka, R. E.; Nakano, Y.; Pape, A. C. H.; Feyen, D. A. M.; van Slochteren, F. J.; Doevendans, P. A.; Sluijter, J. P. G.; Meijer, E. W.; et al. A Fast pH-Switchable and Self-Healing Supramolecular Hydrogel Carrier for Guided, Local Catheter Injection in the Infarcted Myocardium. *Adv. Healthcare Mater.* **2014**, *3*, 70−78.
(194) Herbst, F.; Seiffert, S.; Binder, W. H. Dynamic Supramolecular Poly(Isobutylene)s for Self-Healing Materials. *Polym. Chem.* **2012**, *3*, 3084−3092.
(195) Chen, J.; Yan, X.; Zhao, Q.; Li, L.; Huang, F. Adjustable Supramolecular Polymer Microstructures Fabricated by the Breath Figure Method. *Polym. Chem.* **2012**, *3*, 458−462.
(196) Yan, X.; Xu, D.; Chen, J.; Zhang, M.; Hu, B.; Yu, Y.; Huang, F. A Self-Healing Supramolecular Polymer Gel with Stimuli-Responsiveness Constructed by Crown Ether Based Molecular Recognition. *Polym. Chem.* **2013**, *4*, 3312−3322.
(197) Chen, J.; Yan, X.; Chi, X.; Wu, X.; Zhang, M.; Han, C.; Hu, B.; Yu, Y.; Huang, F. Dual-Responsive Crown Ether-Based Supramolecular Chain Extended Polymers. *Polym. Chem.* **2012**, *3*, 3175−3179.
(198) Gao, L.; Xu, D.; Zheng, B. Construction of Supramolecular Organogels and Hydrogels from Crown Ether Based Unsymmetric Bolaamphiphiles. *Chem. Commun.* **2014**, *50*, 12142−12145.
(199) Zhan, J.; Zhang, M.; Zhou, M.; Liu, B.; Chen, D.; Liu, Y.; Chen, Q.; Qiu, H.; Yin, S. A Multiple-Responsive Self-Healing Supramolecular Polymer Gel Network Based on Multiple Orthogonal Interactions. *Macromol. Rapid Commun.* **2014**, *35*, 1424−1429.
(200) Zhang, Y.; Shi, B.; Li, H.; Qu, W.; Gao, G.; Lin, Q.; Yao, H.; Wei, T. Copillar[5]Arene-Based Supramolecular Polymer Gels. *Polym. Chem.* **2014**, *5*, 4722−4725.
(201) Shi, B.; Xia, D.; Yao, Y. A Water-Soluble Supramolecular Polymer Constructed by Pillar[5]Arene-Based Molecular Recognition. *Chem. Commun.* **2014**, *50*, 13932−13935.
(202) Song, S.; Wang, J.; Feng, H.-T.; Zhu, Z.-H.; Zheng, Y.-S. Supramolecular Hydrogel Based on Amphiphilic Calix[4]Arene and its Application in the Synthesis of Silica Nanotubes. *RSC Adv.* **2014**, *4*, 24909−24913.
(203) Burattini, S.; Colquhoun, H. M.; Fox, J. D.; Friedmann, D.; Greenland, B. W.; Harris, P. J. F.; Hayes, W.; Mackay, M. E.; Rowan, S. J. A Self-Repairing, Supramolecular Polymer System: Healability as a Consequence of Donor-Acceptor π-π Stacking Interactions. *Chem. Commun.* **2009**, 6717−6719.
(204) Harries, J.; Clifton, A.; Colquhoun, H.; Hayes, W.; Hart, L. WO Patent 2014111722 A1, 2014.
(205) Lange, S. C.; Unsleber, J.; Drucker, P.; Galla, H.-J.; Waller, M. P.; Ravoo, B. J. pH Response and Molecular Recognition in a Low Molecular Weight Peptide Hydrogel. *Org. Biomol. Chem.* **2015**, *13*, 561−569.
(206) Hirst, A. R.; Roy, S.; Arora, M.; Das, A. K.; Hodson, N.; Murray, P.; Marshall, S.; Javid, N.; Sefcik, J.; Boekhoven, J.; et al. Biocatalytic Induction of Supramolecular Order. *Nat. Chem.* **2010**, *2*, 1089−1094.
(207) Smith, A. M.; Williams, R. J.; Tang, C.; Coppo, P.; Collins, R. F.; Turner, M. L.; Saiani, A.; Ulijn, R. V. Fmoc-Diphenylalanine Self Assembles to a Hydrogel via a Novel Architecture Based on π−π Interlocked β-Sheets. *Adv. Mater.* **2008**, *20*, 37−41.
(208) Xie, Z.; Zhang, A.; Ye, L.; Wang, X.; Feng, Z.-g. Shear-Assisted Hydrogels Based on Self-Assembly of Cyclic Dipeptide Derivatives. *J. Mater. Chem.* **2009**, *19*, 6100−6102.
(209) Bernet, A.; Behr, M.; Schmidt, H.-W. Supramolecular Nanotube-Based Fiber Mats by Self-Assembly of a Tailored Amphiphilic Low Molecular Weight Hydrogelator. *Soft Matter* **2011**, *7*, 1058−1065.
(210) Bernet, A.; Behr, M.; Schmidt, H.-W. Supramolecular Hydrogels Based on Antimycobacterial Amphiphiles. *Soft Matter* **2012**, *8*, 4873−4876.
(211) Decoppet, J.-D.; Moehl, T.; Babkair, S. S.; Alzubaydi, R. A.; Ansari, A. A.; Habib, S. S.; Zakeeruddin, S. M.; Schmidt, H.-W.; Gratzel, M. Molecular Gelation of Ionic Liquid-Sulfolane Mixtures, a Solid Electrolyte for High Performance Dye-Sensitized Solar Cells. *J. Mater. Chem. A* **2014**, *2*, 15972−15977.
(212) Lin, Q.; Yang, Q.-P.; Sun, B.; Fu, Y.-P.; Zhu, X.; Wei, T.-B.; Zhang, Y.-M. Competitive Coordination Control of the AIE and Micro States of Supramolecular Gel: An Efficient Approach for Reversible Dual-Channel Stimuli-Response Materials. *Soft Matter* **2014**, *10*, 8427−8432.
(213) Stone, D. A.; Hsu, L.; Stupp, S. I. Self-Assembling Quinquethiophene−Oligopeptide Hydrogelators. *Soft Matter* **2009**, *5*, 1990−1993.
(214) Awad, H. A.; Wickham, M. Q.; Leddy, H. A.; Gimble, J. M.; Guilak, F. Chondrogenic Differentiation of Adipose-Derived Adult Stem Cells in Agarose, Alginate, and Gelatin Scaffolds. *Biomaterials* **2004**, *25*, 3211−3222.
(215) Tan, H. P.; Gong, Y. H.; Lao, L. H.; Mao, Z. W.; Gao, C. Y. Gelatin/Chitosan/Hyaluronan Ternary Complex Scaffold Containing Basic Fibroblast Growth Factor for Cartilage Tissue Engineering. *J. Mater. Sci.: Mater. Med.* **2007**, *18*, 1961−1968.
(216) Kirchmajer, D.; Gorkin, R., III; in het Panhuis, M. An Overview of the Suitability of Hydrogel-Forming Polymers for Extrusion-Based 3D-Printing. *J. Mater. Chem. B* **2015**, *3*, 4105−4117.
(217) Thiele, J.; Ma, Y. J.; Bruekers, S. M. C.; Ma, S. H.; Huck, W. T. S. 25th Anniversary Article: Designer Hydrogels for Cell Cultures: A Materials Selection Guide. *Adv. Mater.* **2014**, *26*, 125−148.
(218) Draget, K. I.; Stokke, B. T.; Yuguchi, Y.; Urakawa, H.; Kajiwara, K. Small-Angle X-Ray Scattering and Rheological Characterization of Alginate Gels. 3. Alginic Acid Gels. *Biomacromolecules* **2003**, *4*, 1661−1668.
(219) Jia, J.; Richards, D. J.; Pollard, S.; Tan, Y.; Rodriguez, J.; Visconti, R. P.; Trusk, T. C.; Yost, M. J.; Yao, H.; Markwald, R. R.; Mei, Y. Engineering Alginate as Bioink for Bioprinting. *Acta Biomater.* **2014**, *10*, 4323−4331.
(220) Shoichet, M. S.; Li, R. H.; White, M. L.; Winn, S. R. Stability of Hydrogels used in Cell Encapsulation: An in Vitro Comparison of Alginate and Agarose. *Biotechnol. Bioeng.* **1996**, *50*, 374−381.
(221) Fedorovich, N. E.; Schuurman, W.; Wijnberg, H. M.; Prins, H. J.; van Weeren, P. R.; Malda, J.; Alblas, J.; Dhert, W. J. A. Biofabrication of Osteochondral Tissue Equivalents by Printing Topologically Defined, Cell-Laden Hydrogel Scaffolds. *Tissue Eng., Part C* **2012**, *18*, 33−44.
(222) Fedorovich, N. E.; De Wijn, J. R.; Verbout, A. J.; Alblas, J.; Dhert, W. J. A. Three-Dimensional Fiber Deposition of Cell-Laden, Viable, Patterned Constructs for Bone Tissue Printing. *Tissue Eng., Part A* **2008**, *14*, 127−133.
(223) Catros, S.; Guillemot, F.; Nandakumar, A.; Ziane, S.; Moroni, L.; Habibovic, P.; van Blitterswijk, C.; Rousseau, B.; Chassande, O.; Amedee, J.; et al. Layer-by-Layer Tissue Microfabrication Supports Cell Proliferation in Vitro and in Vivo. *Tissue Eng., Part C* **2012**, *18*, 62−70.
(224) Song, S.-J.; Choi, J.; Park, Y.-D.; Hong, S.; Lee, J. J.; Ahn, C. B.; Choi, H.; Sun, K. Sodium Alginate Hydrogel-Based Bioprinting using a Novel Multinozzle Bioprinting System. *Artif. Organs* **2011**, *35*, 1132−1136.
(225) Arai, K.; Iwanaga, S.; Toda, H.; Genci, C.; Nishiyama, Y.; Nakamura, M. Three-Dimensional Inkjet Biofabrication Based on Designed Images. *Biofabrication* **2011**, *3*, 034113.
(226) Cohen, D. L.; Malone, E.; Lipson, H.; Bonassar, L. J. Direct Freeform Fabrication of Seeded Hydrogels in Arbitrary Geometries. *Tissue Eng.* **2006**, *12*, 1325−1335.

DOI: 10.1021/acs.chemrev.5b00303
Chem. Rev. 2016, 116, 1496−1539

(227) Lee, H.; Ahn, S.; Bonassar, L. J.; Kim, G. Cell(MC3T3-E1)-Printed Poly(ϵ-Caprolactone)/Alginate Hybrid Scaffolds for Tissue Regeneration. *Macromol. Rapid Commun.* **2013**, *34*, 142−149.
(228) Shim, J.-H.; Lee, J.-S.; Kim, J. Y.; Cho, D.-W. Bioprinting of a Mechanically Enhanced Three-Dimensional Dual Cell-Laden Construct for Osteochondral Tissue Engineering using a Multi-Head Tissue/Organ Building System. *J. Micromech. Microeng.* **2012**, *22*, 085014.
(229) Cohen, D. L.; Lipton, J. I.; Bonassar, L. J.; Lipson, H. Additive Manufacturing for in Situ Repair of Osteochondral Defects. *Biofabrication* **2010**, *2*, 035004.
(230) Zhang, Y.; Yu, Y.; Chen, H.; Ozbolat, I. T. Characterization of Printable Cellular Micro-Fluidic Channels for Tissue Engineering. *Biofabrication* **2013**, *5*, 025004.
(231) Pataky, K.; Braschler, T.; Negro, A.; Renaud, P.; Lutolf, M. P.; Brugger, J. Microdrop Printing of Hydrogel Bioinks into 3D Tissue-Like Geometries. *Adv. Mater.* **2012**, *24*, 391−396.
(232) Yan, J.; Huang, Y.; Chrisey, D. B. Laser-Assisted Printing of Alginate Long Tubes and Annular Constructs. *Biofabrication* **2013**, *5*, 015002.
(233) Markstedt, K.; Mantas, A.; Tournier, I.; Martínez Ávila, H.; Hägg, D.; Gatenholm, P. 3D Bioprinting Human Chondrocytes with Nanocellulose−Alginate Bioink for Cartilage Tissue Engineering Applications. *Biomacromolecules* **2015**, *16*, 1489−1496.
(234) Fedorovich, N. E.; Alblas, J.; de Wijn, J. R.; Hennink, W. E.; Verbout, A. J.; Dhert, W. J. A. Hydrogels as Extracellular Matrices for Skeletal Tissue Engineering: State-of-the-Art and Novel Application in Organ Printing. *Tissue Eng.* **2007**, *13*, 1905−1925.
(235) Kim, B. S.; Mooney, D. J. Development of Biocompatible Synthetic Extracellular Matrices for Tissue Engineering. *Trends Biotechnol.* **1998**, *16*, 224−230.
(236) Lee, K. Y.; Mooney, D. J. Alginate: Properties and Biomedical Applications. *Prog. Polym. Sci.* **2012**, *37*, 106−126.
(237) Cohen, D. L.; Lo, W.; Tsavaris, A.; Peng, D.; Lipson, H.; Bonassar, L. J. Increased Mixing Improves Hydrogel Homogeneity and Quality of Three-Dimensional Printed Constructs. *Tissue Eng., Part C* **2011**, *17*, 239−248.
(238) Xu, T.; Zhao, W.; Zhu, J.-M.; Albanna, M. Z.; Yoo, J. J.; Atala, A. Complex Heterogeneous Tissue Constructs Containing Multiple Cell Types Prepared by Inkjet Printing Technology. *Biomaterials* **2013**, *34*, 130−139.
(239) Zhao, Y.; Yao, R.; Ouyang, L.; Ding, H.; Zhang, T.; Zhang, K.; Cheng, S.; Sun, W. Three-Dimensional Printing of Hela Cells for Cervical Tumor Model in Vitro. *Biofabrication* **2014**, *6*, 035001.
(240) Duan, B.; Hockaday, L. A.; Kang, K. H.; Butcher, J. T. 3D Bioprinting of Heterogeneous Aortic Valve Conduits with Alginate/Gelatin Hydrogels. *J. Biomed. Mater. Res., Part A* **2013**, *101A*, 1255−1264.
(241) Wüst, S.; Godla, M. E.; Muller, R.; Hofmann, S. Tunable Hydrogel Composite with Two-Step Processing in Combination with Innovative Hardware Upgrade for Cell-Based Three-Dimensional Bioprinting. *Acta Biomater.* **2014**, *10*, 630−640.
(242) Tan, H. P.; Marra, K. G. Injectable, Biodegradable Hydrogels for Tissue Engineering Applications. *Materials* **2010**, *3*, 1746−1767.
(243) Cheng, J.; Lin, F.; Liu, H.; Yan, Y.; Wang, X.; Zhang, R.; Xiong, Z. Rheological Properties of Cell-Hydrogel Composites Extruding through Small-Diameter Tips. *J. Manuf. Sci., Trans. ASME* **2008**, *130*, 021014.
(244) Landers, R.; Hübner, U.; Schmelzeisen, R.; Mülhaupt, R. Rapid Prototyping of Scaffolds Derived from Thermoreversible Hydrogels and Tailored for Applications in Tissue Engineering. *Biomaterials* **2002**, *23*, 4437−4447.
(245) Mauck, R. L.; Soltz, M. A.; Wang, C. C. B.; Wong, D. D.; Chao, P. H. G.; Valhmu, W. B.; Hung, C. T.; Ateshian, G. A. Functional Tissue Engineering of Articular Cartilage through Dynamic Loading of Chondrocyte-Seeded Agarose Gels. *J. Biomech. Eng., Trans. ASME* **2000**, *122*, 252−260.
(246) Landers, R.; Pfister, A.; Hübner, U.; John, H.; Schmelzeisen, R.; Mülhaupt, R. Fabrication of Soft Tissue Engineering Scaffolds by Means of Rapid Prototyping Techniques. *J. Mater. Sci.* **2002**, *37*, 3107−3116.
(247) Norotte, C.; Marga, F. S.; Niklason, L. E.; Forgacs, G. Scaffold-Free Vascular Tissue Engineering using Bioprinting. *Biomaterials* **2009**, *30*, 5910−5917.
(248) Duarte Campos, D. F.; Blaeser, A.; Korsten, A.; Neuss, S.; Jakel, J.; Vogt, M.; Fischer, H. The Stiffness and Structure of Three-Dimensional Printed Hydrogels Direct the Differentiation of Mesenchymal Stromal Cells toward Adipogenic and Osteogenic Lineages. *Tissue Eng., Part A* **2015**, *21*, 740−756.
(249) Mano, J. F.; Silva, G. A.; Azevedo, H. S.; Malafaya, P. B.; Sousa, R. A.; Silva, S. S.; Boesel, L. F.; Oliveira, J. M.; Santos, T. C.; Marques, A. P.; Neves, N. M.; Reis, R. L. Natural Origin Biodegradable Systems in Tissue Engineering and Regenerative Medicine: Present Status and Some Moving Trends. *J. R. Soc., Interface* **2007**, *4*, 999−1030.
(250) Czaja, W. K.; Young, D. J.; Kawecki, M.; Brown, R. M. The Future Prospects of Microbial Cellulose in Biomedical Applications. *Biomacromolecules* **2007**, *8*, 1−12.
(251) Burdick, J. A.; Prestwich, G. D. Hyaluronic Acid Hydrogels for Biomedical Applications. *Adv. Mater.* **2011**, *23*, H41−H56.
(252) Highley, C. B.; Rodell, C. B.; Burdick, J. A. Direct 3D Printing of Shear-Thinning Hydrogels into Self-Healing Hydrogels. *Adv. Mater.* **2015**, *27*, 5075−5079.
(253) Ferris, C. J.; Gilmore, K. J.; Beirne, S.; McCallum, D.; Wallace, G. G.; in het Panhuis, M. Bio-Ink for on-Demand Printing of Living Cells. *Biomater. Sci.* **2013**, *1*, 224−230.
(254) Du, H. W.; Hamilton, P.; Reilly, M.; Ravi, N. Injectable in Situ Physically and Chemically Crosslinkable Gellan Hydrogel. *Macromol. Biosci.* **2012**, *12*, 952−961.
(255) Oliveira, J. T.; Martins, L.; Picciochi, R.; Malafaya, I. B.; Sousa, R. A.; Neves, N. M.; Mano, J. F.; Reis, R. L. Gellan Gum: A New Biomaterial for Cartilage Tissue Engineering Applications. *J. Biomed. Mater. Res., Part A* **2010**, *93A*, 852−863.
(256) Matricardi, P.; Cencetti, C.; Ria, R.; Alhaique, F.; Coviello, T. Preparation and Characterization of Novel Gellan Gum Hydrogels Suitable for Modified Drug Release. *Molecules* **2009**, *14*, 3376−3391.
(257) Moon, S.; Hasan, S. K.; Song, Y. S.; Xu, F.; Keles, H. O.; Manzur, F.; Mikkilineni, S.; Hong, J. W.; Nagatomi, J.; Haeggstrom, E.; et al. Layer by Layer Three-Dimensional Tissue Epitaxy by Cell-Laden Hydrogel Droplets. *Tissue Eng., Part C* **2010**, *16*, 157−166.
(258) Parenteau-Bareil, R.; Gauvin, R.; Berthod, F. Collagen-Based Biomaterials for Tissue Engineering Applications. *Materials* **2010**, *3*, 1863−1887.
(259) Lee, W.; Lee, V.; Polio, S.; Keegan, P.; Lee, J.-H.; Fischer, K.; Park, J.-K.; Yoo, S.-S. On-Demand Three-Dimensional Freeform Fabrication of Multi-Layered Hydrogel Scaffold with Fluidic Channels. *Biotechnol. Bioeng.* **2010**, *105*, 1178−1186.
(260) Shim, J.-H.; Kim, J. Y.; Park, M.; Park, J.; Cho, D.-W. Development of a Hybrid Scaffold with Synthetic Biomaterials and Hydrogel using Solid Freeform Fabrication Technology. *Biofabrication* **2011**, *3*, 034102.
(261) Jakab, K.; Norotte, C.; Damon, B.; Marga, F.; Neagu, A.; Besch-Williford, C. L.; Kachurin, A.; Church, K. H.; Park, H.; Mironov, V.; et al. Tissue Engineering by Self-Assembly of Cells Printed into Topologically Defined Structures. *Tissue Eng., Part A* **2008**, *14*, 413−421.
(262) Hersel, U.; Dahmen, C.; Kessler, H. RGD Modified Polymers: Biomaterials for Stimulated Cell Adhesion and Beyond. *Biomaterials* **2003**, *24*, 4385−4415.
(263) Hori, K.; Sotozono, C.; Hamuro, J.; Yamasaki, K.; Kimura, Y.; Ozeki, M.; Tabata, Y.; Kinoshita, S. Controlled-Release of Epidermal Growth Factor from Cationized Gelatin Hydrogel Enhances Corneal Epithelial Wound Healing. *J. Controlled Release* **2007**, *118*, 169−176.
(264) Xu, T.; Gregory, C. A.; Molnar, P.; Cui, X.; Jalota, S.; Bhaduri, S. B.; Boland, T. Viability and Electrophysiology of Neural Cell Structures Generated by the Inkjet Printing Method. *Biomaterials* **2006**, *27*, 3580−3588.
(265) Schense, J. C.; Hubbell, J. A. Cross-Linking Exogenous Bifunctional Peptides into Fibrin Gels with Factor XIIIa. *Bioconjugate Chem.* **1999**, *10*, 75−81.
(266) Cummings, C. L.; Gawlitta, D.; Nerem, R. M.; Stegemann, J. P. Properties of Engineered Vascular Constructs Made from Collagen,

DOI: 10.1021/acs.chemrev.5b00303
Chem. Rev. 2016, 116, 1496−1539

Fibrin, and Collagen-Fibrin Mixtures. *Biomaterials* **2004**, *25*, 3699−3706.
(267) Xu, H. T.; Fan, B. L.; Yu, S. Y.; Huang, Y. H.; Zhao, Z. H.; Lian, Z. X.; Dai, Y. P.; Wang, L. L.; Liu, Z. L.; Fei, J.; et al. Construct Synthetic Gene Encoding Artificial Spider Dragline Silk Protein and its Expression in Milk of Transgenic Mice. *Anim. Biotechnol.* **2007**, *18*, 1−12.
(268) Wang, X. H.; Yan, Y. N.; Zhang, R. J. Recent Trends and Challenges in Complex Organ Manufacturing. *Tissue Eng., Part B* **2010**, *16*, 189−197.
(269) Janmey, P. A.; Winer, J. P.; Weisel, J. W. Fibrin Gels and their Clinical and Bioengineering Applications. *J. R. Soc., Interface* **2009**, *6*, 1−10.
(270) Das, S.; Pati, F.; Chameettachal, S.; Pahwa, S.; Ray, A. R.; Dhara, S.; Ghosh, S. Enhanced Redifferentiation of Chondrocytes on Microperiodic Silk/Gelatin Scaffolds: Toward Tailor-Made Tissue Engineering. *Biomacromolecules* **2013**, *14*, 311−321.
(271) Das, S.; Pati, F.; Choi, Y.-J.; Rijal, G.; Shim, J.-H.; Kim, S. W.; Ray, A. R.; Cho, D.-W.; Ghosh, S. Bioprintable, Cell-Laden Silk Fibroin-Gelatin Hydrogel Supporting Multilineage Differentiation of Stem Cells for Fabrication of 3D Tissue Constructs. *Acta Biomater.* **2015**, *11*, 233−246.
(272) Kundu, B.; Rajkhowa, R.; Kundu, S. C.; Wang, X. G. Silk Fibroin Biomaterials for Tissue Regenerations. *Adv. Drug Delivery Rev.* **2013**, *65*, 457−470.
(273) Suntivich, R.; Drachuk, I.; Calabrese, R.; Kaplan, D. L.; Tsukruk, V. V. Inkjet Printing of Silk Nest Arrays for Cell Hosting. *Biomacromolecules* **2014**, *15*, 1428−1435.
(274) Wang, Y. Z.; Kim, H. J.; Vunjak-Novakovic, G.; Kaplan, D. L. Stem Cell-Based Tissue Engineering with Silk Biomaterials. *Biomaterials* **2006**, *27*, 6064−6082.
(275) Snyder, J.; Hamid, Q.; Wang, C.; Chang, R.; Emami, K.; Wu, H.; Sun, W. Bioprinting Cell-Laden Matrigel for Radioprotection Study of Liver by Pro-Drug Conversion in a Dual-Tissue Microfluidic Chip. *Biofabrication* **2011**, *3*, 034112.
(276) Arnott, S.; Fulmer, A.; Scott, W. E.; Dea, I. C. M.; Moorhouse, R.; Rees, D. A. Agarose Double Helix and its Function in Agarose-Gel Structure. *J. Mol. Biol.* **1974**, *90*, 269−284.
(277) Velasco, D.; Tumarkin, E.; Kumacheva, E. Microfluidic Encapsulation of Cells in Polymer Microgels. *Small* **2012**, *8*, 1633−1642.
(278) Normand, V.; Lootens, D. L.; Amici, E.; Plucknett, K. P.; Aymard, P. New Insight into Agarose Gel Mechanical Properties. *Biomacromolecules* **2000**, *1*, 730−738.
(279) Chen, Q.; Zhu, L.; Chen, H.; Yan, H.; Huang, L.; Yang, J.; Zheng, J. A Novel Design Strategy for Fully Physically Linked Double Network Hydrogels with Tough, Fatigue Resistant, and Self-Healing Properties. *Adv. Funct. Mater.* **2015**, *25*, 1598−1607.
(280) Fialho, A. M.; Moreira, L. M.; Granja, A. T.; Popescu, A. O.; Hoffmann, K.; Sa-Correia, I. Occurrence, Production, and Applications of Gellan: Current State and Perspectives. *Appl. Microbiol. Biotechnol.* **2008**, *79*, 889−900.
(281) Freitas, F.; Alves, V. D.; Reis, M. A. M. Advances in Bacterial Exopolysaccharides: From Production to Biotechnological Applications. *Trends Biotechnol.* **2011**, *29*, 388−398.
(282) Khan, T.; Park, J. K.; Kwon, J. H. Functional Biopolymers Produced by Biochemical Technology Considering Applications in Food Engineering. *Korean J. Chem. Eng.* **2007**, *24*, 816−826.
(283) Miyoshi, E.; Takaya, T.; Nishinari, K. Gel-Sol Transition in Gellan Gum Solutions. I. Rheological Studies on the Effects of Salts. *Food Hydrocolloids* **1994**, *8*, 505−527.
(284) Harkness, R. D. Biological Functions of Collagen. *Biol. Rev.* **1961**, *36*, 399−455.
(285) Kadler, K. E.; Baldock, C.; Bella, J.; Boot-Handford, R. P. Collagens at a Glance. *J. Cell Sci.* **2007**, *120*, 1955−1958.
(286) Gomes, S.; Leonor, I. B.; Mano, J. F.; Reis, R. L.; Kaplan, D. L. Natural and Genetically Engineered Proteins for Tissue Engineering. *Prog. Polym. Sci.* **2012**, *37*, 1−17.
(287) Sheu, M. T.; Huang, J. C.; Yeh, G. C.; Ho, H. O. Characterization of Collagen Gel Solutions and Collagen Matrices for Cell Culture. *Biomaterials* **2001**, *22*, 1713−1719.
(288) Kim, J. A.; Kim, H. N.; Im, S.-K.; Chung, S.; Kang, J. Y.; Choi, N. Collagen-Based Brain Microvasculature Model in Vitro using Three-Dimensional Printed Template. *Biomicrofluidics* **2015**, *9*, 024115.
(289) Tan, H. P.; Huang, D. J.; Lao, L. H.; Gao, C. Y. RGD Modified PLGA/Gelatin Microspheres as Microcarriers for Chondrocyte Delivery. *J. Biomed. Mater. Res., Part B* **2009**, *91B*, 228−238.
(290) Choi, Y. S.; Hong, S. R.; Lee, Y. M.; Song, K. W.; Park, M. H.; Nam, Y. S. Study on Gelatin-Containing Artificial Skin: I. Preparation and Characteristics of Novel Gelatin-Alginate Sponge. *Biomaterials* **1999**, *20*, 409−417.
(291) Young, S.; Wong, M.; Tabata, Y.; Mikos, A. G. Gelatin as a Delivery Vehicle for the Controlled Release of Bioactive Molecules. *J. Controlled Release* **2005**, *109*, 256−274.
(292) Sisson, K.; Zhang, C.; Farach-Carson, M. C.; Chase, D. B.; Rabolt, J. F. Evaluation of Cross-Linking Methods for Electrospun Gelatin on Cell Growth and Viability. *Biomacromolecules* **2009**, *10*, 1675−1680.
(293) Kirchmajer, D. M.; Panhuis, M. i. h. Robust Biopolymer Based Ionic-Covalent Entanglement Hydrogels with Reversible Mechanical Behaviour. *J. Mater. Chem. B* **2014**, *2*, 4694−4702.
(294) Smith, G. F. Fibrinogen-Fibrin Conversion - Mechanism of Fibrin-Polymer Formation in Solution. *Biochem. J.* **1980**, *185*, 1−11.
(295) Zhao, W.; Jin, X.; Cong, Y.; Liu, Y. Y.; Fu, J. Degradable Natural Polymer Hydrogels for Articular Cartilage Tissue Engineering. *J. Chem. Technol. Biotechnol.* **2013**, *88*, 327−339.
(296) Ho, W.; Tawil, B.; Dunn, J. C. Y.; Wu, B. M. The Behavior of Human Mesenchymal Stem Cells in 3D Fibrin Clots: Dependence on Fibrinogen Concentration and Clot Structure. *Tissue Eng.* **2006**, *12*, 1587−1595.
(297) Drinnan, C. T.; Zhang, G.; Alexander, M. A.; Pulido, A. S.; Suggs, L. J. Multimodal Release of Transforming Growth Factor-β1 and the BB Isoform of Platelet Derived Growth Factor from PEGylated Fibrin Gels. *J. Controlled Release* **2010**, *147*, 180−186.
(298) Lee, Y. B.; Polio, S.; Lee, W.; Dai, G. H.; Menon, L.; Carroll, R. S.; Yoo, S. S. Bio-Printing of Collagen and VEGF-Releasing Fibrin Gel Scaffolds for Neural Stem Cell Culture. *Exp. Neurol.* **2010**, *223*, 645−652.
(299) Eyrich, D.; Brandl, F.; Appel, B.; Wiese, H.; Maier, G.; Wenzel, M.; Staudenmaier, R.; Goepferich, A.; Blunk, T. Long-Term Stable Fibrin Gels for Cartilage Engineering. *Biomaterials* **2007**, *28*, 55−65.
(300) Gosline, J. M.; Demont, M. E.; Denny, M. W. The Structure and Properties of Spider Silk. *Endeavour* **1986**, *10*, 37−43.
(301) Heidebrecht, A.; Scheibel, T. Recombinant Production of Spider Silk Proteins. *Adv. Appl. Microbiol.* **2013**, *82*, 115−153.
(302) Altman, G. H.; Diaz, F.; Jakuba, C.; Calabro, T.; Horan, R. L.; Chen, J. S.; Lu, H.; Richmond, J.; Kaplan, D. L. Silk-Based Biomaterials. *Biomaterials* **2003**, *24*, 401−416.
(303) Leal-Egana, A.; Scheibel, T. Silk-Based Materials for Biomedical Applications. *Biotechnol. Appl. Biochem.* **2010**, *55*, 155−167.
(304) Schacht, K.; Jüngst, T.; Schweinlin, M.; Ewald, A.; Groll, J.; Scheibel, T. Biofabrication of Cell-Loaded 3D Recombinant Spider Silk Constructs. *Angew. Chem., Int. Ed.* **2015**, *54*, 2816−2820.
(305) Schacht, K.; Scheibel, T. Processing of Recombinant Spider Silk Proteins into Tailor-Made Materials for Biomaterials Applications. *Curr. Opin. Biotechnol.* **2014**, *29*, 62−69.
(306) Langer, R.; Tirrell, D. A. Designing Materials for Biology and Medicine. *Nature* **2004**, *428*, 487−492.
(307) Romano, N. H.; Sengupta, D.; Chung, C.; Heilshorn, S. C. Protein-Engineered Biomaterials: Nanoscale Mimics of the Extracellular Matrix. *Biochim. Biophys. Acta, Gen. Subj.* **2011**, *1810*, 339−349.
(308) Li, C.; Faulkner-Jones, A.; Dun, A. R.; Jin, J.; Chen, P.; Xing, Y.; Yang, Z.; Li, Z.; Shu, W.; Liu, D.; et al. Rapid Formation of a Supramolecular Polypeptide−DNA Hydrogel for in Situ Three-Dimensional Multilayer Bioprinting. *Angew. Chem., Int. Ed.* **2015**, *54*, 3957−3961.

DOI: 10.1021/acs.chemrev.5b00303
Chem. Rev. 2016, 116, 1496−1539

(309) Li, C.; Chen, P.; Shao, Y.; Zhou, X.; Wu, Y.; Yang, Z.; Li, Z.; Weil, T.; Liu, D. A Writable Polypeptide−DNA Hydrogel with Rationally Designed Multi-Modification Sites. *Small* **2015**, *11*, 1138−1143.
(310) Hauser, C. A.; Loo, Y.; Lakshmanan, A.; Ni, M.; Toh, L. L.; Wang, S. Peptide Bioink: Self-Assembling Nanofibrous Scaffolds for 3D Organotypic Cultures. *Nano Lett.* **2015**, DOI: 10.1021/acs.nanolett.5b02859.
(311) Dasgupta, A.; Mondal, J. H.; Das, D. Peptide Hydrogels. *RSC Adv.* **2013**, *3*, 9117−9149.
(312) Apostolovic, B.; Danial, M.; Klok, H.-A. Coiled Coils: Attractive Protein Folding Motifs for the Fabrication of Self-Assembled, Responsive and Bioactive Materials. *Chem. Soc. Rev.* **2010**, *39*, 3541−3575.
(313) Sathaye, S.; Mbi, A.; Sonmez, C.; Chen, Y.; Blair, D. L.; Schneider, J. P.; Pochan, D. J. Rheology of Peptide- and Protein-Based Physical Hydrogels: Are Everyday Measurements Just Scratching the Surface? *Wiley Interdiscip. Rev.: Nanomed. Nanobiotechnol.* **2015**, *7*, 34−68.
(314) Chen, C.; Gu, Y.; Deng, L.; Han, S.; Sun, X.; Chen, Y.; Lu, J. R.; Xu, H. Tuning Gelation Kinetics and Mechanical Rigidity of β-Hairpin Peptide Hydrogels via Hydrophobic Amino Acid Substitutions. *ACS Appl. Mater. Interfaces* **2014**, *6*, 14360−14368.
(315) Haines-Butterick, L.; Rajagopal, K.; Branco, M.; Salick, D.; Rughani, R.; Pilarz, M.; Lamm, M. S.; Pochan, D. J.; Schneider, J. P. Controlling Hydrogelation Kinetics by Peptide Design for Three-Dimensional Encapsulation and Injectable Delivery of Cells. *Proc. Natl. Acad. Sci. U. S. A.* **2007**, *104*, 7791−7796.
(316) Schneider, J. P.; Pochan, D. J.; Ozbas, B.; Rajagopal, K.; Pakstis, L.; Kretsinger, J. Responsive Hydrogels from the Intramolecular Folding and Self-Assembly of a Designed Peptide. *J. Am. Chem. Soc.* **2002**, *124*, 15030−15037.
(317) Yan, C.; Altunbas, A.; Yucel, T.; Nagarkar, R. P.; Schneider, J. P.; Pochan, D. J. Injectable Solid Hydrogel: Mechanism of Shear-Thinning and Immediate Recovery of Injectable β-Hairpin Peptide Hydrogels. *Soft Matter* **2010**, *6*, 5143−5156.
(318) Rughani, R. V.; Branco, M. C.; Pochan, D. J.; Schneider, J. P. De Novo Design of a Shear-Thin Recoverable Peptide-Based Hydrogel Capable of Intrafibrillar Photopolymerization. *Macromolecules* **2010**, *43*, 7924−7930.
(319) Bakota, E. L.; Wang, Y.; Danesh, F. R.; Hartgerink, J. D. Injectable Multidomain Peptide Nanofiber Hydrogel as a Delivery Agent for Stem Cell Secretome. *Biomacromolecules* **2011**, *12*, 1651−1657.
(320) Huang, H. Z.; Shi, J. S.; Laskin, J.; Liu, Z. Y.; McVey, D. S.; Sun, X. Z. S. Design of a Shear-Thinning Recoverable Peptide Hydrogel from Native Sequences and Application for Influenza H1N1 Vaccine Adjuvant. *Soft Matter* **2011**, *7*, 8905−8912.
(321) Huang, H.; Herrera, A. I.; Luo, Z.; Prakash, O.; Sun, X. S. Structural Transformation and Physical Properties of a Hydrogel-Forming Peptide Studied by NMR, Transmission Electron Microscopy, and Dynamic Rheometer. *Biophys. J.* **2012**, *103*, 979−988.
(322) Tsurkan, M. V.; Chwalek, K.; Prokoph, S.; Zieris, A.; Levental, K. R.; Freudenberg, U.; Werner, C. Defined Polymer−Peptide Conjugates to Form Cell-Instructive starPEG−Heparin Matrices in Situ. *Adv. Mater.* **2013**, *25*, 2606−2610.
(323) Wieduwild, R.; Tsurkan, M.; Chwalek, K.; Murawala, P.; Nowak, M.; Freudenberg, U.; Neinhuis, C.; Werner, C.; Zhang, Y. Minimal Peptide Motif for Non-Covalent Peptide−Heparin Hydrogels. *J. Am. Chem. Soc.* **2013**, *135*, 2919−2922.
(324) Thompson, M. S.; Tsurkan, M. V.; Chwalek, K.; Bornhauser, M.; Schlierf, M.; Werner, C.; Zhang, Y. Self-Assembling Hydrogels Crosslinked Solely by Receptor−Ligand Interactions: Tunability, Rationalization of Physical Properties, and 3D Cell Culture. *Chem. - Eur. J.* **2015**, *21*, 3178−3182.
(325) Iwami, K.; Noda, T.; Ishida, K.; Morishima, K.; Nakamura, M.; Umeda, N. Bio Rapid Prototyping by Extruding/Aspirating/Refilling Thermoreversible Hydrogel. *Biofabrication* **2010**, *2*, 014108.
(326) Li, S.; Lu, H.-Y.; Shen, Y.; Chen, C.-F. A Stimulus-Response and Self-Healing Supramolecular Polymer Gel Based on Host−Guest Interactions. *Macromol. Chem. Phys.* **2013**, *214*, 1596−1601.
(327) Zhang, M.; Xu, D.; Yan, X.; Chen, J.; Dong, S.; Zheng, B.; Huang, F. Self-Healing Supramolecular Gels Formed by Crown Ether Based Host−Guest Interactions. *Angew. Chem., Int. Ed.* **2012**, *51*, 7011−7015.
(328) Rodell, C. B.; Kaminski, A. L.; Burdick, J. A. Rational Design of Network Properties in Guest-Host Assembled and Shear-Thinning Hyaluronic Acid Hydrogels. *Biomacromolecules* **2013**, *14*, 4125−4134.
(329) Rodell, C. B.; MacArthur, J. W.; Dorsey, S. M.; Wade, R. J.; Wang, L. L.; Woo, Y. J.; Burdick, J. A. Shear-Thinning Supramolecular Hydrogels with Secondary Autonomous Covalent Crosslinking to Modulate Viscoelastic Properties in Vivo. *Adv. Funct. Mater.* **2015**, *25*, 636−644.
(330) Himmelein, S.; Lewe, V.; Stuart, M. C. A.; Ravoo, B. J. A Carbohydrate-Based Hydrogel Containing Vesicles as Responsive Non-Covalent Cross-Linkers. *Chem. Sci.* **2014**, *5*, 1054−1058.
(331) Kato, K.; Yasuda, T.; Ito, K. Viscoelastic Properties of Slide-Ring Gels Reflecting Sliding Dynamics of Partial Chains and Entropy of Ring Components. *Macromolecules* **2013**, *46*, 310−316.
(332) Katsuno, C.; Konda, A.; Urayama, K.; Takigawa, T.; Kidowaki, M.; Ito, K. Pressure-Responsive Polymer Membranes of Slide-Ring Gels with Movable Cross-Links. *Adv. Mater.* **2013**, *25*, 4636−4640.
(333) Okumura, Y.; Ito, K. The Polyrotaxane Gel: A Topological Gel by Figure-of-Eight Cross-Links. *Adv. Mater.* **2001**, *13*, 485−487.
(334) Yu, J.; Fan, H.; Huang, J.; Chen, J. Fabrication and Evaluation of Reduction-Sensitive Supramolecular Hydrogel Based on Cyclodextrin/Polymer Inclusion for Injectable Drug-Carrier Application. *Soft Matter* **2011**, *7*, 7386−7394.
(335) Ma, D.; Zhang, L.-M. Supramolecular Gelation of a Polymeric Prodrug for its Encapsulation and Sustained Release. *Biomacromolecules* **2011**, *12*, 3124−3130.
(336) Liu, K. L.; Zhu, J.-l.; Li, J. Elucidating Rheological Property Enhancements in Supramolecular Hydrogels of Short Poly[(R,S)-3-Hydroxybutyrate]-Based Amphiphilic Triblock Copolymer and α-Cyclodextrin for Injectable Hydrogel Applications. *Soft Matter* **2010**, *6*, 2300−2311.
(337) Tian, Z.; Chen, C.; Allcock, H. R. Injectable and Biodegradable Supramolecular Hydrogels by Inclusion Complexation between Poly(Organophosphazenes) and α-Cyclodextrin. *Macromolecules* **2013**, *46*, 2715−2724.
(338) Wu, Y.; Guo, B.; Ma, P. X. Injectable Electroactive Hydrogels Formed via Host−Guest Interactions. *ACS Macro Lett.* **2014**, *3*, 1145−1150.
(339) Nakama, T.; Ooya, T.; Yui, N. Temperature-and pH-Controlled Hydrogelation of Poly (Ethylene Glycol)-Grafted Hyaluronic Acid by Inclusion Complexation with α-Cyclodextrin. *Polym. J.* **2004**, *36*, 338−344.
(340) Tomatsu, I.; Hashidzume, A.; Harada, A. Redox-Responsive Hydrogel System Using the Molecular Recognition of β-Cyclodextrin. *Macromol. Rapid Commun.* **2006**, *27*, 238−241.
(341) Loh, X. J. Supramolecular Host-Guest Polymeric Materials for Biomedical Applications. *Mater. Horiz.* **2014**, *1*, 185−195.
(342) Park, K. M.; Yang, J.-A.; Jung, H.; Yeom, J.; Park, J. S.; Park, K.-H.; Hoffman, A. S.; Hahn, S. K.; Kim, K. In Situ Supramolecular Assembly and Modular Modification of Hyaluronic Acid Hydrogels for 3D Cellular Engineering. *ACS Nano* **2012**, *6*, 2960−2968.
(343) Appel, E. A.; Loh, X. J.; Jones, S. T.; Biedermann, F.; Dreiss, C. A.; Scherman, O. A. Ultrahigh-Water-Content Supramolecular Hydrogels Exhibiting Multistimuli Responsiveness. *J. Am. Chem. Soc.* **2012**, *134*, 11767−11773.
(344) Cross, D.; Jiang, X.; Ji, W.; Han, W.; Wang, C. Injectable Hybrid Hydrogels of Hyaluronic Acid Crosslinked by Well-Defined Synthetic Polycations: Preparation and Characterization in Vitro and in Vivo. *Macromol. Biosci.* **2015**, *15*, 668−681.
(345) Hunt, J. N.; Feldman, K. E.; Lynd, N. A.; Deek, J.; Campos, L. M.; Spruell, J. M.; Hernandez, B. M.; Kramer, E. J.; Hawker, C. J. Tunable, High Modulus Hydrogels Driven by Ionic Coacervation. *Adv. Mater.* **2011**, *23*, 2327−2331.

DOI: 10.1021/acs.chemrev.5b00303
Chem. Rev. 2016, 116, 1496−1539

(346) Wang, Q.; Wang, L.; Detamore, M. S.; Berkland, C. Biodegradable Colloidal Gels as Moldable Tissue Engineering Scaffolds. *Adv. Mater.* **2008**, *20*, 236−239.
(347) Bünsow, J.; Erath, J.; Biesheuvel, P. M.; Fery, A.; Huck, W. T. S. Direct Correlation between Local Pressure and Fluorescence Output in Mechanoresponsive Polyelectrolyte Brushes. *Angew. Chem., Int. Ed.* **2011**, *50*, 9629−9632.
(348) Sun, T. L.; Kurokawa, T.; Kuroda, S.; Ihsan, A. B.; Akasaki, T.; Sato, K.; Haque, M. A.; Nakajima, T.; Gong, J. P. Physical Hydrogels Composed of Polyampholytes Demonstrate High Toughness and Viscoelasticity. *Nat. Mater.* **2013**, *12*, 932−937.
(349) Luo, F.; Sun, T. L.; Nakajima, T.; Kurokawa, T.; Zhao, Y.; Sato, K.; Ihsan, A. B.; Li, X.; Guo, H.; Gong, J. P. Oppositely Charged Polyelectrolytes Form Tough, Self-Healing, and Rebuildable Hydrogels. *Adv. Mater.* **2015**, *27*, 2722−2727.
(350) Xu, D.; Liu, C.-Y.; Craig, S. L. Divergent Shear Thinning and Shear Thickening Behavior of Supramolecular Polymer Networks in Semidilute Entangled Polymer Solutions. *Macromolecules* **2011**, *44*, 2343−2353.
(351) Xu, D.; Craig, S. L. Scaling Laws in Supramolecular Polymer Networks. *Macromolecules* **2011**, *44*, 5465−5472.
(352) Jackson, A. C.; Beyer, F. L.; Price, S. C.; Rinderspacher, B. C.; Lambeth, R. H. Role of Metal−Ligand Bond Strength and Phase Separation on the Mechanical Properties of Metallopolymer Films. *Macromolecules* **2013**, *46*, 5416−5422.
(353) Jackson, A. C.; Walck, S. D.; Strawhecker, K. E.; Butler, B. G.; Lambeth, R. H.; Beyer, F. L. Metallopolymers Containing Excess Metal−Ligand Complex for Improved Mechanical Properties. *Macromolecules* **2014**, *47*, 4144−4150.
(354) Lewis, C. L.; Stewart, K.; Anthamatten, M. The Influence of Hydrogen Bonding Side-Groups on Viscoelastic Behavior of Linear and Network Polymers. *Macromolecules* **2014**, *47*, 729−740.
(355) Vatankhah-Varnoosfaderani, M.; GhavamiNejad, A.; Hashmi, S.; Stadler, F. J. Hydrogen Bonding in Aprotic Solvents, a New Strategy for Gelation of Bioinspired Catecholic Copolymers with N-Isopropylamide. *Macromol. Rapid Commun.* **2015**, *36*, 447−452.
(356) Hackelbusch, S.; Rossow, T.; van Assenbergh, P.; Seiffert, S. Chain Dynamics in Supramolecular Polymer Networks. *Macromolecules* **2013**, *46*, 6273−6286.
(357) Fan, J.; Zou, J.; He, X.; Zhang, F.; Zhang, S.; Raymond, J. E.; Wooley, K. L. Tunable Mechano-Responsive Organogels by Ring-Opening Copolymerizations of N-Carboxyanhydrides. *Chem. Sci.* **2014**, *5*, 141−150.
(358) Ji, X.; Jie, K.; Zimmerman, S. C.; Huang, F. A Double Supramolecular Crosslinked Polymer Gel Exhibiting Macroscale Expansion and Contraction Behavior and Multistimuli Responsiveness. *Polym. Chem.* **2015**, *6*, 1912−1917.
(359) Appel, E. A.; Tibbitt, M. W.; Webber, M. J.; Mattix, B. A.; Veiseh, O.; Langer, R. Self-Assembled Hydrogels Utilizing Polymer-Nanoparticle Interactions. *Nat. Commun.* **2015**, *6*, 6295.
(360) Haraguchi, K.; Farnworth, R.; Ohbayashi, A.; Takehisa, T. Compositional Effects on Mechanical Properties of Nanocomposite Hydrogels Composed of Poly(N,N-Dimethylacrylamide) and Clay. *Macromolecules* **2003**, *36*, 5732−5741.
(361) Wang, Q.; Mynar, J. L.; Yoshida, M.; Lee, E.; Lee, M.; Okuro, K.; Kinbara, K.; Aida, T. High-Water-Content Mouldable Hydrogels by Mixing Clay and a Dendritic Molecular Binder. *Nature* **2010**, *463*, 339−343.
(362) Tamesue, S.; Ohtani, M.; Yamada, K.; Ishida, Y.; Spruell, J. M.; Lynd, N. A.; Hawker, C. J.; Aida, T. Linear Versus Dendritic Molecular Binders for Hydrogel Network Formation with Clay Nanosheets: Studies with ABA Triblock Copolyethers Carrying Guanidinium Ion Pendants. *J. Am. Chem. Soc.* **2013**, *135*, 15650−15655.
(363) Wu, L.; Ohtani, M.; Tamesue, S.; Ishida, Y.; Aida, T. High Water Content Clay−Nanocomposite Hydrogels Incorporating Guanidinium-Pendant Methacrylamide: Tuning of Mechanical and Swelling Properties by Supramolecular Approach. *J. Polym. Sci., Part A: Polym. Chem.* **2014**, *52*, 839−847.
(364) Gaharwar, A. K.; Avery, R. K.; Assmann, A.; Paul, A.; McKinley, G. H.; Khademhosseini, A.; Olsen, B. D. Shear-Thinning Nanocomposite Hydrogels for the Treatment of Hemorrhage. *ACS Nano* **2014**, *8*, 9833−9842.
(365) Tan, Z.; Ohara, S.; Naito, M.; Abe, H. Supramolecular Hydrogel of Bile Salts Triggered by Single-Walled Carbon Nanotubes. *Adv. Mater.* **2011**, *23*, 4053−4057.
(366) Du, R.; Wu, J.; Chen, L.; Huang, H.; Zhang, X.; Zhang, J. Hierarchical Hydrogen Bonds Directed Multi-Functional Carbon Nanotube-Based Supramolecular Hydrogels. *Small* **2014**, *10*, 1387−1393.
(367) Hashmi, S.; GhavamiNejad, A.; Obiweluozor, F. O.; Vatankhah-Varnoosfaderani, M.; Stadler, F. J. Supramolecular Interaction Controlled Diffusion Mechanism and Improved Mechanical Behavior of Hybrid Hydrogel Systems of Zwitterions and CNT. *Macromolecules* **2012**, *45*, 9804−9815.
(368) Wang, Z.; Chen, Y. Supramolecular Hydrogels Hybridized with Single-Walled Carbon Nanotubes. *Macromolecules* **2007**, *40*, 3402−3407.
(369) Hui, Z.; Zhang, X.; Yu, J.; Huang, J.; Liang, Z.; Wang, D.; Huang, H.; Xu, P. Carbon Nanotube-Hybridized Supramolecular Hydrogel Based on PEO-b-PPO-b-PEO/α-Cyclodextrin as a Potential Biomaterial. *J. Appl. Polym. Sci.* **2010**, *116*, 1894−1901.
(370) Ogoshi, T.; Takashima, Y.; Yamaguchi, H.; Harada, A. Chemically-Responsive Sol−Gel Transition of Supramolecular Single-Walled Carbon Nanotubes (SWNTs) Hydrogel Made by Hybrids of SWNTs and Cyclodextrins. *J. Am. Chem. Soc.* **2007**, *129*, 4878−4879.
(371) Yang, B.; Zhao, Y.; Ren, X.; Zhang, X.; Fu, C.; Zhang, Y.; Wei, Y.; Tao, L. The Power of One-Pot: A Hexa-Component System Containing $\pi-\pi$ Stacking, Ugi Reaction and Raft Polymerization for Simple Polymer Conjugation on Carbon Nanotubes. *Polym. Chem.* **2015**, *6*, 509−513.
(372) Tamesue, S.; Takashima, Y.; Yamaguchi, H.; Shinkai, S.; Harada, A. Photochemically Controlled Supramolecular Curdlan/Single-Walled Carbon Nanotube Composite Gel: Preparation of Molecular Distaff by Cyclodextrin Modified Curdlan and Phase Transition Control. *Eur. J. Org. Chem.* **2011**, *2011*, 2801−2806.
(373) Mandal, S. K.; Kar, T.; Das, P. K. Pristine Carbon-Nanotube-Included Supramolecular Hydrogels with Tunable Viscoelastic Properties. *Chem. - Eur. J.* **2013**, *19*, 12486−12496.
(374) Zu, S.-Z.; Han, B.-H. Aqueous Dispersion of Graphene Sheets Stabilized by Pluronic Copolymers: Formation of Supramolecular Hydrogel. *J. Phys. Chem. C* **2009**, *113*, 13651−13657.
(375) Adhikari, B.; Banerjee, A. Short Peptide Based Hydrogels: Incorporation of Graphene into the Hydrogel. *Soft Matter* **2011**, *7*, 9259−9266.
(376) Adhikari, B.; Biswas, A.; Banerjee, A. Graphene Oxide-Based Supramolecular Hydrogels for Making Nanohybrid Systems with Au Nanoparticles. *Langmuir* **2012**, *28*, 1460−1469.
(377) Adhikari, B.; Biswas, A.; Banerjee, A. Graphene Oxide-Based Hydrogels to Make Metal Nanoparticle-Containing Reduced Graphene Oxide-Based Functional Hybrid Hydrogels. *ACS Appl. Mater. Interfaces* **2012**, *4*, 5472−5482.
(378) Tao, C.-a.; Wang, J.; Qin, S.; Lv, Y.; Long, Y.; Zhu, H.; Jiang, Z. Fabrication of pH-Sensitive Graphene Oxide-Drug Supramolecular Hydrogels as Controlled Release Systems. *J. Mater. Chem.* **2012**, *22*, 24856−24861.
(379) Cong, H.-P.; Wang, P.; Yu, S.-H. Stretchable and Self-Healing Graphene Oxide−Polymer Composite Hydrogels: A Dual-Network Design. *Chem. Mater.* **2013**, *25*, 3357−3362.
(380) Han, D.; Yan, L. Supramolecular Hydrogel of Chitosan in the Presence of Graphene Oxide Nanosheets as 2D Cross-Linkers. *ACS Sustainable Chem. Eng.* **2014**, *2*, 296−300.
(381) Liu, J.; Chen, G.; Jiang, M. Supramolecular Hybrid Hydrogels from Noncovalently Functionalized Graphene with Block Copolymers. *Macromolecules* **2011**, *44*, 7682−7691.
(382) Wu, L.; Ohtani, M.; Takata, M.; Saeki, A.; Seki, S.; Ishida, Y.; Aida, T. Magnetically Induced Anisotropic Orientation of Graphene Oxide Locked by in Situ Hydrogelation. *ACS Nano* **2014**, *8*, 4640−4649.

DOI: 10.1021/acs.chemrev.5b00303
Chem. Rev. 2016, 116, 1496−1539

(383) Liu, M.; Ishida, Y.; Ebina, Y.; Sasaki, T.; Aida, T. Photolatently Modulable Hydrogels using Unilamellar Titania Nanosheets as Photocatalytic Crosslinkers. *Nat. Commun.* **2013**, *4*, 2029.
(384) Liu, M.; Ishida, Y.; Ebina, Y.; Sasaki, T.; Hikima, T.; Takata, M.; Aida, T. An Anisotropic Hydrogel with Electrostatic Repulsion between Cofacially Aligned Nanosheets. *Nature* **2015**, *517*, 68−72.
(385) Jing, B.; Chen, X.; Wang, X.; Zhao, Y.; Qiu, H. Sol-Gel-Sol Transition of Gold Nanoparticle-Based Supramolecular Hydrogels Induced by Cyclodextrin Inclusion. *ChemPhysChem* **2008**, *9*, 249−252.
(386) Yu, J.; Ha, W.; Sun, J.-n.; Shi, Y.-p. Supramolecular Hybrid Hydrogel Based on Host−Guest Interaction and its Application in Drug Delivery. *ACS Appl. Mater. Interfaces* **2014**, *6*, 19544−19551.
(387) Kar, T.; Dutta, S.; Das, P. K. pH-Triggered Conversion of Soft Nanocomposites: In Situ Synthesized AuNP-Hydrogel to AuNP-Organogel. *Soft Matter* **2010**, *6*, 4777−4787.
(388) Shen, J.-S.; Chen, Y.-L.; Huang, J.-L.; Chen, J.-D.; Zhao, C.; Zheng, Y.-Q.; Yu, T.; Yang, Y.; Zhang, H.-W. Supramolecular Hydrogels for Creating Gold and Silver Nanoparticles in Situ. *Soft Matter* **2013**, *9*, 2017−2023.
(389) Meyer, D. E.; Chilkoti, A. Genetically Encoded Synthesis of Protein-Based Polymers with Precisely Specified Molecular Weight and Sequence by Recursive Directional Ligation: Examples from the Elastin-Like Polypeptide System. *Biomacromolecules* **2002**, *3*, 357−367.
(390) Arul, V.; Gopinath, D.; Gomathi, K.; Jayakumar, R. Biotinylated GHK Peptide Incorporated Collagenous Matrix: A Novel Biomaterial for Dermal Wound Healing in Rats. *J. Biomed. Mater. Res., Part B* **2005**, *73B*, 383−391.
(391) Jun, H. W.; West, J. L. Modification of Polyurethaneurea with PEG and YIGSR Peptide to Enhance Endothelialization without Platelet Adhesion. *J. Biomed. Mater. Res.* **2005**, *72B*, 131−139.
(392) Matsuda, A.; Kobayashi, H.; Itoh, S.; Kataoka, K.; Tanaka, J. Immobilization of Laminin Peptide in Molecularly Aligned Chitosan by Covalent Bonding. *Biomaterials* **2005**, *26*, 2273−2279.
(393) Ranieri, J. P.; Bellamkonda, R.; Bekos, E. J.; Vargo, T. G.; Gardella, J. A.; Aebischer, P. Neuronal Cell Attachment to Fluorinated Ethylene-Propylene Films with Covalently Immobilized Laminin Oligopeptides YIGSR and IKVAV. II. *J. Biomed. Mater. Res.* **1995**, *29*, 779−785.
(394) Wong, J. Y.; Weng, Z. P.; Moll, S.; Kim, S.; Brown, C. T. Identification and Validation of a Novel Cell-Recognition Site (KNEED) on the 8th Type III Domain of Fibronectin. *Biomaterials* **2002**, *23*, 3865−3870.
(395) Lu, H. D.; Soranno, D. E.; Rodell, C. B.; Kim, I. L.; Burdick, J. A. Secondary Photocrosslinking of Injectable Shear-Thinning Dock-and-Lock Hydrogels. *Adv. Healthcare Mater.* **2013**, *2*, 1028−1036.
(396) Wang, H. M.; Shi, Y.; Wang, L.; Yang, Z. M. Recombinant Proteins as Cross-Linkers for Hydrogelations. *Chem. Soc. Rev.* **2013**, *42*, 891−901.
(397) Sorensen, H. P.; Mortensen, K. K. Advanced Genetic Strategies for Recombinant Protein Expression in Escherichia Coli. *J. Biotechnol.* **2005**, *115*, 113−128.
(398) Fahnestock, S. R.; Yao, Z.; Bedzyk, L. A. Microbial Production of Spider Silk Proteins. *Rev. Mol. Biotechnol.* **2000**, *74*, 105−119.
(399) Cregg, J. M.; Cereghino, J. L.; Shi, J.; Higgins, D. R. Recombinant Protein Expression in Pichia Pastoris. *Mol. Biotechnol.* **2000**, *16*, 23−52.
(400) Cereghino, G. P. L.; Cereghino, J. L.; Ilgen, C.; Cregg, J. M. Production of Recombinant Proteins in Fermenter Cultures of the Yeast Pichia Pastoris. *Curr. Opin. Biotechnol.* **2002**, *13*, 329−332.
(401) Barr, L. A.; Fahnestock, S. R.; Yang, J. J. Production and Purification of Recombinant DP1B Silk-Like Protein in Plants. *Mol. Breed.* **2004**, *13*, 345−356.
(402) Heim, M.; Keerl, D.; Scheibel, T. Spider Silk: From Soluble Protein to Extraordinary Fiber. *Angew. Chem., Int. Ed.* **2009**, *48*, 3584−3596.
(403) Maeda, S. Expression of Foreign Genes in Insects Using Baculovirus Vectors. *Annu. Rev. Entomol.* **1989**, *34*, 351−372.
(404) Miao, Y. G.; Zhang, Y. S.; Nakagaki, K.; Zhao, T. F.; Zhao, A. C.; Meng, Y.; Nakagaki, M.; Park, E. Y.; Maenaka, K. Expression of Spider Flagelliform Silk Protein in Bombyx Mori Cell Line by a Novel Bac-to-Bac/BmNPV Baculovirus Expression System. *Appl. Microbiol. Biotechnol.* **2006**, *71*, 192−199.
(405) Heidebrecht, A.; Eisoldt, L.; Diehl, J.; Schmidt, A.; Geffers, M.; Lang, G.; Scheibel, T. Biomimetic Fibers Made of Recombinant Spidroins with the Same Toughness as Natural Spider Silk. *Adv. Mater.* **2015**, *27*, 2189−2194.
(406) Lazaris, A.; Arcidiacono, S.; Huang, Y.; Zhou, J. F.; Duguay, F.; Chretien, N.; Welsh, E. A.; Soares, J. W.; Karatzas, C. N. Spider Silk Fibers Spun from Soluble Recombinant Silk Produced in Mammalian Cells. *Science* **2002**, *295*, 472−476.
(407) Koide, T. Triple Helical Collagen-Like Peptides: Engineering and Applications in Matrix Biology. *Connect. Tissue Res.* **2005**, *46*, 131−141.
(408) Liu, W.; Merrett, K.; Griffith, M.; Fagerholm, P.; Dravida, S.; Heyne, B.; Scaiano, J. C.; Watsky, M. A.; Shinozaki, N.; Lagali, N.; et al. Recombinant Human Collagen for Tissue Engineered Corneal Substitutes. *Biomaterials* **2008**, *29*, 1147−1158.
(409) Olsen, D.; Yang, C. L.; Bodo, M.; Chang, R.; Leigh, S.; Baez, J.; Carmichael, D.; Perala, M.; Hamalainen, E. R.; Jarvinen, M.; et al. Recombinant Collagen and Gelatin for Drug Delivery. *Adv. Drug Delivery Rev.* **2003**, *55*, 1547−1567.
(410) Werkmeister, J. A.; Ramshaw, J. A. M. Recombinant Protein Scaffolds for Tissue Engineering. *Biomed. Mater.* **2012**, *7*, 012002.
(411) Kang, E.; Jeong, G. S.; Choi, Y. Y.; Lee, K. H.; Khademhosseini, A.; Lee, S. H. Digitally Tunable Physicochemical Coding of Material Composition and Topography in Continuous Microfibres. *Nat. Mater.* **2011**, *10*, 877−883.
(412) Betre, H.; Ong, S. R.; Guilak, F.; Chilkoti, A.; Fermor, B.; Setton, L. A. Chondrocytic Differentiation of Human Adipose-Derived Adult Stem Cells in Elastin-Like Polypeptide. *Biomaterials* **2006**, *27*, 91−99.
(413) Chilkoti, A.; Christensen, T.; MacKay, J. A. Stimulus Responsive Elastin Biopolymers: Applications in Medicine and Biotechnology. *Curr. Opin. Chem. Biol.* **2006**, *10*, 652−657.
(414) Urry, D. W. Physical Chemistry of Biological Free Energy Transduction as Demonstrated by Elastic Protein-Based Polymers. *J. Phys. Chem. B* **1997**, *101*, 11007−11028.
(415) McHale, M. K.; Setton, L. A.; Chilkoti, A. Synthesis and in Vitro Evaluation of Enzymatically Cross-Linked Elastin-Like Polypeptide Gels for Cartilaginous Tissue Repair. *Tissue Eng.* **2005**, *11*, 1768−1779.
(416) Chang, D. T.; Chai, R. J.; DiMarco, R.; Heilshorn, S. C.; Cheng, A. G. Protein-Engineered Hydrogel Encapsulation for 3-D Culture of Murine Cochlea. *Otol. Neurotol.* **2015**, *36*, 531−538.
(417) Liu, J. C.; Heilshorn, S. C.; Tirrell, D. A. Comparative Cell Response to Artificial Extracellular Matrix Proteins Containing the RGD and CS5 Cell-Binding Domains. *Biomacromolecules* **2004**, *5*, 497−504.
(418) MacEwan, S. R.; Chilkoti, A. Elastin-Like Polypeptides: Biomedical Applications of Tunable Biopolymers. *Biopolymers* **2010**, *94*, 60−77.
(419) Testera, A. M.; Girotti, A.; de Torre, I. G.; Quintanilla, L.; Santos, M.; Alonso, M.; Rodriguez-Cabello, J. C. Biocompatible Elastin-Like Click Gels: Design, Synthesis and Characterization. *J. Mater. Sci.: Mater. Med.* **2015**, *26*, 1−13.
(420) Li, L.; Kiick, K. L. Resilin-Based Materials for Biomedical Applications. *ACS Macro Lett.* **2013**, *2*, 635−640.
(421) Li, L. Q.; Tong, Z. X.; Jia, X. Q.; Kiick, K. L. Resilin-Like Polypeptide Hydrogels Engineered for Versatile Biological Function. *Soft Matter* **2013**, *9*, 665−673.
(422) McGann, C. L.; Levenson, E. A.; Kiick, K. L. Resilin-Based Hybrid Hydrogels for Cardiovascular Tissue Engineering. *Macromol. Chem. Phys.* **2013**, *214*, 203−213.
(423) Huemmerich, D.; Helsen, C. W.; Quedzuweit, S.; Oschmann, J.; Rudolph, R.; Scheibel, T. Primary Structure Elements of Spider Dragline Silks and their Contribution to Protein Solubility. *Biochemistry* **2004**, *43*, 13604−13612.
(424) Vendrely, C.; Scheibel, T. Biotechnological Production of Spider-Silk Proteins Enables New Applications. *Macromol. Biosci.* **2007**, *7*, 401−409.

DOI: 10.1021/acs.chemrev.5b00303
Chem. Rev. 2016, 116, 1496−1539

(425) Gosline, J. M.; Guerette, P. A.; Ortlepp, C. S.; Savage, K. N. The Mechanical Design of Spider Silks: From Fibroin Sequence to Mechanical Function. *J. Exp. Biol.* **1999**, *202*, 3295−3303.
(426) Leal-Egana, A.; Scheibel, T. Interactions of Cells with Silk Surfaces. *J. Mater. Chem.* **2012**, *22*, 14330−14336.
(427) Müller-Herrmann, S.; Scheibel, T. Enzymatic Degradation of Films, Particles, and Nonwoven Meshes Made of a Recombinant Spider Silk Protein. *ACS Biomater. Sci. Eng.* **2015**, *1*, 247−259.
(428) Rammensee, S.; Huemmerich, D.; Hermanson, K. D.; Scheibel, T.; Bausch, A. R. Rheological Characterization of Hydrogels Formed by Recombinantly Produced Spider Silk. *Appl. Phys. A: Mater. Sci. Process.* **2006**, *82*, 261−264.
(429) Schacht, K.; Scheibel, T. Controlled Hydrogel Formation of a Recombinant Spider Silk Protein. *Biomacromolecules* **2011**, *12*, 2488−2495.
(430) Ramshaw, J. A.; Werkmeister, J. A.; Dumsday, G. J. Bioengineered Collagens: Emerging Directions for Biomedical Materials. *Bioengineered* **2014**, *5*, 227−233.
(431) Frank, S.; Kammerer, R. A.; Mechling, D.; Schulthess, T.; Landwehr, R.; Bann, J.; Guo, Y.; Lustig, A.; Bachinger, H. P.; Engel, J. Stabilization of Short Collagen-Like Triple Helices by Protein Engineering. *J. Mol. Biol.* **2001**, *308*, 1081−1089.
(432) Myllyharju, J.; Nokelainen, M.; Vuorela, A.; Kivirikko, K. I. Expression of Recombinant Human Type I-III Collagens in the Yeast Pichia Pastoris. *Biochem. Soc. Trans.* **2000**, *28*, 353−357.
(433) Martin, R.; Waldmann, L.; Kaplan, D. L. Supramolecular Assembly of Collagen Triblock Peptides. *Biopolymers* **2003**, *70*, 435−444.
(434) Valluzzi, R.; Kaplan, D. L. Sequence-Specific Liquid Crystallinity of Collagen Model Peptides. I. Transmission Electron Microscopy Studies of Interfacial Collagen Gels. *Biopolymers* **2000**, *53*, 350−362.
(435) Hu, K.; Cui, F. Z.; Lv, Q.; Ma, J.; Feng, Q. L.; Xu, L.; Fan, D. D. Preparation of Fibroin/Recombinant Human-Like Collagen Scaffold to Promote Fibroblasts Compatibility. *J. Biomed. Mater. Res., Part A* **2008**, *84A*, 483−490.
(436) Jia, X. Q.; Kiick, K. L. Hybrid Multicomponent Hydrogels for Tissue Engineering. *Macromol. Biosci.* **2009**, *9*, 140−156.
(437) Li, B.; Alonso, D. O. V.; Daggett, V. The Molecular Basis for the Inverse Temperature Transition of Elastin. *J. Mol. Biol.* **2001**, *305*, 581−592.
(438) Meyer, D. E.; Chilkoti, A. Quantification of the Effects of Chain Length and Concentration on the Thermal Behavior of Elastin-Like Polypeptides. *Biomacromolecules* **2004**, *5*, 846−851.
(439) Urry, D. W. Elastic Molecular Machines in Metabolism and Soft-Tissue Restoration. *Trends Biotechnol.* **1999**, *17*, 249−257.
(440) Urry, D. W.; Pattanaik, A.; Xu, J.; Woods, T. C.; McPherson, D. T.; Parker, T. M. Elastic Protein-Based Polymers in Soft Tissue Augmentation and Generation. *J. Biomater. Sci., Polym. Ed.* **1998**, *9*, 1015−1048.
(441) Nagapudi, K.; Brinkman, W. T.; Thomas, B. S.; Park, J. O.; Srinivasarao, M.; Wright, E.; Conticello, V. P.; Chaikof, E. L. Viscoelastic and Mechanical Behavior of Recombinant Protein Elastomers. *Biomaterials* **2005**, *26*, 4695−4706.
(442) Chow, D.; Nunalee, M. L.; Lim, D. W.; Simnick, A. J.; Chilkoti, A. Peptide-Based Biopolymers in Biomedicine and Biotechnology. *Mater. Sci. Eng., R* **2008**, *62*, 125−155.
(443) Betre, H.; Setton, L. A.; Meyer, D. E.; Chilkoti, A. Characterization of a Genetically Engineered Elastin-Like Polypeptide for Cartilaginous Tissue Repair. *Biomacromolecules* **2002**, *3*, 910−916.
(444) Bracalello, A.; Santopietro, V.; Vassalli, M.; Marletta, G.; Del Gaudio, R.; Bochicchio, B.; Pepe, A. Design and Production of a Chimeric Resilin-, Elastin-, and Collagen-Like Engineered Polypeptide. *Biomacromolecules* **2011**, *12*, 2957−2965.
(445) Charati, M. B.; Ifkovits, J. L.; Burdick, J. A.; Linhardt, J. G.; Kiick, K. L. Hydrophilic Elastomeric Biomaterials Based on Resilin-Like Polypeptides. *Soft Matter* **2009**, *5*, 3412−3416.
(446) Fernandez-Colino, A.; Arias, F. J.; Alonso, M.; Rodriguez-Cabello, J. C. Self-Organized ECM-Mimetic Model Based on an Amphiphilic Multiblock Silk-Elastin-Like Corecombinamer with a Concomitant Dual Physical Gelation Process. *Biomacromolecules* **2014**, *15*, 3781−3793.
(447) Haider, M.; Cappello, J.; Ghandehari, H.; Leong, K. W. In Vitro Chondrogenesis of Mesenchymal Stem Cells in Recombinant Silk-Elastinlike Hydrogels. *Pharm. Res.* **2008**, *25*, 692−699.
(448) Wlodarczyk-Biegun, M. K.; Werten, M. W.; de Wolf, F. A.; van den Beucken, J. J.; Leeuwenburgh, S. C.; Kamperman, M.; Cohen Stuart, M. A. Genetically Engineered Silk-Collagen-Like Copolymer for Biomedical Applications: Production, Characterization and Evaluation of Cellular Response. *Acta Biomater.* **2014**, *10*, 3620−3629.
(449) Wang, H. Y.; Cai, L.; Paul, A.; Enejder, A.; Heilshorn, S. C. Hybrid Elastin-Like Polypeptide-Polyethylene Glycol (ELP-PEG) Hydrogels with Improved Transparency and Independent Control of Matrix Mechanics and Cell Ligand Density. *Biomacromolecules* **2014**, *15*, 3421−3428.
(450) Dinerman, A. A.; Cappello, J.; Ghandehari, H.; Hoag, S. W. Swelling Behavior of a Genetically Engineered Silk-Elastinlike Protein Polymer Hydrogel. *Biomaterials* **2002**, *23*, 4203−4210.
(451) Megeed, Z.; Cappello, J.; Ghandehari, H. Controlled Release of Plasmid DNA from a Genetically Engineered Silk-Elastinlike Hydrogel. *Pharm. Res.* **2002**, *19*, 954−959.
(452) Cappello, J.; Crissman, J.; Dorman, M.; Mikolajczak, M.; Textor, G.; Marquet, M.; Ferrari, F. Genetic-Engineering of Structural Protein Polymers. *Biotechnol. Prog.* **1990**, *6*, 198−202.
(453) Megeed, Z.; Cappello, J.; Ghandehari, H. Genetically Engineered Silk-Elastinlike Protein Polymers for Controlled Drug Delivery. *Adv. Drug Delivery Rev.* **2002**, *54*, 1075−1091.
(454) Nagarsekar, A.; Crissman, J.; Crissman, M.; Ferrari, F.; Cappello, J.; Ghandehari, H. Genetic Synthesis and Characterization of pH- and Temperature-Sensitive Silk-Elastinlike Protein Block Copolymers. *J. Biomed. Mater. Res.* **2002**, *62*, 195−203.
(455) Nagarsekar, A.; Crissman, J.; Crissman, M.; Ferrari, F.; Cappello, J.; Ghandehari, H. Genetic Engineering of Stimuli-Sensitive Silkelastin-Like Protein Block Copolymers. *Biomacromolecules* **2003**, *4*, 602−607.
(456) Xia, X. X.; Xu, Q. B.; Hu, X.; Qin, G. K.; Kaplan, D. L. Tunable Self-Assembly of Genetically Engineered Silk-Elastin-Like Protein Polymers. *Biomacromolecules* **2011**, *12*, 3844−3850.
(457) Cappello, J.; Crissman, J. W.; Crissman, M.; Ferrari, F. A.; Textor, G.; Wallis, O.; Whitledge, J. R.; Zhou, X.; Burman, D.; Aukerman, L.; et al. R. In-Situ Self-Assembling Protein Polymer Gel Systems for Administration, Delivery, and Release of Drugs. *J. Controlled Release* **1998**, *53*, 105−117.
(458) Golinska, M. D.; Wlodarczyk-Biegun, M. K.; Werten, M. W. T.; Stuart, M. A. C.; de Wolf, F. A.; de Vries, R. Dilute Self-Healing Hydrogels of Silk-Collagen-Like Block Copolypeptides at Neutral pH. *Biomacromolecules* **2014**, *15*, 699−706.
(459) Parisi-Amon, A.; Mulyasasmita, W.; Chung, C.; Heilshorn, S. C. Protein-Engineered Injectable Hydrogel to Improve Retention of Transplanted Adipose-Derived Stem Cells. *Adv. Healthcare Mater.* **2013**, *2*, 428−432.
(460) Altunbas, A.; Pochan, D. J. Peptide-Based and Polypeptide-Based Hydrogels for Drug Delivery and Tissue Engineering. *Top. Curr. Chem.* **2012**, *310*, 135−167.
(461) Glassman, M. J.; Chan, J.; Olsen, B. D. Reinforcement of Shear Thinning Protein Hydrogels by Responsive Block Copolymer Self-Assembly. *Adv. Funct. Mater.* **2013**, *23*, 1182−1193.
(462) Chen, J. H.; Seeman, N. C. Synthesis from DNA of a Molecule with the Connectivity of a Cube. *Nature* **1991**, *350*, 631−633.
(463) He, Y.; Ye, T.; Su, M.; Zhang, C.; Ribbe, A. E.; Jiang, W.; Mao, C. D. Hierarchical Self-Assembly of DNA into Symmetric Supramolecular Polyhedra. *Nature* **2008**, *452*, 198−202.
(464) Li, Y. G.; Tseng, Y. D.; Kwon, S. Y.; d'Espaux, L.; Bunch, J. S.; Mceuen, P. L.; Luo, D. Controlled Assembly of Dendrimer-Like DNA. *Nat. Mater.* **2004**, *3*, 38−42.
(465) Rothemund, P. W. K. Folding DNA to Create Nanoscale Shapes and Patterns. *Nature* **2006**, *440*, 297−302.
(466) Um, S. H.; Lee, J. B.; Kwon, S. Y.; Li, Y.; Luo, D. Dendrimer-Like DNA-Based Fluorescence Nanobarcodes. *Nat. Protoc.* **2006**, *1*, 995−1000.

DOI: 10.1021/acs.chemrev.5b00303
Chem. Rev. 2016, 116, 1496−1539

(467) Um, S. H.; Lee, J. B.; Park, N.; Kwon, S. Y.; Umbach, C. C.; Luo, D. Enzyme-Catalysed Assembly of DNA Hydrogel. *Nat. Mater.* **2006**, *5*, 797−801.
(468) Nishikawa, M.; Mizuno, Y.; Mohri, K.; Matsuoka, N.; Rattanakiat, S.; Takahashi, Y.; Funabashi, H.; Luo, D.; Takakura, Y. Biodegradable CpG DNA Hydrogels for Sustained Delivery of Doxorubicin and Immunostimulatory Signals in Tumor-Bearing Mice. *Biomaterials* **2011**, *32*, 488−494.
(469) Klinman, D. M. Immunotherapeutic Uses of CpG Oligodeoxynucleotides. *Nat. Rev. Immunol.* **2004**, *4*, 249−259.
(470) Krieg, A. M. Therapeutic Potential of Toll-Like Receptor 9 Activation. *Nat. Rev. Drug Discovery* **2006**, *5*, 471−484.
(471) Roman, M.; Martin-Orozco, E.; Goodman, S.; Nguyen, M. D.; Sato, Y.; Ronaghy, A.; Kornbluth, R. S.; Richman, D. D.; Carson, D. A.; Raz, E. Immunostimulatory DNA Sequences Function as T Helper-1-Promoting Adjuvants. *Nat. Med.* **1997**, *3*, 849−854.
(472) Nishikawa, M.; Ogawa, K.; Umeki, Y.; Mohri, K.; Kawasaki, Y.; Watanabe, H.; Takahashi, N.; Kusuki, E.; Takahashi, R.; Takahashi, Y.; et al. Injectable, Self-Gelling, Biodegradable, and Immunomodulatory DNA Hydrogel for Antigen Delivery. *J. Controlled Release* **2014**, *180*, 25−32.
(473) Guo, W.; Lu, C. H.; Orbach, R.; Wang, F.; Qi, X. J.; Cecconello, A.; Seliktar, D.; Willner, I. pH-Stimulated DNA Hydrogels Exhibiting Shape-Memory Properties. *Adv. Mater.* **2015**, *27*, 73−78.

DOI: 10.1021/acs.chemrev.5b00303
Chem. Rev. 2016, 116, 1496−1539

TEILARBEIT VII

Die Ergebnisse dieses Kapitels wurden bereits in *Nachrichten aus der Chemie* veröffentlicht als:

> "Zellgewebe aus dem Drucker." Schacht, K., Jungst, T., Zehnder, T., Boccaccini, A.R., Groll, J. und Scheibel, T..

Reproduziert aus *Nachrichten aus der Chemie* **2016**, 64: 13-16 mit freundlicher Genehmigung des Verlages John Wiley and Sons.

Zellgewebe aus dem Drucker

Kristin Schacht, Tomasz Jüngst, Tobias Zehnder, Aldo R. Boccaccini, Jürgen Groll, Thomas Scheibel

Die Biofabrikation, also die Verarbeitung von Biotinte, baut mit zellfreundlichen 3-D-Druckverfahren gewebeartige Strukturen auf. Die Zusammensetzung von Biotinten steht daher im Fokus der Materialentwickler, die Gewebe züchten.

◆ Biomaterialforscher, die gleichzeitig Zellen und Polymere verarbeiten, betreiben Biofabrikation. Die Biofabrikation ist noch jung und entwickelt sich schnell – deshalb aktualisierte die Internationale Gesellschaft für Biofabrikation kürzlich die erste Definition, die Mironov et al. im Jahr 2009 aufstellten.[1)] Jetzt bedeutet Biofabrikation „die automatisierte Herstellung biologisch funktionaler Produkte mit struktureller Organisation aus lebenden Zellen, Zell-Aggregaten wie Mikrogeweben, hybriden Gewebekonstrukten, bioaktiven Molekülen oder Biomaterialien durch Biodrucken oder Bioassemblierung und nachfolgender Reifungsprozesse."[2)]

Im klassischen Ansatz der Gewebezucht besiedeln Zellen eine vorgefertigte Trägerstruktur, und zwar isotrop verteilt über die gesamte Trägerstruktur. Durch Reifen, vorzugsweise in einem Bioreaktor, entsteht ein Zell-Materialverbund, der als Gewebeersatz dienen soll.

3-D-Drucke laufen über einen computergesteuerten, automatisierten Schicht-für-Schicht-Prozess. Der baut die gewünschte Struktur direkt ohne Gussform auf. Der automatisierte Prozess gewährleistet reproduzierbare Produkte – das nutzt die Biofabrikation, um Zellen und Materialien direkt in gewebeartigen Strukturen anzuordnen. So entsteht schon vor der biologischen Reifung in Kultur eine Struktur und Morphologie, die natürlichem Gewebe nachempfunden ist. Die Biofabrikation gilt als vorteilhaft, um in vitro funktionale Gewebeanaloga herzustellen, einerseits, weil sie funktionale Komponenten besser ausbildet als die klassische Gewebezucht, und andererseits, weil sie die Reifungszeit minimiert.

Additive Fertigungsverfahren in der Biofabrikation

◆ Der 3-D-Druck von klassischen Werkstoffen läuft teilweise unter extremen Bedingungen ab: Die Schmelzschichtung (fused deposition modeling) etwa verarbeitet Acrylnitril-Butadien-Styrol bei Temperaturen bis zu 230 °C. Im Gegensatz dazu steht die Biofabrikation. Sie muss gewährleisten, dass Zellen überleben, wofür verschiedene Faktoren eine Rolle spielen, darunter Temperatur, wässriges Milieu, eventuell nötige Vernetzungschemie und Druck sowie verwendete Materialien. Zudem muss die Arbeitsumgebung steril sein. Trotz der erschwerten Bedingungen muss die Biofabrikation mechanisch belastbare, formstabile 3-D-Strukturen produzieren. Nur wenige 3-D-Druckverfahren eignen sich hierfür, überwiegend sind das Tintenstrahl- und Dispensdruck sowie laserinduzierter Vorwärtstransfer (Tabelle, S. 14).[3)]

Beim Tintenstrahldruck bauten Forscher zunächst handelsübliche Tintenstrahldrucker um, entleerten und reinigten die Kartuschen und befüllten sie mit Zellsuspensionen. Inzwischen entwickelten sie neue Systeme; neben thermischen wurden piezoelektrische Druckköpfe und elektromagnetische Ventile eingesetzt. Die Hauptvorteile des Tintenstrahldrucks sind der geringe Materialverbrauch, die hohe Überlebensrate von Zellen sowie Strukturen mit einer Auflösung von etwa 75 µm.[3,5)] Allerdings verarbeitet der Tintenstrahldrucker nur Materialien mit einer Viskosität zwischen 3,5 und 12 mPa·s.[3)]

Beim Dispensdrucken kommt die Biotinte in eine Kartusche oder Spritze. Ein computergesteuertes Kontrollsystem bewegt die Kartusche und synchronisiert das Dosieren, was zu 3-D-Strukturen führt. Dieses Verfahren fertigt Konstrukte mit klinisch relevanten Größen in einer Zeit, die sich für die praktische Anwendung eignet – beispielsweise ein Ohr mit den Maßen

◆ QUERGELESEN

- Biotinten bestehen aus Zellen und natürlichen Polymeren wie Alginat oder synthetischen wie Polyethylenglykol.
- Zellfreundlichkeit und Fließeigenschaften der Biotinte entscheiden darüber, ob sie sich für die Biofabrikation eignet.
- Spinnenseidenhydrogele sind wegen ihrer Fließeigenschaften und wegen der Netzwerke, die sie bilden, eine ideale Biotinte.
- Konstrukte aus Spinnenseiden sind nach dem Drucken ohne zusätzliche Quervernetzer und Verdickungsmittel stabil.

Verfahren	Tintenstrahldruck	Dispensdruck	laserinduzierter Vorwärtstransfer
	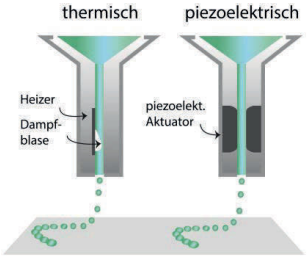	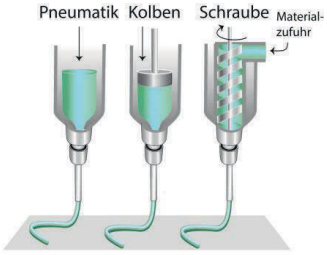	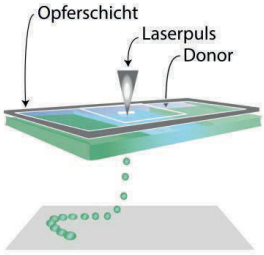
Vorteile	hohe Auflösung hohe Zellvitalität kommerziell erhältlich kosteneffizient	hoher Viskositätsbereich verarbeitbar Aufbau klinisch relevanter Strukturabmessungen möglich kommerziell erhältlich	hohe Auflösung hohe Zellvitalität
Nachteile	eingeschränkter Viskositätsbereich	beschränkte Auflösung	nicht kommerziell erhältlich hohe Kosten limitierte Konstruktgrößen

Für die Biofabrikation gebräuchlichste additive Fertigungsverfahren mit Vor- und Nachteilen.[3,4)]

23 mal 14 mal 5 mm aus rekombinanter Spinnenseide in etwa fünf Minuten. Beim Verdrucken von Zellen verringert sich dadurch jedoch die Auflösung auf etwa 400 µm.[6)] Allerdings ist dieses Verfahren besonders variabel, was die Viskosität des zu verdruckenden Materials angeht: Sie darf zwischen 30 und $6 \cdot 10^7$ mPa·s betragen.[3)]

Der laserinduzierte Vorwärtstransfer ist das Verfahren mit der besten Auflösung, nämlich zwischen 10 und 100 µm, und druckt sogar einzelne Zellen.[7)] Hierbei richtet sich ein gepulster Laser auf den Donor, der aus einem lichtdurchlässigen Trägermaterial, einer Opferschicht und dem zu druckenden Material besteht. Der Laser verdampft lokal die Opferschicht und sorgt damit dafür, dass das Material tröpfchenweise ausgestoßen wird. Dieses Verfahren schließt die Lücke zwischen den beiden anderen Verfahren im Viskositätsbereich von 1 bis 300 mPa·s, verarbeitet aber nur eine geringe Materialmenge pro Donor. Das erschwert es, schnell größere Strukturen aufzubauen.[3)]

Biotinten

◆ In der Biofabrikation beschreibt der Begriff „Biotinte“ druckbare Biomaterialien, die Zellen enthalten. Biotinten sind oft der limitierende Faktor der Biofabrikation, da die Anforderungen an die Materialien hoch sind (Abbildung 1).

Die Biotinte muss druckbar und zellfreundlich sein, das entstehende Konstrukt formstabil.[4)] Es soll außerdem die Eigenschaften des Zielgewebes so gut wie möglich nachahmen. Hydrogele sind die derzeit erfolgversprechendsten Ausgangsmaterialien für Biotinten.[3,8)]

Die wichtigste physikalische Eigenschaft der Biotinte ist ihr Fließverhalten.[4,9)] Vor dem Druck dürfen die Zellen nicht sedimentieren; während des Druckens muss die

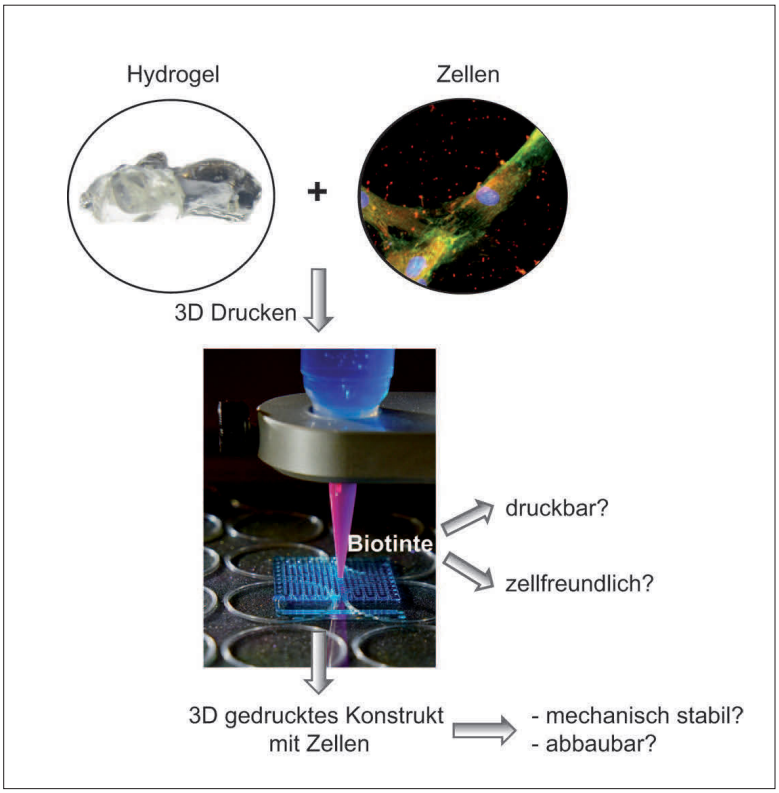

Abb. 1. Beim 3-D-Drucken werden Hydrogele gemischt mit Zellen als Biotinte eingesetzt, um 3-D-Konstrukte mit gesteuerter Mechanik und Abbaubarkeit herzustellen.

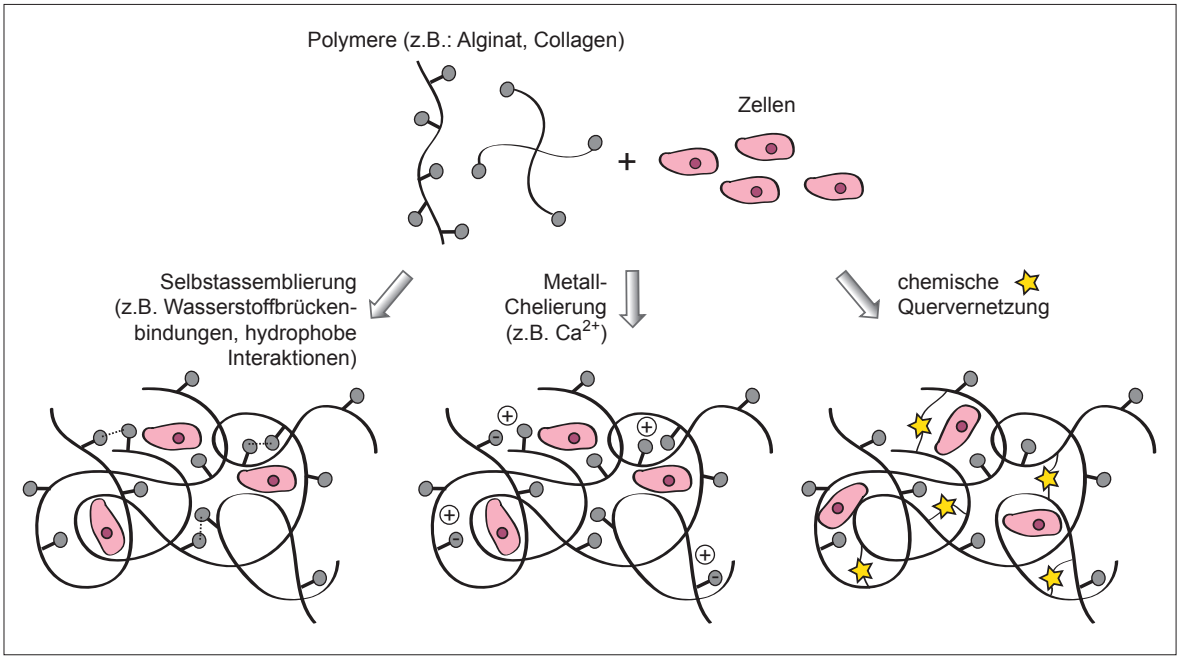

Abb. 2. Vernetzungsmechanismen der Biotinte.

Biotinte gleichmäßig fließen und anschließend schnell aushärten oder gelieren. Ist die Biotinte bereits vor dem Drucken geliert, darf der Druckprozess das Gelnetzwerk nicht irreversibel schädigen.[10] Wenn die Polymere nicht selbstassemblieren, generiert entweder physikalische oder chemische Quervernetzung formstabile Konstrukte (Abbildung 2).

Vorteil der physikalischen Quervernetzung wie auch der Metall-Chelierung ist deren Zellfreundlichkeit. Allerdings ist das Netzwerk oft schwach und der Abbau unkontrolliert. Deshalb müssen viele derart quervernetzte Hydrogele nachträglich chemisch quervernetzt werden, etwa durch Enzyme oder UV-Licht.[4]

Die fertigungsbedingten Anforderungen an Biotinten kollidieren oft mit den biologischen. Im gedruckten Konstrukt müssen eingekapselte Zellen wandern, sich teilen und differenzieren können. Das muss das Material nicht nur zulassen, sondern auch fördern.[11] Zudem muss sich das Biomaterialgerüst ohne schädliche Abbauprodukte in einem Zeitraum zersetzen, in dem sich neues Gewebe bildet und das Gerüst ersetzt.[9]

Biopolymere für den 3-D-Druck

◆ Etablierte Biotinten enthalten natürliche Polymere wie Alginat oder Kollagen und synthetische Polymere wie Polyethylenglykol oder Polylactid sowie modifizierte Varianten und Kombinationen dieser Polymere.[3,9]

Alginat ist ein wichtiger und häufig verwendeter Vertreter der Hydrogele. Es bildet eine zellfreundliche Umgebung, indem es die Zellen mit Nährstoffen und Sauerstoff versorgt. Es lässt sich gut verarbeiten und ermöglicht eine hohe Zellvitalität. Allerdings ist sein Abbau schwer zu steuern, und es hat keine Zelladhäsionsdomänen.

Um die Zellantwort zu verbessern, modifizieren Wissenschaftler Alginat mit Proteinen. Eine Möglichkeit ist, Alginat zu oxidieren und es dadurch kovalent an Gelatine zu binden. Dadurch entsteht ein für die Biofabrikation geeignetes Hydrogel.[12]

Fibrin ist bioabbaubar und geliert schnell, zeigt aber limitierte mechanische Eigenschaften: Das beste Fibrinhydrogel zerfiel innerhalb von drei Wochen.[3] Kollagen ist bioabbaubar, bioverträglich und einfach zu gewinnen. Allerdings variieren kollagenbasierte Biotinten chargenabhängig und haben mit einem Elastizitätsmodul von etwa 1 kPa nur schwache mechanische Eigenschaften. Noch zellfreundlicher als Kollagen ist seine modifizierte Variante, die Gelatine.[3,9]

In neuen Biotinten werden häufig chemisch modifizierte Biopolymere oder Polymermischungen eingesetzt. Die Modifikation soll materialspezifische Eigenschaften wie Zellfreundlichkeit, Verarbeitbarkeit sowie mechanische Eigenschaften und Porosität der Hydrogele optimieren.[8] Beispiele für chemische Funktionalisierungen von Gelatine sind die Methacrylierung und Acetylierung sowie die Vernetzung mit oxidiertem Alginat, was die mechanische und thermische Stabilität erhöht.[12] Um dagegen Alginat biologisch aktiver zu machen, eignen sich Fibrin-Alginat-Mischungen. Allerdings ist es trotz dieser Modifizierungen nötig, neue Biotinten mit verbesserten Eigenschaften zu entwickeln, welche die oft gegenläufigen Anforderungen von Druckprozess und Zellen noch besser vereinen.

Biotinten aus Seide

◆ Seiden sind natürliche Proteinfasern, die Gliederfüßer wie Spinnen oder Insekten etwa beim Spinnen-

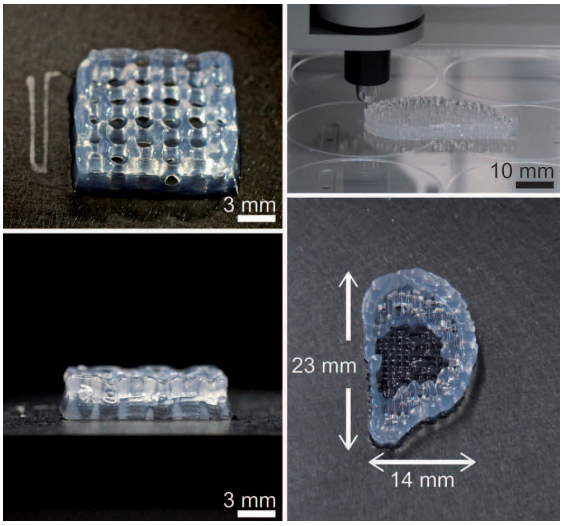

Abb. 3. 3-D-gedruckte Konstrukte aus rekombinantem Spinnenseidenprotein.[9,15]

netz- oder Kokonbau einsetzen. Seide ist bioverträglich, baut sich langsam ab, hat außergewöhnliche mechanische Eigenschaften und ist weder toxisch noch ruft sie Immunreaktionen hervor. Deshalb ist Seide interessant für biomedizinische Anwendungen. Die am besten verfügbare Seide ist die des Seidenspinners *Bombyx mori*, der seit Jahrtausenden industriell kultiviert wird. Biotinten, die auf Seidenspinnerfibroin basieren, sind prinzipiell tauglich für 3-D-Konstrukte – allerdings müssen sie dazu mit Gelatine gemischt werden.[11] Dieser Mix ist notwendig, da Fibroin alleine die Nadel während des Druckprozesses verstopft.

Spinnen produzieren die besten Seiden, sind aber Kannibalen. Folglich sind sie nicht im großen Maßstab züchtbar und eignen sich nicht als natürliche Seidenressource. Deshalb entwickelten Forscher ein biotechnisches Verfahren, das die potenziell bessere Spinnenseide – besser, weil mechanisch stabiler und bioverträglicher – aus rekombinantem Spinnenseidenprotein macht. Dabei helfen Wirtsorganismen, die meist Bakterien sind.[13,14]

Vorteil von rekombinanten Spinnenseidenproteinen ist, dass sie sich in nanofibrilläre Netzwerke selbstassemblieren und außerdem mechanisch stabile Hydrogele bilden. Wissenschaftler nutzten diese Hydrogele bereits als zellfreundliche Biotinte in der Biofabrikation (Abbildung 3).[3,9,15]

Im Gegensatz zu Hydrogelen aus Fibroin zeigen solche aus rekombinanter Spinnenseide ähnlich wie Zahnpasta ein scherverdünnendes Verhalten. Durch die Scherkräfte im Druckkopf fließt die Biotinte während des Druckens. Der Druckkopf legt feine Gerüststrukturen auf der Oberfläche ab, die sofort aushärten – dadurch lassen sich mehrlagige formstabile Gerüste herstellen.[15] Bemerkenswerterweise sind die Spinnenseidenkonstrukte nach dem Drucken stabil, und zwar ohne zusätzliche Quervernetzer oder Verdickungsmittel.

Ausblick

◆ Die Biofabrikation ermöglicht, die Herstellung von Weichgewebeimplantaten zu standardisieren und zu kontrollieren. Das langfristige Ziel ist es, gewebeähnliche Strukturen bis hin zu voll funktionierenden Organen zu produzieren.

Literatur

1) *V. Mironov, T. Trusk, V. Kasyanov et al.,* Biofabrication *2009,* 1, *1.*
2) *J. Groll, J. Burdick, D.-W. Cho et al.,* Biofabrication *2016,* accepted.
3) *T. Jungst, W. Smolan, K. Schacht, T. Scheibel, J. Groll,* Chem. Rev. *2015,* doi: *10.1021/acs.chemrev.5b00303*
4) *J. Malda, J. Visser, F. P. Melchels et al.,* Adv. Mater. *2013,* 25, *5011.*
5) *R. E. Saunders, B. Derby,* Int. Mater. Rev. *2014,* 59, *430.*
6) *C. M. Smith, A. L. Stone, R. L. Parkhill et al.,* Tissue Eng. *2004,* 10, *1566.*
7) *J. A. Barron, D. B. Krizman, B. R. Ringeisen,* Ann. Biomed. Eng. *2005,* 33, *121.*
8) *S. Wüst, R. Müller, S. Hofmann,* J. Funct. Biomater. *2011,* 2, *119.*
9) *E. DeSimone, K. Schacht, T. Jungst, J. Groll, T. Scheibel,* Pure Appl. Chem. *2015,* 87, *737.*
10) *Q. L. Loh, C. Choong,* Tissue Eng., Part B *2013,* 19, *485.*
11) *S. Das, F. Pati, Y. J. Choi et al.,* Acta Biomater. *2015,* 11, *233.*
12) *T. Zehnder, B. Sarker, A. R. Boccaccini, R. Detsch,* Biofabrication *2015,* 7, *1.*
13) *D. Huemmerich, C. W. Helsen, S. Quedzuweit et al.,* Biochemistry *2004,* 43, *13604.*
14) *A. Heidebrecht, T. Scheibel,* Adv. Appl. Microbiol. *2013,* 82, *115.*
15) *K. Schacht, T. Jungst, M. Schweinlin et al.,* Angew. Chem. Int. Ed. *2015,* 54, *2816.*

Kristin Schacht, Jahrgang 1986, studierte molekulare Biologie und Biochemie an der Universität Bayreuth. Seit 2012 promoviert sie bei Thomas Scheibel. Sie beschäftigt sich mit Herstellung und Charakterisierung dreidimensionaler Gerüste aus rekombinanten Spinnenseidenproteinen für biomedizinische Anwendungen.

Tomasz Jüngst, Jahrgang 1984, studierte Nanostructural Engineering an der Universität Würzburg und promoviert seit 2011 unter der Leitung von Jürgen Groll. Sein Forschungsschwerpunkt ist die Herstellung dreidimensionaler Konstrukte für die Gewebezucht.

Tobias Zehnder, Jahrgang 1986, studierte Materialwissenschaften und Werkstofftechnik an der Universität Erlangen-Nürnberg und promoviert seit 2013 bei Aldo R. Boccaccini. Seine Forschung umfasst Herstellung und Charakterisierung von Hydrogel-Zellkonstrukten mit additiven 3-D-Druckverfahren.

Thomas Scheibel, Jahrgang 1969, promovierte 1998 an der Universität Regensburg. Seit 2007 ist er Lehrstuhlinhaber für Biomaterialien an der Universität Bayreuth. Seine Forschungsschwerpunkte liegen auf dem Gebiet bioinspirierter Materialien, die sich von natürlichen Strukturproteinen ableiten.

Jürgen Groll, Jahrgang 1976, ist Lehrstuhlinhaber für Funktionswerkstoffe der Medizin und Zahnheilkunde an der Universität Würzburg. Sein Forschungsfokus liegt auf polymeren Biomaterialien, Nanobiotechnologie und Biofabrikation.

Aldo R. Boccaccini, Jahrgang 1962, ist Lehrstuhlinhaber für Werkstoffwissenschaften (Biomaterialien) an der Universität Erlangen-Nürnberg und Gastprofessor am Imperial College London. Seine Forschungsschwerpunkte sind bioaktive Materialien und Scaffolds für die regenerative Medizin, antibakterielle Beschichtungen und Biofabrikation.

DANKSAGUNG

Zunächst bedanke ich mich bei all denjenigen, die mich auf dem Weg meiner Promotion unterstützt haben und zum Gelingen dieser Arbeit beigetragen haben.

Die vorliegende Arbeit entstand von Februar 2012 bis Februar 2016 an der Universität Bayreuth am Lehrstuhl Biomaterialien unter der Leitung von Prof. Dr. Thomas Scheibel. Zunächst möchte ich mich herzlich bei meinem Doktorvater bedanken, der mich während der letzten Jahre immer unterstützte, mir viele Freiheiten, Vertrauen und Verantwortung entgegen brachte.

Vielen Dank auch an Dr. Stefan Geimer und Prof. Dr. Andreas Fery für die Übernahme meines Mentorats.

Folgenden Kooperationspartnern möchte ich für die spannende und erfolgreiche Zusammenarbeit danken:

- Der Würzburg-Gruppe (Tomasz, Kai, Matthias, Willi, Andrea und Prof. Dr. Jürgen Groll) für die angenehme Zusammenarbeit und hilfreichen Diskussionen für die Fertigstellung der Veröffentlichungen. Mein besonderer Dank geht an Tomasz Jüngst, der mich nicht nur im Labor, sondern auch während meiner privaten Zeit in Würzburg stetig unterstützt hat. Vielen, vielen Dank, denn ohne dich wäre die Arbeit nicht in dieser Form entstanden.
- Elise DeSimone für die tolle, entspannte, lustige und produktive Zusammenarbeit im Labor und bei den Veröffentlichungen. Thank you for all the time we spent together!
- Meinen Studenten (Florian Gisdon, Jan Scheler, Wolfrat Bachert, Jessica Vogt), die eine große Hilfe im Labor waren und die Projekte dadurch zügig vorangetrieben haben. Vor allem danke ich Jessica Vogt für die Datenlieferung und die daraus entstandene Veröffentlichung.
- Bapi Saker, Tobias Zehnder und Prof. Dr. Aldo Boccaccini für die gute Zusammenarbeit im Bioglass® Projekt und dem Review.
- Stefan Geimer und Rita Grotjahn für die Beantwortung von Fragen rund um das TEM und die Hilfestellung am Gerät vor allem bei Problemen.
- Dr. Lutz Heymann, Stephan Jokisch und Gregor Lang für die Hilfe, Unterstützung und Diskussion am Rheometer.
- Alexandra Pellert für die Hilfe in der Zellkultur und das immer offene Ohr.
- Anderl Schmidt und Johannes Diehl für die Fermentation und Proteinreinigung, auch wenn der 30l Fermenter mal gezickt hat.

- Martin Humenik, Steffi Wohlrab, Elena Doblhofer für die Hilfe am FTIR und bei der FSD Auswertung.
- Hendrik Bagel und Johannes Diehl für die REM-Aufnahmen.
- Martin Humenik, Martina Elsner, Joschi Bauer, Tamara Aigner und Aniela Heidebrecht für die Unterstützung und Diskussionen bei der Erstellung von Abbildungen.
- Meinen drei Subgroups: *MedSilk*, *Fiber Processing* und *Biofabrication* für die hilfreichen Diskussionen bei Problemen im Labor und hilfreichen Tipps.

Den TAs (Alex, Anderl, Johannes, Eva, Jasmin, Claudia und Dani) möchte ich danken für die Unterstützung im Laboralltag. Ohne sie wäre die praktische Arbeit wesentlich zeitintensiver gewesen. Außerdem danke ich dem Sekretariat für die Hilfe bei organisatorischen Aufgaben.

Mein besonderer Dank geht an Martin Humenik, Aniela Heidebrecht, Phillip Nowotny, Philipp Neßbach und Thorben Schacht für das Korrekturlesen dieser Arbeit. Durch ihre wertvollen Ratschläge und konstruktive Kritik nicht nur am Ende meiner Promotion haben sie einen wertvollen Beitrag zu dieser Arbeit geleistet.

Allen alten *Fibers* und neuen Biomatlern danke ich recht herzlich für die tolle Arbeitsatmosphäre, für die hilfreichen Tipps im Laboralltag sowie vielen witzigen und amüsanten Momenten im Labor und während der Pausen. Ein besonderer Dank gilt meinen alten und aktuellen Bürokollegen Hendrik, Andrew, Chris, Steffi, Martina, Bruno, Tamara, Elise, Caro und Kiran für die konstruktive und tolle Bürogemeinschaft, die bis zur freundschaftlichen Ebene reichte.

Allen, die die 10 Jahre in Bayreuth zu einer unvergesslichen Zeit gemacht haben, mich auf meinem langen Weg begleitet haben und einen tollen Ausgleich zur Arbeit geschaffen haben, danke ich sehr. Außerdem gilt mein besonderer Dank den Fußball-Jungs und -Mädels sowie meinem Tauzieh-Wettkampfteam, die es ermöglicht haben, auch sportliche Erfolge zu erzielen. Durch Spaß, Anstrengung und blaue Flecken wurde immer wieder eine Ablenkung zur Arbeit geboten.

Mein außerordentlicher Dank geht an meine Familie, die mich immer unterstützt und in jeder Situation bestärkt hat. Sie hatten in allen Lebenslagen ein offenes Ohr und sind das Beste, was man sich wünschen kann. Meinem Freund Philipp Neßbach danke ich für die wertvollen Ratschläge und Hilfe rund um meine Arbeit, aber vor allem für die vielen schönen Momente und dafür, dass du mich zum Lachen brachtest, wenn ich es am meisten brauchte.

Vielen Dank für alles!

ERKLÄRUNG

(§ 8 S. 2 Nr. 6 PromO)

Hiermit erkläre ich mich damit einverstanden, dass die elektronische Fassung meiner Dissertation unter Wahrung meiner Urheberrechte und des Datenschutzes einer gesonderten Überprüfung hinsichtlich der eigenständigen Anfertigung der Dissertation unterzogen werden kann.

(§ 8 S. 2 Nr. 8 PromO)

Hiermit erkläre ich eidesstattlich, dass ich die Dissertation selbständig verfasst und keine anderen als die von mir angegebenen Quellen und Hilfsmittel benutzt habe.

(§ 8 S. 2 Nr. 9 PromO)

Ich habe die Dissertation nicht bereits zur Erlangung eines akademischen Grades anderweitig eingereicht und habe auch nicht bereits diese oder eine gleichartige Doktorprüfung endgültig nicht bestanden.

(§ 8 S. 2 Nr. 10 PromO)

Hiermit erkläre ich, dass ich keine Hilfe von gewerblichen Promotionsberatern bzw. -vermittlern in Anspruch genommen habe und auch künftig nicht nehmen werde.

……

Ort, Datum, Unterschrift